ORIGINAL PAGE IS
OF POOR QUALITY

References.

[1] Brasil-Japan Collaboration ; AIP Conf. Proc. Vol.85(1981) 500
[2] S.Hasegawa; Proceedings Int. Sympo. on Cosmic Rays and particle Physics, Tokyo (1983) 62 and 319
[3] M.Tamada ; 19th ICRC, HE 3.3-6
[4] USSR-Japan joint experiment ; 19th ICRC, HE 3.5-2
[5] H.Bielawska et al. ; Proceedings of Int. Sympo. on Cosmic rays and Particle Physics, Tokyo(1983) 374

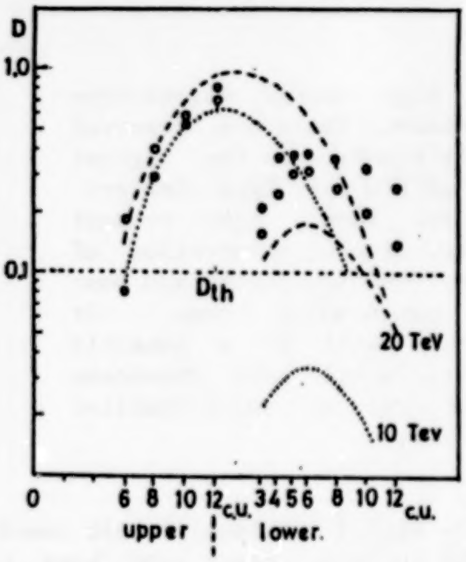

Fig.1 Penetrative nature of high energy(E > 10 TeV) single shower-upper and mini-clusters.
● : single shower-upper
○ : mini-clusters
Dth means threshold darkness of shower spot in X-ray films.

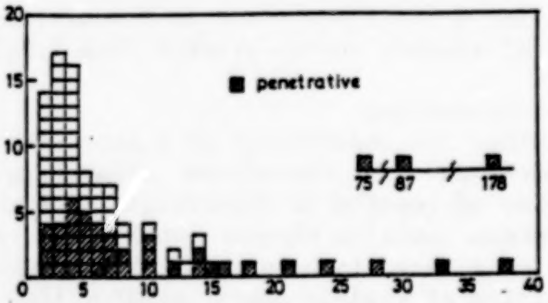

Fig.2 Histogram of shower core number in a mini-cluster.

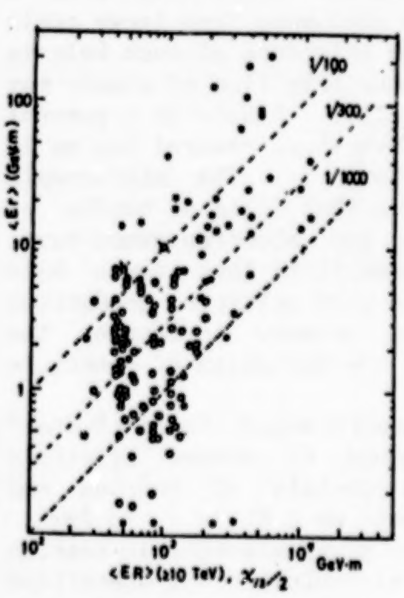

Fig.3 Scatter plot between two spread, <Er> of individual shower clusters and family spread, of Chirons and binocular families.
○ ; Chirons
● ; binocular families.

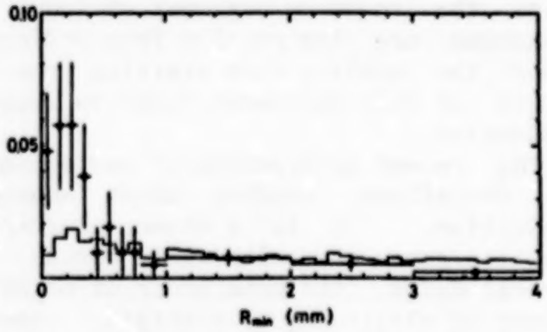

Fig.4 Distribution of relative distance, Rmin, between a hadron and its nearest neighbouring shower. Histogram is background distribution obtained by changing randomly azimuthal angle, ϕ, of hadrons in the observed events.

C-6

N85-35943

Giant Mini-clusters as Possible Origin of "Halo" Phenomena Observed in Super-families

Brasil-Japan Collaboration of Chacaltaya Emulsion Chamber Experiment

ABSTRACT

Among 91 mini-clusters from 30 high energy Chiron-type families in Chacaltaya emulsion chambers, there are observed several extremely large multiplicity clusters in the highest energy range, far beyond the average of ordinary type clusters. We put the name giant mini-cluster for them. The present paper describes some details of microscopic observation of those giants mini-clusters in nuclear emulsion plates and some phenomenological regularity found in common among them. It is discussed such giant mini-clusters will be a possible candidate of origin of narrow symmetric single halo phenomena in X-ray films which is frequently observed in super-families of visible energy greater than 1,000 TeV.

1. Introduction

Since the observation of a super-family with a spectacular halo named "Andromeda" in Chacaltaya chamber no.14 in 1969, there have been a number of reports on observation of such halo phenomena from large scale mountain emulsion chamber experiments, and the existence of such halo is now considered to be a remarkable general characterisitics of cosmic-ray families of visible energy greater than 1,000 TeV. A halo is a general darkened area in X-ray films, ranging from several to several ten mm in diameter, in the central area of super-family. The microscopic observation in nuclear emulsion plates reveals that it is a bundle of great number of shower particles, hadrons and electron/gamma-rays. Since the frequency argument excludes the possibility that those halo phenomena are the results from ordinary type pion multiple production under the scaling rule starting from proton primary incidence, the origin of halo phenomena seems to suggest us new mechanism of particle production.

The recent observation of new shower phenomena named "mini-cluster" in Chacaltaya chamber shows unusual nature of shower particle production. It is a shower cluster which consists of hadrons and electron/gamma-rays with small spread, as small as $\langle E(\gamma)r \rangle$ a few several GeV.m, the same order of magnitude as young atmospheric cascade shower of electromagnetic origin. Among 91 mini-clusters in Chacaltaya chamber no.19, we found several huge mini-clusters with very large multiplicities in higher energy and larger $\langle Er \rangle$ ranges in mini-cluster statistics, far beyond the average of ordinary mini-clusters. The present paper describes some details of such huge mini-clusters, the giant mini-clusters, as the possible origin of halo phenomena in X-ray film observation.

2. Characteristics of huge shower core bundles

We present in Fig.1 the relation between $\Sigma E(\gamma)-N$, total visible energy and multiplicity of shower cores with $E(\gamma) > 1$ Tev, and in Fig.2

< Er > -N, average spread and multiplicity, respectively, for all the observed 91 mini-clusters from 30 Chiron families in Chacaltaya chamber no.19[1] and one from no.18[2]. One sees most of the ordinary mini-clusters gathered around in small N and < Er >, region and, at the same time, we find a group of shower clusters of large multiplicities, say m > 30, with large Σ E and < Er > values as indicated by the mark(◎). Since we see the multiplicity and spread of those clusters are significantly greater than the average of the ordinary mini-clusters, we separate them from the ordinary mini-clusters and put the name "giant mini-cluster" for them. Table 1 gives details of those selected giant mini-clusters.

Table 1. Some details of giant mini-clusters

Event no.	Σ E(γ) (TeV)	N (>1 TeV)	< r > (mm)	< Er > (GeV.m)	family energy (TeV)
#174S-134I	1,056	158	2.88	10.00	1,164 (91 %)
#P06 (no.18)	961	123	1.77	7.40	1,272 (76 %)
#179S-126I	394	86	2.82	7.10	757 (52 %)
#174S-132I	270	98	2.84	4.80	342 (79 %)
# 93S- 56I	169	38	1.33	4.30	182 (93 %)
#165S-126I	126	30	1.79	5.73	156 (81 %)

Figures in bracket mean the energy fraction of giant mini-cluster to total visible family energy.

The following characteristics are remarkable to all the giant mini-clusters above selected. The first, they all show strong penetrative nature into lower chamber and we are able to see not small number of shower cores which could not be attributed to pure electromagnetic cascade originated from atmospheric electrons/gamma-rays. The second, shower bundles show small spread and extremely high rapidity density of number of shower cores in very narrow collimated region, as seen in Fig.3. Since the families are of very simple structure for all, the position of the origin of those giant mini-clusters is estimated to be near above the chamber, say less than 1 km or so. , Microscopic observation in nuclear emulsion plates for central region of giant mini-cluster shows that there are none or very rare of scattered background electron tracks in space among shower cores. Especially, it is reported[2] that the central halo part of the event P06(no.18) is produced ~200 m above the chamber by the triangulation measurement. These facts show the unusual large rapidity density which reflects approximately just the initial state of the production as it is, not severely distorted by the multiplication due to atmospheric degradation. The third, these giant mini-cluster occupy the substantial part of family energy as shown in Table 1, different from the ordinary mini-clusters of Chiron families.

Fig.4 gives the distribution of Er of individual shower cores in giant mini-clusters. The shape of the distribution is the same among them and seems to be well expressed by common exponential law. The average values are given in Table 1.

3. Mini-clusters and giant mini-clusters

At present, we are not able to explain fully the exotic nature seen in either mini-cluster and giant mini-cluster from the present knowledge of the particle production. However, simultaneous observation of those two in the same Chiron family is very suggestive to explore the nature of giant mini-cluster.

At one glance, we immediately noticed that the giant mini-cluster is not of simple symmetrical structure but there are recognized a number of localized sub-clustering. And it is clear enough to hypothesize that giant mini-cluster will be an ensemble of mini-clusters. Then, here is presented the results of sub-clustering into mini-clusters by computer algorithm[3] where the constant is assumed to be $E_c = 6$ GeV.m, which corresponds to assume the giant mini-cluster be an ensemble of mini-clusters with the average spread $\langle Er \rangle = 1 \sim 2$ Gev.m. Fig.5 gives the distribution of E^*r^* of mini-clusters in giant mini-clusters of the present examples, together with the big halo events Ursa-Maior and M.A.III[4] as the reference, for both of them the detailed microscopic observation in nuclear emulsion plates was carried out. We see good regularity of the spread E^*r^* for all the present samples except the case M.A.III, which is wide spread halo in X-ray film observation. The average value is given as $\langle E^*r^* \rangle = 30 \sim 50$ Gev.m. The hypothesis seems to be promising when we are required so rapid energy partition into a large number of minute low energy showers as is seen in experimental results.

4. Discussion

When we see two dimensional contour map of darkness of halo in X-ray films, we find varieties of core configuration. Some cases, it is of narrow single symmetrical core and the other cases, it is of multi-core structure. The event P06(no.18) is of clean single core halo in X-ray film observation, total darkness maximum of which is seen at ∿ 14 c.u. The shower clusters of event #174S-134I passes through the upper chamber before making a single definite halo in X-ray films. From these observation, single and narrow core halo in X-ray films seems to be nothing but huge shower clusters, the giant mini-cluster. When one looks multi-core events, like M.A.III, it seems it is an ensemble of the narrow single cores showing large spread as found in Fig.5.

Acknowledgement

The collaboration experiment is financially supported in part by Conselho Nacional para o Desenvolvimento Cientifico e Tecnologico, Fundacao de Amparo a Pesquisa do Estado de San Paulo, Financiadora de Estudos e Projetos, in Brasil, and Institute forCosmic-Ray Research, University of Tokyo and Grant-in-Aid from the Ministry of Education, in Japan.

Reference

[1] Brasil-Japan Collaboration ; this issues HE 3.5-3.

[2] N.M.Amato, N.Arata and R.H.Maldonardo ; Proc. Intern. Symp. on Cosmic-Rays and Particle Physics (1984) 123

[3] H.Semba ; Suppl. Prog. Theor. Phys. no.76 (1983) 111

[4] S.Yamashita ; Jour. of the Phys. Soci. of Japan Vol.54 No.2(1985) 529

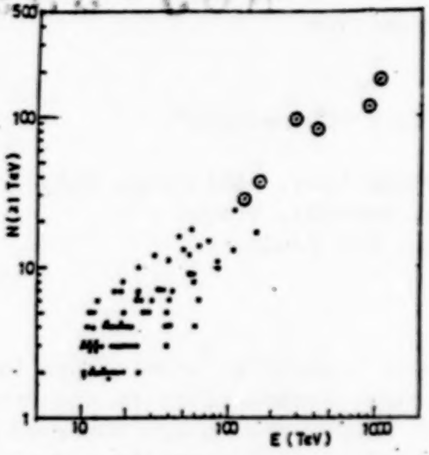

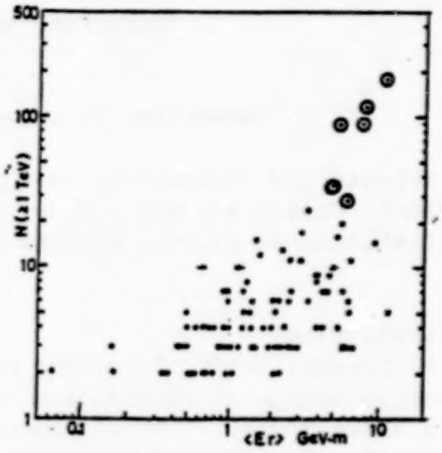

Fig.1 Relation between energy sum, E, and multiplicity, N(>1TeV), of shower cores in mini-clusters.
⊙: giant-mini-clusters (Table 1)

Fig.2 Relation between average spread, <Er>, and N(>1TeV) of shower cores in mini-clusters.
⊙: giant-mini-clusters.

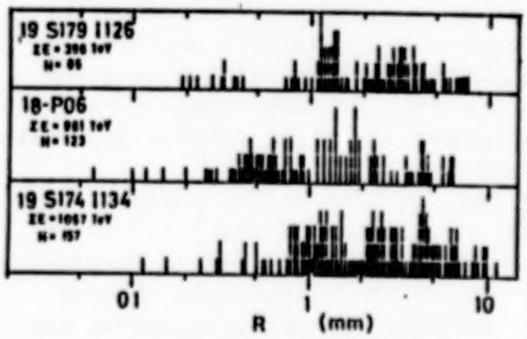

Fig.3 Log r -plot for shower cores of giant-mini-clusters.

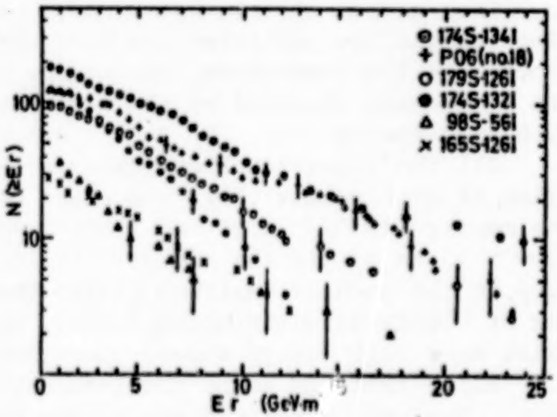

Fig.4 Integral distribution of Er of shower cores in giant-mini-clusters.

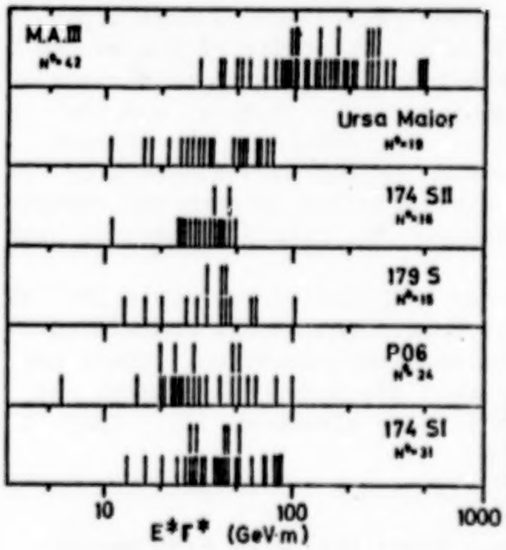

Fig.5 Distribution of E*r* of mini-clusters in giant-mini-clusters and huge core bundles of halo in super-families Ursa-Maior and M.A.III.

ORIGINAL PAGE IS
OF POOR QUALITY

N85-35944

Structure of Super-Families

S. Yamashita, A. Ohsawa+ and J. A. Chinellato°

Science and Engineering Res. Lab., Waseda Univ., Shinjuku, Tokyo.
+Inst. Cosmic Ray Res., Univ. of Tokyo, Tanashi, Tokyo.
°Instituto de Fisica, UNICAMP, Campinas, Sao Paulo.

I. Introduction.

At present study of nuclear interactions induced by cosmic rays is the unique source of information on the nuclear interactions in the energy region above 10^{15} eV. The phenomena in this energy region are observed by air shower array or emulsion chamber installed at high mountain. Emulsion chamber is the pile of lead plates and photo-sensitive layers (nuclear emulsion plate and/or X-ray films) to detect electron showers. High spatial resolution of photographic material used in the emulsion chamber enables us to observe the phenomena in detail, and recently experiments of emulsion chamber with large area are being carried out at high mountains by several groups in the world [1].

They are to observe the mixture of high energy hadronic and e.m. (= electromagnetic) particles produced through the nuclear and e.m. cascade process in the atmosphere, induced by high energy primary cosmic rays. The phenomenon observed by the emulsion chamber is called family, and that with high energy (say, $\Sigma E_\gamma > 10^{15}$ eV) is called super-family.

All the super-families, observed so far, consist of, on N-type X-ray films of high sensitivity, the black core and halo of radius $1 \sim 3$ cm in the center (called halo) and several hundreds of shower spots scattering over ~ 30 cm around the center. It is found by the microscopic observation in the nuclear emulsion plates that the halo is made of numerous number of electrons distributed densely and continuously, and that there exist many high energy shower spots even inside the halo.

Super-families carry the information of high energy nuclear interaction. However, since the events are very complicated, it is most important, we think, at first to make clear the whole structure of the events from the observed data. In other words the first step is to make clear how is the behaviour of the showers incident upon the chamber, and the second is what can produce such behaviour of the showers on the chamber. For the purpose of the first step we assume an appropriate function of energy-lateral distribution for the particles produced through the cascade process, and examine the inter-relation between the halo and detected high energy showers.

The five events analysed here are those with the energy above 10^{15} eV, observed by the series of emulsion chamber experiment at Mt. Chacaltaya (5,200 m, Bolivia), carried out by Brazil-Japan collaboration. Those are among 14 events, observed so far, and the rest are under measurement and analysis. Full description of the events is made elsewhere [2]. Table 1 gives a summary of the events.

II. Energy-Lateral Distribution of Showers

We here approximate the energy-lateral distribution of high energy showers incident upon the chamber, $F(E,r)\,dE\,2\pi r\,dr$, to be,

$$F(E,r) = AC\, r^{s-1} \exp[-\frac{1}{\sigma^2} (\ln \frac{Er}{a})^2] \qquad (1)$$

The distribution, Eq.(1), has the following nature which is fundamental for the particles produced through the cascade process.

(1) The relation, $Er \sim a$, holds with the dispersion σ around $Er = a$ in log-scale.

(2) Integration with respect to r gives the energy spectrum of, $2\pi A(E/a)^{-s}/E$.

The parameters in Eq.(1) are four; *A* relating to the absolute number of showers, *s* to the power index of the energy spectrum, *a* to the lateral spread and σ to the dispersion around the average of the lateral spread. And we determine the four parameters by comparing the energy spectrum and Er-distribution, obtained from the Eq.(1), with the experimental data.

The parameter values determined are tabulated in Table 2 for e.m. and hadronic particles. As to Urça Maior, only several showers have large Er-values and it is difficult to fit the distribution by one set of values.

(a) Lateral distribution of high energy showers.

Fig.1 shows how the lateral distribution, Eq.(1), of high energy e.m. showers, with the parameter values in Table 2, can reproduce the experimental data in case of Andromeda. The expected distribution can reproduce the experimental data in case of shower energy > 5 TeV and > 10 TeV, while the experimental data is short in number for E > 3 TeV. And the agreement becomes good if we adopt the observed number of showers at 3 TeV (the chain line in the figure) instead of the one extrapolated from the energy spec-

Table 1.

	Andromeda	Urça Maior	M.A. I	M.A. II	M.A. III
Halo	$\times 10^{16}$	$\times 10^{14}$	$\times 10^{15}$	$\times 10^{15}$	$\times 10^{15}$
Total energy (eV)	(2.1±0.5)	(9.8±0.2)	(3.2±0.2)	(1.3±0.2)	(5.1±0.5)
e.m. (eV)	1.6×10^{16}				4.4×10^{15}
hadronic (eV)	5.3×10^{15}				6.6×10^{14}
High Energy Showers					
(1) Central region					
Observed number					
e.m.	288	113	96	24	264
hadronic	45	14(22)	11(73)	-	60(101)
Total obs. energy					
e.m. (TeV)	3,585	582	958	437	1,566
hadronic (eV)	1,401(3,417)	281(439)	143(953)	-	516(875)
(2) Outer region					
Observed number					
e.m.	322	108	50	89	227
hadronic	75(183)	25(39)	2(13)	-	92(166)
Total obs. energy					
e.m.	833	355	212	520	782
hadronic	317(773)	267(417)	8(53)	-	622(1,054)

[Numbers in the parenthese are the corrected ones due to the detection efficiency for hadrons.]

trum. The agreement is good for M.A. I, II and III.

Fig.2 is that for the hadrons in the case of Andromeda. Deviation of expected distribution from the experimental data, suggests the hadron distribution is rather of exponential type.

(b) Comparison with halo data.

In this paragraph we examine whether the energy-lateral distribution, Eq.(1), with the parameter values in Table 2, can reproduce the behaviour of the halo. It is to see the behaviour of low energy showers, incident upon the chamber and not to be observed individually.

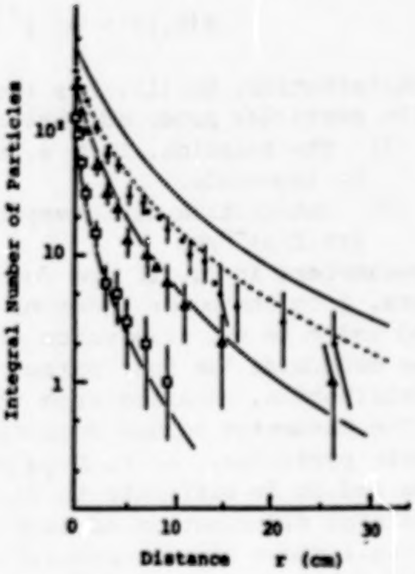

Fig.1. Lateral distribution of e.m. particles in integral form (Andromeda). The marks are for different energy thresholds; ● for E > 3 TeV, △ for E > 5 TeV, and □ for E > 10 TeV. The curves are the expected ones from the assumed energy-lateral distribution with parameter values given in Table 2. The chain line is the case when we adopt the observed number of showers instead of the one expected from the parameter values listed in Table 2.

Energy cut, E_{th}, at the low energy side is necessary to be introduced to reproduce the transition curve of the total electron number in the halo. The values of E_{th} for the events are listed in Table 2. One can see the values for four events except Andromeda are similar to the value of detection threshold of high energy showers of $E_d \sim 3$ TeV. It indicates the observed high energy showers are sufficient to produce the halo in the chamber. In the case of Andromeda the behaviour of the transition curve necessitates a number of low energy showers with the average energy of ~ 0.4 TeV. However, if we assume those showers follow the distribution of Eq.(1), those showers should fall around $r = z_{max}/E = 25$ cm, far from the central region.

Table 4

Event	$A(cm^{-s})$	s	a(TeV·cm)	σ	E_{th}(TeV)	z_{max}(TeV·cm)
(e.m. particles)						
Andromeda	7.8×10^2	1.36	6.7×10^{-1}	1.5	0.1	10.4
Urca Maior	-	1.87	-	-	2.0	-
M.A. I	9.8×10^6	1.94	7.5×10^{-3}	2.0	1.3	3.0
M.A. II	8.3×10^2	1.17	1.0×10^{-1}	2.0	1.0	8.2
M.A. III	5.6×10^5	1.85	2.1×10^{-2}	2.0	2.0	5.7
(hadrons)						
Andromeda	1.9×10	0.97	2.0	1.5		5.0
Urca Maior	-	0.94	-	-		-
M.A. III	8.6×10^2	1.25	2.6×10^{-1}	2.0		38.0

[z_{max} is the value of Er where Er-distribution becomes the maximum.]

ORIGINAL PAGE IS
OF POOR QUALITY

The fact that those showers exist inside the halo to contribute to the transition curve, indicates that they have smaller lateral spread. If these particles have the lateral spread characterized by the e.m. cascade process, their spread is, $r = z_{max}(\text{e.m.})/E = 1.5$ cm, which is consistent with the size of the halo.

It means Andromeda consists of two different kind of showers; one is characterized by $z_{max} = 10$ TeV·cm and the other by $z_{max} = 0.6$ TeV·cm. The former value may be due to nuclear cascade process and the latter due to pure e.m. cascade process.

The lateral distribution of the halo in Andromeda, in terms of track length density, is also consistent with the conclusion of two component of showers, stated above.

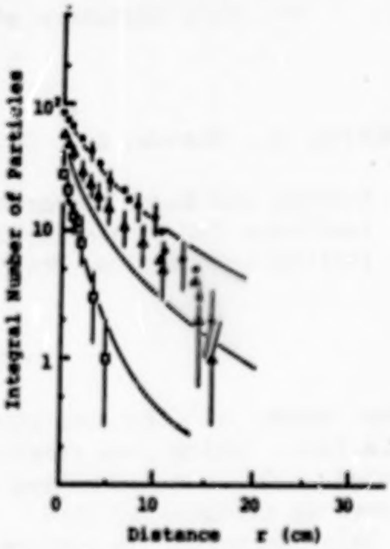

Fig.2 Lateral distribution of hadrons in integral form (Andromeda). See the caption of Fig.1 for the explanation of marks and curves.

III. Conclusion.

We analysed five highest energy events, $\Sigma E_\gamma > 10^{15}$ eV, observed by Chacaltaya emulsion chamber experiment. The results are;

(1) We tried to approximate the behaviour of high energy showers, e.m. and hadronic, by the function Eq.(1). The behaviour of e.m. particles can be described well by Eq.(1), both longitudinally and laterally, while hadrons have the lateral distribution of rather exponential type.

(2) We examined whether the halo can be explained by extrapolating the shower energy to lower energy side in Eq.(1). The four events except Andromeda can be explained by the behaviour of the observed high energy showers, while, as to Andromeda, low energy showers with average energy ∿ 0.4 TeV contribute significantly. And these showers has the spread consistent with that of pure e.m. cascade showers.

The authors thank to the member of Chacaltaya emulsion chamber experiment of Brazil-Japan Collaboration for their valuable discussions.

References

PISCRPP = Proc. Intern. Sympo. on Cosmic Rays and Particle Physics (Tokyo) (1984), Inst. Cosmic Ray Research, Univ. Tokyo, Tokyo.

[1] For example, contributions to PISCRPP and, S. G. Bayburina et al., Nucl. Phys. B191 (1981) 1.

[2] S. Yamashita et al., ICR-report 112-83-6 (1983), Inst. Cosmic Ray Res. Univ. Tokyo, and PISCRPP (1984) 30.

N85-35945

Extremely High Energy Hadron and Gamma-ray Families(III)

— Core Structure of The Halo of Superfamily —

Yamashita, S., Ohsawa, A.*, Chinellato, J.A.**, Shibuya, E.H.**

Science and Engr. Research Lab., Waseda University, Japan
* Institute for Cosmic Ray Research, University of Tokyo, Japan
** Instituto de Fisica, Universidade Estadual de Campinas, Brazil

Abstract

The study of the core structure seen in halo of Mini-Andromeda III(M.A.III), which was observed in Chacaltaya emulsion chamber, is presented. On the assumption that lateral distribution of darkness of the core is exponential type, i.e. $D=D_0\exp(-r/r_0)$, subtraction of D from halo darkness is performed until the cores are gone. The some quantity on cores obtained by this way are summarized. The analysis is preliminary and is going to be developed.

1 Introduction

Since one of the most powerful event, Andromeda(E_{halo} = 21,000 TeV), was observed in 1969, eight events with halo were detected by Brazil-Japan emulsion chamber collaboration experiment, at Mt. Chacaltaya, 5200 m at sea level, in Bolivia(1)(2)(3)(4)(5). The detailed study of halos tells the existence of various pattern of the core structure in halo, i.e., single core structure and/or multi-core structure.

Pamir group of emulsion chamber experiment, already, paid attention to this multi-core structure of halo and has derived the important results such as relative P_t of each core and alignment of the cores, etc.(6)(7).

On the other hand, Chacaltaya group has pointed out that the cores in halo correspond to the Jet-clusters obtained by the clustering analysis for individual high energy shower-particles and to the vestige of the nuclear interaction(5). Then in this article, we pick up the M.A.III for example of typical multi-core event and investigate the characteristic of the core structure in halo. The detailed description on M.A.III is presented elsewhere(5).

2 Method

2-1) Core structure of the halo

Fig.1 shows the two-dimensional distribution of darkness of halo in RR type X-ray film at 10 c.u. on M.A.III. The figure is processed by the micro-computer after getting the data by automatical photometry measurement at Institute for Cosmic Ray Research, University of Tokyo. The measurement is carried out by the square slit with the size of 300 μm and number of steps of measurement are 80 to both horizontal and vertical direction, i.e., the figure is made of the darkness of 80 x 80 cells. The numerals in the figure show the darkness $D(D=-\log_{10} I/I_0)$, where I_0 and I, respectively, express flux of the incident and transmitted light. In the figure, four cores are recognized and are named as H, I, J and L, respectively. The center of halo, $\vec{R}_G$, is defined by the following way to be presented by a mark of + . $\vec{R}_G = \Sigma \vec{r}_i D_i / \Sigma D_i$, where D_i and $\vec{r}_i$, respectively, represent the darkness and position vector of each cell.

2-2) Determination of incident direction

As an air family generally comes into the chamber with inclined direction and halo looks like a elliptical shape which extends to the incident direction, the correction for inclined incidence must be made. For the correction, we make the following way. One subtracts the $D=D_0(x_0,y_0)\exp(-r/r_0)$, (x_0,y_0) is the position of halo center and r_0 is arbitrary, from the all D_i of the cell. As the function, $D=D_0\exp(-r/r_0)$, is a circular symmetrical one on r, subtraction of this function from elliptical halo makes the plus area in both edge of long axis of ellipse and the minus area in both edge of short axis of ellipse when we chose suitable size of r_0. If we can get a line which is joined at two plus area, we determine the direction of the line as incident one and correction for inclined direction is made along the direction. In fact, the coefficient of correlation, R_{xy}, of the first degree is calculated and in the case when absolute value of it is greater than 0.5, we consider there is a linear correlation on x and y and determine the line of incident direction by the least square method.

2-3) Subtraction of the core from halo

We assume that the lateral distribution of the darkness of the core is $D(r,x,y,r_0)dr=D_0(x,y)\exp(-r/r_0)2\pi r dr$, and we input the position of the core, (x,y), and its mean spread, r_0. D_0 is the darkness of the core center and we can get the electron density, ρ_0 $(1/cm^2)$ at $r=0$ by transforming D_0 to ρ_0 .

The distribution, $D(r,x,y,r_0)$, thus defined is subtracted from the darkness of halo made of 80 x 80 cells(contour map) at each r in order of the magnitude of the core size and new contour map is constructed. In this time, correction for inclined incidence is made with the way described in preceding paragraph. Fig.2 shows the new map thus obtained by subtraction of the highest energy core L on the assumption of r_0=1.5 mm. In the figure, we can see the core L disappears and H, I and J cores survive. The same procedures are applied to the second highest core J with r_0= 1.5 mm and to the cores H, I with r_0=0.5 mm, respectively and the new map are shown in Fig.3. In the figure we can see all the four cores disappear.

3 Discussion

Table 1 shows the summary of some quantity on cores H, I ,J and L thus obtained. In the Table 1, ρ_0 and R_0 present electron density of the cores at r=0 and mean lateral spread of the cores, respectively. R is the distance from the center of halo to the core and Ne is a total electron number in the core obtained by $Ne=\int_0^\infty \rho_0 e^{-r/r_0} 2\pi r dr$. According to the simulation calculation by Makio Shibata, we can get the energy of core by transforming the number of electrons in core at 10 c.u. to the energy(8). E in Table 1 shows the energy of each core thus estimated. R_{ij} is a relative distance among each core and Z_{ij} is a quantity induced by Pamir group as $Z_{ij}=R_{ij}(1/N_i+1/N_j)^{-1}$, which is connected with the relative transverse momentum of each core(6)(7). ER_{ij} is the relative lateral spread of each core obtained by $R_{ij}(1/E_i+1/E_j)^{-1}$ using the energy of the cores instead of N_i. Fig.4 shows the scatter plot of the cores in E-R diagram together with that of computer-constructed A-jets. The triangles with capital letters H,I,J and L show the plots of the cores of M.A.III and the closed circles with small letter i,j and l show the A-jets of M.A.III which should correspond to the cores I,J and L as seen in ref.(5). The cores J and L well correspond to the A-jets j and l but correspondence of the core I to A-jet i is not so good. We suppose it is caused by using the unfit r_0. The core H is originated from hadronic component as seen in ref.(5) and the shower development does not still reach the maximum at 10 c.u..

This report is preliminary one and shows the new method of investigation of the core structure. There remain problems to be solved, such as the way of determination of r_0, the order of subtraction of the cores and derivation of the P_t from Z_{ij}, etc.. These problems are under considerations and we will make the answer on their problems in separate publication.

Acknowledgment

The authors would like to express their thanks to all the members of Chacaltaya emulsion chamber experiment. Special thanks are also to Profs. Y. Fujimoto and S. Hasegawa for their kind advices.

Figure captions

Fig.1: Contour map of halo in RR-type X-ray film at 10 c.u. on M.A.III. Cores H, I, J and L are recognized in it. Darkness are shown by numerals in figure.

Fig.2: Contour map of halo on M.A.III after subtracting the core L form Fig.1 with R_0=1.5 mm.

Fig.3: Contour map of halo on M.A.III after subtracting the core J from Fig.2 with R_0=1.5 mm and the cores H and I with R_0=0.5mm.

Fig.4: Scatter plot of the cores in E-R diagram together with that of computer-constructed A-jet. Marks are △ for the cores of M.A.III, ○ for A jet of Andromeda, × for A-jet of Ursa Maior and ● for A-jet of M.A.III.

Reference

(1) A. Ohsawa: ICR-Report-112-83-6(1983)65

(2) J.A.Chinellato: Dr Thesis; Universidade Estadual de Campinas (1981).

(3) K. Sawayanagi : Proc. Int. Sym. on Cosmic Ray and Particle Physics , Tokyo (1984)116.

(4) N.M. Amato et al.: Proc. Int. Sym. on Cosmic Rays and Particle Physics (1984)123.

(5) S. Yamashita: Jour. of the Phys. Soci. of Japan Vol.54 No.2(1985) 529.

(6) Pamir collaboration: Proc. 18th Int. Cosmic-Ray Conf. Vol.5 (1983)126.

(7) L.T. Baradzei et al.: Proc Int. Sym. on Cosmic Rays and Particle Physics, Tokyo(1984)136.

(8) M. Shibata et al.:Uchusen Kenkyu(in Japanese) Vol.26 No.4(1983)13

ORIGINAL PAGE IS
OF POOR QUALITY

Table 1

#	ρ_0(1/cm^2)	R_0(mm)	R(mm)	N_e	E(TeV)
L	2.63×10^7	1.5	1.65	3.72×10^6	580
J	1.91×10^7	1.5	0.55	2.69×10^6	420
H	2.27×10^7	0.5	2.84	3.56×10^5	56
I	6.25×10^6	0.5	1.86	9.81×10^4	15

#--#	R_{ij}(mm)	Z_{ij}(els.mm)	ER_{ij} (TeV.mm)
L--J	2.20	3.44×10^6	536
L--H	3.67	1.19×10^6	187
L--I	3.13	2.99×10^5	46
J--H	2.66	8.37×10^5	131
J--I	1.54	1.46×10^5	22
H--I	1.24	9.58×10^4	14

Fig.1

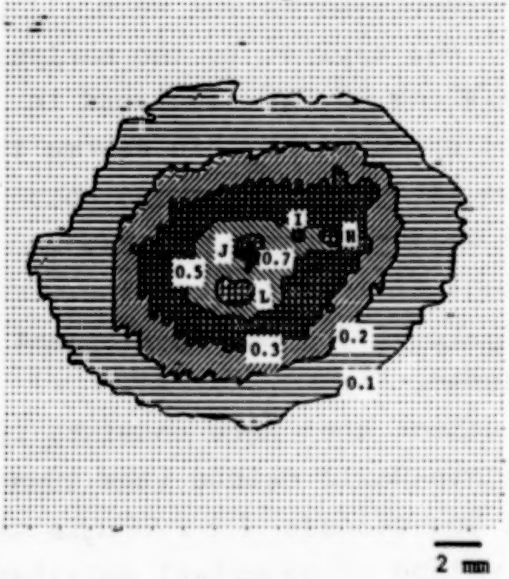

Fig.2

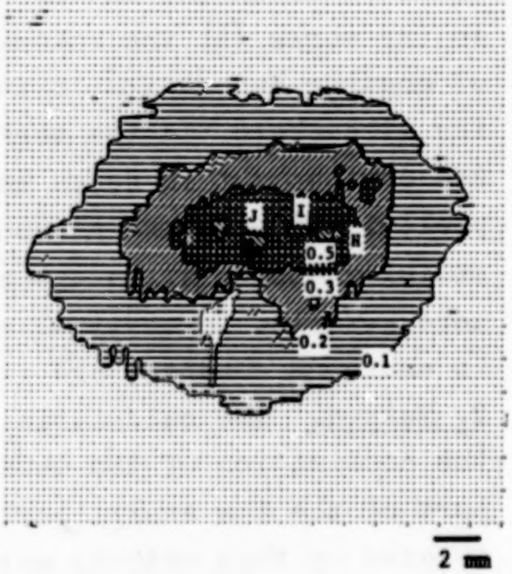

Fig.3

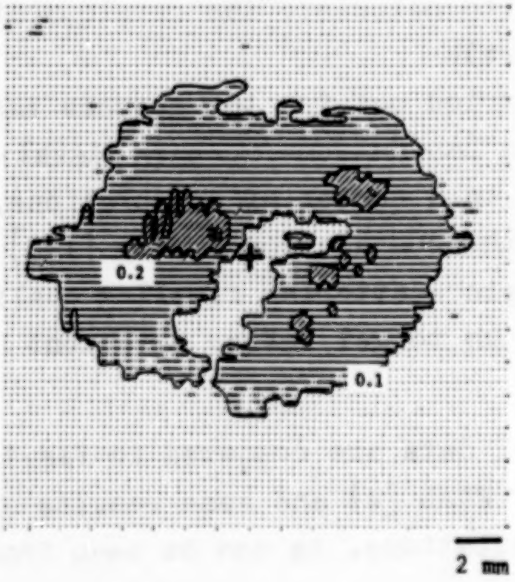

Fig.4

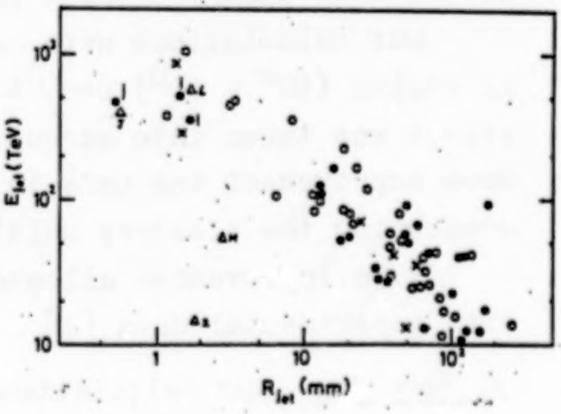

N85-35946

HE 3.5-9

NUMERICAL ANALYSIS OF ELECTROMAGNETIC CASCADES DEVELOPMENT IN EMULSION CHAMBERS

Plyasheshnikov,A.V.,Vorobyev, K.V.
Altai State University, Barnaul,
USSR

1. Introduction. A new calculational scheme of the Monte-Carlo method assigned for the investigation of the development of high and extremely high energy electromagnetic cascades (EMC) in the matter was elaborated in the work [1] . In the works [2] the scheme [1] was applied to the analysis of angular and radial distributions of EMC electrons in the atmosphere. In the work [3] by means of this scheme the EMC development in dense medium is investigated and some preliminary data are presented on the behavior of EMC in emulsion chambers. In the present article the results of more detailed theoretical analysis of the EMC development in emulsion chambers are discussed.

2. Method. The calculational scheme used here consists in the combination of the usual Monte-Carlo method (the transport of the low energy part of the cascade ($E \leq 5 GeV$)is calculated by this method) and a method of numerical solution of adjoint cascade equations (to calculate the development of the high energy cascade part).

Our calculations were carried out for the cascade energy region (10^2 - 10^5) Gev, the Landau-Pomeranchuk-Migdal effect was taken into account in a number of calculations. Some improvement was made in the computational code [1,3] concerning the electron multiple scattering sampling quality.

This improvement allowed us to get better agreement with experimental data [4] .

3. Results. Our calculational data are compared in fig.1 with the experimental data of FNAL [4] and some results of other Monte-Carlo method calculations. As can be seen from

fig.1 our data are in good agreement with experimental results [4] and calculations of Okamoto and Shibata [5] (for $R = 50, 100\ \mu m$ and the upper side of emulsion our results and data [5] practically coincide). At the same time there exists considerable difference of all results presented in fig.1 from the Monte-Carlo method data [6] . To our opinion this difference may be explained by the not quite correct account of the multiple scattering of cascade electrons in [6] .

A comparison of our data for homogeneous medium with analytical data [7] evaluated in the core approximation is given in fig.2. As can be seen, our data for $R = 200\ \mu m$ are in a rather good agreement with analitical results corresponding to the simple saddle point method condition, but there exists considerable disagreement with the data using complicated condition of this method.

It is well known that core approximation data on average number of EMC electrons in a small radius circle are invariant with respect to production E_0R of primary energy E_0 and radius R. Fig.3 shows that such invariance takes place only approximately and only for relatively small values of E_0R.

Fig.4 illustrates the difference in the development of EMC in homogeneous medium of lead and a real emulsion chamber. Analytical data [8] taking into account only single emulsion layer are given there too. A qualitative agreement between numerical and analytical data is observed.

References:

1.Plyasheshnikov,A.V.,Vorobyev,K.V.,(1981),17th ICRC,5,206.
2.Lagutin,A.A.,et.al.,(1981),17th ICRC,5,198;5,202.
3.Plyasheshnikov,A.V.,Vorobyev,K.V.,(1983),18th ICRC,11,73.
4.Hotta,N.,et.al.,(1980),Phys.Rev.D, 22, 1,
5.Okamoto,M.,Shibata,T.,(1981),17th ICRC,5,214.
6.Van Ginneken,A.,(1978),Preprint Fermilab.FN - 309.
7.Fedorova,G.F.,Roganova,T.M.,(1980),Pamir Collaboration Workshop,Gedzina (Poland),p.26.
8.Guzhvin V.V.,Ivanenko,I.P.,et.al,(1975), 14th ICRC,7,2637.

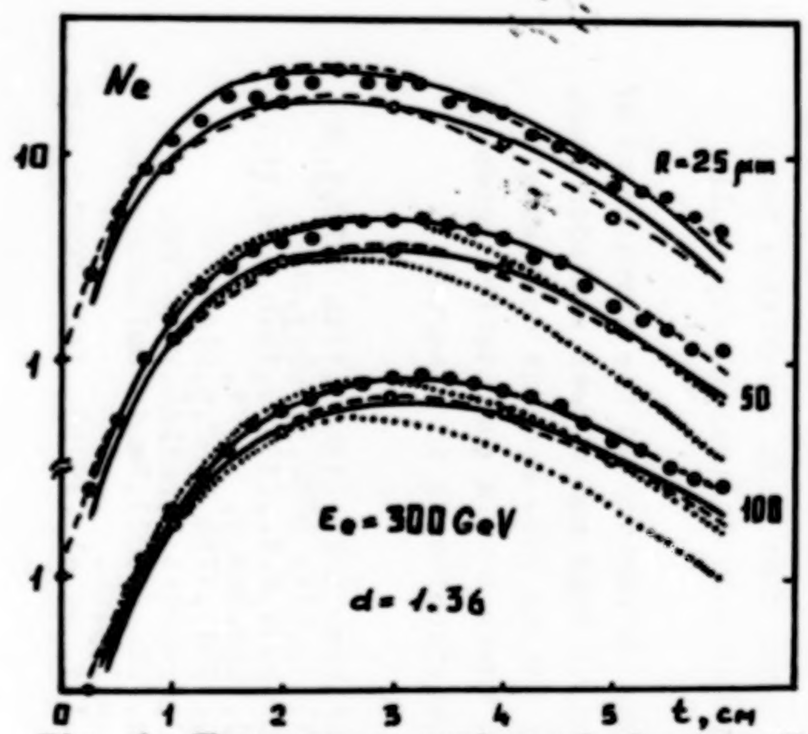

Fig. 1. The average number of electrons N_e within 25,50 and 100 μm for the chamber of the structure described in [4]. ●,○ - experimental data [4] corresponding to the upper (●) and lower (○) emulsion sides, —— - our data, - - - - data [5], ... - data [6]

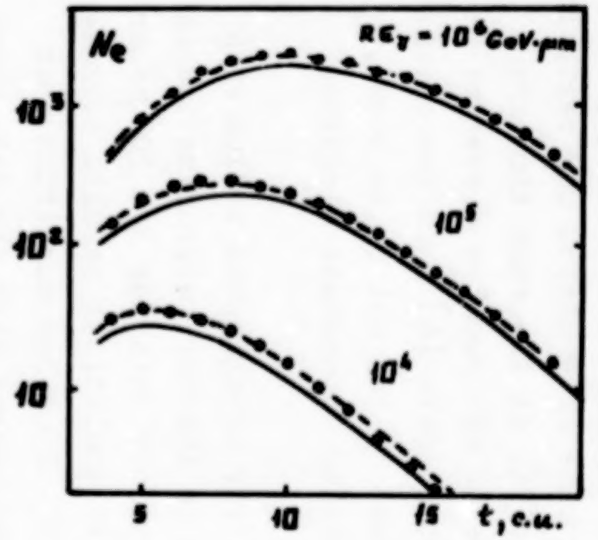

Fig.2. The average number of cascade electrons N_e within radius $R=200\mu m$ for the homogeneous lead absorber. ●- our calculation, curves are the core approximation data [7] corresponding to usual (- - - -) and complicated (——) saddle point method conditions.

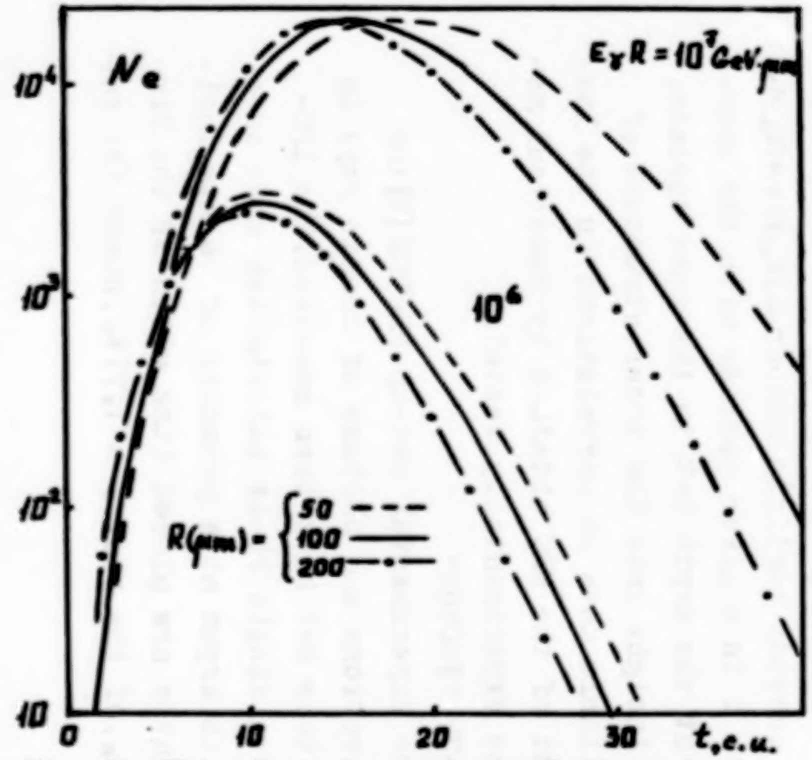

Fig.3. The average number of cascade electrons N_e in the homogeneous lead absorber. The LPM effect is taken into account.

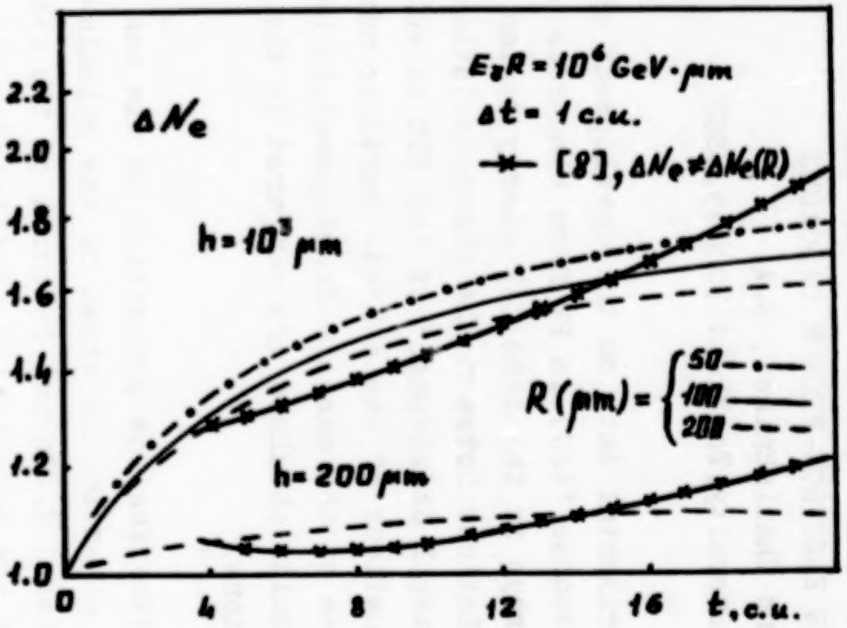

Fig.4. The ratio ΔN_e of average number of electron tracks for homogeneous medium of lead and the lower emulsion side of the chamber having the lead layers thickness Δt = 1c.u. and emulsion (or film) layers thickness h.

N85-35947

AN EXPERIMENTAL STUDY OF CORRELATIONS IN THE DEVELOPMENT OF THE ELECTRON-PHOTON CASCADES

Kratenko, Yu.P. and Charishnikov, S.A.
Tashkent State University,Tashkent 700095,USSR

ABSTRACT

In terms of the experimental data on the development of the electron-photon cascades (EPC) in Pb from electrons and photons of cosmic rays in the tens GeV energy region a calculation of correlations between the characteristics of longitudinal and lateral development of the EPC as well as those between fluctuations of the cascade particle numbers at different stages of the cascade development,is being carried out.The results obtained are compared to the numerical EPC calculations.

1. INTRODUCTION

Among methods characterizing the properties of the cascade processes special attention is drawn to the calculation of correlation between different features of the cascade.Note,a sequence of the correlation coefficients (time-correlation $r(\tau)$) determining a random relation between fluctuations of the cascade particle number $u(E_0,t)=n(E_0,t)-\overline{n(E_0,t)}$ at the depth t in a given cascade with the energy E_0 and $u(E_0,t+\tau)$ at the depth $t+\tau$ in the same cascade, gives a fairly deep insight into the inner structure of the process.The available data on correlations in the longitudinal development of the EPC obtained by numerical methods [1÷4] needs to be experimentally tested.

2. EXPERIMENTAL SET-UP "PHOTON"

With the aid of the experimental set-up PHOTON [5] the EPC's from single electrons and photons of cosmic rays in the energy range of tens GeV have been measured.The EPC-detecting section is a single Pb-Ar calorimeter made as a steel tank filled with argon at a pressure of 16 atm,inside of which 16 Pb plates are placed (the width of the first 11 plates is $0.9t_0$,of the rest 5 - $1.77t_0$,where the radiative unit t_o is 7,4 g/cm^2).Between the plates on the isolators 16 steel strings 0,5 mm of thickness spaced between 3 cm are stretched.Thus obtained 16 ionization chambers(IL) lack in each IL hollow walls and diaphragms,therefore,there is practically no transition effect.To study a spatial development of the EPC strings in the neighbouring IL's were perpendicular placed.PHOTON was exposed at the height of 3160 m over the sea level.Principles of the initial information selection allowed us to take 383 EPC's for analysis. Statistical simulation of experimental conditions and IL calibration showed that the error in measuring E_o,and the number of cascade particles $n(E_o,t)$ is approximately the same being averaged as $\sim 7\%$.

3. RESULTS AND DISCUSSIONS

Comparison of a typical experimental time-correlation $r(\tau)$ with results from[4] by the incomplete Monte-Carlo method shows good agreement (Fig.1).Fit of $r(\tau)$ to the time-correlations of simple autoregression Marcoff and Yule models in Fig.1 is unsatisfactory,especially for large τ .However,the rms deviation of $r(\tau)$ values is known to increase with τ and after a small quantity of runs ($\sim$20-30) is comparable with $r(\tau)$ for large τ,the significance level being $\sim$0,4[6,7].In this case following[7] there are no $u(t)$ fluctuations,a series of $u(t)$ where t is determined by t_o ,can be described by the Marcoff model,i.e. there is a correlation only between $u(t)$ and $u(t+1)$.The corre-

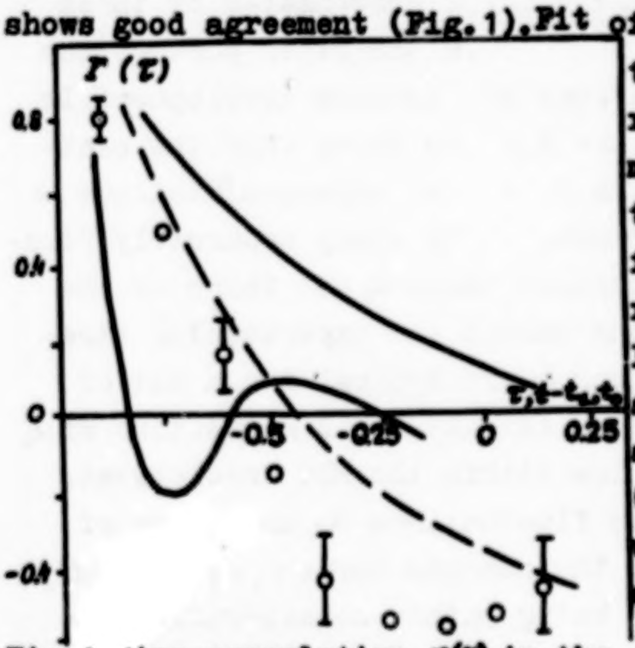

Fig.1 Time-correlation $r(\tau)$ in the EPC.o- the present experiment,(--)- calculation 4 ,1-Marcoff model, 2 - Yule model.

lation interval being $\tau_0 = \int |r(\tau)| d\tau$ [8], or "separation" between depths in t_0 at which cascade fluctuations can be considered as independent, fairly strongly changes with E_0 from $2{,}5 t_0$ for $E_0 \approx 30$ GeV up to $3{,}5 t_0$ for $E_0 = 80$ GeV. Therefore, with the increase of E_0 the values of $r(E_0,t,\tau=1)$ grow through t_0, and the minimum of $r(E_0,t,\tau+1)$ shifts towards the deep depth (Fig.2).

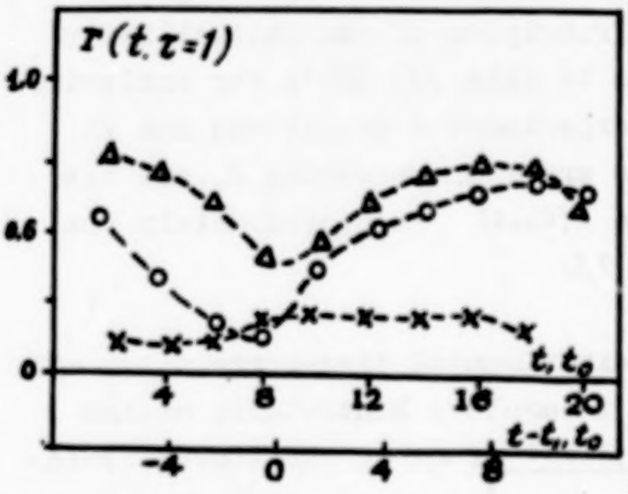

Fig.2 Experimental correlations of $r(t,\tau=1)$. o - E_0=30 GeV, Δ - E_0= 80 GeV, x - for the EPC with E_0 = 80 GeV in the central approach.

The profile of $r(E_0,t,\tau+1)$ coincides with the calculation results [2,3]. Note, that occurence of anticorrelations for large τ is readily explained by the EPC energy conservation law: fluctuations for one region of depths should be compensated by those in the other part of the cascade development. It is known that the central approach [8] allows us to study separately fluctuations directly of the cascade shape u_c and those of the shift u_λ. As our calculations showed the experimental time-correlations for fluctuations u_c are typical for a set of independent random quantities (Fig.2), the distribution of u_c being obeyed to the Gauss law within the EPC development. Consider a relation between fluctuations u_λ and those of the "center-of-gravity" of the cascade curve $t_1 = \int t n(E_0,t) dt / \int n(E_0,t)\, dt$, the latter being rather considerable: $\sigma_{t_1} = 1{,}5$ for E_0=30 GeV. The value of the area under the transition curve $\rho(t)$ can serve as an estimate for the absorbed energy in the cascade, and thus, characterize the cascade particle behaviour [9]. Correlations between $\rho(t)$ at the early stages of the EPC development $(t \leq 2t_0)$ and t_1 turned out to be rather high: ~0,55 and ~0,70 for the EPC^e from the primary electrons and the EPC^γ from photons, respectively. That is, fluctuations of t_1 are generally determined by those of the shift u_1. At the same time a correlation between $\rho(t \leq 2t_0)$ and the second central momentum $\mu_2^{1/2}$, characterizing the longitudinal EPC dimension, is small: for EPC^e ~0,16, for EPC^γ ~0,27. Finally, a correlation between the rms deviation of r_s of the spatial cascade ionization distribution within different depths is not considerable: ~0,3, being independent of the primary particle type and the depth t . A correlation between r_s and $\mu_2^{1/2}$ is practically independent of the primary particle type and E_0 tends towards zero in the region of depths up to $(\ln(E_0/\beta)+2)t_0$, then it gradually grows to 0,4 in the deep depth region. Thus, in the wide range of depths lateral and longitudinal dimensions of the EPC are independent.

References

1. Borkovsky M.I., Reprint of Leningrad Nuclear Physics Institute, No 566, 1980.
2. Betman R.G., Gedalin E.N., in "Nuclear interactions in high energy region", Tbilisi, USSR, 1976, v.2, p.13.
3. Lagutin A.A., Plyasheshnikov A.V., Uchaikin V.V., Vetoshkin V.V. The 17th ICRC, Paris, 1981, v.5, p.198.
4. Kirillov A.A., Lyotov Yu.G. Reprint FIAN USSR, No278, 1982
5. Asimov S.A., Glukhov G.A., Daudov Z.H. et al., Reprint of Tashkent Nuclear Physics Institute, NoP-7-22, 1981.
6. Mendall M.G., Stuart A., Design and analysis and time-series, in Russian, Moscow, Nauka, 1976.
7. Chetyrkin E.M., Kalikhman I.L. Probability and Statistics, Moscow, 1982.
8. Kokoulin R.P., Petruchin A.A. Nucl. Phys. USSR, 1980, v.32, 4(10), p.1030.
9. Ivanenko I.P. Electromagnetic cascade processes.- Moscow, 1972.

N85-35948

THE ELECTROMAGNETIC COMPONENT OF ALBEDO FROM SUPERHIGH ENERGY CASCADES IN DENSE MEDIA

Golynskaya R.M., Hein L.A., Plyasheshnikov A.V., Vorobyev K.V.

Institute of Nuclear Physics, Moscow State University,
Moscow 119899, USSR

Albedo from cascades induced in iron by high-energy gamma-quanta were Monte-Carlo simulated. Thereafter the albedo electromagnetic component from proton-induced cascades were calculated analytically. The calculations showed that the albedo electromagnetic component increases more rapidly than the nuclear-active component and will dominate at sufficiently high energies.

1. Introduction. When a calorimetric installation is used to detect high energy particles essential methodical difficulties are caused by albedo from absorber. Experiment shows that at energies of several TeV the nuclear-active component contributes the most into the albedo effect, and the dependence of albedo on primary energy is rather weak, i.e. logarithmic. Calculations of the albedo from electron-photon cascades so far performed to energies of 100 GeV show that the albedo electromagnetic component increases more rapidly, according to a power law. It indicates that further rapid increase being present, the electromagnetic component will dominate and provide a rapid increase with energy of the overall albedo flux.

A semi-analytical Monte-Carlo method described in /1/ allowed calculations of albedo from the electron-photon showers to highest energies of interest now. In /2/, the results for lead have been reported. We present here the results on the albedo from iron. The results obtained were used to calculate the electromagnetic component of albedo from a primary proton-induced cascade. Since, according to the calculations, the albedo electron flux is 2-3 orders less than the gamma-quantum flux, results on the gamma-quantum albedo only are presented.

2. Results for primary gamma-quantum. Fig.1 shows the energy dependence of the albedo gamma-quantum flux for three angles of incidence of a primary gamma-quantum. One can see that this dependence is, with a high accuracy, a pure power law $N_\gamma \sim E^\delta$.

Fig.2 presents the albedo gamma-quantum flux versus cascade production depth. The results are for two primary energies and two incidences(production depth is measured along the normal to the entrance plane). It can be noted that i) the exponent $N_\gamma(t) \sim e^{-\mu t}$ provides a good description; ii) the rate of albedo attenuation somewhat increases with energy, e.g. μ (3 GeV)=.92, $\mu(10^3$ GeV)=.71.
iii) the results for various incidence angles demonstrate a very high similarity. In Fig.3 the dependence of the mean

energy of albedo gamma-quanta on the primary gamma-quantum energy is shown for three incidence angles. The mean energy can be seen to somewhat increase with primary energy.

In Fig.4, the energy spectrum of albedo gamma-quanta is presented for a primary energy of 10^3 GeV and a normal incidence. It can be noted that about 90% of the photons are confined within the energy interval to 1 MeV.

Fig.5 shows the rms radius versus primary energy. We present the results for a normal incidence and two production depths t=0 and t=2. With an increase of primary energy the area of albedo emission first apparently broadens, but at higher energies one could suppose some narrowing. In Fig.6, the albedo gamma-quanta radial distribution is shown for energy 3 GeV and a normal incidence.

The angular distribution of albedo gamma-quanta is practically izotropic in the angular range from 30° to 70°, the mean cosine being eqaal to $\cos$=.7 and independent of both energy and shower incidence angle.

3. Discussion of results for primary gamma-quantum. We make here an attempt to obtain the general features of the albedo behaviour by constructing a rather simple model of its production and applying the results of cascade theory. It proved to be feasible to deduce a simple formula which represents a good reflection of the dependence of albedo on energy and incidence angle $N_\gamma(E,t,\cos\Theta) \sim \left(\frac{E}{\beta}\right)^s e^{-\mu t} / -\lambda_1(s)$ where β is the critical energy, $\lambda_1(s)$ being the known cascade theory function, and s is found from the equation $\lambda_1(s) = \mu\cos\Theta$.

This formula can be thought to be approximating over E, t, and $\cos\Theta$, i.e. the values of N and μ being once taken from calculations for one energy, the albedo values can be found for all energies and incidences. The agreement with calculations is demonstrated by the following comparison: if the value of μ at E=3 GeV is taken, $N \sim E^{.48}$/calculations yield $E^{.48}$/ is obtained for a normal incidence and $N \sim E^{.62}$ /calculated value is $E^{.63}$/ for the incidence angle $\cos\theta$=.6.

4. Primary proton. The above discussed features of the behaviour of albedo from a primary gamma-quantum allowed analytical going over to the albedo from a primary proton. The expression for the mean albedo value reads

$$N_\gamma^p = \left\{\frac{2}{s+1}\,\frac{f_{N\pi}(s)}{\mu\lambda_N+1-f_{NN}(s)}\left[1+\frac{2f_{\pi\pi}(s)}{\mu\lambda_\pi+1-2f_{\pi\pi}(s)}\right]\right\} N_\gamma^\gamma(E_p)$$

Here $f_{ij}(s) = \int dx\,\frac{x^s}{\sigma_{ij}}\,\frac{d\sigma_{ij}}{dx}$

in the $h_i+A=h_j+x$-reaction, where a h_{ij} hadron is either nucleon or pion, λ_i being the nucleon or pion interaction length. The above expression shows that the contribution of the secondary interactions is about 25%, i.e. the albedo is mainly determined by the first interaction characteristics and primary proton path. Only the variation of these characteristics and μ with energy provides a weak energy dependence of the expression in the figure brackets, i.e. the albedo energy dependence maintains to be a power law with about the same exponent S. For the inclusive distributions and interaction lengths corresponding to the modern accelerator data the calculated values for the coefficient of transition from a primary gamma-quantum to a proton/expression in the figure brackets/ are the following

$$\{\ldots\}_{\cos\theta=1} = 0.16\ , \quad \{\ldots\}_{\cos\theta=0.6} = 0.082$$

5.Conclusion. The gamma-quantum albedo indicates a rapid power law increase of $N \sim E^s$, where $s \gtrsim 0.5$, to the highest energies for which the calculation was performed. The mean energy of albedo gamma-quanta slightly increases with primary energy, the lateral distribution becomes broader, and the angular distribution maintains its shape, being close to the izotropic one. We should notice finally, our simulations do not incorporate the Landau-Pomeranchuk effect. The effect should reveal itself in Fe at energies $>10^{14}$ eV, i.e. providing far deeper cascade development the albedo should sharply decrease with energy (see /2/).

References

1. Plyasheshnikov A.V., Vorobyev K.V., 1981, Proc. 17th ICRC, 5, 206.
2. Plyasheshnikov A.V., Vorobyev K.V., 1983, Proc. 18th ICRC, 11, 73.

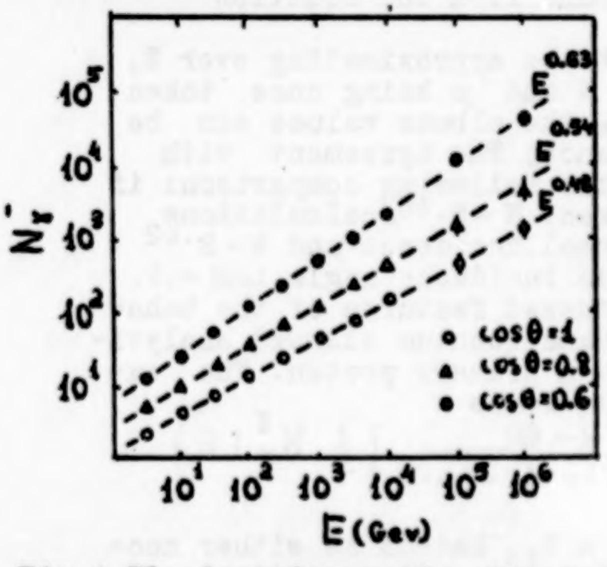

Fig.1.The dependence of the albedo flux on the energy of the primary gamma-quantum. Lines are for the power approximation.

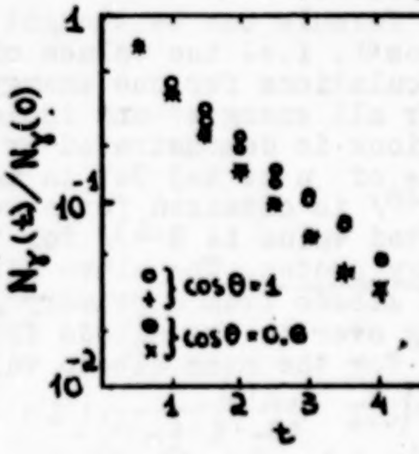

Fig.2.The albedo attenuation with the shift of the cascade generation point.

Crosses are for primary energy $E = 3$ GeV;
circles - 10^3 GeV.

ORIGINAL PAGE IS
OF POOR QUALITY

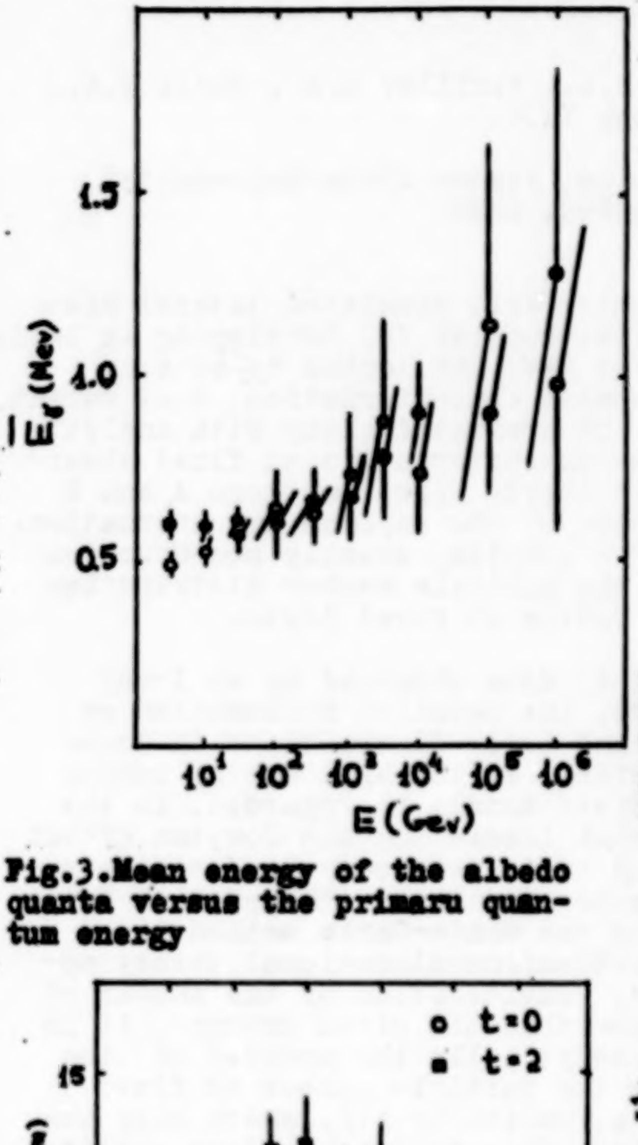

Fig.3.Mean energy of the albedo quanta versus the primaru quantum energy

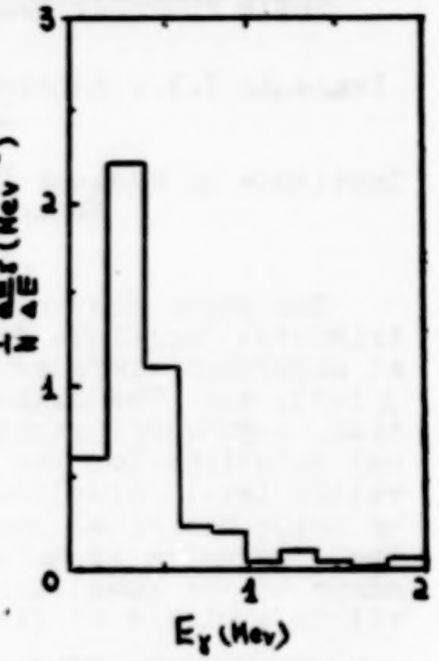

Fig.4.The energy spectra of the albedo quanta. The primary quantum energy is 10^3 GeV, normal incidence

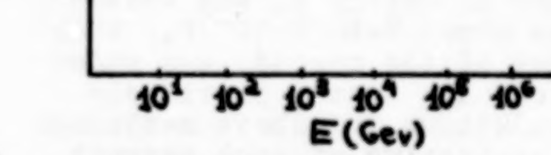

Fig.5.The albedo RMS radius vs primary energy, for two depths of the cascade generation, normal incidence

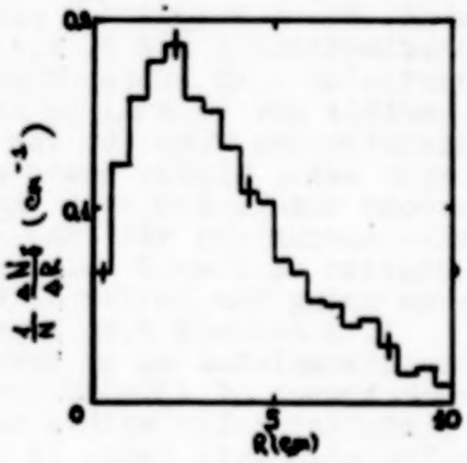

Fig.6.The albedo quanta radial distribution. Primary energy is 3 GeV, normal incidence

N85-35949

INTEGRAL FUNCTIONS OF ELECTRON LATERAL DISTRIBUTION AND THEIR FLUCTUATIONS IN ELECTRON-PHOTON CASCADES

Ivanenko I.P., Kanevsky B.L., Kirillov A.A., Linde I.A.,
Lyutov Yu.G.

Institufe of Nuclear Physics, Moscow State University,
Moscow 119899, USSR

The paper presents Monte-Carlo simulated lateral distribution functions for electrons of EPC developing in lead, at superhigh energies (.1-1 PeV) for depths $t \lesssim 60$ c.u. $\Delta t=1t_0$ c.u. The higher moment characteristics, i.e. variation, asymmetry, excess, are presented along with analytical solutions for the same characteristics at fixed observation level calculated to theory approximations A and B by using numerical inversion of the Laplace transformation. The conclusion is made of a complex, usually non-Gaussian shape of the function of the particle number distribution within a circle of given radius at fixed depth.

To analyse experimental data obtained by an X-ray emulsion chamber technique, the detailed information on mean EPC characteristics and their fluctuations in dense media is necessary. Therefore, in the high energy region The Landau-Pomeranchuk effect should be regarded, in the low energy region ionization losses and the Compton effect should be allowed for, and it is necessary to describe rather correctly the scattering processes. The problem being extremely complex requires the Monte-Carlo method to be used. For a simplified problem(one-dimensional theory approximations A and B, i.e. consideration of the number of particles with energy higher than the given energy), it is possible now to analyse analytically the problem of the distribution function for the particle number at fixed depth using higher moments, unlike to /1/, where only the second moment has been used. This approach allows qualitative comparison with the Monte-Carlo results and is of interest in itself as an approbation of the technique(e.g. when using the latter to analyse quark-gluon cascades).

1. A cascade from a primary of energy E_0 was Monte-Carlo simulated up to energies about $E=10^{-2}-10^{-3}E_0$, then each branch of 130-150 branches of the cascade was ended by statistically with a mean cascade from a previously calculated data bank. In calculations the above mentioned processes were regarded, and scattering at each segment of the free path was considered in the Fermi approximation/2/. An estimate by the method of standards assuming the initial distribution to be non-Gaussian/3/, showed that, in the range $(1/2 \div 2)t_{max}$, where t_{max} is the depth of a mean shower maximum($t_{max} \gtrsim 20t_0$), a statistics of 100 events yielded an error(standard) of the mean to be 2-3%,

of variation ~ 10%, of asymmetry 20-30%, and of excess 40-80%. Calculations were made on a net of 14 radii (1-400 um) given uniformly in logarithm of spatial variable, (lgr), that made it feasible to plot the differential $P(E_0,r,t)$ lateral distribution function: the particle number at distance r from the axis at depth t. The obtained differential functions were integrated and approximated.

Figs.1 and 2 compares our calculations (see the solid lines) with the experiment/4/ for the differential and integral distribution functions. The experimental results are presented for front-side film of a type C-chambers woth delution factor d=1.18 leading to a decrease of the particle number in cascade with increasing depth.

Fig.3 shows the results for 8 values of primary γ. The bundles of curves are parametrized by the product E_0R. The point in Fig.3 are for the results/5/. This figure illustrates violation of the core approximation of the Landau-Pomeranchuk effect. The investigation of fluctuations of the particle number within a circle of given R substantiates the general picture of evolution of the density distribution function/6/ - at $t \lesssim 1/2\ t_{max}$ and $t \gtrsim 3/2\ t_{max}$, the distributions are narrow-peaked and skewed towards the small particle number (to the left), at $1/2\ t_{max} \lesssim t \lesssim 3/2\ t_{max}$ these distributions shift to the right transforming through symmetric distributions into asymmetric ones with a flat maximum(or several maxima), Gaussian distributions in the region of t_{max} are rather an exclusion than a rule. The results under consideration give a considerable qualitative clarification of the earlier data and allow investigation of the dependence on R or, what is the same, on the efficient value of threshold energy. Figs.4-6 shows $Var(E_0,t)=\sigma/m$, $As(E_0,t)=m_3/\sigma^3$, $Ex(E_0,t)=m_4/\sigma^4-3$ where $m_i=\frac{1}{n}\sum(N(E_0,R,t)-m)^i$ the numbers are for energy in TeV, R=140 um(a) and radii in um(b). The influence of the Landau-Pomeranchuk effect can be clearly seen in Fig.4 - the curve minimum at E_0 10 TeV (see Fig.4a); degrading(see Fig.4b) with increasing R corresponds to a decrease of efficient threshold energy, i.e. a weaker influence of the Landay-Pomeranchuk effect on a cascade.

2. To analyse analytically the set of equations for higher moments of the function of distribution over the particle number in approximation A, it is written in the similar form as in /1/. The solution of this set of equations can be obtained to approximation A for homogeneous cross sections and any moment using the Mellin transformation in energy E_0/1/. For the first, second, third etc. moments of the functions of distribution over the particle number in a shower induced by a primary electron the solutions can be represented as follows /7/:

$$\overline{N_e^1}(E_0,E,t)=\frac{1}{2\pi i}\int_{-i\infty+A}^{+i\infty+A}ds\,(E_0/E)^s\,\varphi_1(s,t)\,\frac{1}{s}$$

$$\overline{N_e^2}(E_0,E,t)=\frac{1}{(2\pi i)^2}\iint_{-i\infty+A}^{+i\infty+A}ds_1\,ds_2\left(\frac{E_0}{E}\right)^{s_1+s_2}\varphi_2(s_1,s_2,t)\,\frac{1}{s_1s_2}$$

$$\overline{N_e^3}(E_0,E,t)=\frac{1}{(2\pi i)^3}\iiint_{-i\infty+\Delta}^{+i\infty+\Delta} ds_1\,ds_2\,ds_3\left(\frac{E_0}{E}\right)^{s_1+s_2+s_3}\psi_3(s_1,s_2,s_3)\,\frac{1}{s_1s_2s_3}$$

etc.

In the cascade theory approximation B similar formulae for higher moments can be obtained. These integrals for a moderate values (n =1,2,3,4) can be calculated using the numerical Laplace inversion. These calculational results are listed in Table 1 and show qualitative agreement with the simulation results. Around the shower maximum we can perform the detailed analysis of higher moments and structure of the distribution function at $E_0/E(E_0/\beta)$. Using the saddle point method ($S_{s.p.}-1$) it can be shown that in the region of shower maximum

$$Var \sim A_2/\sqrt{\ln E_0/E}$$

i.e. Var decreased slowly, as $\sqrt{\ln E_0/E}$, with increasing ratio E_0/E/8/. Asymmetry and excess increases

$$A_x \sim A_3\sqrt{\ln E_0/E}\,,\quad E_x \sim A_4 \ln E_0/E$$

This behaviour of higher moments contradicts the assumption of the Gaussian shape of the distribution functions for the particle number.

The investigation showed that fluctuations of the distribution functions for the particle number within a circle of fixed radius and those of the function of the number of particles with energy higher than the given energy are of similar character, oscillations of higher moments show evidence of a complex structure of the distribution functions and indicate that Gaussian distribution is rather an exclusion than a rule.

References

1. Yanoshi L., JETP, 26, 386, 518, 1954.
   Gerasimova N.M., Trudy FIAN, 26, 192, 1964.
2. Belenky S.Z. Shower processes in cosmic rays, Gostechizdat, 243, 1948.
3. Kramer G. Mathematical methods of statistics, "Mir", Moscow, 648, 1976.
4. Hotta N. et al. Phys. Rev. D1, 22, 1, 1980.
5. Vorobyev K.V., Plyasheshnikov A.B., Uchaikin V.G., Half-analytical Monte-Carlo method. Dep. VINITI, 120, 1984.
6. Ivanenko I.P. et al. Proc. 16th ICRC, 9, 247, 1979.
7. Kanevsky B.L., Linde I.A. Proc. 17th ICRC, 6, 268, 1981,
8. Gerasimova N.M. Proc. 16th ICRC, 9, 216, 1979.

Table 1

t	N	Var^2	A_s	N	Var^2	A_s	N	Var^2	A_s
2	64.8	.25	1.0	30.1	.17	1.92	.12+2	.25	.99
4	415	.14	.3	110.2	-.11	-.12	.13+4	.15	.52
6	982	.7-1	-.45	157.9	.48-1	-1.1	.45+4	.94-1	-.4-2
8	1333	.31-1	-.78	145	.33-1	-1.3	---	---	-.2+1
10	1272	.17-1	-1.26	91.9	.76-1	.76-1	.12+5	.24-1	-3.34

N85-35950

ORIGINAL PAGE IS
OF POOR QUALITY

Table 1(continued)

t	$\bar{N}$	Var^2	A_s	$\bar{N}$	Var^2	A_s	$\bar{N}$	Var^2	A_s
14	600	.9-1	.6	24.5	.49	1.75	.95+4	.15-1	.87
18	167	.43-1	.91	4.44	2.29	4.99	.40+4	.10	1.77

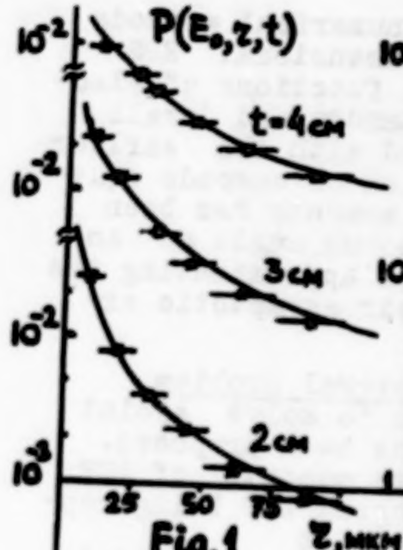

Fig.1

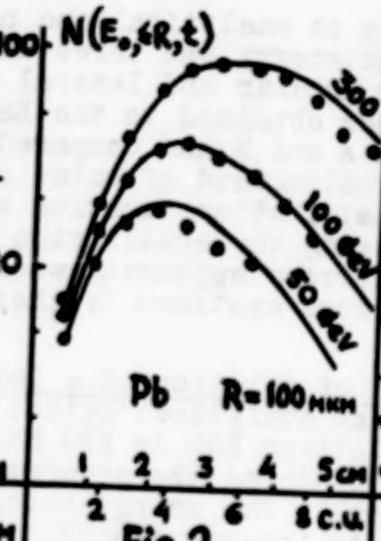

Fig.2

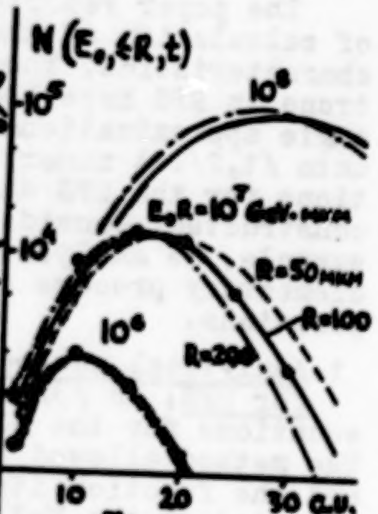

Fig.3

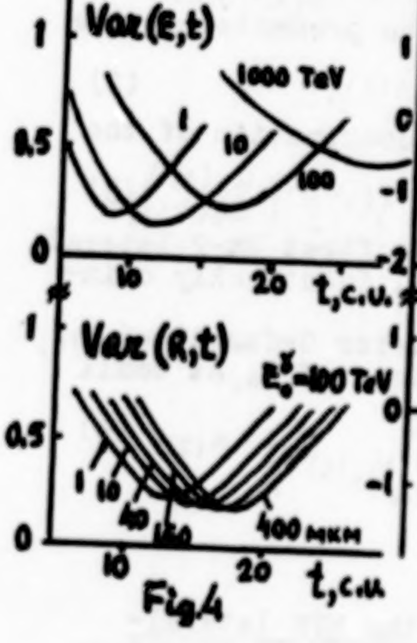

Fig.4

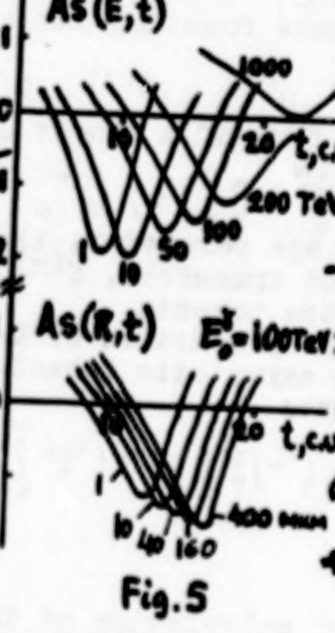

Fig.5

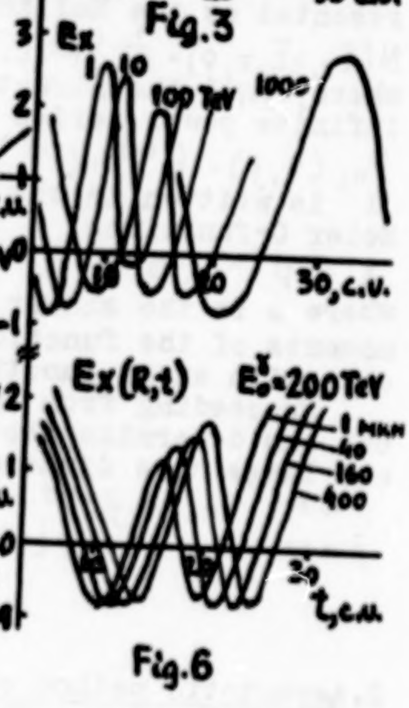

Fig.6

N85-35950

HE 3.5-13

ANALYTICO-NUMERICAL METHODS OF CALCULATIONS OF ENERGY AND THREE-DIMENSIONAL PARTICLE DISTRIBUTIONS IN ELECTROMAGNETIC CASCADES

Ivanenko I.P., Kanevsky B.L., Roganova T.M., Sizov V.V.,
Triphonova S.V.

Institute of Nuclear Physics, Moscow State University,
Moscow 119899, USSR

The paper reports on analytical and numerical methods of calculation of the energy and three-dimensional EPS characteristics. The angular and lateral functions of electrons in EPS have been obtained to the Landau and small angle approximations A and B and compared with the earlier data /1,2/. A numerical method of solution of cascade equations for the EPS distribution function moments has been constructed. Considering the equilibrium rms angle as an example, we analyse errors appearing when approximating the elementary process cross sections by their asymptotic expressions.

1. Analytical method of solution of a lateral problem for EPS. In /3/, an analytical method to solve ajoint equations for the electron LDF in EPS has been proposed. The method allowed obtaining the accurate moments of LDF and the function itself. The energy-integral LDF being represented as the Mellin inverse transformation

$$N(E_0,>E,t,\rho)=\frac{1}{2\pi i}\int ds(E_0/E)^s\,\frac{1}{s}\,H_1(s)\,e^{\lambda_1(s)t}\,P_{n_2}(s,\tilde\rho), \qquad (1)$$

where $\tilde\rho=\rho E/E_0$, the structure function can be presented as the infinite power series

$$P_{n_2}(s,\tilde\rho)=P^{(0)}+(P^{(1)}-P^{(0)})+(P^{(2)}-P^{(1)})+\ldots \qquad (2)$$

Δ is written in the form of a linear combination of the Meier G-functions

$$\Delta=P^{(n)}-P^{(n-1)}=\sum_{k=0}^{2n}C_k(s)\,G^{60}_{26}\left(f(s)\tilde\rho^{2}\,\middle|\,\begin{matrix}a_p(s)\\ b_q(s)\end{matrix}\right), \qquad (3)$$

where s is the shower age parameter, the first 2n-2 lateral moments of the function transform, $N^{(n)}$, identically coincide with exact function moments.

Proceeding from the properties of Meier G-functions/4/, one can determine the asymptotic behaviour of P_{n_2} at small and large core distances

$$\begin{aligned}&\tilde\rho\to 0 \qquad P_{n_2}\sim\tilde\rho^{\,2-s}\\ &\tilde\rho\to\infty \qquad P_{n_2}\sim\exp\left[-4f^{1/4}\sqrt{\tilde\rho}\right]\tilde\rho^{\,2-s+\frac{1-s}{4}}\sum_{k=0}^{\infty}M_k(s)\,\tilde\rho^{\,-k/2}\end{aligned} \qquad (4)$$

2. Asymptotic method of calculation of the EPS lateral-angular functions. The method proposed consists in reducing the solution for angular and lateral functions to a (3)-type contour integral based on the known asymptotics of the solution and calculation of the latter by a saddle-point method. The angular and lateral parts of a cascade equation solution in approximation A can be presented in

the form /2/

$$P(s,\theta)=\frac{1}{4\pi^2 i}\int dp\,\Gamma(p+1)\,m_\theta(p,s)\left(\frac{\theta E}{E_k}\right)^{-2p}\frac{1}{\theta^2} \qquad (5)$$

$$P(s,r)=\frac{1}{4\pi^2 i}\int dp\,\Gamma(p+1)\,m_r(p,s)\left(\frac{rE}{E_k}\right)^{-2p}\frac{1}{r^2}$$

The asymptotics of angular and lateral functions(5) at $p\to-$ $(z\to\infty)$ and $t\gg1$ reads, respectively

$$m_\theta(p,s)\sim\Gamma(p+1)\,a_\theta(s)^{-2p}\;;\quad m_r(p,s)\sim\Gamma(3p+1)\,a_r(s)^{-2p} \qquad (6)$$

In the region $\mathrm{Re}\,p<0$ $(z\to0)$ the energy-integral angular and lateral distribution functions have the closed singularities

$1/p+1,\ 1/p+s/2$ (7)

Patching of the two asymptotics for the angular and lateral functions yields, respectively:

$$m_\theta(p,s)\sim\frac{\Gamma(p+1)\Gamma(p+s/2)}{\Gamma(s/2)}\,a_\theta(s)^{-2p}\;;\; m_r(p,s)\sim\frac{\Gamma(2p+2)\Gamma(2p+s)}{\Gamma(s)}\,a_r(s)^{-2p} \qquad (8)$$

The integral in (5) is then represented as a product of singularities by some function G(p,s) without singularities in the region $-s/2<\mathrm{Re}\,p<\infty$.

The function G(p,s) is developed into Taylour series in the vicinity of a point p_0

$$G(p,s)=G(p_0,s)+(p-p_0)G'(p_0)+(p-p_0)^2/2\,G''(p_0)+\dots \qquad (9)$$

and a term with the first derivative $G(p_0)$ is required to be zero. From this condition we find a point "p_0" and calculate integrals (5):

$$P(s,\theta)=K_{(2-s)/2}(2a_\theta z_\theta)(a_\theta z_\theta)^{\frac{2+s}{2}}G_\theta(p_0,s)+\dots;\; P(s,r)=K_{2-s}(2\sqrt{a_r z_r})(a_r z_r)^{\frac{2+s}{2}}G_r(p_0,s)\dots \qquad (10)$$

where

$$p_0^{(\theta)}=-1+K_{(2-s)/2}(2a_\theta z_\theta)\,a_\theta z_\theta/K_{(2-s)/2}(2a_\theta z_\theta);\; p_0^{(r)}=-1+K_{3-s}(2\sqrt{a_r z_r})\sqrt{a_r z_r}/K_{2-s}(2\sqrt{a_r z_r}) \qquad (11)$$

The expression for the angular part of the distribution function at $G=1$ coincides with the Belenky's function/1/. However, in the expression for $a_\theta(s)$ in /1/ $a=\sqrt{f(\lambda)}/\lambda$ at $\lambda=\lambda_1(s)$. In the present case, $a_\theta(s)$ is determined from the condition of coincidence of first moments of angular distribution function (9) with a point. If the functions are normalized to the first moment, an accuracy of the functions obtained from (9) is considerably better, and in the core approximation region $(z\to0)$ these functions practically coincide. At $-s/2<p<3$ $G_\theta(p)\sim1$, and the term with second derivative is negligible. A parameter $a_r(s)$ for the lateral distribution function is determined from a condition of coincidence of the second moments with a point and approximation function. In the integer points$(p=n)$ the function G(n,s,t) is thought to be known, since the lateral function moments in approximation A are known. In a wide range of the variable $-s/2<p_0<3$, $G_r(p_0)$ varies slightly and a term with $G_r''(p_0)$ can be neglected. Table 2 compares lateral distribution function (9) with Kamata-Nishimura's calculations /2/. Within 5-10%, even zero approximation yields good results. The lateral-angular distributions can be similarly constructed in cascade theory approximation /5/.

3. Numerical method of solution of cascade theory problems for EPC. To solve analytically the cascade theory problems, simplified expressions for elementary process cross secti-

ons are used. The influence of these simplifications on the results of calculations is considered for an "equilibrium" rms angle. A numerical method of cascade equation solution has been reported in /6/. For showers induced in lead and air by a primary electron, Fig.1 shows the rms angles of electrons, (see the dashed curves) devided by the Landau analytical expressions /7/ for these magnitudes(see their table below the figure). The top of Fig.1 presents the values of $\overline{\theta^2_r}$ obtained for scattering described in the Landau approximation, in the standard theory approximation A and in approximation C allowing for ionization losses, realistic expressions for bremsstrahlung and pair production cross sections and the Compton effect. The values of $\overline{\theta^2_r}$ obtained to Approximation C for air and lead considerably differ from those in Approximation A and from each other. At the bottom of Fig.1, the curves calculated to Approximation A for scattering described realistically are shown - the Thomas-Fermi equation was taken to present atomic potential, a nucleus being considered to be a uniformly charged sphere. By comparing these curves with curves (A) at the figure top a physical accuracy of the Landau approximation can be estimated. On the whole, it can be stated that the differential angular characteristics are sensitive to the details of a description of elementary interactions in the energy range, where their cross section differs from the asymptotic values.

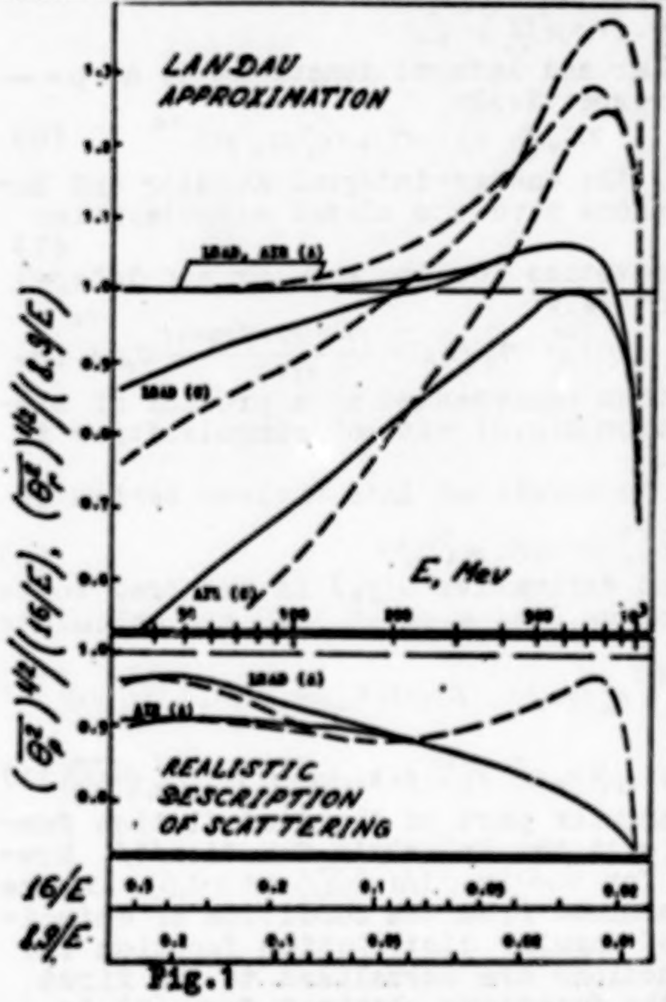

Fig.1

References.

1. Belenky S.Z. Shower processes in cosmic rays, M.: Gastechizdat, 1949, 243p.
2. Nishimura J.N. Handbuch der Physic, Berlin, Springer Verl., 1967, 46/2, 1-113.
3. Roganova T.M., Triphonova S.V., Proc. 18th ICRC, 1983,

5, 32.
4. Luke J.L. The special functions and their approximations, New York, 1969.
5. Ivanenko I.P., Kanevsky B.L. Asymptotic methods of solution of lateral-angular problems in cascade theory (in print).
6. Ivanenko I.P., Ivanova E.V. Maximenko V.M., Sizov V.V. Preprint FIAN, 1985.
7. Landau L.D. JETP, 1940, 10, 1107.

Table 1

The ratio of moments of exact and approximate function for normalization to the first moment and at

	$s = 0.6$		$s = 1$		$s = 2$	
1	1	0.82	1	0.87	1	0.95
2	0.90	0.60	0.92	0.67	0.96	0.83
3	0.82	0.41	0.87	0.48	0.90	0.60

Table 2

The EPS lateral function in cascade theory Approximation A. Comparison with the Nishimura-Kamata's calculation /2/ for the zero approximation, parameter $a_r(s)$ being normalized to the second moment

$s \backslash \xi$	0	0.01	0.03	0.1	0.3	1.0	3.0
0.6	0.38	0.33	0.26	0.15	---	0.04	0.00006
	0.38	0.34	0.27	0.17	0.05	0.04	0.00009
1	1.12	0.91	0.71	0.4	---	0.017	0.00050
	1.01	0.91	0.70	0.38	0.15	0.019	0.00065
1.4	2.5	1.8	1.31	0.72	---	0.038	0.0016
	2.5	1.9	1.35	0.69	0.27	0.041	0.0019
	0.53	3.0	1.9	0.94	---	0.060	0.0040
	0.54	2.7	1.8	0.99	0.37	0.060	0.0037

N85-35951

MULTIDIMENSIONAL ANALYSIS OF DATA OBTAINED IN EXPERIMENTS WITH X-RAY EMULSION CHAMBERS AND EXTENSIVE AIR SHOWERS

A.A.CHILINGARYAN, S.KH.GALFAYAN, M.Z.ZAZYAN
Yerevan Physics Institute, Markarian st.2
375036, Yerevan, Armenia, USSR

A.M.DUNAEVSKII
Lebedev Physical Institute
Leninsky prospect 53, Moscow, USSR

1. Introduction

The traditional approach to the analysis of data available from experiments with X-ray emulsion chambers consists in considering one-dimensional distributions or the dependences of one experimentally observed value on the other.

Recently the analysis of two- and three-dimensional distributions /1/ as well as the presentation of averages of two variables together with their errors led to the possibility of drawing a conclusion on the scaling violation in the secondary particle fragmentation region at the energies $\sim 10^{16}$ eV and estimating the degree of its violation /2/.

Thus, the increase of simultaneously analyzed features seems to be attractive, but it is apparent that the analysis of three and more features is connected with the necessity to have the quantitative measure of distinction of multidimensional distributions presented by limited samples.

The other main problem of cosmic ray physics may be formulated as the problem of determining the portion of experimental events belonging to one of described types. That is the problem of determining the portion of photon-hadron (γ - h) families generated by various primary nuclei or the determination of the primary component chemical composition by the EAS data.

In the present paper we shall show that the solution of the above problems may be realized in the multidimensional space by the nonparametric statistic methods developed in /3,5/. Note that the use of these methods for processing the experimental data from the cosmic ray physics installations has demonstrated their advantage over the traditionally applied techiques /4,6,7/.

This is a methodical work, i.e. the experimental events are replaced by the model ones. Thus we have an opportunity to determine the limits of applicability of the methods suggested and to estimate the expected accuracies of determining the desired physical values.

Among the models used, there is a pure-scaling one - M6, the models with increasing cross section and scaling violation in the pionization region - M4, Femin, Femax (the detailed description of the models may be found in /8/). Some models are obviously nonrealistic (e.g. M6), but for the methodical purposes the use of the family banks corresponding to these models is admissible.

2. The Distinction of Strong Interaction Models

The selection of the feature set optimal for the discrimination purposes is performed with account of the averages differences and the correlation information. The feature pairs with the statistically significant difference in correlations are included in the set. Finally each set is characterized by the so-called Bayesian risk R - the probability to misclassify the models (or the model and experimental data) in classification procedure performed with the optimal Bayesian decision rule (for details of the method and used features see /9/).

The R^{B} use in one-dimensional analysis leads to the same conclusions as the standard statistical methods of two samples averages difference significance calculation (T-test and Wilcoxon test). The more is the difference between R and 0.5 (corresponding to the classes total overlapping) the stronger is the difference between the distributions.

The Bayesian risk calculation method /10/ allows to obtain unbiased effective estimates and to judge of the model describing the experiment in the best way by the successive comparison of the experimental and alternative model training samples.

The estimation accuracy depends on the sizes of the used training samples. Besides there is an interrelation between the sample size and maximum dimensionality of the space where one may realize the effective local reconstruction of the probability multidimensional density. As we see from Table 1, the samples limitation (100÷400) leads to that the addition of low-informative features may even deteriorate the discrimination due to the scarcity of points in N-dimensional feature space.

Table 1. The comparison of the M4 and M6 models by means of γ-family various characteristics.

Combination	Space dimensionality	R^{B}
$\bar{R}_\gamma$	1	0.38±0.3
$\bar{R}_\gamma$, $\overline{ER}_\gamma$	2	0.37±0.3
$\bar{R}_\gamma$ $\Sigma' E_\gamma$, d'_γ	3	0.35±0.3
$\bar{R}_\gamma$, $\Sigma' E_\gamma$, d'_γ b'_γ	4	0.34±0.3
ΣE_γ, n_γ, $\bar{R}_\gamma$, $\overline{ER}_\gamma$, d_γ, $\Sigma' E_\gamma$, …	10	0.38±0.3
$\Sigma' E_\gamma$, n'_γ, $\bar{R}'_\gamma$, $\overline{ER}'_\gamma$, d'_γ, b_γ, …	15	0.40±0.3

The comparison of the M4 and M6 models by means of various feature combinations has shown that the addition of information from the hadronic block or the shower installation to the γ-family information does not reduce the classification errors. That is, in the problems related to the study of strong interaction cross sections and scaling violation in the pionization region it is enough to analyze only the photon family characteristics.

3. Separation of Families from the Light and Heavy Nuclei. Determination of the Portion of Families from Fe Nuclei.

Let us take as prototypes (training samples) the samples containing the events from the light nuclei and, respectively, the events from the banks Femin and Femax. Various combinations of both types from the events not included in the training samples will be taken as the "experimental" one. Such a choice imitates the case of precise knowledge of the strong interaction model. The portion of "iron" events in these samples is set to be $P_H = 0.05$, 0.07, 0.1.

The estimate of the portion of families initiated by the Fe nuclei will be obtained after the experimental data classification and calculation of the probabilities to misclassify the events of both types.

$$\hat{R}_H = \frac{R_H^* - R_{L\to H}}{1 - R_{H\to L} - R_{L-H}}$$

where P_H^* is the portion of families referred to the "iron" type, $P_{L\to H}$ and $R_{H\to L}$ are the probabilities of the classification possible errors.

Table 2 shows that the reconstructed P_H value is rather close to the true one. Besides, it may be shown that the classification allows one to enrich 5÷7 times the selected events with the families from the heavy nuclei, this possibly enabling one to study Fe - N^{14} interaction at the energies more than 10^{16} eV.

Table 2. Reconstruction of the portion of families from the Fe nuclei. The training and control samples are taken from the banks M6 and Femin.

Installation	Features	P_H	P_H^*	$\hat{P}_H$
γ-block	$\Sigma E_\gamma, \bar{R}_\gamma, \alpha_\gamma$	0.05	0.194	0.042±0.060
		0.07	0.202	0.055±0.058
		0.1	0.217	0.080±0.058
γ-block + shower part	$\Sigma E_\gamma, \bar{R}_\gamma, \alpha_\gamma, E_0$	0.05	0.09	0.048±0.025
		0.07	0.115	0.074±0.024
		0.1	0.138	0.098±0.023
γ-h -block	$\bar{R}_\gamma, n_h, \bar{R}_h$	0.05	0.125	0.044±0.028
		0.07	0.149	0.076±0.026
		0.1	0.171	0.099±0.025

However, if the strong interaction model is unknown (this case was simulated by the use of "experimental" data from the banks not coinciding with the prototypes), the reconstruction is carried out with great errors. Therefore, to treat the real experimental data one should use either more realistic models or combinations of features weakly dependent on the strong interaction model, but simultaneously highly sensitive to the primary nucleus type.

4. Conclusion

The use of nonparametric statistic methods allows one to carry out the quantitative comparison of the model and experimental data. The same methods enable one to select the events initiated by the heavy nuclei and to determine the portion of the corresponding events. For this purpose it is necessary to have the banks of artificial events describing the experiment sufficiently well. At present, the model with the small scaling violation in the fragmentation region /11/ is the closest to the experiments. Therefore, the treatment of γ-families obtained in "Pamir" experiment is being carried out at present with the application of these models.

REFERENCES

/1/ Danilova T.V., Erlykin A.D., VANT, ser.tekhn.fiz.eksp., issue 1(13), p.13-19, 1983.
/2/ Pamir Collaboration, 18th ICRC, v.5, p.425-428, 1983.
/3/ Chilingaryan A.A., VANT, ser.tekhn.fiz.eksp., issue 2(8), p.59-68, 1981.
/4/ Chilingaryan A.A., VANT, ser.tekhn.fiz.eksp.,issue 3(12), p.90-91, 1982.
/5/ Chilingaryan A.A., 18th ICRC, v.5, p.524-526, 1983.
/6/ Chilingaryan A.A., VANT, ser.tekhn.fiz.eksp., issue 1(13), p.81-84, 1983.
/7/ Chilingaryan A.A., VANT, ser.tekhn.fiz.eksp., issue 1(13), p.61-68, 1983.
/8/ Dunaevskii A.M., Uryson A.V., Preprint FIAN, No.150.
/9/ Chilingaryan A.A., Galfayan S.Kh., Zazyan M.Z., Dunaevskii A.M., 18th ICRC, v.5, p.487-490, 1983.
/10/ Galfayan S.Kh., Chilingaryan A.A., in: Statistical Problems of Control, issue 66, Vilnius, 1985.
/11/ Vernov S.N., Khristiansen G.B. et al., 15th ICRC, v.8, p.32-35, 1976.

HE 3.6-3

N85-35952

A NEW METHOD OF DIFFERENTIAL STRUCTURAL ANALYSIS OF γ-FAMILY BASIC PARAMETERS

L.G.MELKUMIAN, S.V.TER-ANTONIAN

Yerevan Physics Institute, Markarian st. 2
375036, Yerevan, Armenia, USSR

YU.A.SMORODIN

Lebedev Physics Institute, Leninsky Prospekt 53
117312 Moscow, USSR

ABSTRACT

The maximum likelihood method is used for the first time to restore parameters of electron-photon cascades registered on X-ray films. The method allows to carry out a structural analysis of the γ-quanta family darkening spots independent of the γ-quanta overlapping degree and to obtain maximum admissible accuracies in estimating the energies of the γ-quanta composing a family. The parameter estimation accuracy weakly depends on the value of the parameters themselves and exceeds by an order the values obtained by integral methods.

In our previous papers /1,2/ we have proposed for the first time to use the maximum likelihood method for the solution of the traditional inverse problem of X-ray emulsion experiments. The essence of the method consisted in the reconstruction of source parameters (the energy E, zenith and azimuth angles Θ and φ, the spot center coordinates X, Y) of the darkening spot on the X-ray emulsion film according to the matrix of darkening densities $\{\rho_{ij}\}$ measured by a densitometer in the cells (i,j) $i = 1, \ldots, N_i$, $j = 1, \ldots, N_j$. The scanning cell dimensions Δx, Δy and the number of cells $n_i \cdot n_j = N$ are fixed. It has been shown in /1,2/ that the maximum likelihood method gives consistent, efficient and nonshifted estimates for the parameters E, Θ, φ, X, Y in the wide range of scanning cell dimensions $\Delta X = \Delta Y = 10$ [illegible] 50 μkm. The accuracy of parameter estimation slightly depends on the value of the parameters themselves and exceeds by an order the values obtained by the momenta method and by integral methods.

The results of /1,2/ are obtained for the darkening spots caused by a single γ-quantum (electron) with the energy E in the range 2 ÷ 100 TeV and zenith angle in the interval 1 ÷ 0.5.

In /3/ the results of solution of the inverse problem for the general case - the number of the darkening spot sources (γ -quanta) is greater than 1 with the strongly marked structure of the spot overlapping, are given.

Remaining within the framework of notations accepted in /1,2/, one may present the likelihood function for the realized density matrix $\{\rho_{ij}\}$ at the unknown but fixed vector of parameters $\vec{\eta} = \eta(E_1, \dots E_n, X_1, \dots X_n, Y_1, \dots Y_n, \Theta, \varphi)$ in the form

$$\Phi(\{\rho_{ij}\} | \vec{\eta}) = \prod_{i=1}^{N_i} \prod_{j=1}^{N_j} f_\ell(n_{ij}/\vec{\eta}), \qquad (1)$$

where $n_{ij} = \rho_{ij} \cdot S$ is the number of electrons in the cell (i, j); $S = \Delta X \cdot \Delta Y$ is the cell area; N_i, N_j is the corresponding number of scanning cells along the X and Y axes; $f_\ell(n_{ij}/\vec{\eta})$ is the probability of n_{ij} electrons having been registered in the cell (i, j) at the given $\vec{\eta}$ vector of parameters; $\ell = 1$, if $n_{ij} < m_{min}$; $\ell = 0$, if $n_{min} \leq n_{ij} \leq n_{max}$; $\ell = 1$, if $n_{ij} > n_{max}$. The boundary values of the electron number are defined by the operation properties of the film and are chosen by us as in /1-3/ $\rho_{max} = n_{max}/S = 0.5 \mu km^{-2}$, $\rho_{min} = n_{min}/S = 0.002 \mu km^{-2}$. The distribution function $f_\ell(n/\vec{\eta})$ is assumed to be Poisson with the mean value $\bar{n} = \sum_{n_\gamma} \bar{n}_m + \bar{n}_\Phi$, where n_γ is the number of γ-quanta (electrons), $\bar{n}_m(E_m, X_m, Y_m, \Theta, \varphi)$ is the average number of electrons in the cell (i, j) generated by the source with the energy E_m, whose trajectory crosses the film at the point X_m, Y_m at the zenith and azimuth angles Θ and φ respectively; $\bar{n}_\Phi$ is the average number of "background" electrons ($\rho_\Phi = \bar{n}_\Phi / S = 0.04 \mu km$).

The determination of the $\vec{\eta}$ vector components is performed numerically by minimizing the likelihood function negative logarithm:

$$\Omega_0 \equiv \min \Delta(\vec{\eta})_{n_\gamma} \equiv \min \left\{ -\ln \Phi(\{\rho_{ij}\} / \vec{\eta}_{n_\gamma}) \right\} \qquad (2)$$

The inverse problem may also be solved in the case when the number of darkening spot sources n_γ is unknown. In this case one should minimize the functional

$$\Omega_1 \equiv \min \left\{ \min \Delta(\vec{\eta}) \right\}_{n_\gamma}, \; n_\gamma = n_0, n_0 + \Delta n, \dots, n', \qquad (3)$$

where n_0 and n' determine the boundaries of search for the darkening source number.

The inverse problem was solved by the maximum likelihood method basing on the density matrix $\{\rho_{ij}\}$ generated by the Monte-Carlo method at the given vector of parameters $\{\rho_{ij}\}$. The average number of equivalent electrons in the cell (i, j) was calculated according to the cascade theory axial approximation. Fluctuations were assumed to be Poisson-distributed. The BESM-6 computer main memory allowed one to analyze the rasters with the cell number $N_i \cdot N_j \leq 7000$ and the summary number of unknown parameters $3(n_\gamma + 1) \leq 99$.

Consider the possibilities of the elaborated method at

1) $n_\gamma = 1$, 2) $n_\gamma = 2$, that is of interest for calibrating the emulsion technique on $\pi^0 \to 2\gamma$ decays; 3) $n_\gamma > 2$ for processing γ-families; 4) $n_\gamma = ?$, i.e. when the number of the darkening spot sources is the component of parameter vector and is unknown.

1. $n_\gamma = 1$

The simulated rasters parameter reconstruction was carried out for discrete series of γ-quanta energy ($E_0 = 2,5,10,20,50,100$ TeV) $\Delta X = \Delta Y = 10,20\,\mu$km cell dimensions and various thicknesses of absorbers (d).

The relative accuracy of estimates of E, θ, φ made a few per cent. The accuracy of the definition of the spot center coordinates is 2-5 μkm.

2. $n_\gamma = 2$

For the darkening spot pair the calculations were performed at various energies $E_1 = 2 \cdot E_2 (2,4,5,10,20$ TeV) and distances between the spot centers $\mathcal{D} = (0.1 \div 100\,\mu$km) at the scanning step of 10,20,50 μkm.

The results may be formulated as follows:

a) the accuracy of determining the zenith θ and azimuth φ angles differs insignificantly from the single spot results and makes $\sigma_{\cos\theta} \le 5 \div 7$ %;

b) the accuracy of determining the spot center coordinates is $\sigma_x \approx \sigma_y \le \Delta X/2$, the distances between centers are $\sigma_{\mathcal{D}} \approx \Delta X$

c) the accuracy of determining the energy for the overlapping spots is not worse than 10% at the summary energy reconstruction accuracy of 5-7%.

3. $n_\gamma > 2$

For the overlapping families of γ-quanta the inverse problem was solved for the energies distributed uniformly in the 2-20 TeV interval. The number of γ-quanta was varied in the region 2-20 over the area 0.25 mm .

The accuracies of determining the parameter vector components at $3 \le n_\gamma \le 10$ were independent of the n_γ number and on the average equalled the corresponding values at $n_\gamma = 2$.

The accuracy of determining the zenith angle cosine made $4 \div 5$ % and also was independent of n_γ .

4. $n_\gamma = ?$

The n_γ value varied in the interval $1 \div 5$ due to the complexity of solving the problem at the unknown number of the darkening spot sources.

No noticeable variation of the estimation accuracy was observed. Note also that at the known values of $n_\gamma \le 10$ the efficiency of solving the inverse problem equalled $90 \div 100$ %. At the unknown n_γ the efficiency decreased to 80%, and the computer counting time grew 5 - 7 times.

REFERENCES

/1/ Melkumian L.G., Ter-Antonian S.V., Preprint EPI-649(39)-83, Yerevan, 1983.
/2/ Melkumian L.G., Ter-Antonian S.V., Preprint EPI-725(40)-84, Yerevan, 1984.
/3/ Melkumian L.G., Ter-Antonian S.V., (1984), sb. Voprosi atomnoi nauki i tekhniki, ser.tekhn.fiz.eksp., 3(20), p.60-64.

LPM EFFECT AND PRIMARY ENERGY ESTIMATIONS

N85-35953

M.F. Bourdeau and J.N. Capdevielle
Laboratoire de Physique Théorique, Université de Bordeaux I
Rue du Solarium, 33170 GRADIGNAN, FRANCE

1. Introduction

The distorsion of the electron cascade development under LPM effects is now currently admitted (1, 2, 3) ; it consists in an increase of depths of showers origin, of shower maximum T_{max}, a decrease of the number of particles at maximum N_{max} and results in a flattening and a widening of the cascade transition curve. Connected with the influence of multiple Coulomb scattering on basic electromagnetic processes (bremstrahlung, pair production), this effects appears at high energy with a threshold dependent on the density of the medium (more than 10 TeV for lead, more than 10^6 TeV in air).

We examine here, consequently, the electromagnetic components of hadron induced showers in lead and EAS in air, calculated for the same hadronic cascades in the different alterlative, including or not LPM effect.

2. Analytical representation of cascade curve

We have used in lead our Monte-Carlo data (1) to estimate from numerical values of γ-induced showers the different moments at fixed primary photon energy E_o

$$p_n(E_o) = \int_0^\infty t^n N_e(E_o,t)\, dt$$

The longitudinal spread τ and the integral track length S_o have therefore been obtained from the relations between appropriate moments

$$[\tau(E_o)]^2 = \frac{p_2(E_o) - [p_1(E_o)]^2/p_o(E)}{p_o(E)}$$

and

$$S_o(E_o) = \sqrt{2\pi}\, \tau(E_o) N_{max}(E_o) = \int_o^\infty p(E_o,t)\, dt$$

We found convenient to describe the data including LPM effect by the following formula (replacing Greisen's formula when $E_o > 1$ TeV in lead) :

$$N_e(E_o,t) = 15.3[1 + \alpha_2 B_o^{\beta_2}]^{-1} E_o^{0.9773} \exp[-(t-T_o)^2/2\tau^2]$$

with $T_o = T_{max}^{LPM}$, $\tau = \tau^{LPM}$ and $B_o = \text{Ln}(E_o/10^3)$, where

$$T_{max}^{LPM} = 4.98 + \text{Ln}\, E_o + \alpha_1[\text{Ln}\, E_o]^{\beta_1} \quad (\alpha_1 = 0.0001477,\ \beta_1 = 4.64)$$

and

$$\tau^{LPM} = 3.78(1 + \alpha_2 B_o^{\beta_2})\, E_o^{\delta} \quad (\alpha_2 = 0.008446\ ;\ \beta_2 = 2.7936)$$

This formula is inserted in our Monte-Carlo programm of hadronic cascade for all γ rays of different energy emitted at different depth.

Similar procedure has been adopted for air, from Monte-Carlo data (2) leading to the formula for $E_o \geqslant 10^5$ TeV

$$N_e(E_o,t) = 0.00825\ E_o(100.-0.88B_o-1.62B_o^2)\ \exp\left[-(t-T_o)^2/2\tau^2\right]$$

where $B_o = \mathrm{Ln}\ (E_o/10^8)$, $T_o = 1.363B_o + 21.09$

$$\tau = 5.2 \quad \text{if } E_o \leqslant 10^{10}\ \text{GeV}$$

$$\tau = 5.2 - 0.426\ \mathrm{Ln}\ (E_o/10^{10}) \quad \text{if } E_o \geqslant 10^{10}\ \text{GeV}$$

(E_o in GeV, t in c.u.). This formula is also inserted in our hydrid Monte-Carlo-analytic simulation in air in place of Greisen's formula.

3.Simulation in lead calorimeters

The model used for production of secondary hadrons is SBM extended in lead following HE 4.1-9 with $< \nu > = 3.2$. The energy lost in disintegration of the struck nucleus is $E_D(\text{MeV}) = 124\ N_H + 30$, the number of tracks N_H being obtained from $N_H = 3.46E^{0.33}A^{0.19}$ (4). The Monte Carlo procedure gives the quantities E_{ion}, E_d, E_{out} at different depth of a calorimeter 1000 g/cm^{-2} deep built with lead plates of 50 $g.cm^{-2}$.

$$E_{ion} = (N_1 + N_2 + 0.75\ N_3)\ 32 \times 7.4\ (\text{MeV})$$

$$(N_1 = ½(N(100+N(200))\ ,\ N_2 = ([N(300)+N(400)]/2)\ldots)$$

is the energy lost by secondary particles and γ initiated cascades, E_D is the total energy spent by disintegration, E_{out} is the energy leaking out the considered slide (or the bottom of the calorimeter) estimated as the sum of the individual energies of outgoing hadrons. The behaviour of those quantities with depth are given in fig. 1 for incoming protons of 10^5 GeV. E_{ion} is given with and without LPM It can be ascertained that for short calorimeters ($\sim 3\lambda$) E_{ion} is 1.6 times lower at 10^6 GeV when LPM is taken into account and a systematic underestimation, rising with energy, occurs when the primary E_o is estimated from E_{ion} without consideration of LPM. A first approach of the amended Grigorov spectrum is shown in fig. 2. Similar consequences will also be detailed for emulsion chamber data.

4. EAS with LPM

EAS induced by proton have been simulated between 10^9-10^{11} GeV, for scaling model (5) and CKP model. For 1st model according to the small number of more energetic secondaries secondaries an important distorsion occurs in cascade curve (fig. 3 - 4) at 10^{10} and 10^{11} GeV. The discrepancy is not visible at 10^9 GeV. For CKP model, LPM can be neglected even at 10^{10} GeV. If we postulate, following (6) the validity of scaling at such energies, the primary energy near 10^{11} GeV estimated from the Fly's eye could be underestimated by 30% without LPM correction.

5. Conclusion

LPM effect implies higher intensities near 10^6 GeV, estimated from direct measurements. The tendancy of fig. 2 where Grigorov

ORIGINAL PAGE IS
OF POOR QUALITY

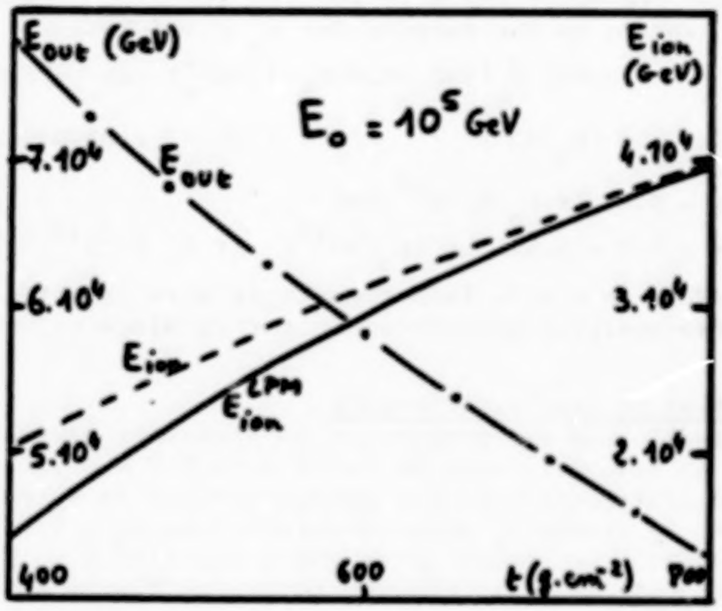

Fig. 1

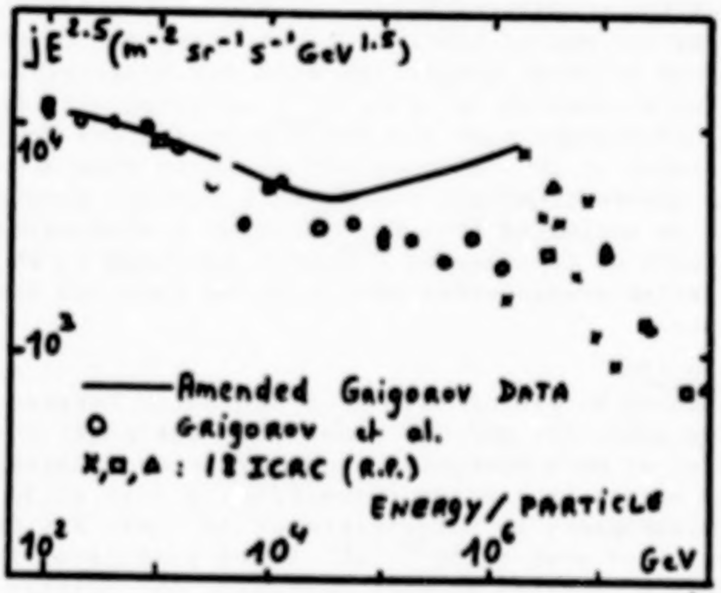

Fig. 2

ORIGINAL PAGE IS
OF POOR QUALITY

amended spectrum is nearer of EAS data (7) could be stronger, if we consider in nuclear model the decrease of inelasticity with primary energy (HE 4.1-9,10). In atmosphere, it's difficult to know at present if scaling model is valid at so high energy, but we have considered here at least, the extremal distorsion due to LPM.

References

1. Bourdeau M.F. et al., 1981, J.Phys. G7, 1571.
2. Misaki A. et al., 1981, 17th ICRC, Paris, 5, 162.
3. Aminova T.P. et al., 1984, Proc.Symp.Cosmic Rays and Particle Physics, Tokyo, 420.
4. Bourdeau et al., 1977, Proc. 15th ICRC, Plovdiv, 15, 133.
5. Capdevielle J.N. et al., 1981, Proc. 17th ICRC, Paris, 6, 66.
6. Linsley J. et al., 1981, Phys.Rev.Lett. 46, 459.
7. Wdowczyk J., 1984, 9th ECRS, Kosice

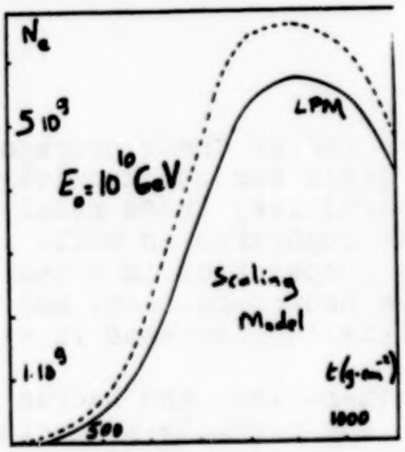

Fig. 3

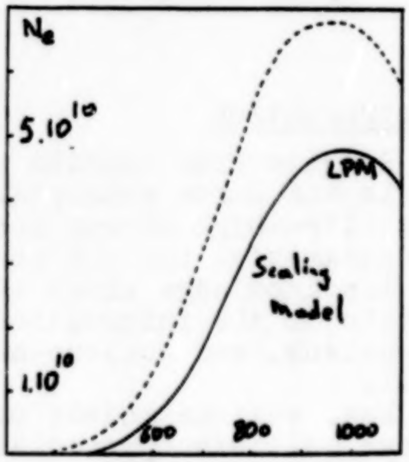

Fig. 4

N85-35954

EXPERIMENTAL BASIS FOR THE MODELS OF CASCADE PROPAGATION IN ATMOSPHERE

Strugalski Z.

Institute of Physics of the Warsaw Technical University
ul. Koszykowa 75
00-662 Warsaw, Poland
and
Joint Institute for Nuclear Research, High Energy Labor.
Dubna, USSR

ABSTRACT

The picture of the hadron-nucleus collision process is presented as emerged on the basis of newly obtained experimental data. The picture is applicable for models of cascade propagation in Earth atmosphere.

1. Introduction

Results from studies of cascades ond of their propagation in the Earth atmosphere form a basis for our knowledge about ultra-high energy cosmic ray particles; these results are fundamental for the cosmic ray astrophysics as well. But, the knowledge about the cascade propagation in a medium rests on the information about the hadron-nucleon, hadron-nucleus, and nucleus-nucleus collision processes first of all.

Now, various models of the hadron-nucleon and hadron-nucleus collision processes, and of the particle-producing reactions in them, are in use, based on different almost arbitrarily introduced physical processes assumed. The assumptions do not correspond in many cases to the reality - they are inadequate. The question: "Is an assumption adequate or not ?" should find its answer primarily in experiments.

We have studied experimentally the hadron-nucleus collisions at the conditions when the reaction outcome was almost totally identified, Strugalski Z. et al. (1981 a, b; 1982 a - c; 1983 a -e); experimental data have been obtained as well on the hadron-nucleon collision processes in their initial stages - before decays of produced resonances, using massive target nuclei as detectors, Strugalski Z. (1981 a,b; 1982; 1984 a-d; 1985). The results are crucial for any model of the hadron-nucleon, hadron-nucleus, and nucleus-nucleus collisions and, therefore, for a more adequate model of the cascade propagation in media - in the Earth atmosphere in particular.

2. Experimental procedure

In experiments, the 26 and 180 litre xenon bubble chambers, Kanarek T. et al. (1959), Kuznetsov E. V. et al. (1970), were used. The smaller chamber was exposed to beams of pions with 2.34, 5, and 9 GeV/c momentum from the synchrophasotron of the Joint Institute for Nuclear Research in Dubna; the bigger chamber was exposed to pion beam at 3.5 GeV/c momentum from the accelerator of the Institute of Experimental and Theoretical Physics in Moscow.

General experimental information about the pion-xenon nucleus collisions is contained in series of Communications of the JINR: Strugalski Z. et al. (1981, 1982, 1983, 1984, 1985). Additional appropriate information has been found in various emulsion works: Andersson B. et al. (1978), Babecki J. and Nowak G. (1978), Bannik B.P. et al. (1980), Gurtu A. et al. (1979), Meyer H. et al. (1963), Otterlund I. et al. (1978), Tsai-Chü et al. (1977), Winzeler H. (1965); the accelerator data there are at energies up to about 400 GeV in the lab, the cosmic ray data are up to a few thousands GeV.

3. Results

Four main phenomena are usually observed, when hadrons collide with atomic nuclei: a) The emission of nucleons with energies from about 20 up to about 400 MeV; b) The production of particles; c) The evaporation of target fragments; d) The fission of residual target nucleus.

3.1. Nucleon Emission. Any hadron with kinetic energy higher than the pion production threshold may pass through some layer of nuclear matter before to come into particle - producing reaction in it; there are events in which incident hadrons with energies of a few GeV traverse nuclei or are stopped in them without causing particle production. In any case, are the particles produced or not, any hadron causes emission of nucleons in passing through atomic nucleus. The number n_N of the emitted nucleons equals the number of nucleons contained within the volume $v = \pi D_o^2 \lambda$ centered on the hadron path λ in nuclear matter, where D_o is the diameter of the nucleon. The particle production process does not effect an influence on the nucleon emission.

Any hadron loses its kinetic energy monotonically along its path in nuclear matter, by nucleon emission. Energy spectra and angular distributions of emitted nucleons are practically the same in pion-xenon nucleus collisions with and without particle production; they do not depend neither on the multiplicity of emitted protons nor on the multiplicity of produced pions. The spectra and distributions are the same for pion-xenon collisions at 3.5 GeV/c momentum and for the proton-nucleus collisions in emulsions at 400 GeV/c.

3.2. Particle Production. Particles are produced via intermediate objects, we have called them "generons", created firstly in 2 ⟶ 2 type endoergic reactions and decaying after the lifetimes $\tau \approx 10^{-22}$ s into particles and resonances. Generons behave themselves in passage through nuclear matter as usual hadrons do it - in particular, they can produce new generons in colliding with the downstream nucleons. A quasilinear cascade of generons may develop in nuclear matter, therefore. This way, the outcomes in hadron-nucleus collisions at an energy E are the compositions of m outcomes in hadron-nucleon collisions at energies in average E/m, where m is the number of particle-producing collisions of the incident hadron.

The nucleon emission process does not depend on the particle production process. The region of the particle production process in the target nucleus is not larger than the region of the nucleon emission, therefore; it is rather almost linear and situated collinearly with the incident hadron course in predominant number of collisions.

3.3. Evaporation of Target Fragments. Relation between the multiplicity of the emitted protons and the mean multiplicity of the charged fragments in collisions with a given proton multiplicity allows to determine the size and localization of the fragment evaporation region, Strugalski Z. (1984). Nuclear fragments are evaporated from the surface of the damaged part of the target nucleus; the damage is due to the nucleon emission process accompanying the passage of any hadron through nuclear matter.

3.4. Fission of the Residual Target Nucleus. In any hadron-nucleus collision the target nucleus is damaged, and relatively large part of it is removed, as it may be concluded from experimental results on the nucleon emission and target fragment evaporation. Obviously, such damaged nucleus is instable and it must decay into stable smaller nuclei in the final state.

More information about the experimental picture of the hadron-nucleus and hadron-nucleon collision processes can be found in series of works: Strugalski Z. (1982, 1984, 1985).

References

Andersson B. et al., 1978, Phys. Lett., 73B, 343.
Babecki J. et al., 1978, Acta Phys. Polon., B142, 445.
Bannik B.P., 1980, Comm. JINR, Dubna, R1-13055.
Gurtu A. et al., Pramana, 3, 311.
Meyer H. et al., 1963, Nuovo Cim., 28, 1399.
Otterlund I. et al., 1978, Nucl. Phys., B142, 445.
Strugalski Z. et al., Comm. JINR, Dubna: 1982, a) E1-82-718, b) E1-82-719, c) E1-82-841; 1983, a) R1-83-68, b) R1-83-237, c) R1-83-564, d) R1-83-568, e) R1-83-234.
Strugalski Z. Communications JINR, Dubna: 1981 a) E1-81-576, b) E1-81-577; 1982, a) E1-82-718, b) E1-82-719, c) E1-82-841; 1983, a) E1-83-155, b) E1-83-850; 1984, a) E1-84-195, b) E1-84-268, c) E1-84-853, d) E1-84-854; 1985, E1-85-231.
Tsai-Chü et al., 1977, Nuovo Cim. Lett., 20, 257.
Winzeler H., 1965, Nuclear Phys., 69, 661.

N85-35955

HE 3.6-7

RELATION BETWEEN GAMMA-RAY FAMILY AND EAS CORE
- MONTE-CARLO SIMULATION OF EAS CORE -

Tomotake YANAGITA
Takakura-cho 5-4-301, Nishinomiya, 662 JAPAN

ABSTRACT

Preliminary results of Monte-Carlo simulation on EAS($Ne=10^5$) core is reported. As the first collision at the top of atmosphere, high multiplicity (high rapidity density) and large Pt (1.5GeV average) model is assumed. The most of the simulated cores show complicated structur.

1. Introduction. Several simulation studies on the EAS core structure were performed previously(Ref.1). Although various models or assumptions (fire ball, CKP, heavy primary or energy dependent Pt etc.) were tested in these works, the prominent frequency of the multi- or complicated core structure has not been simulated.

Recently, in the direct and pseudo-direct observation of nuclear interaction by EC (JACEE and CONCORDE, Ref.2, 3), very high multiplicity (high rapidity density) and comparatively large transverse momenta events were detected. The feature of these events gives us a motive for another EAS core simulation. We performed the core simulation taking these interaction feature in the simple model.

2. Simulation. The final output of the simulation calculation is the electron density map. We postulate 16*10 of packed array consist of 50*50 cm^2 density detectors, then area is 40 m^2 which is similar to the Norikura Spark Chamber Array(Ref.4).

The first collision depth (hereafter it is abreviated as Zo) is not sampled randomly, but is fixed to 10, 50 and 100 g/cm^2. The nuclear cascade is traced to observation depth(750g/cm^2) and the gamma-rays produced through neutral pion decay are filed (x,y,z-coordinate, directional cosine and the energy). From the gamma-ray file the core density map is generated superposing each electromagnetic cascade. As the electron lateral distribution function of the electromagnetic cascade, the NKG-formula is used.

Tracing the nuclear cascade, only the forward region in the rapidity space is concerned but the central and backward regions are neglected in each interaction.

Model and Postulate for the first interaction :
- survival particles are not in concern
- total energy of produced particles is fixed to 600TeV.
- multiplicity of charged hadrons is fixed to 20.
- multiplicity of neutral pion is fixed to 10.
- production energy spectrum is exponential type.
- transverse momentum distribution is exp(-Pt/Po),
  Po = 1.5 GeV/c

Other Interaction :
- collision mean free path is 90 g/cm^2.

ORIGINAL PAGE IS
OF POOR QUALITY

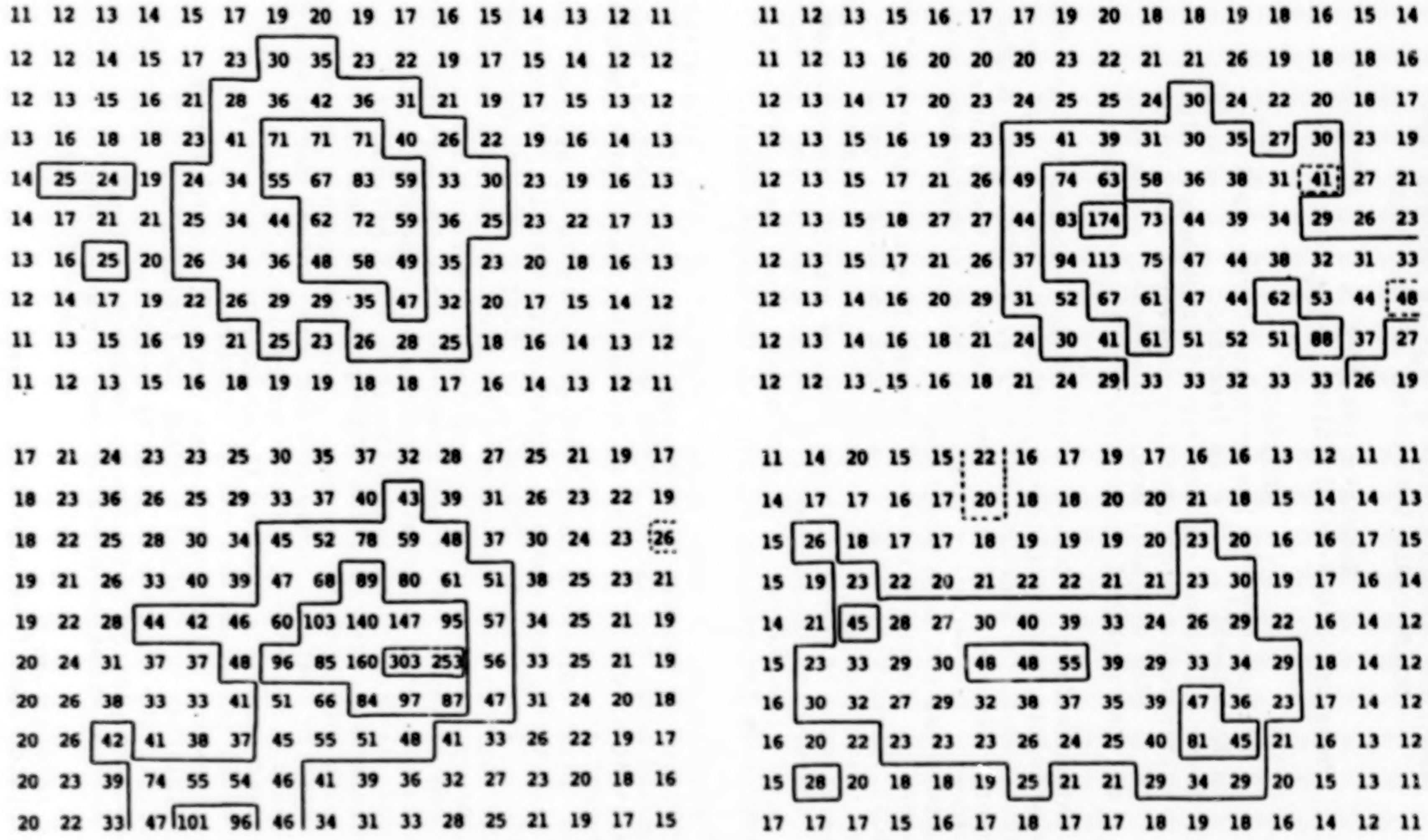

11	12	13	14	15	17	19	20	19	17	16	15	14	13	12	11
12	12	14	15	17	23	30	35	23	22	19	17	15	14	12	12
12	13	15	16	21	28	36	42	36	31	21	19	17	15	13	12
13	16	18	18	23	41	71	71	71	40	26	22	19	16	14	13
14	25	24	19	24	34	55	67	83	59	33	30	23	19	16	13
14	17	21	21	25	34	44	62	72	59	36	25	23	22	17	13
13	16	25	20	26	34	36	48	58	49	35	23	20	18	16	13
12	14	17	19	22	26	29	29	35	47	32	20	17	15	14	12
11	13	15	16	19	21	25	23	26	28	25	18	16	14	13	12
11	12	13	15	16	18	19	19	18	18	17	16	14	13	12	11

11	12	13	15	16	17	17	19	20	18	18	19	18	16	15	14
11	12	13	16	20	20	20	23	22	21	21	26	19	18	18	16
12	13	14	17	20	23	24	25	25	24	30	24	22	20	18	17
12	13	15	16	19	23	35	41	39	31	30	35	27	30	23	19
12	13	15	17	21	26	49	74	63	58	36	38	31	41	27	21
12	13	15	18	27	27	44	83	174	73	44	39	34	29	26	23
12	13	15	17	21	26	37	94	113	75	47	44	38	32	31	33
12	13	14	16	20	29	31	52	67	61	47	44	62	53	44	48
12	13	14	16	18	21	24	30	41	61	51	52	51	88	37	27
12	12	13	15	16	18	21	24	29	33	33	32	33	33	26	19

17	21	24	23	23	25	30	35	37	32	28	27	25	21	19	17
18	23	36	26	25	29	33	37	40	43	39	31	26	23	22	19
18	22	25	28	30	34	45	52	78	59	48	37	30	24	23	26
19	21	26	33	40	39	47	68	89	80	61	51	38	25	23	21
19	22	28	44	42	46	60	103	140	147	95	57	34	25	21	19
20	24	31	37	37	48	96	85	160	303	253	56	33	25	21	19
20	26	38	33	33	41	51	66	84	97	87	47	31	24	20	18
20	26	42	41	38	37	45	55	51	48	41	33	26	22	19	17
20	23	39	74	55	54	46	41	39	36	32	27	23	20	18	16
20	22	33	47	101	96	46	34	31	33	28	25	21	19	17	15

11	14	20	15	15	22	16	17	19	17	16	16	13	12	11	11
14	17	17	16	17	20	18	18	20	20	21	18	15	14	14	13
15	26	18	17	17	18	19	19	19	20	23	20	16	16	17	15
15	19	23	22	20	21	22	22	21	21	23	30	19	17	16	14
14	21	45	28	27	30	40	39	33	24	26	29	22	16	14	12
15	23	33	29	30	48	48	55	39	29	33	34	29	18	14	12
16	30	32	27	29	32	38	37	35	39	47	36	23	17	14	12
16	20	22	23	23	23	26	24	25	40	81	45	21	16	13	12
15	28	20	18	18	19	25	21	21	29	34	29	20	15	13	11
17	17	17	15	16	17	18	17	17	18	19	18	16	14	12	11

Fig.1-a,b,c,d. Core density maps for Zo=10g/cm^2. One of the most simple example is in (a). Typical complicated examples are in (b), (c) and (d).

(a)	(b)
(c)	(d)

ORIGINAL PAGE IS
OF POOR QUALITY

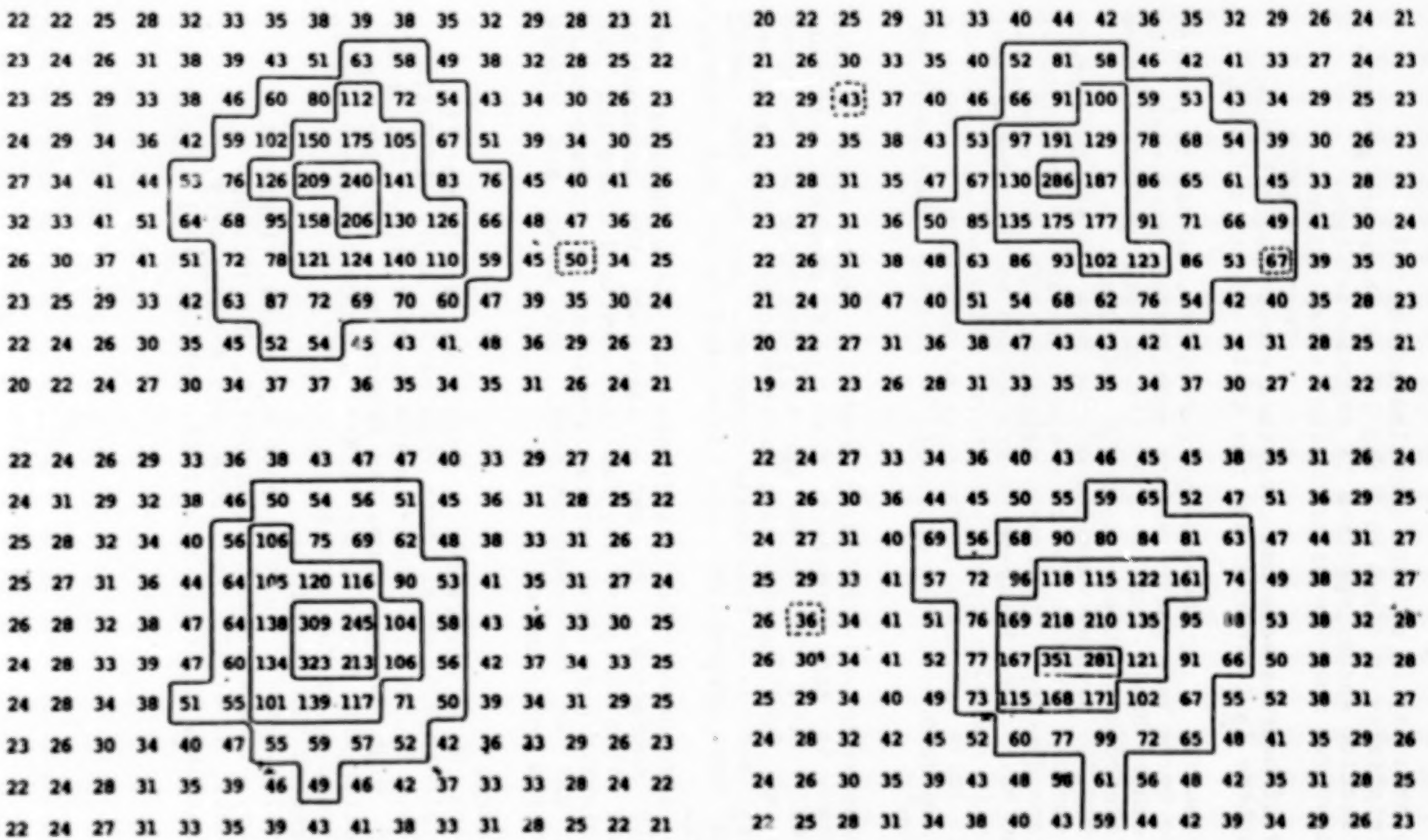

(e)

22	22	25	28	32	33	35	38	39	38	35	32	29	28	23	21
23	24	26	31	38	39	43	51	63	58	49	38	32	28	25	22
23	25	29	33	38	46	60	80	112	72	54	43	34	30	26	23
24	29	34	36	42	59	102	150	175	105	67	51	39	34	30	25
27	34	41	44	53	76	126	209	240	141	83	76	45	40	41	26
32	33	41	51	64	68	95	158	206	130	126	66	48	47	36	26
26	30	37	41	51	72	78	121	124	140	110	59	45	50	34	25
23	25	29	33	42	63	87	72	69	70	60	47	39	35	30	24
22	24	26	30	35	45	52	54	45	43	41	48	36	29	26	23
20	22	24	27	30	34	37	37	36	35	34	35	31	26	24	21

(f)

20	22	25	29	31	33	40	44	42	36	35	32	29	26	24	21
21	26	30	33	35	40	52	81	58	46	42	41	33	27	24	23
22	29	43	37	40	46	66	91	100	59	53	43	34	29	25	23
23	29	35	38	43	53	97	191	129	78	68	54	39	30	26	23
23	28	31	35	47	67	130	286	187	86	65	61	45	33	28	23
23	27	31	36	50	85	135	175	177	91	71	66	49	41	30	24
22	26	31	38	48	63	86	93	102	123	86	53	67	39	35	30
21	24	30	47	40	51	54	68	62	76	54	42	40	35	28	23
20	22	27	31	36	38	47	43	43	42	41	34	31	28	25	21
19	21	23	26	28	31	33	35	35	34	37	30	27	24	22	20

(g)

22	24	26	29	33	36	38	43	47	47	40	33	29	27	24	21
24	31	29	32	38	46	50	54	56	51	45	36	31	28	25	22
25	28	32	34	40	56	106	75	69	62	48	38	33	31	26	23
25	27	31	36	44	64	105	120	116	90	53	41	35	31	27	24
26	28	32	38	47	64	138	309	245	104	58	43	36	33	30	25
24	28	33	39	47	60	134	323	213	106	56	42	37	34	33	25
24	28	34	38	51	55	101	139	117	71	50	39	34	31	29	25
23	26	30	34	40	47	55	59	57	52	42	36	33	29	26	23
22	24	28	31	35	39	46	49	46	42	37	33	33	28	24	22
22	24	27	31	33	35	39	43	41	38	33	31	28	25	22	21

(h)

22	24	27	33	34	36	40	43	46	45	45	38	35	31	26	24
23	26	30	36	44	45	50	55	59	65	52	47	51	36	29	25
24	27	31	40	69	56	68	90	80	84	81	63	47	44	31	27
25	29	33	41	57	72	96	118	115	122	161	74	49	38	32	27
26	36	34	41	51	76	169	218	210	135	95	88	53	38	32	28
26	30	34	41	52	77	167	351	281	121	91	66	50	38	32	28
25	29	34	40	49	73	115	168	171	102	67	55	52	38	31	27
24	28	32	42	45	52	60	77	99	72	65	48	41	35	29	26
24	26	30	35	39	43	48	58	61	56	48	42	35	31	28	25
22	25	28	31	34	38	40	43	59	44	42	39	34	29	26	23

Fig.1-e,f. Core density maps for Zo=50g/cm^2.
Fig.1-g,h. Core density maps for Zo=100g/cm^2.

inelasticity is uniform distribution of 0-1.
multiplicity is fixed to 9 and 1/3 of these are pi-zero.
production energy spectrum is exponential type.
transverse momentum distribution is exp(-Pt/Pm),
Pm = 0.4 GeV/c.

Decay of hadrons were not concerned except neutral pion. Atmosphere is isothermal and the scale height is 7.0 km.

3. Results. In the case of Zo=10g/cm^2, almost 50 percent of the cores have multi- and/or complicated structure. On the other hand, scarce cores (10 or less percents) have complicated structure, when Zo=50 and 100g/cm^2.

In Fig.1, typical examples of the core map are presented. The contour lines in the maps are drawn at the densities of (average density of the 16*10 detectors)*2^n, where n=0, 1, and so on. Small sub-peaks are marked by the broken line.

Even in the most simple structured cores, we can find some small scale sub-peaks in the case of Zo=10g/cm^2. There is no examples having well separated multi-core, when Zo=50 and 100g/cm^2.

4. Discussion and Concluding Remarks. Multi-cored EAS was observed at the prominent rate at a mountain altitude (Ref.4). And, the baloon and airplane born EC detected gamma-ray families with large multiplicity, high rapidity density and large transverse momentum. And in the JACEE events the projectiles are identified to He and heavier nuclei.

Our simulation results indicate that these phenomena are closely connected. It can be said that the interaction feature like the gamma-ray families mentiond above and the sufficiently high first interaction point can produce multi-cored EAS at the prominent rate, but steep and simple structured cores scarcely.

References:

1. Ogita, N. et al. Canad. J. Phys., Vol.46, (1968)S164.
Thielheim,K.O. et al. Acta Physica 29, Supl.3(1970)519.
Dake, S. et al. Contribution to Workshop on Cosmic Ray and High Energy Gamma Ray Experiments for the Space Station Era, Baton Rouge (1984), and ICR-Report=121-85-2, University of Tokyo, (1985).
2. Burnett, T.H. et al.
3. Iwai, J. et al. Nuovo Cimento A, Vol.69, (1982)295.
4. Kino, S. et al. Rpoc. ICCR, Vol.8, EA(1977)79.
Sasaki, H. et al. Proc. ICCR, Vol.8 EA(1979)190.
5. Nakatsuka, T. et al. proc.ICCR, Vol.11, (1981)326.

N85-35956
HE 3.6-8

COMPARISON OF BIG EVENT WITH CALCULATIONS OF THE AIR SHOWER DEVELOPMENT

Niwa,M., Misaki,A. and Matano,T.
Department of Physics, Saitama University,
338 Urawa, Japan
Honda,K., Tsushima,I., Kawasumi,N. and Hashimoto,K.
Department of Physics, Yamanashi University,
400 Kofu, Japan

ABSTRACT

We calculate high energy hadrons and electron-photons in air showers at various stages of developments.

We use the numerical calculation for solving the diffusion equation for nuclear cascade following Dedenko and the analytical calculation for cascade shower induced gamma rays. From these calculation, we can get the longitudinal development of high energy hadron and electron-photon component, and energy spectra of these components at verious depth of air shower development. The total number of hadron(N_H) and electron-photon component(N_γ) are related according to stages of air shower development and primary energy as shown in Fig.1. From such a figure, we can understand the relation between both components. We can show the relation of the total energy of hadron and electron-photon component above the threshold energy as Fig.2. The energy balance between both components is also useful parameter to study high energy events accompanying air showers. The relation of N_H and fractional hadronic energy($\Sigma E_H^\gamma/(\Sigma E_H^\gamma+ \Sigma E_\gamma)$) is calculated like Fig.3. This relation is helpful to understand the stage of air shower development(t) and primary energy(E_P).

These calculations has been done and compared with experimental results,especially Big event.

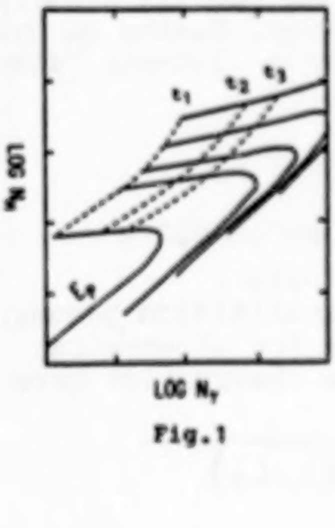

Fig.1

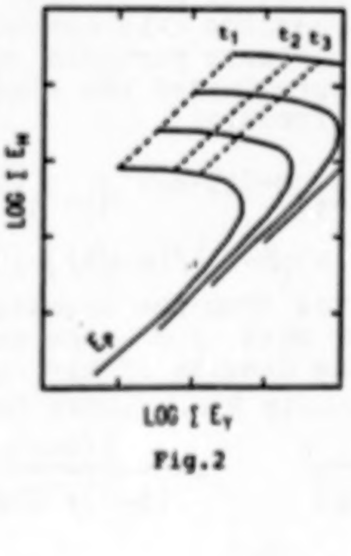

Fig.2

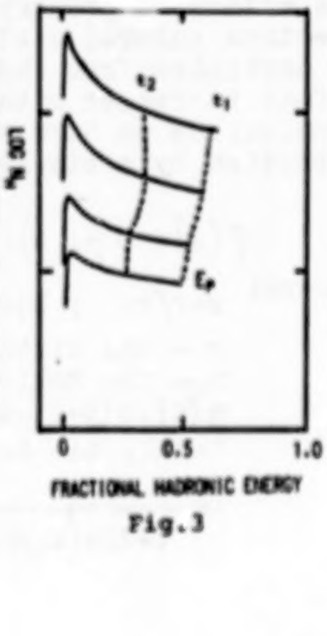

Fig.3

THE LATERAL DISTRIBUTIONS OF CHARGED PARTICLES OF ENERGY GREATER THAN 0.3 E_{crit} IN ELECTRON-PHOTON CASCADES IN LEAD AND AIR

N85-35957

A. Wasilewski[x], B. Kryś[xx]
[x]Institute of Nuclear Studies, Łódź, Poland
[xx]University of Łódź, Phys. Department, Łódź, Poland

In the recent investigations, both theoretical and experimental, the disagreement between cascade theory and experimental data is pointed out. In the present paper the radial distributions obtained from the Monte-Carlo simulations are compared with the well known results of the analytical theory for all particles in cascades. In the paper the data on mean radius of the electron lateral distribution in air are compared with these in lead

Lateral development of the electromagnetic cascades

In order to study the three dimensional behaviour of electromagnetic cascades, our simulation was made for the cascades initiated at the top of atmosphere and at a depth of 712 g/cm^2 for different energies. It shows, that the lateral distributions of particles are narrower than the NKG distributions with an age parameter describing the longitudinal development of the cascades /6,7/. We also found that the initiating point of the cascade development has an effect on the width of the electron lateral distribution. It appeared that the width of the distribution is determined by the density of the atmosphere at so-called effective height above the considered level and this gives the possibility of removing the differencies in the shape of distributions for different starting points of the cascades. The effective height was estimated as equal to 2 cascade units. The investigation of the effect of primary particle energy on the width of the electron lateral distribution shows that the mean distance of particles from the cascade axis corrected for the density effect increases with primary particle energy. Basing on our simulations we have approximated the electron lateral distribution by a simple formula:

$$\rho(x) = C(s,z)\cdot X_1^{\,s+0.5\cdot z-2}\cdot(1+X_1)^{z-5.3}$$

where: $x=r/r_0$; $X_1 = x\cdot\eta(t-2)/(m\cdot\eta(t))$; $m=0.8-0.2\cdot s$

r - the distance from the cascade axis ;

r_0 - the Molier unit ; C - the normalization param.,

$\eta(t), \eta(t-2)$ - the density of air for the observation level, the density 2 c.u. above the observation level

$$s=\frac{3t}{t+2\ln(E_0/\varepsilon_k)} \qquad z=\frac{3(t-2)}{(t-2)+2\ln(E_0/\varepsilon_k)}$$

From that formula we derived the value of so-called the local age parameter for different distances from the cascade axis. The local age parameter is defined as the age parameter obtained from the NKG formulae on the basis of particle density at two distances from the axis. The result is shown in Fig.1 . This analysis shows that the local age parameter changes form a value clearly greater than the NKG age parameter at small distances to significantly lower one at distances greater than the 0.1 Molier unit. It means that the method of describing the lateral distributions of electrons by the NKG function with one parameter can lead to different results depending on the distances at which this parameter is estimated .

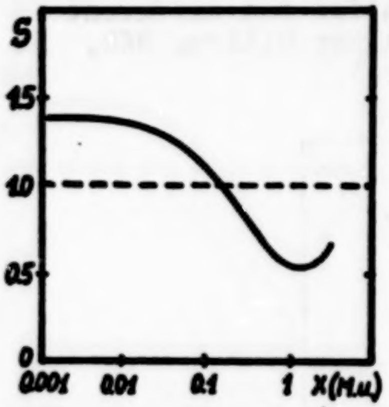

Fig.1 The value of the local age parameter as a function of distance X from the cascade axis : solid line - our approximation , broken line - the age parameter describing the longitudinal development. The ratio of electron densities at distances form the axis X_{i-1} and X_i where $X_i = X$, lg X_{i-1}/X_i was taken.

The comparison of simulation of the electromagnetic cascades with the other results

In this part we compare our approximation with those proposed by Nishimura-Kamata/1/, Greisen/2/, Hillas/4/ and Uchaikin/5/.

The comparison of the mean distances of particles from the cascade axis obtained from our results with the Hillas ones is shown in Fig.2a. Comparison of the analytical results

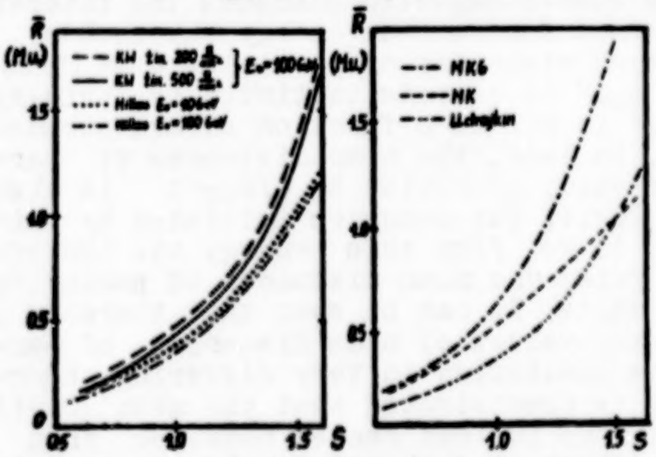

Fig.2 The mean distances of electrons from the cascade axis as a function of age parameter s .

for the same stage of the cascade development /NKG, NK and Uchaikin formulae / is shown in Fig.2b. Thus it is seen that reconstruction of such parameters as age parameter and number of particles on the basis of the proposed lateral distributions cannot give the same results.

The comparison of the relative numbers of particles at small distances from the cascades axis for two different stages of the cascade development with the Hillas, NKG, NK and Uchaikin formulae is shown in Fig.3

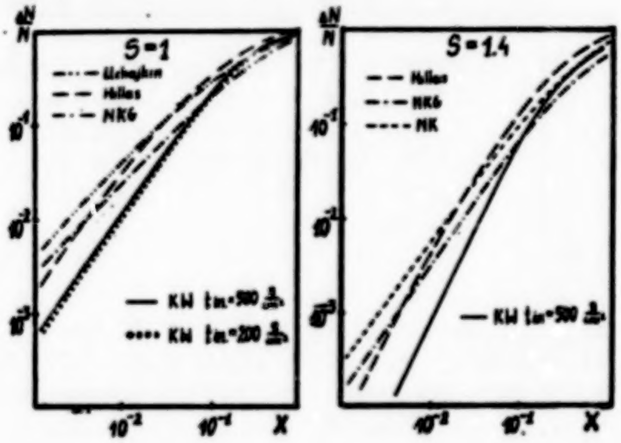

Fig.3 The relative numbers of electrons as a function of X

The present situation is such that near the axis the evident differencies between the curves exist. These deviations have significant consequancies for the experimental investigations. For instance, that flat distributions of electrons at small distances from the axis would lead to underestimation of the energy in subcores in EAS.

The comparison of simulation of the electromagnetic cascades with various energy threshold in different absorbers.

In simulations of the electromagnetic cascades the lateral distributions were obtained for various energy thresholds. The comparison of the mean distances of particles with threshold 30 m_ec^2 and 60 m_ec^2 in cascade initiated by primary photon of energy 50 GeV in air as a function of age parameter is shown in Fig.4. In lead, the mean distances of particles with the similar value of ratio E_{thr}/E_{crit} is also shown /E_{thr}=4 m_ec^2/. in Fig.4. for cascades initiated by primary photons of energy 10 GeV /for this energy the LPM effect does not play any role/ The mean distances of particles are compared in Molier units. It can be seen that there is a good agreement between the values of meas distances of particles obtained from the simulation in very differing absorbers - lead and air. It is demonstrated that the mean radii of the lateral distributions in lead can be obtained from those in air, if the same ratio of the threshold energy to the critical energy is taken.

ORIGINAL PAGE IS OF POOR QUALITY

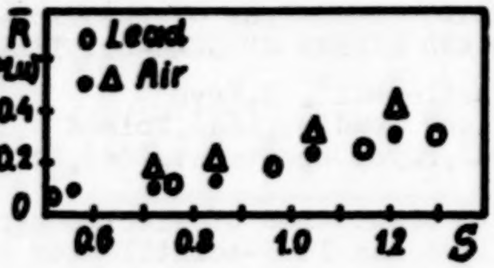

Fig.4 The mean distances of electrons with threshold $30\ m_ec^2$ and $60\ m_ec^2$ in air and $4\ m_ec^2$ in lead for cascades initiated by primary photons of energy 50 GeV at the depth 712 g/cm^2 in air and 10 GeV in lead.

Conclusions

The method applied in EAS research for estimation of parameters / i.e. age parameter and a number of particles / is based on assumption that the lateral distributions of particles in air showers are of the same type as in the electro magnetic cascades. The lateral distributions are always reconstructed by fitting the NKG function to the experimentally measured densities of particles at several distances from the shower axis. The signalized incoherences in EAS research / 8 / i.e. change of the age parameter with distances can be explained as a results of applying the incorrect formula / NKG ones /. This effect may be still better visible for higher energy threshold of secondary particles.

The formula proposed by us though not so easy for direct use in EAS research explain the discrepancies between experimental data and NKG formula, for instance the change of age parameter with distance.

The present results show that the applied Monte - Carlo method for significantly different absorbers seems to be good.

Acknowledgments

We would like to express the sincere thanks to Prof. J.Wdowczyk from the Institute of Nuclear Studies for helpful discussions.

References

/1/ Kamata.K,Nishimura J.,Suppl.Prog.Theor.Phys. 6,93,1958
/2/ Greisen K,Progress of Cosmic Ray Physics, 1956
/3/ Allan H., XIV ICRC,Munich,6,3071,1975
/4/ Hillas A.M.,Lapikens J., XV ICRC, Plovdiv,8,460,1977
/5/ Uchaikin V.V., XVI ICRC, Kyoto,7, 1979
/6/ Kryś E.,Wasilewski A., IX ECRC,Kosice,1984
/7/ Kryś E., Acta Physics Polonica,v B16,1985
/8/ Miyake, XVII ICRC,Paris, 10, 1981

RESULT OF MONTE-CARLO SIMULATION OF ELECTRON-PHOTON CASCADES IN LEAD AND LAYERS OF LEAD-SCINTILLATOR

A. Wasilewski[x], E. Kryś[xx]
[x]Institute of Nuclear Studies, Łódź, Poland
[xx]University of Łódź, Phys. Department, Łódź, Poland

Results of Monte-Carlo simulation of electromagnetic cascade development in lead and lead-scintillator sandwiches are analysed. It is demonstrated, that the structure function for "core approximation" is not applicable in the case in which the primary energy is higher than 100 GeV. The simulation data has shown that introduced inhomogeneous structure of chamber gives subsequent reduction of secondary particles.

Introduction.

In this paper we present results of detailed simulations, including the LPM effect, of electromagnetic cascades in lead and lead-scintillator sandwiches which are often used in emulsion chamber experiments. The following processes were taken into account in calculations: pair production, bremstrahlung including LPM effect with energy dependent cross - sections /Fig.1/, ionisations loss, Compton effect, single and multiple Coulomb scattering, the electron and positron inelastic scattering, photoelectric effect, annihilation of the positron.

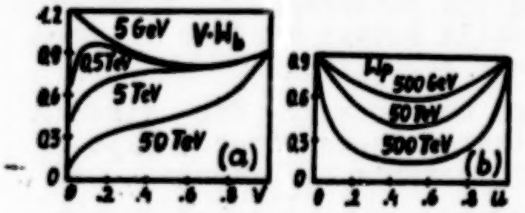

Fig.1.a The product of differential cross-section of bremstrahlung and v, where $v=E/E_0$; b The differential cross-section of pair production, where $u=E/E_0$.

The simulations were performed:

- in lead, for primary photons of energy 100 GeV, 10 TeV and 100 TeV and for primary electrons of energy 100 GeV,
- in sandwiches of lead and scintillator: for primary electrons of energy 100 GeV /Tab.1, No.1/, primary photons of energy 10 TeV and 100 TeV /Tab.1, No.2/.

absorber		Pb	Sc	Pb	Sc	Pb	Sc	Pb	Sc	Pb	Pb
thickness of aborb. /cm/	1	1	.5	.5	.5	.5	.5	.5	.5	.5	.5
	2	4	2	1	2	1	90	3	2	1	1

Tab.1 The structure of chambers investigated in our simulation. No.1: this sandwich is similar to that used in FNAL experiment[1]. No.2: this one is similar to the big gamma-hadron detector used in cosmic rays research /for instance Pamir Collaboration [2] /.

General procedure was following. All particles with energies exceeding certain value of $k=E_0/E_k$ were followed individually. Particles below E_k down to the threshold energy were followed using the so-called "thinning" method. The value of k was usually taken to be 1000 or 100 and the threshold energy was 2 $m_e c^2$.

Longitudinal and lateral development of the electromagnetic cascades

In the emulsion chamber technique, the energy of an incoming electron or photon is measured by the behaviour of cascade showers near the shower axis. In "core approximation" is assumed that the lateral structure functions depend on $E_0 r/K_s$ and s only and not of separate variables E_0 and r. In this paper we analyse validity of this statement for wide range of energies and for different structure of chambers. In Fig.2 one can see the transition curves for primary electrons and photons of energy 100 GeV for shower radii 100 um together with the cascades obtained in chamber C_1 of FNAL experiment.

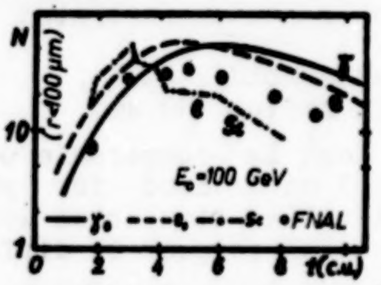

Fig.2 Cascades curves of electrons in photon and electron initiated showers for radius 100 um.

Our results are presented separately for cascade passing only throught lead and for cascades initiated in lead-scintillator /sandwich No.1/. As can be seen the introduced scintillator plays important role, giving subsequent reduction of secondary particle numbers. The transition curve obtained for sandwiche's structure shows similar tendence as is seen in experiment, i.e. the smaller electron size than in pure lead chamber. We conclude that the agreement with experiment can be achieved by emploing as an absorber in our simulations the precise structure of FNAL sandwiches.

Let's compare the shape of transition curves when the energy of primary particles increases.

In Fig.3a we present the transition curves with $E_{thr}=2m_e c^2$ for E_0= 10 TeV and E_0= 100 TeV for pure lead chamber and for sandwich No.2. Fig.3b gives the transition curves for "core approximation" i.e. for shower radius 100 um and for the same primary energies of particles. For these cascades the LPM effect plays an important role in transition curves as the energy increases giving a deeper position of shower maximum and smaller size at maximum. In Fig.3 one can see that even primary photons of energy 10 TeV can penetrate through all chamber /sandwich No.2/. This effect is stronger when the primary energy of photon increases. The most of EAS experiments have one or more layers of carbon: this enhances the detector capability to discriminate hadrons from photons and electrons. The insteresting results of the present simulations is that the number of particles after penetration of the thick /90 cm/ scintillator and 3 cm lead increases if the lead follow this scintillator. Furthermore the numbers of electrons after first 4-5 cm in lead is comparable with ones after 90 cm of scintillator and 3 cm of lead for primary photons of energy 100 TeV. A detailed simulation would be necessary to quantify this effect with respect to different experiment.

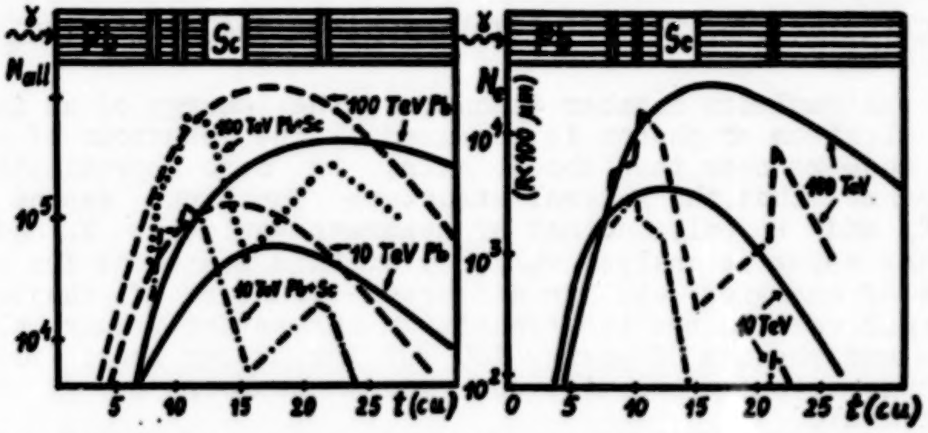

Fig. 3 Cascade curves of electrons in photon initiated shower.
a. for all particles with threshold 2 m_ec^2 ,
b. the same threshold but in radius 100 um.

The comparison of the simulation transition curves for different energies shows that validity of statement "core approximation" for all range of energies and depths is not good - Fig.4 .

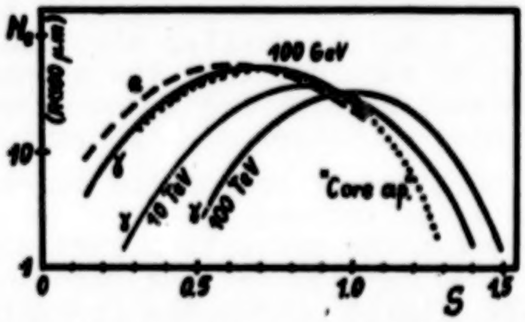

Fig.4 The transition curves of electrons obtained in our simulation /solid ones/ are compared with "core approximation" /the numbers of electrons for 10 TeV and 100 TeV are scaled to 100 GeV - i.e. divided by 100 and 1000 respectively/.

Our results show that applied "core approximation" for lower energies than 100 GeV is rather good, but for higher energies LPM effect makes this relation wrong.

On the basis of presented transition curves we estimated the energy of primary particle for different depths of development cascades according to "core approximation". It is shown in Tab.2 . The value of energy determinated from our data changes from a value lower than the energy of primary particle at low s to the value greater than ones at higher s. In the other words, our results show that the method of describing lateral distributions of electrons by "core approximation" leads to underestimation of the energy of the primary particle at low value of s and to overestimation at higher s.

	s	0.5	0.6	0.7	0.8	0.9	1.0	1.1	1.2	1.3	1.4
a	t /cm/ E_e/TeV/	2.9 5.0	3.6 7.1	4.5 9.2	5.3 10.1	6.3 12.8	7.3 15.0	8.5 17.0	9.7 22.3	11.2 26.6	12.8 31.0
b	t/cm/ E_e/TeV/	6.6 7.0	8.3 21.0	10.1 40.0	12.0 77.0	14.2 107.0	16.6 170.0	19.2 280.0	22.1 370.0	25.3 670.0	29.0 1000.

Tab.2 The comparison of the energy of primary photon estimated according to "core approximation". The energy of primary photon is : a. 10 TeV and b. 100 TeV.

As one can see, these discrepancies depend on the depth of the observation level and on the primary energy of particles.

Conclusions

1. It was stated that inhomogeneous structure of chamber has an effect on the transition curves. It appeared that numbers of secondary particles / for constant radii and constant primary photon energy / is determined by thickness, the kind of absorbers and their place in sandwiches.

2. It is not possible to describe the lateral dsitributions of particles with "core approximation" independent of the primary particle energy because the LPM effect plays an important role in transition curves. The method of describing lateral distributions of electrons by the "core approximation" used in chamber experiments lead to underestimation of the primary photon energy at low values of s and overestimation at higher s .

Acknowledgements

We would like to express the sincere thanks to Prof. J. Wdowczyk from the Institute of Nuclear Studies for critical advise about various aspects of interpreting the data discussed here. Thanks are also due to dr J.A. Wrotniak for his informations about "thinning" method.

References

[1] Hotta N et al., 1980 Phys.Rev.D 22 1
[2] Trudy FIAN, v.154, Moskva 1984

ON 'MINI-CLUSTER' OBSERVED BY CHACALTAYA EMULSION CHAMBER EXPERIMENT

T. Tati
Otsuka 6-36-8, Bunkyo-ku, Tokyo 112, Japan

N85-35959

It is mentioned that the phenomena of 'Mini-Cluster' observed by Chacaltaya emulsion chamber experiment support the model of hadronic matter based on the theory of finite degree of freedom.

1. Introduction

The world of elementary particles has been more and more enlarged and diversified and, at the same time, unifying relations in it have gradually been established basing on the quantum field theory. In this case, the quantum field theory itself has been unchanged in its foundation, though basic fields and their interactions have been effectively selected. The quantum field theory gives divergent results showing that the theory is not completely defined. The difficulty is avoided for practical problems by choosing the renormalizable type of theories. Even in the renormalizable case, the theory contains an undefined part left to future theories. The renormalization theory evades the divergence difficulty by replacing arbitrarily the undefined divergent part by an appropriate finite constant and considers only things independent of details of the undefined part. We want to consider, however, the difficulty or inconsistency in the fundamental theory as a moment for deeper recognition of the existence of elementary particles.

The divergence difficulty is due to the infinite degree of freedom of the quantum field given by the set of all possible values of momentum or equivalently of position of the particle associated to the field. The quantum field with a finite degree of freedom is contradictory to the space-time description so that the theory of finite degree of freedom requires the reformation of the concept of space-time based on the non-space-time description [3]. The theory of finite degree of freedom suppresses the high momentum part of the degree of freedom referring to a universal timelike vector[1] and gives consequences for the part left undefined in the renormalization theory[3].

The ultrahigh energy nuclear interactions have long been investigated by the emulsion chamber experiments of Brasil-Japan collaboration and Soviet group. They found various kinds of fireballs as intermediate states of multi-hadron productions[4,5]. It is considered that the approach using phenomenological models is effective for the interpretation of fireball phenomena. In this case, when the models reflect a basic idea, its validity can be tested by experimental facts. The model of hadronic matter[2] of which hadrons are made based on the theory of finite degree of freedom seems to give a picture which explains qualitatively the characteristic properties of hadrons and hitherto found fireballs[4,5].

The hadronic matter is made mainly of a great number of virtual urbaryon pairs (quark pairs) generated by vacuum polarization. Due to the finite degree of freedom of urbaryon, it is an extended matter with a fairly uniform density and a volume generally proportional to its mass apart from individualities. Recently the Brasil-Japan collaboration observed bundles of electromagnetic showers with very small transverse momenta (some 10 MeV) accompanied by decay products of Chiron-type fireballs (Chiron and Geminion)[6]. The bundle of electromagnetic showers is called 'Mini-Cluster'. It is mentioned in this paper that the phenomena of 'Mini-Cluster' support the picture of fireballs made of the hadronic matter based on the theory of finite degree of freedom.

2. A Picture of Hadrons and Fireballs made of the Hadronic Matter

The basic particle (urbaryon) of the hadronic matter is a bare quark q having color and flavor and obeying the theory of finite degree of freedom. 'bare' is to distinguish q from the physical quark Q[8] mentioned below but we call q simply quark in the following. The hadronic matter consists of a certain number of quarks carrying quantum numbers of the system and a large number of virtual quark pairs generated by vacuum polarization. The position degree of freedom of the field of basic particle distributes with a density (1/v) in the hyperplane perpendicular to a universal timelike vector N_μ, that is, the space in the Lorentz system (we call N-system) in which $N_\mu = (1,0,0,0)$. The relative velocity between the N-system and our laboratory system on the earth is considered some $10^{-3}c$ (c is the light velocity) on cosmological grounds so that our laboratory system is considered approximately the N-system for high energy phenomena[3]. The volume v is given by

$$(4\pi/3)K_1^3 v \approx (2\pi\hbar)^3,$$

when the effective cutoff of the momentum degree of freedom is K_1. (The cutoff function should have a sufficiently long tail.)

Due to the Fermi statistics, only a finite number of quarks can occupy the volume v. This acts to extend the volume of the system and to make its density uniform. Hadronic matter is assumed to be a superposition of states confined with the maximum compactness so that the mass is, apart from individualities, e.g. vibrational excitations, in general given by

$$M \approx \rho V \approx \rho(n/f)v,$$

where ρ is the density being a constant, f is the number of quarks in v and, V and n are expectation values of the volume and the number of quarks of the system, respectively. The quantum field theory implies that the hadronic matter has its proper V and n for each quantum state. In a broad view, it is assumed that all colorless ground states (hadrons) have nearly the same V and n given by

$$V \approx V_N \approx (4\pi/3)(1/M_N)^3 \ , \quad n \approx n_N \approx f(V_N/v),$$

where M_N is the nucleon mass. Hadron resonances are considered excited states of hadrons by surface vibrations.

We consider that there exists a free physical quark Q clothed in a cloud of virtual quark pairs like a physical electron in QED clothed in a cloud of virtual electron pairs. In our picture, when Q and anti Q combine to form a meson $(Q'\bar{Q}')$ (Q' represents a deformed physical quark in the hadron), hadronic matter of the volume $2V_Q - V_N$ should disappear. This corresponds to the binding energy

$$B \approx \rho(2V_Q - V_N) \approx 2M_Q - M_N,$$

where M_Q is the physical quark mass. Conversely, in order to decompose $(Q'\bar{Q}')$ into Q and $\bar{Q}$, we should produce hadronic matter of the volume $2V_Q - V_N$. The produced giant hadronic matter is, however, a colorless fireball which decays into hadrons. This is a limited color confinement in our picture. For definiteness and simplicity, we assume that all colored ground states have nearly the same V and n given by

$$V \approx V_Q \approx 10\ V_N, \quad n \approx n_Q \approx 10\ n_N,$$

so that $M_Q \approx 10\ M_N$.

The effective cutoff momentum K of hadronic matter of size n is given by

$$K \approx nK_1,$$

where K_1 is the effective cutoff momentum of the basic particle (quark). The production probability of hadronic matter is suppressed when the momentum surpasses its effective cutoff K, although it can be accelerated when it is stable, e.g. by an electromagnetic field, far beyond K due to a long tail of the cutoff function. The effective cutoff for the Lorentz factor is given by, in the N-system,

$$\Gamma \approx K/M \approx (nK_1)/(\rho nv) \approx (K_1/\rho v),$$

which is insensitive to the size of hadronic matter. Cosmic ray experiments seem to suggest that there exists an effective cutoff around 10^4- 10^5 for Lorentz factors of fireballs insensitive to their sizes. When we take $K_1 \approx 10\ M_N$ (in this case, $n_N \approx 10^4$), we have $\Gamma \approx 10^5$.

Hitherto found fireballs are three kinds of ordinary fireballs H, SH and UH quanta having masses about 3 GeV, 30 GeV and 300 GeV, respectively, which decay mainly into pions and four kinds of exotic fireballs Mini-Centauro, Centauro, Geminion and Chiron, the decay products of which contain almost no pions. The masses of Mini-Centauro and Geminion are about 30 GeV and the masses of Centauro and Chiron are considered as being around 300 GeV.

We assume that the fireballs decay in accordance with the schema mentioned below and, in each step of decays, the sum of masses of decay products is about equal on an average to half of the mass of the decaying fireball. This scheme gives the right order of magnitude of multiplicity and transverse momenta of decay products characterizing each fireball.

H quantum decays into several pions. SH quantum decays into several H quanta. UH quantum decays into several SH quanta. Mini-Centauro decays into several nucleon pairs $(N\bar{N})$'s. Centauro decays into several Mini-Centauros. Geminion decays into a physical quark pair $Q\bar{Q}$[8]. Chiron decays into several Geminions.

In view of the model of hadronic matter, H, SH and UH quanta are the hadronic matter of the volume around V_N, 10 V_N and 100 V_N, respectively. (H quantum is considered an excited state hadronic matter of $V \approx V_N$ by volume vibration. In this case, H quantum is not a superposition of hadron resonances.) Centauro and Mini-Centauro are interpreted as UH quantum and SH quantum, respectively, in which the production of the participating H quanta in their decays is suppressed due to that the momenta of the H quanta surpass their effective cutoff and, instead of each H quantum, a nucleon pair $N\bar{N}$ is produced for which the effective cutoff momentum is larger than that of H quantum[7]. Chiron is interpreted as UH quantum in which the production of the participating SH quanta in the decay is suppressed due to that the momenta of the SH quanta surpass their effective cutoff and, instead of each SH quantum, a physical quark pair $Q\bar{Q}$ is produced for which the effective cutoff momentum is larger than that of SH quantum. The physical quark pair thus produced instead of a SH quantum is, regardless of whether the SH quantum belongs to decay products of a larger fireball or not, considered to be a Geminion.

3. 'Mini-Cluster'

The decay products of exotic fireballs have definite nuclear collision mean free paths so that they are considered to be indestructible. In our picture, the decay products of Centauro type and Chiron type fireballs are nucleons and physical quarks, respectively. In this case, in order to produce physical quarks in the p-$\bar{p}$ collider interaction, the colliding particles should have at least $\Gamma M_{CM} \simeq 10^6$ GeV which is far beyond the present collider energies[10]. The observed collision mean free path of the decay product of Chiron type fireballs is considerably short compared with that of the nucleon. This fact is in accord with our model, since the physical quark is an indestructible hadronic matter of the volume much larger than that of the nucleon.

Owing to that the nuclear matter is a fairly homogeneous many body system, the liquid drop model is applied to heavy nuclei and the excitations being considered due to surface vibrations are observed. The hadronic matter in our picture is also a fairly homogeneous many body system so that the excitations due to surface vibrations should be observed. We consider that the hadron resonances are due to surface vibrations. The surface vibration of the physical quark should also have observable effects.

The frequencies of stationary surface waves of liquid drop is[11]

$$\omega_\ell = [(4\pi\epsilon/3M_d)\ell(\ell-1)(\ell+2)]^{1/2}, \quad \ell = 2, 3, \ldots ,$$

where ϵ is the surface energy per unit area and M_d the mass of the drop. When ϵ is assumed to be the same for all hadronic matter and M_Q is taken to be 10 GeV, the ratio $\hbar\omega_\ell(Q)/\hbar\omega_\ell(N)$ of the quantum $\hbar\omega_\ell$ for the physical quark to that for the nucleon is about 1/3. In our picture, $\hbar\omega_\ell(N)$ is the spacing of hadron resonances for $\Delta J = 2$ and is about 500 MeV. Then $\hbar\omega_\ell(Q)$ turns out to be about the pion mass. In view of the oversimplification of our model, it is possible that $\hbar\omega_\ell(Q)$ is considerably smaller than the pion mass, e.g. some 10 MeV. In this case, the n quantum excited state of surface vibration of the physical quark, $E_n = n\hbar\omega_\ell(Q)$, decays emitting n photons of energy $\hbar\omega_\ell(Q)$. The transition probability per unit time for the γ emission of the liquid drop is given by[11]

$$(\Gamma_\gamma/\hbar) = (1/4)[\omega_\ell(Q)/c]^5[QM]^2/\hbar ,$$

where $[QM]$ is the quadrupole moment of the emitting system. The quark is considered to move fairly freely in its massive neutral clothes of virtual pairs. (For the hadronic matter, just as heavy nuclei, the liquid drop model and the degenerate Fermi gas model are considered valid for collective motions and individual particle motions, respectively.) Then the life time of the γ emission of the physical quark is estimated to be around 10^{-18} sec. (Γ_γ is the γ ray width.)

Thus we consider that the recently observed 'Mini-Cluster' accompanied by a decay product of the Chiron type fireballs is due to the surface vibration of the physical quark and accordingly supports the model of hadronic matter based on the theory of finite degree of freedom.

1 T. Tati, Prog. Theor. Phys. 24 (1960), 1.
2 T. Tati, Prog. Theor. Phys. 43 (1970), 1596.
3 T. Tati, Prog. Theor. Phys. Suppl. No. 76 (1983), 186.
4 C.M.G. Lattes et al., Phys. Rep. 65 (1980), 152.
5 Brasil-Japan EC Collab., Proc. 17th ICRC 11 (1981), 100.
6 Brasil-Japan EC Collab., Proc. 18th ICRC 11 (1983), 77.
7 T. Tati, Proc. 13th ICRC 3 (1973), 2311.
8 T. Tati, Proc. 16th ICRC 7 (1979), 367.
9 T. Tati, Proc. 17th ICRC 5 (1981), 356.
10 T. Tati, Proc. 18th ICRC 5 (1983), 495.
11 H.A. Bethe, Rev. Mod. Phys. 9 (1937), 69.

N85-35960

HE 3.7-1

A COMPARATIVE ANALYSIS OF GAMMA AND HADRON FAMILIES AT THE SUPERHIGHT ENERGIES RECORDED IN EXPERIMENT "PAMIR"

Azimov S.A.,Mulladjanov E.J.,Nosov A.N.,Nuritdinov H.
Talipov D.A.,Halilov D.A.,Yuldashbaev T.S.

Physical-Technical Inatitute of Academy of
Sciences of the Uzbek SSR, USSR

In the paper a comparative analysis of hadron and gamma families were undergone the decascading procedure is made. Receive results are compared with different models of interactions. In hadron families with energies $\Sigma E_\gamma^h > 20$ TeV as well as in gamma families with energies $\Sigma E_\gamma > 70$ TeV increasing azimuthal anyzotropy in events with large ER is observed.

INTRODUCTION

It's of interest compare different characteristics of the gamma and hadron families at superhight energies. However, electromagnetic multiplication of the initial γ-quanta in the atmosphere has a great influence on observed characteristics of the γ-families decreasing sensitiveness these characteristics (especially longitudinal) to different models of strong interaction. Hadron families characteristics are free the influence of those effects.

The decascading procedure suggested in /I/ allow to reduce essentialy the influence of electromagnetic cascading multiplication of the initial γ-rays in the atmoaphere. All particles paires satisfied the condition $Z_{ik} < Z_o$ were combined in single group (initial quantum), where $Z_{ik}=R_{ik}(I/E_i+I/E_k)^{-I}$, R_{ik} -the mutual distance of particle pair in mm, E_i, E_k -their energies in TeV. The decascading parameter was set equal to Z_o=IO TeV·mm. Thus the observed γ_o-families are transformed in the initial γ_i-family. The comparison characteristics of the hadron-families (h-families) with such γ_i-families is a more corred procedure than comporison with observed families.

The experimental data about spatial characteristics of the γ_i and h-families compare with simulated families calculated on different assumptions about mechanism of the strong interaction. Different assumptions about chemical composition of the primary cosmic radiation exert essential influence on the results of such analysis. Consequently, in the paper an new selecting criteria of γ-families are formed by primary nuclei or protons is proposed.

We considered such spatial characteristics as $\bar{R}$ ($\bar{R} = \sum_{i=1}^{n_\gamma} R_i / n_\gamma$, R_i -distance of the γ-quanta from axis of family, n_γ -number particles of family) and α proposed in the work /2/ for analyse the structure of the families.

$\alpha = \sum_{i\neq j}^{n} \mathrm{Cos}2\varepsilon_{ij}/(n(n-I))$, where ε_{ij} -the angle between the momentum projections of i-th and j-th particles in azimuthal XY-plane, perpendicular to the primary particles direction, n -number of particles in family.

The value α reachs magnitude $\alpha = I$ for the completely complanar events and become minimal $\alpha_{min} = - I/(n-I)$ in the case of an isotropic, uniform distribution of azimuthal angles.

I. The characteristics of the hadron and gamma families

To analyse the spatial structure of γ-families it is impotant to have more complete information about particles with large transverse momenta. Consequently it's were investigated the experiment "Pamir" data obtained under conditions when film scanning and particle selection were realised within the radius R = 30 sm relatively the energy weighted center of γ-family. In the result were selected N=326 γ-families with energies ΣE_γ=60÷500 TeV and number of particles $n_\gamma \geqslant 4$. The minimum energy of the γ-quants in the families was set E_γ=4 TeV. Particle scanning and selection h-families were realised within the radius R=30 sm too. The minimum energy of the cascades in the h-families was set E_γ^h =4 TeV. It were selected N=18I h-families with energies E_γ^h =20÷500 TeV.

At the analysis of the hadron families on record by " "Pamir" carbon chamber, it is nesessary to take account the formation structured events that is the groups of spots with mutual distances less than ~I mm in X-ray film. These narrow groups of spots corresponds to one hadron above the chamber and originate from spatial fluctuations in nuclear-electromagnetic cascad (NEC) in the chamber /3/.

In the paper the groups of the electron-photon cascades (EPC) with mutual distanse less than I.7 mm are considered as one cascade is produced by only hadron.

In table presents data about $<\bar{R}>$ and $\bar{\alpha}$ obtained from experiment and from CS -scaling and CSČj -models /4/.

TABLE

	EXPERIMENT		CALCULATION		
	γ_i-fam.	h-fam.	CS γ_i-fam.	CSČj γ_i-fam.	CSČj h-fam.
$<\bar{R}>$	44.6±2.I	45.3±3.4	29.I±I.3	42.I±3.8	47.3±4.8
$\bar{\alpha}$	0.I9±0.0I	0.26±0.02	0.II±0.0I	0.2I±0.02	0.28±0.03

In CSČj-model the inelastic charge-exchange of leading charge pion into neutral one $\pi^{\pm}\rightarrow\pi^{0}+\ldots$ and the jet production processes was taken into account. The generation cross section of jets with large transverse momenta P_{tj} is calculated according to /5/. As one can see from table I only jet generation model is in good agriment with experiment.

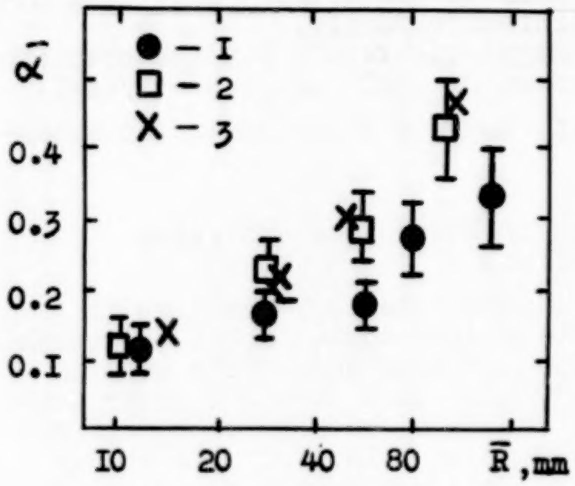

Fig. I

Fig.I presents data about the dependence of the value $\bar{\alpha}$ on the spatial parameter $\bar{R}$ of γ_i and hadron families (I - γ_i-families, 2 -h-families, 3 -h-families from CSCj-model). As one can see from figure I, the essential incrising of the azimuthal correlation in the range of the large values $\bar{R} > 50$ mm of the hadron and γ_i-families is observed. These results are in a good agriment with the jet production model while CS-model is led to smaller values $\bar{\alpha}$, $\bar{R}$, than in experiment.

2. Gamma-families originated from nucleus-nucleus (AA) and proton-nucleus (PA) interactions

In the paper the selecting criteria of that families obtained from the analysis of the γ-families simulated on the basis MSF-model /6/.

The criterion: $\bar{R} > 40$ mm and $\alpha < 0.2$ for selection of γ-families, originated from nucleus-nucleus interactions (AA-families) is proposed, as for as AA-families are more wide (the majority of the families have the value $\bar{R} > 40$ mm) and isotropic in the azimuthal plane than PA-families. That criterion select 65% AA- and 35% PA- of simulated families with energy $\Sigma E_\gamma = 70-500$ TeV, contained EPC with energies $E_\gamma \geqslant 2$ TeV, lying within the radius R=30 sm from family center.

The using such criterion to experimental data showed, the fraction AA-families at the observation level is 15 ± 4%. This value is agree with assumption about normal chemical composition of the primary cosmic radiation at energies $E_0 \geqslant 10^{15}$ eV.

Other proposed criterion: $d = n_o / n_i$ where n_o and n_i - number of the observed and initial γ-quants in the families. According to MSF-model, families with $d \geqslant 1.6$ originated from protons (the admixture of AA-families compose ~ 9%), and events with $d \leqslant 1.2$ originated mainly from nucleus-

-nucleus collisions (among them 70% AA- and 30% PA-families).

At the Fig.2 data about the dependence azimuthal correlations from value $\overline{ER}$ (E -energy R -distance of the γ -quanta from axis of family, I -experimental families with d $\geqslant$ I.6 , 2 -experimental families with d $\leqslant$ I.2 , 3 -CSČj-model, 4 -MSF-model for events with d $\leqslant$ I.2) is presented.

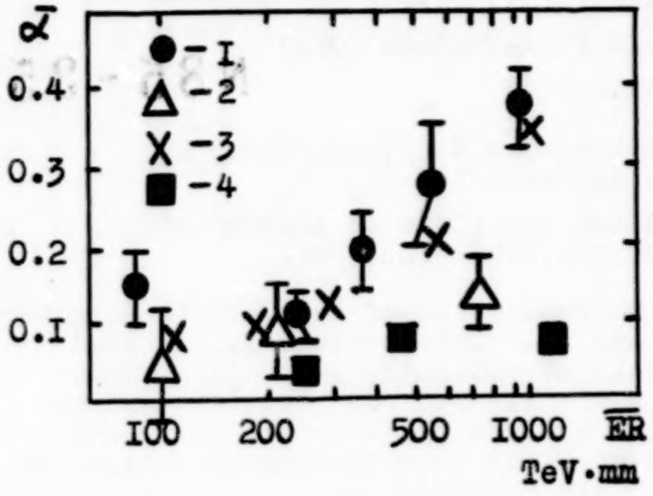

Fig. 2

How one can see from Fig.2, effect of the azimuthal correlations increasing in the range of the large values $\overline{R}$ and $\overline{ER}$ connected with proton-nucleus interactions and described by CSČj-model. On the other hand for the nucleus-nucleus interactions the increasing azimuthal correlations is not observed.

REFERENCES

I. L.T.Baradzey, Yu.A.Smorodin, E.A.Solopov Preprint FIAN N I03, I974
2. S.A.Azimov, T.S.Yuldashbaev et.el. Zeszyty Naukove Universitety Lodzkiego, Lodz I977, z.60, s.II, p.28I
3. G.G.Leptuh et.el. Proc. of International Symposium on Cosmic Rays and Particle Physics, Tokyo, March I9-23, I984, p.26I
4. S.A.Azimov, E.J.Mulladjenov, H.Nuritdinov, D.A.Talipov, D.A.Halilov, T.S.Yuldashbaev Proc. I8-th ICRC, Bangalor, India I983, v.5, p.458
5. L.V.Gribov, E.M.Levin, M.G.Ryskin Phys.Lett. I2IB, 65, I983
6. R.A.Mukhamedshin Proc. I7-th ICRC, Paris I98I, v.5, p.343

ORIGINAL PAGE IS
OF POOR QUALITY

A STUDY OF γ-FAMILIES GENERATED IN NUCLEON-NUCLEUS (NA) AND PION-NUCLEUS (πA) INTERACTIONS

N85-35961

Azimov S.A., Mullajanov E.J., Nuritdinov H.,
Yuldashbaev T.S.

Physical-Technical Institute of Academy of
Sciences of the Uzbek SSR, USSR

In the paper the separation of the γ-families generated in NA and πA interactions is realized from the analysis of simulated γ-families. Some characteristics of NA and πA families and the influence of the process of inelastic charge-exchange of charged pions into neutral ones type of $\pi^{\pm}A \rightarrow \pi^{0}+\ldots$ are studied.

In the paper the characteristics of γ-families generated in pion-nuclear πA-interactions (π-families) and nucleon-nuclear NA-interactions (N-families) in atmosphere is investigated.

The selecting criteria of π and N-families is proposed from the analysis of γ-families simulated on the basis of scaling CS and CSČ -models.

The CS -model is based on extrapolation to the superhight energies of the interaction characteristics known in the accelerater energies in the assumption of Feynman sca - ling validity. For that there is made no difference between NA and πA interactions mechanism.

In the CSČ -model the inelastic charge-exchange of leading charge pion into neutral one $\pi^{\pm}\rightarrow\pi^{0}+\ldots$ was taken into account. The inelastic charge-exchange probability W is set equal to 0.2 at $x_1 = E_1/E_0 \geqslant 0.5$ (x_1 -Feynman's variable for leading particle, E_0 -energy ofcolliding particle).

The families are considered as a formed mainly in the pion-nuclear interactions (π-families), if the fraction of the energy from pion interactions

$$K^{\pi} = \frac{\Sigma E_{\gamma}^{\pi}}{\Sigma E_{\gamma}} ,$$

where ΣE_{γ}^{π} -the summary energy of the cascades from πA - interactions, was satisfied the relation: $K^{\pi} > 0.5$ .If the value

$$K^{N} = \frac{\Sigma E_{\gamma}^{N}}{\Sigma E_{\gamma}} ,$$

where ΣE_{γ}^{N} -the summary energy of the γ-quanta from nucleon-nuclear cascades, was satisfied the relation: $K^{N} > 0.5$, than such families are considered as a formed in the nucleon-nuclear interactions (N-families) (ΣE_γ -the total energy of γ-family).

The spatial characteristic of the simulated γ-families $\bar{R} = \sum_{i=1}^{n_\gamma} R_i / n_\gamma$ (where R_i -distanse of γ-quanta from axis of family, n_γ -number of γ-quants in the family) is considered too. The simulated families were selected according to criteria analogous to those in Pamir experiment: the family summary energy $\Sigma E_\gamma = 30 \div 500$ TeV, the number of particles $n_\gamma \geqslant 3$, the minimal energy of quanta was equal to $E_\gamma = 2$ TeV, only those quanta is included in families which were found in the round with radius $R = 30$ sm from the center. As we showed in the work /I/, the simulated families with $\bar{R} > 40$ mm mainly consist of the π-families (them fraction compose $70 \div 85\%$ for both models), and families for which angles of arrival on plant $\theta \leqslant 20^\circ$ and $\bar{R} < 20$ mm mainly consist of the N-families. Therefore, those conditions used as a selecting criteria of π and N-families in the work.

The characteristics of simulated γ-families were compared with the experiment "Pamir" data. The film scanning and particle selection were realised within the radius $R =$ 30 sm relatively the energy weighted center of γ-family. In the result it were selected $N = 539$ γ-families with energies $\Sigma E_\gamma = 30 \div 500$ TeV and number of particles $n_\gamma \geqslant 3$. The minimum energy of the γ-quants in the families was set $E_\gamma = 2$ TeV. At this, the conditions near to experimental in the simulated families were introduced. The registration efficiency of γ-quants $E_\gamma = 2 \div 4$ TeV in the energy region change from 0.3 to I.0 . The registration efficiency of γ-families reach I.0 at energy $\Sigma E_\gamma \geqslant 70$ TeV. The error δE in the energy measuring and real spatial resolution of the close situated quants (quants, situated on distanse $r_{I,2} =$ $40 \div 100$ μm with energies $E_I + E_2 = 25 \div 50$ TeV, were considered as an unified) were taken account.

In the paper an distributions of families arrived the installation under different angles θ to vertical investigated. In the experiment the errors of the angles determination for the families arrived under small angles to vertical are large.

The registration probability of γ-quanta decrease in the large angles range $\theta > 36^\circ$. Therefore, events with angles of arrival situating in interval $9^\circ \leqslant \theta \leqslant 36^\circ$ were selected for analyse. At this, the error in the angle measuring of the arrival $\Delta\theta \sim 1^\circ$ introduced in the simulated families.

All events divided on the groups of families arrived the installation under angles $\Delta\Theta_1 = 9^\circ \div 18^\circ$ (number this families N_I), and arrived under angles $\Delta\Theta_2 = 18^\circ \div 36^\circ (N_2)$.

The value

$$F = \frac{P_2}{P_I}$$

where $P_I = N_I/(N_I + N_2)$ -the fraction of families arrived on plant under angles $\Delta\Theta_1 = 9^\circ \div I8^\circ$ and $P_2 = N_2/(N_I + N_2)$ -the fraction of families arrived under angles $\Delta\Theta_2 = I8^\circ \div 36^\circ$ is calculated for families of experiment "Pamir" and simulated families. In consequence an following values F: 0.82 ± 0.08 (CS -model), I.45 ± 0.I5 (CSČ -model) and I.64 ± 0.I6 (experiment) were obtained.

Like that, the experimental data relatively value F agree with CSČ -model.

In the paper the families selected according to selecting criteria of π and N -families ($\bar{R} > 40$ mm and $\bar{R} < 20$ mm) is investigated. At this, for value $\Delta = N_\pi / N_N$, where N_π -number of π -families, N_N -number of N -families the following values were obtained: 0.5 ± 0.07(CS-model), 0.78 ± 0.I2 (CSČ-model) and 0.73 ± 0.09 (experiment).

How one can see from analyse of the angulas distributions of γ-families and the correlation between π and N-families, the experimental data are described by CSČ-model in that the inelastic charge-exchange of leading charge pion into neutral one $\pi^\pm \to \pi^0 + \dots$, was taken account.

REFERENCE

I. S.A.Azimov, E.J.Mulladjanov, H.Nuritdinov, T.S.Yuldashbaev Proc. I8-th ICRC, Bangalor, India I983, v.5, p.462

N85-35962

HADRONS REGISTRATION IN EMULSION CHAMBER WITH CARBON BLOCK

A. Tomaszewski and Z. Włodarczyk

Institute of Physics, University of Lodz, Lodz, Poland and
Institute of Physics, Pedagogical University
Kielce 25-509, Lesna 16, Poland

NEC in X-ray emulsion chambers with carbon block, which are usually used in the "Pamir" experiment, was Monte-Carlo simulated. Going over from optical density to ΣE_γ is discussed. Role NEC in the interpretation of energy spectra is analysed.

1. Introduction. As a result of the nuclear-electromagnetic cascade (NEC) in C-layer and Pb-layer of haderonic block, we get a spot on X-ray film of emulsion chamber and then we get several optical densities of the spot corresponding to several radii of a photometer diaphragm. General methodical problem of the hadronic block measurements is how to obtain a value of energy of the hadron - E_0 (or energy of electromagnetic component of a cascade initiated by the hadron-ΣE_γ) from the data of the optical densities D.

2. Simulation Assumptions. Spots of the individual NEC were simulated. We took into account a chamber consisting of 6 cm Pb gamma block (0.35 λ, 10.5 c.u.) and hadronic block having 65 cm C-generator (0.95 λ, 2.7 c.u.) and 4 cm Pb-layer (0.23λ 7.0 c.u.). The calculation were divided into following parts:
a. For purely proton spectrum with integral slope $\gamma=2$, NEC in the chamber was Monte - Carlo simulated, useing scaling model
b. For each particles of electromagnetic component at energy $E_\gamma > 0.05$ TeV the mean cascade function for electron density $\rho(E_\gamma, r, t)$ at depths t was used. Target diagramme was constructed on the area $300\times300\ \mu m^2$ with cells $12\times12\ \mu m^2$ each.
c. The electron density diagramme was transformed to the flux of light diagramme, assumed the characteristic curve $D(r) = 4.0\{1-\exp[-3.25\,\rho(r)]\}$ of X-ray film. At a position of diaphragm for X-ray film at depth 4 cm of Pb-layer was obtained.

ORIGINAL PAGE IS
OF POOR QUALITY

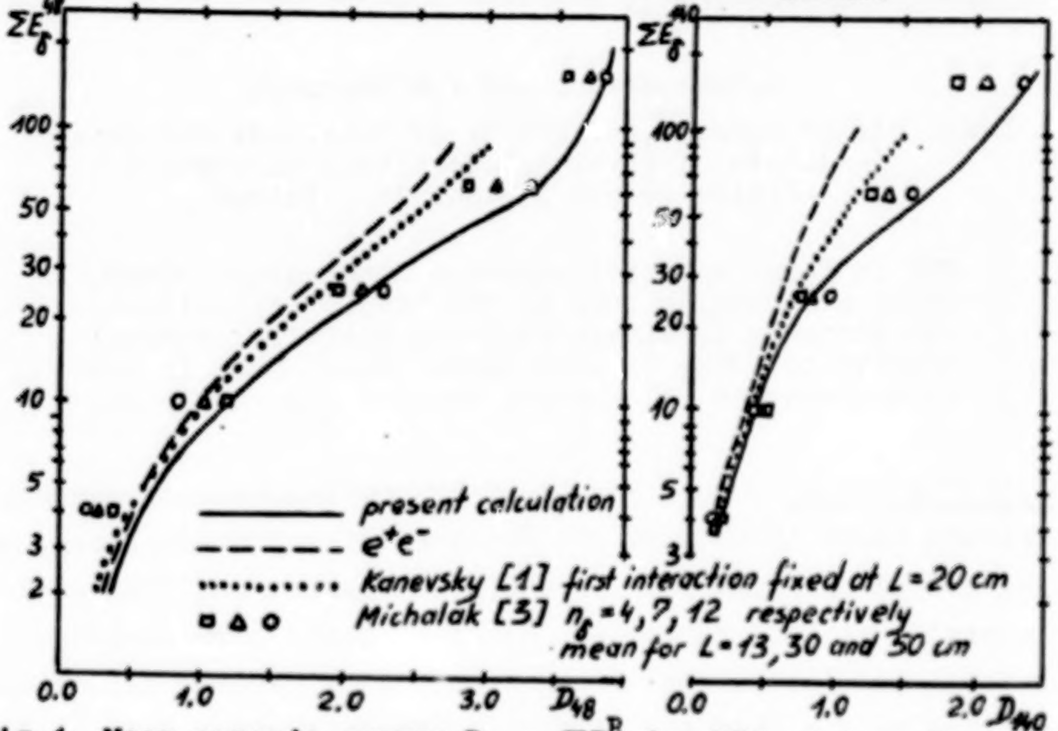

Fig.1. Mean cascade curves $D_R - \Sigma E_\gamma^R$ for NEC at 4 cm Pb.

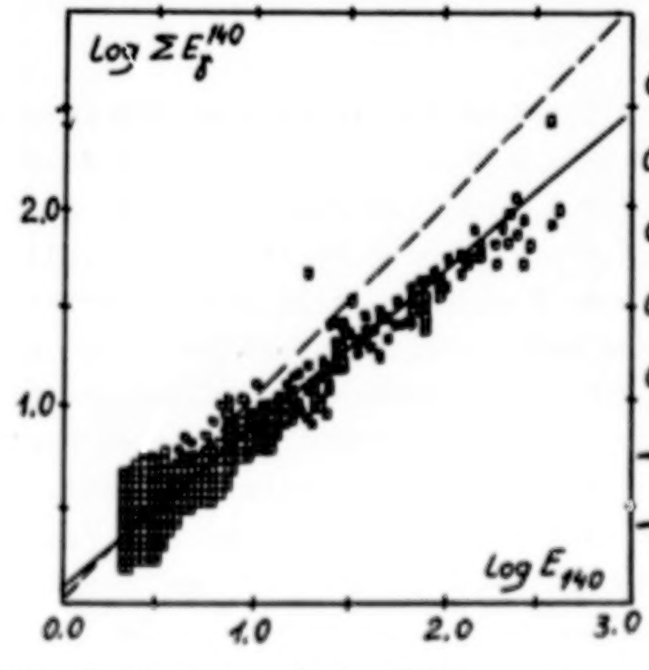

Fig.2. Scatter plot of ΣE_γ versus E for R = 140 μm and Δt = 0. Dasched line is the dependence for the case Δt = -2.0 c.u.

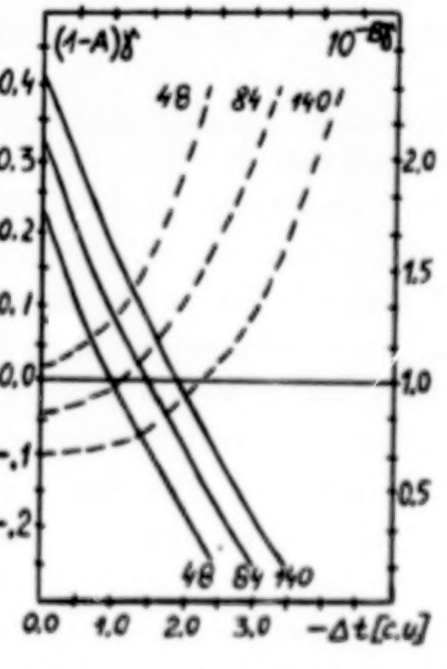

Fig.3. Dependence of $(1-A)\gamma$ and $10^{-B\gamma}$ on the Δt (solid and dashed curves, respectively).

ORIGINAL PAGE IS
OF POOR QUALITY

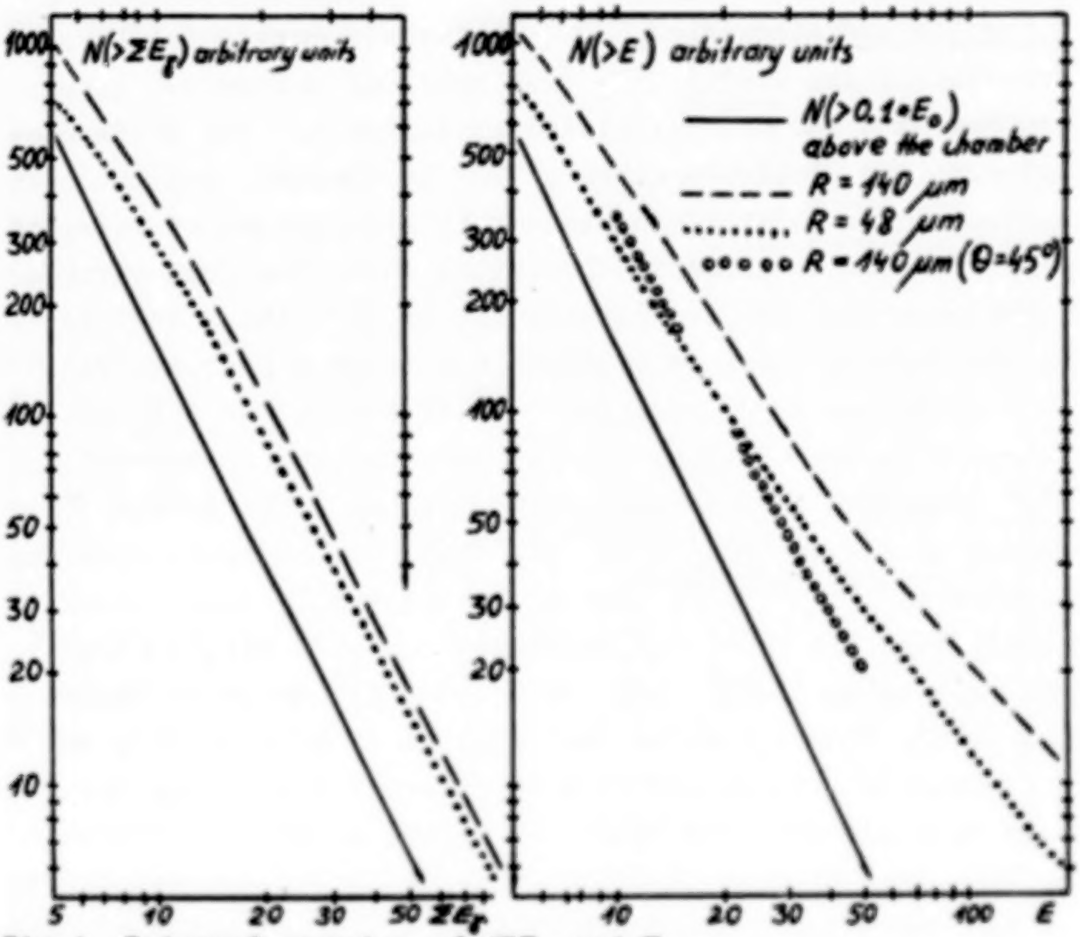

Fig.4. Integral spectra of ΣE_γ and E.

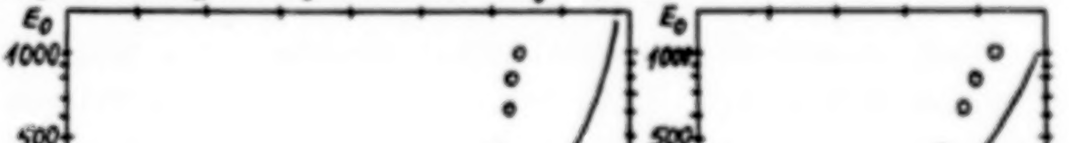

Fig.5. Mean cascade curves D_R-E_0 for NEC recorded at 4 cm Pb.

3. Results and Discussion. Mean cascade curves for D_R as a function of the energy ΣE_γ^R (for radii of photometer diaphragm R=48 and 140 μm) are ploted in Figure 1. The difference between the densities given by NEC in chamber and the ones corresponding to electron cascade is significant at energies above 30 TeV. The present calculation shows the much stronger difference than the one pointed out by [1] (the difference in the C-block thick is negligible at high energy, see Fig.5)

In Figure 2 we presented scatter plot of ΣE_γ and of energy E obtained useing the "average transition curves" for e^+e^- (recorded by diaphragm with R=140 μm). The energy ΣE_γ depend on E as $\Sigma E_\gamma = 10^B E^A$. Then the observed spectrum $N(>E)=C\ 10^{-B\gamma} E^{(1-A)\gamma} E^{-\gamma}$ should be flatten by power index of $(1-A)\gamma$ than the injection spectrum on ΣE_γ: $N(>\Sigma E_\gamma)=C(\Sigma E_\gamma)^{-\gamma}$. The quantities $(1-A)\gamma$ and $10^{-B\gamma}$ are presented in Figure 3 (at $\Delta t=0$). Figure 4 shows the integral spectra of ΣE_γ and E

Roughly , it is possible to estimate the energy spectra took into account the thick of carbon layer Δt penetrated by NEC. Nevertheless this manner is dangerous, because deepen in NEC development the difference is not so significant (see Figure 4 , curve for $\theta = 45$ deg : $t = 4.0/\cos(45)$ Pb).

Mean cascade curves for optical density as a function of hadron energy E_0 are ploted in Figure 5. The difference between present calculation and Kanevski [2] data are caused by the difference in transition $\Sigma E_\gamma \rightarrow D$ mentioned above.

4. Conclusion. Useing $D(\Sigma E_\gamma)$ corresponding to e^+e^- cascade or these calculated by [1,2] provide to flattenens of the observed hadron spectrum and decreases of attenuation m.f.p. (calculated from zenith angle distribution) at $\Sigma E_\gamma > 30$ TeV.

References

[1] Kanevsky B.L., in: Electron-Photon Cascade at High Energy Cosmic Rays, Moscow (1980), in Russian

[2] Kanevsky B.L., et al., 17 th ICRC, 5, 335, Paris (1981) and Moscow State University Report-in Russian

[3] Michalak W., Acta University of Lodz, 60, 137, Lodz (1977)

HE 3.7-4

NEW ANALYSIS OF NUCLEAR INTERACTION OBSERVED BY MT. KANBARA EMULSION CHAMBER EXPERIMENT

N85-35963

Nanjo. H
Hirosaki University, Hirosaki, Japan

1. Introduction. Up to date, the analysis of air cascade family has been performed mainly by using a full Monte Carlo simulation, because of the large fluctuation of the air cascade. Recently it has become clear, however, that it is difficult to draw a definite conclusion about the interaction mechanism by using only this kind of simulation, due to too many assumptions in relation to the amount of information.

On the other hand, some attempts to reproduce the original γ-ray at the interaction point, for example `decascading[1]', have also been made. This kind of method makes it possible to observe the interaction directly and to analyze the data from various angles. All of these methods, however, assume the constant ER in cascade shower, where E is energy and R is the distance from the center of cascade shower. This character is all-inclusive and changes according to the energy and the interaction height of original γ-ray. It is impossible, therefore, to reproduce the exact interaction height and energy by these methods. This work adopts a quite different way from the ER constant method; that is, a relative method in separating one cascade shower from others. This new method makes it possible to estimate the interaction height and energy by using information about the lateral spread of the cascade shower.

2. New method. Fig.1 (a) shows the correlation between E and R of γ-rays in a simulated family event. Open circle and closed circle represent the γ-ray produced by one original γ-ray and other original γ-rays, respectively. In this figure, we can find an energy gap at the boundary between groups of cascade shower γ-rays. The new method is nothing but a way to classify one cascade shower group from others by using of this energy gap.

We make a classification of each cascade shower according to the following procedure.

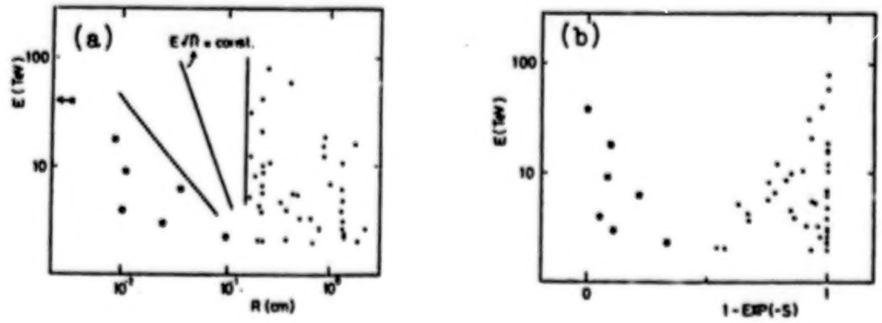

Fig.1 (a) Correlation between E and R in a simulated family event. Open and closed circle represent the γ-ray produced by one original γ-ray and othe γ-rays, respectively. (b) Transformed figure of (a) in order to represent the energy gap symmetrically.

C-7

1) Take the i-th γ-ray as a temporary center of a cascade shower group. The selection of the i-th γ-ray is performed according to size of energy, because a high energy γ-ray should be located near the true center.
2) Calculate the following quantity Sij representing a spread between the i-th γ-ray of a temporary center and all other γ-rays ($j = 1 \sim n$),

$$S_{ij} = (E_i+5)R_{ij}\sqrt{E_j}/15 \qquad (1)$$

where Rij is a length between the i-th and j-th γ-rays. As is seen in Fig.1 (a), a straight line of $R\sqrt{E}$ = constant has a mean inclination between the line of ER=constant and R=constant.
3) Caluculate the energy density for the following quantity Wj,

$$W_j = 1-\exp(-S_j) \qquad (2)$$

for fixed i. Wj ranges from 0 to 1 and is effective to search for an energy gap impartially among various cases. The correlation between E and W is shown in Fig. 1 (b) for the same sample as in (a). We can see a symmetrical valley of energy in this Figure.

The energy density is defined as

$$P_j = \sqrt[3]{E_j \cdot E_{j+1} \cdot E_{j+2}}/(W_{j+2}-W_j) \qquad (3)$$

The boundary is set up the position Wmin where Pj has the minimum value.
4) Select candidates, which satisfy the following criteria, as members of the same cascade shower with the i-th γ-ray.

$$W_j < W_{min} \quad \text{and} \quad E_j < E_i$$

5) Proceed to the next γ-ray to be set as a temporary center. The γ-rays which have been already selected in (4) are excluded as new centers.
6) When a γ-ray is selected as a candidate of more than two groups, it is decided to belong the group which gives the smallest distance from its center.

3. Estimation of energy and production height. The energy and production height of γ-ray are estimated by using the mean spread of clusterized γ-ray as members of a cascade shower. The mean lateral spread <R> is defined as,

$$\langle R\rangle = \Sigma R/N \quad (\text{cm}) \qquad (4)$$

where R is a distance from the energy weighted center and N is the number of γ-rays in a cluster. Close investigation of the simulation data drew the estimation formula of energy Ees and interaction height Hes at Mt. kanbara height (5500m) as follows,

$$E_{es} = \Sigma E \cdot 10^{2.5\langle R\rangle} \quad (\text{TeV}) \qquad (5)$$

$$H_{es} = 17000 \cdot \langle R\rangle^{1.5} \quad (\text{m}) \qquad (6)$$

4. Check of new analysis method. Reproducibility by the new method was checked by using artificial data in a full Monte Carlo simulation. For the purpose of checking, only the standard model simulation was necessary. An outline of the simulation[2] is as follows.

(1) Proton primary with energy spectrum as

$$I(E)dE \propto E^{-\beta-1}dE \quad (\beta=1.7)$$

(2) Particle production spectrum is scaling law

$$f(X)dX \propto (1-X)^{3.5}/XdX$$

where $X=E/E_0$, E and E_0 are secondary and primary energy, respectively.

(3) Interaction mean free path

$$\lambda = \begin{cases} 80\ \mathrm{g/cm^2} & \text{for proton} \\ 96\ \mathrm{g/cm^2} & \text{for secondary pion} \end{cases}$$

(4) Mean transverse momentum

$$\langle Pt \rangle = \begin{cases} 330\ \mathrm{MeV/c} & \text{for secondary particle} \\ 500\ \mathrm{MeV/c} & \text{for leading particle} \end{cases}$$

For the investigation of large Pt, the double value $\langle Pt \rangle = 660$ MeV/c was also used.

All of the clusterized groups have not always one to one correspondence to the expected one. In the case of no one to one correspondence, the original γ-ray which gives the highest energy ratio within the cluster is selected as corresponding γ-ray and used for checking.

Fig.2 (a) shows the distribution of Nes/N_0, where Nes is the number of γ-rays in an actual clusterized group and N_0 is the expected number in the corresponding cascade shower. The peak at $Nes/N_0=2$ is due to the case of $N_0=1$. Figure shows fairly strong agreement and the validity of the new method was confirmed.

Fig.2 (b) and (c) show the comparison of estimated energy Ees and estimated interaction height Hes of original γ-ray with expected true ones E_0 and H_0, respectively. Fig. (c) for interaction height shows broad distribution. This is due to mainly the fluctuation in the traveling distance of the original γ-ray from the interaction point to the first pair creation point. We need the statistical analysis for the interaction height.

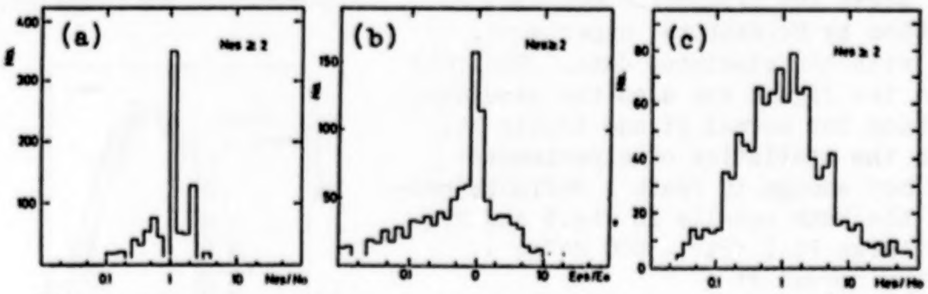

Fig.2. Comparison of the estimated value by new method with the expected one (a) Number of γ-rays in a clusterized shower (b) energy and (c) interaction height of original γ-ray

Fig.3 shows the reproducibilty of the transverse momentum Pt distribution, (a) for normal Pt and (b) for double Pt. The full and broken lines represent the distribusions of the estimated Pt and of the expected Pt of all γ-rays at the interaction point. The estimated and expected distribtion does not necessarily coincide because of the detection bias and the error of estimated value. The positions of peak, however, coincide with each other, and the estimated distribution for normal Pt and for large Pt reproduce just a double difference. It is worth notice that the estimated Pt distribution has a large error but is independent of the interaction model.

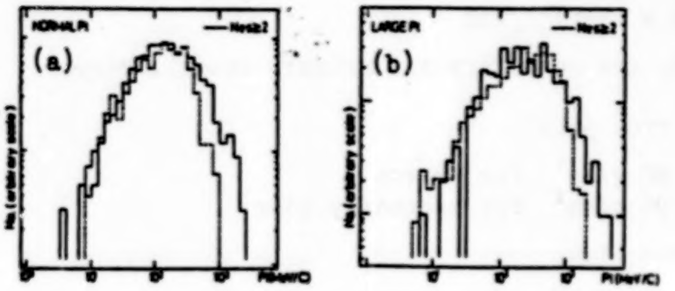

Fig.3 The transverse momentum Pt distribution of reproduced γ-ray for (a) normal Pt (b) double Pt, compared with the distribution of all γ-rays produced by the interaction (broken line).

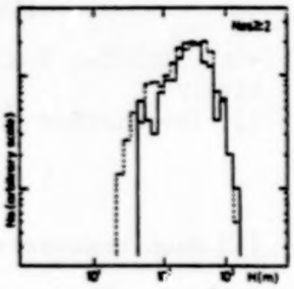

Fig.4 The interaction height distribution, compared with the simulated data(broken line)

5. Results. In Fig.4, is shown the result of the interaction height of the reproduced original γ-ray by the experimental data of the Mt. Kambara emulsion chamber experiment, compared with the result of simulated data (broken line). The experimental data does not contradict the prediction of the simulation.

Fig.5 shows the lateral spread R distribution, where R is the distance between an energy weighted center of a family and of γ-rays in a cluster. Smoothed curves represent the distribution of the simulated data in the case of normal Pt and double Pt.

Fig.6 shows the transverse momentum Pt distribution by Mt.Kanbara experiment, compared with the simulated data. Smoothed curves in the figure are also the simulated distribution for normal Pt and double Pt.

Though the statistics of experimental data are not enough to reach a definite conclusion, the both results in Fig.5 and Fig. 6 prefer large Pt (<Pt> ~ 600 MeV/c) rather than normal Pt.

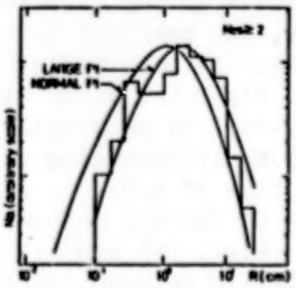

Fig.5 The lateral spread distribution of original γ-ray. Smoothed curves represent the simulated data for normal Pt and large Pt.

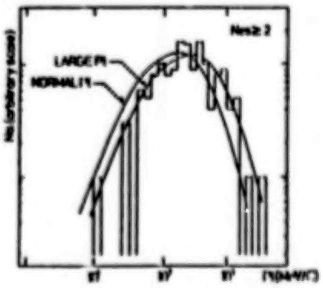

Fig.6 The transverse momentum Pt distribution of reproduced original γ-ray, compared with the simulated distribution for normal Pt (<Pt>=330 MeV/c) and large Pt (660 MeV/c)

6. Acknowledgments. The author would like to express his thanks to the members of the Mt. Kanbara group for allowing the use of experimental data. He is much indebted to Dr. Shibata of Yokohama National University for using the Monte Carlo simulation method. The auther thanks Mr. Y. Noto of Hirosaki University for help in calculation of the simulation.

References
1. H. Semba Prog. Theor. Phys. Suppl. No. 76, 111 (1983)
M. Amenomori et al. Phys. Rev.D 25, 2807 (1982)
2. M. Shibata Phys. Rev.D 24, 1847 (1981)

N85-35964

ON THE MEAN CHARACTERS OF FAMILY EVENTS OBSERVED AT MT.KANBALA

China-Japan Emulsion Chamber Collaboration *

ABSTRACT

General features of family events with $\Sigma E\gamma > 200$ TeV, observed by the emulsion chambers at Mt.Kanbala, are presented in comparison with the Monte Carlo simulation. The lateral and cluster structure, and the energy spectra of constituent gamma-rays and hadrons are shown to be consistent with the Monte Carlo results calculated under the assumption of heavy-enriched primary, scaling, QCD jets and increasing cross-section.

1.Introduction.

Upto now, the total amount of exposure of emulsion chambers(ECs) at Mt. Kanbala has reached about 420 m^2year. We already observed 10 big family events with energies $\Sigma E\gamma > 1000$ TeV. The main purpose of our experiment is to clarify what kinds of phenomena are new in the energy region beyond 10^{16} eV, though the problem of primary composition at these energies is inevitably interwined with this subject.

In this paper we present the average behaviour of the family events in comparison with the Monte Carlo simulation made by an assumption on primary and interaction. First, we discuss the flux of gamma-families at Mt.Kanbala, since this is known to be very sensitive to the model of both interaction and primary composition. Then the average features of family events are shown.

2.Experiment.

Two types of chambers are assembled on the Mt.Kanbala station. One is the Pb-EC, usually used at the mountain experiments, and the other the Fe-EC. The exposure list is shown in ref. 1).

In our data processing, hadrons are defined as showers with its starting point deeper than 6 c.u. and/or with accompanying successive interactions in the EC, and others are identified as gamma-rays. The minimum energy of showers accepted in our analysis is set to be 4 TeV. The detection efficiency of hadrons is estimated to be about 40 % for Pb-EC and about 80 % for Fe-EC in an average.

Here, we use only the data taken from the Pb-chambers

ORIGINAL PAGE IS
OF POOR QUALITY

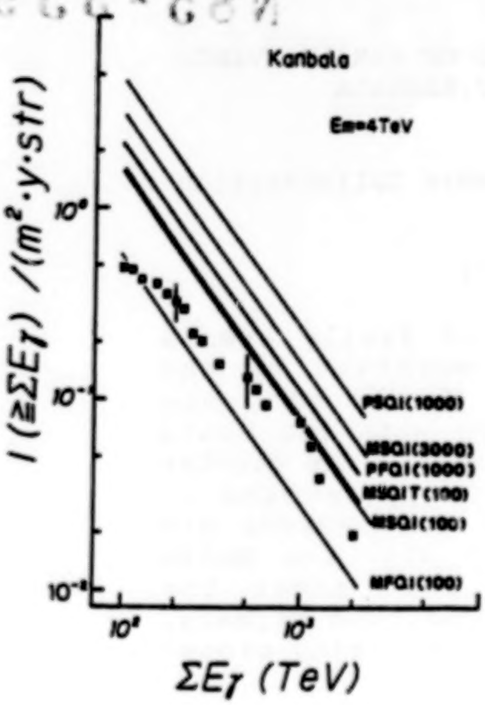

Fig. 1.

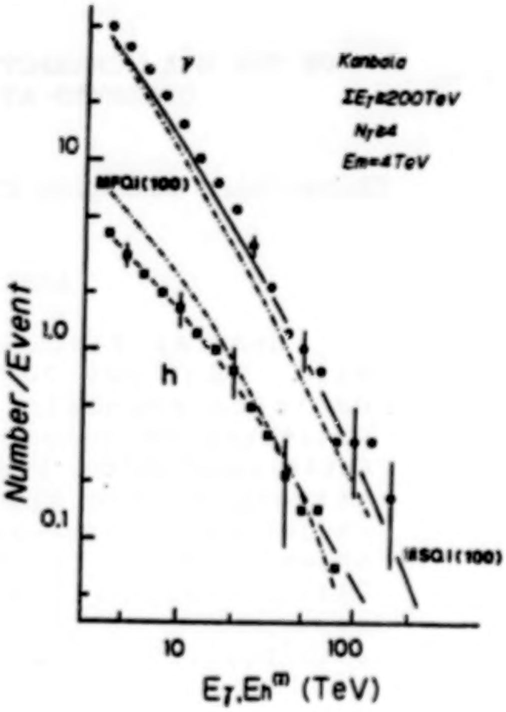

Fig. 2.

because the amount of exposure of the Fe-chambers is still insufficient to get quantitative results.

3. Monte Carlo simulation.

In order to make a standard picture on family phenomena and also to learn the size of its fluctuations, we have done the Monte Carlo simulations based on the conventional model of interaction and primary composition. Details of the simulation calculation are found in ref. 2). The meaning of the symbols appeared in this text is as follows ; M : Mixed chemical composition with a significant amount of heavy nuclei. The spectrum of Proton/He/L/M/H/VH/Fe becomes steeper at a bending energy (E_b) from 1.7/1.7/1.7/1.6/1.6/1.6/1.5 to 2.0 (all). The bending energy of proton spectrum is denoted in the bracket, and other nuclei steepen at energy of Z^*E_b. P : Proton dominant primary (In both cases, the total flux is normarized to the Grigorov's total spectrum at 10^{15} eV). S : Scaling in the fragmentation region. F : Fire-ball model normalized at 150 TeV. Q : QCD-jet. I : Increasing cross-section as $E^{0.06}$. T : Increasing average P_t as $E^{0.04}$.

4. Results

4.1. Intensity of gamma-families at Mt.Kanbala.

The absolute flux of gamma-families is compared with the Monte Carlo calculations as shown in Fig. 1. As learned from

ORIGINAL PAGE IS
OF POOR QUALITY

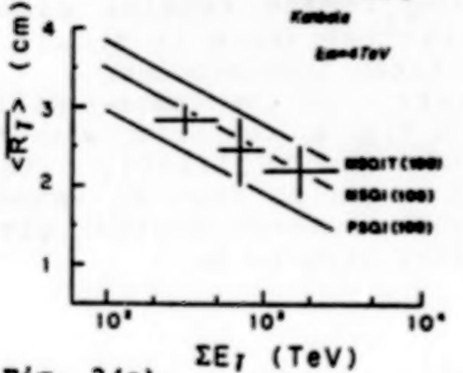

Fig. 3(a).

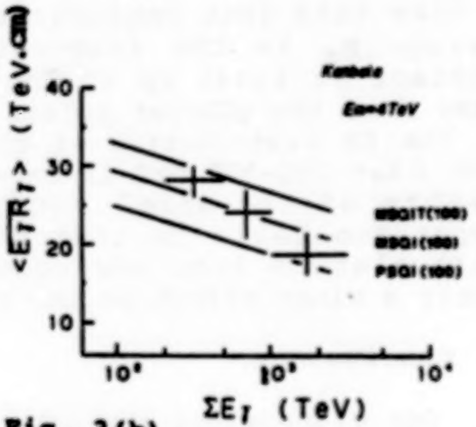

Fig. 3(b).

this figure, both cases of the model PSQI(1000) and MSQI(3000) give too high intensity compared with our data. In order to accord with the data, the proton spectrum must be bent at around 10^{14} eV. In this case, the fraction of protons and irons to the total is estimated to be about 20 % and 40 % at around 10^{15}eV, respectively. Even if we adopt the fire-ball model, the fraction of protons doesn't exceed 50 %.

4.2 Energy spectra of gamma-rays, hadrons.

Figure 2 shows the energy spectrum of gamma-rays and hadrons superposed in the energy interval of $\Sigma E_\gamma > 200$ TeV. The solid and dotted line corresponds to the model MSQI(100) and MFQI(100), respectively. No clear difference is found between the data and the model MSQI(100) both on the number of showers and the slope of spectrum. However, the fire-ball model (MFQI, heavy enriched primary and scaling break) gives steeper spectrum compared with the experiment. That is, strong scaling break is incompatible with the heavy enriched primary and requires the proton dominant primary.

4.3 Lateral structure of gamma-families.

The mean values of <R> and <ER> of gamma-rays averaged in the respective energy range are shown with the Monte Carlo results in Fig. 3(a), (b). Our data come between the model MSQIT(100) and PSQI(1000), and remain close to the MSQI(100). At accelerator energy regions, the mean P_t near central region seems to increase with energy as $E^{0.04}$. But, it is also well confirmed that the behaviour of

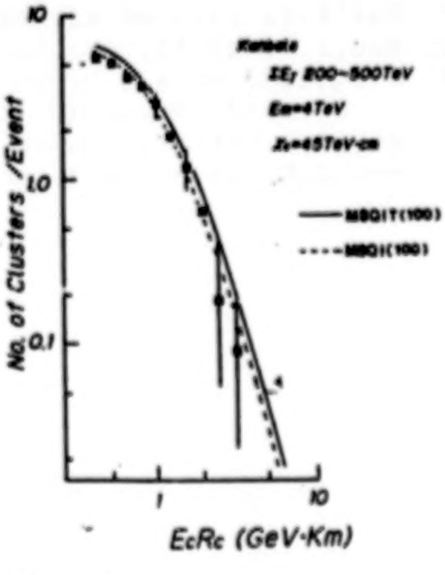

Fig. 4.

gamma-families is sensitive to the fragmentation region. If we take this into consideration, then we may say that the average P_t in the fragmentation region remains almost constant at least up to about 10^{15} eV (Here it should be noted that the QCD-jet effect is taken into account.).

The ER distribution of clusters in the gamma-families with ΣE_γ= 200-500 TeV is shown in Fig. 4, comparing with the results of the model MSQIT(100) and MSQI(100). This comparison tells us that the increasing mean P_t (smooth extrapolation from the accelerator energy region) gives merely a minor effect on the cluster structures.

5. Conclusions.

Our discussions are summarized as follows,

1) Scaling in the fragmentation region, increasing cross-section as E^δ , δ=0.04-0.06, and the heavy enriched primary spectrum can well explain our experimental data.
2) A fraction of protons and irons to the total flux takes a value of about 20 % and 40-60 % at around 10^{15} eV, respectively. The proton spectrum should steepen at around 10^{14} eV .
3) The energy dependence of average P_t is very weak in the fragmentation region.

These conclusions are compatible with other data, i.e., uncorrelated gamma-ray/hadron spectrum and the behaviour of super-families3). We also observed several family events with a peculiar structure, and some of these events are described in other paper4).

This work is financially supported in part by IHEP, Academia Sinica in China and ICR, University of Tokyo, and Grant-in Aid from the Ministry of Education in Japan. Data analysis was made by using the Computer FACOM M380R of INS, University of Tokyo.

* For full list of authors, see HE 3.1-2.

1) Ren,J.R. et al, HE3.1-2, in this volume.
2) Ding,L.K. et al, Proc. Int. Symp. on Cosmic Rays and Particle Phys.(ICR, Univ. of Tokyo, 1984), p142.
3) Ren,J.R. et al, HE3.4-9, in this volume.
4) Ren,J.R. et al, HE3, in this volume.

N85-35965

HE 3.7 - 7

STRUCTURED EVENTS IN "PAMIR" CARBON X-RAY CHAMBERS

G.G.Leptukh

Institute of Physics of Academy of Sciences of the
Georgian SSR,Tbilisi,380077,USSR

ABSTRACT

Results of experimental and theoretical investigations of Structured Events or Narrow Groups of Hadrons in "Pamir" carbon chambers are presented.

It is shown that these events are formed by the usual fluctuations in in-chamber development of NEC initiated by a single hadron from the atmosphere.

1.Introduction. In the present article the revised data on Structured Events or Narrow Groups of Hadrons[1,2]are presented along with the final results of their Monte-Carlo simulation.

A Structured Event(SE) is a group of density spots on X-ray film in Hadron(H)-block of carbon emulsion chamber with mutual distances between spots in the interval (0.1 - 1.0) mm and energy registered in each spot $E_h^{(\gamma)} \geq 2$ Tev.

Anomalously small distances in SE link these events with the so-called "Chiron"-type events and "mini-clusters" registered by Brazil-Japan Collaboration[3,4]and with the certain ones observed by Pamir Collaboration[5,6].Usually, these phenomena are interpreted as an indication on an existance of narrow groups of particles in the atmosphere.However,to insist in this hypothesis the thorough investigation of all possibilities to obtain the observed events by the known physical processes is needed.This work has been performed for SE case and has led to the conclusion of SE origin triviality.

2.Properties of experimental Structured Events. From the data of 2 x 46 m^2 area of two-storey "Pamir-77/78" C-chamber(60 cm of C and 5 cm of Pb in each H-block) as much as 85 SE have been selected.Since SE as a rule are consisted of two density spots the properties of two-spot SE are presented here:

a)The fraction of SE of the total number of registered hadrons with $E_h^{(\gamma)} \geq 4$ Tev is:

$$\langle F \rangle = (8 \pm 2)\ \%, \qquad (1)$$

while the ratio of SE fraction in lower H-block to the one in upper H-block is:

$$\langle Q \rangle = 1.3 \pm 0.3. \qquad (2)$$

b)The spatial distribution within SE,i.e. the distribution of distances between spots in SE,is very narrow,concentrates at the lower edge of allowed interval and vanishes at 0.5 mm.The first two momenta of the distribution are:

$$\langle R\rangle = (0.21 \,{}^{+0.03}_{-0.01})\ \text{mm}, \quad \sigma = 0.10\ \text{mm}. \qquad (3)$$

Spatial distributions in both H-blocks are almost identical.

c)Energy-weighted spatial distribution in SE has the following mean value:

$$\langle E_h^{(\gamma)} R\rangle = (0.38 \pm 0.03)\ \text{Tev.mm}. \qquad (4)$$

d)The average energy of SE as a whole is:

$$\langle \sum_{1}^{l} E_h^{(\gamma)}\rangle = (9.1 \pm 0.5)\ \text{Tev}. \qquad (5)$$

3.Out-of-chamber sources of Structured Events. Usually,to estimate the average height of parent interaction the⟨ER⟩ characteristics of events under investigation is used along with the average transverse momentum of gammas produced in nuclear interaction ($\langle P_T^{\gamma}\rangle = 0.2$ Gev/c).In case of SE one obtains the following:

$$\langle H\rangle = 0.4\ \text{Tev.mm} / 0.2\ \text{Gev} = 2\ \text{m}, \qquad (6)$$

i.e. a source of SE seems to be above the chamber.

Investigations of possible out-of-chamber sources of SE have excluded them because in addition to the smallness of SE fluxes from these sources the experimental approximate equivalence of SE fractions in both H-blocks and narrowness of SE spatial distribution are not reproduced.For example,Monte-Carlo simulation of NEC in the atmosphere in the framework of quasiscaling model of strong interaction has resulted to almost uniform distribution of distances between hadrons in narrow groups of particles at the installation level:

$$\langle R\rangle = (0.61 \pm 0.06)\ \text{mm}, \quad \sigma = 0.30\ \text{mm}, \qquad (7)$$

which is in the striking discrepancy with the experiment.

4.Sources of SE inside the chamber. As the average height of the usual nuclear interaction in the chamber is estimated to be equal to ≈40 cm above the observation level,i.e. above the level of X-ray films under investigation,it is possible to estimate the average transverse momentum of gamma-rays in interactions giving rise to SE:

$$\langle P_T^{\gamma}\rangle = 0.4\ \text{Tev.mm} / 400\ \text{mm} = 1\ \text{Gev}, \qquad (8)$$

which is five times higher than usually accepted value.

However,simulation of high-P_T processes in the chamber have yield the negligible flux of SE[1].This is due to the smallness of high-P_T processes cross-section,the smallness of transverse jet average energy and high energy threshold of X-ray film.

To check whether SE can be produced-hadron interactions inside the chamber the direct problem of NEC simulation in C-chamber has been solved along with the inverse problem of event processing,measurement and energy restoration[2].

Each simulated event is presented at the observation level in the form of secondary electron number density distribution(two-dimensional histogram,80 x 80 channels).Note, that this allows a study of density spot microstructure on X-ray films in Hadron-block.

As regions of low density are not visible on film due to the latter low sensitivity it is obvious that only peaks of the distribution can be seen as density spots.Investigation of these distributions in simulated events in Gamma- and Hadron-block has shown the difference in their shapes: gamma-initiated events are of one-peaked narrow distribution whereas hadron-initiated ones result in rather wide comlicated structure of electron number density distribution.It is evident that if two or more sufficiently well separated peaks(local maxima) of the latter distribution are above the certain threshold the event is seen as SE on X-ray film.

To select the required SE among the simulated ones a special method has been developed for the computer-search of local maxima which are candidates for separate density spots.The experimental procedure of optical density measurement by means of microphotometer with round diaphragm has been also simulated.Only peaks of electron number density distributions with corresponding energies above the accepted threshold value have been considered.

5.Results. The following properties of simulated SE have been obtained to be compared with similar ones in Sect.2:

$$\begin{aligned} \langle F \rangle &= (20 \pm 4)\ \%, \\ \langle R \rangle &= (0.23 \pm {}^{0.03}_{0.01})\ \text{mm}, \qquad (9) \\ \langle E_h^{(\gamma)} R \rangle &= (0.39 \pm 0.03)\ \text{Tev.mm}, \\ \langle \Sigma E_h^{(\gamma)} \rangle &= (10.6 \pm 0.6)\ \text{Tev}. \end{aligned}$$

As it can be seen the experimental and theoretical values are in good agreement.The excess in SE fraction in simulated events is related to its high sensitivity to handling parameters whereas it has been found the spatial and energy properties to be rather stable.

The interesting result is that the average energy of hadron interacted in the chamber and resulted in non-structured(usual)spot with $E_h^{(\gamma)} \geq 4$ Tev is just the same as the average energy of hadron that generates SE.It means that SE are quiet normal events with $E_h^{(\gamma)} \geq 4$ Tev and the selection of SE at the experiment does not biased energies of hadrons fallen on the installation from the atmosphere.

6.Discussion. Now the question is why simple estimates based on $\langle ER\rangle$ and $\langle P_T'\rangle\langle H\rangle$ relation have failed so drastically?

To study sources of this contradiction the genealogies of the certain number of simulated events have been analysed, i.e.it has been examined where from particles which form distant spots are originated.The investigation has shown that spots at distances greater than 0.1 mm from event's center are formed by rather low-energy particles from NEC nuclear interactions in the upper part of the chamber.All other particles in NEC give rise to more energetic central spot.When measuring optical density of distant spot the corresponding particle energy is overestimated due to overlapping effect.This effect was investigated in Gamma-block 7 where it was shown that "tails" of neighbouring electron-photon cascades(EPC) overlapped thus "amplifying" corresponding optical densities.In H-block the effect is stronger due to high multiplicity and narrowness of NEC secondary particles at film level.Overlapped EPCs of these particles form high "pedestal" for distant low-energy particle and lead to to visible distant spot.

The second,rather trivial,source of simple formula(8) failure is that it can not be used in case of cascade. That is why in case in-chamber NEC the average P_T was once more overestimated.

7.Conclusion. The investigation performed have shown that SE as a whole corresponds to a single hadron from the atmoshere.Distant spots in SE are formed by the usual fluctuations in in-chamber NEC development.Corresponding energies are overestimated due to overlapping effect.

It is recommended to treat SE as single "hadron" and to determine its energy by measuring optical density of SE as a whole by means diaphragm of highest radius.

8.Acknowledgments. The author is indepted to N.N.Roinishvili,I.P.Ivanenko,V.I.Galkin,B.L.Kanevsky and A.K.Managadze for the aid in research and useful discussions.

References.

1.Khizanishvili,L.A. et al,(1983),Proc.18th ICRC,Bangalor, vol.11,p.133.
2.Leptukh,G.G. et al,(1984),Proc.Intern.Symp.on Cosm.Rays and Particle Physics,Tokyo,p.414.
3.Hasegava,S,(1984),ibid,p.319.
4.Tamada,M,(1984),ibid,p.352.
5.Bielawska,H. et al,(1984),ibid,p.360.
6.Bayburina,S.G. et al,(1984),ibid,p.426.
7.Denisova,V.G.,Managadze,A.K.,(1984),Lebedev P.N.Phys. Inst. preprint No.20.

N85-35966

ULTRA HIGH ENERGY EVENTS IN ECHOS SERIES AND PRIMARY ENERGY SPECTRUM

Capdevielle J.N.,lab.Phys.Théorique,Bordeaux,rue du Solarium,33170 Gradignan,France
Iwai J. and Ogata T.,ICR,University of Tokyo,Japan

1.ECHOS series. EMULSION chambers with X-ray film are boarded on the supersonic Concorde Air France liner from October 1978.Since, 6 chambers have been exposed at the highest altitude(about 16Km). The different flights of the French-Japanese collaboration(often quoted as Concorde Collaboration)have been scheduled on Atlantic between Paris and New York as listed in table 1.(ECHOS-Emulsion Chamber On Supersonic).

ECHOS	Altitude $g\text{-}cm^{-2}$	Exposure (hours	Area m^2	Depth c.u.	Type	Period
1	106	200	0.1	8.5	producer no prod.	9-11 78
2	"	"	0.2	7.5	prod.	1-2 80
3	"	"	0.25	6.5	+spacer	1-2 82
4	"	"	0.2	8.5	+TLS sheet	8-10 82
5	"	500	0.2	8.5		11/84-8/85

Table 1

A description of the different chambers and sensitive materials can be found in previous reports(1,2,3) as well as the collection of remarkable events in ECHOS1,2,3 between 10^6-10^7GeV; we examine hereafter those events,jets,stratospheric ray family in view to point out some signature of phase transition quark gluon plasma and try from a general review of the data of flying experiments(Concorde,JAL cargo jets,JACEE) to situate the tendancy of primary cosmic ray spectrum.

2Correlation rapidity density-$\langle p_T\rangle$. A survey of ISR and $\overline{P}$-P data has been taken from Hagedorn's compilation and joined to our data and analysis of cosmic ray jets (2) on Fig.1.The accelerator data suggested a clear increase of $\langle p_T\rangle$ with rapidity density dn/dy and also that $\langle p_T\rangle$ levels off at highest densities (16).The total p_T distribution has been derived from well collimated and localized jets in emulsion chambers like JF1af1 In Concorde(2),Texas Lone Star in stack,C-C and Ca-C collisions in JACEE(5,6)or in Chacaltaya experiment(7).Admitting that $\langle p_T\rangle$ is the same for nucleon-nucleus collision,we can extend the behaviour of $\langle p_T\rangle$ versus dn/dy by one order of magnitude(fig.1).Inside the exprimental errors,the prediction of Barshay

$$\langle p_T\rangle = 0.32\exp\left[\frac{1}{7}\,\mathrm{Ln}\left(1+\frac{3}{\exp(-0.519\frac{dn}{dy}^2)Ei(-0.0519)}\right)\mathrm{Ln}\left(3-\exp(0.0516\frac{dn}{dy}^2)E_i(-0.0516\frac{dn}{dy}^2)\right)\right]$$

looks in better agreement than the hybrid model containing thermodynamic coupled with collective motions,which links phase transition and $\langle p_T\rangle$ flattening.(4)

3.Pseudo-rapidity distributions and phase transition.

It was advanced that the bumps occuring in pseudo-rapidity distribution could also be a signature of transition to quark-gluon plasma(8).We have carried out a Monte-Carlo simulation of 1500 p-Aluminium collisions for specific comparison with our typical event JFaf1 produced in Concorde cabin wall.The multicluster phenomenological model(MPM)has been used to extrapolate the collider data(see HE4.1-9,10),assuming simultaneous rise in Lns of height anf width of plateau,random production of small clusters decaying with Gaussian distribution and finally inclination of plateau for nucleon-nucleus collision.The average number $\langle\nu\rangle$ of successive collisionss in Al target has been taken as 2 at low energy.

The pseudo-rapidity distribution plotted on fig.2 for $E_o=2\,10^6$ GeV includes all the possible fluctuations in multiplicity and inelasticity for p-Al collisions(where $\bar{n}_c=73$).If the discrepancy of the left part can be easily explained by the γ-ray threshold of 100 GeV,the simulation cannot explain the large number of γ rays emmitted(about 50%) at very high rapidity.Substracting the forward part of simulated from experimemtal distribution,we obtain superposition of two components,one being consistent with the extrapolation of accelerator data(containing near 80 γ's) ,also for n_c estimated to 45 in JFaf1, and one additive component characterized by a narrow peak with gaussian distribution centered at 2.7 unit of rapidity in CMS with FWHM near 1unit.

This could be the rapidity signature of an explosive decay of phase transition fireball after compression of the projectile fragmentation fireball in the target.(the target fragmentation fireball cannot be seen with γ rays in emulsion chamber).Such procedure rep eated with $E_o= 10^6$ GeV lead to similar results even more pronounced.

5.Primary energy spectrum.

Using the relations previously developed between E_o,$\sum E_\gamma$,r_γ, $\langle E_\gamma R_\gamma\rangle$for stratospheric γ ray family with SBM model by Monte-Carlo simulation,we make a first attempt(now repeated with MPM) to estimate the integral primary spectrum from the primary energy E_o of ultra high energy jets in our Concorde and JAL cargo data(table2,3) in "average conditions".

Name	$\sum E_\gamma$ (TeV)	Commant	E_o (GeV)
JF2f1	1589	1Km above chamber	$0.9\ 10^7$
JF1af1	260	From cabin wall	$1.9\ 10^6$
JF3-1	55	jet	$4\ 10^5$
JF3-2	51	jet	$3.9\ 10^5$
JF1af2	34	600m above	$2.3\ 10^5$
JFa1	18	jet	$1.55\ 10^5$

Table 2.Concorde data.

ORIGINAL PAGE IS
OF POOR QUALITY

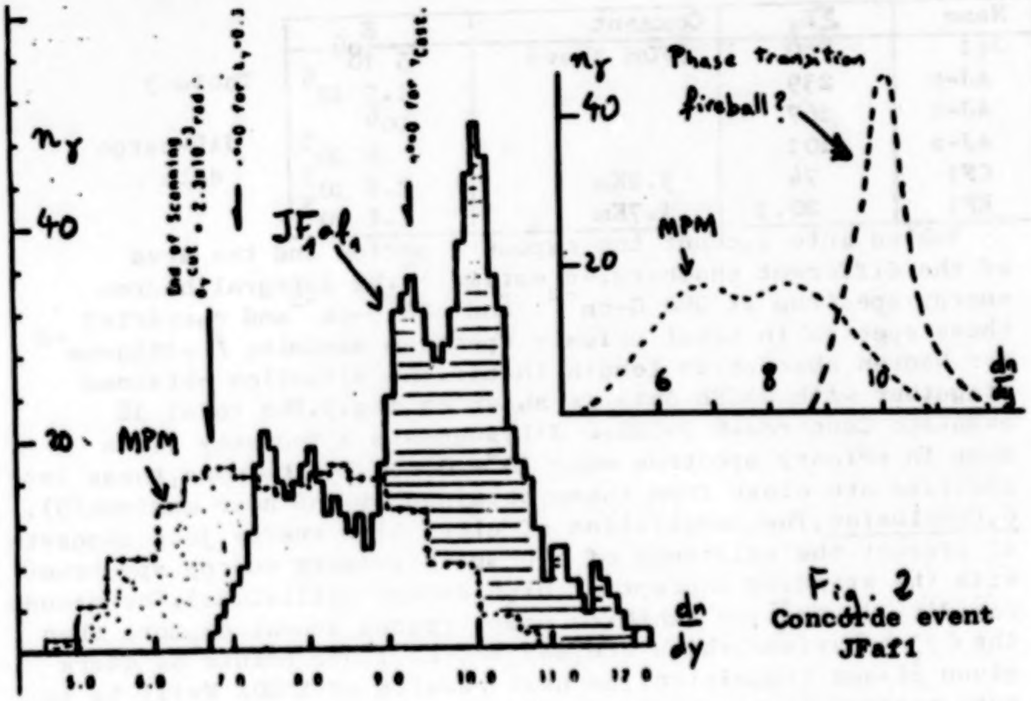

Fig. 2
Concorde event
JFaf1

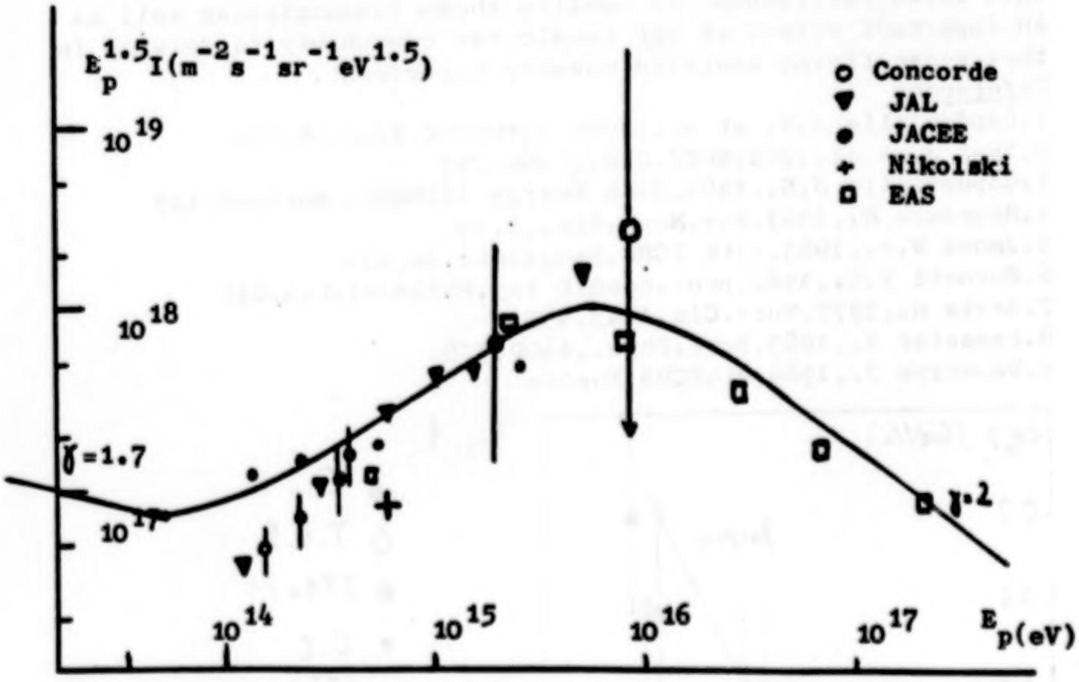

Fig.3

Name	ΣE_γ	Comment	E
0#1	760	770m above	$5\ 10^6$
AJ-c	239		$1.5\ 10^6$
AJ-b	167		10^6
AJ-a	101		$6\ 10^5$
CF1	74	3.2Km	$2.8\ 10^5$
EF1	20.5	1.7Km	$1.2\ 10^5$

Table 3

JAL-cargo data

Taking into account the exposure period and the area of the different chambers, we estimate the integral hadron energy spectrum at 260 G-cm^{-2} and 105 g-cm^{-2} and converted those spectra in total primary spectrum assuming Λ =105g-cm^{-2} for hadron absorption length in air. The situation obtained, together with JACEE data is shown on fig.3. The total 18 events (6 Concorde+6 JACEE+6 JAL) suggests a tendancy for a bump in primary spectrum near $10^6 - 10^7$ GeV. Furthermore, those intensities are close from those obtained by EAS near maximum(9).

6.Conclusion. The compilation of ultra high energy jets suggests at present the existence of a bump in primary energy spectrum(with the standard concept of high energy collisions). The pseudo rapidity distribution exhibits some typical anomalies, more than the $\langle p_T \rangle$ behaviour, which are, may be, the fingerprints of quark gluon plasma transition. The next results of ECHOS Vwill be in both cases determinant to confirm those tendancies, as well as an important effort of the cosmic ray communauty to develop in that sense flying emulsion chamber experiment.

References

1.Capdevielle J.N. et al.,1979,16th ICRC,Kyoto,6,324
2.Iwai J.et al.1982,NUOV.CIM.,A69,295
3.Capdevielle J.N.,1984,High Energy ASTROPH.,Moriond,129
4.Hagedorn R.,1983,Riv.Nuov.Cim.,6,10
5.Jones W.v.,1983,18th ICRC,Bangalore,12,279
6.Burnett T.h.,1982,proc.cosmic ray,Philadelphia,236
7.Arata n.,1978,Nuov.Cim.A,43,455
8.Faessler A.,1983,Nucl.Phys.,A400,578c
9.Wdowczyk J.,1984,9thECRS,Kosice

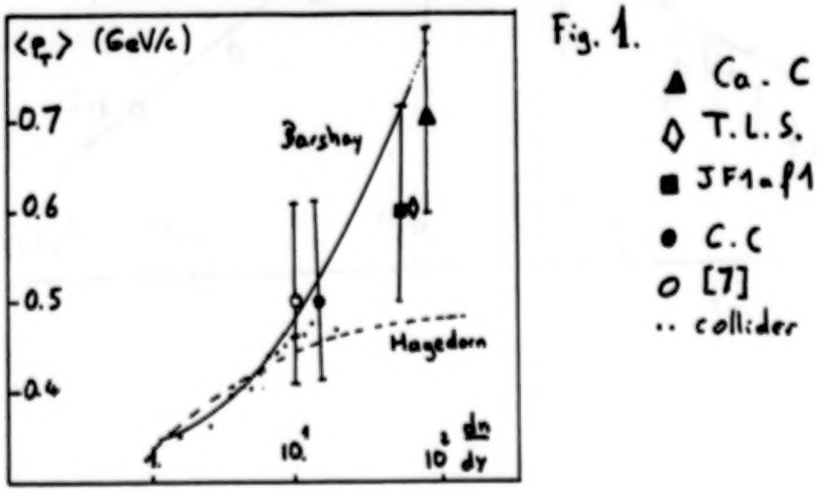

Fig. 1.

ORIGINAL PAGE IS
OF POOR QUALITY

N85-35967

HE 3.7-IO

Peculiarities of gamma-quanta distribution at 20 Tev energy

P.M.Ermakov, A.A.Loktionov, Yu.T.Lukin, T.Kh.Sadykov.

HEPI of Kazakh Academy of Sciences, Alma-Ata, USSR.

The angular distribution of protons from the fragmentational region was analized. The gamma-quanta families were generated in a dense target by cosmic ray particles at 20 Tev energy. There were found the families which had dense groups (spikes) of gamma-quanta where the rapidity density was 3 times more than the average value determined for all registered families. The experimental data were compared with the results of artificial families simulation.

The fluctuations of particles density in the rapidity scale which were discovered in accelerator experiment [I] were discussed before when gamma-quanta families were studied in cosmic ray experiments [2]. It becomes interesting to study these fluctuations again because the mechanism of their appearance is connected with the effect of quark retention which leads to length restriction of gluons emission [3] Thus, in the paper [4] there was discovered a structure of the angular correlations of charged secondaries in the inelastic proton-proton interactions at 400 Gev which gives new information about quart retention character.

The data concerning cosmic particles interaction were received by means of the installation consisting of the 9 m^2 ionization calorimeter and X-ray and emulsion chamber (XREC) of the same area, which was disposed just on the ionization calorimeter. At 11 m above the ionization calorimeter there was the paraphine target of 60 m^2 area and of I5 g/cm^2 thickness.

The photosensitive layers of XREC consisted of X-ray film RT-6 and nuclear emulsion R-2T. The registration energy threshold for gamma-quanta for about I00% detection efficiency was equal to $I.5 \cdot IO^{I2}$ ev for X-ray films and $0.5 \cdot IO^{I2}$ for nuclear emulsion.

The comparison of electron-nuclear cascades in the ionization calorimeter with dark spots in the X-ray film and emulsion chamber was made using coordinates of an entrance point of a high energy particle, zenith and azimuth angles and neutral pions energies measured by the ionization calorimeter and the XREC.

On ionization calorimeter and XREC give incomplete information about each individual interaction: not all secondaries are registered by XREC, besides, it is impossible to separate particles from first and second interactions. The limited spatial resolution of a calorimeter leads to confluence of electron-nuclear cascades initiated by near particles. Thus, the peculiarities of the experiment don't exclude the possibility of systematic distortion of some hadron-nucleons interaction characteristics. To reveal these systematic distortions there were made simulations of electron-nuclear and electromagnetic cascades applicable to the experimental conditions [5] .

It was considered three-dimensional picture of electron-nuclear and electromagnetic cascade development for the case when cosmic particles went through layers of substance having different atomic weights, densities, cascade units and interaction mean free pathes. The height was taken as 5200 m above sea level for simulation of artificial interactions. For this height there is known the experimental data concerning the composition and energy spectra of handrons and electrons.

In the simulations of hadron-nuclear interactions there was used the model which was based on an extrapolation of accelerator data into more than 10^{13} ev energy region. The model assumed scaling conservation in the fragmentational region.

The experimental statistics was 203 families of gamma-quanta initiated by particles at the mean energy which was equaled to 20 Tev. The mean number of gamma-quanta with energies above registration threshold was equaled to: $\langle N_\gamma \rangle \simeq 6.5$

The dense gamma-quanta jets (spikes) were looked for among the families with the number of gamma-quanta $N_\gamma > 4$

Photon groups were taken for spikes when $N_\gamma \geq 4$ and the densities on the rapidity scale were $N_\gamma/\Delta\eta \geqslant 9$. Such spikes were found in I23 families.

Fig.I gives the rapidity-distribution of the family photons against the spike rapidity. It can be seen that photons in spikes are in rather narrow rapidity interval. The width of the peak at half-height is iqualed to: $\Delta\eta = 0.5$.

Fig.2 shows the number of spikes distribution against gamma-quanta density per rapidity unit.

Fig.3 shows the spike-distribution against the number of photons in the spikes (K).

Fig.4 gives the distribution of the families against emission angles of jets in center-of-mass system. The emission angles in CMS range from I° to I5°, the most probable value being 5-6°.

The estimations of the process of gamma-quanta generation with high density on rapidity scale are, probably, underrated becouse there were not taken into account the possible double-modal distributions of gamma-quanta in the families with high multiplicity.

Bibliography.

I.Rushbrooke J.G. Preprint CERN-EP/84-39,(I984).
2.Amanov K.A. et al., ICRC papers, Paris, v.5, p.307,(I98I).
3.Dremin I.M.,Nuclear Physics,v.37,p.649,(I983).
4.Dremin I.M. et al., Letters to JETP ,v.40,p.320,(I984).
5.Ermakov P.M.,Shorin B.F., Preprint HEPI, n.84-I6,p.I-22, Alma-Ata,(I984).

ORIGINAL PAGE IS
OF POOR QUALITY

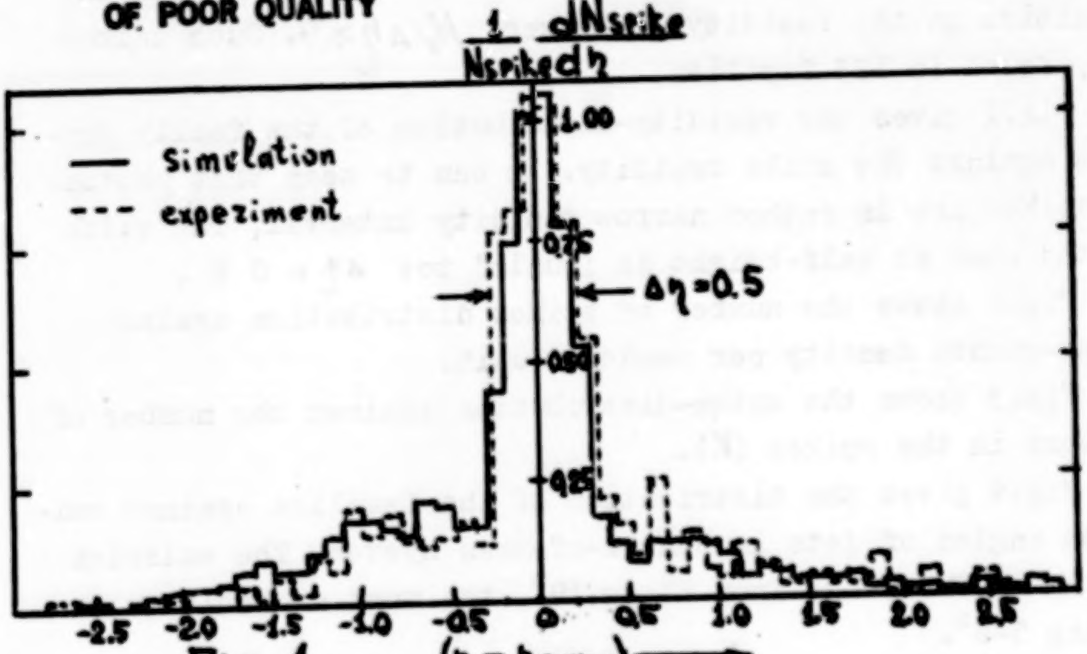

Fig. 1

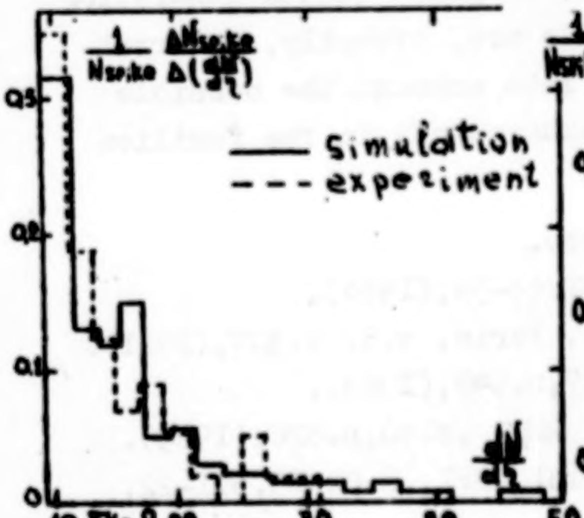

Fig. 2

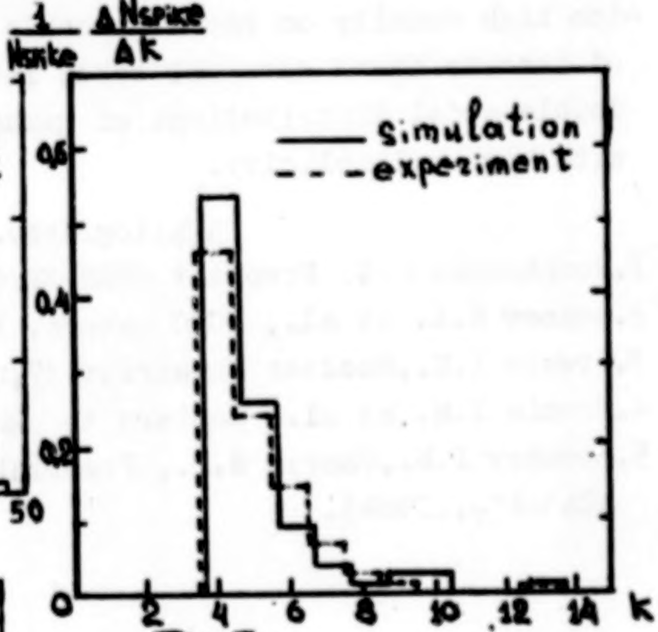

Fig. 3

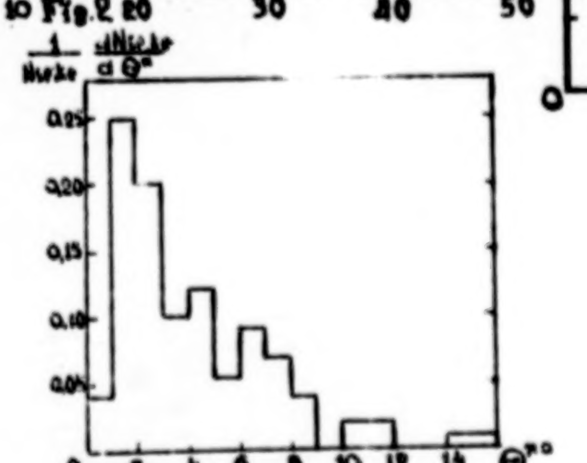

Fig. 4

AUTHOR INDEX

AGUIRRE, C
296,300
AIZU, H
239
ALEEM, FE
21
AMATO, NM
292,320
324,356
AMEEV, SSH
180
AMENOMORI, M
208,348
336
AMINEVA, TP
200
AMMIRAJU, P
28
AOKI, H
200,280
356
ARATA, N
292,320
324,356
ATWATER, TW
100,184
AVAKIAN, VV
64,17
AZARIAN, MO
64
AZIMOV, SA
428,424
200
AZIMOV, ZA
200
BAI, GZ
278,336
BAKHTIGIREEV, SE
200
BALASUBRAHMANYAN, VK
137
BALTRUSAITIS, RM
5
BARADZEI, LT
200
BELLANDI, J
356
BHATTACHARYYA, S
220
BIELAWSKA, H
200
BLOKH, YAL
236
BOBODJANOV, IB
200
BORISOV, AS
200
BOURDEAU, MF
400
BRASIL-JAPAN,
360
BRAZIL-JAPAN,
250
BURNETT, TH
172,156
164,160
152,76,168
CANANOV, SD
216
CANANOV, SB
200
CAO, PY
278,336
CAPDEVIELLE, JN
447,400
CASSIDAY, GL
5
CHADRANYAN, EKH
216
CHADRANYAN, LK
200
CHAE, IK
188
CHARISHNIKOV, SA
376
CHASNIKOV, IYA
274
CHEN, MY
25
CHERDYNTSEVA, KV
254,200
CHILINGARYAN, AA
392
CHINA-JAPAN COLLABORATION,
317,313
309,204
439
CHINELLATO, JA
364,356
368
CHOU, TT
43
CHUBENKO, AP
96,254
COOPER, R
5
DAKE, S

AUTHOR INDEX

DAKE, S
172,156
164,160
152,76,305
168
DANILOVA, TV
35
DEMIANOV, AI
270
DENISOVA, VG
200
DERRICKSON, JH
160,152
DING, L
212
DOBRIGKEIT, C
356
DOBROTIN, NA
200
DOKE, T
68
DREMIN, IM
145
DUBOVY, AG
254
DUNAEVSKII, AM
392
DUNAEVSKY, AM
200
EBY, PB
133
EGIYAN, KSH
64
ELBERT, JW
5
ELLSWORTH, RW
55
EMELYANOV, YA
200
EREMENKO, YUA
274
ERLYKIN, AD
92,35
ERMAKOV, PM
451
EROFEEVA, IN
196
FAUTH, AC
243
FIXSEN, DJ
104
FOUNTAINS, W
160
FREIER, PS
FREIER, PS
100,104
184
FUJII, M
239
FUJIMOTO, Y
200,356
FUKI, M
172,156
164,160
152,76,168
FUNAYAMA, Y
200,284
356
GAISSER, RK
55
GAISSER, TK
47,9,328
GALFAYAN, SK
392
GARSEVANISHVILI, LP
258
GENG, QX
278,336
GERHARDY, PR
5
GOLYNSKAYA, RM
380
GOULD, RJ
149
GREGORY, JC
172,156
164,160
152,76,168
GUBAR, NE
200
GULOV, YA
200
GUSEVA, ZM
200
HAGUENAUER, M
68
HALILOV, DA
424
HALZEN, F
47
HASEGAWA, S
200,356
HASHIMOTO, K
296,300
411
HAYASHI, R
152
HAYASHI, T

HAYASHI, T
172,156
164,160
152,76,168
HAYASHI, TO
160
HEIN, LA
380
HE, M
278,336
HE, RD
278,336
HOLYNSKI, R
172,60,156
164,160
152,76,168
HONDA, K
296,300
411
HOTTA, N
208,301
305,348
336
HUANG, RQ
25
HUO, AX
278,336
ILIJINA, NP
200
INNOCENTE, V
68
IVANENKO, IP
384,388
200
IWAI, J
172,156
164,160
152,76,447
168
JAPAN-USSR,
352
JING, C
212
JING, G
212
JONES, WV
172,156
164,160,76
168
JONEW, WV
152
JURAK, A
172,156
164,160
JURAK, A
152,76,168
JUSKIEWICZ, B
200
KAMBEROV, G
88
KANEVSKAYA, EA
200
KANEVSKY, BL
31,384,388
KARAGJOZIAN, GV
17
KASAHARA, K
68,208,301
348,336
KASHIWAGI, T
68
KAWAMOTO, M
305
KAWASUMI, N
296,300
411
KAZANAS, D
137
KAZUNO, M
239
KEMPA, J
51
KEROPIAN, MI
17
KERTZMAN, MP
184
KHALILOV, DA
200
KHISANISHIVILI, LA
200
KHIZANISHVILI, LA
216
KIKUCHI, J
68
KIM, CO
72,188
KIM, DH
188
KIM, SN
72,188
KIRILLOV, AA
384
KLOSINSKI, J
141
KOBAYASHI, T
208,348
KOBAYSHI, T
239

AUTHOR INDEX

KONISHI, E
208,348
KOSLOV, VD
5
KOTLYAREVSKI, DM
258
KRATENKO, YUP
376
KRUGLOV, NA
270
KRUTIKOVA, NP
92,254
KRYS, E
412,416
KUANG, HH
278,336
KUBIAK, G
51
KUCHIN, IA
80,84
KUMANO, H
200,246
356
KUSUNOSE, M
305
LADARIA, NK
216,258
LANZANO, S
68
LATTES, CMG
356
LAZAREVA, TV
200
LEPTUKH, GG
443,200
LI, GJ
278,336
LI, JY
278,336
LILAND, A
224
LINDE, IA
384
LINSLEY, J
1
LITVINOV, VA
266
LIU, ZH
278,336
LOH, EC
5
LOKTIONOV, AA
451
LORD, JJ
LORD, JJ
172,156
164,160
152,76,168
LUKIN, YUT
451
LU, SL
278,336
LYUTOV, YG
384
MACHAVARIANI, SK
96
MACHIDA, M
296,300
MACIASZSZYK, A
200
MADIGOZHIN, DT
274
MAGNANI, R
300
MALDONADO, RHC
292,320
324,356
MALINOWSKI, J
200
MAMIDJANIAN, EA
64,17
MANAGADZE, AK
200
MANDRITSKAYA, KV
228
MARTINIC, NJ
296,300
MARTIROSOV, RM
17
MASUDA, K
68
MATANO, T
296,300
411
MAXIMENKO, VM
200
MEEFAN, CA
152
MEEGAN, CA
160
MELKUMIAN, LG
396
MENON, MJ
356
MIKHAILOVA, IA
31,200
MIKUMO, E
208,348

AUTHOR INDEX

MILCZAREK, K
200
MISAKI, A
411
MITO, I
208,348
336
MITSUMUNE, T
305
MIYAMURA, O
172,156
164,160
152,76,168
MIZUMOTO, Y
5
MIZUTANI, K
204,208
348,336
MUKHAMEDSHIN, RA
200
MULLADJANOV, EJ
424
MULLAJANOV, EG
200
MULLAJANOV, EJ
428
MURAKAMI, H
68
MURAKI, Y
68
MURZINA, EA
200
MURZIN, VS
196
NAKADA, T
68
NAKAMOTO, A
68
NAKATSUKA, T
305
NAM, RA
200
NANJO, H
208,348
336,435
NAVIA, CE
296,300
356
NEDEL'KO, OE
200
NESTEROVA, NM
254
NIKOLAEV, LP
200
NIKOLSKAJA, NM
254
NIKOLSKY, SI
96,254
NISHIKAWA, K
305
NISHIMURA, J
239
NISHIO, A
239
NIWA, M
411
NOMURA, Y
239
NORMURADOV, F
200
NOSOV, AN
424
NURITDINOV, H
428,424
NURITDINOV, K
200
ODA, H
164,160
152,168
OGATA, T
172,156
164,160
152,76,447
168
OHANIAN, GZH
64
OHMORI, N
305
OHSAWA, A
364,200
356,368
OHTA, I
336
OLIVERIRA CASTRO, FM
356
OLSZEWSKI, A
76
ORLOV, AM
145
OVSEPIAN, GG
17
PAMILAJU, OA
356
PAMIR COLLABORATION,
232,344
192,340,39
PARK, IG
72

AUTHOR INDEX

PARNELL, TA
172,156
164,160
152,76,168
PASHKOV, SV
200
PIOTROWSKA, A
51
PLYASHESHNIKOV, AV
372,380
POMELOVA, EI
200
POPOVA, EG
200
POPOVA, L
88
PROSKURYAKOV, AG
270
PUCHKOV, VS
200
RAKOBOLSKAYA, IV
31,200
REN, GX
25
REN, JR
278,336
ROBERTS, E
160,152
ROGANOVA, TM
388,200
ROGOVAYA, SI
236
ROINISHIVILI, NN
200
ROINISHVILI, NN
216
RYABOVA, NG
200
SADYKOV, TKH
274,451
SAITO, T
172,156
164,160
152,76,301
305,168
SAKATA, M
301,305
SALEEM, M
21
SARYCHEVA, LI
270
SASAKI, H
305
SATO, K
SATO, K
208,348
SAWAYANAGI, K
243,356
SAZHINA, GP
228
SEMBA, H
200,356
SHABEL'SKI, YUM
258
SHABELSKI, YM
92
SHERER, NI
258
SHIBATA, M
208,348
336
SHIBATA, T
356
SHIBUYA, EH
332,200
356,368
SHIMA, M
301,305
SHIRAI, T
239,208
348,336
SHMONIN, VL
180
SHOBORONOV, K
200
SILES, L
300
SIVOKLOKOV, SYU
196
SIZOV, VV
388
SLAVATINSKY, SA
200
SMIRNOVA, LN
196,270
SMIRNOVA, MD
200
SMORODIN, YA
200
SMORODIN, YUA
396
SOKHOYAN, SO
17
SOKOLSKAYA, NV
228
SOKOLSKY, P
5
STANEV, T

AUTHOR INDEX

STANEV, T
55,328
STECK, D
5
STEMANETYAN, GZ
258
STRAUSZ, S
172,164
160,76
STREITMATTER, RE
137
STRUGALSKI, Z
404,108
112,115
118,122
125,129
SUGIMOTO, H
208,348
SUKHATME, UP
9
SU, S
278,336
SVANIDZE, MS
200
SVESHNIKOVA, LG
31,200
SZABELSKI,
51
SZARSKA, M
164,152,76
TABUKI, T
172,156
164,160
152,76,168
TAIRA, K
208,348
TAIRA, T
239,208
348,336
TAKAHASHI, Y
172,156
164,160,76
133,168
152
TALIPOV, DA
424,200
TAMADA, M
200,284
288,356
TATALASHVILI, NG
258
TATEYAMA, N
239,208
348,336
TATI, T
420
TER-ANTONIAN, SV
64,396
TOMASZEWSKI, A
431,200
TOMINAGA, T
172,156
164,160
168
TOMINAGA, Y
76
TORII, S
239,208
301,348
336
TRETYAKOVA, MI
145
TRIPHONOVA, SV
388
TSOMAYA, PV
258,262
TSUSHIMA, I
296,300
411
TUKISH, EI
254
TURTELLI, A
356
UCHAIKIN, VV
266
VARDANYAN, IN
270
VARKOVITSKAYA, AYA
228
VERBETSKI, YG
258
VILDANOV, NG
254
VOINOV, VG
274
VOROBYEV, KV
372,380
WADDINGTON, CJ
104
WANG, CR
278,336
WANG, SZ
278,336
WANG, YX
278,336
WASILEWSKI, A
412,416
WATTS, J

AUTHOR INDEX

WATTS, J
172
WATTS, JS
152
WATTS, JW
164
WDOWCZYK, J
51
WEFEL, JP
164,76
WILCZYNSKA, B
172,156
164,160
152,76,168
WILKES, RJ
172,156
164,160
152,76,168
WLODARCZYK, Z
431
WOLTER, W
172,156
164,160
152,76,168
WOSIEK, B
172,176
156,164
160,152,76
168
WOZNIAK, K
60
WROTNIAK, JA
56,328
XUE, YG
336
YAKOVLEVA, TI
254
YAMAMOTO, Y
301,305
YAMASHITA, S
364,200
356,368
YANAGITA, T
407
YANG, CN
43
YEREMIAN, SHS
13
YERSHOV, AA
270
YODH, GB
9,56
YOKOI, K
200,356
YOON, CS
72
YOSHIDA, A
239
YUDA, T
68,208,301
348,336
YULDASHBAEV, TS
428,424
YULDASHBAYEV, TS
200
ZAITSEVA, EG
200
ZAMCHALOVA, EA
228
ZAPATA, J
300
ZATSEPIN, GT
200
ZATSEPIN, VI
228
ZAZYAN, MZ
392
ZELEVINSKAYA, NG
200
ZHAMKOCHIAN, VM
13
ZHANG, NJ
278,336
ZHDANOV, GB
200
ZHOU, WD
278,336
ZHOU, YZ
25
ZHU, Q
212
ZIMIN, MV
200

BIBLIOGRAPHIC DATA SHEET

1. Report No. NASA CP-2376 Volume 6	2. Government Accession No.	3. Recipient's Catalog No.

4. Title and Subtitle
19th International Cosmic Ray Conference
Conference Papers

5. Report Date
August 1985

6. Performing Organization Code
665

7. Author(s)
Frank C. Jones, compiler

8. Performing Organization Report No.

9. Performing Organization Name and Address
Laboratory for High Energy Astrophysics
Goddard Space Flight Center
Greenbelt, MD 20771

10. Work Unit No.

11. Contract or Grant No.

13. Type of Report and Period Covered
Conference Publication

12. Sponsoring Agency Name and Address
National Aeronautics and Space Administration
Washington, D. C. 20546

14. Sponsoring Agency Code

15. Supplementary Notes

16. Abstract

These volumes contain papers submitted for presentation at the 19th International Cosmic Ray Conference, held on the campus of the University of California, San Diego in La Jolla, CA., August 11-23, 1985. The conference is held every other year. The present volume contains papers with Paper Codes HE 1.1 through HE 3.6 and deals with cross sections, particle production, nuclei and nuclear matter, cosmic-ray jets, and emulsion chamber simulations.

17. Key Words (Selected by Author(s))
cross sections, particle production, nuclei, nuclear matter, jets, emulsion chamber, simulations

18. Distribution Statement
Unclassified - Unlimited

Subject Category - 93

19. Security Classif. (of this report) Unclassified	20. Security Classif. (of this page) Unclassified	21. No. of Pages	22. Price*

*For sale by the National Technical Information Service, Springfield, Virginia 22161

STAR 23 SEP 20 1985

NASA-CP-2376-Vol. 7

19TH INTERNATIONAL COSMIC RAY CONFERENCE

LA JOLLA, USA AUGUST 11-23, 1985

(NASA-CP-2376-Vol-7) NINETEENTH INTERNATIONAL COSMIC RAY CONFERENCE. HE SESSIONS, VOLUME 7 (NASA) 398 p HC as boxed set only $200/MF A01 per volum CSCL 03B G3/93
N85-35968
THRU
N85-36065
Unclas
20934

CONFERENCE PROGRAM

SESSIONS VOL. 7

19TH INTERNATIONAL COSMIC RAY CONFERENCE

LA JOLLA, USA   AUGUST 11-23, 1985

CONFERENCE PAPERS

HE

SESSIONS
VOL. 7

PUBLICATION COMMITTEE

F.C. Jones, Chm.
J. Adams
G.M. Mason

NASA Conference Publication 2376

Published by
Scientific and Technical Information Branch
National Aeronautics and Space Administration
Washington, D.C. 20546

August 1985

For sale by the National Technical Information Service, Springfield, VA 22151

PREFACE

The 19th International Cosmic Ray Conference, under the auspices of the Cosmic Ray Commission of the International Union of Pure and Applied Physics, is being held on the campus of the University of California, San Diego, on 11 through 23 August 1985. In keeping with the tradition begun in 1971 by the Australian organisers of the 12th ICRC, the Proceedings of this conference are appearing in two sets of volumes. The first set, consisting of volumes 1 through 8, is being distributed to all participants at the beginning of the conference. This set contains the contributed papers. The second set, distributed after the conference, contains invited, rapporteur, and highlight papers. The papers are reproduced here exactly as they were received from the authors, without refereeing.

For the 19th ICRC, the scientific program was organised according to three major divisions-- OG (cosmic rays and gamma rays of Galactic Origin), SH (Solar and Heliosphere), and HE (High Energy). Technical papers are included in each of the three divisions.

This conference depended on funds from several agencies of the United States government, including major financial support from the National Aeronautics and Space Administration and support from the National Science Foundation, the Department of Energy, and the Air Force Geophysics Laboratory. Important financial support also came from the Center for Astrophysics and Space Sciences of the University of California, San Diego, from the California Space Institute of the University of California, from the Department of Physics and Astronomy of the University of Maryland, College park, from the International Union for Pure and Applied Physics, and from several corporate sponsors who will be acknowledged by name in the post-conference volumes.

We appreciate the confidence placed in the conference organisers by the Cosmic Ray Commission, and acknowledge with thanks the role of the Commission members in setting up the rules for the conference and in advising the organisers during its planning.

We are grateful to all of the members of the various organising committees listed at the front of this volume. The three Program Committees went to great effort to organise a coherent scientific program and to schedule four parallel sessions with a minimum of conflicts. The Local Organising Committee has worked long and hard to ensure efficient and hospitable accommodations for all the participants, both in the scientific sessions and outside them. The Publications Committee not only took great pains to assemble these volumes but also maintained an orderly data base of papers and authors which was extremely helpful to the program committees. The General Organising Committee made important contributions of ideas and efforts to make the conference possible; this committee included international representation from all of North America, thus the departure from the traditional name of National Organising Committee. And the entire effort was coordinated by the dedicated members of the Steering Committee.

Martin H. Israel, Chairman
General Organising Committee

August, 1985

LETTER FROM THE EDITORS

This conference marks a departure from previous conferences in this series in that the publication of the Conference Papers was carried out an entire continent away from the activities of Local Organising Committee. This posed some problems but, to the considerable surprise of the Publications Committee members, the one that was expected to be the most trouble turned out not to be significant. The overwhelming majority of those submitting papers and abstracts sent them to the correct address, not to La Jolla as was feared. We wish to thank our many authors for their alertness and commend them for handling a complicated situation so well.

There are eight volumes to be distributed to the conference participants in addition to the Conference Program and Author Index: three volumes for OG, two for SH and three for HE. the detailed makeup of these volumes is described in the prefaces written by the Scientific Program chairmen for their respective volumes. Out of some 1100 abstracts that were accepted by the Scientific Program Committees for inclusion in the conference some 929 papers were finally received in time for inclusion in the Conference Papers. This represents a response of approximately 84 percent, a modest improvement. Even if one excludes the 42 one page papers that should be considered as "confirming abstracts", even though there was no such formal category, the response was somewhat higher than that of recent years. We attribute this to the carrot of a later deadline than before coupled with the stick of there being no printing of post deadline contributed papers. We believe that this decision of the General Organizing Committee was a wise one. Of course invited, rapporteur, and highlight talks will be printed in volumes to be distributed to the participants after the conference as usual.

The Publications Committee had much generous help in performing its duties: from Goddard Space Flight Center we had the help of B. Glasser, L. Harris, E. Schronce, N. Smith, J. Esposito and T. Smith. From the Naval Research Laboratory we were helped by T. Mazzotta, and at the University of Maryland M. L. Snidov and J. Mucha gave much needed assistance. Special thanks are due to Caryl Short, the lone staff member of the Publications Committee. She maintained the computer data base, organized the abstracts as they arrived, and kept track of the papers themselves to see that the finally arrived in the right place at the right time. Without her help the job would have been far more difficult than it was.

PUBLICATIONS COMMITTEE August, 1985

Frank C. Jones, Chm.
Jim Adams
Glen M. Mason

HE SESSIONS
VOLUME VII

19th INTERNATIONAL COSMIC RAY CONFERENCE
LA JOLLA, USA
AUGUST 11–23, 1985

INTERNATIONAL UNION OF PURE AND APPLIED PHYSICS
MEMBERS OF THE COMMISSION ON COSMIC RAYS OF IUPAP

A.E. Chudakov, Chm.
F.B. McDonald
G.C. Castagnoli
P.H. Fowler
D. Hovestadt
J. Kota
T.O. Montmerle
H. Moraal
J.R. Prescot
B.V. Sreekantan
K. Suga
J. Wdowczyk

STEERING COMMITTEE

F. McDonald, Chm.
G. Burbage
M. Forman
T. Gaisser
M. Israel
F. Jones
R. Lingenfelter
R. Mewaldt
L. Peterson

GENERAL ORGANIZING COMMITTEE

M. Israel, Chm.
M. Bercovitch
P. Freier
R. Gall
R. Jokipii
L. Jones
V. Jones
S. Krimiges
J. Kurfess
J. Lockwood
P. Meyer
B. Price
R. Ramaty
F. Reines
M. Shapiro
M. Shea
J. Simpson
E. Stone
D. Venkatesan
J. Waddington
S. White

PROGRAM COMMITTEES

OG SESSIONS	SH SESSIONS	HE SESSIONS	PUBLICATIONS
R. Mewaldt, Chm.	M. Forman, Chm.	T. Gaisser, Chm.	F. Jones, Chm.
G. Cassiday	H. Hudson	K. Lande	J. Adams
C. Fichtel	G. Mason	J. Linsley	G. Mason
A. Harding	B. McKibben	E. Loh	
J. Matteson	M. Pomerantz	G. Yodh	
D. Muller			
W. Webber			

LOCAL ORGANIZING COMMITTEE

L. Peterson, Chm.
G. Burbidge
R. Lingenfelter
R. Rothschild
J. Arnold
W. Baity
A. Buffington
M. Burbidge
W. Fillius
R. Gall
R. Gould
H. Hudson
J. Linsley
K. Marti
G. Masek
J. Matteson
C. McIlwain
R. Mewaldt
O. Piccioni
M. Thiemens
W. Thompson
H. Ticho
R. White

Sponsored by
National Aeronautics and Space Administration
National Science Foundation
Department of Energy
Center for Astrophysics and Space Science, University of California, San Diego
California Space Institute, University of California
Department of Physics and Astronomy, University of Maryland, College Park

Preface to HE Volumes

Papers contributed to the XIX International Cosmic Ray Conference were arranged into three major divisions: Origin and Galactic phenomena (OG), Solar and Heliospheric (SH), and High Energy (HE). The HE sessions at this conference comprise all the subjects formerly included in the muon and neutrino sessions (MN) and the extensive air shower sections (EA) as well as those on high energy interactions, new particle searches and emulsion chamber results, which were previously classified in HE. In addition, technical papers have not been classified separately, but have been inserted in appropriate subject sections. All the papers now classified as HE are contained in volumes 6, 7 and 8.

Volume 6 includes sessions HE1 (cross sections and interactions of particles and nuclei at high energy) and HE3 (emulsion chamber results). Extensive air shower papers (HE4) are in volume 7. Papers on muons and neutrinos (HE5), searches for new particles and processes (HE6) and some on new techniques (HE7) are in volume 8.

Altogether some 380 abstracts were received for the HE sections. These were divided into the 25 groups listed in the tables of contents of the HE volumes. (These groups correspond only approximately to the 26 contributed paper sessions at the conference.)

Four rapporteurs were selected to cover the subjects of the HE sessions:

L.W. Jones	High Energy Interactions and New Particle Searches (HE1 & HE6);
M. Shibata	Emulsion Chamber Observations and Interpretation (HE3);
R.W. Clay	Extensive Air Showers (HE4);
K. Sivaprasad	Muons and Neutrinos (HE5).

The written versions of the rapporteur talks are contained in the post-conference volume together with highlight and invited papers.

The work of arranging the HE program was shared by a committee consisting of

T.K. Gaisser (Bartol), Chairman
K. Lande (Pennsylvania)
E.C. Loh (Utah)
J. Linsley (New Mexico)
G.B. Yodh (Maryland)

This conference is the 19th in a series. Previous conferences in this series were held at:

Cracow, Poland - 1947
Como, Italy - 1949
Bagneres-de-Bigorre, France - 1953
Guanjuato, Mexico - 1955
Varenna, Italy - 1957
Moscow, USSR - 1959
Kyoto, Japan - 1961
Jaipur, India - 1963
London, UK - 1965
Calgary, Canada - 1967
Budapest, Hungary - 1969
Hobart, Australia - 1971
Denver, USA - 1973
Munchen, FRG - 1975
Plovdiv, Bulgaria - 1977
Kyoto, Japan - 1979
Paris, France - 1981
Bangalore, India - 1983

ORIGINAL PAGE IS
OF POOR QUALITY

HE 4.1
EXTENSIVE AIR SHOWER THEORIES AND SIMULATIONS

PAPER CODE		PAGE
HE 4.1-2	ELECTRONS, MUONS AND HADRONS IN EXTENSIVE AIR SHOWERS AND HOW DO THEY DEPEND ON NUCLEAR INTERACTION MODEL (PART II) JA WROTNIAK,GB YODH	1
HE 4.1-3	ANALYSIS OF EQUI-INTENSITY CURVES AND NU DISTRIBUTIONS OF EAS G TANAHASHI	5
HE 4.1-5	ANALYSIS OF THE HADRONIC COMPONENT IN E. A. S. OBSERVED AT 700 G.CM**-2 BY A SCALE BREAKING MODEL ? J PROCUREUR,JN STAMENOV,PV STAVREV SZ USHEV	9
HE 4.1-7	ELECTRONS, MUONS AND HADRONS IN EXTENSIVE AIR SHOWERS AND HOW DO THEY DEPEND ON THE NUCLEAR INTERACTION MODEL (PART I) JA WROTNIAK,GB YODH	12
HE 4.1-8	SIMULATION OF EAS PROPERTIES ON THE BASIS OF HIGH ENERGY INTERACTION MODEL DEDUCED FROM THE ACCELERATOR DATA G KUBIAK,J SZABELSKI,J WDOWCZYK	16
HE 4.1-9	NEW ASPECTS IN NUCLEON-NUCLEUS COLLISIONS AND EAS PROPERTIES AROUND 10**6 GEV JN CAPDEVIELLE,J GAWIN	20
HE 4.1-10	SMALL AIR SHOWERS AND COLLIDER PHYSICS JN CAPDEVIELLE,J GAWIN,B GROCHALSKA	24

HE 4.1-11 HIGH ENERGY HADRONS IN EXTENSIVE AIR SHOWERS — 28
SC TONWAR

HE 4.1-13 DEPENDENCE OF THE AVERAGE SPATIAL AND ENERGY CHARACTERISTICS OF THE HADRON-LEPTON CASCADE ON THE STRONG INTERACTION PARAMETERS AT SUPERHIGH ENERGIES — 32
NG BOYAADJIAN,PYU DALLAKYAN,AP GARYAKA
EA MAMIDJANIAN

HE 4.1-14 HADRONIC COMPONENTS OF EAS BY RIGOROUS SADDLE POINT METHOD IN THE ENERGY RANGE BETWEEN 10**5 AND 10**8 GEV — 36
M SINHA,S ROY

HE 4.1-15 ABOUT THE INCREASE OF THE LARGE P1 PROCESSES FRACTION IN HA INTERATIONS AT ENERGIES 5.10**14 - 10**16 EV ACCORDING TO THE DATA ON EAS HADRONS — 40
TV DANILOVA,AG DUBOVY,AD ERLYKIN
NM NESTEROVA,AP CHUBENKO

HE 4.1-17 PHENOMENOLOGY OF SOFT HADRON INTERACTIONS AND THE RELEVANT EAS DATA — 44
NN KALMYKOV,GB KHRISTIANSEN,MV MOTOVA

HE 4.1-19 THE MAXIMUM DEPTH OF SHOWER WITH E SUB O > 10**17 EV ON AVERAGE CHARACTERISTICS OF EAS DIFFERENT COMPONENTS — 48
AV GLUSHKOV,NN EFIMOV,IT MAKAROV
MI PRAVDIN,LG DEDENKO

HE 4.1-20 SENSITIVITY OF DEPTH OF MAXIMUM AND ABSORPTION DEPTH OF EAS TO HADRON PRODUCTION MECHANISM — 52
RA ANTONOV,VI GALKIN,LA HEIN
IP IVANENKO,BL KANEVSKY,VA KUZMIN

HE 4.2
EXTENSIVE AIR SHOWER CORES AND DENSITY SPECTRA

PAPER CODE PAGE

HE 4.2-1 A CRITICAL ANALYSIS OF AIR SHOWER STRUCTURE FUNCTIONS AND SIZE SPECTRUM MEASUREMENTS WITH THE NBU AIR SHOWER ARRAY 56

N CHAUDHURI,DK BASAK

HE 4.2-2 MEASUREMENT OF THE LOCAL DENSITY SPECTRUM 60

ZH LIU,JG LIU,GJ LI,GZ BAI,QX GENG
J LING,WE HAZEN,ES HAZEN

HE 4.2-3 CHARACTER OF ENERGY FLOW IN AIR SHOWER CORE 64

K MIZUSHIMA,K ASAKIMORI,T MAEDA
T KAMEDA,Y MISAKI

HE 4.2-4 OBSERVATION OF EAS USING A LARGE WATER TANK 68

K INOUE,H SAKUYAMA,N SUZUKI,T SUZUKI

HE 4.2-5 THE DEVELOPMENT OF AIR SHOWER IN THE IRON ABSORBER 69

M HAZAMA,S DAKE,K HARADA,M KAWAMOTO
M SAKATA,T SUGIHARA

HE 4.2-6 APPLICATION OF PHOTODIODIES TO THE DETECTION OF ELECTROMAGNETIC BURSTS 73

Y FUKUSHIMA,T SAITO,M SAKATA,M SHIMA
Y YAMAMOTO

HE 4.2-9 CORE STTRUCTURE OF EAS IN 10**15EV TO 10**17EV 77

T HARA,Y HATANO,N HAYASHIDA,T KIFUNE
M NAGANO,G TANAHASHI

HE 4.2-10 PARTICLE DISTRIBUTIONS IN ~10**14 - 10**16 EV AIR SHOWER CORES AT SEA LEVEL 81
AL HODSON,AG ASH,RM BULL

HE 4.2-11 THEORETICAL STUDY OF EAS CORE STRUCTURE ? 85
L POPOVA

HE 4.2-15 MONTE CARLO SIMULATIONS OF ELECTRON LATERAL DISTRIBUTIONS IN THE CORE REGION 10**13 - 10**16 EV AIR SHOWERS 89
AG ASH

HE 4.2-16 COMPARISON OF SIMULATION RESULTS WITH SEA-LEVEL EXPERIMENTAL DATA ON 10**14 - 10**16 AIR SHOWER CORES 93
AG ASH

HE 4.2-18 PARTICLE DISTRIBUTION IN ~ 10**13 - 10**16 EV AIR SHOWER CORES AT MOUNTAIN ALTITUDE AND COMPARISON WITH MONTE CARLO SIMULATIONS 94
AG ASH

HE 4.2-19 TSKHRA-TSKARO COMPLEX INTENDED FOR THE INVESTIGATION OF EAS SPATIAL CHARACTERISTICS NEAR AXIS ? 98
YA GROMOV,YG VERBETSKI,DM KOTLYAREVSKI
LP GARSEVANISHVILI,AA NOVALOV
IV PAZIASHVILI,NS RUSISHVILI
LS KHACHATURYAN,NG TATALASHVILI
L KHACHATURYAN,GZ STEMANETYAN

VOLUME 7

HE 4.3
EXTENSIVE AIR SHOWER MUONS AND ELECTRONS

PAPER CODE PAGE

HE 4.3-1 A NEW STUDY OF SHOWER AGE DISTRIBUTION IN NEAR VERTICAL SHOWERS BY NBU AIR SHOWER ARRAY 101

N CHAUDHURI,DK BASAK,GC GOSWAMI,B GHOSH

HE 4.3-2 A NEW STUDY OF MUONS IN AIR SHOWERS BY NBU AIR SHOWER ARRAY 105

N CHAUDHURI,N MUKHERJEE,S SARKAR
DK BASAK,B GHOSH

HE 4.3-3 LATERAL DISTRIBUTION OF ELECTRONS OF AIR SHOWERS 107

K ASAKIMORI,T MAEDA,T KAMEDA
K MIZUSHIMA,Y MISAKI

HE 4.3-4 DETAILED STUDIES OF THE ELECTRON LATERAL DISTRIBUTION IN EXTENSIVE AIR SHOWERS WITH ENERGIES AROUND 10**16 EV 111

T DZIKOWSKI,J GAWIN,J WDOWCZYK

HE 4.3-6 STUDY OF MUONS NEAR SHOWER CORES AT SEA LEVEL USING THE E594 NEUTRINO DETECTOR 114

JA GOODMAN,SC GUPTA,H FREUDENREICH
K SIVAPRASAD,SC TONWAR,GB YODH
RW ELLSWORTH,MC GOODMAN,D BOGERT
R BURNSTEIN,R FISK,S FUESS,J MORFIN
T OHSKA,J BOFILL,W BUSZA,R MAGAHIZ
T MATTISON,A MUKHERJEE,L OSBORNE,R PITT
L ROSENSON,A SANDACZ,M TARTAGLIA
FE TAYLOR,R VERDIER,S WHITAKER,GB YEH
B STRONGIN,M ABOLINS

HE 4.3-7 CORRELATION OF HIGH ENERGY MUONS WITH PRIMARY COMPOSITION IN EXTENSIVE AIR SHOWER 115

C CHO,S HIGASHI,N HIRAOKA,S OZAKI
T SATO,T SUWADA,T TAKAHASHI,H UMEDA

HE 4.3-8 MEASUREMENT OF LOW ENERGY MUONS IN EAS AT ENERGY REGION LARGER THAN 10**17 EV 119
Y MATSUBARA,T HARA,N HAYASHIDA,K KAMATA
M NAGANO,H OHOKA,G TANAHASHI,T TESHIMA

HE 4.3-9 MUON FLUCUATION STUDIES OF EAS > 10**17 EV 123
PR BLAKE,M LUKSYS,WF NASH,AJ SEPHTON

HE 4.3-10 AVERAGE FEATURES OF THE MUON COMPONENT OF EAS >= 10**17 EV 127
PR BLAKE,M LUKSYS,WF NASH,AJ SEPHTON

HE 4.3-11 MEASUREMENT OF SHOWER ELECTRONS AND MUONS USING A SMALL AIR SHOWER ARRAY 131
SK CHAN,LK NG

HE 4.3-12 THE LONGITUDINAL DEVELOPMENT OF MUONS IN COSMIC RAY AIR SHOWERS AT ENERGIES 10**15 - 10**17 EV 135
T CHEUNG,PK MACKEOWN

HE 4.3-13 TOPOLOGICAL ASPECTS OF AGE PARAMETER 139
JN CAPDEVIELLE,J GAWIN

HE 4.3-14 MONTE CARLO SIMULATION OF E.A.S. GENERATED BY 10**14-10**16 EV PROTONS 143
EJ FENYVES,BC YUNN,T STANEV

HE 4.3-15 LATERAL DISTRIBUTION OF CHARGED PARTICLES IN EAS 147
LG DEDENKO,GV KULIKOV,VI SOLOVJEVA
VP SULAKOV

HE 4.3-16 LATERAL DISTRIBUTION OF HIGH ENERGY MUONS IN EAS OF SIZES N SUB E~10**5 AND N SUB E ~10**6 151

YUN BAZHUTOV,GG ERMAKOV,YUA FOMIN
VI ISAEV,ZV JAROCHKINA,NN KALMYKOV
BA KHRENOV,GB KHRISTIANSEN,GV KULIKOV
MV MOTOVA,IP PROSHKINA,VP RUKOVICHKIN
VI SOLOVJEVA,VP SULAKOV,AV SHKURENKOV
AV TRUBITSYN,VV VASHKEVICH

HE 4.4
CERENKOV SIGNALS AND EXTENSIVE AIR SHOWER ENERGY CALIBRATION

PAPER CODE		PAGE
HE 4.4-1	ENERGY CALIBRATION OF THE FLY'S EYE DETECTOR RM BALTRUSAITIS,GL CASSIDAY,R COOPER R ELBERT,PR GERHARDY,VD KOSLOV,EC LOH Y MIZUMOTO,P SOKOLSKY,D STECK	155
HE 4.4-2	THE STRUCTURE OF EAS AT E>0.1 EEV RM BALTRUSAITIS,GL CASSIDAY,R COOPER JW ELBERT,PR GERHARDY,EC LOH,Y MIZUMOTO P SOKOLSKY,D STECK	159
HE 4.4-4	STANDARD VALUE FOR THE RADIATION LENGTH IN AIR J LINSLEY,J LINSLEY	163
HE 4.4-5	LONGITUDINAL TRIAL FUNCTIONS AND THE COSMIC RAY ENERGY SCALE J LINSLEY	167
HE 4.4-7	EAS DEVELOPMENT CURVE AT ENERGY OF 10**16 - 10**18 EV MEASURED BY OPTICAL CERENKOV LIGHT T HARA,M DAIGO,M HONDA,K KAMATA T KIFUNE,Y MIZUMOTO,M NAGANO,Y OHNO G TANAHASHI	171
HE 4.4-8	MISSING ENERGIES AT PAIR CREATION AA EL-ELA,S HASSAN,ER BAGGE	175
HE 4.4-9	TRANSITION EFFECT OF AIR SHOWER PARTICLES IN PLASTIC SCINTILLATORS K ASAKIMORI,T MAEDA,T KAMEDA K MIZUSHIMA,Y MISAKI	179

HE 4.4-10 THE SYSTEM OF EAS TIME ANALYSIS 183

AZ KHALAFYAN,VM MKHITARYAN,JS OGANEZOVA
GL BASHINDJAGHYAN,NB SINEV,LI SARYCHEVA

HE 4.4-13 ON THE DETERMINATION OF THE DEPTH OF EAS DEVELOPMENT MAXIMUM USING THE LATERAL DISTRIBUTION OF CERENKOV LIGHT AT DISTANCES < 150 M FROM EAS AXIS 187

N ALIEV,T ALIMOV,M KAKHKHAROV
BM MAKHMUDOV,N RAKHIMOVA,R TASHPULATOV
NN KALMYKOV,GB KHRISTIANSEN,VV PROSIN

HE 4.4-14 STUDY OF THE ENERGY SPECTRUM OF PRIMARY COSMIC RAYS; EAS SIZE FLUCTUATIONS AT A FIXED PRIMARY ENERGY 191

N ALIEV,T ALIMOV,N KAKHKHAROV,N KHAKIMOV
N RAKHIMOVA,R TASHPULATOV
GB KHRISTIANSEN

HE 4.4-15 STUDY OF THE SHOWER MAXIMUM DEPTH BY THE MEHTOD OF DETECTION OF THE EAS CERENKOV LIGHT PULSE SHAPE 195

N ALIEV,T ALIMOV,M KAKHKHAROV
N KHAKIMOV,BM MAKHMUDOV,N RAKHIMOVA
R TASHPULATOV,GB KHRISTIANSEN,VV PROSIN
VYU ZHUKOV

HE 4.4-16 ANALYSIS OF CERENKOV PULSES RECORDED SIMULTANEOUSLY AT TWO SITES 199

DF LIEBING,JR PATTERSON

HE 4.4-17 PRELIMINARY RESULTS OF THE CERENKOV EAS FLASHES OBSERVATIONS ON THE MULIT-MIRROR INSTALLATION OF THE CRIMEAN ASTROPHYSICAL OBSERVATORY 203

BM VLADIMIRSKY,YL ZYSKIN,YI NESHPOR
AA STEPANIAN,VP FOMIN,VG SHITOV

HE 4.4-18 THE EXPERIMENTAL CASCADE CURVES OF EAS AT E > 10**17 EV OBTAINED BY THE METHOD OF DETECTION OF CHERENKOV PULSE SHAPE 207

YUA FOMIN,NN KALMYKOV,GB KHRISTIANSEN
MV MOTOVA,YUA NECHIN,VV PROSIN,VY ZHUKOV
NN EFIMOV,VM GRIGORIEV,ES NIKIFOROVA

VOLUME 7

HE 4.4-19 LATERAL-ANGULAR AND TEMPORAL CHARACTERISTICS OF EAS OPTICAL RADIATION 211

TA CHUYKOVA,VI GALKIN,IP IVANENKO
TM ROGANOVA

HE 4.5
GAMMA-RAY AIR SHOWERS

PAPER CODE PAGE

HE 4.5-1 THE IDENTIFICATION OF GAMMA-RAY INDUCED EAS 215
PR BLAKE,WF NASH

HE 4.5-3 MUONS IN GAMMA SHOWERS 219
T STANEV,CP VANKOV,F HALZEN

HE 4.5-4 MUON SPECTRUM IN AIR SHOWERS INITIATED BY GAMMA RAYS 223
SA STEPHENS,RE STREITMATTER

HE 4.5-5 DEVELOPMENT OF ELECTROMAGNETIC CASCADES IN THE ATMOSPHERE INCLUDING THE LANDAU-POMERANCHUK-MIGDAL EFFECT 227
RE STREITMATTER,SA STEPHENS

HE 4.5-6 ELECTROMAGNETIC AND MUONIC STRUCTURE OF SHOWERS INITIATED BY GAMMA-RAYS AND BY HADRONS 231
AMM HILLAS

HE 4.5-7 THE MUON CONTENT OF GAMMA-RAY SHOWERS 235
PG EDWARDS,RJ PROTHEROE

HE 4.5-9 THE HUMP IN THE CERENKOV LATERAL DISTRIBUTION OF GAMMA RAY SHOWERS 239
S SINHA,MVS RAO

HE 4.5-10 SIMULATION OF GAMMA-INITIATED SHOWERS 243
JN STAMENOV,K VANCOV,T VODENICHAROVA

HE 4.5-11 PHENOMENOLOGICAL CHARACTERISTICS OF ? ELECTRON COMPONENT IN GAMMA-QUANTA INITIATED SHOWERS 247
SI NIKOLSKY,JN STAMENOV,SZ USHEV

HE 4.5-13 ✓A THREE-DIMENSIONAL MONTE CARLO CALCULATION OF THE PHOTON INITIATED SHOWERS AND KIEL RESULT 251
✓ A OKADA,Y MURAKI

HE 4.5-14 ✓CONSTRUCTION OF A COSMIC RAY AIR SHOWER TELESCOPE 252
LK NG,SK CHAN

HE 4.5-15 ✓AN UNDERGROUND COSMIC RAY MUON TELESCOPE FOR OBSERVATION OF COSMIC RAY ANISOTROPY 256
✓ YW LEE,LK NG

HE 4.5-16 ✓NUCLEAR CASCADES IN ELECTROMAGNETIC SHOWERS PRODUCED BY PRIMARY GAMMA-QUANTA IN THE ATMOSPHERE 260
/TV DANILOVA,AD ERLYKIN,AV MIRONOV
EI TUKISH

VOLUME 7

HE 4.6
EXTENSIVE AIR SHOWER TECHNIQUES

PAPER CODE PAGE

HE 4.6-2 ON THE POSSIBILITES OF LARGE-SCALE RADIO AND FIBER OPTICS DETECTORS IN COSMIC RAYS 264

GA GUSEV,MA MARKOV,IM ZHELEZNYKH

HE 4.6-3 RADIO SIGNALS FROM VERY LARGE AIR SHOWERS 268

K SUGA,F KAKIMOTO,K NISHI

HE 4.6-4 ON THE PRODUCTION MECHANISM OF RADIO-PULSES FROM LARGE EXTENSIVE AIR SHOWERS 272

P DATTA,KM PATHAK

HE 4.6-5 A NEW STUDY ON THE EMISSION OF EM WAVES FROM LARGE EAS 276

KM PATHAK,GKD MAZUMDAR

HE 4.6-6 AIR FLUORESCENCE DETECTION OF LARGE AIR SHOWERS BELOW THE HORIZON 280

P HALVERSON,T BOWEN

HE 4.6-7 INVESTIGATION OF COSMIC RAYS IN VERY SHORT TIME SCALES 284

J PELTONEN,E VALTONEN,JJ TORSTI
H ARVELA,M LUMME,M NIEMINEN,E VAINIKKA

HE 4.6-8 A FACILITY FOR INVESTIGATION OF MULTIPLE HADRONS AT COSMIC-RAY ENERGIES 288

E VALTONEN,JJ TORSTI,H ARVELA,M LUMME
M NIEMINEN,J PELTONEN,E VAINIKKA

HE 4.6-9 A POSSIBLE EAS ARRAY ABOVE THE SOUDAN II DETECTOR 292

K SIVAPRASAD

HE 4.6-10 FAST SCINTILLATION COUNTER SYSTEM AND PERFORMANCE 293

H SASAKI,A NISHIOKA,M KUSUNOSE
T NAKATSUKA,T NAKATSUKA,T HORIKI
Y HATANO

HE 4.6-11 PERFORMANCE OF A LOCAL ELECTRON DENSITY TRIGGER TO SELECT EXTENSIVE AIR SHOWERS AT SEA LEVEL 297

T ABBAS,J MADANI,F ASHTON

HE 4.6-13 MICROPROCESSOR-BASED SINGLE PARTICLE CALIBRATION OF SCINTILLATION COUNTER 301

GKD MAZUMDAR,KM PATHAK

HE 4.6-14 SAMARKAND COMPLEX SET-UP FOR INVESTIGATION OF COSMIC RAY VARIATION IN THE ENERGY RANGE OF 7.10**9 - 10**15EV 304

LI DORMAN,F VALIHODZHAEV,BM MAKHMUDOV
N SIRODZHEV,R TASHPULATOV

HE 4.6-15 RADIO WAVE EMITTED BY AN EXTENSIVE AIR SHOWERS IN 10 KHZ TO 1 MHZ REGION 308

J NISHIMURA

HE 4.7
EXTENSIVE AIR SHOWER ARRIVAL TIMES AND MINI-ARRAYS

PAPER CODE		PAGE
HE 4.7-1	STRUCTURE OF THE SHOWER DISK OBSERVED AT MT. NORIKURA H SASAKI,A NISHIOKA,N OHMORI,M KUSUNOSE T NAKATSUKA,T HORIKI,Y HATANO	312
HE 4.7-2	STRUCTURE OF AIR SHOWER DISK NEAR THE CORE N INOUE,M KAWAMOTO,Y MISAKI,T MAEDA T TAKEUCHI,Y TOYODA	316
HE 4.7-3	PROPERTIES OF 10**18 - 10**19 EV EAS AT FAR CORE DISTANCE M TESHIMA,M NAGANO,T HARA,Y HATANO N HAYASHIDA,CX HE,M HONDA,F ISHIKAWA K KAMATA,Y MATSUBARA,M MORI,H OHOKA G TANAHASHI	320
HE 4.7-4	LONGITUDINAL DEVELOPEMENT OF MUONS IN LARGE AIR SHOWERS STUDIED FROM THE ARRIVAL TIME DISTRIBUTIONS MEASURED AT 900M ABOVE SEA LEVEL F KAKIMOTO,I TSUCHIMOTO,T ENOKI,K SUGA K NISHI	324
HE 4.7-5	ARRIVAL TIME DISTRIBUTIONS OF ELECTRONS IN AIR SHOWERS WITH PRIMARY ENERGIES ABOVE 10**18 EV OBSERVED AT 900M SEA LEVEL F KAKIMOTO,I TSUCHIMOTO,T ENOKI,K SUGA K NISHI	328
HE 4.7-6	THE THICKNESS OF THE SHOWER DISC AS OBSERVED IN SHOWERS PRODUCED BY PRIMARIES ABOVE 10**19 EV MA LAWRENCE,AA WATSON,AA WEST	332

HE 4.7-7 METHODS FOR ROOF-TOP MINI-ARRAYS 336

WE HAZEN,ES HAZEN

HE 4.7-8 EXPECTED RATES WITH MINI-ARRAYS FOR AIR SHOWERS 339

WE HAZEN

HE 4.7-9 FAST SCINTILLATION COUNTER PREAMPLIFIER FOR THE OBSERVATION OF LINSLEY EFFECT 343

LK NG

HE 4.7-10 A MINI-ARRAY FOR LARGE AIR SHOWERS 347

LK NG,LK NG,SK CHAN,WE HAZEN,ES HAZEN

HE 4.7-12 A NOTE ON SOME STATISTICAL PROPERTIES OF THE RISE TIME PARAMETERS USED IN MUON ARRIVAL TIME MEASURES 351

DJ VAN DER WALT,EJ DE VILLIERS

HE 4.7-13 SUB-LIMINAL PULSES FROM COSMIC RAY AIR SHOWERS 355

J LINSLEY

HE 4.7-14 THICKNESS OF THE PARTICLE SWARM IN COSMIC RAY AIR SHOWERS 359

J LINSLEY

HE 4.7-15 STUDY OF THE TIME-DIFFERENTIATED PARTICLE FLUX DENSITY AT VARIOUS DISTANCES FROM EAS AXIS 363

VG ATRASHKEVICH,RJ CHERNYKH,YUA FOMIN
GK GARIPOV,GB KHRISTIANSEN,GV KULIKOV
AP LEBEDEV,SJ MATSENOV,VJ NAZAROV
AA SILAEV,VJ SOLOVYEVA,VP SULAKOV
AV TRUBITSYN,OV VEDENEEV

N85-35969

ELECTRONS, MUONS AND HADRONS IN EXTENSIVE AIR SHOWERS AND HOW DO THEY DEPEND ON NUCLEAR INTERACTION MODEL
(Part II)

J.A.Wrotniak and G.B.Yodh

Department of Physics and Astronomy
University of Maryland
College Park, MD 20742, U.S.A.

Here we present some of the results of Monte Carlo simulations of extensive air showers for nuclear interaction models as outlined in our contribution HE 4.1-7 to this Conference.

In the notation used below, numbers in brackets () denote mean square errors in last decimal digit units. k, M, G, T and E stand for appropriate powers of 10. For the scarcity of place, the radial data on showers are not included.

Table 1. Average shower size at 1000 g/cm²

E[eV]	Primary protons					Primary iron	
	P-Y00	M-Y00	M-F00	M-F01	R-F01	FF-Y00	RM-F00
20 T	1.09(6)k		1.17(5)k			.25(1)k	.31(1)k
100 T	10.8(5)k	11.6(5)k	8.5(4)k	10.7(4)k	10.2(6)k	2.12(4)k	2.41(4)k
500 T	88(3)k		64(3)k			22.3(6)k	21.8(3)k
2 P	539(20)k		331(14)k			165(4)k	139(3)k
10 P	3.21(6)M	2.99(7)M	2.28(6)M	2.69(8)M	2.21(7)M	1.47(5)M	1.08(2)M
50 P	20.2(4)M		15.2(4)M			10.9(1)M	7.7(2)M
200 P	92(1)M		69(2)M			58(1)M	40(1)M
1 E	507(7)M	519(5)M	411(10)M	451(7)M	391(6)M	378(4)M	261(4)M

Table 2. Fluctuations of the shower size at 1000 g/cm² (s.d.of Log[base 10] Ne)

E[eV]	Primary protons					Primary iron	
	P-Y00	M-Y00	M-F00	M-F01	R-F01	FF-Y00	RM-F00
20 T	.42		.44			.13	.12
100 T	.33	.33	.34	.35	.34	.13	.13
500 T	.22		.26			.12	.10
2 P	.18		.19			.08	.07
10 P	.13	.14	.17	.19	.17	.07	.07
50 P	.10		.15			.05	.05
200 P	.07		.11			.04	.05
1 E	.06	.05	.09	.09	.09	.03	.04

ORIGINAL PAGE IS
OF POOR QUALITY

Table 3. Average depth of shower maximum (g/cm²)

E[eV]	Primary protons					Primary iron	
	F-Y00	M-Y00	M-F00	M-F01	R-F01	FF-Y00	RM-F00
20 T	486(6)		481(5)			307(2)	306(2)
100 T	557(7)	562(7)	521(6)	537(7)	532(8)	377(2)	368(2)
500 T	621(7)		570(6)			447(3)	433(2)
2 P	698(10)		602(7)			509(3)	481(3)
10 P	735(6)	712(6)	653(5)	671(6)	639(7)	583(4)	535(3)
50 P	801(8)		708(7)			643(3)	587(3)
200 P	> 865(8)		729(6)			701(4)	622(4)
1 E	> 920(8)	> 872(7)	777(10)	784(6)	742(4)	773(5)	669(4)

Table 4. Average shower size at maximum (exactly: geometric mean values)

E[eV]	Primary protons					Primary iron	
	F-Y00	M-Y00	M-F00	M-F01	R-F01	FF-Y00	RM-F00
20 T	10.6(1)k		10.9(1)k			7.82(4)k	7.50(3)k
100 T	56.9(7)k	56.0(7)k	58.3(6)k	65.2(7)k	63.7(8)k	40.9(2)k	39.6(2)k
500 T	289(3)k		310(3)k			225(1)k	223(1)k
2 P	1.15(2)M		1.26(2)M			957(4)M	982(4)k
10 P	5.74(5)M	6.01(6)M	6.55(4)M	6.95(5)M	7.18(6)M	5.12(2)M	5.38(2)M
50 P	28.8(3)M		33.3(3)M			26.2(1)M	28.8(2)M
200 P	111(2)M		134(1)M			106(1)M	118(1)M
1 E	552(9)M	614(5)M	662(7)M	703(5)M	726(3)M	530(3)M	610(2)M

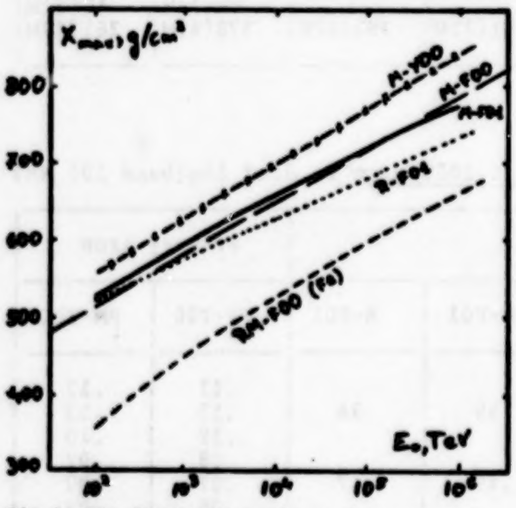

Fig.1. The depth of maximum for some of our models.

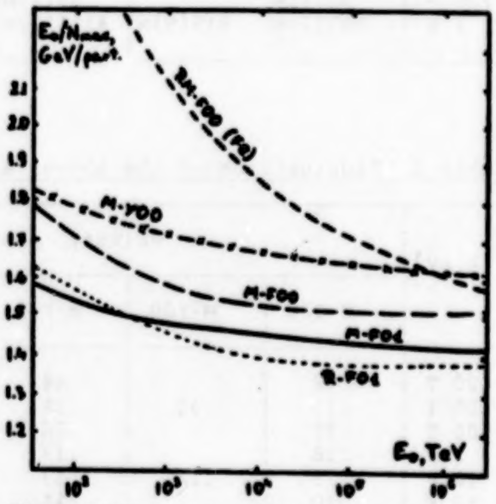

Fig.2. Energy per electron at the shower maximum.

Table 5. Fluctuations in shower size at maximum (s.d.of Log [base 10] Ne[max])

E[eV]	Primary protons					Primary iron	
	F-Y00	M-Y00	M-F00	M-F01	R-F01	FF-Y00	RM-F00
20 T	.10		.09			.032	.033
100 T	.08	.08	.08	.07	.07	.027	.029
500 T	.07		.06			.021	.022
2 P	.06		.05			.017	.014
10 P	.06	.06	.04	.05	.04	.015	.015
50 P	.06		.04			.014	.011
200 P	.07		.04			.009	.014
1 E	.07	.04	.04	.04	.02	.013	.008

Model M-F00 was also run at primary proton energy of 100 EeV (or 10^{20} eV); 151 showers at 1000 g/cm^2 and 64 at 1400 g/cm^2 were simulated. Number of electrons at 1000 g/cm^2 was 59.5(5) G, its fluctuations .04, at maximum (average depth 906(5) g/cm^2): 66.1(5) G and .024, respectively.

Table 6. The average muon number at 1000 g/cm^2.

(a) at E > 2 GeV

E[eV]	Primary protons					Primary iron	
	F-Y00	M-Y00	M-F00	M-F01	R-F01	FF-Y00	RM-F00
20 T	.36(1)k		.34(1)k			.64(1)k	.64(1)k
100 T	1.55(3)k	1.53(2)k	1.43(3)k	1.09(2)k	1.06(2)k	2.32(2)k	2.30(2)k
500 T	6.6(1)k		6.1(1)k			9.57(6)k	9.24(4)k
2 P	22.4(5)k		21.0(3)k			34.2(2)k	32.3(3)k
10 P	90(2)k	91(2)k	82(1)k	52.9(6)k	51.9(8)k	147.6(6)k	136.1(6)k
50 P	337(6)k		334(4)k			612(2)k	567(3)k
200 P	1.03(3)M		1.08(2)M			2.03(2)M	1.90(1)M
1 E	3.71(14)M	4.54(9)M	4.14(7)M	2.33(4)M	2.38(3)M	7.87(5)M	7.60(3)M

(b) at E > 200 GeV

E[eV]	Primary protons					Primary iron	
	F-Y00	M-Y00	M-F00	M-F01	R-F01	FF-Y00	RM-F00
20 T	3.1		2.9			<.1	<.1
100 T	8.4	8.5	8.7	8.5	8.6	7.8	7.5
500 T	29		32			73	77
2 P	83		97			207	223
10 P	299	330	342	254	279	692	773
50 P	1.03 k		1.24 k			2.43 k	2.71 k
200 P	2.88 k		3.96 k			7.11 k	8.25 k
1 E	10.5 k	13.6 k	13.8 k	9.3 k	10.7 k	24.5 k	30.1 k

ORIGINAL PAGE IS
OF POOR QUALITY

Table 7. The average hadron number above 2 GeV at 1000 g/cm².

E[eV]	Primary protons					Primary iron	
	F-Y00	M-Y00	M-F00	M-F01	R-F01	FF-Y00	RM-F00
20 T	4.3(3)		4.8(3)			2.0(2)	4.2(3)
100 T	34(3)	38(3)	27(2)	17(2)	19(2)	11(1)	17(1)
500 T	244(11)		168(8)			88(3)	96(2)
2 P	1.33(6)k		701(32)			554(15)	500(13)
10 P	6.7(2)k	5.9(2)k	3.7(2)k	1.95(9)k	1.65(9)k	4.41(9)k	3.19(6)k
50 P	34(2)k		18.3(7)k			28.8(4)k	18.0(5)k
200 P	131(4)k		65(3)k			131(3)k	78(2)k
1 E	566(19)k	550(15)k	293(12)k	130(6)k	106(5)k	711(10)k	388(8)k

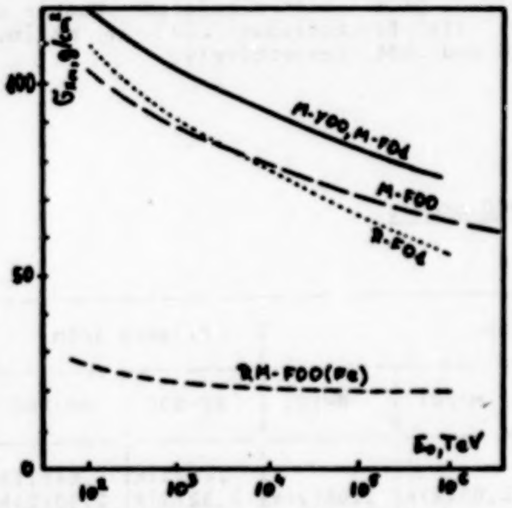

Fig.3. Fluctuations in the depth of maximum.

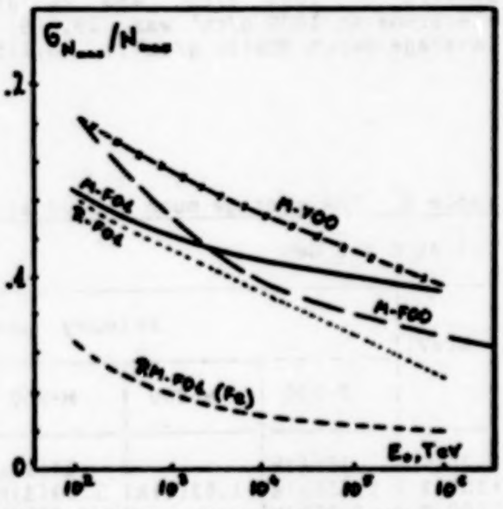

Fig.4. Relative fluctuations of the shower size at maximum.

[One more model was used for EAS generation: M-F10, with all features exactly like M-F00, but with quite different multiplicity distributions. All shower characteristics checked by us were in statistically good agreement between these models].

In principle, the data shown here should speak for themselves. We would like, however, conclude with three remarks:

* The most significant part of scaling violation effect is generated by the inclusion of rising cross-section.
* Among the models considered the lowest value for Eo/N[max] is obtained when rapidly rising cross-section and charge exchange are both included (model R-F01). The value is still 1.38 GeV/electron.
* Except at the highest energies, the sensitivity to atomic mass of the primary is greater than to specific assumptions about multiple production.

N85-35970

ANALYSIS OF EQUI-INTENSITY CURVES AND N_μ DISTRIBUTION OF EAS

G.TANAHASHI

Institute for Cosmic Ray Research, University of Tokyo
Tanashi, Tokyo, 188 Japan

ABSTRACT

The distribution of the number of muons in EAS and the equi-intensity curves of EAS are analyzed on the basis of Monte Carlo simulation of various cosmic ray composition and the interaction models. Problems in the two best combined models are discussed.

1. Introduction

Many analyses of EAS data have been reported to investigate the cosmic ray composition and their interaction. For example, the comprehensive work was reported by Gaisser et al(1) in 1978. After then, the equi-intensity data of Chacaltaya was revised(2) and the other data of Akeno experiment was added to it(3). Akeno experiment also gave a distribution of the number of muons(>1Gev) of EAS at fixed shower size with a good statistics(4). In this report we make an analysis of these data with use of the Monte Carlo simulation described in 2.

2. One dimensional simulation of EAS

Among the parameters used in the interation model of the cosmic ray with the air nucleus, the collision m.f.p. is assumed to be $\lambda=\lambda o/(1+0.07(\log E_0(Tev)+1)^{1.5})gcm^{-2}$ where $\lambda o=80$ and 120 for proton and pion interaction respectively, and Eo is the cosmic ray energy. The value of λ are shown in Fig.1 together with $\sigma=290.Eo(Tev)^{0.06}mb$ obtained in the Akeno experiment(5). The assumptions of the other parameters are following.

The leading particle carrys the energy Es fluctuated uniformly between 0-Eo. The partition of the rest of the energy between the fragmentation and the central region is half to half. The energy spectrum of the produced particles in the fragmentation is $\exp(-E/E^*)$ where E^* is 0.6Es and Es for proton and pion incident respectively. In the central region the spectrum is assumed to be a plateau shaped one whose energy spread is shown in Fig.2 for various models. Resultant multiplicity-energy relation , multiplicity distribution, scaling behavior and inclusive rapidity distribution are checked to fit the data of accelerator experiments. Produced particles are to be pions or kaons, and the proportion of the kaon production is to increase with the energy as $0.05\log E_0(Gev)$.

Interation models shown in Fig.2 are used for the EAS calculation. They are SC(scaling), STD(standard, which is scaling + the extension of the central distribution in 10^{14}ev to the higher energies), SC1/2(scaling + increasing multiplicity with $E_0^{1/2}$ in the central region above 10^{14}ev), SCM(scaling + particles nearly at rest in CM system above 10^{14}ev) and CCM (no fragmentation particles and all particles nearly at rest in CM system above 10^{14}ev).

We have further two kinds, I and II, in each of the above models. I includes the generation of the high energy neutral pion as the leading particle, and the forward and backward symmetry of the produced particles in CM system. II includes no production of the energetic neutral pion as the leading , and the enhanced particle production in the backward three times more than the forward as the effect of target nucleus. The details

ORIGINAL PAGE IS
OF POOR QUALITY

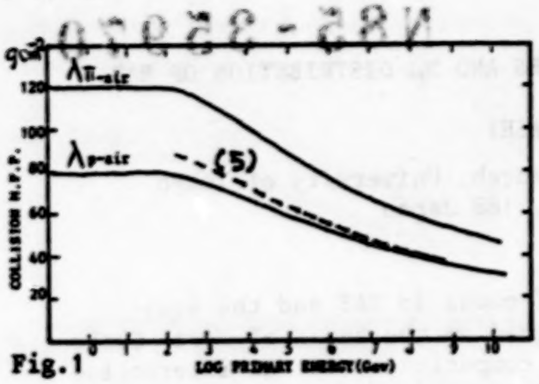

Fig.1

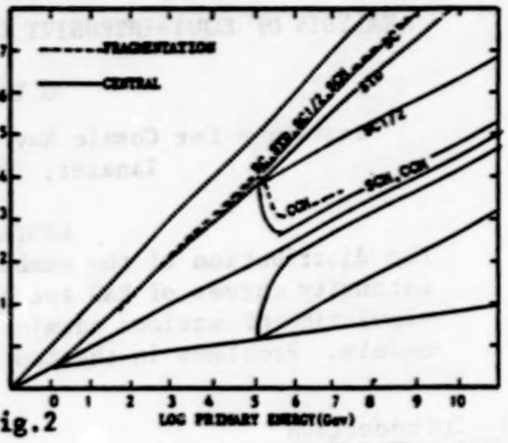

Fig.2

of these assumptions will be described elswhere.

The shower curves of electrons and muons of STD based on I, II are shown in Fig.3. It is seen that the attenuation of particles between 1000-1600gcm^{-2} is nearly exponential and has almost the same attenuation length(180-190gcm^{-2} in I and 190-200gcm^{-2} in II) irrespective of the primary energies above 10^{13}ev. In the same figure, the shower curves of the constant cross section are also shown for the comparision. The reason that the attenuations are almost the same comes mainly from the increasing cross sections. The other result is that the muon content in II is almost 3 times larger than I's.

In Fig.4 the shower curves of various models are shown in comparison. All of them are based on model I. It is found again the attenuation byond 1000 gcm^{-2} are almost parallel. The difference among SC, STD and SC1/2 are very small, and this

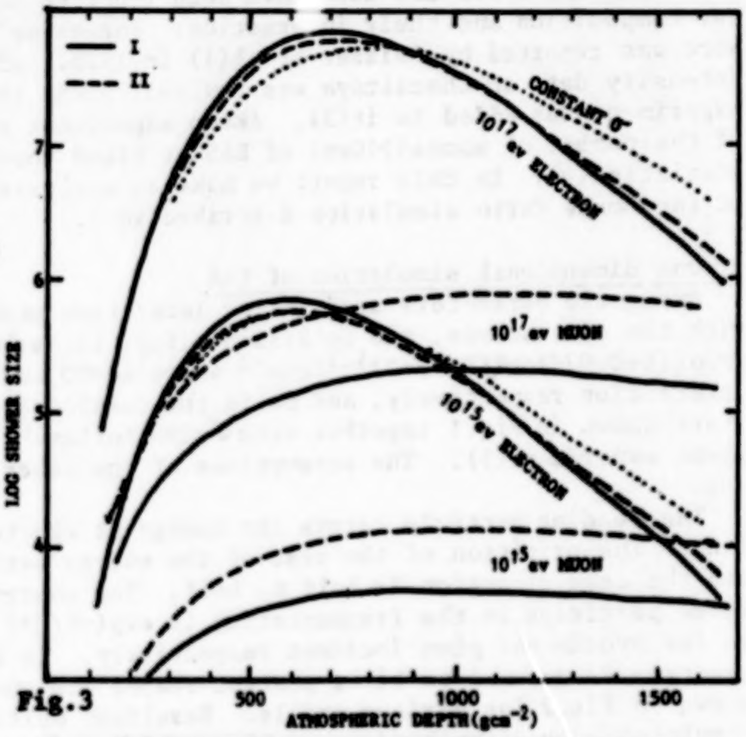

Fig.3

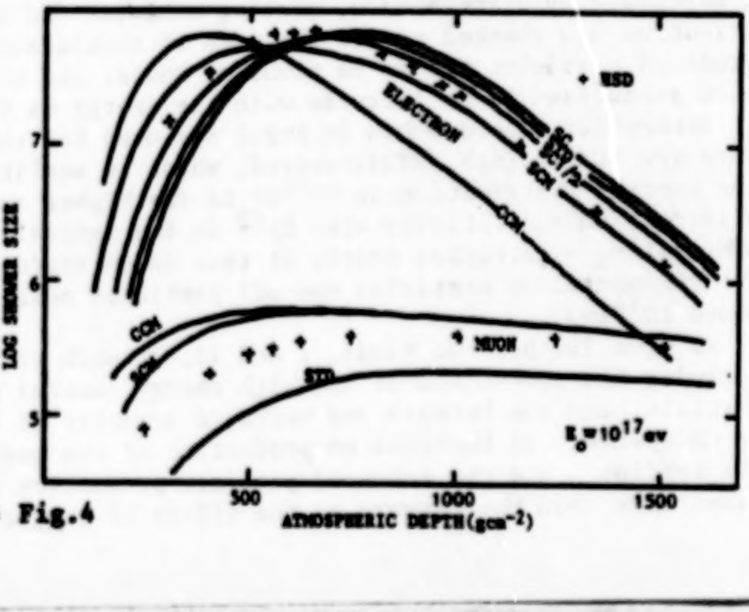

Fig.4

ORIGINAL PAGE IS
OF POOR QUALITY

means that the energy distribution in the central region does not affect much the shower curve except the extreme case like SCM. The crosses in the figure show the iron shower curve(HSD) based on the superposition of STD.

3. Nμ distribution of fixed Ne

The Nμ distributions of EAS of different primary component (mass number A=1,4,15 and 50) are calculated under the condition of fixed Ne assuming the primary integral energy spectrum to be E^{-2}. These Nμ distributions include the error which comes into Nμ in the course of the data reduction and also the error due to the possible fluctuation of muon lateral distribution. The distribution of A>4 are almost due to these errors. These Nμ distributions of each component are superposed to fit the experiment(5) as shown in Fig.5. The conclusions obtained from this comparision are (i)low Nu tail requires the existence of proton showers more than several % (ii)the Nu distribution of the proton shower must be as broad as in STD, that is, the very high multiplicity models are avoided because of their narrow distribution of Nμ (iii)the avrage Nμ of each component must be spread over more than factor 3 for fixed Ne.

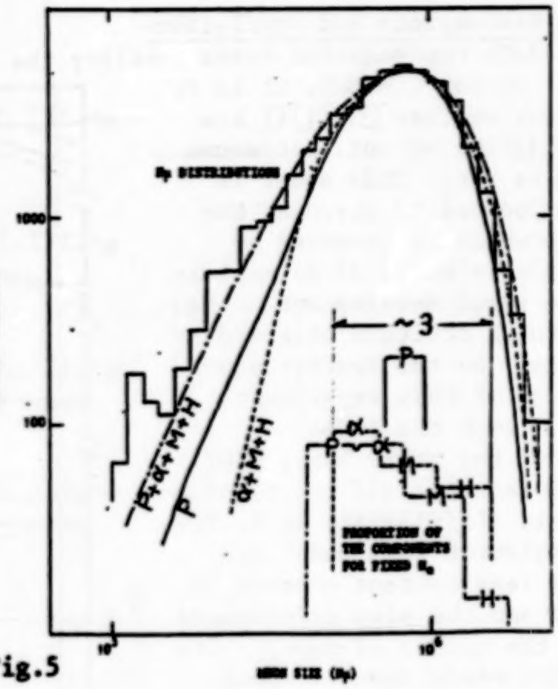

Fig.5

4. Equi-intensity curves of EAS

Equi-intensity curves of a mixed composition are related to each shower curves as follows. Assume that the shower curves are energy independent in the required energy region, that is N(E,x)=E.N(x) where N(e,x) is the shower curve of energy E in depth of x. The intensity ratio of the heavy to the proton shower in fixed shower size is

$$\Delta(x)=(Ih/Ip)_N=(Ih/Ip)_E.(Nh(x)/Np(x))^{\gamma}$$

where $k=(Ih/Ip)_E$ is the intensity ratio in fixed energy and γ is the integral exponent of the primary energy spectrum. Putting $\gamma=2$, $\Delta(x)$ can be calculated with use of the values of Nh(x), Np(x) as the funtion of k. Equi-intensity curves $\overline{N}(x)$ are obtained from

$$\overline{N}(x)=Np(x)/(1+\Delta(x))+Nh(x).\Delta(x)/(1+\Delta(x))$$

$\Delta(x)$ and $\overline{N}(x)$ are calculated for the following combinations of the proton and the heavy showers.

proton shower	STD	STD	STD	SCM
heavy shower	HSD	SCM	CCM	CCM
notation	HSD/STD	SCM/STD	CCM/STD	CCM/SCM

The $\overline{N}(x)$ are shown in Fig.6 for k=0.1, 1.0 and 10 together with the experimental data(2)(3). In general, the attenuation length between 800-1400 gcm^{-2} are steeper than either prediction, but two cases(HSD/STD and k=10)

ORIGINAL PAGE IS
OF POOR QUALITY

(CCM/SCM and k=0.1) barely fit the experiment as shown in the figure in dotted curves after the normalization of the intensity. SCM/STD and CCM/STD do not fit because of too much difference of proton and heavy shower curves. This differenc makes the composite curves flat.

5. Discussions and conclusion

Both two selected cases satisfy the requirement (i) in 3.

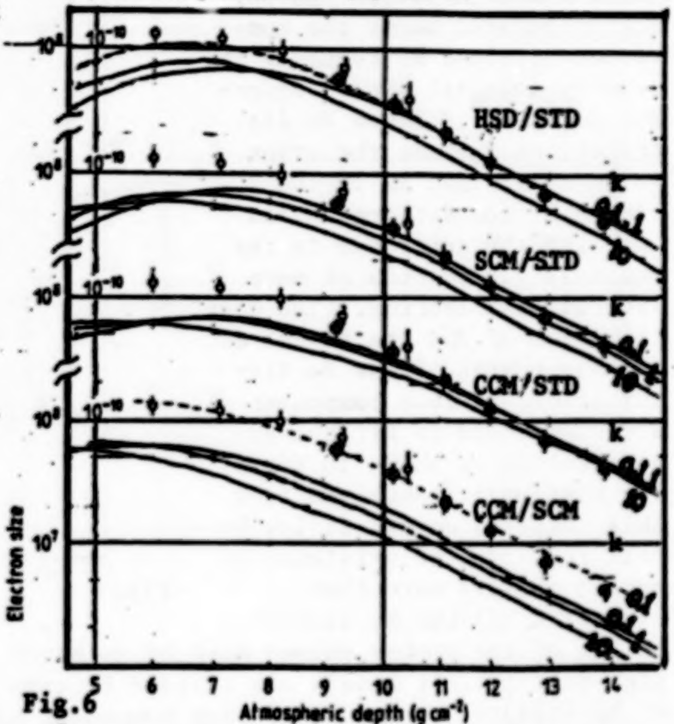

Fig.6

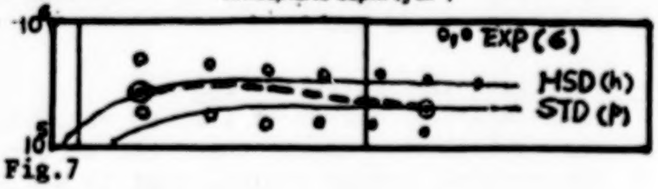

Fig.7

As for CCM/SCM, it is not clear whether (ii)(iii) are satisfied or not, but seems to be not. This model is introduced to approach the one which is proposed by Kakimoto et al(2) to explain the rapid development of EAS in high altitude observed by them. So the further progress of this experiment will test the model.

On the other hand, HSD/STD satisfys all the requirements (i)(ii)(iii) in 3. The problems of this model are the less content of muons in EAS and the slow development of the number of muons. The model needs about 2 times more muons. If we adopt model II instead of I, the number of muons increases but the attenuation length also increases apart further from the experiment. As for the slow development of muon in this model, we can scarcely fit the experiment by taking the number of muons of iron showers in 600 gcm^{-2} and of proton showers in 1100gcm^{-2}(Fig.7). If the Nμ difference of the proton and the heavy nucleus shower is larger in some model, such a model is better in this problem.

Acknowledgements

The EAS simulation are done by FACOM 380 at the computer room, Institute for Nuclear Study, University of Tokyo.

References

(1) Gaisser, T.K. et al.	Rev. Mod. Phys., 50, 859	1978
(2) Kakimoto, F. et al.	J. Phys. G; Nucl. Phys. 9, 339	1983
(3) Nagano, M. et al.	J. Phys. G; Nucl. Phys. 10, 1295	1984
(4) Hara, T. et al.	Proc. 18th ICRC(Banbalore), 11, 285	1983
(5) Hara, T. et al.	Phys. Rev. Lett. 50, 2058	1983
(6) Hara, T. et al.	Proc. 18th ICRC(Bangalore), 11, 281	1983

ANALYSIS OF THE HADRON COMPONENT IN E.A.S. OBSERVED AT 700 $g.cm^{-2}$ BY A SCALE BREAKING MODEL

J. Procureur
Laboratoire de Physique Théorique
Université de Bordeaux 1
rue du Solarium
33170 Gradignan (France)

J.N. Stamenov, P.V. Stavrev, S.Z. Ushev
Institute of nuclear research and nuclear energy
Bld. Lenin 72
Sofia (Bulgaria)

ABSTRACT

The Tien Shan experimental results about the hadron component in E.A.S. with sizes 10^4-10^6 are analysed with help of a scale breaking model. It is shown that the secondary particles multiplicity depends on the interaction energy stronger as predicted from accelerator experiments and the primary mass composition is rich on protons at energies 10^5-10^6 GeV

1. Introduction. Hadrons in extensive air showers provide direct informations about high energy interactions.

In the rule the biases pertaining to different shower array arrangements have a relative large influence for the basic phenomenological characteristics of the E.A.S. hadron component.

In this situation, the problem of the correct comparison between model calculated and experimental characteristics is of great importance for the reliability of the derived conclusions about the high energy interaction characteristics.

This is why we take carefully into account the triggering conditions of the Tien Shan array and the characteristic procedures for the statistical data treatment.

2. Method The characteristics of the E.A.S. hadron component were calculated on the basis of a scale breaking model under the assumption of a pure proton primary composition.

Details on the model of simulation are given in the proceedings of this conference (HE 5.4-8) and in ref (1).

The different observables computed from simulation characterize the "pure development" of the showers.

Then, to be compared with the results obtained in Tien Shan experiment, pseudo-experimental values were determined with help of the IMEAT algorithm which takes into account all internal characteristics of this array.

By this way we obtained results for showers with fixed sizes 10^4-10^6 and with average zenith angle $\bar{\theta} = 22°$

3. Results

The dependences of hadron numbers $N_h(>E_h)$ on the shower size were analysed in the size interval 10^4-10^6 and at Tien Shan observation level.

Simulations were made for different threshold energies for the hadrons : $E_h > 0.6$; 1 and 10 TeV.

It is seen fig. 1 that the experimental dependences (2-4), $N_h \sim N_e^{\alpha}$ for $E_h > T_r$, are much steeper than those predicted from the adopted Scale Breaking Model.

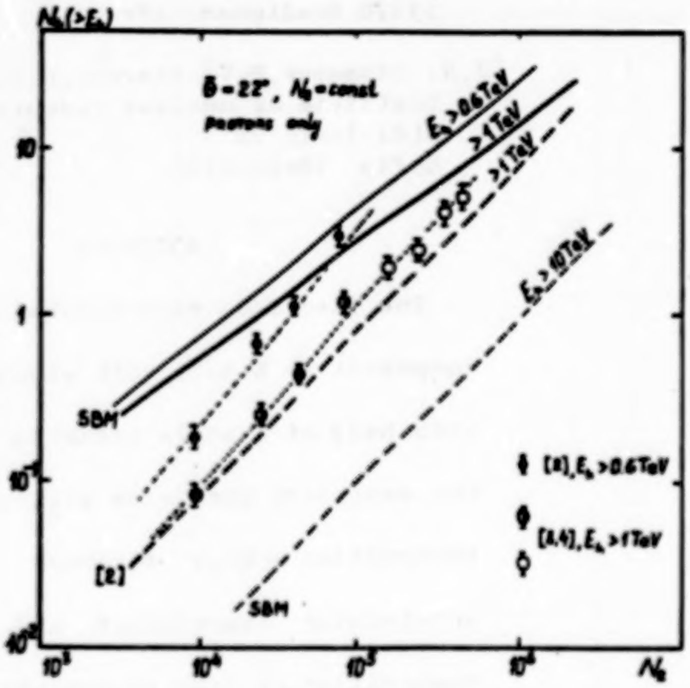

fig. 1

Their comparison with the results obtained by Erlykin et al. (2) and the analysis of the both models show that the main reason for the discrepances between the experimental and calculated curves lies in the adopted energy dependence of the secondary particles multiplicity :

$$\langle n_s \rangle = \alpha + \beta \ln s + \gamma (\ln s)^2 \quad (1)$$

For a better agreement with experiment, it is necessary to adopt a stronger energy dependence of the multiplicity. Indeed, our determination of $\langle n_s \rangle$ coming from the p-$\bar{p}$ collider is equivalent to $E^{0.13}$ whereas the multiplicity used in ref. (2) takes into account the p-air interaction and is $\langle n_s \rangle \alpha E^{0.25}$.

On fig. 2 are shown the integral energy spectra of hadrons for different fixed sizes and at observation level 700 g.cm^{-2}

It is seen that the calculated integral spectra $N_h(>E_h)$ become as expected harder with the rising of the size N_e.

The shape of the hadron energy spectra in E.A.S. is well described with calculation results, carried out with help of the used scale breaking model (1).

The correct agreement for the shape of these spectra is a good indication for the predominance of protons in the primary mass composition at energies 10^5-10^6 GeV.

ORIGINAL PAGE IS
OF POOR QUALITY

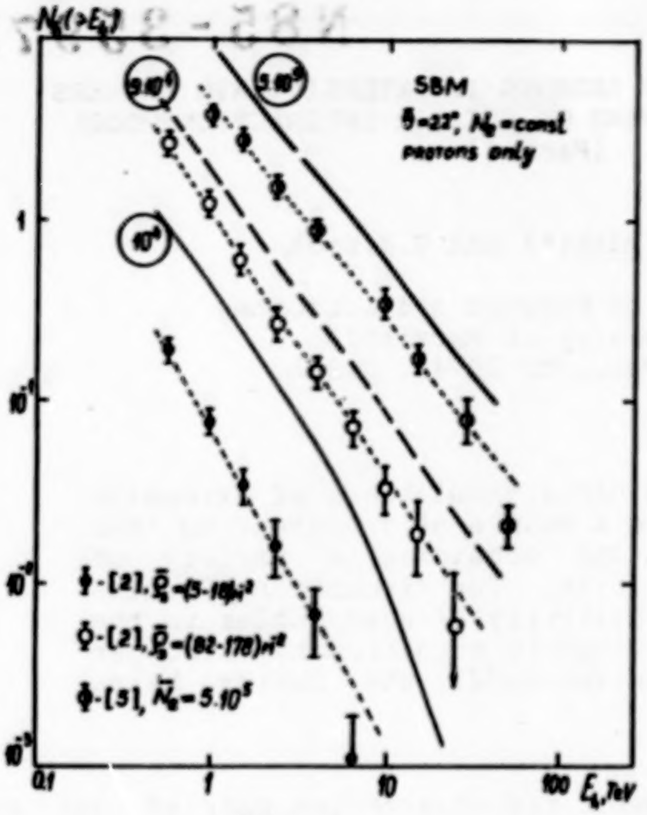

fig. 2

4. Conclusions

The analysis of Tien Shan hadron component data on the basis of the used scale breaking model shows that the average multiplicity $\langle n_s \rangle$ of secondary particles increases essentially more than predicted by the p-$\bar{p}$ collider, $\langle n_s \rangle \propto E^{0.13}$, under the supposition that the protons play the main role (5-6) in the primary mass composition for energies 10^5–10^6 GeV.

References.

(1) J. Procureur, J.N. Stamenov et al., 1985, to be published in J. Phys. G
(2) T.V. Danilova et al., 1984, Moscow, preprint FIAN n° 14
(3) V.S. Aseikin et al., 1982, Moscow, preprint FIAN n° 215
(4) N.M. Nesterova, A.G. Dubovy, 1979, Proc. 16th ICCR, Kyoto, 8, 345
(5) V.A. Romakhin, N.M. Nesterova, 1979, Trudy FIAN v 109, 77
(6) J.N. Stamenov et al., 1983, Proc. 18th ICCR, Bangalore OG4-11

N85-35972

ELECTRONS, MUONS AND HADRONS IN EXTENSIVE AIR SHOWERS AND HOW DO THEY DEPEND ON NUCLEAR INTERACTION MODEL
(Part I)

J.A.Wrotniak(*) and G.B.Yodh

Department of Physics and Astronomy
University of Maryland
College Park, MD 20742, U.S.A.

We performed Monte Carlo simulations of extensive air showers, using a couple of different nuclear interaction models and obtaining a variety of shower characteristics. The discussion of these shows, that the sensitivity of observables to the primary mass spectrum is significantly stronger than to the interaction model, the latter being quite weak.

The interpretation of cosmic ray observation carried out at various depths in the atmosphere requires detailed simulations of the propagation of nuclear-electromagnetic cascades generated by primary cosmic rays in the atmosphere. These calculations demand quantitative prescription for the following inputs necessary to carry out the simulation:

1. Chemical composition and energy spectrum of primary cosmic rays beyond where direct measurements were made (>50 TeV/nucleus);
2. Inclusive cross-sections for particle production in hadron-air nucleus collision at high energies - beyond (and not only, cf [1]) those available at SPS pp and Tevatron II;
3. High energy nucleus-nucleus cross-sections and fragmentation properties.

In addition, photons and electrons produced in the simulation tree must be propagated down to earth using electromagnetic theory and semi-empirical distribution functions. Thus the simulation is complex, multivariate enterprise. Quite often it is difficult to intercompare results from simulations of different groups because of not only disparity of the input,

---

(*) On leave from Łódź University, Poland.

(**) This work (and its continuation, HE 4.1-2) was supported in part by the U.S.National Science Foundation under Grant No. PHY 8207425

but also due to the simulation structure and algorithms.

In this paper together with HE 4.1-2 in this volume (see also [1]) we examine the sensitivity of air shower observations to changes in the interaction model and the nature of the primary by carrying out rather complete simulations over a wide energy range using the same program structure for shower generation, but changing the parameters, mostly one at a time, in the interaction models, for both proton and iron primaries. The energy range covered is from 20 TeV to 1 EeV (10**18eV). The interaction models vary from one with constant cross-section and scale invariant production distributions to a model with rapidly rising cross-section, large violation of scaling in both forward and central regions and charge exchange for the leading particle.

Nuclear interaction models

Particle production distributions in p-air and meson-air collisions are approximated by p-p and meson-p collisions. Two basic models of our variety are briefly compared in Table 1; the corresponding inclusive cross-sections are shown in Figs.1 and 2.

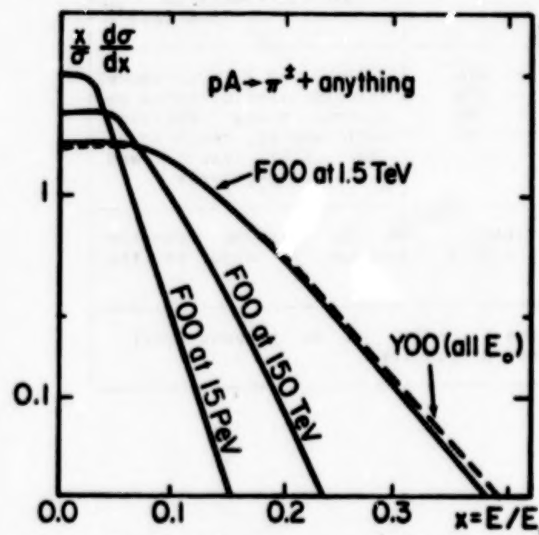

Fig.1. The distributions of $x=E/E$[int] for models used in our study.

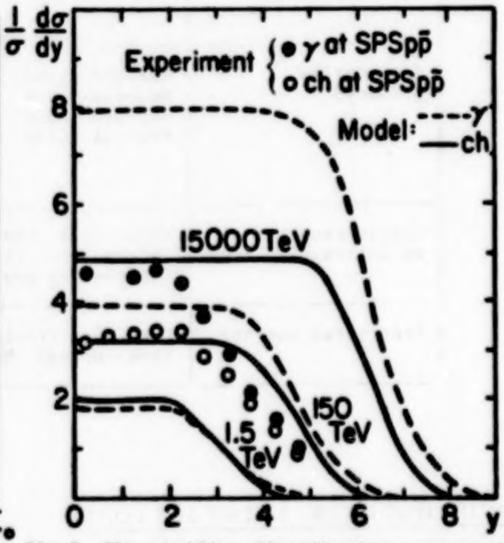

Fig.2. The rapidity distributions compared with pseudorapidity data from SPSpp.

Some other models were tried out, too, in order to check effects due to some particular differences in the assumptions:

- M-YOO - same as F-YOO, but the cross-sections in hadron-air interactions rise as in M-FOO (this is what the M before the hyphen means),

* M-F01 - adding a possibility of charge exchange to M-F00: interacting pion emerges from the collision with equal probabilities in any of three possible isospin states, and a kaon - in any of the four (the charge exchange possibility is denoted with the last "1" in the model notation),
* R-F01 - similar to M-F01, but with faster rise in cross sections: mean free paths for nucleons decrease in "M" case from 84 to 55 g/cm^2, and in "R" - from 86 to 37 g/cm^2 between 1 TeV and 1 EeV.

Table 1 Comparison of features of two basic models used.

	Model F-Y00	Model M-F00
Mean free paths for inelastic interaction	Energy-independent: nucleons: 75 g/cm^2 pions: 110 g/cm^2 kaons: 130 g/cm^2	Below 1 TeV nucleons: 84 g/cm^2 pions,kaons: 117 g/cm^2 Above 1 TeV $L(E) = L_0/(1+.0383*\mathrm{Ln}\ E)$
Inelasticity	Uniform in (0,1) for nucleons and (1/3,1) for mesons	
Inclusive distributions in x = E/E[interaction] for secondaries	Energy-independent: scaling extrapolation of the ISR data	Below 1 TeV as Y00; above: the functional shape is unchanged, but the scale x-value decreases as $1/E[\mathrm{int}]^{.125}$
Secondaries produced	Charged pions - 60% Neutral pions - 30% Charged kaons - 5% Neutral kaons - 5%	Below 1 TeV as Y00; above: the fractions of kaons and neutral pions increase with energy, reaching at 1EeV 6.8% (each) and 53.7%, respectively
Charge exchange of an interacting meson	None (i.e. the leading particle emerging from the interaction is always identical in kind to the interacting one)	
Transverse momenta	See [3]; irrelevant here, as we present only longitudinal EAS properties	

Nucleus-Nucleus interactions

For nuclei other than protons the interaction cross-sections had to be assumed, as well as some nucleus interaction/fragmentation model. Once again, the detailed description of the fragmentation algorithm may be found in [3]; it is based on the data compiled in [4] by J.E.Nowicka et al. The mean free paths for nucleus-air interaction were assumed in two different ways:

@ Energy-independent values [4] ranging from 37 g/cm^2 (alpha particles) to 16 g/cm^2 (iron). These were used for heavy nuclei-initiated EAS generated with model F-Y00, therefore denoted as FF-Y00;

@ R - rising cross-sections in Gaisser parametrization [2], consistent with "R" pA ones, e.g. for the iron group the mean free paths decrease from 12.2 to 10.6 g/cm^2 between 100 TeV and 1 EeV. These were used in combination with "M-" or "R-" models, therefore denoted as e.g. RM-F00 or RR-F01.

Other simulation assumptions

For hadrons and muons three-dimensional Monte-Carlo simulation was performed down to the threshold energy of 2 GeV (1 GeV for of pi-zeros). Photons and electrons emerging in the simulation tree were accounted for down to 170 MeV. However, the electromagnetic showers were followed the Monte-Carlo way only to a 200 GeV threshold; as soon as a photon or electron reached energy between 170 MeV and 200 GeV, the number of cascade electrons due to it was estimated from the Greissen formula. [This approach is more exact, than a non-Monte-Carlo treating of each electromagnetic shower from the very beginning].

The assumed cascade unit was 36.7 g/cm^2 and the critical energy - 84.2 MeV. (The c.u. value turned out to be quite important; changing it by just 1 g/cm^2 results in 6-7% change in 200 TeV shower sizes at sea level!). In the high-energy part (i.e.above 200 GeV) only pair creation, bremmstrahlung and Coulomb scattering were included into simulation.

As far as the main aim of this work was to check the model sensitivity, we limit this presentation to only vertical showers in the U.S.Standard atmosphere; the detection level was at the depth of 1000 g/cm^2.

Above 1 PeV initial energy, the thinning technique invented by Hillas [5] was used (to save the CPU time); performed checks proved, that this did not affect either the average values or the width of fluctuations (at least those checked by us).

The review of results obtained as described here may be found in our contribution HE 4.1-2 to this Conference.

References

1. J.A.Wrotniak and G.B.Yodh; HE 1.2-6 in the present volume
2. T.K.Gaisser et al.; 18th ICRC, Bangalore, 5, 174 [1983]
3. J.A.Wrotniak; SHOWERSIM/84, Univ.Md.Rep. PP 85-191 [1985]
4. J.E.Nowicka et al; Univ.Md.Rep. PP 85-190 [1985]
5. A.M.Hillas; 17th ICRC, Paris, 8, 193 [1981]

ORIGINAL PAGE IS
OF POOR QUALITY

SIMULATION OF EAS PROPERTIES ON THE BASIS OF HIGH ENERGY INTERACTION MODEL DEDUCED FROM THE ACCELERATOR DATA

G.Kubiak, J.Szabelska and J.Wdowczyk
Institute of Nuclear Studies
90-950 LODZ 1, Box 447
POLAND

A.W.Wolfendale
University of Durham, Durham DH1 3LE
ENGLAND

1. Introduction. Calculations of extensive air showers in atmosphere have been performed using formulae describing p-p and p-air nucleus interactions presented elsewhere in this proceedings /HE 1.2-4/. The formulae fitted to the accelerator data have been extrapolated taking the same trend up to 10^{16} eV. Above that energy it was assumed that the degree of scaling violation /α -parameter/ is saturating or even decreasing. The latter assumption follows from earlier work of some of us /Wdowczyk and Wolfendale, 1984/ where we found that without this restriction shower maxima at the highest energies are located too high in the atmosphere. Results of calculations have been compared with experimental data. The comparison was made separately for the curves obtained from the so called equal intensity cuts and for the Cerenkov data.

2. Method of calculations. In the first stage using Monte Carlo method there were calculated EAS longitudinal development curves for three different requirements. These requirements are: fixed primary energy, fixed size of shower at every observation level and fixed size at the sea level. Examples of the curves for proton primaries with energies around 10^{16} eV are given in figure 1. In the next stage the curves calculated for fixed sizes at every observation level and for different primary masses are combined according to the assumed mass composition. The mass composition have been taken according to the two component model of the galactic cosmic rays /Wdowczyk, 1984, also see OG 5.4-6 this proceedings/.

3. Results. In figure 2. the longitudinal development curves are compared with experimental data. In figure 3. the position of the shower maxima obtained from the equal intensity cuts are compared with predictions /here the predictions are taken for fixed shower sizes at the observation levels/. Finally in figure 4. the data on shower maxima positions obtained from the Cerenkov observations are compared with the predictions /in that case the predictions are taken for the fixed size at sea level as the observations are performed usually at sea level/. Separately are shown curves obtained under the assumption that the scaling violation parameter $\alpha = 0.25$ above 10^{16} eV and

ORIGINAL PAGE IS
OF POOR QUALITY

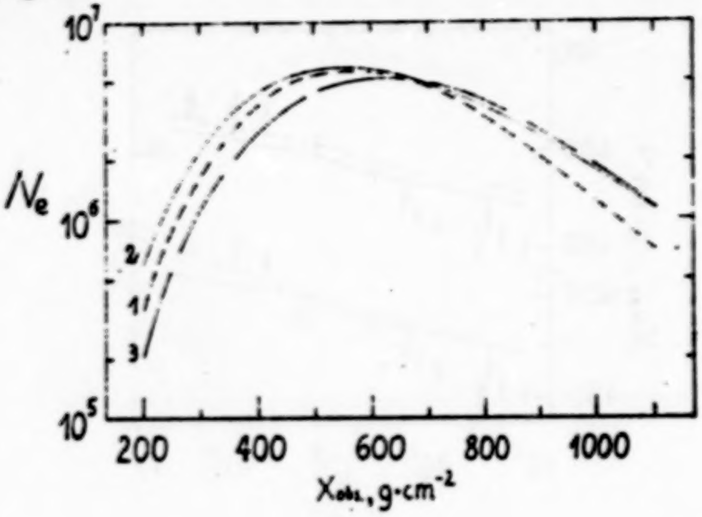

Fig.1. EAS longitudinal developement curves. 1-fixed primary energy, 2-fixed size of the shower at every observation level, 3-fixed size at sea level.

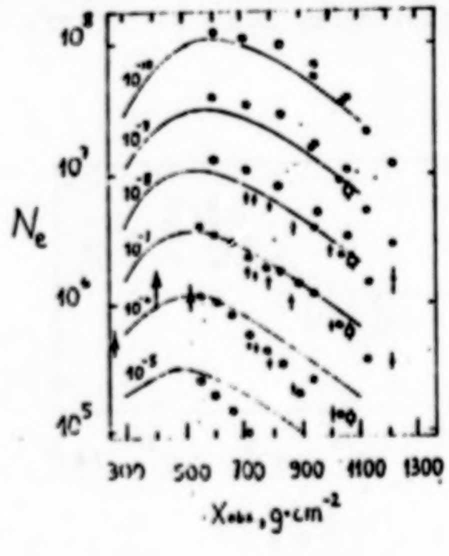

Fig.2. The longitudinal developement of EAS in the atmosphere obtained for proton-air nucleus interactions compared with the experimental data, see J.Gawin et al., /1984/.

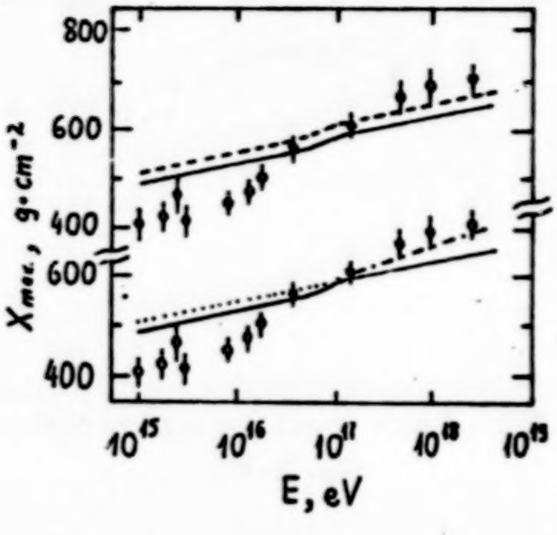

Fig.3. The positions of shower maxima. Calculations were performed with fixed shower sizes at every observation level.Experimental points are from equal intensity cuts.Predictions are from the following models: proton-proton interactions /– – –/,proton-air nucleus interactions with full mass composition /———/ and with primary protons only /····/, Scaling sets for energies higher then 1E16 eV /–··–/.

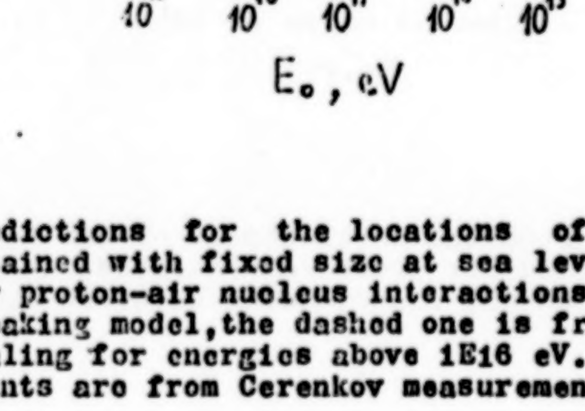

Fig.4. Predictions for the locations of shower maxima obtained with fixed size at sea level.Full line is for proton-air nucleus interactions with scale-breaking model,the dashed one is from the model with scaling for energies above 1E16 eV. The experimental points are from Cerenkov measurements.

assuming that effectively scaling sets at that energy.

In figures there are given results of calculations obtained with the farmula for proton - air nucleus interactions. In figure 3. for comparison there is also shown the development curve obtained using formula for proton-proton interactions /we may say for a proton atmosphere/.

4. Conclusions. If we use the model based on direct extrapolation of the accelerator data the predicted variation of the shower maximum position is different than that obtained from the observations. The predicted positions of shower maxima are located too low at energies 10^{15}-$3x10^{16}$ eV and too high for energies above. The situation can not be significantly improved by the variation of the primary particle mass as the used composition is already proton dominated at energies above 10^{16} eV and reasonably heavy below that energy.

Practically sufficient improvement is obtained if it is assumed that some sort of scaling is introduced above 10^{16} eV. By term of scaling we mean hare that the multiplicity of the secondary particles at these energies saturates.

It seems extremely difficult to restore the agreement with the data at energies 10^{15} - 10^{16} eV. Introduction of heavy particles here is not only insufficient but also contradictory with other observations /for instance multiple muons/. It seems that the observations require an assumption about existence of some new feature at energies around few times 10^{15} - 10^{16} eV. That reqirement is strengthened by the fact that the same tendency is observed both in the data obtained from the equal intensity cuts and those from the Cerenkov observations.

Important point which follows from the comparisons made in figures 3. and 4. is that the positions of shower maxima should be calculated differently for the case of the equal intensity cuts and for the case of the Cerenkov observations.

References

1. Gawin, J. et al., /1984/, Acta Universitatis Lodziensis, Folia Phisica 7, 59.
2. Wdowczyk, J., /1984/, Proceedings of the Int. School of Cosmic Ray Astrophysics, Erice, Sicily, November 4-15.
3. Wdowczyk, J., Wolfendale, A. W., /1984/, J. Phys., A: Nucl. Phys., 10, 257.

NEW ASPECTS IN NUCLEON-NUCLEUS COLLISIONS AND EAS PROPERTIES AROUND 10^6 GeV

N85-35974

J.N. Capdevielle
Laboratoire de Physique Théorique, Bordeaux, France

and

J. Gawin
Institute of Nuclear Studies, Lodz, Poland

1. Introduction

At energies higher than 2.10^5 GeV, we have very few information on detailed properties of nucleon-nucleon collision ; the rare elements are coming from "jets", and, as non direct improvements from γ-ray families. The results exhibit some conflicting features, or, at least, very large fluctuations like copious production of γ-rays in opposition to Centauro-like events,sometimes suggest that phase transition to quark gluon plasma occurs in nucleus-nucleus collisions and even in nucleon-nucleus collision (1) (2). The multicluster phenomenological model (MPM) is here extrapolated for EAS simulation up to 5.10^6 GeV to put in evidence some significant deviation between experimental data and prediction.

2. Extrapolation of short range order picture, nucleus-nucleus collision

The emission of small clusters from nucleon-nucleon collision is taken following (3) assuming always that the width of the plateau of rapidity is rising with Ln s (and also the height); the secondary particles are generated by decay of those clusters like in (4) but the truncated Poissonian distribution has been replaced by a Gaussian distribution. The width of this Gaussian has also been parametrized versus Ln s at ISR and $\bar{p}$-p energy and extrapolated in continuity of HE 4.1-9. The extension to p-air collision is also not different.

The most convenient was in this last case to generate directly the clusters from an inclined plateau, the rapidity of a cluster in CMS y_c being obtained from

$$\int_{-y_o}^{y_c} R(y)dy = \xi \int_{-y_o}^{y_o} R(y)dy$$

(ξ simple random number) and decay those clusters like for nucleon-nucleon collision in center of mass system. About KNO violation and asymptotic limit for fluctuations of multiplicity, as well as correlation between $< p_t >$ and central rapidity density we assume strict continuity with the previous description at energies higher than 2.10^5 GeV, as well as for proportion of different species $K^{\pm}$, $p,\bar{p}$ (taken as in ref. (1) of HE 4.1-9).

Nethertheless, we introduced here one variant in MPM concerning the production of secondary η mesons : herealso, a Ln s increase has been taken from the invariant mass distribution of the two-photon sample in UA2 experiment and the rate previously estimated in ISR. In this version, about half of the photons produced in a collision of 10^6 GeV are coming from η mesons (fig. 1).

A typical characteristic of the multicluster phenomenological model is the constant decrease of total inelasticity $< K >$ for nucleon-nucleon collision (underlined in HE 4.1-9) and consequently for p-air collision (fig. 1), estimated by summation of the energy carried by secondaries in Laboratory system.

The extension to nucleus-nucleus collision follows ref.(6) in HE 4.1-9 : the plateau of rapidity is transformed like for p-nucleus, assuming an increase of multiplicity in collision of nuclei A and B

$$R\left(\frac{AB}{PP}\right) \sim \tfrac{1}{2} < \nu_A > + < \nu_B > = \tfrac{1}{2} P$$

B being the air constituent target nucleus.(ν is defined as for p-nucleus and P is the number of participating nucleons). In the EAS Monte-Carlo simulation, we have treated separately the contribution coming directly from the participating nucleons and the contribution governed by the behaviour of the "spectators".

3. Comparison with experimental data

We obtain with 5 GeV muon in Tian-Shan a better agreement than with models previously used (fig.2, 4.1-9) ; muon content after 10^6 GeV deviates from MPM, but if we consider the version assuming η meson production the agreement is restored up to $5 \cdot 10^6$ GeV. This can be explained by the larger number of γ's produced in the η channels decay with lower individual energies than in π^0 decay.The muon of 220 GeV are also in agreement with KGF data (fig. 3 HE 4.1-9) and Moscow data for muons of the same energy (5); the flattening in the experiment after $N_e = 10^6$ is up to now not confirmed in Moscow and it could be an effect of the small statistics. Very good agreement is also obtained at Tian-Shan level for high energy hadrons, and also for the $< E_H r_H >$ factor (fig. 2). Up to now, $< E_H r_H >$ was decreasing with energy with a majority of models but in one case, including decrease of $< K >$ versus rising s (6). We note that in MPM this circumstance is also the cause of the large number of energetic hadrons surviving at Tian-Shan altitude.

Satisfactory situation appears also for maximum depth T_{max} versus energy (fig. 3); for instance, T_{max} near 10^6 GeV is measured near 520 $g.cm^{-2}$ by Cerenkow method (5) when MPM gives 550 $g.cm^{-2}$ for proton. We observe that the maximum depth from Cerenkow measurements is located at deeper altitude than in previous experiments with lower number of detectors and smaller resolution. If η meson production is assumed, the maximum depth decreases by about 35g. cm^{-2}. Furthermore, very good agreement is obtained with the most recent data on T_{max} measurements (7).

4. Conclusion

If we consider the good agreement obtained with age parameter data in Akeno (HE 4.3-13), we can conclude that the multicluster phenomenological model gives an acceptable description of EAS data and can be extended at least at one decade higher than the $\bar{p}$-p energy. If we include η meson production, it can be even accepted at energies near 10^7 GeV. A rise of rapidity plateau in Ln s (simultaneously in width and height) appears sufficient and

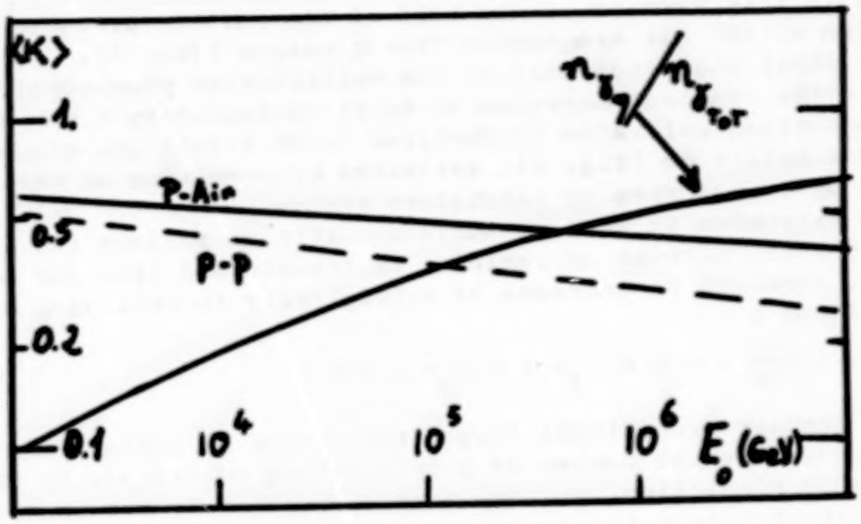
⟨K⟩
1.
0.5
0.2
0.1
$n_{\gamma_\gamma}/n_{\gamma_{TOT}}$
P-Air
P-P
10^4
10^5
10^6
E_0 (GeV)

Fig. 1

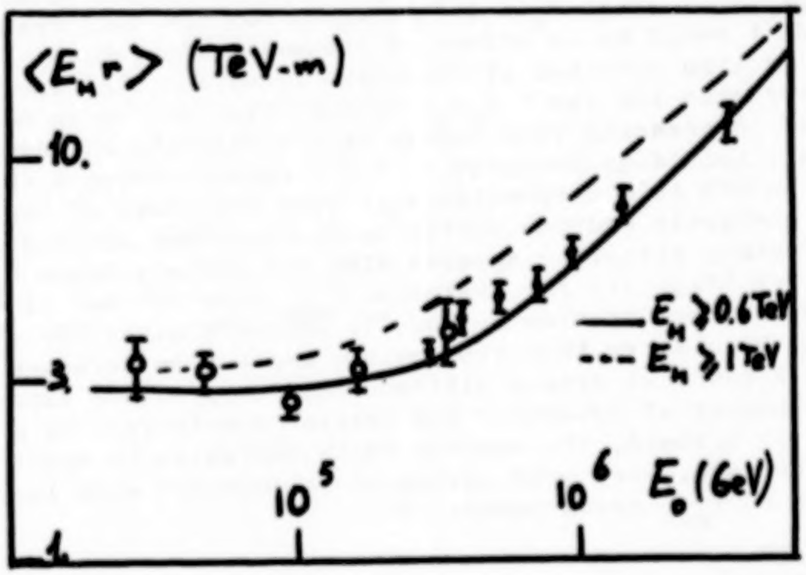
⟨$E_H r$⟩ (TeV.m)
10.
3.
1.
10^5
10^6
E_0 (GeV)
$E_H \geq 0.6$ TeV
$E_H \geq 1$ TeV

Fig. 2

ORIGINAL PAGE IS
OF POOR QUALITY

differently with previous models we don't need any exotic change in composition or in multiplicity to explain in this kinematical range the experimental data. At least, it appears no necessity of any enhancement of heavy nuclei in primary component. A very large fraction of the rapidity plateau is compatible, and, may be, only in the central region we cannot exclude a more important rise of rapidity density.

References

1. J.N. Capdevielle et al., 1984, J.Phys. G10, 705.
2. A. Faessler, 1983, Nucl.Phys. A400, 578c.
3. B. Degrange, 1985, private communication, Paris.
4. K. Alpgard et al., 1983, Phys.Lett. 123B, 108.
5. G.B. Kristiansen, 1984, private communication, Moscow.
6. A. Antonov et al., 1984, Proc.Symp. Cosmic ray and particle physics, Tokyo, 431.
7. N. Inoue et al., 1985, J.Phys. G11, 657.

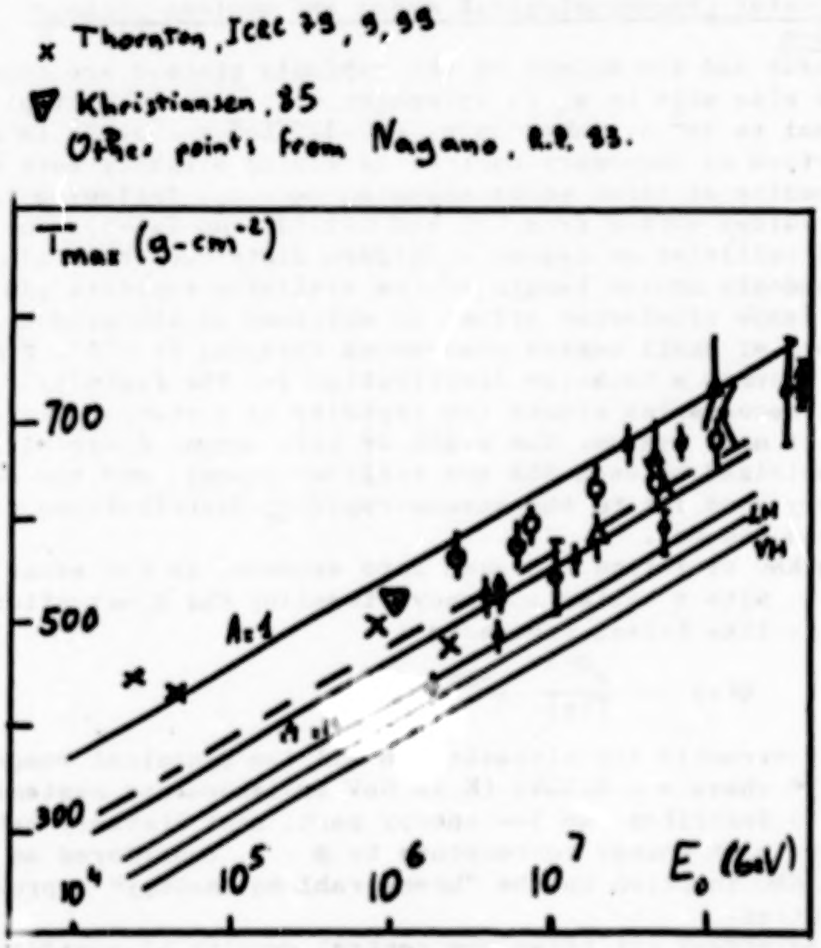

Fig. 3

SMALL AIR SHOWERS AND COLLIDER PHYSICS

N85-35975

J.N. Capdevielle
Laboratoire de Physique Théorique, Bordeaux, France
and
J. Gawin, B. Grochalska
Institute of Nuclear Studies, Lodz, Poland

1. Introduction

At energies lower than 2.10^5 GeV (in Lab. system), we have now more accurate information on nucleon-nucleon collision ($\bar{p}$-p collider (1)) and on primary composition (JACEE data (2)). The behaviour of those both basic elements in cosmic ray phenomenology from ISR energy suggests some tendencies for reasonable extrapolation in the next decade 2.10^5 - 2.10^6 GeV (paper HE 4.1-10).

Small showers in altitude, recorded in the decade 2.10^4-2.10^5 GeV offers a good tool to testify the validity of all the Monte-Carlo simulation analysis and appreciate how nucleon-air collision are different from nucleon-nucleon collisions.

2. Multicluster phenomenological model and nucleon-nucleus collision

The width and the height of the rapidity plateau are together assumed to rise with Ln s, in agreement with a total multiplicity proportional to $\ln^2$ s, taken as $n_s = 0.127 \text{ Ln}^2 s + 0.584 \text{ Ln } s + 0.57$. The proportion of secondary neutral is rising slightly more rapidly, on the opposite of other works assuming $n_\gamma = n_s$, following the numerical values quoted from UA5 and UA1 (1) (HE 5.1-5). For each individual collision we assume a uniform distribution of clusters, choosen randomly on the length of the available rapidity plateau. The short range clustering effect is obtained by the production in large number of small masses resonances decaying in $\pi^+\pi^-$, $\pi^+\pi^o$,... (K=2). We assumed a Gaussian distribution for the rapidity of the individual secondaries around the rapidity of corresponding cluster in center of mass system. The width of this normal distribution has been parametrized between ISR and collider energy, and the model gives a very good fit to the pseudo-rapidity distributions at E_{cm} = 53 and 540 GeV.

Strong KNO violation is taken into account, in the sense shown in HE 5.1-5, with a better accuracy, treating the fluctuations of multiplicity like Erlang processes :

$$\Psi(z) \sim \frac{z^{\alpha-1}}{\Gamma(z)} e^{-\alpha z}$$

describing correctly the situation in all the dynamical range if $\alpha = 100 \, aE^{-a}$ where a = 0.1042 (E in GeV in laboratory system). The values $\alpha = 6$ describes the low energy part, near Slattery behaviour and the very high energy corresponds to $\alpha = 2$, considered as an asymptotic KNO function in the "bremstrahlung analogy" approach to multiproduction.

For each individual collision the central density of rapidity ρ_o is estimated by counting the secondaries contained in 2/3 of the plateau length and the average $< p_t >$ is correlated with ρ_o(3)

according to

$$< p_t > = \frac{C}{[-e^z E_i(-z)]^{\gamma}}$$

($C = 0.38$ GeV/c, $\gamma = \frac{1}{8}$ at 155 TeV and here $z = \frac{\pi}{4}[n/\bar{n}(s)]^2$), the the invariant cross section being parametrized by the same formula for π's and K's in function of the transverse mass $m_T = \sqrt{m^2+p_t^2}$.

We observed that the model described up to here reproduced also the decrease of inelasticity by 30% between ISR and $\bar{p}$-p collider, after summation of the energies $E_i = m_T \cosh y_i$ carried by individual secondaries (E_i, y_i in Lab. system) (4).

The model is extended to hadron-air collision by introducing the number of participating nucleons $< \nu > = A \; (\sigma_{in}^{pp}/\sigma_{in}^{pA} = 1.325 + 0.0543 \ln E$ established from hadron-nucleus data (5) (6) with $R_A = < n(pA)>/< n(pp)> \sim \frac{1}{2}(< \nu > + 1)$. Considering rapidity distribution normalized by rapidity distributions of p-p interactions of the same energy, we describe the rate

$$R(y) = \frac{(dn/dy)_{p\text{-}Air}}{(dn/dy)_{p\text{-}p}} \sim my + m_o$$

on plateau basis ($m_o = \rho_A/\rho_o$) and finally generate directly the clusters from the corresponding "inclined plateau" ; the value R(y) obtained by the adapted Monte-Carlo procedure for all secondaries is shown on fig. 1 for 3000 p-air collisions with $E = 10^6$ GeV.

For hadron-nucleus collision we adopt $< p_t >_{p\text{-}A} = < p_t >_{p\text{-}p}$ as predicted by dual parton model (7) and fluctuations of multiplicity similar to p-p collisions. We refer hereafter this model as MPM (multicluster phenomenological model).

3.Comparison with Tian-Shan and KGF data (8,9)

Mixed component is taken as energy constant with 39.5% nucleons, 28.7% α, 13.5% CNO, 11.5% LH, 6.9% iron groups, with $\gamma = 2.7$ (2). The situation is shown in fig. 2 for MPM and nucleons, as well as for MPM and mixed. (The extension to nucleus-nucleus collision and the introduction of secondary η-mesons are discussed in HE 4.1-10), and also in fig. 3 for 220 GeV muons recorded in KGF (for nucleons primary only). The hadron behaviour versus size is shown on fig. 4 for $E_H > 0.6$ TeV and $E_H \geqslant 1$ TeV at Tian Shan level.

4. Conclusion

The multicluster phenomenological model, adapted to p-air collision is in surprising good agreement with EAS data at energy smaller than 2.10^5 GeV ; this agreement is obtained without an increase of primary mass or multiplicity, even for higher energy muons in KGF (220 GeV) and high energy hadrons (0.6 to 1 TeV), suggesting agreement non only in central region, but in all the dynamical rapidity range.

5. Aknowledgements J.N.C. is indebted to Professor B. Degrange for drawing his attention on multicluster models.

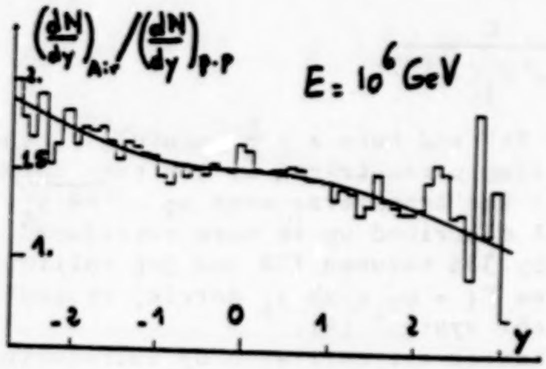

Fig. 1

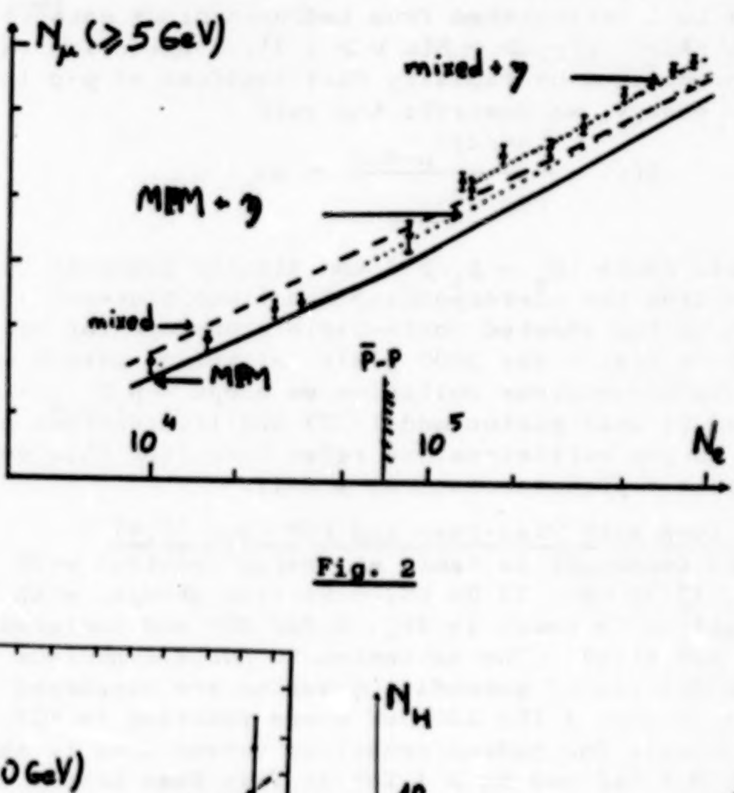

Fig. 2

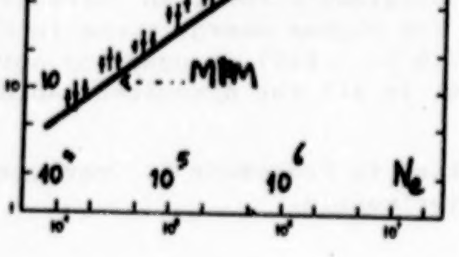

Fig. 3

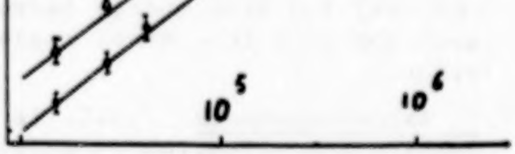

Fig. 4

References

1. P. Carlson, 1983, Proc. 17th Inter. Winter meeting on fundamental Physics, JEN Madrid, 11.
2. JADE collaboration, 1984, Burnett T.H. et al., Int. Symp.Cosmic rays and particle Physics, Tokyo, 468.
3. S. Barshay, 1984,Phys.Rev. D29, 1010.
4. G.N. Fowler et al., 1984, Phys.Lett. 145B, 407.
5. J.E. Elias et al.,1980, Phys.Rev. D22, 13.
6. M.A. Faessler, 1984, CERN EP/84-165.
7. C. Pajares, 1983, Proc. 11th Int. Winter meeting on fundamental Physics, JEN Madrid, 257.
8. V. Aseikin et al., 81, 1982, FIAN reprint 178 and 215.
9. B.S. Acharya, 1983, Ph.D. Thesis, Tata Institute, Bombay.

HIGH ENERGY HADRONS IN EXTENSIVE AIR SHOWERS

N85-35976

S.C. Tonwar

Tata Institute of Fundamental Research
Homi Bhabha Marg, Colaba, Bombay-400 005
India

ABSTRACT

Experimental data on the high energy hadronic component in extensive air showers of energies ~ 10^{14} - 10^{16} eV, when compared with expectations from Monte Carlo simulations have shown the observed showers to be deficient in high energy hadrons relative to simulated showers. We attempt here to understand these anamalous features with more accurate comparison of observations with expectations, taking into account the details of the experimental system. Results obtained from this analysis and their implications for the high energy physics of particle interactions at energies ~ 10^{15} eV are presented.

Studies on the characteristics of particle interactions at energies above those available at particle accelerators are being carried out either with emulsion chambers at mountain altitudes or through experiments on the high energy hadron component in extensive air showers. Results obtained on the hadron component in air showers of energies ~ 10^{14} - 10^{16} eV over the last 15 years or so have presented a baffling picture. Initial attempts to interpret the observed characteristics of high energy hadron component in EAS were undermined by the apparent large differences between the results reported by different groups. However, during the last few years, our group[1,2] has been able to show that these differences are mostly due to instrumental facters and there indeed is a basic disagreement between the experimental results and the expectations from Monte Carlo simulations which use data available from CERN $\bar{P}P$ experiments. These disagreements relate to (i) the number of high energy hadrons per shower and(ii) the charged to neutral ratio among these hadrons. The present situation regarding the comparison between experimental results from four groups and our simulations[1] is shown in figure 1. It is seen from this figure that the most accurate measurements (represented by the line RHV) made using multiplate cloud chamber show the observed number of hadrons in a shower to be almost an order of magnitude smaller than the expected number. Electronic detectors (like single layer scintillators used as burst detectors), which integrate partially the energies of hadrons incident over the hadron detector, represented by lines RVS and BVS, expectedly overestimate the number compared to the measurements made with multiplate cloud chamber. Large area hadron calorimeters which integrate over the energies of the

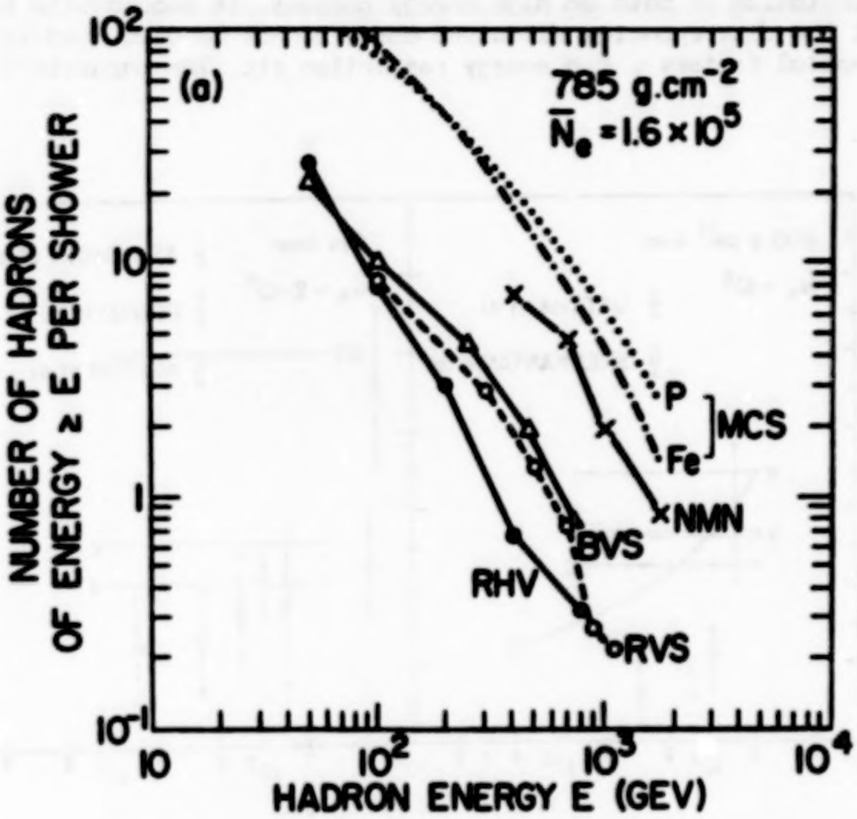

Figure 1 : Comparison of the observed integral energy spectrum for high energy hadrons in air showers of average size ~1.6 x 10^5 at mountain altitudes (from reference 1)

hadrons incident over the detector fully, represented by the line NMN, give a much larger number for the high energy hadrons as expected.

It is clear from figure 1 that some major changes are required in interaction model at energies ~ 10^6 GeV to account for this large discrepancy. A constraint on the range of models that can be proposed to account for this discrepancy is imposed by the observed charged to neutral ratio[2] for these high energy hadrons at mountain altitudes as shown in figure 2. It is seen from this figure that the observed C/N ratio is less than half of the value expected from simula--tions. Since charged pions constitute the largest component of the charged hadrons, protons and charged kaons being much smaller in number and neutrons and neutral kaons constitute most of the neutral hadrons, the results fron C/N ratio suggest that dominance of pions among secondary particles may be less in interactions at air shower energies. Of course, another cosntraint on the range of models is imposed by the fact that observations on electron and muon components in air showers seem to agree well with expectations[3]. It should be remarked here that

our lack of firm knowledge of primary composition at air shower energies which plays a very significant role in interpretation of observations on electron and muon components, does not have any important role in the interpretation of data on high energy hadrons. It should also be noted that the discrepancies discussed above cannot be accounted in terms of experimental factors , e.g energy resolution etc. The parameters that are readily available for changing the interaction model, without invoking an altogether new type of interaction such as suggested by the observat--ations[4] of Chirons, Geminions, and Centauros, etc. type of events in emulsion chamber experiments at mountain altitudes, are (i) interaction cross-sections, (ii) composition of secondary particles, (iii) transverse momentum distributions, and (iv) longitudinal momentum distributions. Note that the average multiplicity as well as its distribution are essentially controlled by the forms of distributions for (iii) and (iv). The simulations already incorporate the increase in cross-sections[5] consistent with observations upto $\bar{P}P$ Collider energies and in fact are consistent with observations upto the highest energies $\sim 10^{18}$ eV. Changing the composition of secondary particles towards lowering the pion content among secondaries and increasing the baryon content helps in reducing the C/N ratio but does not reduce the expected number of high energy hadrons significantly. The fact that large p_t tail and jets seem to play an important role at very high energies has already been

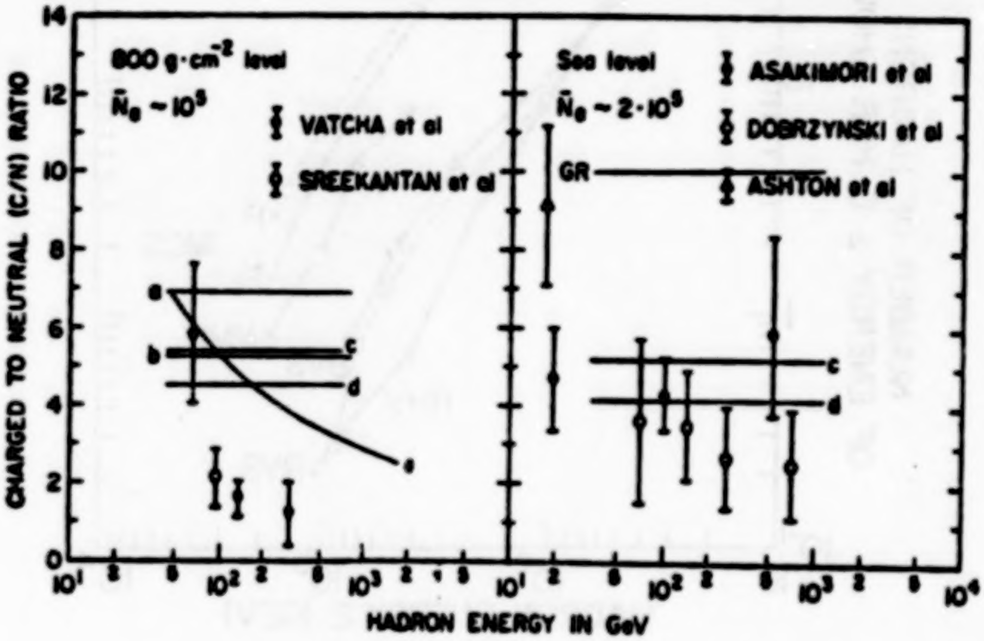

Figure 2: Comparison of the observed charged to neutral (C/N) ratio with expectations from simulations as a function of the hadron energy (from reference 2)

incorporated in the calculations, though not specifically as jets but as an energy dependent component of large p_t particles. It may also be noted here that consistency of the observed lateral distribution of hadrons with simulations approximately, poses same restraints on the range of large p_t cross-section that can be assumed. Softer x distribution is being tried in simulations at present and analysis is being carried out of showers simulated with various assumptions. Progress in this work will be discussed at the Conference.

ACKNOWLEDGEMENT

It is a pleasure to thank Prof. B.V. Sreekantan for many fruitful discussions.

REFERENCES:

1. Sreekantan, B.V., S.C. Tonwar, and P.R. Viswanath, Phys. Rev. D 28, 1050 (1983)
2. S.C. Tonwar, in Proton-Antiproton Collider Physics-1981, proceedings of the Workshop on Forward Collider Physics, Madison, eds. V.Barger, D.Cline, and F. Halzen (AIP, New York, 1982), p.562.
3. G.B. Yodh et al, Phys. Rev. D 29, 892 (1984)
4. S. Hasegawa, Proceedings of International Symposium on Cosmic Rays and Particle Physics, Tokyo, 1984, eds. A. Ohsawa and T. Yuda (Institute for Cosmic Ray Research, Tokyo, 1984), p.718
5. S.C. Tonwar, preprint (1985).

N85-35977

DEPENDENCE OF THE AVERAGE SPATIAL AND ENERGY CHARACTERISTICS OF THE HADRON-LEPTON CASCADE ON THE STRONG INTERACTION PARAMETERS AT SUPERHIGH ENERGIES

N.G.BOYADJIAN, P.YU.DALLAKYAN, A.P.GARYAKA,
E.A.MAMIDJANIAN

Yerevan Physics Institute, Markarian st. 2
375036, Yerevan, Armenia, USSR

ABSTRACT

A method for calculating the average spatial and energy characteristics of hadron-lepton cascades in the atmosphere is described. The results of calculations for various strong interaction models of primary protons and nuclei are presented. The sensitivity of the experimentally observed EAS characteristics to variations of the elementary act parameters is analyzed.

The theoretical analysis of hadron-lepton cascade propagation in the atmosphere is possible at present by two methods: a) Monte-Carlo cascade simulation; b) solving the set of kinetic equations. Despite the advantages, the Monte-Carlo method is at the same time the most cumbersome and demands much computer time. The main drawback of the second method is that shower characteristics for fixed primary energy are obtained, whereas in the experiment the showers with fixed N_e are studied. However the comparison of the results obtained by both methods shows that the dependence of the average shower characteristics on the strong interaction parameters turns out to be qualitatively the same, while the quantitative difference is small. As an example of this, we may point out the conclusion that the average experimental characteristics of EAS can be described using the strong interaction model with increasing cross sections, growing plateau in the pionisation region and asymptotic scaling in the fragmentation region; this conclusion, being made from the solution of diffusion equations /1/, was confirmed by the Monte-Carlo simulation results /2/.

In the present paper we describe a method of solving the three-dimensional set of kinetic equations for shower components, based on the calculation of the contributions from the successive generations by Monte-Carlo evaluation of the corresponding multidimensional integrals.

The integral spectrum of the (i + 1)-th pion generation in EAS for depth Z and primary energy E_0 can be presented in the form:

$$\Pi_{i+1}(>E,z) = \int \frac{dz'}{\lambda_\pi} e^{-\frac{z-z'}{\lambda_\pi}} \int\limits_{E_{i+1}>E} \frac{d^3p_{i+1}}{E_{i+1}} \; \frac{d^3p_i}{E_i} * \tag{1}$$

$$* [N_i(\vec{P}_i, z') f_{\pi N}(\vec{P}_{i+1}, \vec{P}_i) + \Pi_i(\vec{P}_i, z') f_{\pi\pi}(\vec{P}_{i+1}, \vec{P}_i)$$

where $\Pi(>E, z)$, $\Pi(\vec{p}, z)$ and $N(\vec{p}, z)$ are the integral and differential momentum spectra of pions and nucleons at depth Z, and $f_{\pi N}(\vec{p}, \vec{p}_0)$ and $f_{\pi\pi}(\vec{p}, \vec{p}_0)$ are the invariant inclusive spectra of pion production in NA and πA interactions. The expressions for the nucleon and muon spectra can be written in the same manner. For Monte-Carlo computation of integral (1) a set of interaction depths in the atmosphere and particle momenta are randomly simulated. From the known momenta and depths, we calculate the diatance from the shower axis to the particle's arrival point at the observation level. The value of the integrand is calculated for the simulated set. Further on, knowing the energy and the distance of the particle from the axis, we can obtain the integral and differential spectra over E and r . The spatial distribution function (SDF) of electrons is obtained multiplying the γ -production spectrum $\Gamma(E, z, r)$ by the SDF for photon initiated showers in the approximation of ref./3/. The accuracy of the calculation of the integral depends on the variance and the number of simulations of the integrand values. The integral was smoothed to minimize the dispersion. The method will be described in detail in a forthcoming paper.

This work presents the results of calculations for the models of multiple production. The first one is the so-called "standard" model of the scaling type, where the inclusive spectra are taken in the Hillas parametrization /4/, and $\langle p_\perp \rangle = 0.37$ GeV. The second is the model of quark-gluon jets /5/, where the target nuclei effects are taken into account according to ref./6/. In this model, as is well known, there takes place the cross section rise, the plateau grows and the scaling is weakly violated in the fragmentation region. In this model the spectra differ quantitatively from those used earlier, mainly in the fragmentation region. The mean transverse momentum in this model increases logarithmically with energy.

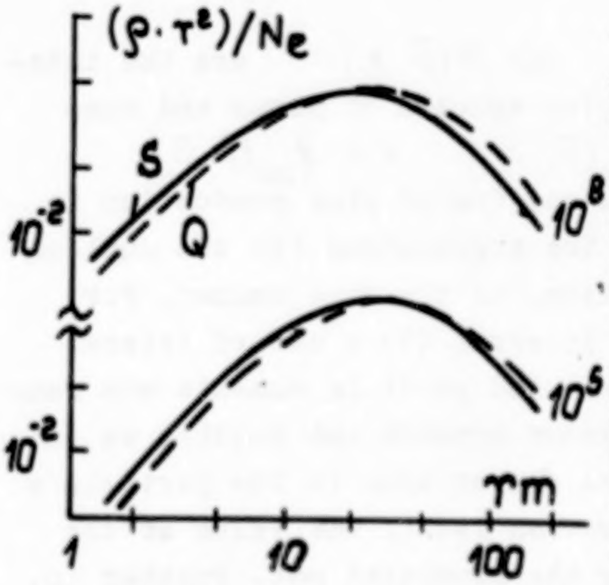

Fig. 1

Figure 1 shows the radial distribution of $\rho_e \cdot r^2/N_e$, where $\rho_e(r)$ is the SDF at 700 g/cm^2. The figures near the curves denote the primary energy in GeV. S labels the "standard" model curve, Q - the models of the quark-gluon jets. The curves differ insignificantly, since the SDF of EAS is mostly due to the electromagnetic interactions. However in the model a more rapid energy dissipation takes place and the SDF is a bit wider.

Figure 2 presents hadron and muon distribution in a circle of radius   with E > 5 GeV. The same is shown in

Fig.3 for an energy cut-off 1 TeV. The small energy particles number and the SDF show weak moel dependence. As expected, the high-energy hadrons are concentrated in the narrow region near the shower axis. The same is true for high-energy muons. The SDF of high-energy hadrons is the most model-dependent characteristic. In the Q model the total number of muons with energy > 5 GeV is greater than in the S model, whereas the number of muons with E > 1 TeV is almost the same but the SDF in the Q model is wider which is due to both rise of the cross section and the average transverse momentum. The total number of hadrons with E > 1 TeV is larger in the S model as compared to that in the Q model by a factor of ~ 2.5 in the range of E_0 and r .

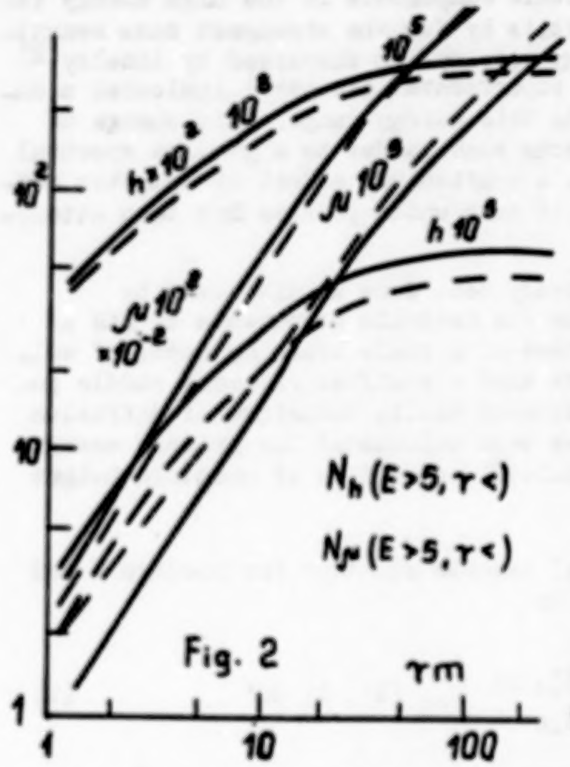

Fig. 2

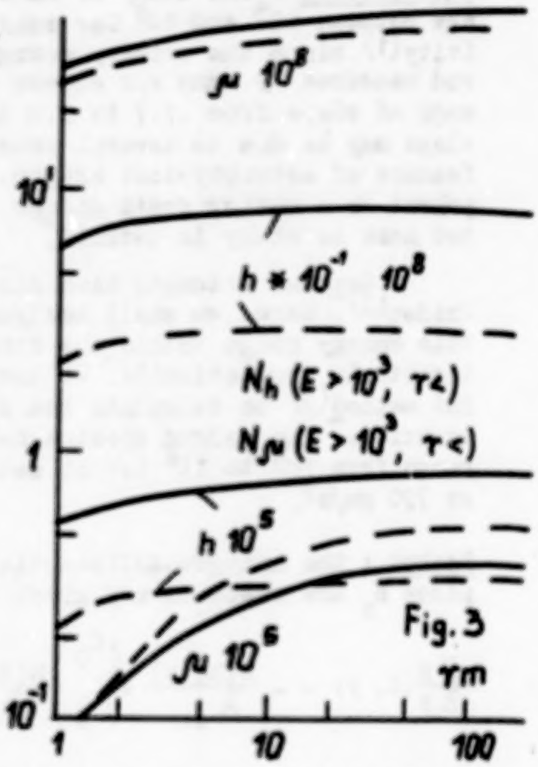

Fig. 3

The authors are indebted to the participants of the ANI-84 workshop for useful discussions.

REFERENCES

/1/ Boyadjian N.G. et al. Proc.17th ICRC,Paris,1981,6,280.
/2/ Kalmykov N.,Khristiansen G. Proc.18th ICRC,1983,7,330.
/3/ Lagutin A.A. et al. Proc.16th ICRC,Kyoto,1979,7,18.
/4/ Hillas A. Proc.Workshop on Casc.Simul.,Paris,1981,p.13.
/5/ Kaidalov A.,Ter-Martirosian K. Yad.Fiz.,1984,39,545;40,211.
/6/ Anisovich V.V. et al. Yad.Fiz.,1984,39,932.

HADRONIC COMPONENTS OF EAS BY RIGOROUS SADDLE POINT METHOD IN THE ENERGY RANGE BETWEEN 10^5 AND 10^8 GEV.

N85-35978

Malabika Sinha and Sisir Roy
Indian Statistical Institute
Calcutta 700035, India

Introduction : The study of hadronic components in the high energy range between 10^5 and 10^8 Gev exhibits by far the strongest mass sensitivity(1) since the primary energy spectrum as discussed by Linsley(2) and measured by many air shower experimental groups(3) indicates a change of slope from -1.7 to 2.0 in this energy range. This change of slope may be due to several reasons such as due to a genuine spectral feature of astrophysical origin, a confinement effect of galactic component or a rather rapid change of mass which problem has been attempted here to study in details.

Several attempts have already been done as discussed by Grider(3). Here, we shall analyse the hadronic components of EAS at this energy range within the scheme of a scale breaking model of multiparticle production(4). We have used a modified rigorous saddle point method(5) to calculate the inverse Mellin transform of diffusion equations. The hadron spectra has been calculated for primary energy range from 10^5 to 10^8 Gev at sea-level as well as at mountain height at 720 gm/m^2.

Method : The integro-differential cascade equation for nucleon N and pions N_π are respectively given by

$$\frac{\partial N}{\partial y}(E, y) = -\frac{N(E, y)}{\lambda_{in}} + \int_E^{E_0} \frac{N(E', y)}{\lambda_{in}} W_{NN}(E', E)\, dE' \tag{1}$$

$$\frac{\partial N_\pi}{\partial y}(E, y) = -\left(\frac{1}{\lambda_{in}} + \frac{B}{Ey}\right) N_\pi(E, y) + \int_E^{E_0} \frac{N(E', y)}{\lambda_{in}} W_{N\pi}(E, E')\, dE' + \int_E^{E_0} \frac{N_\pi(E', y)}{\lambda_{in}} W_{\pi\pi}(E', E)\, dE' \tag{2}$$

For simplification, we have considered (i) the nucleon interaction length $\lambda_N \approx$ pion interaction length λ_π at high energy(6). (ii) Limiting fragmentation is assumed to hold for F_{NN}. The unknown function $N_\pi(E, y)$ can be expressed in the form

$$N_\pi = n_\pi(E, y)\, e^{-y/\lambda_\pi} = n_\pi(E, y)\, e^{-y'} \tag{3}$$

ORIGINAL PAGE IS
OF POOR QUALITY

Let $\sigma_{in} = \sigma_{in} (1 + a \ln E/100)$ (4)

i.e. $\frac{1}{\lambda_\pi} = (1 + a \ln E/100)$ where $a \simeq .037$.

Initially, this rigorous saddle point method was proposed for scaling model(5) where

$$n_\pi + N_n = \frac{C_0}{E}\sqrt{\frac{\pi}{y'}}\, e^{y' (g(s) - 1) - \bar{s}_0 \ln w} \tag{5}$$

So is given by $\frac{dg}{ds}\Big|_{s = s_0} = \frac{\ln w}{y'}$ and $\bar{s}_0$ by $= s_0 - ay' + 1$

But according to our model the inclusive cross-section and the average multiplicity are given by

$$\frac{1}{\sigma_{in-el}} E \frac{d\sigma}{d^3p}\Bigg|_{pp \to \pi \bar{x}} \simeq \frac{9}{\langle n \rangle \pi^-} \cdot \frac{25}{4} \cdot \frac{1}{4\pi} \frac{f_\rho \pi w}{16\pi^2} \exp[- \frac{26.88}{\langle n \rangle_{\pi^-}} \cdot \frac{P_T^2}{(1-x)}]$$

$$\exp [- 2.38 \langle n \rangle_{\pi^-} x] \frac{mb}{Gev^2} \tag{6}$$

where $\langle n \rangle_{\pi^+ pp} = \langle n \rangle_{\pi^- pp} = \langle n \rangle_{\pi^0} = 0.35 S^{\frac{1}{3}}$ (S in Gev^2)

Thus $F_{N\pi} = 1.06\, e^{-2.38 \langle n \rangle_\pi \cdot x}$

$$F_{\pi\pi} = 1.062\, e^{-2.38 \times 5/9 \langle n \rangle_\pi . x}$$

Now at high energy we can write $F_{N\pi} = 1.06\, e^{-2.38 . 2^{\frac{1}{3}} x^{\frac{1}{3}} E_0^{\frac{1}{3}}}$ (7)

where $E/E' \sim E/E_0$.

Here x be the Feynman scaling variable as used in the previous paper on saddle point method(5). So we can use the previous method to our case also. Now after some calculations it can be shown that s_0 admits of an approximate representation in terms of gamma function i.e.

$$\frac{dg}{ds}\Big|_{s = s_0} = \frac{\ln w}{y'}$$

Here the following approximation has been taken for gamma function

$$(s) = 1 + a_1(s - 1) + a_2 (s - 1)^2 + a_3 (s - 1)^3 + a_4 (s - 1)^4 + a_5(s - 1)^5$$

where $a_1 = 0.5748$, $a_2 = 0.95123$, $a_3 = - 0.699$, $a_4 = 0.4245$
$a_5 = - 0.10106$.

Results : In Fig.1, the several data are shown together with the hadron spectrum obtainted by us from our model and also with that calculated by Grieder. These data cover a large size range centred around Ne = 10^5 and this corresponds to primary energy 10^6 Gev. So different types of detecting system with large size window, explain this large dispersion of data.

But even with this dispersion we can emphasise from the comparison of these data with our prediction for iron and proton initiated showers of same total energy i.e. 10^6 Gev, that this energy range of primary spectrum can not be dominated by iron nuclei.

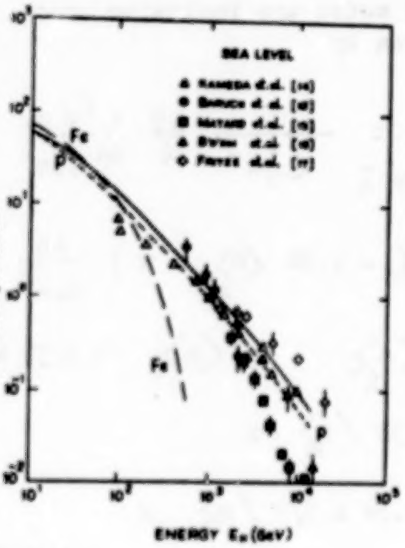

FIG.1

Hadron energy spectra at sea level in proton initiated showers of 10^6 Gev primary energy obtained from our present work (solid line). Dashed and dot lines are from Grieder [1].

In Fig.2, we have compared the data obtained by Dubovy et al(7) at 720 gm/m^2 which shows a nice agreement with our predicted hadron spectra with proton as primary particles whereas the spectra expected by taking heavy particle (Fe = 56) as primary is showing a sharp cut off supporting our conclusion.

Now it is evident from the above results that in the critical energy region under consideration i.e. between 10^5 and 10^7 Gev, in particular around 10^6 Gev, is not dominated by iron primaries.

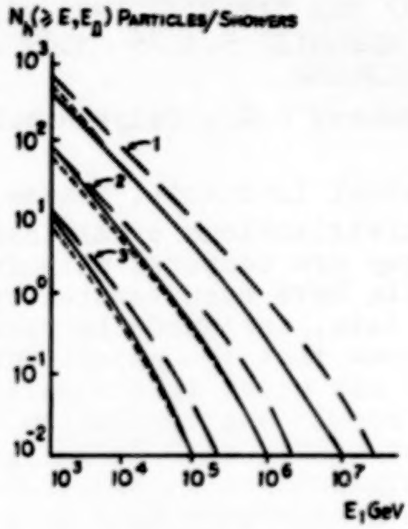

ORIGINAL PAGE IS
OF POOR QUALITY

FIG. 2

Integrated energy spectra of hadrons in EAS as calculated for $y = 720$ gm/cm^2 and primary energy E_0 (Gev) 1-10^8, 2-10^7, 3-10^6 and compared with those from Boyadshyn et. al. [22] for $a_n = a_\pi = 0$ (dashed curves), $a_n = a_\pi = 0.03$ (dot curves) and prediction from present model (solid curves).

References :

1] P.K.F. Grieder : 15th PICRC 8, 370 (Plodiv 1977).

2] J. Linsley : 18th PICRC, 12, 135 (Bangalore 1983), and references therein.

3] P.K.F. Grieder : 18th PICRC, EA 2-23, 328 (Bangalore, 1983).

4] P. Bandopadhyay et. al. Nuovo Cimento, 49A, 133 (1979) and references therein.

5] J. Sidhanta et. al. Phys. Rev. D 28, 1113 (1983).

6] J. Sidhanta and Rajkumar Roychoudhury, Z. Naturforsch 39a (1984).

7] A.G. Dubovy and N.M. Nestarova, Brief Communication on Physics No. 8, Phys., Inst., Acad., Sci. (USSR), 1978, p. 18.

ABOUT INCREASE OF THE LARGE $p_\perp$ PROCESSES FRACTION IN hA INTERACTIONS AT ENERGIES $5\cdot10^{14}-10^{16}$ eV ACCORDING TO THE DATA ON E.A.S. HADRONS

Danilova T.V., Dubovy A.G., Erlykin A.D., Nesterova N.M., Chubenko A.P.

P.N.Lebedev Physical Institute, Moscow, 117924,USSR

The lateral distributions of EAS hadrons obtained at Tien-Shan array are compared with the simulations. The simulation data have been treated by the same way as experimental data, included the recording method. The comparison shows that the experimental hadron lateral distributions are wider than simulated ones. On the base of this result the conclusion is drawn that the fraction of processes with large $p_\perp$ increases in hadron-air interactions at energies $5\cdot10^{14}-10^{16}$ eV compared with accelerator data in p-p interactions at lower energies.

Introduction. The hadron lateral distributions of EAS detected by Tien-Shan array /I/($N_e > 1.3\cdot10^5$; $p_0 = 690\ g\cdot cm^{-2}$) were published previously /2,3/. It was found that the experimental distributions were wider than simulated ones and the difference increased with EAS size N_e. The more rapid rise with energy of the transverse momentum in hadron-air nuclei interactions has been assumed at primary energies $E > 5\cdot10^{14}$ eV compared with the lower energies.

It is difficult to explain this result by variation of the primary mass composition, because calculations show a weak dependence of hadron lateral distribution at distances R=1,5-5 m from EAS axis on primary composition.

Method. EAS electron-photon component parameters (N_e-size; X_0, Y_0 - axis coordinates; θ, φ -zenith and azimuth angles; S - "age" and so on) have been determined by means of the multichannel scintillation and G.M.counter system. The energy and coordinates of hadrons have been determined by means of the ionization calorimeter ($\sigma_{tot} = 36\ m^2$). The descriptions of methods and accuracies were given in /1,2,3/.

The hadron density has been calculated as $\rho_a(R) = n_a(R)/\sigma$ for various distances R; (n_a is the number of hadron cascades detected in the calorimeter; $\sigma(R, X_0, Y_0, \theta, \varphi)$ is the area within the bounds of the calorimeter). The special simulation /3/ demonstrated the correctness of $n_a(R)$ to $\rho_a(R)$ restoration and the small influence of coordinate location inaccuracies. It is necessary to take into account the limited lateral resolution of hadron detectors (ionization chambers). It is possible that the hadron cascades in the calorimeter could be formed by several hadrons separated by distances smaller than the chamber size (0.25 x 3) m^2.

In this report Tien-Shan experimental results on lateral distributions of hadron cascades in the calorimeter: $n_a(R, \Delta E, N_e)$ are compared with the simulation data

ORIGINAL PAGE IS
OF POOR QUALITY

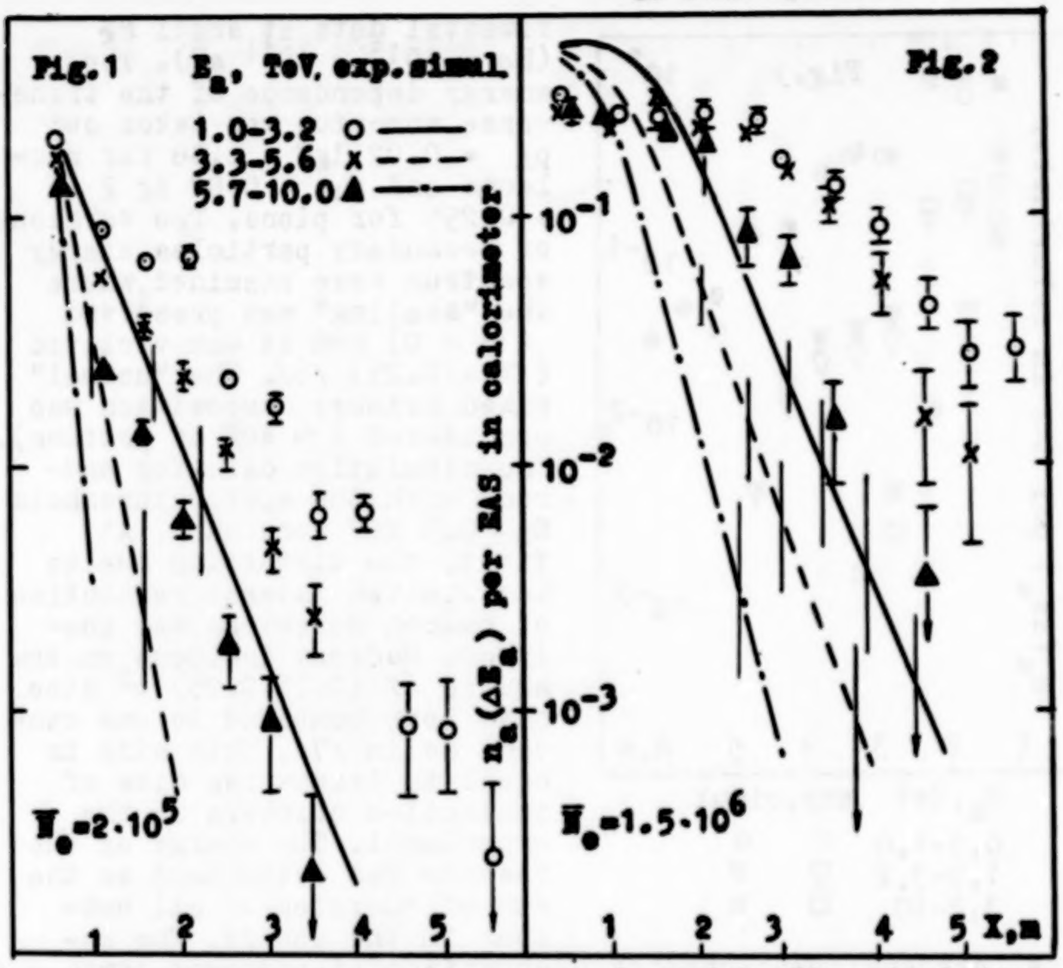

based on atmospheric nuclear cascade model. The simulation data have been treated by the same way as experimental ones (selection, recording and processing criteria).

Experiment. On the base of ~ 5000 EAS the dependence of hadron cascade number in calorimeter on R was obtained at distances R = 1-6 m from axis in various intervals of energies E_a (ΔE_a) from 0.5 to 10 TeV and various intervals of N_e. The showers with axes passed through the upper plane of the calorimeter have been selected. EAS axis parameters (X_0, Y_0, Θ, φ) were estimated by scintillation counters for the selection and after that they were corrected with the help of lateral parameters of hadron cascade with maximum energy. The cascade energy has been measured at 150-820 g.cm^{-2} of Pb absorber in the calorimeter. The special calculation shows that this energy is equal to the energy of incident hadron on the average. The cascades which passed through the side chambers were not taken into account. The experimental results are presented in fig.1 and 2.

Simulations. The results of Monte-Carlo atmospheric nuclear cascade simulation were used to compare with the experiment. The detailed interaction characteristics at accelerator energies have been taken into consideration /4,5/. Previously the results of the calculation were checked by EAS expe-

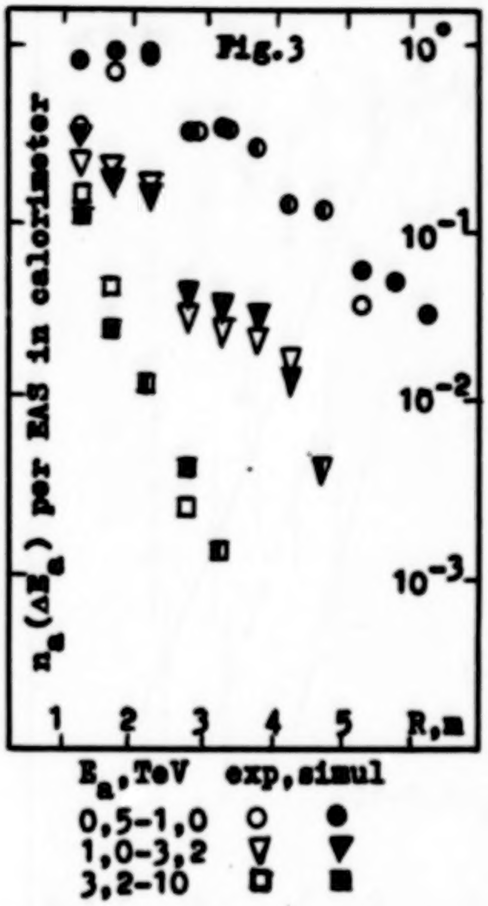
Fig.3

rimental data at small N_e ($E_o = 10^{13} - 10^{14}$ eV). The energy dependence of the transverse momentum was taken as: $p_\perp = 0.02 \lg E + 0.38$ for nucleons and $p_\perp = 0.02 \lg E + 0.295$ for pions. Two versions of secondary particles energy spectrum were examined,where the "scaling" was preserved ($\alpha = 0$) and it was violated ($\alpha = 0.25$) /6/. The "normal" mixed primary composition was considered (~ 40% of protons). The simulation data for hadrons with the energy threshold $E_a \geqslant 0.5$ TeV were used. At first, the distortion due to the limited lateral resolution of hadron detectors was analysed. Hadrons incident on the square of (0.25x0.25) m^2 size have been combined to one cascade as in /7/. This size is equal to transverse size of ionization chambers in the experiment. The energy of the cascade was determined as the sum of energies of all hadrons in the square. The mutual perpendicular chamber disposition at adjacent rows allows to select the cascades in this square.

In fig.3 the simulation results for the number of separate hadrons are compared with the number of hadron cascade in the calorimeter. The data are presented for showers of $\bar{N}_e = 6.10^5$, $\theta < 45^\circ$ in three intervals of E_a : $\Delta E_a = (0.5-1); (1-3.2); (3.2-10)$ TeV. The data in fig.3 show that the number of hadron cascades on (0.25x0.25) m^{2}square does not differ so much from separate hadron number at distances (1-5) m from axis.

The experimental and simulation result comparison. On the base of simulations one can conclude that the previous experimental data /2,3/ of hadron lateral distribution are not almost distorted by detection methods at distances R = 1-5 m from the EAS axis.

In oder to avoid the errors due to possible wrong identification of hadron cascades in two projections in the calorimeter, the new treatment of experimental and simulation data has been carried out by examination of only on X projection. In this case the total thickness of absorber above the chamber has been taken into account in the treatment of the experiment and the hadrons incident on the area (0.25x3) m^2 (the size of the ionization chamber) are combined to cascades in simulation.

In fig.1,2 the experimental data on hadron cascade number n_a (X, ΔE_a, N_e) passed through the calorimeter at different X distances are compared with the simulations for the version of "scaling" model treated by the same way as experimental ones. The data for three intervals of E are presented for two intervals of N_e : $N_e = (1{,}3-3{,}2).10^5$; $\overline{N}_e = 2.10^5$ and $N_e = (10-32).10^5$; $\overline{N}_e = 1.5.10^6$. The experimental results are shown by figures, the simulated ones are by lines. It is seen from fig.1,2 the experimental distributions are wider than simulation ones. The preliminary additional calculation indicates: if hadrons with energies $E_a < 0.5$ TeV are taken into account the result changes not so much.

Conclusions. The analysis of lateral-energy EAS hadron characteristics has been carried on the base of experimental statistical material several times greater than before /2,3/. Atmospheric nuclear cascade simulations made within assumption of "normal" weak rise of $p_\perp$ (E) were carried out in the same conditions of detection and treatment as in the experiment. The comparison experimental and simulation results indicates the increase of large transverse momentum $p_\perp$ (E) processes in hadron-air nuclear interactions at energies $5.10^{14}-10^{16}$ eV compared with lower accelerator energies in p-p interactions. It permits one to assume that the fraction of hadron "jets" with large $p_\perp$, observed at accelerator experiments, increases with energy. This effect is predicted by QCD-theory /8/ in processes of deep inelastic scattering af partons. The special calculation is necessary to determine influence of these processes on the EAS hadron lateral distribution at $E_0 > 5.10^{14}$ eV. However, the approximate estimation has been carried out by us on the base of QCD-theory /8/ indicates to possibility to explain Tien-Shan experimental data by means of the large $p_\perp$ "jet" production.

Acknowledgements. We would like to thank Romakhina N.S. for her help in treatment of data.

References

1. A.D. Erlykin, N.M. Nesterova et.al. 9th ICRC, London, 1965, 2, 731
2. V.A. Romakhin, N.M. Nesterova, A.G. Dubovy 15th ICRC, Plovdiv, 1977, 8, 107
3. A.G. Dubovy, N.M. Nesterova, V.A. Romakhin Kratkie soob., Lebedev Institute, 1978, 10, 8

4,5. Danilova T.V., Erlykin A.D., Machavariani S.K. 17th ICRC, Paris, 1981, 6, 18th ICRC, Bangalore, 1983, 6, 78

6. Wdowczyk J., Wolfendale A.W. Nuovo Chim., 1979, 54A, N4, 433
7. Dubovy A.G., Dunaevsky A.M., Nesterova N.M. et al 17th ICRC, Paris, 1981, 6, 199.
8. Gribov L.V., Levin E.M., Ryskin M.G. Phys.Lett.B, 1983, 121, 65

PHENOMENOLOGY OF SOFT HADRON INTERACTIONS AND THE RELEVANT EAS DATA

N.N.Kalmykov, G.B.Khristiansen, M.V.Motova
Institute of Nuclear Physics, Moscow State University,
Moscow II7234, USSR

I.Introduction. The interpretation of the experimental data in superhigh energy cosmic rays requires the calculations using various models of elementary hadron interaction. One should prefer the models justified by accelerator data and giving definite predictions for superhigh energies. The model of quark-gluon pomeron strings (the QGPS model) satisfies this requirement.

2.Model of quark-gluon pomeron strings. The QGPS model combines the supercritical pomeron theory with the modern quark-gluon pattern of hadron interactions. (The term supercritical pomeron theory was used in the works /3,4/ where EAS calculations were first made in terms of the QGPS model) The QGPS model, called also the dual parton model /5,6/, allows at present to calculate all necessary characteristics of hadron-nucleon and hadron-nucleus interactions /7-9/.

The QGPS model gives a good agreement with experimental EAS data /3,4/ and describes also the main data on gamma-families /I0/. The calculations in /3,4,I0/ were made at $\Delta=\alpha_p(0)-I=0.07$ (see /I,2/), where $\alpha_p(0)$ is the intercept of Regge pomeron trajectory. In this work we present the results of the EAS calculations in terms of the QGPS model with the parameters specified using the ISR and SPS data. The value of Δ is now $0.I2\pm0.02$ /8/. That gives a stronger violation of scaling than $\Delta=0.07$. Besides, the hadron-nucleus interactions are also treated in the QGPS model, so we don't need the additive quark model (AQM) that was used in /3,4/. It should be noted that values of function

$$R(x)=\left(\frac{1}{\sigma_{in}^{hA}}\times\frac{d\sigma^{hA}}{dx}\right)\Big/\left(\frac{1}{\sigma_{in}^{hN}}\times\frac{d\sigma^{hN}}{dx}\right)$$

for AQM and QGPS models are the same with a good accuracy

(~I0%).

3.Comparison with EAS data. Fig. I shows the inelastic nucleon cross-section in air calculated at Δ=0.I2 in terms of the Glauber model. The result is almost the same as in work /3/ up to the energies of ~I0^5 GeV but the cross-section increases more rapidly at higher energies than at Δ=0.07. The calculation results agree with the estimates obtained in cosmic ray experiments /II,I2/.

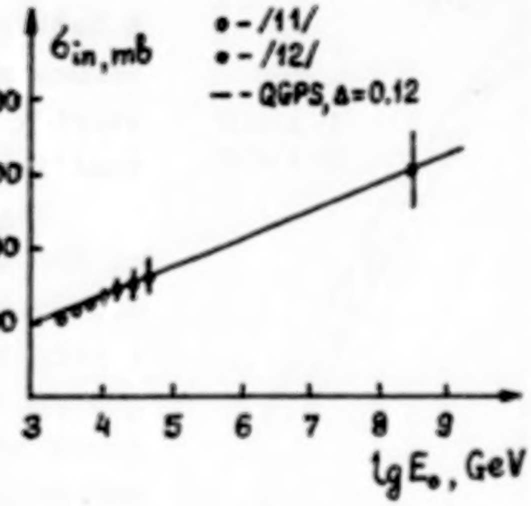

Fig.I. The inelastic nucleon cross-section in air.

Fig.2 shows the dependence of the >I0 GeV muon number N_μ on the EAS electron size N_e at sea level. The model gives a good fit to experimental data if allowance is made for the complex primary composition (40% of protons and I5% of fractions of nuclei with A=4,I5,29 and 56). The fit is better at Δ=0.I2 than at Δ=0.07. The small difference (~0.05) between the calculated and experimental values of α in relation

$$N_\mu \sim N_e^\alpha$$

may be easily compensated considering the possible changes of the composition with energy in terms of the diffusion model /I3/ or the increase of the kaon and barion fractions of secon-

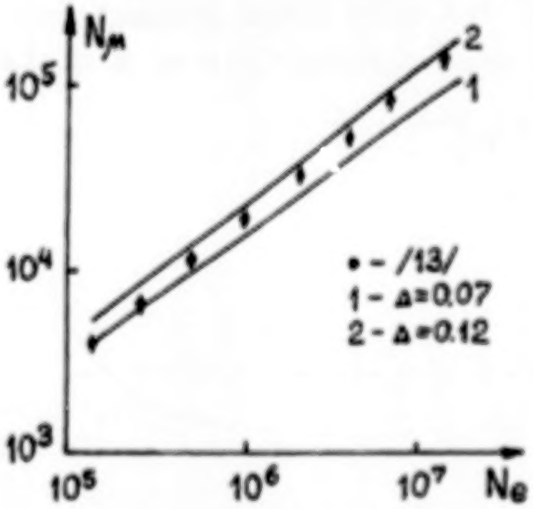

Fig.2. The number of >I0 GeV muons as function of the EAS electron number at sea level.

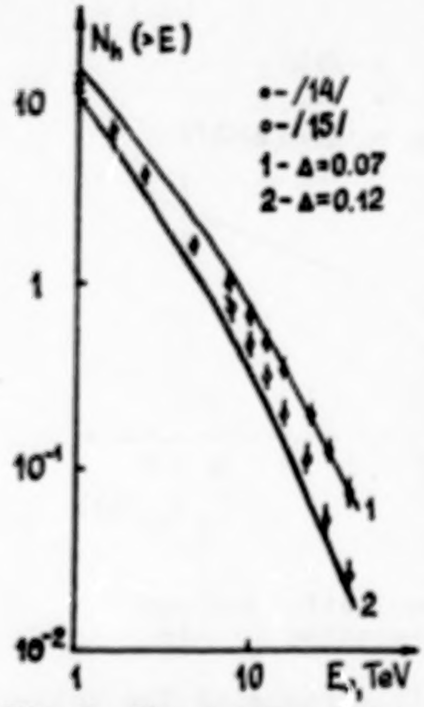

Fig.3. The energy spectrum of hadrons in EAS with $N_e \approx 9\cdot 10^5$ at mountain level.

daries as the energy increases /8/. A better agreement in the absolute values may be attained by slightly varying the primary cosmic ray composition.

Fig.3 shows the energy spectrum of EAS hadrons at mountain level and experimental data /I4/. Considering that incidence of hadron groups onto EAS array causes difference between the hadron spectrum and measured spectrum of energies released in the ionisation calorimeter at $E_h \sim$ I0 TeV /I5/ one can claim that transition to Δ=0.I2 improves the fit to experimental data.

The EAS maximum depth varies little as a function of primary energy (by I0-20 g/cm^2) at different E_0, so the earlier conclusions concerning the agreement of the QGPS model predictions with experimental data /3,4,I0/ remain valid.

Thus a certain variation of the QGPS model parameters improves the description of EAS experimental data as a whole.

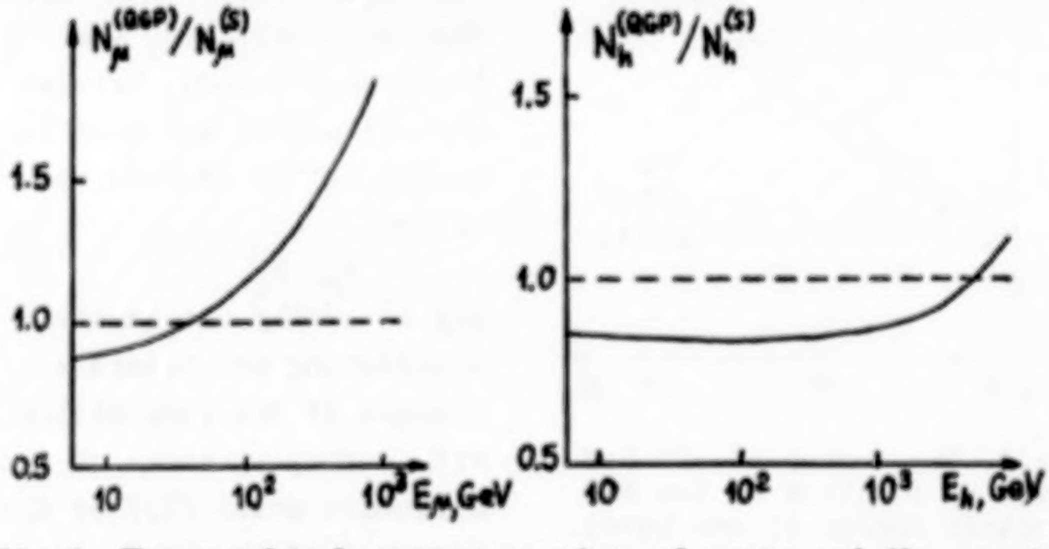

Fig.4. The sea-level energy spectra of muons and the mountain level energy spectra of hadrons in nucleus generated EAS.

4.Quark-gluon plasma. The possible production of quark-gluon plasma in nucleus-nucleus collisions has been intensively discussed since recently /I6,I7/. This model predicts significant cumulative effects (production of particles with energy $>E_0/A$) and a large number of secondary kaons and barions. Fig.4 shows some characteristics of nucleus generated EAS ($A=56$, $E_0=I0^6$ GeV) calculated in terms of quark-gluon plasma model /I6,I7/ the results being normalised to the traditional superposition model predictions. The calculations have shown that the shower maximum shifts as little as by 20 g/cm^2. The significant variations take place for hadron spectrum at energy region close to E_0/A and for muon spectrum at energies above I00 GeV. So to establish the existence of the quark-gluon plasma one should study hadron and muon spectra in nuclei generated showers at sufficiently high energies.

5.Acknowlegement. The authors are indebted to A.B.Kaidalov and Yu.M.Shabelsky for important discussions.

6.References.

I. Kaidalov A.B.,Phys.Lett.,I982,BII6 ,459.
2. Kaidalov A.B.,Ter-Martirosyan K.A.,Phys.Lett.,I982,BII7, 247.
3. Kalmykov N.N.,Khristiansen G.B.,Pisma ZhETF,I983,37,247.
4. Kalmykov N.N.,Khristiansen G.B.,Proc.I8 ICCR,Bangalore, I983,v.II,330.
5. Capella A.,Tran Thanh Van J.,Z.Phys.C,I983,I8,85.
6. Aurenche P. et al.,Z.Phys.C,I984,23,67.
7. Kaidalov A.B.,Ter-Martirosyan K.A.,Sov.Nucl.Phys.,I984, 39,I545; I984,40,2II.
8. Kaidalov A.B.,Piskunova O.I.,Preprint ITEP-I49,Moscow, I984.
9. Kaidalov A.B.,Preprint ITEP-II6,Moscow,I984.
I0.Kalmykov N.N. et al.,Sov.Nucl.Phys.,I985,4I,947.
II.Nam R.A. et al.,Proc.I8 ICCR,Bangalore,I983,v.5,336.
I2.Cady R. et al.,Proc.I8 ICCR,Bangalore,I983,v.II,398.
I3.Khristiansen G.B. et al.,Cosmic rays of superhigh energies. Karl Thiemig Verlag,Munchen,I980.
I4.Nesterova N.M.,Dubovy A.G.,Proc.I6 ICCR,Kyoto,I979,v.8,345.
I5.Dubovy A.G. et al.,Proc.I8 ICCR,Bangalore,I983,v.6,I63.
I6.Anishetty R. et al,,Phys.Rev.D,I980,22,2793.
I7.Elbert J.W.,Stanev T.,Proc.I8 ICCR,Bangalore,I983,v.5,526.

N85-35981

THE MAXIMUM DEPTH OF SHOWER WITH $E_0 > 10^{17}$ eV ON AVERAGE CHARACTERISTICS OF EAS DIFFERENT COMPONENTS

A.V.Glushkov, N.N.Efimov, I.T.Makarov, M.I.Pravdin

Institute of Cosmophysical Research & Aeronomy,
Lenin Ave., 31, 677891 Yakutsk, USSR

L.G.Dedenko

Scientific-Research Institute of Nuclear Physics,
Moscow, USSR

ABSTRACT

EAS development model independent method of the determination of a maximum depth of shower (X_m) is considered. X_m values obtained on various EAS parameters are in a good agreement.

1. Introduction. Investigations of the shower maximum depth X_m are carried out at various arrays and by different methods but the significant scattering of the obtained data is still available (Table 1). A reason of most of discrepancies is mainly due to methodical difficulties associated with the transition from the observed EAS parameters $P=P(X_m)$ to X_m. Thereby one had to use the theoretical conceptions on EAS development difficult to test experimentally.

2. Method. We considered one more method of X_m determination on the experimental data obtained at the Yakutsk EAS array. By computer calculations such parameters were found which are the functions of $P=P(X_m/X)$ or $P=P(X-X_m)$ type in wide limits of initial conditions: $X=1020\cdot\sec\theta$. The calculations were carried out at various E_0 and θ on two, quite different models of EAS development. The first model corresponded to scaling [10], the second one - to scaling at $E<10^{14}$ eV

Table 1

Parameter	E_0	X_m	Work
n_Q	$1{,}6\cdot10^{17}$	660±30	[1]
$\tau_{1/2}(Q)$	$1{,}4\cdot10^{17}$	700±15	[2]
	$2\cdot10^{17}$	681±20	[3]
	$1{,}2\cdot10^{17}$	706±36	[4]
	10^{17}	620±20	[5]
	10^{17}	545±20	[5]
	10^{17}	500±20	[5]
	$2\cdot10^{17}$	680±20	[6]
LDF(Q)	$2\cdot10^{17}$	627±20	[7]
	$1{,}5\cdot10^{17}$	600±50	[8]
$\Psi(\mu)$	$3\cdot10^{17}$	684±30	[9]
$\lg(\rho_c/\rho_\mu)$	$3\cdot10^{17}$	750±30	[9]
LDF(ρ_c)	$3\cdot10^{17}$	609±3	[9]

ORIGINAL PAGE IS
OF POOR QUALITY

[10] and to $n_s \sim E^{0,25}$ at $E \geqslant 10^{14}$ eV. The cross-sections in inelastic processes on both models changed with energy according to [10]. The index of the LDF of electrons n_e at the distance interval R=200-600 m from the shower core ($\rho_e \sim R^{-n_e}$) and ratios of densities of the EAS Cerenkov light to electrons $\lg(Q/\rho_e)$ and of electrons to muons $\lg(\rho_e/\rho_\mu)$ at R=300 m were considered. The above parameters are satisfactorily measured at the Yakutsk EAS array ($\rho_e = \rho_s - \rho_\mu$).

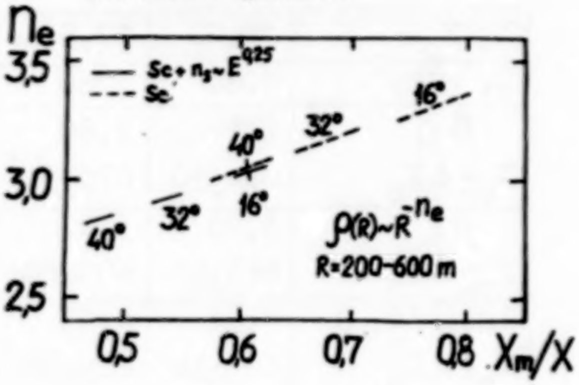

Fig.1

3. Results. Calculation results at E_o = 10^{17}-10^{18} eV and Θ = 16, 32 and 40° are shown in Figs.1-3. From Fig.1 it is seen that n_e is unambigiously associated with X_m/X independently of E_o, Θ and characteristics of nuclear interactions. We use this peculiarity of electron LDF to find X_m:

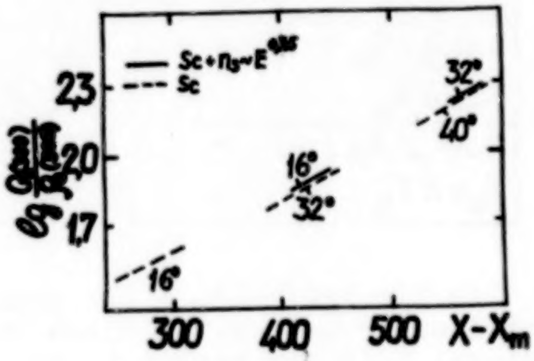

Fig.2

$$X_m = \left(\frac{n_e - 2,11}{1,7}\right) \cdot X, \ g/cm^2 . \qquad (1)$$

The obtained X_m are given in Table 2. The parameter $\lg(Q/\rho_e)$ which is the function of $X-X_m$ possesses the analogous feature (Fig.2).

$$X_m = X - 423(\lg\frac{Q}{\rho_e} - 0,88). \qquad (2)$$

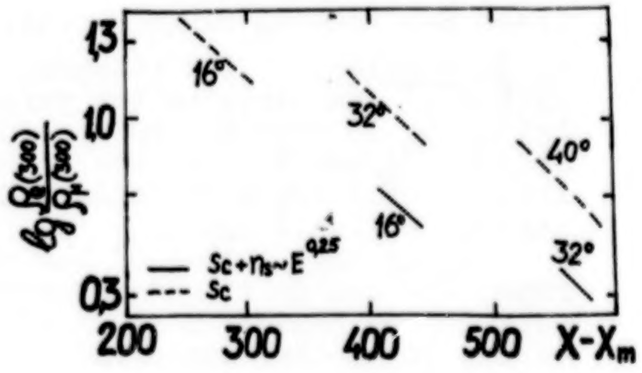

Fig.3

Table 2

$\lg E_0$	17,20	17,55	18,02	18,42	18,94
X, g/cm^2	1060	1060	1070	1080	1060
n_Q	2,57	2,60	2,70	2,78	2,80
$X_m \pm \Delta X_m$	660±30	675±30	725±30	765±30	755±40
n_e	3,18	3,22	3,26	3,31	3,31
$X_m \pm \Delta X_m$	665±60	690±60	720±60	760±60	750±60
$\lg(Q/\rho_e)$	1,94	1,91	1,79	1,71	1,59
$X_m \pm \Delta X_m$	615±30	625±30	685±40	730±40	760±45
$\lg(\Phi/N_e)$	5,37	5,31	5,19	5,19	5,0
$X_m \pm \Delta X_m$	640±40	665±40	725±40	735±40	800±40
$\lg E_0$	-	17,56	17,91	18,39	18,79
X, g/cm^2	-	1090	1080	1080	1080
$\lg(\rho_e/\rho_\mu)$	-	0,76	0,82	0,99	1,04
$X_m \pm \Delta X_m$	-	670±20	670±20	715±20	725±25
$\lg(N_e/N_\mu)$	-	1,17	1,28	1,47	1,54
$X_m \pm \Delta X_m$	-	665±35	670±35	720±35	735±35

As for $\lg(\rho_e/\rho_\mu)$ the unambiguity condition due to the zenith angle is broken. Therefore the experimental and calculational data are needed to be compared at similar Θ.

The averaging of data in Table 2 results in the following expression:

$$X_m = (700 \pm 35) + (66 \pm 6)(\lg E_0 - 18),\ \text{g/cm}^2. \qquad (3)$$

Note that all the above parameters were experimentally obtained at fixed $\rho_s(300)$ and calculations were also carried out under such condition. If to make calculations at fixed E_0, then X_m value becomes ~ 50 g/cm^2 less.

4. Discussion. The integral values $\lg(\Phi/N_e)$ and $\lg(N_e/N_\mu)$ are close to the parameters $\lg(Q/\rho_e)$ and $\lg(\rho_e/\rho_\mu)$. Here Φ is the total flux of the EAS Cerenkov light; N_μ and N_e are the total numbers of muons and electrons. Their dependences on $X-X_m$ are analogous to ones presented in Figs.2 and 3.

Apply this method of the analysis of data to other arrays. One can do it without additional calculations with respect to the parameter $\lg(\rho_c/\rho_\mu)$ [9], since it is similar to our parameter. According to [9] at R=300 m, $E_0=10^{17}$ eV and $\Theta \approx 15°$ we have $\lg(\rho_c/\rho_\mu)=0,3$. To recount from ρ_c measured at the Haverah Park array to ρ_e at R=300 m we use the ratio $\rho_e/\rho_c \approx 1{,}8$ [11]. Then lg(ρ_e/ρ_μ)$\approx$0,58 and from Fig.3 we find $X_m \approx 620$ g/cm^2, i.e. much higher than in Table 1.

5. Conclusion. The analysis of various EAS components based on the method of "model independent" parameters yields $X_m=700\pm35$ g/cm^2 at $E_0=10^{18}$ eV and at fixed $\rho_s(300)$.

References

1. Efimov, N.N. et al., (1983), Proc. 18-th ICRC, Bangalore, vol.6, 176.
2. Kalmykov, N.N. et al., (1979), Proc.16-th ICRC, Kyoto, vol.9, 73.
3. Protheroe, R.J. and Turver, K.E. Nuovo Cimento, 51A, (1979), 277.
4. Thornton, B. and Clay, R., (1980), Phys.Rev.Lett., vol.45, 1463.
5. Inoue, N. et al., (1981), Proc.17-th ICRC, Paris, vol.11, 270.
6. Hammond, P.T. et al., (1978), Nuovo Cimento, 1C, 315.
7. Dyakonov, M.N. et al., (1981), Proc.17-th ICRC, Paris, vol.6, 106.
8. Hara, T. et al., (1981), Proc.17-th ICRC, Paris, vol.11, 277.
9. McComb, T.J.L. and Turver, K.E., (1982), Nucl.Phys., vol.8, 1119.
10. Hillas, A.M., (1979), Proc.16-th ICRC, Kyoto, vol.9, 13.
11. Kellermann, E.W. and Towers, L., (1969), Preprint, Univ.Leeds.

N85-35982

SENSITIVITY OF DEPTH OF MAXIMUM AND ABSORPTION DEPTH OF EAS TO HADRON PRODUCTION MECHANISM

Antonov R.A., Galkin V.I., Hein L.A., Ivanenko I.P.,
Kanevsky B.L., Kuzmin V.A.

Institute of Nuclear Physics, Moscow State University,
Moscow 119899, USSR

Comparison of experimental data on depth of EAS development maximum in the atmosphere, t_m, and path of absorption, λ, in the lower atmosphere of EAS with fixed particle number in the energy region $E_0 = 10^{15}-10^{18}$eV with the results of calculation show that these parameters are sensitive mainly to the inelastic interaction cross section and scaling violation in the fragmentation and pionization region. The data are explained in a unified manner within the framework of a model in which scaling is violated slightly in the fragmentation region and strongly in the pionization region at primary cosmic rays composition close to the "normal" one and a permanent increase of inelastic interaction cross section. It is shown that, while interpreting the experimental data, disregard of two methodical points causes a systematic shift in t_m: i) shower selection system; ii) EAS electron lateral distribution when performing the calculations on basis of which the transfer is made from the Cerenkov pulse FWHM to the depth of shower maximum, t_m.

Two models (I,II)[1] were used as basic ones in our simulation. In the both models, an increase in cross section of hadron-air nuclei interaction was taken in the form

$\sigma_h^{in}(E_0) = \sigma_h^{in}(E')(1+\alpha_h \ln(E_0/E'))$ where $E' = 100$ GeV, $\alpha_h = 0.04$. In model I, at $E_0 = 10^{14}-10^{15}$eV scaling is violated in both pionization and fragmentation regions, model II being quasi-scaling.

For a set of fixed values of E_0 the double distributions over particle number at sea level and t_m were obtained. Using the Baiece theorem the distribution over E_0 at fixed particle number was derived regarding the power-law primary energy spectrum ($I(>E_0) \sim E_0^{-\gamma}$).

Table 1 lists the results of calculations for a 1030 g/cm^2 obseravtion depth. For each version 100 showers were simulated. The values of the threshold energy Ethr of tracing a nuclear cascade are listed in Table 1. Mixed composition of primary radiation was regarded (see Table 2).

An examination of Table 1 shows that at a fixed particle number at sea level, N, the value t_m^{meas} is sistematically overestimated regardless of a measurement method. The overestimate depends on E_0 and the interval width Δ N. E_0 increasing up to $\sim 10^{18}-10^{19}$eV, the overestimation decreases to zero.

Fig.1 illustrates the difference of distributions over t_m in the case of a fixed primary energy and in the case

Table 1

E_o, eV	E_{thr}, GeV	Model I			Model II		
		$\bar{t}_m$, g/cm^2	$\bar{t}_m^{meas}-\bar{t}_m$, g/cm^2		$\bar{t}_m$, g/cm^2	$\bar{t}^{meas}-\bar{t}$, g/cm^2	
			$\gamma=1.7$	$\gamma=2.2$		$\gamma=1.7$	$\gamma=2.2$
10^{14}	5	427±7	+220	+240	467±9	+235	+251
10^{15}	5	490±7	+206	+226	541±8	+184	+210
10^{15}	10	485±7	+161	+181	---	---	---
$3\cdot10^{15}$	5	520±7	---	---	---	---	---
10^{16}	5	---	---	---	618±8	+158	+170
10^{17}	50	---	---	---	667±15	+57	+67

of a fixed particle number at observation level.

Table 2

A	1	4	14	26	50-56
%	41	9	15	17	18

Table 3 compares results of Cerenkov light FWHM calculations regarding(τ_2) and disregarding(τ_1) shower lateral distribution. The latter approximation assumes all photons to be delayed as if they were emitted from the shower core. Further we present the values of differences between t_m evaluated using τ_1 and τ_2 : one can see that the use of $t_m(\tau_1)$ dependence instead of $t_m(\tau_2)$ leads to an overestimation of t_m.

Table 3

E_o, eV	R, m	τ_1, ns	τ_2, ns	$\Delta t_m = t_m(\tau_2) - t_m(\tau_1)$, g/cm^2
10^{15}	200	8.5	4.1	110
10^{15}	300	25.2	16.9	90
10^{15}	400	40.6	33.9	50
10^{17}	200	19.5	13.2	150
10^{17}	400	54.3	63.4	50

Fig.2 compares the summary of experimental data on t_m with the results of our calculation. At chemical composition close to the normal one the experimental data are well described by model I.

Fig.3 presents the comparison of the experimental data from /3/ on absorption path of EAS with fixed particle number N near sea level with our calculation. Calculation in terms of model I at α_h=0.04 and "normal" composition is consistent with the experiment.

References

1. Antonov R.A., Ivanenko I.P., Kuzmin V.A., Roganova T.M., Yadernaya Fizika, 1984, v.40, vyp. 5(11), 1222.
2. Ivanenko I.P., Kanevsky B.L., Roganova T.M., Pis'ma v JETP, 1978, 28, 704; Yadernaya Fizika, 1979, 29, 694; Preprint FIAN N 001, Moscow, 1979.
3. Nagano M. et al., J. Phys. G.: Nucl. Phys., 1984, 10, L235.

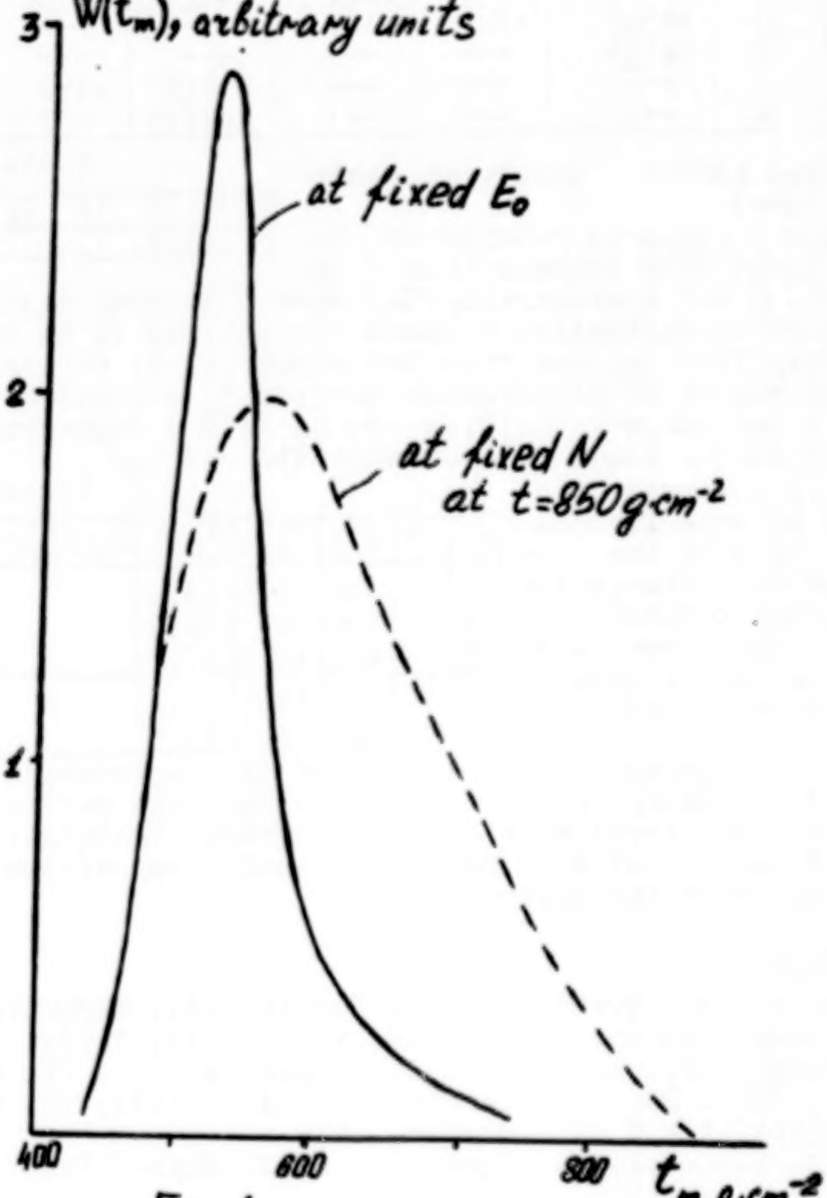
W(t_m), arbitrary units
3
2
1
at fixed E_0
at fixed N
at t=850 g·cm^-2
400
600
800
t_m, g·cm^-2

Fig. 1

ORIGINAL PAGE IS
OF POOR QUALITY

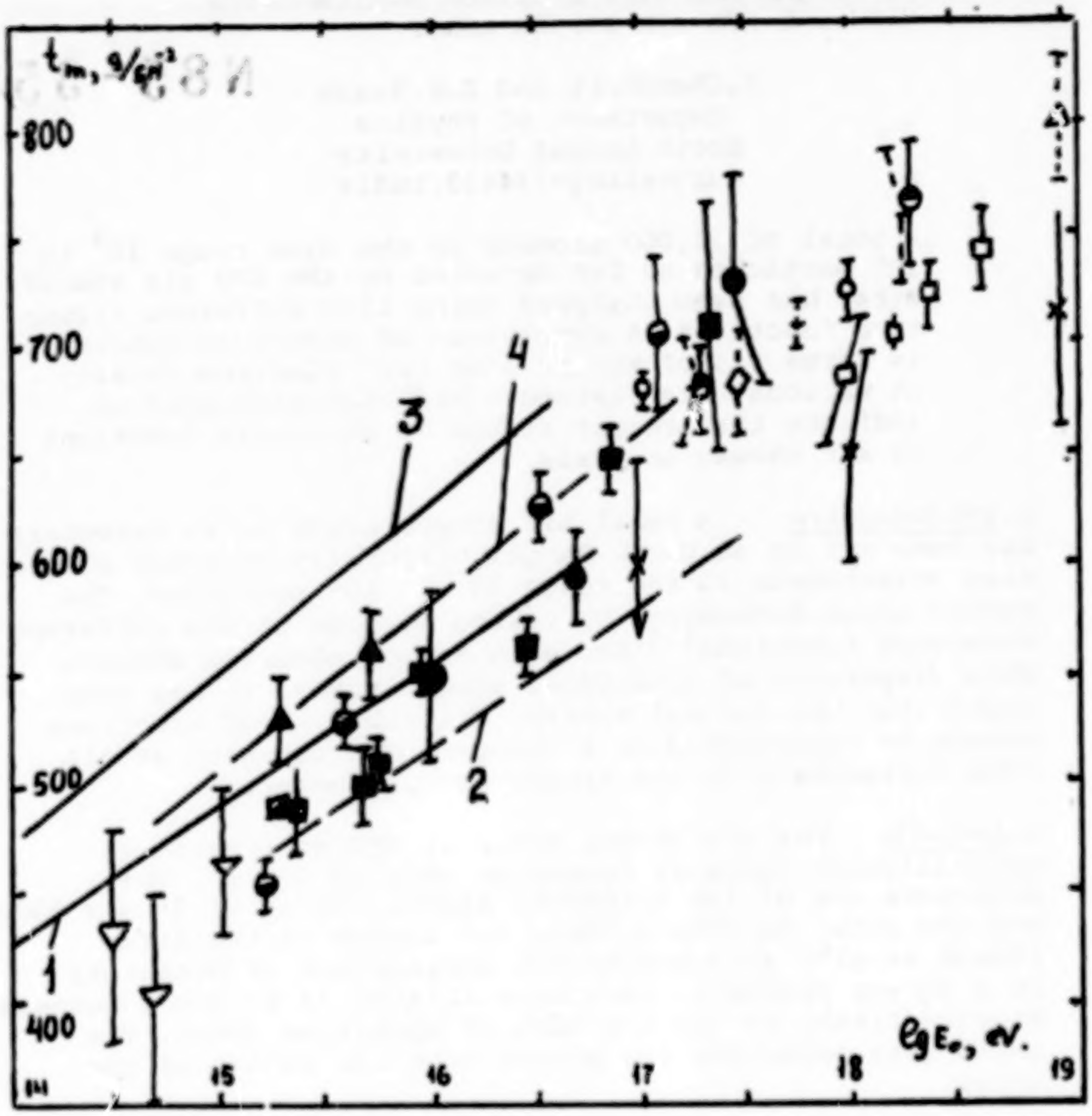

Fig 2.

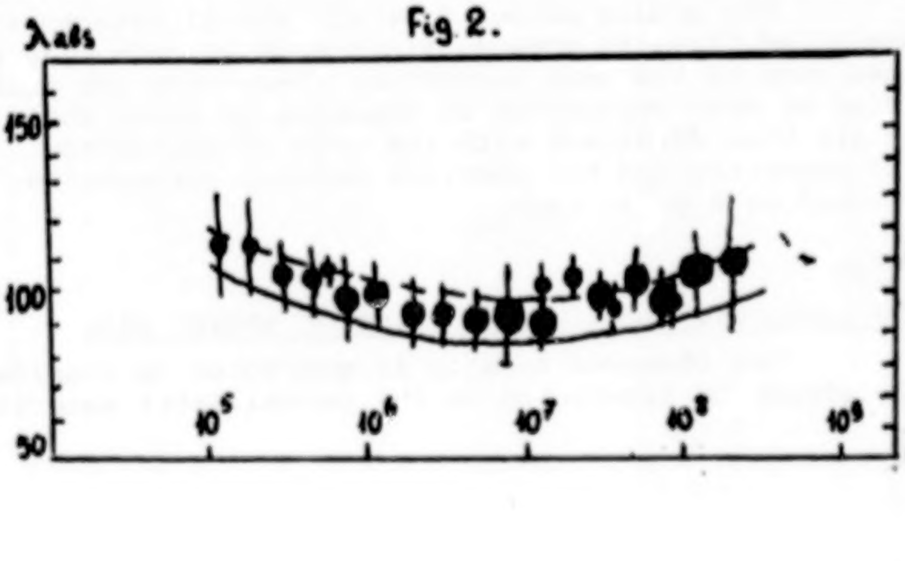

Fig 3

A CRITICAL ANALYSIS OF AIR SHOWER STRUCTURE FUNCTIONS AND SIZE SPECTRUM MEASUREMENTS WITH THE NBU AIR SHOWER ARRAY

N85-35983

N.Chaudhuri and D.K.Basak
Department of Physics
North Bengal University
Darjeeling-734430,India

A total of 11,000 showers in the size range 10^4 to 10^6 particles so far detected by the NBU air shower array has been analysed using five different structure functions. A comparison of structure functions in terms (i) of shower size (ii) electron density at various core distances has been discussed to indicate the present status of structure functions in air shower analysis.

1.Introduction A small air shower array of 21 detectors has been set up at North Bengal University to cover shower size measurement in the range 10^4 to 10^6 particles. The shower sizes determined by taking any one of the different structure functions[1-5] for each set of observed showers show dispersion of individual shower sizes. It has been found that the lateral density distribution of electrons cannot be represented by a standard NKG function at all core distances with the single age parameter.

2.Methods The air shower array at NBU comprising 21 scintillation counters covers an area of 900 m^2. The detectors are of two different sizes. One is of 25cm x 50cm and the other is 50cm x 50cm. The layout of the array (Basak et al[6]) is based on the arrangement of detectors in a square symmetry. Each scintillator is of 5cm thickness mounted firmly on the box made of aluminium sheet. The small area detectors are placed near the centre of the array.

The analog pulses from all the 21 detectors are amplified first by preamplifiers each of gain ≈ 30 and are then sent to the main laboratory where they are again amplified by main amplifiers of appropriate gain. These pulses are then digitised with the help of analog-to-digital converter and the observed density information are printed on a paper tape.

3.Results

3.1.The structure functions in terms of shower size

The observed density is corrected by considering the effect of transition in the scintillator material and aluminium box using the formula of Asakimori et al[7] as given below

$$\Delta_c = \Delta_o/(1.192 - 0.136 \log r)$$

where Δ_c is the corrected density and Δ_o is the observed density, and r is the core distance in metre.

The structure functions in terms of shower sizes computed by taking NKG function and any one of the other structure functions for each observed shower are shown in Figs. 1 to 4. It is found that Fig. 1 shows the dispersion of individual shower sizes about the expected undeviated shower size line. However Fig.4 shows a significant deviation between the expected and deviated line fitting the dispersion of the computed shower sizes using NKG and Hillas function. The important characteristics of air showers is the size spectrum which has been determined from the density distribution. The differential size spectrum can be represented by a power-law of the type

$$F(N_e) = (0.42 \pm 0.02) \times 10^{-8}(N_e/10^4)^{-2.51 \pm 0.01}$$

$$m^{-2}sec^{-1}sr^{-1}particle^{-1}.$$

It is important in the sense that if the size-primary energy relation is known, then the primary particle energy spectrum can be derived from the size spectrum.

3.2. The structure functions in terms of electron density distribution

The structure functions in terms of published electron density distribution functions[1-5] have been compared with the observed density distribution for different shower size and age values as shown in Figs. 5 and 6. We find that the observed electron density distribution follows the Hillas distribution more accurately than other density distribution functions.

4. Discussion The structure functions in terms of size indicate that the change of shower age from 1.2 to 1.1 (Figs. 1 to 4) causes a shift of core coordinates and a consequent decrease of shower size from Hillas function by about 35%. The use of distribution function by Lagutin et al[4] yields shower sizes somewhat smaller than those computed by NKG function, whereas in the electron density distribution, the Hillas function gives better distribution with observed density distribution. The differential size spectrum determined using the Hillas function gives an exponent of 2.51 for showers of size range 10^4 to 10^6 electrons.

5.Conclusions It can be concluded that the data on electron lateral distribution are in agreement with Hillas distribution function and the size spectrum obtained from Hillas function with average age of 1.2 compares well with the spectrum by KGF group[8] as

$$F(N_e) = (1.37 \pm 0.07) \times 10^{-8}(N_e/10^4)^{-2.42 \pm 0.02} m^{-2} sec^{-1} sr^{-1} particle^{-1}$$

6.Acknowledgements The authors are grateful to the Department of Atomic Energy, Govt. of India for the financial assistance for carrying out research work at North Bengal University.

References

1. Greisen,K., (1960), Ann.Rev.Nucl.Sci., 10,63.
   Nishimura,J. & Kamata,K., (1950),(1951),(1952), Prog.Theor.Phys. 5,899,6,628,7,185.
2. Hillas,A.M. and Lapikens,J., (1977), Proc. 15th ICRC, Plovdiv, 8,460.
3. Dedenko, L.G. et al, (1975), Proc. 14th ICRC, Munich 8,2731.
4. Lagutin, A.A. et al, (1979), Proc. 16th ICRC, Kyoto, 7,18.
5. Capdevielle, J.N. et al, (1983), Proc. 18th ICRC, Bangalore, 11,307.
6. Basak, D.K. et al, (1984), Nucl.Intr.Meths.,227,167.
7. Asakimori, K. et al, (1981), Proc. 17th ICRC, Paris, 11,301.
8. Rao, S. (1981), Ph.D. thesis, TIFR, University of Bombay, India.

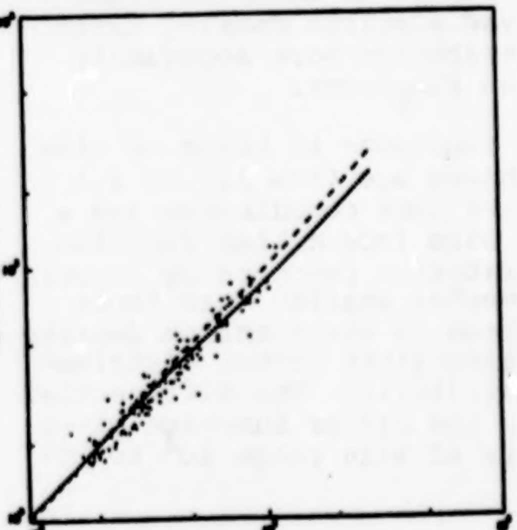

FIG. 1. THE DISPERSION OF SIZES OBTAINED FOR THE SAME SET OF SHOWERS USING THE FUNCTIONS OF HILLAS [illegible] AND NKG FOR s = 1.2.

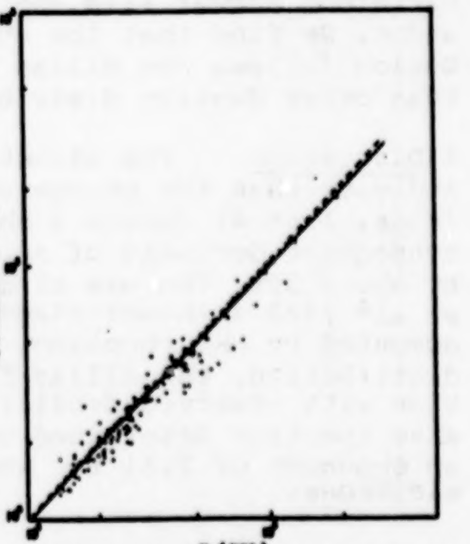

FIG. 2 THE DISPERSION OF SIZES OBTAINED FOR THE SAME SET OF SHOWERS USING THE FUNCTIONS OF [illegible] AND NKG FOR s=1.2.

ORIGINAL PAGE IS OF POOR QUALITY

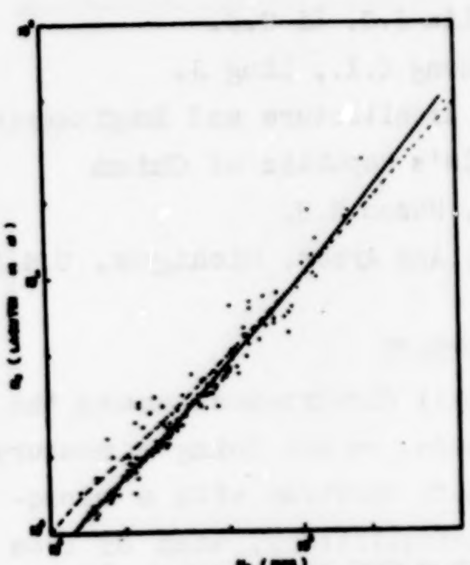

FIG.3. THE DISPERSION OF SIZES OBTAINED FOR THE SAME SET OF SHOWERS USING THE FUNCTIONS OF LAGUTIN et al[4] AND GKG FOR s = 1.2.

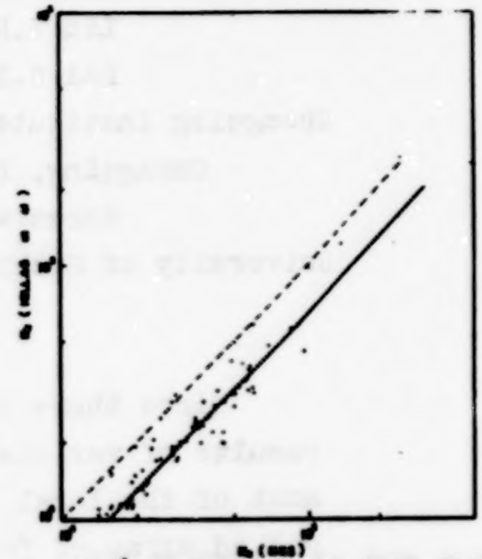

FIG.4. THE DISPERSION OF SIZES OBTAINED FOR THE SAME SET OF SHOWERS USING THE FUNCTIONS OF HILLAS et al[2] AND GKG FOR s = 1.1.

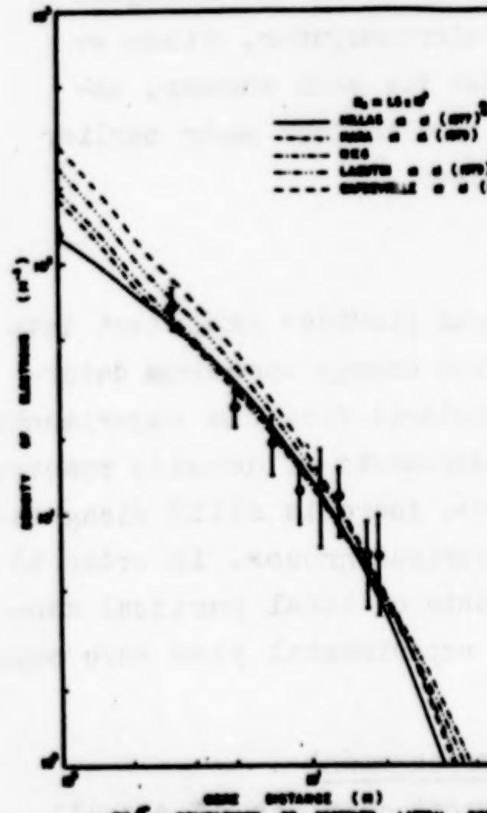

FIG.5. COMPARISON OF OBSERVED LATERAL DISTRIBUTION OF ELECTRONS WITH THE THEORETICAL DISTRIBUTIONS ACCORDING TO VARIOUS STRUCTURE FUNCTIONS FOR $N_e = 1.5\times10^5$ & s = 1.2

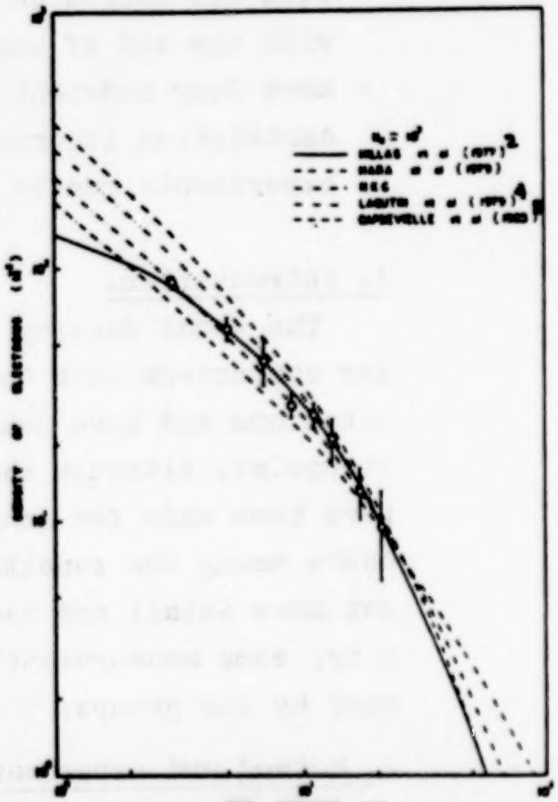

FIG.6. COMPARISON OF OBSERVED LATERAL DISTRIBUTION OF ELECTRONS WITH THE THEORETICAL DISTRIBUTIONS ACCORDING TO VARIOUS STRUCTURE FUNCTIONS FOR $N_e = 10^5$ AND s = 1.2

N85-35984

HE 4.2-2

MEASUREMENT OF THE LOCAL DENSITY SPECTRUM

Liu Z.H., Liu J.G. Li G.J.
Bai G.Z., Geng Q.X., Ling J.
Chongqing Institute of Architecture and Engineering
Chongqing, People's Republic of China
Hazen W.E., Hazen B.S.
University of Michigan, Ann Arbor, Michigan, U.S.A.

ABSTRACT

Since there is still disagreement among the results of various groups, we are doing a measurement of the local density spectrum with a close-packed array of four scintillators, each of area 0.14 m^2. Data are taken with conventional electronics, supervised by an on-line microcomputer. The data are stored on audio cassettes and analyzed with the aid of another microcomputer. Since we have four indepent samples for each shower, uncertainties inherent in results from many earlier experiments can be minimized.

1. Introduction.

The local density spectrum provides important data for comparison with those from energy spectrum determinations and have some advantages from the experimental viewpoint. Although the measurements of density spectrum have been made for many years, there is still disagreements among the reuslts of various groups. In order to get more detail and useful data of local partical density, some measurements and experimental plan have been made by our groups.

2. Method and experimental arrangement

The experimental arrangement consists of a small array of four plastic scintillators and a computerized recording and analysing system. The area of each scintillator is 0.14 m^2 and the thickness is 2.5 cm. The light signals are collected by a photomultiplier of model GDB-44 with a photocathode area of 15.2 cm^2. The scintillator is closed packed in a container of aluminum cone shell, and the inside surface of the container has been well polished, so the light of scintillator will be uniformly diffused.

The output from the scintilltor counter has been calibrated against the response of a single particle to determine the particle number.

In order to obtain the correct value, the pre- and main amplifier has been well adjusted.

3. Computerized recording system.

Fig. 1 shows the associated recording and discriminating system.

The output signal from each photomultiplier are digitized through the electronics and transmitted to the computer's memory, therfore the data of each detector can be analysed separately. Use of the microcomputer offers advantages in data handling as well as provides overall system simplicity and flexibility.

4. Discussion.

Since we have four independent samples for each shower, uncertainties inherent in results from many earlier experiments can be minimized.

In the present measurement, only four scintilltors have been operated, but it may be increased up to 8 photomultipliers.

5. Acknowledgements.

This work was supported by Chongqing Science and Technology Committee. We are grateful for the interest and support of Professor B.E.Wei, and we are also thank

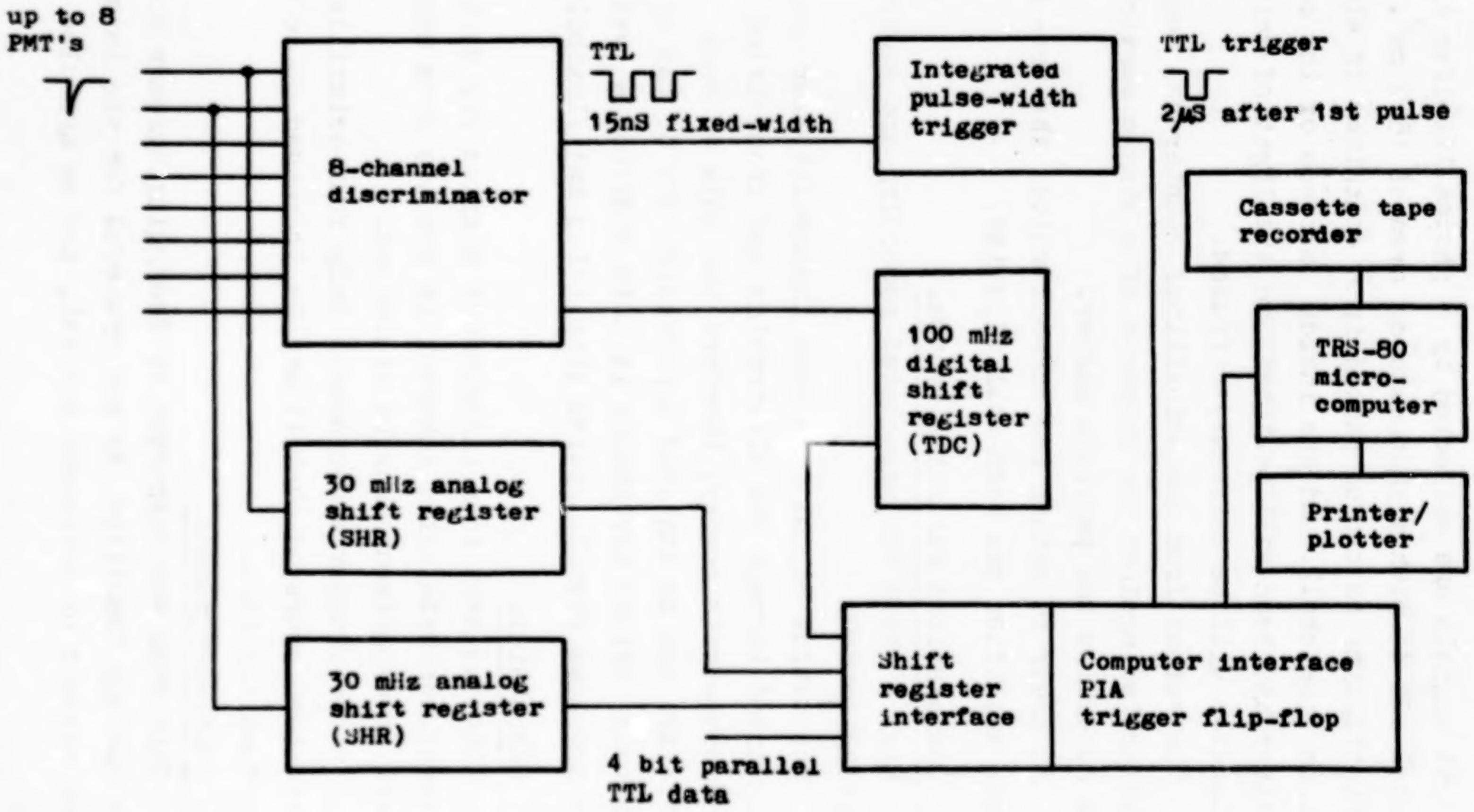
up to 8
PMT's
TTL
15nS fixed-width
8-channel discriminator
Integrated pulse-width trigger
TTL trigger
2µS after 1st pulse
Cassette tape recorder
100 mHz digital shift register (TDC)
TRS-80 micro-computer
Printer/ plotter
30 mHz analog shift register (SHR)
30 mHz analog shift register (SHR)
Shift register interface
Computer interface
PIA
trigger flip-flop
4 bit parallel TTL data

Fig. 1. Block Diagram of the Computerized Recording System

to Mr Y.H.Tam and Mr Y.F.Dai for valuable discussion.

References

(1) Porter, M.R. et al., 17th ICRC, Conference Papers, Vol. 6, 308, 1981.

(2) Hatano Y. et al., 16th ICRC, Conference Papers, Vol. 11, 161, 1979.

(3) Hazen W.E. and Hazen E.S., 18th ICRC, Conference Papers, Vol. 6, 14, 1983.

N85-35985

HE 4.2-3

ORIGINAL PAGE IS
OF POOR QUALITY

Character of Energy Flow in Air Shower Core

K.Mizushima

Kobe Women's Junior College, Chuo-Ku,
Kobe 650, Japan

K.Asakimori and T.Maeda

Department of Physics, Kobe University
Nada-Ku Kobe 657, Japan

T.Kameda

Kobe Women's University, Suma-Ku, Kobe 654, Japan

Y.Misaki

Research Center for Nuclear Physics,
Osaka University, Ibaraki, Osaka 567, Japan

ABSTRACT

Energy per charged particle near the core of air showers was measured by 9 energy flow detectors, which were the combination of Cerenkov counters and scintillators. Energy per particle of each detector was normalized to energy at 2m from the core. We obtained the following results as to the energy flow ;-
i) integral frequency distribution of mean energy per particle (averaged over 9 detectors) is composed of two groups separated distinctly,
ii) Showers contained in one group show an anisotropy of arrival direction.

1 Introduction As it is clear that energy flow is an importamt parameter of air showers, we have pursued it from various points of view. Some results were reported elsewhere (1) (2). One of the most interesting results was the possible existence of an anisotropy of arrival direction seen among the showers having large relative deviation. However, number of the showers selected was small in the previous report, and so there lies a fear that the anisotropy is a pretense due to small samples. Also the criterion of large relative deviation was not clear enough. To confirm these points the experiment has been carried out, and the data analized augmented in number by twice and a half time compared to ones reported previously.

2 Experiment and Results Arrangement of nine energy flow detectors in the air shower array of Kobe University and the characteristics of them were reported in (1) and (2).

The measurement was carried out during the period from October 1981 to November, 1983. 2606 showers whose axes hit within 3m from the center of the assembly of energy flow detectors less than 30° of zenith angle, were selected. We denote the energy flow in i-th Cerenkov counter by Eobi, where i=1,2,----,9, and put Ei= Eobi/Ni, where Ni is the number of charged particle measured by the scintillator just above the Cerenkov counter. Next, to obtain mean energy per charged particle at 2m from the axis, Ei is normalized at 2m using the average lateral distribution of energy flow which is approximately independent on shower size and on age for showers of size range $10^5 \sim 10^6$. Because of strict condition of selection ($\theta \leq 30°$, $r \leq 3$m) and characteristics of lateral distribution of Ei, errors induced in normalization are small. Each Ei normalized is ordered from maximum to minimum ,and is expressed by E2i (i=1,-----9), where i=1 corresponds to maximum, and i=9 to minimum.

Using these E2i, we put ME9=$\sum_{i=1}^{9}$E2i/9 and ME4=$\sum_{i=1}^{4}$E2i/4.

Fig.1 shows the relation between ME9 and size of showers. Showers of large value of ME9 are found in region of smaller size ($\leq 3\times10^5$). Fig.2 shows the integral spectra of ME9, corresponding to showers of different size region, $10^5 \leq N < 1.5\times10^5$, $1.5\times10^5 \leq N < 3\times10^5$, and $3\times10^5 \leq N$, and we denote these spectra as SP1,SP2,and SP3 respectly.

If we approximate these spectra by power function, SP1 and SP2 have at least two different powers, suggesting that showers in the small size region have at least two different kinds of shower groups. Considering the bending point in SP1 and SP2 as critical energy, we divide showers into two groups and denote showers above the critical energy as H-group. Straight line in Fig.1 is the boundary of two groups. In Fig.3 are plotted arrival directions of showers H-group. They seem to show an anisotropy in the region of galactic north pole. Fig.4 shows the integral spectrua in two regions of Right Ascension,12h ~ 16h and the remainder. From these two spectra the anisotropy occurs at ME9 $\gtrsim$ 0.9 Gev and this value corresponds to the bending of SP1 and SP2 in Fig.2.

Fig.5 and Fig.6 show the relation between ME4 and size of showers and that between ME4 and age parameter. As ME4 is interpreted to be energy flow of background particles, it is supposed to reflect the longitudinal development of air showers. The figures prove such interpretation to be right.

Fig.7 shows the relation between ME4 and E2$_1$-ME4 (denote MAXE) in showers of different age regions. Detailed analysis of ME4 and MAXE is now being carried out.

3 Discussion The criterion imposed vaguely on the boundary of large relative deviation previously is now clarified, and the boundary indicates the crossing point of two different groups. And in the group above the boundary (H-group) is seem an anisotropy to be exist. In spite of augmented data by factor 2.5, an anisotropy remaines still in the region near the galactic north pole.

ORIGINAL PAGE IS
OF POOR QUALITY

If the anisotropy found here is confirmed by further accumulation of data, and if H-group has any difference of characteristics from the remainder, it is safely said that H-group reflects some composition of the primary cosmic rays. It seems to be also interesting to study the relevance of the anisotropy mentioned here to that found in μ-rich showers and N-rich ones.

Considering these items, we intend to investigate the characteristics of indivisual shower in H-group in detail.

References

(1) Asakimori, K. et al.: 17th ICRC at Pris, 6(1981) 187.
(2) Asakimori, K. et al.: 18th ICRC at Bangalore, EA 1.1-27

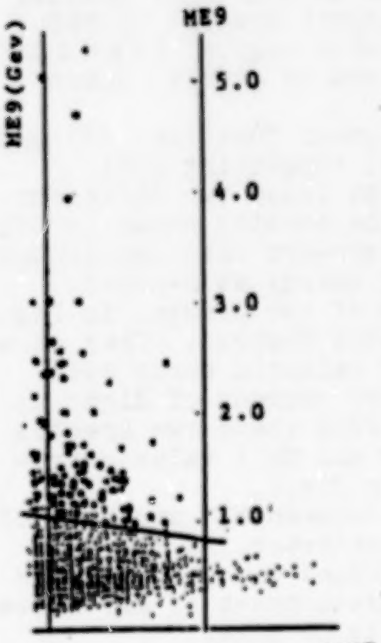

Fig. 1

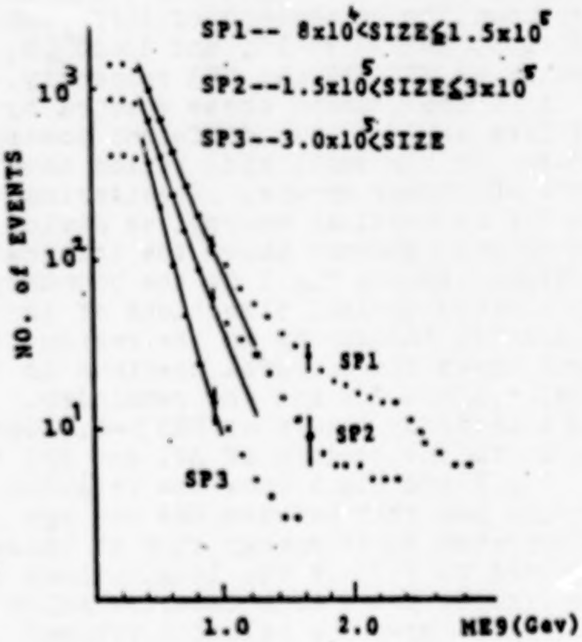

Fig. 2

ORIGINAL PAGE IS
OF POOR QUALITY

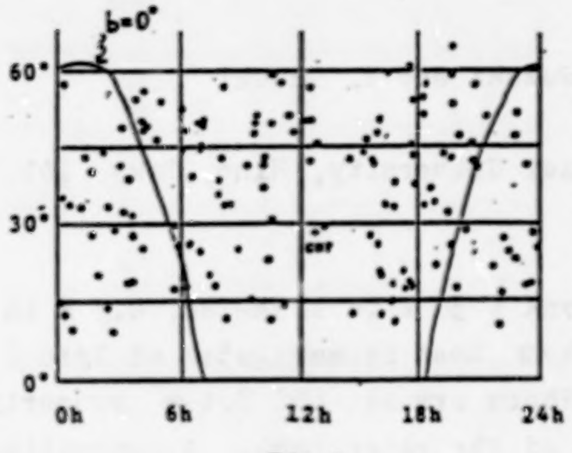

Fig.3

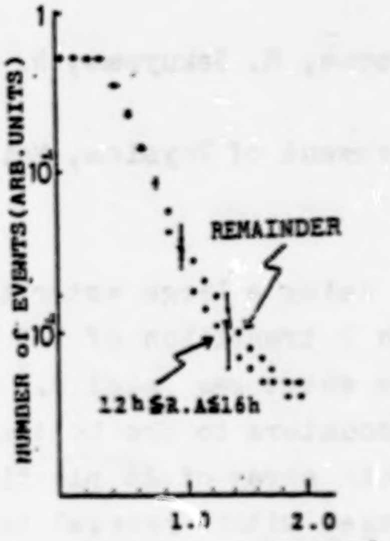

Fig.4

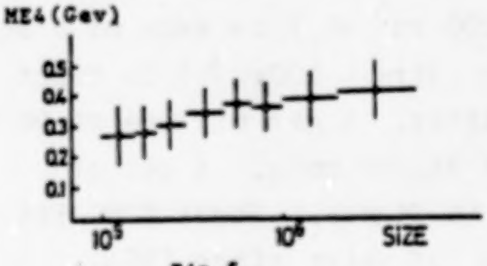

Fig.5

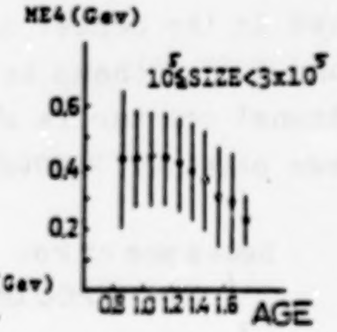

Fig.6

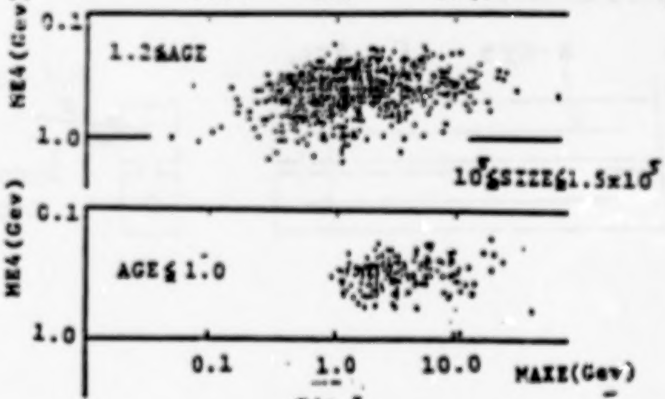

Fig.7

N85-35986

Observation of EAS using a large water tank

K. Inoue, H. Sakuyama, N. Suzuki and T. Suzuki

Department of Physics, Meisei University, Hino, Tokyo 191

Using a large water tank (30 m in diameter, 4.5 m in depth) transition of EAS has been investigated at Taro (200 m above sea level). There are set 150 0.4 m^2 proportional counters to the bottom of the water tank. A conventional EAS array of 25 plastic scintillation detectors has been arranged within several tens meter from the water tank. Proportional counter (10x10x200 cm^3 x2) is made of a square shaped pipe of iron. Tungsten wire ($100 \mu m \phi$) is tight stretched in the center of counter. A gas mixture of 90 % argon and 10 % methane is used at 760 mmHg. A set of proportional counter is shown in figure. About 3000 EAS have been obtained through 1 m of water since 1984.

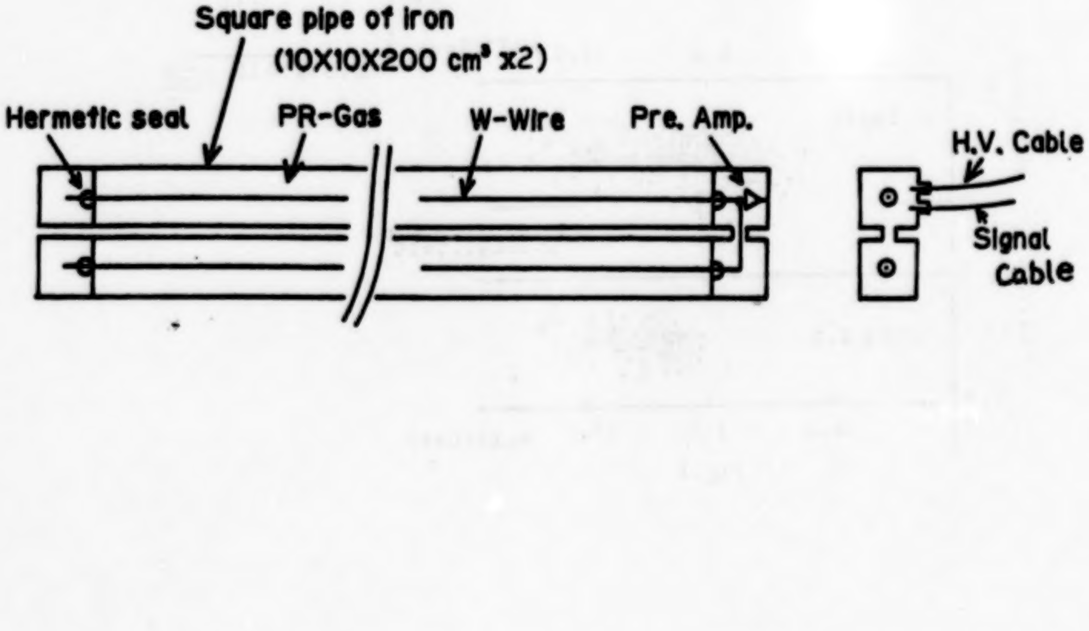
Square pipe of iron
(10X10X200 cm³ x2)
Hermetic seal
PR-Gas
W-Wire
Pre. Amp.
H.V. Cable
Signal Cable

HE 4.2-5

N85-35987

The Development of Air Shower in the Iron Absorber

M. Hazama:
Aichi Women's College, Nisshincho Aichi

S. Dake and K. Harada:
Department of Physics, Kobe University, Kobe

M. Kawamoto:
Natural Science, Kobe University, Kobe

M. Sakata and Y. Yamamoto:
Department of Physics, Konan University, Kobe

T. Sugihara:
College of Liberal Arts, Kobe University, Kobe

ABSTRACT

The iron open-sandwich experiments to observe one dimensional development of individual air showers were carried out at Akeno Observatory. One dimensional energy flow, incident energy and production height of shower is estimated using the data of size and age obtained from the above experiment and simple calculation.

1. Introduction.

In order to study the total development of individual air showers, two general methods to observe at different altitudes or to catch the generation gap of air showers from the difference of their arrival directions at the same altitude, have been used. But it is impossible to observe the longitudinal development of a shower and only able to grasp its average features.

The experiments to measure the particle density of each generation of a shower using the multiple detectors set top and bottom sndwiching some materials such as water, iron, led etc. as absorber between them and arranged over the range of 3 - 7 m, mainly to study the longitudinal development of the central parts of an air shower, have been carried out.(1-4) But the cost of experiment increases when the sandwich type arrangement mentioned above is adopted to observe the total longitudinal development of individual air shower, because the whole range of lateral spread of an air shower must be covered with the detectors.

Now, the new observation method so called "open sandwich" has been proposed as follows. Some different kinds of air shower arrays are arranged over the range enough to observe whole features of air shower.

The types of air shower array are classified by the thickness of the substance piled on the scintillation counter. The transition of the particle densities of an air shower is known when it passes through a substance by comparing the particle densities obtained from some different kinds of air shower arrays, and in the result the total longitudinal development of an air shower can be observed by the smaller number of detectors.

2. Experimental procedure.

Iron open sandwich experiment was carried out at s1 station in Akeno Observatory (920g/cm2) for three months (December 1980 - March 1981). The array consists of 100 scinttilation counters which covered an area of 50X50m2, they are 30 counters, on which 5 iron plates are laid (4.5cm iron thick and called 2Fe array), 28 counters 10 iron plates(9cm thick,4Fe array) and 42 counters non iron plate(0Fe array) in which 4 counters to detect arrival direction are included. The unit area of 96 scintillation counters is 0.5mx0.5m and of 4 detectors for arrival directions is 1mx1m.

The air shower array was triggered by the condition of any six fold coincidence out of central eight scintillation counters discriminating of 6 particles per counter. Thus 12,070 air showers were obtained in the above observation period.

3.1 Analysis of air showers.

The coordinates of shower axis (Xc ,Yc)and the set of the parameters size No and age So (No,So) on top of the iron plate, where So denotes lateral spread of air shower, are determined by fitting lateral density distribution curve obtained from 0Fe data to the theoretical lateral curves(NKG lateral structure function) by means of the least square method.

Another two sets of size and age (N2 ,S2) and (N4 ,S4) for the axis of 0Fe array are also obtained by the same method as above using the data from 2Fe and 4Fe array respectively.

The arrival direction(zenith angle θ) is determined by the difference of time arriving at the 4 counters to detect zenith angle.

1,308 air showers whose axces hit near the central part of the array and the parameters sizes and ages are determined with high precision, which are suitable for analysis, are selected and analyzed. They satisfy the following conditions: $\theta < 30^\circ$, $r = \sqrt{X_c^2 + Y_c^2} < 8.0$ m, $\sqrt{\Sigma dN_0(i)^2/42} < N_0$, $\sqrt{\Sigma dN_2(i)^2/30} < N_2$, $\sqrt{\Sigma dN_4(i)^2/28} < N_4$, where $dN_0(i)$, $dN_2(i)$ and $dN_4(i)$ are the difference between the number of particles detected by the i-th detector of 0Fe, 2Fe, or 4Fe array and one estimated as the value of i-th detector from the sets of parameters (No ,So), (N2 ,S2) or (N4 ,S4) respectively.

3.2 Models, energy and production height of air shower.

An air shower starts from the gamma rays decayed from neutral pi mesons which are produced when a primary cosmic ray interacts with an air nucleus. The number of gamma rays and the energy distribution of the gamma rays are assumed as follows.
In 1-gamma ray model(e1) 1 gamma ray is emitted and in CKP model (e2) the number and the energy of gamma ray follow CKP distribution. One third of incident energy transfers to electromagnetic cascade in both models.
The age parameter of an air shower Sl, which denotes longitudinal development of air shower, can not to be measured directly.

From the experimental results that in electromagnetic cascade the age for lateral development agrees with the one for longitudinal development when they are measured in the range one Moliele unit, which presents order of lateral spread of air shower and about 91 m at Akeno, Sl is substituted for So in usual. However, they are essentially diffrent to each other, then following two models about age parameter of individual air shower are assumed as
Sl = So.... (sa) and Sl = So + 0.2.... (sb).

The combination of 2 models for energy distribution and 2 models for age makes the 4 models; (e1-sa), (e2-sa), (e1-sb) and (e2-sb) called model A,B,C and D respectively.
The primary energy Eo and production height T of the air shower were determined by selecting the set of (Eo,T) which corresponds to the set of (No,Sl) obtained from calculation of electro magnetic cascade depending on models mentioned above, and yet agrees with experimental value.

3.3 Determination of energy flow.

The calculation for energy flow of the air shower has been carried out by the assumption that the electromagnetic component consists of electrons only because it has been difficult to know the energy distribution of gamma rays.
Now, new attempt to estimate the energy flow of electron or gamma ray individually has been made by giving each energy distribution based on electromagnetic cascade theory, and the age for electron or gamma rays is also determined separately.
The energy distribution of electron or gamma ray composed of the shower, on top of the iron plate, is given by electromagnetic cascade theory respectively as follows,

$NedE = AeE^{-(1+Se)}dE$ and

$NgdE = AgE^{-(1+Sg)}dE.$

Where, age Se is substituted for Sl assumed above, and age for gamma ray Sg is given by the set of (Eo ,T) determined above.

4. Results and discussions

The energy determination of air shower ever been used is to multiply size No by the average energy which is obtained some simulations. (5) Age is taken into account as well as size in this method. The present results agree with those published before in model A and B. (5) The average value of the ratio Eo to No and one of energy flow per electron Ef are in Table 1. The values of Ef are consistent with ones of other works. (6) The ratio N4/N2 corrrelates with age So as shown in Fig. 1. Fig. 2 sohws the correlation of mean energy per shower electron or total energy flow to So at Akeno altitude. The correlation between the ratio of total energy flow to incident energy Ef/Eo and So is shown in Fig. 3.

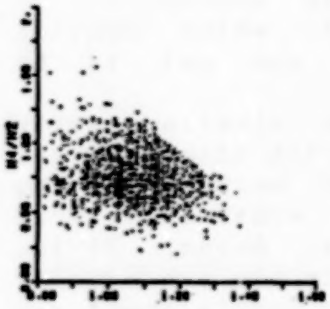

Fig. 1

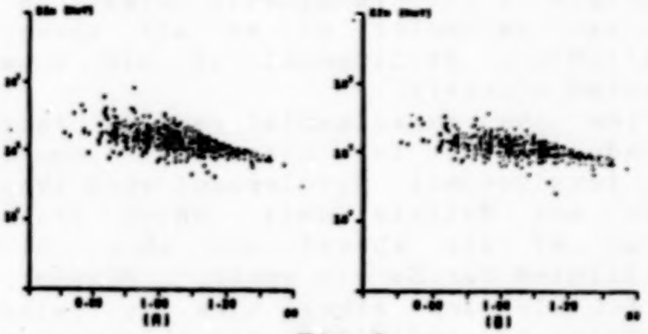

Fig. 2

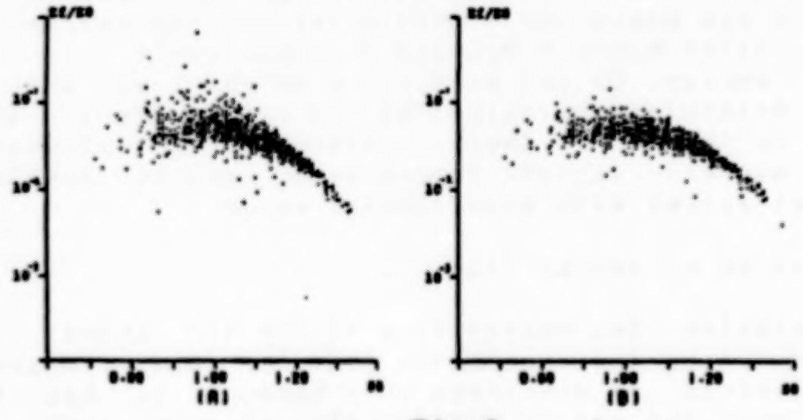

Fig. 3

model	$\langle E_0/N_0\rangle$(Gev)	$\langle E_f\rangle$(Mev)
A	4.27	140
B	3.33	117

Table-1

References

1. Y. Toyoda, J. Phys. Soc. Japan, 17(1962)415
2. S Dake et al., Nuovo Cim., 41B(1977)55
3. Y. Matano et al., Acta Phys. Hungariae 29 Suppl. 3(1970)451
4. S. Miyake et al., J. Phys. Soc. Japan., 18(1963)692
5. K. Kamata et al., ICR. Rep., 43(1984)3
6. G. Tanahashi et al., J. Phys. Soc. Japan, 20(1965)883

N85-35988

Application of Photodiodes to the Detection of Electromagnetic Bursts

Fukushima, Y., Saito, To., Sakata, M., Shima, M., Yamamoto. Y.
Department of Physics, Konan Univ., higashinada, Kobe, 658, Japan.

Abstract

A new type of photodiode + scintillator ($1\ m^2 * 1\ cm$) detector is developed to detect the large electro-magnetic burst under a EX-chamber. The threshold burst size is found to be $4.3*10^5$ particles at the center of the scintillator. Therefore a gamma-ray family of 10 TeV is detectable by it, when it is set under 14 r.l. of iron. In addition, a very fast (2.4 nsec width) and very bright (correspond to 10^6 particles) scintillation pulse has become avarable for this study.

1. Introduction.

Simultaneous observations of EAS and gamma-ray family have been made by two groups (1)(2). In these observations it is important, for successful joining of a EAS event with its corresponding gamma-ray family, to detect the distribution of electromagnetic cascade burst in the EAS core area. The burst distribution is detected by scintillation counter array beneath emulsion and X-ray film (EX) chambers. In our case (1), an unit burst detector is composed of a plastic scintillator ($50*50*3\ cm^3$) and a 2" photomultiplier tube (PMT), and the detecting range for burst size is 10^3 - 10^6 particles/$0.25m^2$.

A new type of photodiode, recently developed, may be useful instead of PMT for detection of such a large burst. The sensitivity of the photodiode is not comparable to that of PMT as yet, detection of large size burst as these observation may be possible. Photodiode have many advantages in comparison with PMT : low cost, miniature size and high stability, and one can make burst detector covering large area with low cost.

Large burst events emit scintillation light of considerable luminosity and of very short duration of a few nsec. Then we, first of all, make a pulsed light source which emits very bright pulsed scintillation light of 2.4 nsec. It is obtained by irradiating plastic scintillator ultraviolet laser pulse of short width less than 1 nsec.

2. Pulsed Light Source and Light Response Checker.

Short ultraviolet light of 337.1 nm is made by the method of transverse excited nitrogen laser of Blumlein type (3). Figure 1 illustrates the cross sectional view of the laser device; the electrodes of which have a gap of 3 mm and length of 5 cm and is operated by 14 kV - 22 kV DC high voltage. The flow of N_2 gas is about 3 ℓ/min under the atmospheric pressure. From this laser oscillator about 10 different spectral lines are emitted and the 337.1 nm line is the most eminent in them. In order to cut off the visible lines we use a interference

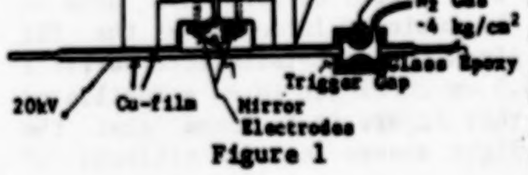

Figure 1

filter of passing only (337±15) nm. The specifications of this device are presented in Table 1. The pulse shape of the 337.1 nm is detected by a biplaner photo tube (R1193U, Tr = 0.27 nsec, HAMAMATSU) and a oscilloscope (7904, 500 MHz, Tektronix). In Fig. 2(a), the shape of it is shown. Because of the limit of the oscilloscope's response the FWHM will be smaller than 0.9 nsec which is known from Fig. 2(a). The shape of a scintillation light made by the laser light is shown in Fig. 2(b), from which one can observe the pulse shape of real scintillation light of width 2.4 nsec. The stability of this laser output is less than 5% after preliminary heating of a half hour as is seen in Fig. 3.

Spectral Output	:	337.1 nm
Repetition Rate	:	3-40 Hz
Pulse Width	:	≤1 nsec
Output Stability	:	10 %
Beam Dimension (At Exit)	:	1.5*3 mm^2 (Vertical* Horizontal)
Beam Divergence (Half Angle)	:	7.7*7.7 mrad^2
Trigger	:	N_2 Gas Pressurized Spark Gap (~4 kg/cm^2)

Table 1

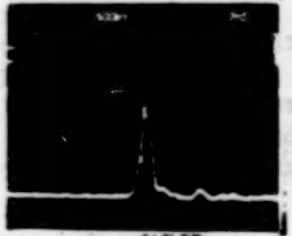

Figure 2(a)
0.5V/div.,2nsec/div.

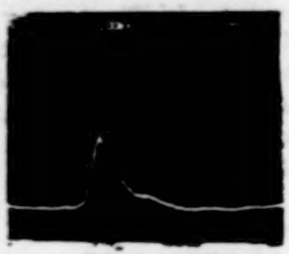

Figure 2(b)
0.1V/div.,2nsec/div.

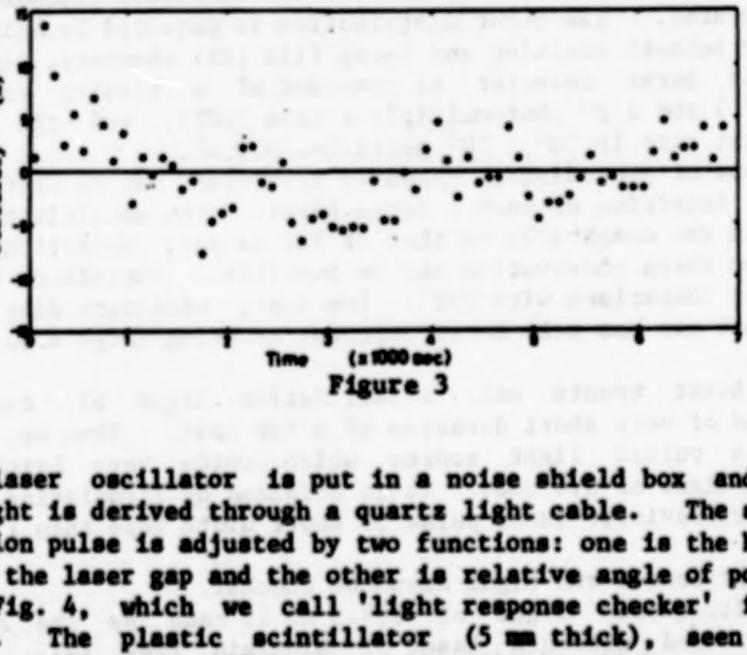

Figure 3

The laser oscillator is put in a noise shield box and only the pulsed light is derived through a quartz light cable. The strength of scintillation pulse is adjusted by two functions: one is the high voltage applied on the laser gap and the other is relative angle of polarizers as seen in Fig. 4, which we call 'light response checker' for PMT or photodiode. The plastic scintillator (5 mm thick), seen in Fig. 4, converts the 100% of the 337.1 nm to scintillation light.

Figure 5 shows the response curve of PMT system which is composed of PMT, preamplifier and mainamplifier, where output of the mainamplifier is square wave and whose pulse width corresponds to logarithm of pulse height from preamplifier. In addition, the "number of particles" used as the unit of abscissa in Fig. 5 means the luminous intensity at the PMT window; intensity of "one particle" is given when a relativistic particle vertically traverse a scintillator of 3.5 cm thick set in a scintillator box of our standard use (1). From this figure it is found that the maximum luminosity generated by this light source is a few millions of particles.

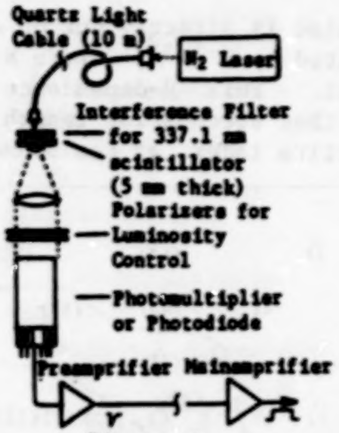
Quartz Light
Cable (10 m)
N₂ Laser
Interference Filter
for 337.1 nm
scintillator
(5 mm thick)
Polarizers for
Luminosity
Control
Photomultiplier
or Photodiode
Preamprifier Mainamprifier

Figure 4

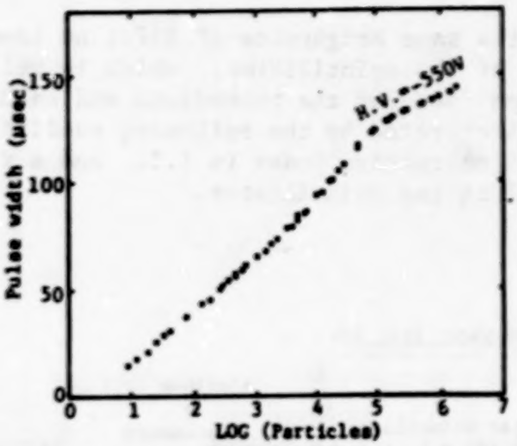

Figure 5

3. Response of PIN Type Photodiodes.

We use PIN type photodiodes (S1723-01,HAMAMATSU) which have large sensitive area ($10*10\ mm^2$) and very high speed of response in both rise and decay times (Tr = 15 nsec). The preamplifier circuit for this photodiode is shown in Fig. 6, which has field effect transistor and function of current-voltage converter. Pulse height of the preamplifier shows a good linear relation with luminous intensity as shown in Fig. 7.

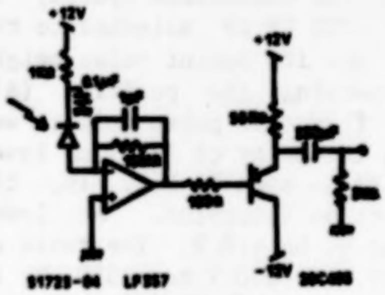
+12V
+12V
-12V
S1723-04
LF357

Figure 6

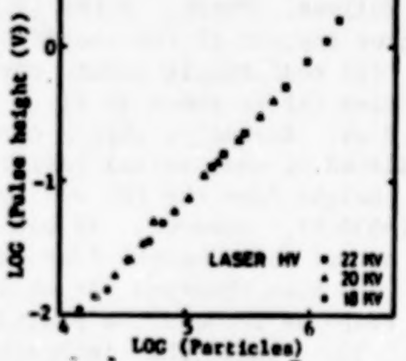

Figure 7

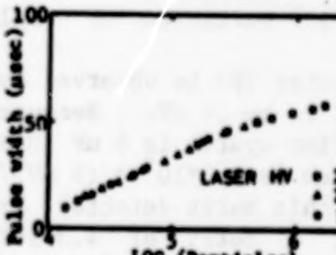

Figure 8

The output pulse width from the mainamplifier, the same type as used for PMT system, does not show a linear relation with them as shown in Fig. 8. From this result, however, we can conclude that this PIN photodiode-amplifier system is useful for detection of local burst size higher than a few 10^4 particles when we use it instead of PMT in the standard type scintillator box before mentioned.

4. A Burst Detector of $1\ m^2$ Unit Detected by Photodiodes.

An unit pack of photodiode and preamplifier is attached to the each corner of the scintillator whose size is $100*100*1\ cm^3$, and the whole unit is wrapped with aluminum foil as shown in Fig. 9. The uniformity of response is measured, as illustrated in Fig. 10. Numbers in the figure show the values of relative pulse heights of the preamplifier output, where the same brightness of 337.1 nm laser pulse is directly put on each point of the scintillator, which is well fitted by $R^{-1.55}$, where R is distance between the photodiode and each point. This R-dependence is well interpreted by the following conditions that attenuation length is 1 m, a refractive index is 1.5, and a reflective index at the boundary is 0.97 in the scintillator.

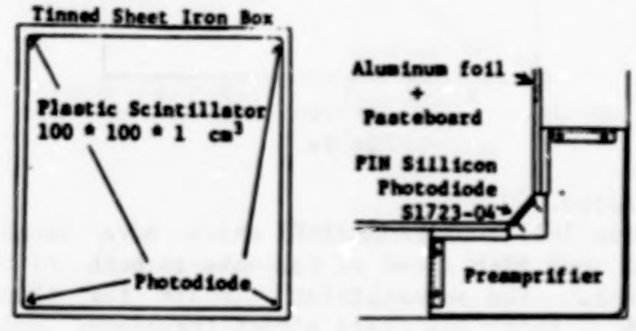

Figure 9

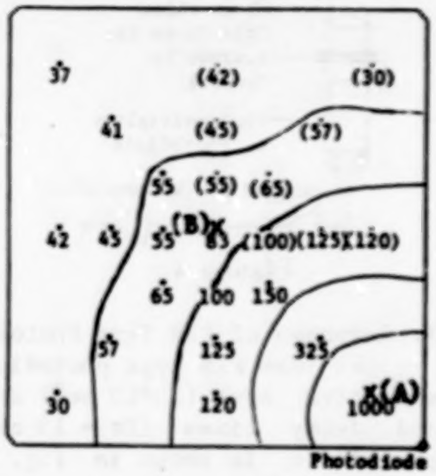

Figure 10

The threshold burst size, detectable by the photodiode system, is estimated as follows. First, a PMT (H.V. = -800 V) is attached to the 1 m^2 scintillator instead of the photodiode, and its output pulse height was measured for real single cosmic ray traversing the position (A), where the position (A) is shown in Fig. 10. Then this pulse height was found to be 4.5 mV. Secondly, when a certain intensity of 337.1 nm laser pulse is irradiated to the central position (B) as seen in Fig. 10, the output pulse height from the PMT was found to be saturated. At lower H.V. of PMT (-550 V), however, it was found to be 4.0 V. The ratio of decrease of output pulse height from the H.V. = -800 V to -550 V is 0.079, which has been observed for this PMT. On the other hand, the difference of response between the positions (A) and (B) was 1000 : 83 as seen in Fig. 10. Then the intensity of 337.1 nm laser in this irradiation is found to correspond to scintillation light of
$(4.0\ V)/((0.0045\ V) * 0.079 * (83 / 1000)) = 1.3*10^5$ particles of real cosmic rays.
When the same laser light irradiated at the same point (B) is observed by the photodiode, the preamplifier output is found to be 24 mV. Because the threshold voltage of this photodiode-preamplifier system is 8 mV (S/N = 3), the threshold particle number for this system is $1.3*10^5 * (8\ mV / 24\ mV) = 4.3*10^4$ particles at position (B). If this burst detector is set beneath a EX-chamber with 14 r.l. of iron, a burst of $4.3*10^4$ electrons and positron will be generated by a cosmic gamma-ray of about 10 TeV, so that we can conclude that a gamma-ray family of $\Sigma E_\gamma = 10$ TeV, at least, is detectable by this new burst detector.

References

(1) Nakatsuka, T. et al., 18-th ICRC, Bangalore, 1983, conf. Vol. 11,346.
(2) Matano, T. et al., 18-th ICRC, Bangalore, 1983, conf. Vol. 11, 342.
(3) Mitani, T. J. Appl. Phys. 52(5), May, 1981, P.3159

HE4.2-9

N85-35989

CORE STRUCTURE OF EAS IN 10^{15}ev TO 10^{17}ev

T.Hara, Y.Hatano, N.Hayashida, T.Kifune, M.Nagano and G.Tanahashi

Institute for Cosmic Ray Research, University of Tokyo
Tanashi, Tokyo, 188 Japan

ABSTRACT

With use of Akeno calorimeter, the attenuation of particles in concrete is analized as the function of the shower size of 10^5 to 10^7. The attenuation length does not depend much on the shower size but depends a little on the shower age. The average value is $\sim 150 \mathrm{gcm}^{-2}$ for s=0.5-0.85 and $\sim 140 \mathrm{gcm}^{-2}$ for s=0.85-1.15. These values and their fluctuations are consistent with the equi-intensity curves of EAS.

1. Introduction

Akeno calorimeter has an area of about 10mx10m and has the proportional counter arrays at 5 different depths(0, 115, 230, 345 and $633 \mathrm{gcm}^{-2}$ in concrete) with 10cm resolution in one dimension(1). We report the preliminary result of energy flow or the attenuation length measurement with use of the calorimeter. In this paper the attenuation length(Λ) is defined as

$$\text{Energy flow} = \beta\int_{x_o}^{\infty} N(x)dx = \beta\, N(x_o)\int_{x_o}^{\infty}\exp(-x/\Lambda)dx$$

where β ; the energy loss/particle. unit mass
$N(x)$; shower size in the depth x
x_o ; observation depth, $930 \mathrm{gcm}^{-2}$ in Akeno

The data are of the latter half of 1982, and about 13,000 vertical showers are analyzed whose sizes are between 10^5 and several times of 10^7. Only 3 shower cores hit the calorimeter area above the size of 10^7.

2. Average attenuation length of EAS

The analysis is only for the vertical showers with $\sec\theta = 1.0-1.1$. EAS data are sorted in the shower size(N) bin of $10^{5.0-5.5}$, $10^{5.5-6.0}$, $10^{6.0-6.5}$, $10^{6.5-7.0}$ and $>10^{7.0}$, and also in the age(s) bin of 0.50-0.85, 0.85-1.15 and 1.15-1.50. The average lateral distribution of particles and the shower sizes in each concrete depth are determined in every combinations of the above sorting. Fig.1 shows the average local attenuation lengths as the function of core distance in $N=10^{6.0-6.5}$ and in all s. They are defined in 1 replacing N(x) by $\Delta(x)$, the particle density in a unit of 10 proportional counters(5mx1m). The average shower sizes in each concrete depth are obtained by integrating $\Delta(x)$ over the core distance. They are shown in Fig.2. A systematic difference of the particle densities measured by the scintillation counters and by the proportional counters are corrected in the figure, that is $\Delta pc/\Delta sc$ is about 1.5 at $\Delta=10$, 1.3 at $\Delta=10^2$ and 1.15 at $\Delta=10^3$. The shower sizes are normalized within each size bin. The error bars only show the uncertainty due to the threshold of the counter output, and in most cases the true values are considered to be rather close to the lower limit. The data of size=10^7 and age=0.85-1.15 are not reliable because of the poor statistics of the core events.

The attenuation lengths from these transition data are $150 \pm 10 \mathrm{gcm}^{-2}$ for s=0.50-0.85 and $140 \pm 10 \mathrm{gcm}^{-2}$ for s=0.85-1.15, and not much depend on the shower size. These values are smaller than $\sim 180 \mathrm{gcm}^{-2}$ predicted for the proton showers of the standard interaction, and also for the iron showers as shown in Fig.3(2), where "standard" means the increasing cross section as $\sigma \propto E^{0.06}$, Feynman scaling and the extrapolation of the known central energy distribution to the higher energies.

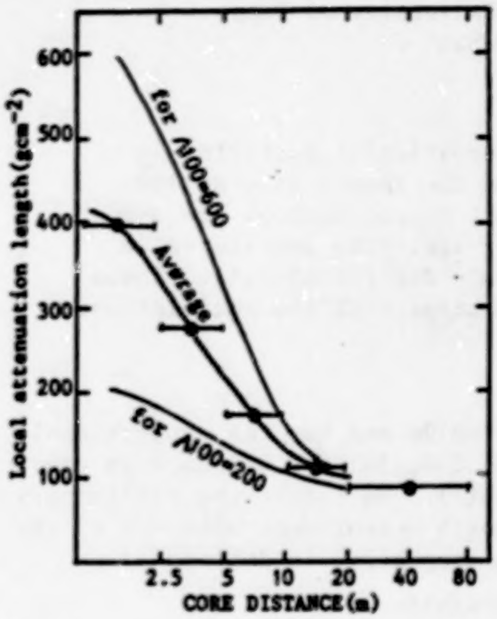

Fig.1

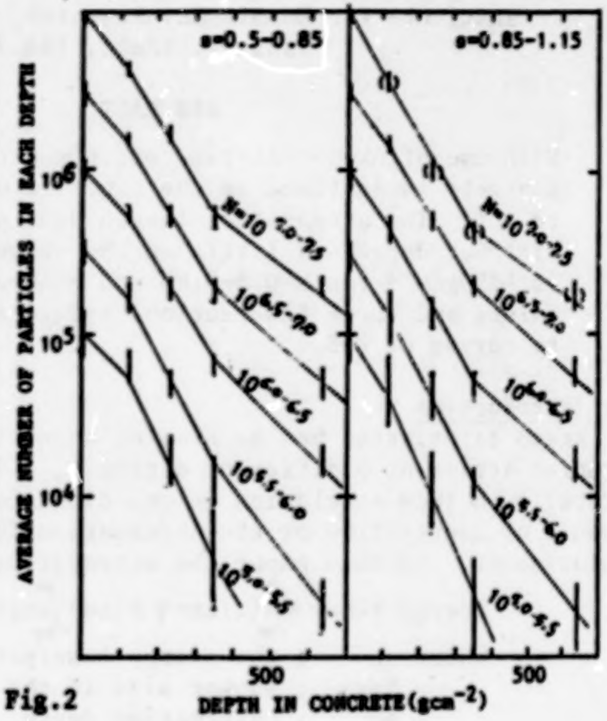

Fig.2

3. Relation of 3 attenuation lengths ΛE, ΛI, ΛN

To see the consistency of the result with others, three attenuation lengths are taken into account. Their definitions are as follows.

(i) ΛE of the fixed energy shower

ΛE is obtained from the shower calculation of the fixed energy, and in the case of the simulation, the average value of many showers is used. ΛE is about 180gcm^{-2} in 10^{16}ev and in >950gcm^{-2} for the standard proton showers(Fig.3).

(ii) ΛI of equi-intensity cut

ΛI is obtained from the equi-intensity cut of the size spectra in the different depths. The experimental value is 160-170gcm^{-2}(3) in 10^{16}ev to 10^{17}ev and >950gcm^{-2}.

(iii)ΛN of the fixed size in the fixed level

The attenuation length obtained in the calorimeter experiment is ΛN. The experimental value is 140-150gcm^{-2} as described in 2.

In what follows we make a simple calculation of these Λs to see how the cosmic ray composition affects these values. The composition is assumed to be two components, the proton and the heavy nuclei. Each shower curve is to be the exponential form, say $Np.\exp(-x/\Lambda p)$ for proton and $Nh.\exp(-x/\Lambda h)$ for heavy nuclei. $Np=Nh=10^9$, $\Lambda p=180$gcm^{-2} and $\Lambda h=140$gcm^{-2} in 10^{16}ev as shown in Fig.3. The reason to adopt the small value of Λh is that the usual models of heavy nuclei shower can not give a appreciably smaller attenuation than the proton's. The fluctuations of the longitudinal development are ignored. The integral energy spectrum is to be E^{-2}, and the intensity ratio at the same energy $k=Ih/Ip$ is to be a parameter of the calculation. ΛE, ΛI and ΛN are given as follows.

$\Lambda=(x2-x1)/\ln(N1/N2)$
for ΛE, $N1/N2=(ex1p+k.ex1h)/(ex2p+k.ex2h)$
for ΛI, $N1/N2=((ex1p^2+k.ex1h^2)/(ex2p^2+k.ex2h^2))^{0.5}$
for ΛN, $N1/N2=(ex1p^2+k.ex1h^2)/(ex1p.ex2p+k.ex1h.ex2h)$
where N1 and N2 are the shower size at the depth of x1 and x2 respectively and $ex1p=\exp(-x1/\Lambda p)$, $ex1h=\exp(-x1/\Lambda h)$, $ex2p=\exp(-x2/\Lambda p)$, $ex2h=\exp(-x2/\Lambda h)$.

The relations between k and Λs are shown in Fig.4. It is seen that ΛN has almost the same value as ΛI in the whole range of k. This means that the difference of ΛI(160-170gcm^{-2}) and ΛN(140-150gcm^{-2}) can not be explained by means of the different response of proton and heavy nuclei showers.

The other possible explanation is to attribute it to the fluctuation of the shower development. Fig.5 shows two distributions of simulated attenuation lengths of fixed energy and of fixed size for the proton showers. The positions of the distribution maximum are almost the same, but the average value of the fixed energy one is larger than that of the fixed size. As the attenuation length of fixed energy is nearly equal to that of the equi-intensity cut in single component showers, this can explain the difference provided that the primary cosmic rays contain a proper amount of protons.

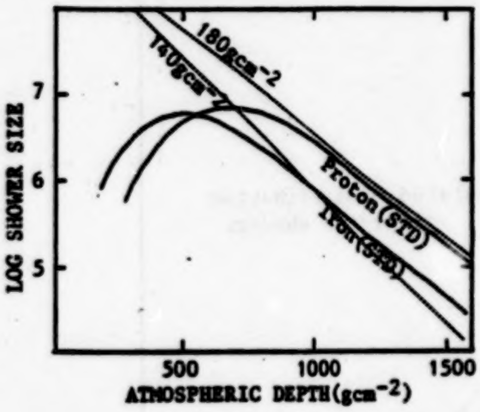

Fig.3

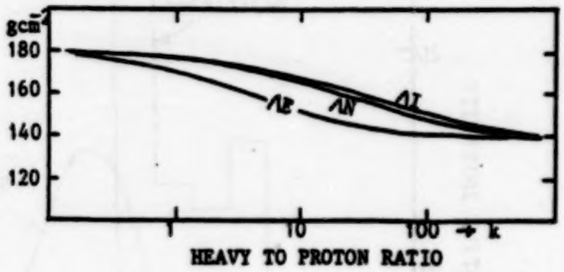

Fig.4

4. Fluctuation of the attenuation length

The attenuation length of each shower can not be directly obtained from the data, and only "the attenuation length within 10mx10m(Λ100)" are obtained. The histogram in Fig.6 shows the Λ100 distribution(bottom side scale) of the showers which hit the central part(5mx5m) of the calorimeter. This kind of fluctuation decreases with the core distance, and gets remarkably smaller beyond 15m down to 80-90gcm^{-2}. So, for the core hitting showers, we can convert Λ100 to the attenuation length assuming the local attenuation lengths are continuous between 5m and 20m.

The conversion depends on how to interpolate the attenuation between 5m and 20m. The most gentle one is that the local attenuation lengths fluctate around the average in proportion to the central Λ100 in the region above 80-90gcm^{-2} like the two curves in Fig.1. The attenuation lengths obtained with use of this conversion are shown in the top side scale of Fig.6. In the same figure, the distribution of the attenuation length is compared with the one simulated for proton showers(the same one in Fig.5). The observed distribution does not agree with the prediction. Some part of the disagreement may be the contribution of the heavy nuclei showers, but the further discussion needs the further detailed analysis, especially the improvement of Λ100 conversion to the attenuation length.

Fig.5

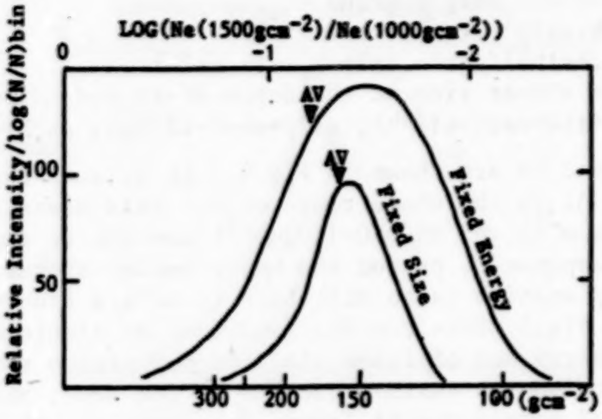

Fig.6

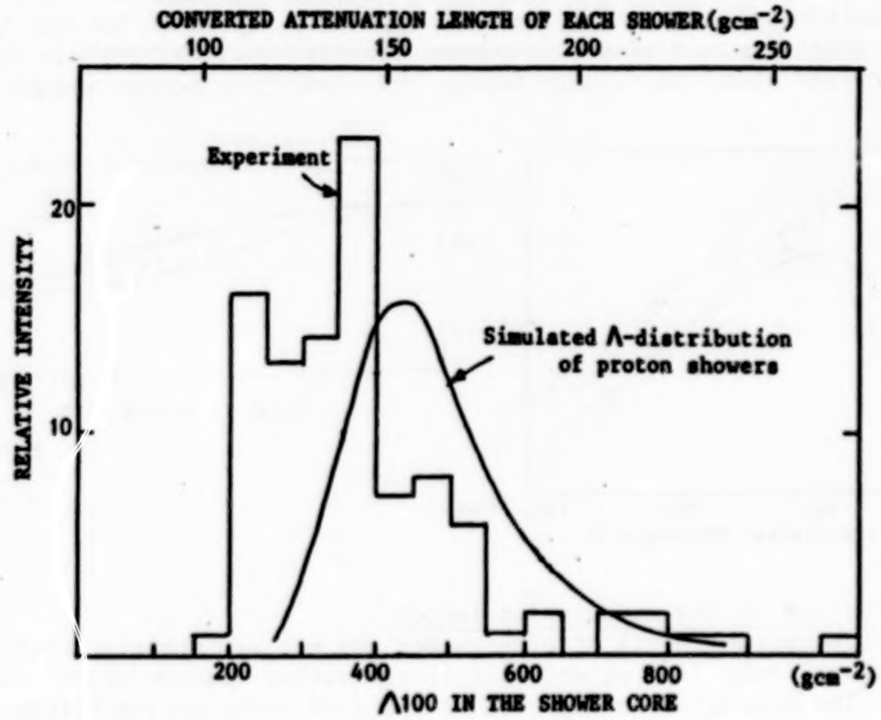

Acknowledgements

The authors are indebted to the technical staffs in Akeno crew. The data reductions and the EAS simulation are done by FACOM 380 at the computer room, Institute for Nuclear Study, University of Tokyo.

References

(1) Hara, T. et al. Proc. 16th ICRC(kyoto), 8, 135 1979
(2) Tanahashi, G. HE 4.1-3 in this conference
(3) Nagano, M. et al. J. Phys. G; Nucl. Phys. 10, 1295, 1984

N85-35990

HE 4.2-10

PARTICLE DISTRIBUTIONS IN $\sim 10^{14} - 10^{16}$ eV AIR SHOWER CORES AT SEA LEVEL

A.L. Hodson*, A.G. Ash*, and R.N. Bull+

*Department of Physics, University of Leeds, Leeds, U.K.
+Department of Physics, University of Nottingham, Nottingham, U.K.

ABSTRACT

At the Bangalore Conference we reported experimental evidence for the 'steepening' of the differential density spectra for known fixed distances (0, 1·0, 2·5 and 4·0 m) from the shower centres and for 'core flattening', the cores becoming flatter, on average, as the shower size (primary energy) increases. With improved statistics on 4192 cores, the previous results are exactly confirmed.

1. Introduction. At the Bangalore Conference we reported the first measurements of the differential density spectra for cosmic-ray air showers at known fixed distances from the centres of shower cores (Hodson et. al., 1983a) and also evidence that as the shower size increases the cores, on average, become flatter (Hodson et.al.,1983b). In this paper we report data on a total of 4192 shower cores, increasing the statistics previously available. The conclusions regarding 'steepening' of the density spectra and 'core flattening' given at Bangalore are confirmed and it is shown that the flattening effect extends to at least 2·5 m radius from the shower centre.

2. Data and results. The data on particle distributions near to the cores of $10^{14} - 10^{16}$ eV air showers at Leeds (80 m above mean sea level, $1020\,\mathrm{g\,cm^{-2}}$) were obtained from a 7 m × 5 m array of discharge chambers. A particular feature of the apparatus is the precision (usually $\sim$0·1 m) with which the centres of symmetry of the shower cores can be located. The experimental arrangement, triggering system, and data analysis were exactly as described in the above 1983 papers. An additional 1589 shower cores have now been analysed and the combined data are given in Figures 1 and 2.

Figure 1 shows the differential spectra for densities $\rho(r)$ measured at r = 0, 1·0, 2·5, and 4·0 m from the shower centres. All four spectra are of a similar shape which may be approximated by two power law lines; all four spectra are consistent with a power law index of $\lesssim -2$ at low densities before steepening to an index of $\sim -3{\cdot}5$ at high densities. Deviations from the −2 power law at the lowest densities shown in Figure 1 are attributed to trigger and scanning bias. The 'central density' spectrum (Figure 1a) steepens at $\rho(0) \sim 800\,\mathrm{m^{-2}}$; for r = 1·0, 2·5, and 4·0 m the spectra steepen at lower density values. The 'join point' between the two power law lines occurs at about the same differential rate in each of the four spectra (horizontal dashed lines).

Figure 2 expresses the data on core flattening. The quantity $\langle\rho(r)\rangle$ is defined as the average density for all shower cores in a particular interval of $\rho(4{\cdot}0)$. The closer the ratio $\langle\rho(r)\rangle/\langle\rho(r')\rangle$ is to unity, where $r' < r$, the flatter is the particle distribution in the region between r' and r from the shower centre. In the absence of data on the

ORIGINAL PAGE IS
OF POOR QUALITY

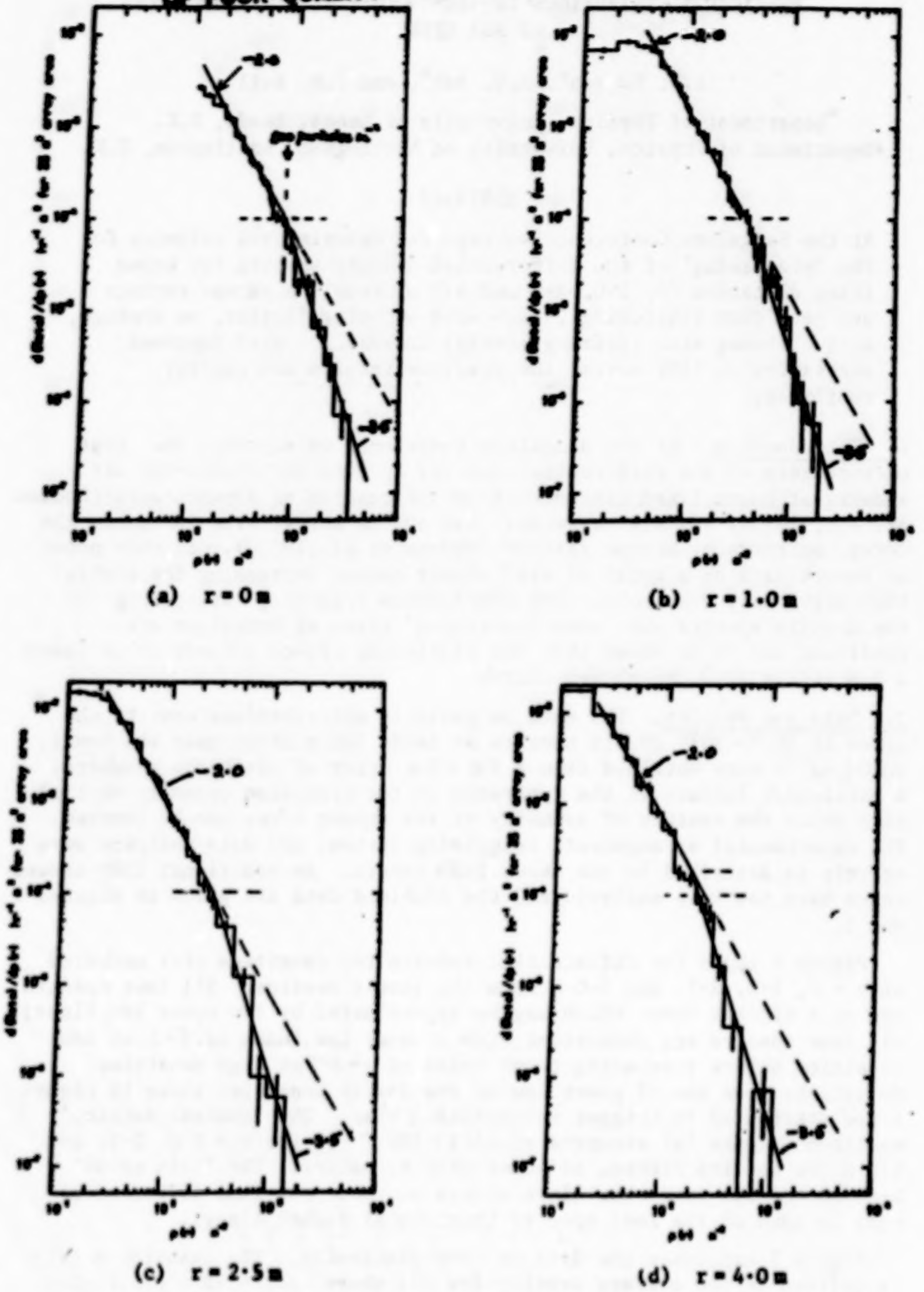

(a) r = 0 m (b) r = 1·0 m

(c) r = 2·5 m (d) r = 4·0 m

Figure 1. Experimental differential density spectra at known fixed distances (r) from the shower centre.

Total no. of shower cores: 4192; Run time: 7033 hours

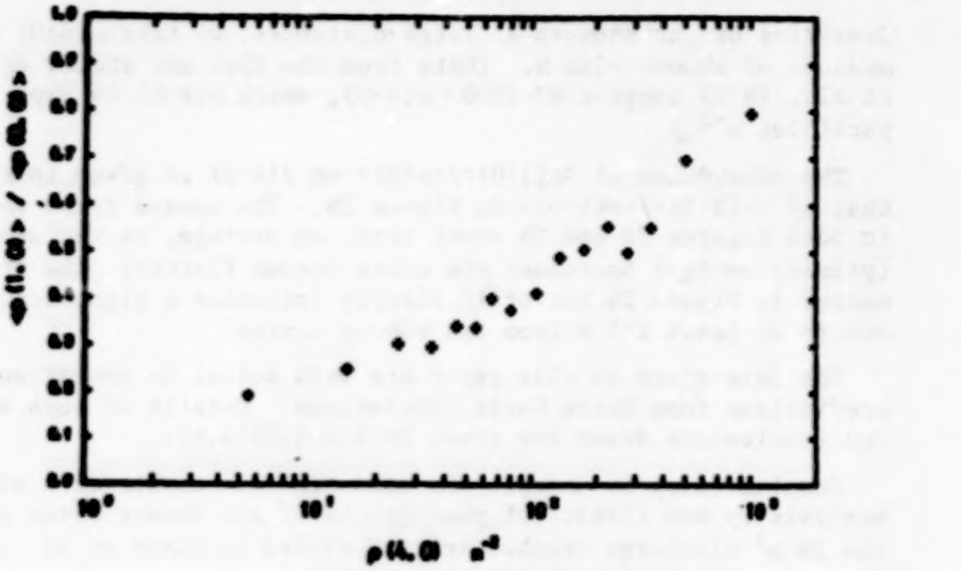

(a) 'Core flattening' between 0 and 1·0 m from the shower centre

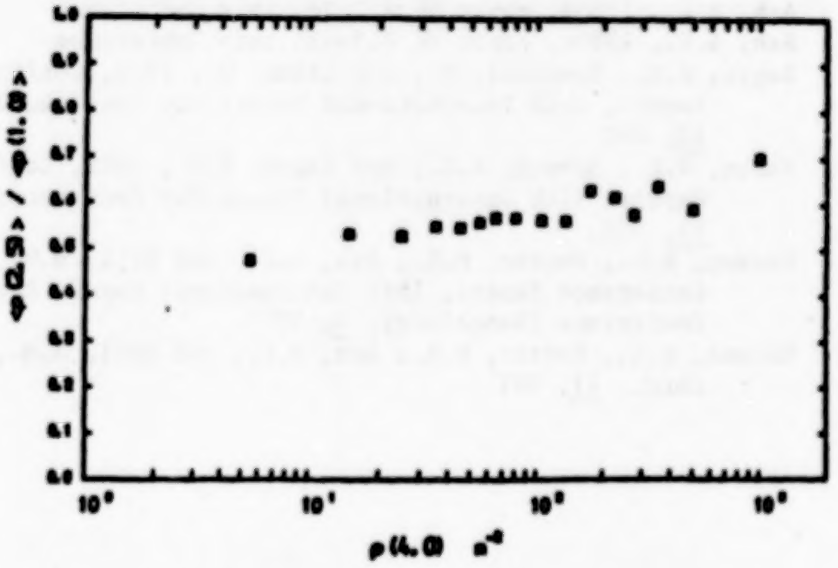

(b) 'Core flattening' between 1·0 and 2·5 m

Figure 2. Data showing that the particle distribution in shower cores becomes flatter, on average, as the shower size increases.

(The ordinate is a measure of the flatness of the distribution; the abscissa is an approximate measure of shower size.)

densities of our showers at large distances, we take $\rho(4\cdot0)$ as a rough measure of shower size N. (Data from the Kiel air shower array (Bagge et al., 1979) suggest $N \sim 2000 \times \rho(4\cdot0)$, where $\rho(4\cdot0)$ is expressed in particles m^{-2}.)

The dependence of $\langle\rho(1\cdot0)\rangle/\langle\rho(0)\rangle$ on $\rho(4\cdot0)$ is given in Figure 2a, that of $\langle\rho(2\cdot5)\rangle/\langle\rho(1\cdot0)\rangle$ in Figure 2b. The upward trend towards unity in both Figures 2a and 2b shows that, on average, as the shower size (primary energy) increases the cores become flatter; the trend is less marked in Figure 2b but still clearly indicates a significant flattening out to at least 2·5 m from the shower centre.

The data given in this paper are well suited to comparison with predictions from Monte Carlo simulations. Details of such simulations and conclusions drawn are given by Ash (1985a,b).

Complementary to the present data are the results of a similar analysis by Ash (1985c) of photographs of air shower cores observed in the 20 m^2 discharge chamber array operated by Hazen et al. (1981) at Sacramento Peak (730 g cm^{-2}), New Mexico.

3. Acknowledgements. This work was supported by the Science and Engineering Research Council. We especially thank our film scanners, Mrs J Barker and Mrs J Wilson, for their painstaking work.

References

Ash, A.G., 1985a, paper HE 4.2-15, this Conference
Ash, A.G., 1985b, paper HE 4.2-16, this Conference
Ash, A.G., 1985c, paper HE 4.2-18, this Conference
Bagge, E.R., Samorski, M., and Stamm, W., 1979, Conference Papers, 16th International Cosmic Ray Conference (Kyoto), 13, 260
Hazen, W.E., Hendel, A.Z., and Hazen, E.S., 1981, Conference Papers, 17th International Cosmic Ray Conference (Paris), 11, 350.
Hodson, A.L., Porter, M.R., Ash, A.G., and Bull, R.M., 1983a, Conference Papers, 18th International Cosmic Ray Conference (Bangalore), 6, 23
Hodson, A.L., Porter, M.R., Ash, A.G., and Bull, R.M., 1983b, *ibid.* 11, 201

N85-35991

HE 4.2 - 11

THEORETICAL STUDY OF EAS HADRONIC STRUCTURE

L. Popova
Institute of Nuclear Research and Nuclear Energy
Bld. Lenin 72, Sofia, Bulgaria

1. General remarks on the experimental data The structure of EAS is determined mainly by the energetic hadrons. They are strongly collimated in the core of the shower and essential difficulties are encountered for resolution of individual hadrons. The properties for resolution are different of the variety of Hadron detectors used in EAS experiments. This is the main reason making it difficult to obtain a general agreement between actually registered data with different detectors.

The most plausible source for disagreement is the uncertainity in determination of the energy of individual hadrons. A principal factor might be the incidence of multiple hadrons over large area detectors. Such measurements do not distinguish between events with one or more hadrons over the detectors and thus, provide an upper limit to the hadron energy flow/1/. For example, hadron measurements in Kolar Gold Fields/2/ performed with a deep iron calorimeter, include leakage of energy flow in the energetic electron component which arrives through the top layers and, particularly, through the sides of the calorimeter for inclined showers. This is valid, to a lesser extent for the measurements at Tian Shan/3,4,5/ performed with smaller ionisating detector. The measurements at Pic du Midi/6/ with flash tube hodoscope were relatively less affected due to the thickness of the detectors. In the scintilator burst detectors, distortion in hadron energy due to multiple hadron incidence is expected to play a significant role even though the individual scintilators occupy relatively small area as in the case of Norikura experiment/7/.

Many efforts during the last few years were devoted to estimation of the effect from multihadron incidence/8/. The signals observed in Ooty experiment/8/ with burst detectors were converted/9/ to hadron energy using conversion factor obtained with Monte Carlo simulations/1/. There was pointed out a reasonably good agreement/6/ between the results in Ooty experiment, and those from Pic du Midi. Nevertheless, significent difference is observed with the calorimeter measurements/2,3/. This situation is shown in fig.1 and 2, where we compared the experimental data of hadrons in EAS at different levels. All data are normalized assuming that the attenuation length of hadrons is 350 g.cm^{-2} /5/.

2. Analysis of the model calculations In the begining we want to point out an unespected effect revealed from the theoretical investigations, e.g. the change in the assumptions about the main parameters of high energy interactions, as well as for the nature of the primary particles, are relatively slightly affecting the properties of hadronic component in EAS at mountain altitudes. For example, the lateral distribution of hadrons (E_h>300 Gev) calculated by us on the basis of our new phenomenological model/10/, in which is assumed breaked scaling variable $x_s = x.\sqrt{s}^{\omega}$, is very similar to that

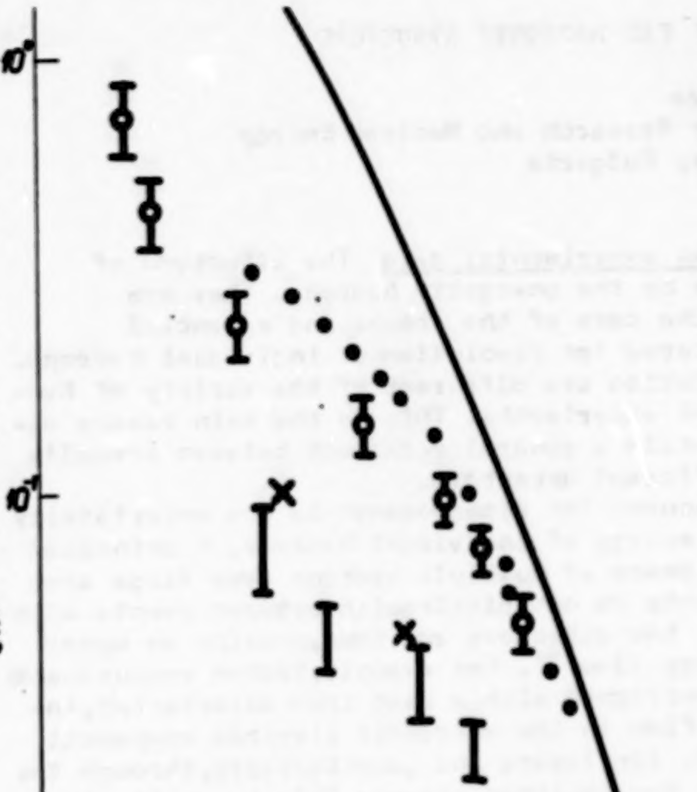

Fig.1 Lateral distribution of hadrons 300 Gev in EAS falling at mountain altitudes with intensity 1.6 $10^{-5}\mathrm{m}^{-2}\mathrm{s}^{-1}\mathrm{sr}^{-1}$
- Tien Shan data /3-5/
- ● Kollar Gold Fields data /2/
- ✕ Pic du Midi data /6/
- I Doty burst data /9/

ORIGINAL PAGE IS OF POOR QUALITY

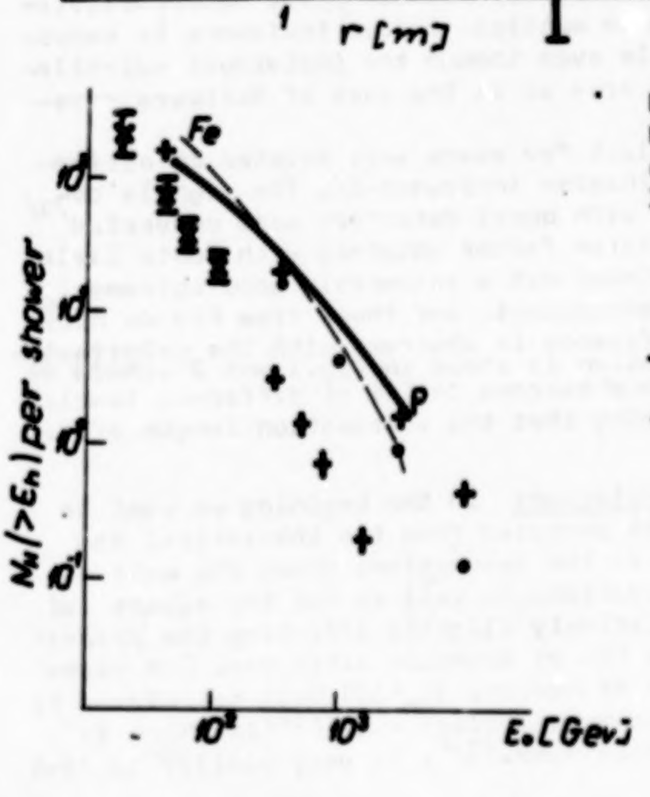

Fig.2 Energy spectrum of hadrons at mountain altitudes in EAS with intensity $10^{-5}\ \mathrm{m}^{-2}\mathrm{s}^{-1}\mathrm{sr}^{-1}$.
- ● Tien Shan data /3,4/
- ✚ Kolar Gold Fields data /2/
- Norikura data /7/
- Pic du Midi data /6/
- —— present calculations for proton showers,
- – – present calculations for iron primaries.

ORIGINAL PAGE IS
OF POOR QUALITY

obtained by Grieder/11/ assuming standard model with multiplicity $n_s \sim E^{0.437}$ in the both extreme cases of proton and iron primary spectrum. Similar small effect from the change of interaction models on EAS hadrons with different energies and in wide range of shower sizes is observed in comparing our breaked scaling model calculations with those of Kempa/12/ assuming standard model with different multiplicity laws ($n_s \sim E^{1/4}$ and $n_s \sim E^{1/2}$). All those facts are showing that in general, the number of hadrons at mountain altitudes is not very sensitive to the change of multiplicity law.

By means of the results obtained recently by Sreekantan et al/9/ with similar breaked scaling model we can see in fig.3 the influence of the assumption about the energy spectrum of the secondary particles, characterized by the scaling violation parameter α. They have assumed slight increase of α that equalizes our parameter ($\alpha = 0.13$ in Lab.system) at energies about 2.10^5 Gev. The steeper shape of curve 2 can be connected with the larger coefficient of inelasticity (0.72) in pion collisions assumed by Sreekantan et al.

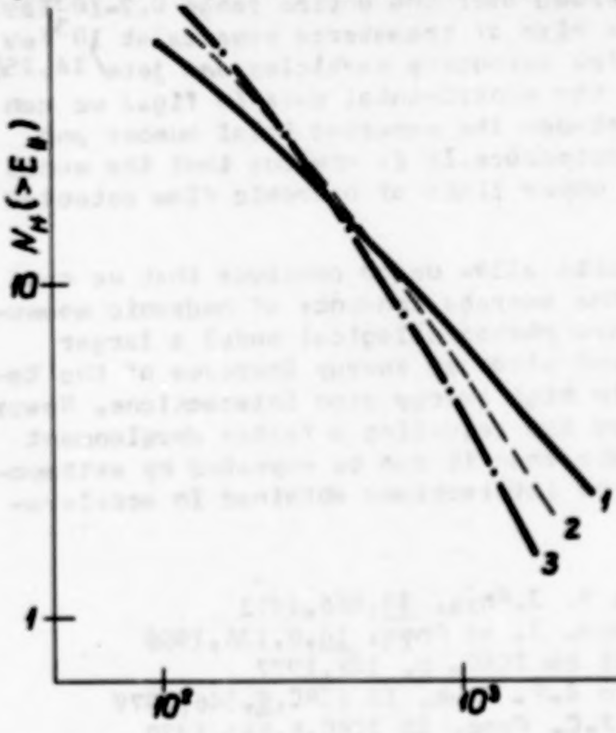

Fig.3 Comparison of the theoretical predictions for the energy spectrum of hadrons in EAS with size 1.5 10^5 at 785 $g\,cm^{-2}$ according to the present calculations for proton showers (1) with the estimations of Sreekantan et al/9/ for proton (2) and iron (3) primary spectrum

Similar effect give the calculations of Danilova et al/13/. Assuming $k_{\pi-air} = 0.84$ they obtain less number of hadrons in extensive showers (with a factor of 2) than we have calculated with $k_{\pi-air} = 0.5$

More essential is the effect from energy increase of the inelastic cross section. The number of hadrons calculated in/9/ for $\sigma^{in}_{p-air} = 260 + 11 \ln\left(\frac{E}{500}\right)^{1.4}$ is about 2 times smaller than in the case of logarithmic increase of σ^{in} assumed in our calculations.

The effect of primary particle mass on the properties of hadron component is illustrated in both figures 2 and 3 . We can see that even for the two extreme cases of pure proton and pure iron primary composition there is relatively small change in the energy spectrum of hadrons.

ORIGINAL PAGE IS
OF POOR QUALITY

3. Comparison with experimental data In fig.1 we have compared the results for hadron lateral distribution obtained in our calculations with breaked scaling model and hadron densities compiled from different mountain experiments. It is seen that the slope of the theoretical curve differes from the experimental distribution. That difference is substantial near the core of showers, where the effect of multiple hadrons in hadronic detection is rather strong. Appart the apparatus effect, the observed disagreement can be due to the fact that in our model calculations we have neglected the possibility for appearence of secondary pions with large transverse momentum (above 1.4 Gev/c). In fact there is observed in accelerator experiments up to 2.10^5Gev slight decrease in the slope of p_t-distribution. Certainly, existence of such pions should cause a flatter lateral distribution of shower hadrons near the core. However, drastic change of p_t-distribution, needed to explain the contradiction in fig.1 was not observed over the entire range $0.2-10^3$Tev. It might be supposed that the rise of transverse momenta at 10^3Tev could be attributed to only few secondary particles and jets/14,15/.

From the comparison with the experimental data in fig.2 we can see an apparent difference between the expected total number and the measurements with burst detectors. It is obvious that the model calculations are fitting the upper limit of hadronic flow detected with calorimeters.

4. Conclusion The above results allow us to conclude that we can get a better agreement with the average tendency of hadronic measurements if we assume in our new phenomenological model a larger coefficient of inelasticity and stronger energy increase of the total inelastic cross section in high energy pion interactions. Nevertheless, EAS data above 10^5Gev are revealing a faster development of hadronic cascades in the air than it can be expected by extrapolating the parameters of hadron interactions obtained in accelerator measurements.

References

1. Tonwar S.C. and Sreekantan V. J.Phys. A4,868,1971
2. Chatterjee B.K. et al. Canad. J. of Phys. 16,8,136,1968
3. Romachin V. et al. Proc. 15 th ICRC, 8, 107,1977
4. Nesterova N.M. and Chubenko A.P. Proc. 16 ICRC,8,346,1979
5. Nesterova N.M. and Dubovy A.C. Proc. 16 ICRC,8,845,1979
6. Van Staa R. et al. J.Phys. A1,135,1974
7. Miyake S. et al. Proc. 16 ICRC, 13,165,1979
8. Vatcha R.H. and Sreekantan S.V. J.Phys. A6,1050,1057,1973
9. Sreekantan R.V. et al. Phys. Rev.(in press),1983
10. Popova L. Acta Universitatis Lodziensis,1984,Lodz, Poland
11. Grieder P.K. Proc. 17 ICRC 8, 288,1981
12. Kempa J. Nuovo Cimento 31, 568,1979
13. Danilova T.V. and Erlykin A.D. Preprint Number 85 of Lebedev
   Institute of Physics,Moscow,1984
14. Nikolski S.I. Journal of Theoretical and Experimental Physics
   51,80,1966
15. Brasil-Japan Emulsion Chamber Collab.-AIP Conf.Proc.49,New Yourk
   145,1979.

N85-35992
HE4.2-15

MONTE CARLO SIMULATIONS OF ELECTRON LATERAL DISTRIBUTIONS IN THE CORE REGION OF $10^{13}-10^{16}$ eV AIR SHOWERS

A.G. Ash

Department of Physics
University of Leeds
Leeds LS2 9JT
U.K.

ABSTRACT

This paper contains details of computer models of shower development which have been used to investigate the experimental data on shower cores observed in the Leeds 35m^2 and Sacramento Peak (New Mexico) 20m^2 arrays of current-limited spark ("discharge") chambers. The simulations include predictions for primaries ranging from protons to iron nuclei (with heavy nuclei treated using both superposition and fragmentation models).

1. Introduction

Analysis of photographs of $10^{14}-10^{16}$ eV air shower cores in arrays of current-limited spark chambers at Leeds (1020 g cm^{-2}) and Sacramento Peak (730 g cm^{-2}) has provided data on particle distributions within a few metres of the shower axis in the form of density spectra and density averages measured at known fixed distances from the shower centre (Ash, 1985a, Hodson et al., 1983a,b, 1985). Comparison of these results with Monte Carlo simulation predictions by Ash (1985a,b) has demonstrated the failure of the scaling model. Details of the calculations are presented in this paper (see also Ash, 1984).

2. Hadron collision models

Simulation techniques based in the laboratory frame were used, and the models generated only pions and leading nucleons; nuclear target effects were neglected. The energy-splitting algorithms of Hillas (1981) were used to generate "radial scaling" secondary energy spectra in pion collisions (Fig.1a) and nucleon collisions (Fig.1b), except that for the latter, the flat leading nucleon spectrum given was replaced by a more accurate form (Hillas, 1979a): the elasticity $X = E_{nuc}/E_o$ was sampled using $X = 0{\cdot}76a + 0{\cdot}24a^4$ (instead of $X = a$) where a is a random number (0·0....1·0). (If, as a result, E_{nuc} was less than the nucleon rest energy mc^2 then $E_{nuc} = mc^2$). For $E_o \gg mc^2$ the resulting average elasticity is equal to 0·42.

Transverse momenta were sampled from the energy-independent distribution $h(p_t)dp_t = p_t e^{-p_t/p_o}$ with p_o equal to 0·24 GeV/c for secondary pions (in both pion and nucleon collisions) and equal to 0·28 GeV/c for leading nucleons. (If $p_t > p$ then the secondary was considered to be going backwards and was dropped from the cascade.)

Mean free paths for nucleon-'air' nucleus collisions (Fig.2) based on nucleon-nucleon cross sections rising as $\ln^2 s$ at high energy were as

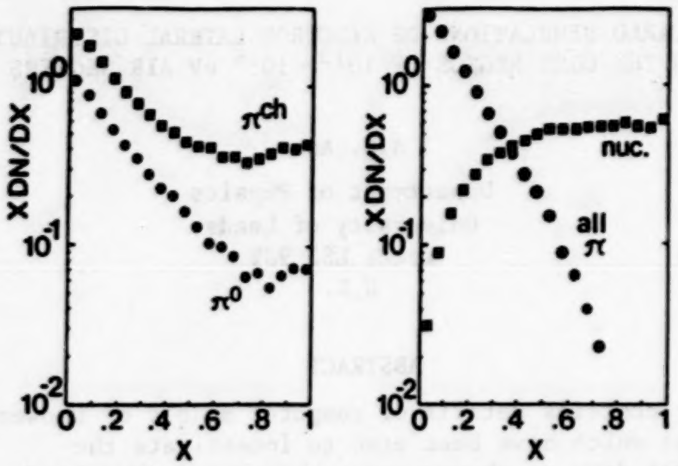

(a) Pion collisions (b) Nucleon collisions

Fig. 1 Particle production spectra in simulated 100 GeV hadron-'air' nucleus collisions. X is the secondary energy divided by the projectile energy, both measured in the laboratory frame

given by Hillas (1979b); those for pion collisions were obtained by scaling up the nucleon mean free paths by (114/86) at all energies.

3. Nuclear fragmentation models

The "superposition model" was used i.e. a shower with primary mass number A, energy E_{prim}, was taken as a co-axial superposition of A proton showers with energy E_{prim}/A. A more realistic treatment of primaries ranging from helium nuclei to iron nuclei was given in the one-dimensional "fragmentation model" which is based mainly on emulsion data and follows quite closely the Bartol model (Gaisser et al., 1982) with which it is in good agreement for the average distribution in the atmosphere of the "first" inelastic collisions of primary nucleons. Excellent agreement with Freier and Waddington's (1975) simulation predictions of the average rate of release of nucleons from projectile nuclei as a function of atmospheric depth is obtained using the Cleghorn nucleus-nucleus cross sections, adopted by them, instead of the larger cross-sections of Gaisser et al. (1982) normally used.

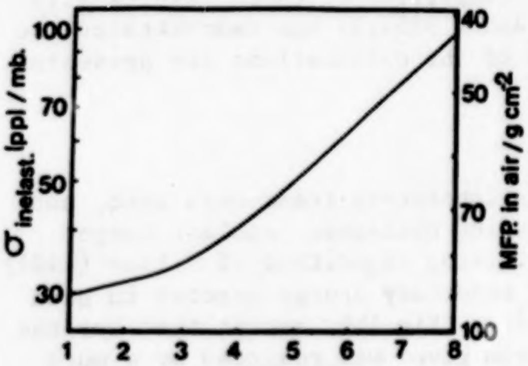

Fig. 2 Inelastic pp cross-sections and corresponding mean-free-paths in air used in simulations

4. Propagation model

A non-isothermal atmosphere was used. Coulomb scattering and ionisation loss (2·2 MeV per $g\,cm^{-2}$) were applied to hadrons, but were neglected for projectile nuclei in the "fragmentation model". Geomagnetic effects were neglected.

5. Electromagnetic cascade function

An average development function based on unpublished Monte Carlo calculations for photon-initiated cascades by A.M. Hillas was used. The electron density at 1020 g cm^{-2} (Leeds) for cascades due to vertical photons was

$$\rho(r) = \frac{1}{2\pi r}\frac{dn(r)}{dr}(1 + r/45)^{-3}\ \mathrm{m}^{-2} \quad \text{with} \quad n(r) = \frac{a}{\sqrt{y}}\, e^{t(1 + \ln f/0{\cdot}72)}$$

$$\text{and} \quad a = 0{\cdot}460/(1 + 0{\cdot}380/x) \qquad x = E.r/5{\cdot}8093$$

$$f = 1 - 0{\cdot}72(1 - y/t) \qquad y = \ln(1 + 2{\cdot}390x)$$

E is the photon energy in GeV, and t is the vertical thickness (r.l.) between the photon production point (π^0 decay) and the observation level. A radiation length of 36·1 g cm^{-2} was used. If a cascade was inclined this was taken into account by multiplying the density calculated from the formula by the cosine of the zenith angle and taking t equal to the slant thickness, and r equal to the perpendicular distance from the cascade axis.

The cascade function has been used directly for each photon (EMC Model I) or in conjunction with a simple Monte Carlo technique to simulate fluctuations in the formation of the first e^+e^- pair (EMC Model II).

Mountain level calculations involved rescaling the above electromagnetic cascade lateral distributions according to the lower air density.

6. Simulation of the electron distribution in the shower core

(a) Calculations for Leeds

A map of the core region was obtained by superposing electromagnetic cascades, taking into account the direction and location of their axes. In each shower simulation the shower primary was directed at the centre of a square of side 10·2 m located in the observation plane. The square was subdivided into $(51)^2$ equal squares, and the counts of electrons deposited in each of them determined using the cascade function. Computing time consumed in doing this was saved by ranking photons so as to concentrate the most detailed calculations on photon cascades with the densest "cores", and by "thin sampling" (Hillas, 1981) of low energy hadrons. Calculations for photon energies down to 1 GeV from π^0 decay could therefore be made on a routine basis.

After calculating the electron counts the simulation program searched for a shower centre (centre of symmetry) in the central $(7{\cdot}6)^2\,\mathrm{m}^2$ of the mapping area (most of the shower centres, located to within ∿5cm, fall within 0·5 m of the centre of the mapping area). The shower was discarded if a shower centre was not found in the "search area", and also if the electron density, averaged over 2 × 2 adjacent square elements of the mapping area, did not exceed 50 m^{-2} somewhere in the mapping area.

If the shower was not discarded then densities at various radial distances from the shower centre were obtained, as in the experimental work (Hodson et al., 1983a,b, 1985), from counts made in an "annular grid", in this case, "superposed" over the mapping area. The grid used consisted, as in the experiment, of a series of concentric circles, starting with a radius of 0·25 m and then with radii increasing in 0·5 m steps. For the above experimental work the annuli were divided into equal areas of $\pi/16m^2$. However for the simulations it was more convenient to divide the annuli angularly each into 16 sections ("sampling bins") by common radii from the centre. The difference between the two procedures is not significant: both give densities for the same radial widths.

Counts were obtained in the "sampling bins" with the "annular grid" centred on the shower centre. The central count, calculated by integrating the electron density over the area of the central bin, gave the density corresponding to the experimental central density $\rho(0)$. Counts in the annuli at 1·0, 2·5 and 4·0 m were derived from the mapping area counts and gave densities corresponding to the experimental densities $\rho(1{\cdot}0)$, $\rho(2{\cdot}5)$ and $\rho(4{\cdot}0)$ respectively. These results were supplemented by counts, determined as above, in the remaining annuli out to 4·5 m and by densities calculated at points in the mapping plane further out. The radial density distribution was thus sampled at intervals of 0·5 m out to 7·0 m from the shower centre.

(b) Calculations for Sacramento Peak

Both the calculations and the experimental analysis are made using the corresponding Leeds-level grids with dimensions in array space scaled up according to the lower air density found at mountain level.

7. Construction of density spectra etc.

Predictions of the average lateral distribution and density spectra at fixed distances from the shower centre have been obtained for a wide choice of primary composition and energy spectra. A technique of weighting the simulated showers according to the primary fluxes assumed was used to obtain results for different primary energy spectra.

8. Acknowledgements

The author thanks Dr A.M. Hillas for his help with this work, and the Science and Engineering Research Council for support in the form of a Post-Doctoral Research Fellowship.

References

Ash, A.G., 1984, Ph.D.thesis, University of Leeds
Ash, A.G., 1985a, paper HE4.2-18, this Conference
Ash, A.G., 1985b, paper HE4.2-16, this Conference
Freier, P.S. and Waddington, C.J., 1975, Astrophys.Sp.Sci., 38, 419
Gaisser, T.K. et al., 1982, Phys.Rev., D25, 2341
Hillas, A.M., 1979a, Haverah Park Note, September 1979
Hillas, A.M., 1979b, 16th ICRC, Kyoto, 6, 13
Hillas, A.M., 1981, 17th ICRC, Paris, 8, 193
Hodson, A.L. et al., 1983a, 18th ICRC, Bangalore, 6, 23
Hodson, A.L. et al., 1983b, 18th ICRC, Bangalore, 11, 201
Hodson, A.L. et al., 1985, paper HE4.2-10, this Conference

N85-35993

HE 4.2-16

COMPARISON OF SIMULATION RESULTS WITH SEA-LEVEL EXPERIMENTAL DATA ON $10^{14}-10^{16}$ eV AIR SHOWER CORES

A.G. Ash

Department of Physics, University of Leeds, Leeds LS2 9JT, U.K.

ABSTRACT

Simulation predictions for the Leeds 35 m^2 horizontal discharge chamber array for proton primaries with a $\sim E^{-2.7}$ spectrum extrapolated from balloon data to 10^{16} eV give power law $\rho(r)$-spectra with constant slope ~ -2 consistent with the experimental data up to the point at which they steepen but overshooting them at higher densities, and at high shower sizes predicted cores which are significantly steeper than those observed. Further comparisons with results for heavy nuclei primaries (up to A = 56) point to the inadequacy of changes in primary composition to account for the observed density spectra and 'core flattening', and the shower size spectrum together, and point, therefore, to the failure of the scaling interaction model at $\sim 10^{15}$ eV primary energy.

PARTICLE DISTRIBUTIONS IN $\sim 10^{13} - 10^{16}$ eV AIR SHOWER CORES AT MOUNTAIN ALTITUDE AND COMPARISONS WITH MONTE CARLO SIMULATIONS

A.G. Ash

Department of Physics, University of Leeds, Leeds LS2 9JT, U.K.

ABSTRACT

Photographs of 521 shower cores in an array of current-limited spark ('discharge') chambers at Sacramento Peak (2900m above sea level, 730 g cm^{-2}), New Mexico, U.S.A., have been analysed and the results compared with similar data from Leeds (80m above sea level, 1020 g cm^{-2}). It was found that the 'central' density differential spectrum is consistent with a power law index of -2 up to $\sim 1500 m^{-2}$ where it steepens, and that shower cores become flatter on average with increasing size.

Scaling model predictions for proton primaries with a $\propto E^{-2.71}$ energy spectrum account well for the altitude dependence of the data at lower densities. However, deviations at higher densities indicate a change in hadron interaction characteristics between $\sim$ few $\times 10^{14}$ and 10^{15} eV primary energy causing particles close to the shower axis to be spread further out.

1. Introduction. Experimental data on particle distributions within a few metres of the axes of air showers at Sacramento Peak (2900m above sea level, 730 g cm^{-2}), New Mexico, U.S.A., are described. The data are the results of the author's analysis of photographs of showers in an array of current-limited spark chambers ('discharge' chambers) operated by Hazen et al. (1981). These photographs were originally obtained as part of a search for high-p_t subcores.

The results are compared with similar data from the $35 m^2$ discharge chamber array at Leeds (80m above sea level, 1020 g cm^{-2}) (Hodson et al., 1985) and predictions from Monte Carlo simulations.

2. Experimental Details. The array was housed under a canvas tent and was photographed from above using a small camera. During the experimental runs used as the basis for the present work the array consisted of 20 $1 m^2$ discharge chambers (nearly identical to those used at Leeds) arranged into 4 parallel rows each of 5 chambers, with $\sim$30cm gaps (walkways) between adjacent rows and the chambers in each row close-packed to give in most cases only $\sim$3cm width of dead space between them. The trigger condition was a particle density $\gtrsim 50 m^{-2}$ in a scintillator near the centre of the array in coincidence with at least one particle in a scintillator a few metres outside the array. The trigger rate was $\sim 10 hr^{-1}$.

3. Analysis and Results. The methods of analysis of the shower photographs follow closely those of Hodson et al. (1983a,b) for the Leeds data. The photographs (negatives on 35mm film) were projected at a linear demagnification of 8 in array space and scanned by eye for cores. Core location and subsequent density measurements made use of an annular grid, superposed over the projected image, identical in pattern to that used for the Leeds photographs (see Hodson et al., 1983a) but with its dimensions (in array space) linearly scaled up by a factor s=(1020/730). This was to take approximately into account the effect of the difference in air density on particle densities when comparing the data for Leeds and Sacramento Peak. As in Hodson et al. (1983a) the grid was used to determine a shower centre (centre of symmetry) for the particle distribution of each core located in the array area and, with the grid

centred on the shower centre, densities at various radial distances were determined. To reduce the effects of trigger bias and scanning bias the analysis excluded all showers with centres located in the walk-ways between the rows of chambers, those with centres falling in the 4 corner chambers and any in the remaining outer chambers with centres falling within 0.4m of the edge of the array. The total collecting area for shower cores was then equal to $\simeq 12\text{m}^2$.

A count of discharges in the centre circle (radius 0·25s m) of the grid gave the 'central' density; when a walk-way overlapped part of the centre circle (maximum 50%) then symmetry was used to obtain the count for the whole of its area. Counts in the angular sections of the annuli at the scaled distances s m and 2·5s m gave densities at these distances. (In general, counts were made in only one randomly-selected section in each of these annuli.)

In the rest of this paper, observed particle densities per m^2 (i.e. count/actual bin area in array space) are given, rather than densities scaled up by a factor s^2.

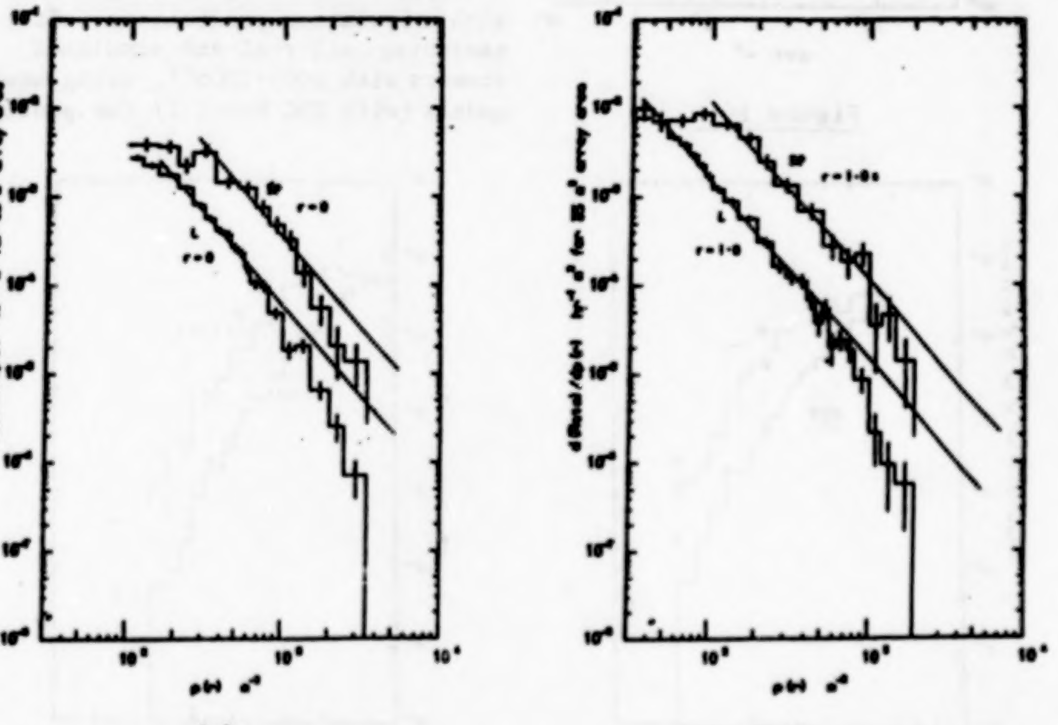

(a) (b)

Figure 1 Differential density spectra ρ(r) observed at Leeds (L) and Sacramento Peak (SP)

Figure 1 shows the differential density spectra for 521 cores at 0, 1·0 s, and 2·5 s m from the shower centre (normalised to a 35m^2 collecting area) as observed at Sacramento Peak, compared with the corresponding experimental data for Leeds. Power law lines of index −2 have been superposed on the spectra to show the steepening at high densities in the Leeds data (see Hodson et al., 1985) and for comparison with Sacramento Peak. (The deviations of the spectra from the −2 power law at low densities are due to trigger and scanning bias.) In Figure 1(a) there is evidence of a

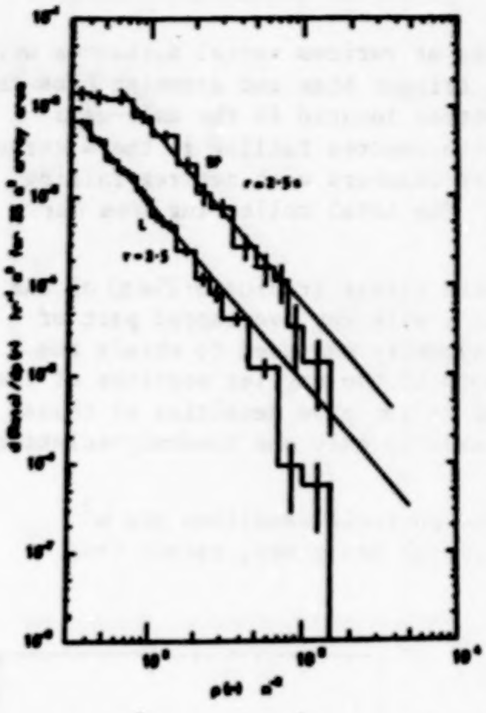

Figure 1(c)

steepening from the -2 power law in the Sacramento Peak ρ(0) spectrum at ~1·5.10^{3}m^{-2}; the spectra further out (Figures 1(b) and 1(c)) may also steepen around 10^{3}m^{-2} but this is less clear.

Figure 3 gives a plot of core 'flatness', <ρ(1·0 s)>/<ρ(0)>, versus ρ(2·5 s) (used as a measure of shower size, as ρ(4·0) in Hodson et al., 1985); this shows a tendency for shower cores to become flatter within s(=1·4)m as the showers become larger (as also reported for the Leeds data (Hodson et al., 1985)). Taking Figures 1 and 3 together, steep dense shower cores are observed at a lower rate than might be expected by extrapolation.

Figures 2 and 3 give comparisons with simulation predictions, after excluding all real and simulated showers with ρ(0)<100m^{-2}, using scaling models (with EMC Model I) for proton primaries, described by Ash (1985a). The full detailed core-mapping calculations were used for comparison with the Leeds data; for Sacramento Peak a simpler calculation was used, with the shower centre assumed to coincide with the shower axis. For the present purposes this

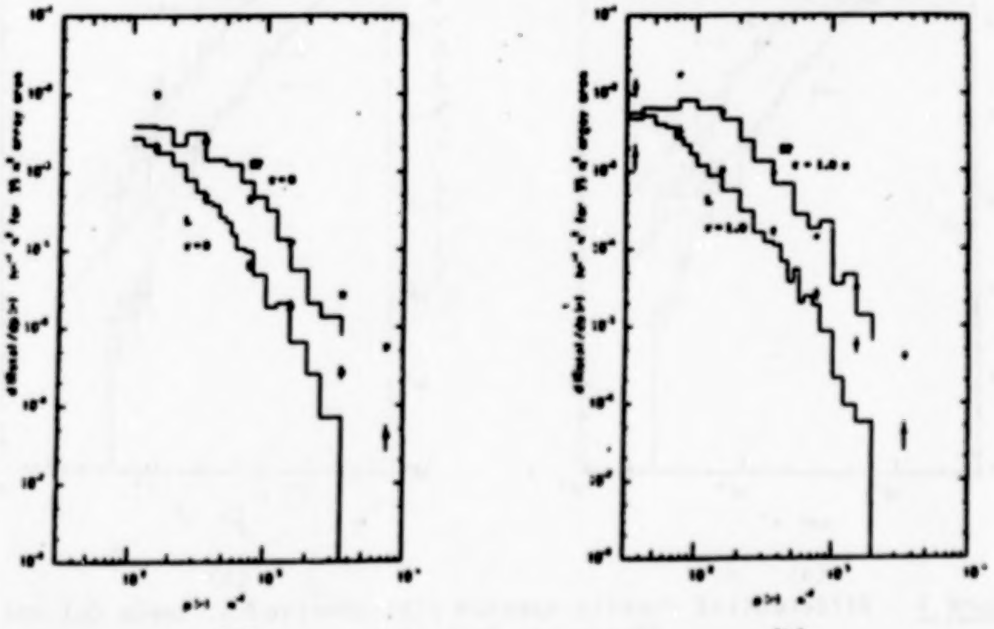

(a) (b)

Figure 2 Comparison of observed differential density spectra (histograms) at Leeds (L) and Sacramento Peak (SP) with simulation predictions (points)

ORIGINAL PAGE IS
OF POOR QUALITY

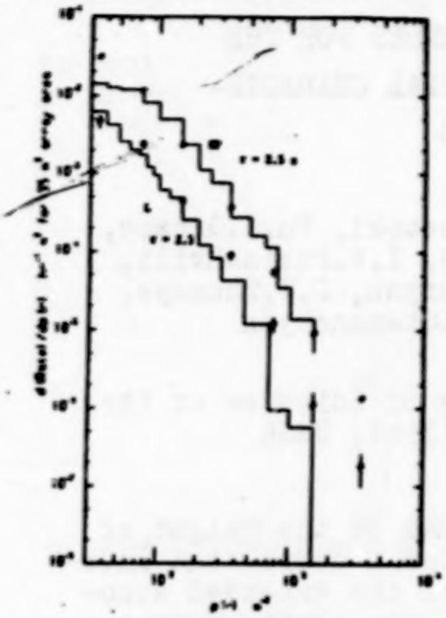

Figure 2(c)

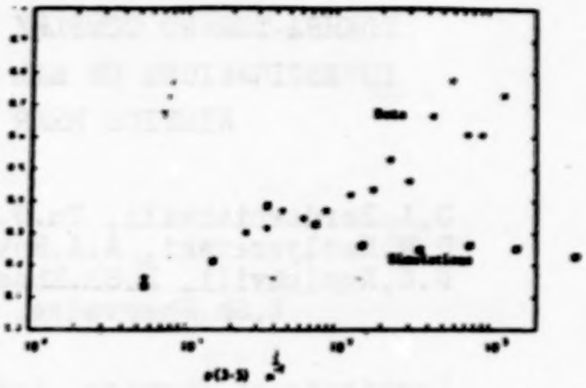

Figure 3 'Core flattening' at Sacramento Peak

difference is unimportant. The proton primary energy spectrum was $dn/dE = 1{\cdot}36 \times 10^4 E^{-2.71}$ Gev^{-1} m^{-1}sr^{-1} s^{-1}, consistent with balloon-based observations, here extrapolated to 10^{16} eV. The predictions agree well with the observed spectra both in slope and in absolute rates in the −2 power law region, where proton showers would be expected to dominate the spectra. At higher densities, all the Leeds spectra and the Sacramento Peak $\rho(0)$ spectrum are clearly steeper than those predicted.

Figure 3 shows that the predicted large proton showers have much steeper cores, on average, than those observed, as was also found for the Leeds data (Ash, 1985b).

4. Discussion.

It is interesting to consider the mean primary energy $\langle E \rangle$ of showers with a given $\rho(r)$ at Sacramento Peak. At $\rho(0) = 1{\cdot}5 \times 10^3$ m^{-2} the proton simulations predict $\langle E \rangle = 6 \times 10^{14}$ eV; if the steepening of the $\rho(0)$ spectrum is due to a rapid increase in the slope of the proton primary energy spectrum then a clear steepening should also occur for similar values of $\langle E \rangle$ in the density spectra further out. At 2·5 m and 5 m from the shower centre $\langle E \rangle = 6 \times 10^{14}$ eV corresponds to densities of ∼200m^2 and 400m^{-2} respectively; no steepening is evident at around these densities. This, together with the observed core flattening, lends support for a significant change in hadron interaction characteristics between primary energies of ∼ a few × 10^{14} and 10^{15} eV. A natural explanation might be found in a mechanism which spreads particles out from within ∼1m of the shower centre. Complete understanding probably requires the combined effect of interaction changes plus some steepening in the proton energy spectrum.

5. Acknowledgements.

Grateful thanks go to Professor W.E. Hazen for loan of the Sacramento Peak shower photographs, to Dr A.L. Hodson for help in preparing this paper, and to Dr A.M.Hillas for his advice. The Science and Engineering Research Council provided a Post-Doctoral Fellowship.

References (ICRC = International Cosmic Ray Conference)

Ash, A.G., 1985a, paper HE 4.2-15, this Conference
Ash, A.G., 1985b, paper HE 4.2-16, this Conference
Hazen, W.E., Hendel, A.Z., and Hazen, E.S., 1981, 17th ICRC (Paris), 11, 330
Hodson, A.L., Porter, M.R., Ash, A.G., and Bull, R.M., 1983a, 18th ICRC (Bangalore), 6, 23
Hodson, A.L., Porter, M.R., Ash, A.G., and Bull, R.M., 1983b, *ibid*, 11, 301
Hodson, A.L., Ash, A.G., and Bull, R.M., 1985, paper HE 4.2-10, this Conference

N85-35995

TSKHRA-TSKARO COMPLEX INTENDED FOR THE INVESTIGATIONS OF EAS SPATIAL CHARACTERISTICS NEAR AXIS

O.L.Berdzenishvili, Yu.G.Verbetski, Yu.A.Gromov,
D.M.Kotlyarevski, A.A.Novalov, I.V.Paziashvili,
N.S.Rusishvili, L.Sh.Khachaturyan, P.V.Tsomaya,
Z.Sh.Sharvadze, G.Z.Stemanetyan

Institute of Physics, Academy of Sciences of the
Georgian SSR, Tbilisi, USSR

Tskhra-Tskaro EAS complex located at the height of 2500 m above sea level is intended for a correlated investigation of three main components of the extended atmospheric showers (EAS) - hadron, muon and electron-proton ones - near the shower axis. This complex is aimed at the investigation of proton and primary cosmic radiation nucleus interactions with the nuclei of air atoms within the energy range $10^{14} - 10^{16}$ eV.

The complex will consist of the following basic parts (see Fig.1):

1. Shower part of the complex for the measurement of the shower electron-proton component (N°3,4,5,8).
2. Mobile master device (N°9).
3. The installation for the investigation of hadron nuclear interactions BAS-„ЯВА" (N°1,6).
4. „Video-EAS" installation (N°2,7).
5. μ-detector installation (Fig.2, N°6).

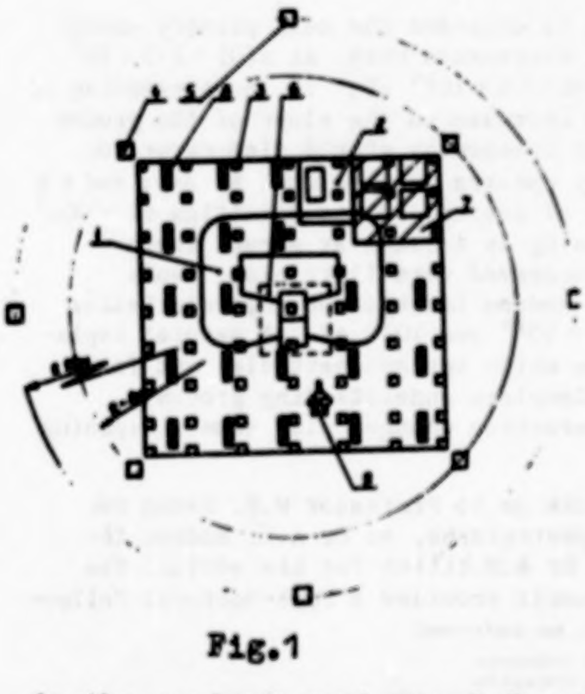

Fig.1

I The shower part is an installation of central type including scintillation and ionization sensors for the measurements of the energy and direction of the particle generating an EAS, the avalanche age, the spatial behaviour of its basic components, EAS axis restoration.

The dimensions of scintillators (3 cm thick) used in the central part are 0.5 x 0.5 m^2 the information pick-up from the detector corner.

The scintillators are 1.5 m distant from each other, filling an area of ~ 160 m^2. It is also planned to locate on this area paired ionization chambers ~ 5 m distant from each other (see Fig.1). Thus, a sufficiently detailed reproduction of the EAS central part is achieved.

The periphery of the shower part of the complex consists of two groups of scintillation detectors. One of them (4 detectors) will be situated along a circumference with a radius of 8 m centered in the geometric centre of the complex, while the second similar group of detectors will be situated at a radius of ~ 50 m with respect to the geometric centre (see Fig.1). In the peripheric scintillators, the detectors 3 cm thick with the dimensions of 1 x 1 m^2 are used, with the information pick-up from the top.

II. Mobile master device represents three scintillation counters close to each other and switched for coincidence with the dimensions 0.5 x 0.5 x 0.5 m^3 (Fig.1, N°9), which will detect the atmospheric showers with the energy $E \geqslant 10^{14}$ eV and define the axis position.

Moving the singling-out system within the distance of 0 ÷ 15 m from the spark chambers, one may obtain the averaged spatial distribution of EAS components by measuring the particle density in spark chambers.

III. The installation " ЯВА" has been working at the station for 10 years serving for the investigation of hadron interaction with nuclei within the energy range 0.1 ÷ 10 TeV. This unit includes a magnetic spark spectrometer (MSS) and a „small" ionization calorimeter (SIC). Spark chambers (Fig.1, N°5, Fig.2, N°1,5) intervaled with targets 0.1 nuclear interaction length thick are situated in the upper part of the magnet gap. This unit serves to determine the direction of an incident charged hadron and the characteristics of secondary particles.

IY. "Video EAS" apparatus is intended for a detailed investigation of EAS characteristics near the axis, as well as correlations between them, using spark and ionization chambers. The apparatus contains a large ionization calorimeter (BIC) (Fig.2, N°3), and its depth is supposed to reach 1000 g/cm^2. At present, ~ 200 g/cm^2 of the absorbent is laid, and one layer of ionization chamber with a total number of the registration channels equal to 16 is mounted.

A part of the spark chambers of the "Video EAS" apparatus is mounted under the large ionization calorimeter (Fig.2, N°4) and serves for the simultaneous observation of hadron and muon EAS components. In the course of the experiment, muon registration threshold will be increasing beginning from $E \geqslant 0.5$ GeV at the BIC thickness of 0.2 kg/cm^2. (Hadron registration threshold are approximately 50 times higher).

In the other part of spark chambers located in the immediate vicinity of BIC, the electron-photon EAS component with the energy threshold of ~ 2 MeV is registered. The upper and lower walls of the chambers are transparent, and the inner volume is photographed with the cameras.

Y. μ-detector is located under the SIC of apparatus and consists of two-spark chambers interleaved with magnetized iron (the magnetic field intensity is ~ 2 T) and scintillation starting device. The distance between the layers of chambers is ~ 145 cm. The photographing will be accomplished using the cameras RFK-5 constitutingstereopairs, which is necessary to restore the spatial pattern and momentum measurements. The energy threshold of registration depends on μ-meson direction and varies within $3 \div 10$ GeV.

VI. At the Institute of Physics of the Academy of Sciences of the Georgian SSR, a two-level system of using microcomputer "Electronics-60" at the first level and the computer "SM-4" at the next one is developed. According to our plans, the computer "Electronics-60" will be carry out the calibration of scintillators and ionization chambers, the spectra treatment, etc., while the total complex treatment of the whole system will be carried uot by the computer SM-4.

VII. The problems, solved using the above complex.

The complex character of the device permits to study a wide range of nuclear-physical, cosmophysical and astrophysical problems.

It is planned to study the character of transverse pulse behaviour near the axis, momentum and angular correlations between hadrons and muons and each other, to investigate the secondary particle composition (the relationships between neutron and charged components) and to study μ-meson group fluctuations in order to obtain the information on the primary composition, to study in detail the behaviour of primary particle and nuclei spectra within the energy range of $10^{14} \div 10^{16}$

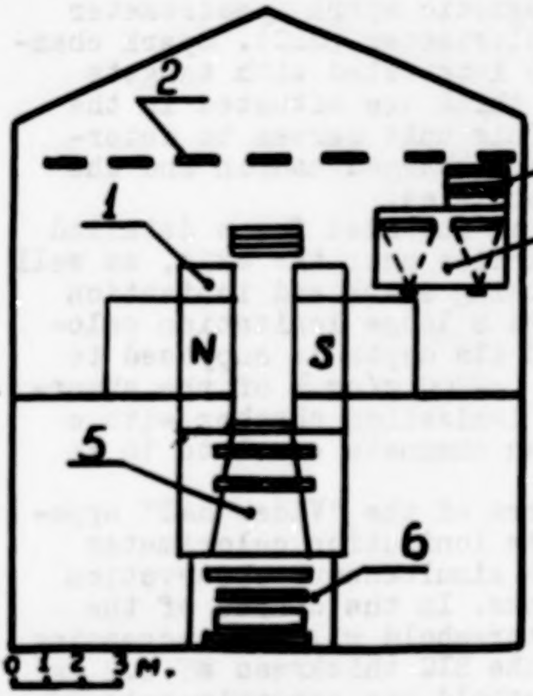

Fig.2

Each unit of the complex described above has been tested. It is planned to put Tskhra-Tskaro installation in operation by the end of 1986.

N85-35996

HE 4.3-1

A NEW STUDY OF SHOWER AGE DISTRIBUTION IN NEAR VERTICAL SHOWERS BY NBU AIR SHOWER ARRAY

N.Chaudhuri, D.K.Basak, G.C.Goswami and B.Ghosh
Department of Physics
North Bengal University
Darjeeling - 734430, India

The air shower array has been developed since it started operation in 1981. The array covering an area of 900 m^2 now incorporates 21 particle density sampling detectors around two muon magnetic spectrographs. The air showers are detected in the size range 10^4 to 10^6 particles. A total of 11000 showers has so far been detected. Average values of shower age have been obtained in various shower size ranges to study the dependence of shower age on shower size. The core distance dependence of shower age parameter has also been analysed for presentation in the conference.

1. Introduction The age parameter which was calculated by fitting a particular shower with a given structure function is not constant over all core distances and shower sizes. Moreover the lateral distribution function does not fit well over all distances with the single age parameter. The age determination has been done using NKG as a reference function and also the forms of Hillas et al[1], and Lagutin et al[2]. In all the cases of shower analysis it has been found that the age lies between 0.8 to 1.7 for various shower sizes in the range 10^4 to 10^6 particles. In the present study the shower size 'N_e' and shower age 's' (average and local shower age) have been determined through standard χ^2 - method using NKG and various structure functions.

2. Methods In an array of 21 detectors covering an area of 900 m^2, the density of the particles is estimated from the printed recording of the shower particles in each detector.

The shower age which is estimated by fitting the shower densities (r) with the help of the χ^2-minimisation method is shown in the figures for showers falling within zenith angle 0° - 30°. The fitting of NKG function for extensive air shower lateral electron distribution for a single age parameter gives some systematic errors. Hence the term 'local age parameter' (l.a.p.) S(r) is defined by Capdevielle et al[3] as

$$S(r) = \frac{1}{2x+1}\left[(x+1)\frac{\partial \ln f}{\partial \ln x} + (2+\beta_0)x + 2\right]$$

ORIGINAL PAGE IS
OF POOR QUALITY

which gives the best fit in the neighbourhood of r for a given structure function f. Where $\beta = 4.5$ if f is NKG function and $X = r/r_0$, r_0 = Moliere radius.

The value of S(r) is numerically estimated in a small band of distance $[r_i, r_j]$

$$S_{ij} = \frac{\mathrm{Ln}\,[F_{ij}\, X_{ij}^{2}\, Y_{ij}^{4.5}]}{\mathrm{Ln}\,[X_{ij}\, Y_{ij}]}$$

where $F_{ij} = f(r_i)/f(r_j)$,

$X_{ij} = r_i/r_j$ and $Y_{ij} = (X_i + 1)/(X_j + 1)$

and $S_{ij} \rightarrow S(r)$ if $r_i \rightarrow r_j$
with $r = (r_i + r_j)/2$.

3. Results

3.1. Age distribution The age is calculated over a particular shower size range and a typical age 's' distribution is shown in Fig.1. We find that for showers falling within zenith angle 30° having sizes in the range 10^4 - 2×10^4 particles the individual shower age lies between 0.3 and 1.25.

3.2. Variation of l.a.p. with core distance

The l.a.p. distribution is shown in Figs. 2.1 and 2.2 in the core distance range 1-20m. For showers in the size range $4.0 < \log N_e < 4.5$, the l.a.p. increases with the increase of core distance, whereas for showers in the size range $4.5 < \log N_e < 5.3$, the l.a.p. decreases very slowly from 2.5m to 10m and then increases from 10m to 20m.

3.3. Variation of l.a.p. with the shower size

The l.a.p. distribution is shown in Fig.3 for core distances in the range from 3-10m and from 10-20m. It has been found that the l.a.p. decreases as the shower size increases from 10^4 to 10^5 particles for both the distance ranges.

3.4. Variation of average age parameter distribution with shower size

The average age for a shower group was determined and plotted as a function of shower size as shown in Fig.4 along with the similar data of Khristiansen et al[4], Asakimori et al[5], Abdullah et al[5] and Gerhardy et al[7]. The average age is nearly constant over a shower size range 10^4 - 10^6 particles.

4.Discussion Each shower was fitted to the Hillas function to obtain the core coordinates and shower age. The average age for a shower group is consistent with other experiments. The present data on the l.a.p. shown in Figs. 2.1 and 2.2 show the constancy of l.a.p. in the core distance range 2-20m. The dependence of l.a.p. on shower size in two core distance regions shown in Fig. 3 shows near constancy of l.a.p. in the size range $10^4 - 10^5$ particles.

5.Conclusions It can be concluded from the plotted data that the determination of average age and l.a.p. from the present experiment is consistent with the measurements of other workers mentioned above.

6.Acknowledgements The Department of Atomic Energy, Govt. of India is thanked for the financial assistance for the DAE Project at North Bengal University.

References

1. Hillas, A.M. et al (1977), Proc. 15th ICRC, Plovdiv, 8, 450.
2. Lagutin, A.A. et al, (1979), Proc. 16th ICRC, Kyoto, 7, 13.
3. Capdevielle, J.N., (1983), Proc. 18th ICRC, Bangalore, 11, 303.
4. Khristiansen, G.B., et al, (1981), Proc. 17th ICRC, Paris, 6, 39.
5. Asakimori, K., et al, (1981), Proc. 17th ICRC, Paris, 11, 301.
6. Abdullah, M.M., et al, (1981), Proc. 17th ICRC, Paris, 6, 151.
7. Gerhardy, P.R., et al, (1981), Proc. 17th ICRC, Paris, 6, 152.

ORIGINAL PAGE IS
OF POOR QUALITY

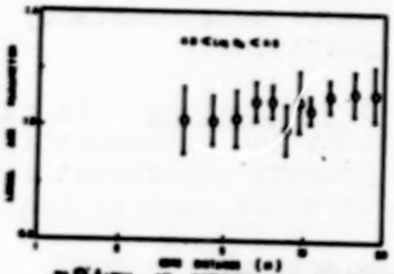

FIG. 5. LOCAL AGE DISTRIBUTION WITH CORE DISTANCE.

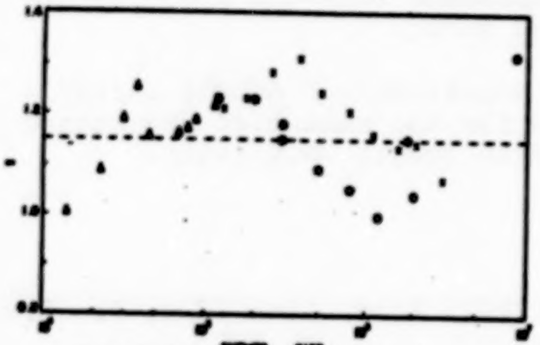

FIG. 4. VARIATION OF AVERAGE AGE PARAMETER WITH SHOWER SIZE. - - - - [illegible] (19[illegible]) ○-ABDULLAH [illegible] (19[illegible])[6] ○-ASAKIMORI [illegible] (19[illegible]) x-GERASIMOV [illegible] (19[illegible]) AND Δ-PRESENT EXPERIMENT.

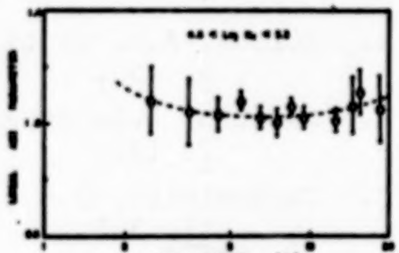

FIG. 6. LOCAL AGE DISTRIBUTION WITH CORE DISTANCE.

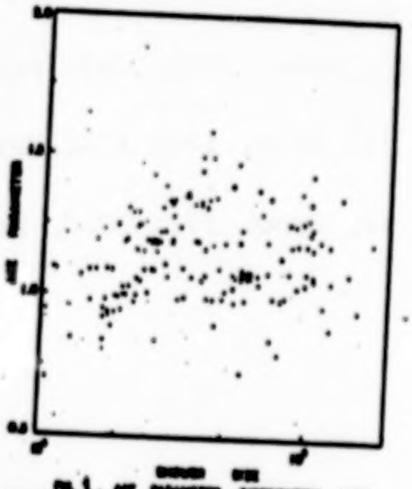

FIG. 3. AGE PARAMETER DISTRIBUTION WITH SHOWER SIZE OF SELECTED SHOWERS.

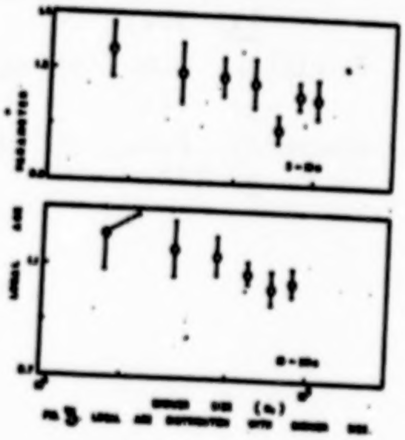

FIG. 7. LOCAL AGE DISTRIBUTION WITH SHOWER SIZE.

N85-35997

HE 4.3-2

A NEW STUDY OF MUONS IN AIR SHOWERS BY NBU AIR SHOWER ARRAY

N.Chaudhuri, N.Mukherjee, S.Sarkar
D.K.Basak and B.Ghosh

Department of Physics
University of North Bengal
Darjeeling - 734 430, India

The NBU air shower array has been in operation in conjunction with two muon magnetic spectrographs. The array incorporates 21 particle density sampling detectors around the magnetic spectrographs covering an area of 900 m^2. The layout of the array (Basak et al[1]) is based on the arrangement of detectors in a square symmetry. The array set up on the ground level is around a 10 m high magnetic spectrograph housing. This magnetic spectrograph housing limits the zenith angular acceptance of the incident showers to a few degrees. The array of detectors is sensitive to air showers initiated by cosmic primaries of energy in the range 10^{14}-10^{15} eV. The detectors are scintillator counters made of plastic scintillators of two different sizes : 0.25 m^2 and 0.125 m^2. Each scintillator is of 5 cm thick mounted firmly within a box made of aluminium sheets. A DUMONT 6364 photomultiplier tube mounted suitably to view the scintillator forms a detector. The pulses from the detectors are digitised by an analog-to-digital converter and the density information from all the detectors is printed out on a paper tape by a line printer. Two muon magnetic spectrographs at a separation of 4 m have been installed in a housing which is located near the centre of the array of detectors.

A 2-metre neon flash tube (NFT) chamber which has been used as a low energy muon detector in the NBU air shower array consists of 9 layers of neon flash tubes installed in a chamber with a cover of 5 cm of lead to get rid of electrons. Each layer contains 54 tubes arranged in such a way that a single muon passing through the flash chamber must discharge the tubes lying on the trajectory of the particle. The NFT chamber covers an area of 1 m x 1 m for the localisation of muon trajectories.

An absorber of 1000 gm/cm^2 of concrete on the roof about 1 m above the spectrograph units is provided to remove the electronic component. Additional lead absorber could be placed above the top tray of the spectrograph for this purpose. The information on muon triggered neon flash tube glows for the location of particle trajectory is obtained by a set of cameras. From the recorded coordinates of the passing muon at the four levels of detection in the spectrograph, its deflection in the magnetic field is calculated. The momentum of a muon is determined from the relation

$$P = 21.96/\Delta \ \text{GeV/c}$$

where Δ is the deflection in t.s.unit (1 t.s. = 1.999 + 0.0002 cm) and the constant in the numerator is the product of the geometrical factor of the spectrograph and the line integral of the magnetic induction.

Three hundred muons in the fitted showers of size range 10^4 - 10^5 particles have so far been scanned and the momenta determined in the momentum range 2 - 440 GeV/c. More than 1500 recorded showers are now in the process of scanning and fitting. Shower records that will be obtained till June '85 will be incorporated. A lateral distribution of muons of energy greater than 300 MeV in the shower size range 10^5 - 7×10^5 has been obtained from the record of NFT chamber.

The Department of Atomic Energy, Govt. of India, is supporting the air shower work at North Bengal University.

References

1. Basak,D.K. et al, (1984), Nucl. Instr. Meths., 227, 167.

HE 4.3-3

Lateral Distribution of Electrons of Air Showers

K.Asakimori and T.Maeda
Department of physics,
Kobe University, Nada-Ku, Kobe 657, Japan

T.Kameda
Kobe Women's University, Suma-Ku, Kobe 654,Japan

K.Mizushima
Kobe Women's Junior College, Chuo-Ku,
Kobe 650, Japan

Y.Misaki
Research Center for Nuclear Physics,
Osaka University, Ibaraki,
Osaka 567, Japan

ABSTRACT

Lateral distribution of electrons (abbreviated to LDE) of the air showers of size $10^5 \sim 10^6$ was studied within one MU.
The results are summarized as follows:
i) LDE of the air showers observed is well represented by NKG function except for vicinity of the core,
ii) LDE measured by thin scintillators does not differ from that measured by thick ones of 50mm thickness.

1 Introduction, Lateral distribution of shower particle is usually approximated by NKG function. However, several authors reported recently that the lateral distribution is not expressed by NKG function of single age parameter, and that number of particles measured by scintillator of 50 mm thickness distorts remarkably the lateral distribution near the core of air showers because of multiplication of the particles in scintillator (1)(2). Basing on these results, change of age parameter with distance from the core and its physical meanings are discussed among some reseachers of air showers.

LDE of the air showers within one MU from the core and the effect of thickness of the scintillators on the lateral distribution were studied by the air shower array of Kobe University. The latter is investigated by means of scintillators of various thickness. From the results obtained by these measurements; change of age parameter with the distance from the core (local age parameter) is obtained.

2. Experiment and Results, Nine plastic scintillators of area 1 m^2 and thickness of 50 mm and 67 plastic scintillators of area 0.25 m^2 and thickness of 50 mm were used for the measurement of densities of charged particles of air showers of size $\gtrsim 10^5$, within 1 MU from the core. In addition to these scintilators, scintillators of various thickness were placed among

them to study the effect of the thickness of scintillators on densities of particles (3).

Assuming LDE is expressed by NKG function, NKG function of best fit for indivisual shower was obtained. The shower array of Kobe University and the method of best fit were reported in detail elsewhere (4).

About ten thousands showers were observed during the period from December 1983 to June 1984.

The average LDE of showers of size $10^5 \sim 10^6$ and less than 30° of zenith angle normalized to the showers of size 10^6 are shown in Fig.1 for several sections of age parameter. Solid line in the figure is NKG function of mean age parameter for the showers classified in each section. Number of particles is corrected for the transition effect using the correction formulae (4).

From the figure, it is pointed out that LDE is well represented by NKG function except for the showers of $1.4 \leq s \leq 1.6$ and for distance within 3 m from the core. Large disparity of showers of the latters from NKG function of the same age parameter is considered to be caused by any small samples of showers, or the inadequateness of the method of best fit for these showers, or any physical reason, but nothing is known now definitely.

In Fig.2, are shown the average LDE of showers, which are measured by thin scintillators and have size $\geq 10^5$, zenith angle $\leq 30°$, and age parameter $1.0 \leq s < 1.2$. The figure indicates that LDE is not different from those in Fig.1.

This result obviously show that the effect of the thickness of scintillators on density measurement is so small that one may safely use thick ones of 50 mm thickness. The local age parameter defined by Capdevielle and Gawin is obtained basing on LDE in Fig.1 and Fig.2 (5). The results are shown in Fig.3 and Fig.4. Local age parameter decreases slowly with increasing distance from the core, and farther than 3 m it is nearly constant, and does not show any tendency of decrease. Furthermore, local age parameter obtained by thin scintillators does not show any remarkable difference from that obtained by the scintillators of 50 mm thickness.

These results reveal that the variation of thickness of the scintillators does not significantly affect the value of age parameter, and that NKG function approximates well LDE.

3. Conclusion. LDE of air showers is approximated well by NKG function except for the neighborhood of the core and for the showers of old age parameter. Change of local age parameter is not recognized but for the vicinity of the core, and this shows the validity of approximation of LDE by NKG function of single age parameter. LDE obtained by thin scintillators does not differ largely from that obtained by those of 50 mm thickness, and this result shows that multiplication and absorption of particles in the scintillators are not so large.

Our results are in disagreement with those of Akeno group with respect to the variation of local age parameter and the

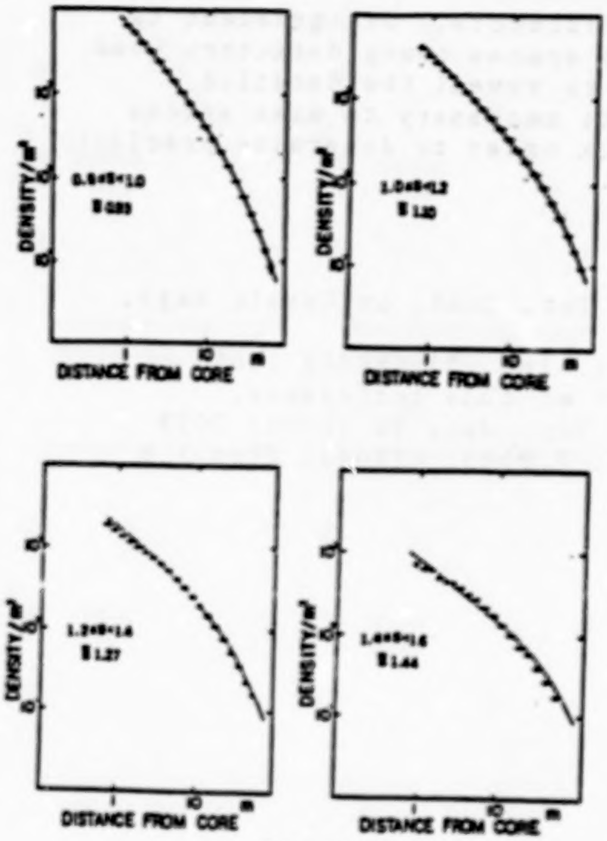

Fig.1

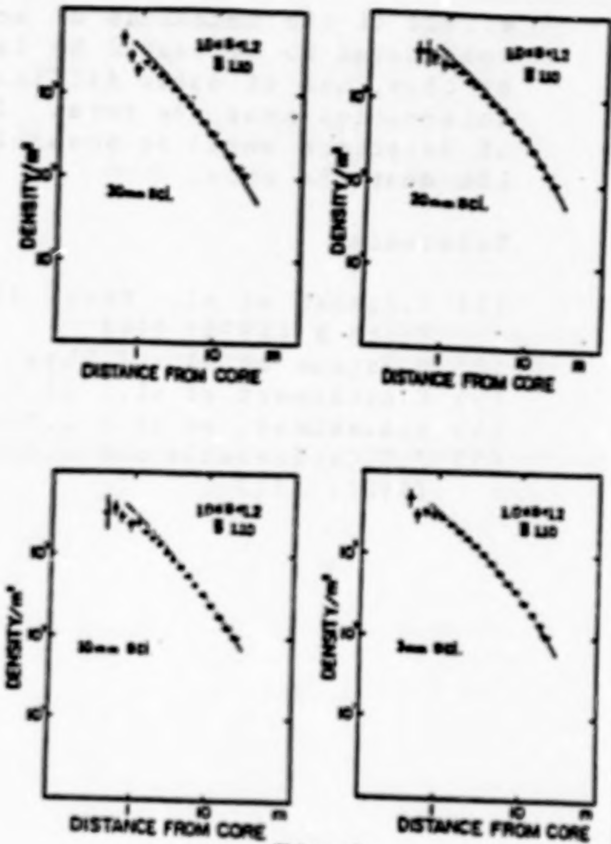

Fig.2

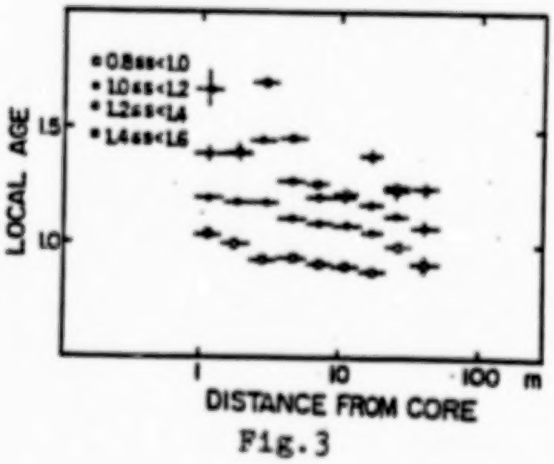

Fig.3

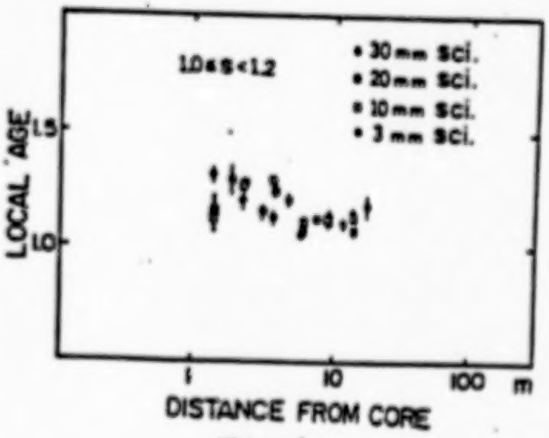

Fig.4

effect of the thickness of scintillators. Disagreement is considered to be caused by large spaces among detectors used by them, and it makes difficult to reveal the detailed information near the core. It is necessary to make spaces of detectors small as possible in order to determine precisely LDE near the core.

References

(1) T.Kaneko et al.: Proc. 14th Int. Conf. on Cosmic Rays, Münch 8 (1975) 2747
(2) M.Nagano et al.: J.Phys. Soc. Jpn. 53 (1984) 1667
(3) K.Asakimori et al.: HE 4.4-9 of this conference.
(4) K.Asakimori et al.: J.Phys. Soc. Jpn. 51 (1982) 2059
(5) J.N.Capdevielle and J.Gawin: J.Phys. G(Nucl. Phys.) 8 (1982) 1317

ORIGINAL PAGE IS
OF POOR QUALITY

N85-35999

HE 4.3-4

DETAILED STUDIES OF THE ELECTRON LATERAL DISTRIBUTION IN EXTENSIVE AIR SHOWERS WITH ENERGIES AROUND 10^{16} eV.

T.Dzikowski, J.Gawin and J.Wdowczyk

Institute of Nuclear Studies and
University of Łódź, Cosmic Ray Laboratory
90-950 Łódź 1, box 447, Poland.

I. The experimental procedure.

Using the Lodz extensive air shower array, we have performed detailed studies of the electron lateral distribution in extensive air showers. The showers were grouped according to their particle densities around 20 m from the core. The grouping was made in very narrow intervals of the densities. For every group of showers and for every distance interval /changing by 5 m/ histograms of the numbers of electron counters discharged have been obtained. The trays of G.M counters were located at following distances from the centre of the triggering detectors array : 16 m, 76 m, 117 m, 137 m, 141 m and 147 m, /Dzikowski et al., 1979/.

Every histogram then has been fitted with particle density spectrum described by the gamma distribution

$$P(\varrho) = \frac{b^{p}}{\Gamma(p)}\, \varrho^{p-1} \exp(-b\varrho)$$

taking into account the exact probabilities of the discharge of the given number of counters. The parameters p and b were calculated from the experimental histograms. Those parameters gives the average density and the width of fluctuations from the formulae /Dzikowski et al., 1977/.

$$\langle\varrho\rangle = \frac{p}{b} \qquad \frac{\sigma}{\langle\varrho\rangle} = \frac{1}{\sqrt{p}}$$

In the present work we are analysing only the average densities as a function of the shower core distance.

ORIGINAL PAGE IS
OF POOR QUALITY

The errors of the densities were obtained by Monte Carlo method following way. Taking the experimentally obtained distribution of densities in the form of the gamma function histogram of the expected discharged counters has been simulated. This procedure has been repeated 10 times. For every obtained histogram new values of the p, b parameter have been obtained. The spreads of the parameters values have been taken as a measure of the errors.

II. Results.

The obtained lateral distributions are compared in fig.1 with the commonly used Nishimura, Kamata, Greisen /N K G/ formula. As it is known the formula is /Greisen, 1956/

$$\rho(r) = \frac{N_e}{r_1^2} C(s) \left(\frac{r}{r_1}\right)^{s-2} \left(1+\frac{r}{r_1}\right)^{s-4.5}$$

where s is the formal age parameter and r_1=79 m the so called Moliere distance unit. The values of the obtained shower sizes and age parameters are given in table I.

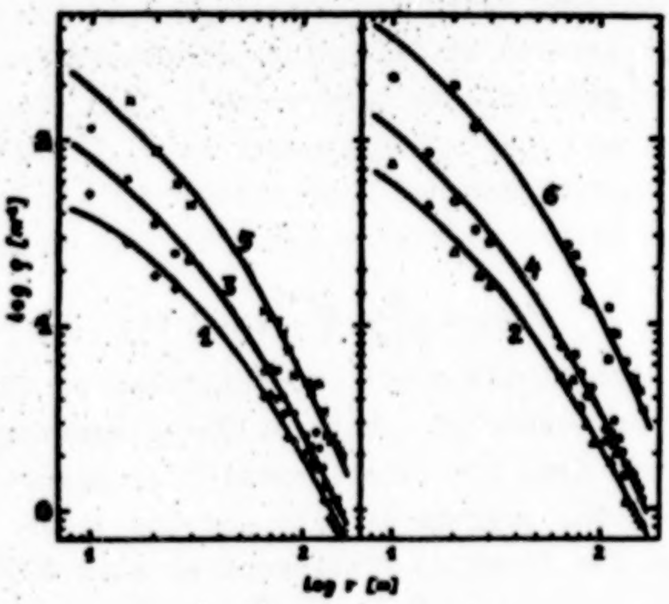

Figure 1. Experimental elektron lateral distribution for different shower sizes. The curves represent lateral distribution calsulated from N K G formula for parameters summarised in table I.

ORIGINAL PAGE IS
OF POOR QUALITY

Table I.

Number and symbol	N_e	s
1. +	3.99×10^5	1.59
2. △	4.59×10^5	1.50
3. ●	5.53×10^5	1.45
4. ○	7.07×10^5	1.42
5. ×	1.13×10^6	1.39
6. □	2.26×10^6	1.41

It is interesting to note that the obtained lateral distributions are relatively wide /high value of the „s" parameters/ and that the NKG formula relatively well describes the lateral distributions at the distances above 50 meters from the core, whereas at the smaller distances the experimental distributions are slightly steeper.

III. Conclusions.

The electron lateral distribution at distances 60-150 m from the core seems to be well described by the NKG function with relative large values of the shower age parameter. The curves at smaller distances appear to go lower then the experimental points.

References.

Dzikowski, T. et al., J. Phys. G: Nucl. Phys., 3,1591/1977/

Dzikowski, T. et al., Proc. XVI-th Int. C. R. Conf. Kyoto, 8,276 /1979/

Greisen, K., Progress in Cosmic Ray Physics, 3,1 /1956/

N85-36000

STUDY OF MUONS NEAR SHOWER CORES AT SEA LEVEL USING THE E594 NEUTRINO DETECTOR

Goodman, J.A.,[1] Gupta, S.C.,[1] Freudenreich, H.,[1] Sivaprasad, K.,[1] Tonwar, S.,[2]
Yodh, G.B.,[1] Ellsworth, R.W.,[3] Goodman, M.C.,[4] Bogert, D.,[5] Burnstein, R.,[6]
Fisk, R.,[5] Fuess, S.,[5] Morfin, J.,[5] Ohska, T.,[5] Bofill, J.,[7] Busza, W.,[7]
Eldridge, T.,[7] Friedman, J.I.,[7] Kendall, H.W.,[7] Kostoules, I.G.,[7] Lyons, T.,[7]
Magahiz, R.,[7] Mattison, T.,[7] Mukherjee, A.,[7] Osborne, L.,[7] Pitt, R.,[7]
Rosenson, L.,[7] Sandacz, A.,[7] Tartaglia, M.,[7] Taylor, F.E.,[7] Verdier, R.,[7]
Whitaker, S.,[7] Yeh, G.B.,[7] Strongin, B.,[7] Abolins, M.,[8] Brock, R.,[8]
Cohen, A.,[8] Ernwain, J.,[8] Perkins, G.,[8] Hatcher, R.,[8] and Werthmann, A.[8]

[1] Univ. of Maryland, College Park, MD
[2] Tata Inst. of Fundamental Research, Bombay, India
[3] George Mason University, Fairfax, Virginia
[4] Argonne National Laboratory, Argonne, Illinois
[5] Fermi National Lab., Batavia, Illinois
[6] Illinois Inst. of Technology, Chicago, Illinois
[7] Massachusetts Inst. of Technology, Cambridge, MA
[8] Michigan State University, East Lansing, Michigan

ABSTRACT

The E594 neutrino detector has been used to study the lateral distribution of muons of energy > 3 GeV near shower cores. The detector consists of a 340 ton fine grain calorimeter with 400,000 cells of flash chamber and dimensions of 3.7 m x 20 m x 3.7 m (height). The average density in the calorimeter is 1.4 gm/cm^2 and the average Z is 21. The detector was triggered by four 0.6 m^2 scintillators placed immediately on the top of the calorimeter. The trigger required ≥ 2 p/m^2 in at least two of these four counters. The accompanying EAS was sampled by 14 scintillation counters located up to 15 m from the calorimeter.

Several off-line cuts have been applied to the data. Demanding five particles in at least two of the 'trigger' detectors, a total of 20 particles in all of them together, and an arrival angle for the shower < 45° reduced the data sample to 11053 events. Of these in 4869 cases, a computer algorithm found at least three muons in the calorimeter. To take into account the failure of the computer algorithm to estimate the number of muons when the ionisation deposited in the calorimeter was very large, an upper limit on the total 'trigger' electrons was imposed. A limit of 100 electrons reduced the data set to 9657 events out of which 4803 events had more than three muons in the calorimeter. These cuts were also applied to the Monte Carlo simulated predictions (as described elsewhere at this conference) based on two different primary spectra; the first spectrum is dominated by heavy primaries while the second by protons. A preliminary comparison of the rates of predicted and observed triggers favors the first spectrum. Comparison of the detailed electron and muon numbers and their averages is carried out.

N85-36001

CORRELATION OF HIGH ENERGY MUONS WITH PRIMARY COMPOSITION IN EXTENSIVE AIR SHOWER

C.Cho, S.Higashi, N.Hiraoka, S.Ozaki, T.Sato,
T.Suwada, T.Takahashi and H.Umeda

Depertment of Physics, Osaka City University

Osaka, Japan

Abstract

An experimental investigation of high-energy muons above 200 GeV in extensive air showers has been made for studying high-energy interaction and primary composition of cosmic-rays of energies in the range $10^{14} \sim 10^{15}$ eV.

The muon energies are estimated from the burst sizes initiated by the muons in the rock, which are measured by four layers of proportional counters, each of area 5 x 2.6 m^2, placed at 30 m.w.e. deep, Funasaka tunnel vertically below the air shower array. The air shower array, area of about 30 x 40 m^2 contains 21 plastic scintillation counters, of which five are for fast timing and all used for density determination.

The lateral distributions of high-energy muons above 200 GeV has been determined in the size range $10^4 \sim 10^6$ particles and in the lateral range $0 \sim 20$ m. These results are compared with Monte Carlo simulations based on the scaling model and the fireball model for two primary compositions, all proton and Mixed.

1. Introduction

High-energy muons in cosmic-rays keep information with characteristics of nucleus interaction and composition of primary cosmic-rays. An experimental investigation of high-energy muons in EAS with other components of the shower has been performed to take accurate information on both aspects. In this experiment the energies of muons are determined from the burst sizes initiated by them in the rock above the detector and incoming directions are also determined by the use of the center of gravity of burst. By the use of this direction and the data from the shower array, we can determined the shower size N_e, age parameter S and distance between shower core and muon. Here we present results from an investigation of muon component (≥200 Gev) of EAS in size range $4 \times 10^4 \sim 10^6$ particles.

2. Experimental Arrangement and Method of Analysis

The apparatus consists of a scintillation counter array for the detection of air showers and four layers of proportional counters at the underground to observe bursts initiated by muons. Sixteen scintillation counters, 1 x 1 m^2 and 10 cm thick, are used to record the densities correspond to 1 to 2000 particles. Five, 50 x 50 cm^2 and 10 cm thick, counters are used for fast timing. These counters are distributed as shown in Fig. 1. Four layers of proportional counters are used to measure the size and the two dimensions lateral spread of the shower particles which are produced in the rock by high-energy muons. The area of each layer is 2.6 m x 4.5 m, the spatial resolution, i.e., distance of adjacent two wires, are 5 cm along 2.6 m and 10 cm along 4.5 m, and the distance between the top and the bottom layer is 94 cm. The burst detector is located inside the Funasaka Tunnel whose depth is 30 m.w.e. (1) and which is 18 m below the air shower array. Data are taken when each layer of the burst detector has more than 10 particles and any one of 16 scintillation counters has more than 6 particles. Lateral distribution of particles in observed burst is flat which is produced by multi-muon, or convex by a muon. Then convex bursts are selected by the following conditions which are determined on the basis of the analysis of bursts without air shower.

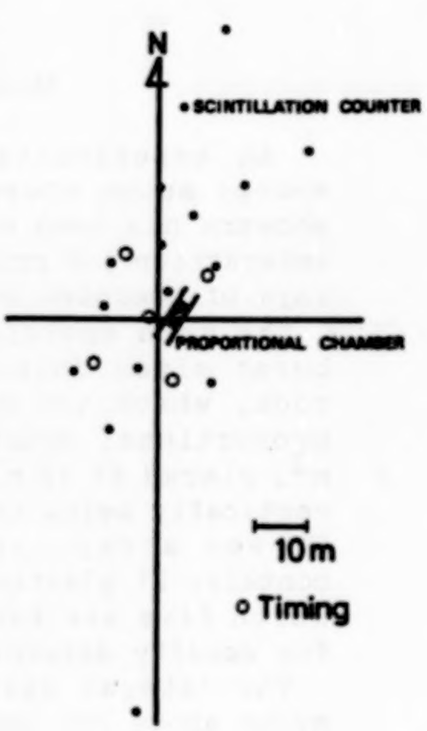

Fig.1 Plan of extended particle array. ○, timing and particle density; ●, particle density.

1) $\beta_2 \geq 3$, ≥ 30 particles for each layer, where

$$\beta_2=\mu_4/(\mu_2)^2,\ \mu_k=\Sigma f_i(r_i-\langle r\rangle)^k/n,\ n=\Sigma f_i,\ \langle r\rangle=\Sigma f_i r_i/n,$$

f_i, r_i : particle number and position of i-th wire,
Σ : sum of wires within a burst for each layer.

2) ratio of numbers of particles in a layer is between 0.5 and 2.0.

For the selected data, center of gravity of burst size is calculated for each layer. Incoming direction of muon, namely, of air shower is determined from these 4 points. The energy of muon is determined from the burst size (N_b) using the next equation:

$$E\ (\text{ GeV })= 0.67N_b^{-1.03}.$$

Size (N_b) is obtained from the average of four layers and zenith angle correction is applied. This equation is obtained from the conversion of burst size spectrum to energy spectrum. The air shower parameters, size (N_e), core location (X,Y) and age parameter (S), are determined by a least square fit of observed densities to NKG lateral distribution (2). We estimate the errors of these parameters, $\sigma(X,Y)=\pm 2$ m and $\sigma(\theta,\psi)=\pm 6^{\circ}$ from analysis of artificial showers. The probability of finding muon within interval r' for muon of core distance r is calculated by Monte Carlo method using the $\sigma(X,Y)$ and $\sigma(\theta,\psi)$, and the result is presented in Fig. 2.

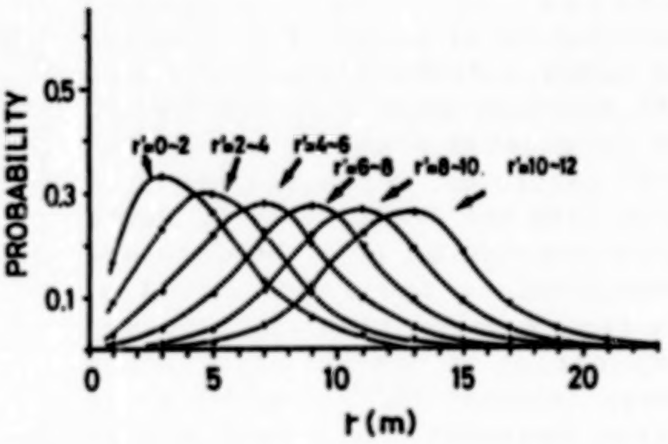

Fig.2 Probability distribution of finding muon within interval r' for muon core distance r.

3. Results and Conclusion

During the 13666 hours, 2776 events have been obtained which are satisfied with burst conditions and air shower conditions. Only 103 events in which muon energy is ≥ 200

GeV are survived after next five conditions are applied.

1) air shower sizes N_e are in the range $4 \times 10^4 \sim 10^6$ particles,
2) zenith angles θ are in the range $0 \sim 35^o$,
3) modified χ^2 values for lateral fit are in the range $0 \sim 5$,
4) core distance are in the range $0 \sim 20$ m.

Four conditions are on the basis of analysis of artificial showers. Under these conditions, correction factor of the acceptance-area is estimated to be 1. Relative densities of muon are obtained from 103 events by acceptance-area and finding probabilities. The density in the range 0 to 2 m becomes low because of flat lateral distribution of burst. Fig. 3 shows the lateral distribution of muons with energies more than 200 GeV in the associated shower size $4 \times 10^4 \sim 10^6$ particles. Comparing the data curve with the predictions of Monte Carlo simulation (3), the data are normalized at the range $2 \sim 4$ m. The figure shows that the primary composition of cosmic-rays in the energy interval $10^{14} \sim 10^{14.5}$ eV is proton dominant. Data have errors due to energy estimation of air shower, short range of core distance and poor statistics, but the conclusion that the primary composition of cosmic-rays in the energy range till $10^{14.5}$ eV are proton dominant, as other experiments suggest (4), may be correct. It is necessary to increase the range of shower size and core distance.

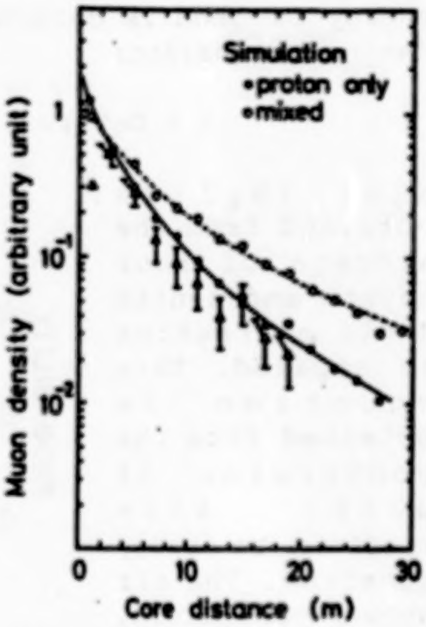

Fig.3
Density distribution of muon above 200 GeV against core distance.

References

(1) Higashi,S. et al. ,16th ICRC, Kyoto, 10, 208,(1979).
(2)This fitting program has been presented from the air shower group of Kobe University of Japan.
(3) Mizutani, K. et al. , this Conference Paper, OG 5.2-9.
(4) See, for example, Acharya, B.S. et al, 16th ICRC, Kyoto, 8, 304, (1979). ; Burnett, T. H. et al. , Phys. Rev. Lett., 51, 1010, (1983).

Measurement of Low Energy Muons in EAS at Energy Region Larger than 10^{17}eV.

Y.Matsubara , T.Hara, N.Hayashida, K.Kamata, M.Nagano,
H.Ohoka, G.Tanahashi and T.Teshima*
Institute for Cosmic Ray Research, University of Tokyo,
Tanashi, Tokyo, 188 Japan
* Department of Physics, Kyoto University,
Sakyo-ku, Kyoto, 606 Japan

Abstract

A measurement of low energy muons in EAS (threshold energies are 0.25, 0.5, 0.75 and 1.38 GeV) was carried out. The density under the concrete shielding equivalent to 0.25 GeV at core distance less than 500 m and 0.5 GeV less than 150 m suffers contaminations of electromagnetic components. Therefore the thickness of concrete shielding for muon detectors for the giant air shower array is determined to be 0.5 GeV equivalence. Effects of photoproduced muons are found to be negligible in the examined ranges of shower sizes and core distances. The fluctuation of the muon density in 90 m^2 is at most 25 % between 200 m and 600 m from the core around 10^{17}eV.

1. Introduction

Constrution of muon detectors for the giant air shower array starts from 1984 at Akeno. One of the purposes of this experiment is to determine the appropriate absorber thickness. Muons in EAS must be measured under the shielding in order to eliminate electromagnetic components. On the other hand, the thickness of shielding is desired to be as thin as possible from the economical point of view. Another purpose is to examine whether effects of photoproduced muons appear appreciably in giant air showers when we measure such low energy muons.

2. Experiments and Data Analysis

The measurement was done by using a large calorimeter of 100 m^2 area (effective area 90 m^2) at the center of Akeno EAS Array (Hara et al. 1979), which consists of four layers of proportional counters under the concrete shielding as is shown in Fig.1. The threshold energies for muons at each layer correspond to 0.25, 0.5, 0.75 and 1.38 GeV respectively. Counters are made of iron square pipes of size 10 cm x 10 cm x 500 cm filled with P10 gas (Hayashida and Kifune 1980). The trigger condition is 7-fold coincidence with more than 4 particles out of 38 scintillation counters in Akeno EAS Array, which are arranged in lattice shape with mutual spacing of 120 m. 18000 showers are analyzed and the conditions for data

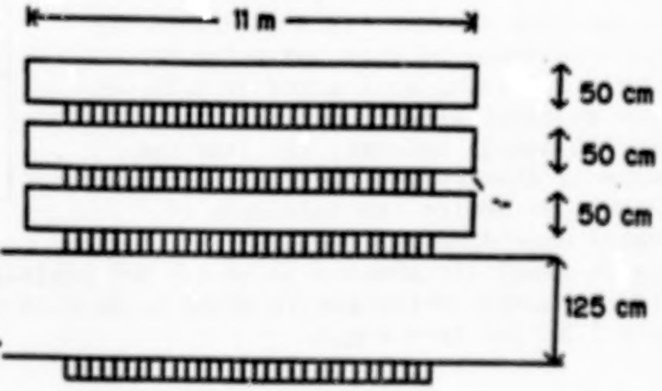

Fig.1 The structure of the colorimeter

selection are as follows; shower size lager than 10^7, core distance larger than 50 m from the calorimeter and chi square for the fitting of shower sizes and directions reasonably small. Only vertical showers are examined in this paper except those shown in Fig.4. Present data are compared with those by other nine muon stations of 25 m^2 each, where the thickness of the concrete shielding corresponds to threshold energy 1 GeV .

3. Results and Discussions

The lateral distribution of muons of energy more than 1 GeV is given by Greisen's formula (Greisen 1960)

$$\rho_\mu(R) = C(R/R_0)^{-0.75}(1+R/R_0)^{-2.5} \quad \text{... (A)}$$

from the data of muon stations in Akeno EAS Array, where R is a core distance, C is a normlization factor depending on sizes and zenith angles, and R_0 is a characteristic distance which varies with zenith angles (Hara et al. 1983). Greisen presents also the lateral distribution as a function of muon energy $E\mu$ as follows (Greisen 1960)

$$\rho_\mu(>E\mu,R) = (A) \times (51/(50+E\mu)) \times (3/(2+E\mu))^{f(R)} \quad \text{... (B)}$$

where $f(R) = 0.14 \times R^{0.37}$. We use this function as a reference, though the Greisen's formula were derived from the data of lower sizes and larger energy regions of muons than are considered now.

(1) Lateral distribution

Fig.2 shows the lateral distribution of the density at each layer for vertical showers. Curves are those given by the formula (B) with R_0=280 m. Densities under shieldings equivalent to 0.5, 0.75 and 1.38 GeV at more than 150 m from the core can be fit well to this formula, but those under the shielding equivalent to 0.25 GeV show larger values than this curve. The lateral distribution of the density ratio of each layer to the fourth layer in three shower sizes is shown in Fig.3, where the density of the lowest layer is taken as a reference value. Curves are given by the formula (B). It is suggested from both figures that the concrete shielding equivalent to 0.25 GeV can not prevent the leakage of electromagnetic components at the core distance less than 500 m , and 0.5 GeV less than 150 m also. Fig.4 is the zenith angle dependence of this ratio for the concrete shielding equivalent to 0.25 GeV x secθ at equal size. The higher the threshold energy becomes, the less the leakage of electromagnetic components is observed. We decide the thickness of concrete shielding for the observation of muons in giant air showers to be 0.5 GeV equivalence for safety, though the minimum absorber thickness is found to be 0.34 GeV (this is the case for secθ = 1.3-1.4) from Fig.4.

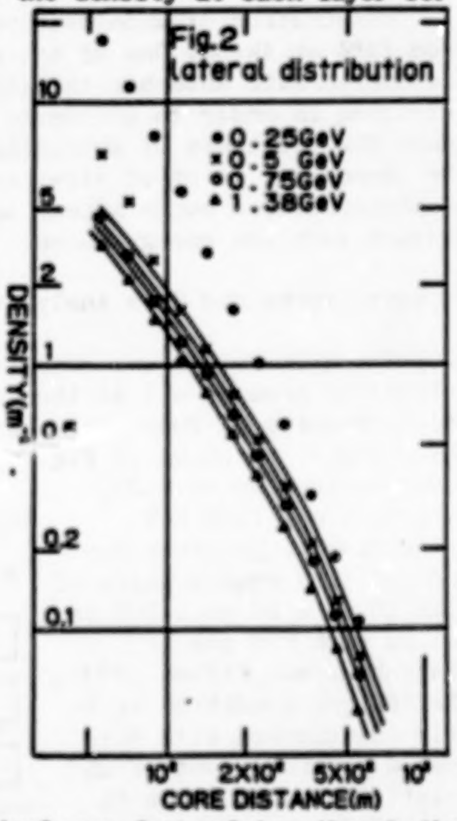
Fig.2 lateral distribution

ORIGINAL PAGE IS
OF POOR QUALITY

(2) Effects of photoproduced muons

The number of photoproduced muons in EAS is proportional to the primary energy E_0, while the number of muons in nuclear cascades to E_0^a $(a<1)$. Therefore, the contribution of photoproduced muons to total muons becomes significant in larger shower sizes. According to the simulation (McComb et al. 1979), if the density of photoproduced muons takes over that from pionization, 'α' in $\rho_\mu \propto Ne^\alpha$ becomes 1. Fig.5 shows the relation between the muon density and the shower size, and between the muon size and the shower size. There exists no significant tendency that the power 'α' becomes larger as the shower size becomes larger. Effects of photoproduced muons may be negligible in the examined ranges of shower sizes and core distances.

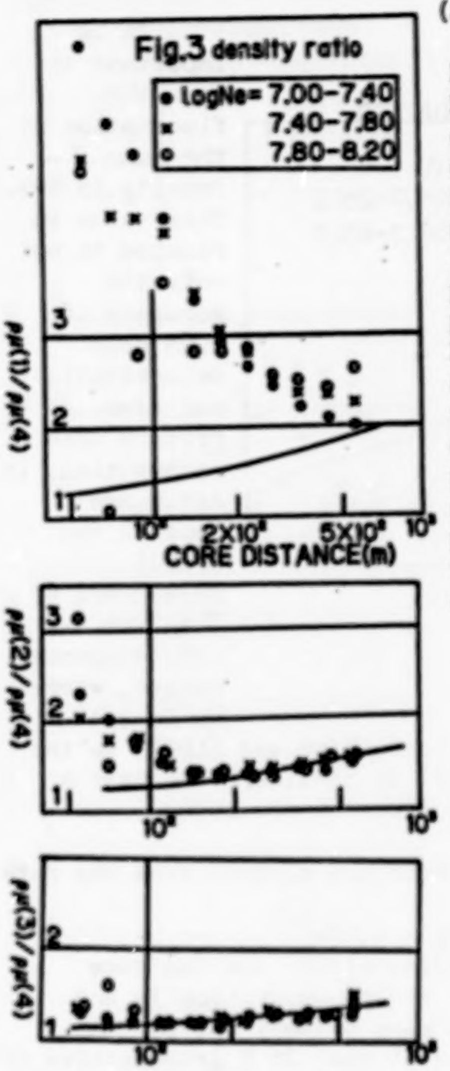

Fig.3 density ratio

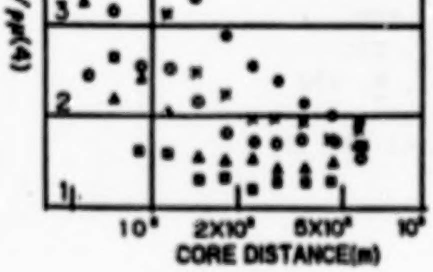

Fig.4 zenith angle dependence of density ratio (logNe=7.00-7.40)

Fig.5 size dependence of Nμ and ρμ

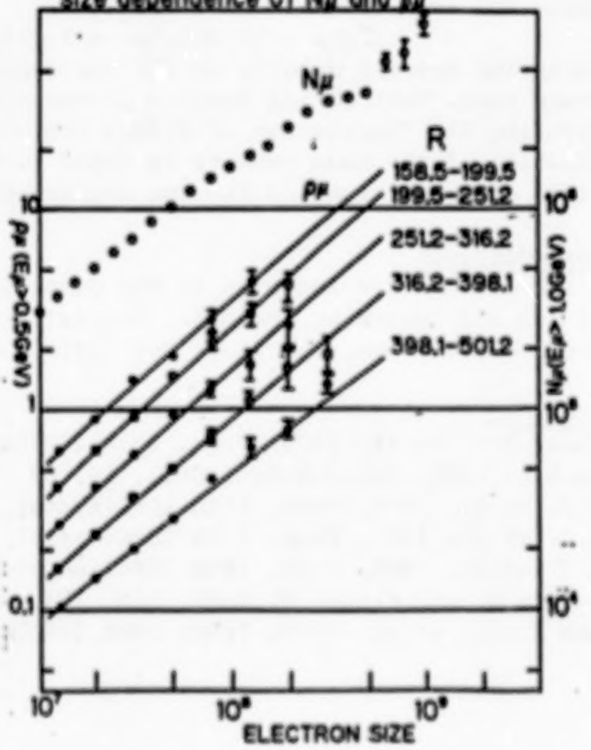

(3) Fluctuation of muons

Fig.6 S(600) dependence of density fluctuation

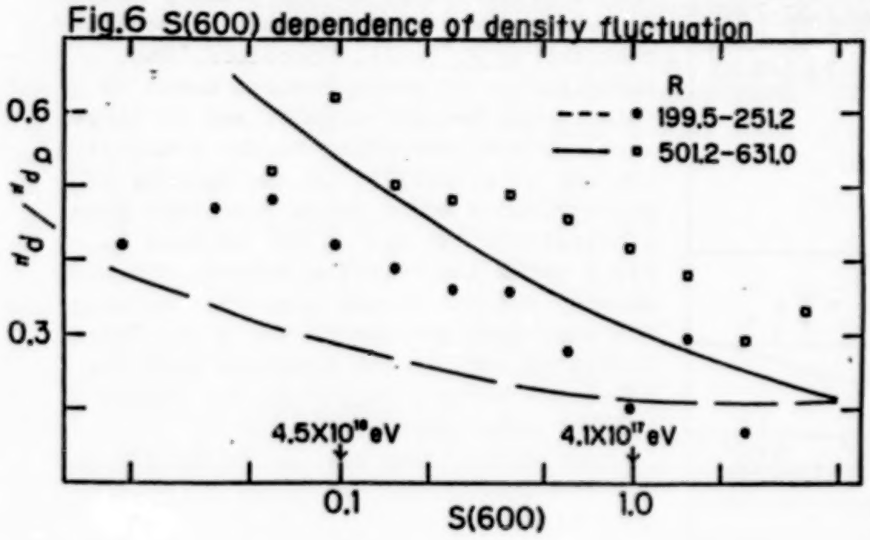

It is important to know the fluctuation of the muon density in EAS. This value is related to not only the accuracy of muon size determination, but also to the primary mass composition. In Fig.6 are plotted the S(600) dependence of σ/ρ_μ for two core distance ranges, where ρ_μ is the density of 0.5 GeV muons in 90 m^2, σ is its fluctuation and S(600) is the electron density at 600 m from the core. S(600) is considered to have a good relation to the primary energy E_0 as (Glushkov et al. 1979)

$$E_0 = 4.1 \times 10^{17} (S(600))^{0.96}$$

Curves in Fig.6 are the experimental errors which are derived from the data of Akeno EAS Array (Hara et al. 1981),

$$\sigma/\rho_\mu = (0.668/\rho_\mu^2 + 1.42/\rho_\mu + 0.04)^{1/2}$$

by using the average density in the corresponding S(600) and two core distance bins. Subtracting these experimental errors quadratically and considering the fluctuation of S(600) for the same primary energy, the fluctuation of the muon density is found to be at most 25 % irrespective of the core distance examined for the primary energy around 10^{17} eV.

Acknowledgements

The authors are indebted to the other members of Akeno group for obtaining and analyzing the data. The data analysis is done by FACOM M380 at the Computer Room, Institute for Nuclear Study, University of Tokyo.

References

Glushkov A.V. et al. 1979, Proc. 16th ICRC(kyoto), 8, 158
Greisen K. 1960, Ann.Rev.Nucl.Sci., 10, 63
Hara T. et al. 1979, Proc. 16th ICRC(Kyoto), 8, 135
Hara T. et al. 1981, Proc. 17th ICRC(Paris), 11, 231
Hara T. et al. 1983, Proc. 18th ICRC(Bangalore), 6, 122
Hayashida N. and Kifune T. 1980, NIM, 173, 431
McComb T.J.L. et al. 1979, Proc. 16th ICRC(kyoto), 9, 126

HE 4.3-9

N85-36003

MUON FLUCTUATION STUDIES OF EAS > 10^{17} eV

P. R. BLAKE, M. LUKSYS, W. F. NASH and A. J. SEPHTON
University of Nottingham, England.

1. Introduction Fluctuation studies need to compare a parameter which is sensitive to longitudinal fluctuations against a parameter which is insensitive. Cascade calculations indicate that the shower size parameter at Haverah Park, $\rho(500)$, and the muon density are insensitive while parameters that significantly reflect the longitudinal development of a particular EAS include the muon/water Cerenkov response ratio and the muon arrival time dispersion. This paper presents conclusions based on muon fluctuation studies of EAS measured between 1976 and 1981 at Haverah Park.

2. Description of Muon Detectors Three 10 m^2 shielded scintillators situated at 0, 150 m and 250 m from the centre of the Haverah Park array. Due to practical considerations the detectors had slightly different absorber thicknesses leading to calculated vertical muon thresholds of 317, 431 and 488 MeV respectively. Two of the muon detectors (those at 0 m and 150 m) had immediately neighbouring large area water Cerenkov detectors so that a local response ratio between the two detectors could be directly measured. The recording of the three detectors was triggered from the water Cerenkov 500 m array by the arrival of EAS with primary energies $\geq 10^{17}$ eV.

3. Fluctuations in μ/c Ratio The ratio of the density response of the muon detectors to the density of the water Cerenkov detectors (symbolised by μ/c) was used to study fluctuations between EAS. For a data set consisting of those EAS with two direct measurements of μ/c an analysis of variance (AOV) was carried out in order to extract the between-EAS variance (σ_B^2) from the total measured variance (σ^2).

R(m)	secθ	Number of EAS	$\sigma_B/(\mu/c)$	F	P
120	1.0-1.1	61	22.4% (±10)	2.44	<0.01
→220	1.1-1.2	36	19.7% (±12)	2.57	<0.01
	1.2-1.3	28	24.7% (±20)	2.23	0.01<p<0.025
220	1.0-1.1	83	0.0% (-0 +15)	0.74	>0.1
→320	1.1-1.2	52	19.9% (±19)	1.46	0.05<p<0.1
	1.2-1.3	37	23.4% (±12)	3.15	<0.01
320	1.0-1.1	54	0.0% (-0 +27)	0.94	>0.1
→420	1.1-1.2	36	1.1% (-1 +40)	1.00	>0.1
	1.2-1.3	23	4.4% (-4 +35)	1.02	>0.1

Table 1 Between-EAS fluctuations in μ/c.

Because the different energy thresholds lead to different μ/c ratios the AOV was carried out using standard residuals defined by S.R. = $[(\mu/c) - (\overline{\mu/c})]/\sigma$, where μ/c is the normalised measured ratio, $(\overline{\mu/c})$ is the average value and σ the standard deviation for the interval under consideration. The results of the AOV are presented in Table 1.

Also included in the table are the F ratio (mean square deviation between EAS to mean square deviation within EAS) and p, the probability that random variations in the data could account for the quoted between-EAS fluctuations. The results indicate that at core distances ~200 m the magnitude of the between-EAS fluctuations is ~20%. Such a result would be consistent with at least a 50% proton primary flux at ~10^{17} eV [eg. Marden et al, 1971].

4. Fluctuations in Muon Risetime The muon arrival timespread at each of the 10 m^2 muon detectors is characterised by the time interval between 10% and 70% of the full pulse amplitude (T_{70}). The instrumental response was found to be T_{70} = 32 ns. For a specific R and θ, fluctuations in T_{70} occur arising from fluctuations in the longitudinal development. AOV techniques allow between-shower fluctuations in T_{70} to be separated from within EAS fluctuations. Such analysis leads to a value of σ_B/T_{70} = 10.7(±2) ns/63 ns = 17% at 325 m, for secθ = 1.1.

Detailed cascade model calculations relating to T_{70} fluctuations remain to be carried out. As a consequence the significance of the T_{70} fluctuations is treated in Section 7 in terms of fluctuations in the height of electromagnetic maximum

5. Correlations of μ/c and η_c The water Cerenkov response lateral distribution function used by the University of Leeds group to analyse the EAS is of the form:

$$\rho_c = k\,R^{-(\eta_c + R/4000)}$$

It has been found that η_c is sensitive to EAS longitudinal development. Thus a strong correlation is expected between fluctuations in μ/c and η_c. Table 2 gives the derived correlation coefficients for the data sets from two muon detectors and also the significance of the correlation.

Detector	secθ	N	r	P
A	1.0-1.1	190	0.449	<0.001
	1.1-1.2	81	0.342	<0.01
	1.2-1.3	40	0.420	<0.01
	1.3-1.4	20	0.598	<0.001
C	1.0-1.1	117	0.398	<0.001
	1.1-1.2	52	0.595	<0.001
	1.2-1.3	34	0.515	<0.01
	1.3-1.4	10	0.618	<0.1

Table 2 Correlation between fluctuation in μ/c and fluctuation in η_c. r = correlation coefficient.

The strong correlation confirms that μ/c and η_c are sensitive parameters to EAS development.

6. Correlation of μ/c and T_{70} A small positive correlation is found between the values of SR(μ/c) and SR(T_{70}) at all zenith angles (see Table 3).

Detector	secθ	No of EAS	r	P
A - μ/c	1.0-1.1	20	0.032	>0.1
B - T_{70}	1.1-1.2	15	-0.306	>0.1
	1.2-1.3	4	0.541	>0.1
	1.3-1.4	7	-0.405	>0.1
A - μ/c	1.0-1.1	32	0.016	>0.1
C - T_{70}	1.1-1.2	19	0.278	>0.1
	1.2-1.3	25	0.172	>0.1
	1.3-1.4	10	0.438	>0.1
C - μ/c	1.0-1.1	44	0.203	>0.1
A - T_{70}	1.1-1.2	31	0.006	>0.1
	1.2-1.3	25	0.245	>0.1
	1.3-1.4	12	0.323	>0.1
C - μ/c	1.0-1.1	15	0.122	>0.1
B - T_{70}	1.1-1.2	16	0.013	>0.1
	1.2-1.3	12	-0.197	>0.1
	1.3-1.4	9	0.382	>0.1

Table 3 Correlation between μ/c and T_{70} fluctuations

Because of the different core distance dependences the two correlating parameters were measured simultaneously from two different muon detectors. The significance of the correlation coefficients in Table 3 is statistically limited due to the small amount of data available for the analysis.

7. Fluctuations in Depth of Electromagnetic Maximum Fluctuations in the depth of maximum (X_{max}) are closely related to the mass spectrum of the primary particles. It is not possible to measure X_{max} directly at Haverah Park. However the fluctuation in X_{max} can be determined indirectly from the measurement of some shower parameters, eg. μ/c which is sensitive to X_{max}. Assuming

$$\Delta X_{max} = \frac{X_{max}}{X} \; \frac{(\mu/c) - (\overline{\mu/c})}{\partial(\mu/c)/\partial X}$$

and using the AOV carried out on the μ/c fluctuations observed at two detectors (for core distances 120 m < R < 220 m and secθ < 1.3) yields:-

N	σ_B(g cm^{-2})	F	p
125	73.2	2.39	<0.01

The value of σ_B is the between-shower fluctuation (in g cm^{-2}) obtained from the AOV and gives an initial estimate of the fluctuation in X_{max}. The values of F and p show that highly significant between-EAS fluctuations are present in the data. Removing the spurious contribution to σ_B from the pressure correction, the corrected fluctuations in depth of maximum, $\sigma(X_{max})$ for EAS in the energy range 10^{17} - 10^{18} eV is given by $\sigma(X_{max}) = (71 \pm 12)$ g cm^{-2}). Using a similar technique the fluctuations in T_{70} yield $\sigma(X_{max}) = (69 \pm 28)$ g cm^{-2}.

Measurement of $\sigma(X_{max})$ at energies above 10^{17} eV have been reported by other groups from a variety of studies. The values obtained above are in good agreement with these other measurements.

8. Conclusions It was stated in section 3 that the μ/c fluctuations are consistent with at least a 50% proton primary flux at ~10^{17} eV. This conclusion is supported by the $\sigma(X_{max})$ results. None of the different model predictions available give such a large $\sigma(X_{max})$ value based on a pure iron primary beam [eg. Gaisser et al (1982), Chantler et al (1983)]. Since the value of $\sigma(X_{max})$ measured in the present work, 71 (± 12) g cm^{-2}, is ~3.5 σ above even the largest calculated estimate for iron nuclei it is extremely unlikely that cosmic rays in the energy range 10^{17} - 10^{18} eV are dominantly iron nuclei. This measurement of $\sigma(X_{max})$ is however consistent with a pure proton mass composition on the basis of the calculations of Chantler et al (1983) [$\sigma(X_{max}) = 60$ g cm^{-2}].

Large fluctuations in X_{max} can arise if several masses are present in the primary beam. For a mixed composition in which P:He:(Mg:CNO):Fe is 50:19:19:12, it is found that $\sigma(X_{max}) = 57$ gcm^{-2} based on Gaisser et al (1982).

In conclusion the fluctuation in X_{max} seen at energies in the range 10^{17} - 10^{18} eV can be accounted for by a mass composition in which > 50% of the primaries are protons. Primaries at these energies cannot be dominantly iron.

REFERENCES

Chantler, M. P., Craig, M. A. B., McComb, T. J. L., Orford, K. J., Turver, K. E. and Walley, G. M. J. Phys. G 9 L27 (1983).

Gaisser, T. K., Stanev, T., Freier, P. and Waddington, C. J. Phys. Rev. D, 25, 2341 (1982).

Marsden, D. J., Hillas, A. M., Hollows, J. D. and Hunter, H. W. 12th Int. Cos. Ray Conf., Hobart p.1013 (1971).

N85-36004

HE 4.3-10

AVERAGE FEATURES OF THE MUON COMPONENT OF EAS $\geq 10^{17}$eV

P. R. BLAKE, M. LUKSYS, W. F. NASH and A. J. SEPHTON
University of Nottingham, England.

1. Method Three 10 m^2 liquid scintillators were situated at approximately 0 m, 150 m and 250 m from the centre of the Haverah Park array. The detectors were shielded by lead/barytes giving muon detection thresholds of 317 MeV, 431 MeV and 488 MeV respectively. During part of the operational period the 431 MeV threshold was lowered to 313 MeV for comparison purposes. For risetime measurement fast phototubes were used and the 10% to 70% amplitude time interval was parameterised by T_{70}.

2. The Muon Density Lateral Distribution A muon lateral density distribution of the form $\rho_\mu(R,\theta) = k[\rho(500)]^{0.94}\ 1/R(1 + R/490)^{-\eta}$ has been fitted to the data for 120 m < R < 600 m and 0.27 < ρ(500) < 2.55. The shower 'size' parameter ρ(500) is the water Cerenkov response at 500 m from the core of the EAS and is relatable to the primary energy (eg Hillas model A gives $E_p = 3.87 \times 10^{17}$ $[\rho(500)^{1.018}]$). Table 1 shows the best fit values of k and η to the data for near vertical EAS. The results show general consistency.

SECθ RANGE	DETECTOR THRESHOLD MeV	NO. OF EAS	BEST FIT k	UNCERTAINTY IN k	BEST FIT η	UNCERTAINTY IN η
1.0-1.1	313	320	2060	± 150	2.77	± 0.15
	317	1056	2000	± 90	2.69	± 0.09
	431	925	1980	± 80	2.96	± 0.09
	488	803	1890	± 90	3.11	± 0.10

Table 1 Best fit values of k and η in the muon density lateral distribution.

Table 2 compares the values of muon density derived at 100 m core distance intervals from the Nottingham detectors for ρ(500) = 1.15. Also labelled are the data from other arrays where the intercalibration has been carried out on the basis of flux rates [Blake et al (1975) and (1981)]. The Akeno data is taken from Nagano et al (1984).

CORE DIST (m)	NOTTM SCINT S-L 313MeV	NOTTM SCINT S-L 317MeV	NOTTM SCINT S-L 431MeV	NOTTM SCINT S-L 488MeV	SYDNEY SPARK CHAMB S-L 700MeV	GREISEN (1960) S-L 1GeV	YAKUTSK SCINT S-L 1GeV	AKENO PROP $930gcm^{-2}$ 1GeV
100	14.00	13.80	13.00	12.10	-	6.60	6.90	8.50
200	4.55	4.54	4.10	3.72	2.86	2.29	2.20	2.82
300	2.09	2.10	1.83	1.63	1.35	1.09	0.96	1.28
400	1.12	1.14	0.96	0.84	0.72	0.60	0.52	0.70
500	0.67	0.69	0.56	0.48	0.42	0.37	0.30	0.42
600	0.43	0.44	0.35	0.30	0.26	0.24	0.20	0.27

Table 2 Comparison of muon density lateral distribution (Muons m^{-2} for $\theta < 25°$ and $E_p = 3.87 \times 10^{17}$ eV). [S-L = sea level]

Allowing for the different thresholds and altitudes the results show reasonably consistent agreement. Figure 1 plots the muon density data at 300 m as a function of threshold energy.

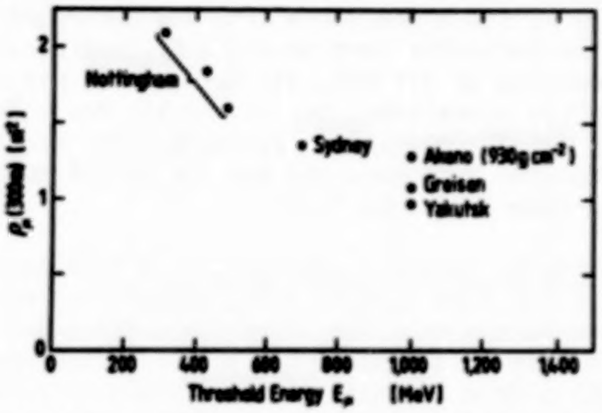

Figure 1 Muon density at 300 m as function of threshold energy.

The errors on individual points are estimated as ~10% and arise mainly from the intercalibration procedure.

Most nuclear cascade models yield distributions in agreement with the experimentally derived lateral distributions as regards slope.

Clearly absolute muon density predictions depend on both the primary mass composition assumed as well as the details of the cascade model.

3. Muon-water Cerenkov Ratio Figure 2 displays the muon-water Cerenkov density ratio as a function of R and θ for $\rho(500) = 1.15$ and $E_\mu = 317$ MeV. Again, on the whole, models predict the observed shape of the observed lateral distribution with reasonable closeness. however whilst Hillas (1971) model A fits the absolute value of the ratio well with a 100% proton primary beam; the Gaisser et al (1978) predictions require A ~ 56 to be compatible.

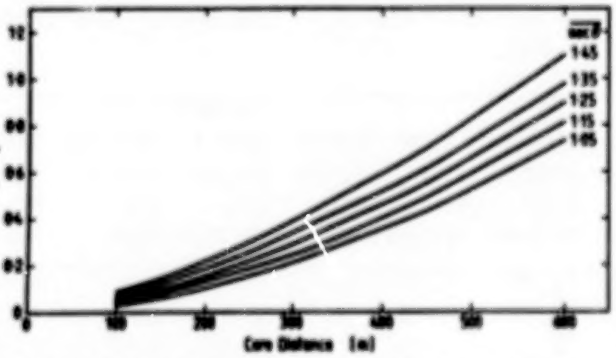

Figure 2 Muon-water Cerenkov density ratio (ρ_μ/ρ_c) as a function of core distance and secθ.

4. The Average Time Spread ($\bar{T}$). Fast phototubes and electronics enable the time spread of the muons (T_{70} = 10% to 70% full amplitude) to be determined including an instrumental response T_{70}=32 ns.

Table 3 lists the derived values for T_{70} as a function of R for three of the threshold energies.

R(m)	313 MeV	431 MeV	488 MeV
200	57.9 ns	54.2 ns	53.4 ns
250	64.4 ns	59.2 ns	59.4 ns
300	70.9 ns	64.2 ns	65.4 ns
350	77.4 ns	69.2 ns	71.4 ns
400	83.9 ns	74.2 ns	77.4 ns
450	90.4 ns	79.2 ns	83.4 ns
500	96.9 ns	84.2 ns	89.4 ns

Table 3 Derived values of T_{70} for $\rho(500) = 1$ and $\sec\theta = 1$.

Figures 3 and 4 compare the experimentally derived data for T_{70} (at 431 MeV threshold) with the cascade calculations of McComb and Turver (1981). Clearly the experimental data are faster than the predictions even assuming a 100% iron primary flux.

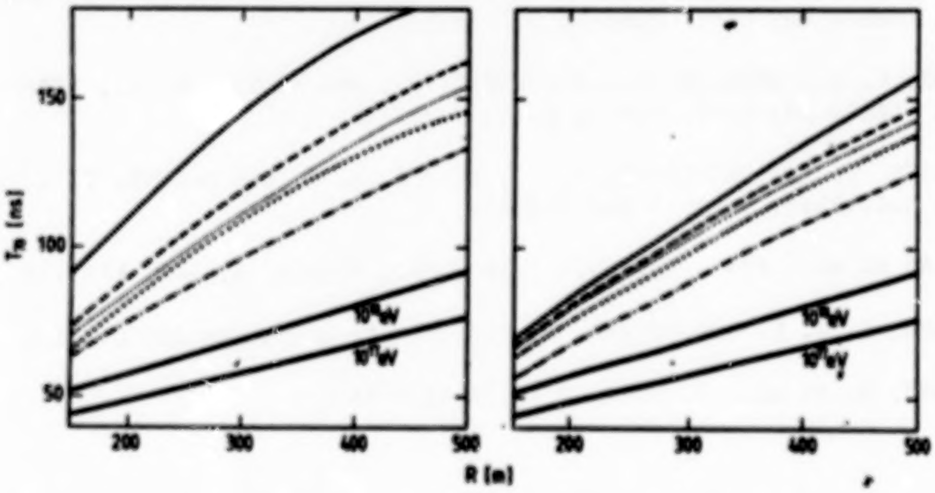

Figure 3 & 4 Comparison of predictions and experimental measurements of T_{70} as a function of R.

——— Experimental data best fits. McComb and Turver (1981) simulations with

—·—·— scaling, σ = const   - - - - - - Landau, $E^{1/4}$, σ = const

······ Landau, $E^{1/3}$, σ = const   ...... Scaling, $\sigma = \ln^2 s$

-·-·-· Landau, $E^{1/3}$, $\sigma = \ln^2 s$ Fig. 3 Proton   Fig. 4 Iron primaries

5. Elongation Length Both of the two parameters (μ/c and T_{70}) can be used to determine the 'elongation rate' of the EAS. The technique used has been described elsewhere (Blake et al, 1983). Calculations based on the data presented in this paper lead to an

elongation rate = 66(±10)g cm^{-2} $decade^{-1}$ from (μ/c) and 73(±23)g cm^{-2} $decade^{-1}$ from T_{70}.These results are in substantial agreement with other experimental data in the same energy range.

6. Conclusions The average lateral distribution of both the density and time speed of muons in EAS have been measured. The density measurements fit in well with those from other arrays and thus serve successfully for cross-checking of array calibrations.

The fast average risetime of the muons indicates early EAS development and little contribution from photoproduced muons at these primary energies.

Both the muon density and muon time spread are sensitive to small changes in threshold detection energy (both ~6% per 100 MeV at ~400 MeV threshold). Both measurements yield 'elongation rates' (~70 g cm^{-2} $decade^{-1}$) in close agreement with other work.

These results support the general conclusion that the primary beam contains a significant proportion of light elements at these energies.

REFERENCES

BLAKE, P. R., NASH, W. F., PRESCOTT, I. C. and STRUTT, R. B., 14th Int. Cosmic Ray Conf. Munich, 8, (1975).

BLAKE, P. R., NASH, W. F., O'CONNELL, B., and STRUTT, R. B., 17th Int. Cosmic Ray Conf. Paris, 6, 8, (1981).

GAISSER, T. K., PROTHEROE, R. J., TURVER, K. E. and McCOMB, T. J. L. Rev. Mod. Phys. 50 no.4 859 (1978).

HILLAS et al. Proc. Int. Cos. Ray Conf., Hobart, 3, 1007 (1971).

McCOMB, T. J. L. and TURVER, K. E., private communication (1981).

NAGANO, M. et al. J. Phys. G 10, 1295 (1984).

ORIGINAL PAGE IS
OF POOR QUALITY

N85-36005

HE 4.3 - 11

Measurement of Shower Electrons and Muons using a Small Air Shower Array

S.K. Chan and L.K. Ng
Physics Department, University of Hong Kong
Hong Kong

Abstract

A small air shower array has been used to measure the size spectrum of air showers at sea level in the size range $6.10^3 - 10^6$. The result fitted with the power law gives an index -2.79±0.11 for the differential spectrum. Lateral distribution of electrons fitted with the well known NKG function results in an age parameter $s = 1.35$ for core distances less than 30m and $s = 0.8$ for longer core distances. Lateral distribution of muons follows the general shape of Greisen's relation but is much higher in intensity. Muon and electron densities at the same observation point are also compared.

1. Introduction. Cosmic rays of energy around 10^{14}eV are of particular interest with the present day availability of accelerator data. It was with this in mind that the present experiment was constructed.

The air shower array used has been described in a previous experiment (Chan et al 1979) and the accuracy of core location is typically ±6m. The present addition at the centre of the array is a flash tube assembly shown in figure 1. The upper trays of flash tubes (each 1m x 6.5mm diameter) are for measuring the total particle density, while the lower trays shielded by iron plates (threshold 0.3 GeV) are for determining the muon density simultaneously. The maximum observable density is $30m^{-2}$.

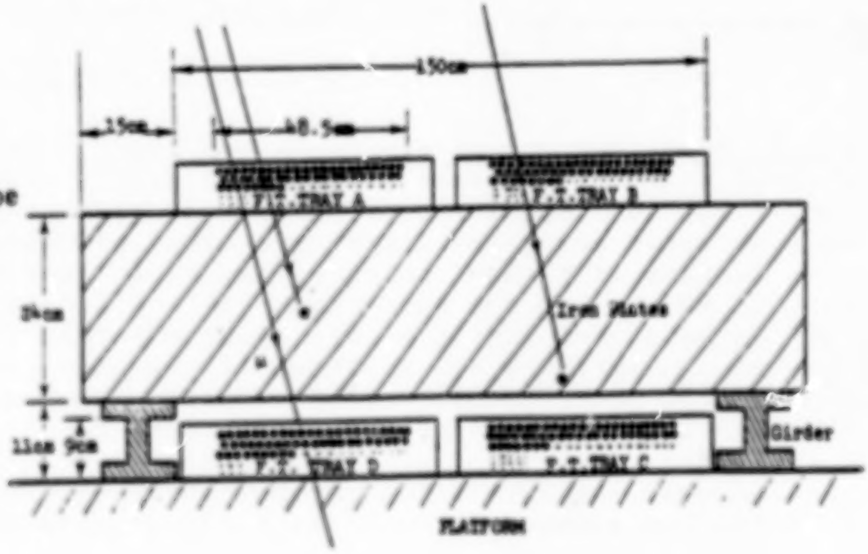

Fig. 1
Flash tube
assembly

However, as the result below reveals, most air showers observed at sea level may be just old showers with primary energies greater than 10^{14}eV, which are above the accelerator energy range. Nevertheless, it is still worthwhile to report on the measured results obtained.

2. The shower size spectra. The differential and integral size spectra in figures 2 and 3 respectively were computed from 6798 measured events taken in the period July - December, 1981. Fitting each spectrum with a power law gave agreeable slope indices, -2.79 ± 0.11 for the differential and -1.83 ± 0.1 for the integral. The latter is compared with other workers' results in figure 3.

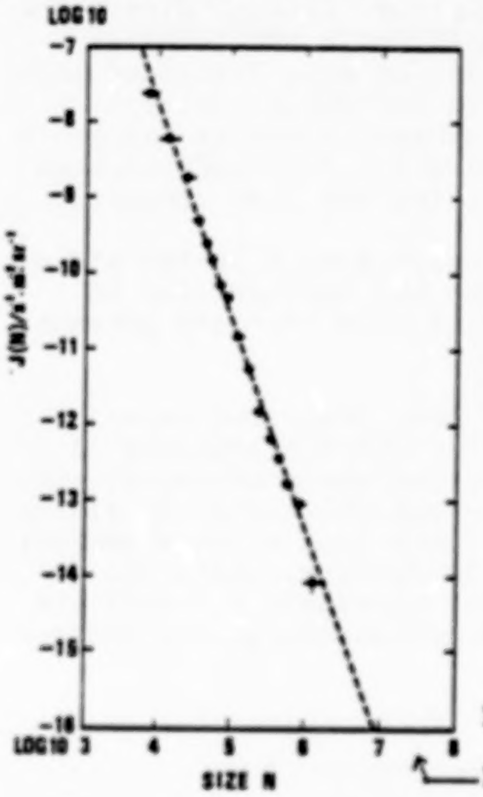

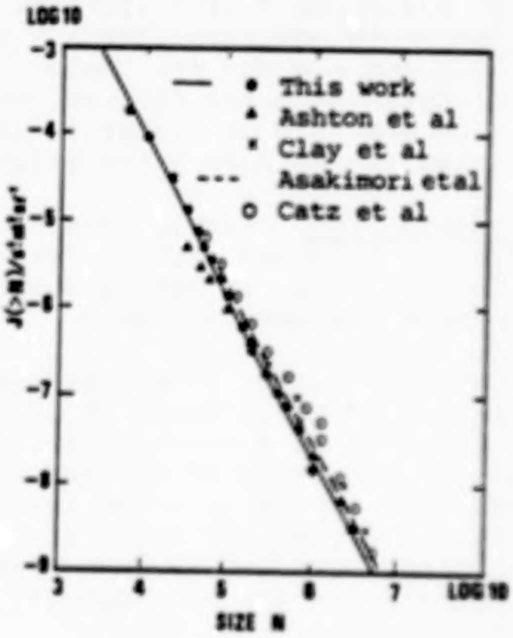

Fig.3 Integral size spectrum.

Fig.2 Differential size spectrum

3. Lateral distributions of electrons and muons. Results in the figures 4 and 5 are based on particle tracks observed from the flash tube assembly. Difference in track intensity between the upper and lower flash tube trays provides the electron density at a known location and known size of a shower. For showers in the size range 10^4 - 4.10^4, the results can be fitted with the well known NKG function with a single age parameter s = 1.3. Those in the size range 4.10^4 -2.10^6 are more complicated, giving a fairly large age parameter(s ~ 1.35) at smaller core distances, but a very small parameter (s ~ 0.8) at larger core distances. A straight forward interpretation is that those falling close to our detection assembly were in fact old showers well

passed their point of maximum development, and those further away were developing young showers.

The data presented in figure 6 for the muon lateral distribution are based on the track count in the lower flash tube trays. Local bursts in the iron absorber were rejected since they were mostly hadron events. The distribution follows the general shape of the classical relation (Greisen 1960), but the intensity is about three times as large.

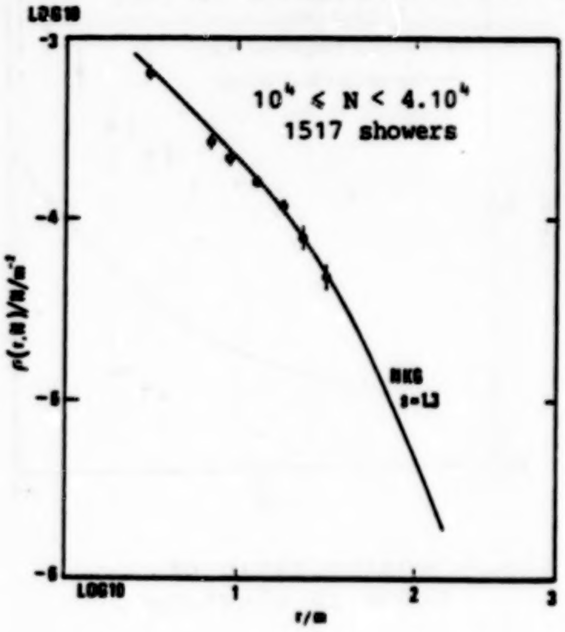

Fig. 4
Lateral distribution
of electrons.

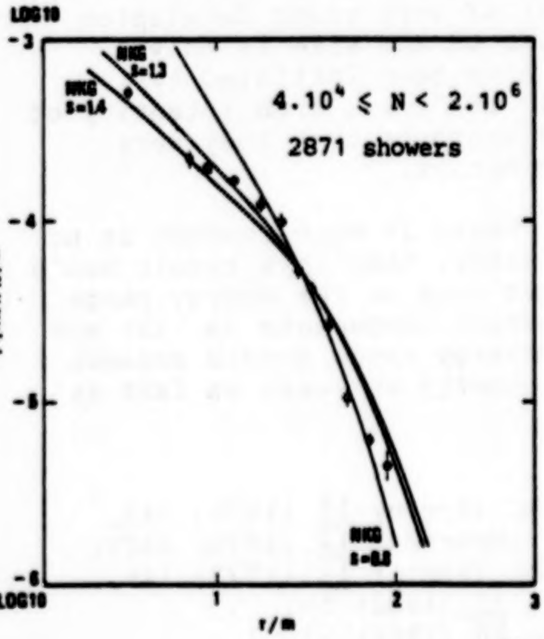

Fig. 5
Lateral distribution
of electrons.

C-3

ORIGINAL PAGE IS
OF POOR QUALITY

4. Density ratios of muons to electrons. Figure 7 presents the density relation between shower muons and electrons at the same location from each core. The pioner results due to Cocconi (Hayakawa 1969), and rough estimates based on Greisen's relation and the NKG function with mean shower size $2.23.10^4$ are also shown for comparison. Again our ratios are expected to be much higher.

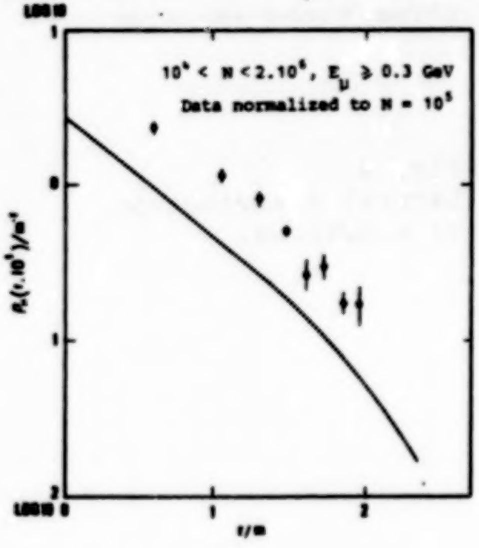

Fig.6 Lateral distribution of muons.

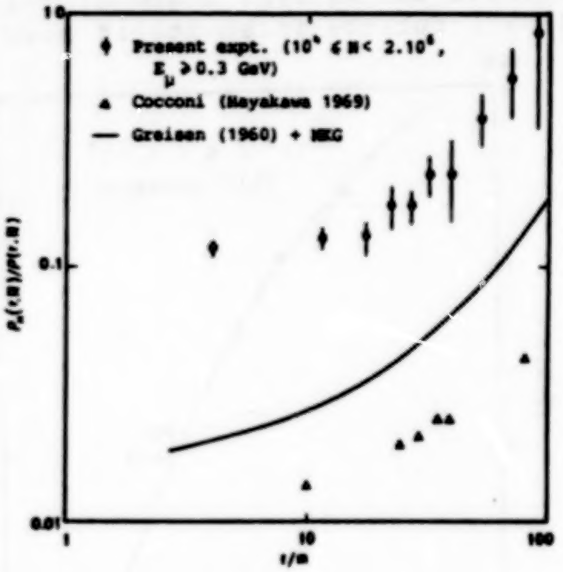

Fig.7 Density ratio of muons to electrons.

5. Discussions. If the observed shower events are either old declining showers ($s \sim 1.3$) or very young developing showers ($s \sim 0.8$), the smallness of the size is only phenomenological and may not have been initiated by primaries of small energies ($\sim 10^{14}$eV). High intensity of muon component in the showers supports that they were initiated by higher energy primaries.

Alternatively, if the richness in muon content is not due to the phenomenological factor, then this result would suggest that the primary cosmic rays at the energy range concerned are dominated by heavier components ($A \sim 15$) and that p-p interaction at this energy range should possess multiplicity which rises with energy at least as fast as $n_s \alpha E^{\frac{1}{4}}$.

References.

Ashton F et al, Proc. 16th ICRC (Kyoto) 13 (1979) 243.
Catz P et al, Proc. 14th ICRC (Munchen) 12 (1975) 4329.
Chan S K et al, Proc. 16th ICRC (Kyoto) 11 (1979) 149.
Clay R W et al, Aust. J. Phys. 35 (1982) 59.
Greisen K, Ann. Rev. Nucl. Sc. 10 (1960) 63.
Hayakawa S, Cosmic Ray Physics N.Y.Wiley-Interscience(1969).

N85-36006

HE 4.3-12

THE LONGITUDINAL DEVELOPMENT OF MUONS IN COSMIC RAY AIR SHOWERS AT ENERGIES 10^{15}-10^{17}eV

T. Cheung and P.K. MacKeown
Department of Physics
University of Hong Kong
HONG KONG

ABSTRACT

The relationship between longitudinal development of muons and conventional equi-intensity cuts is carefully investigated. The development of muons in EAS has been calculated using simulation with a scaling violation model at the highest energies and mixed primary composition. Profiles of equi-intensity cuts expected at observation altitudes of 550, 690 and 930 gcm^{-2} can fit the observed data very well.

1. Introduction In recent years estimates of the longitudinal development of muons in EAS have been presented by several groups, based on equi-intensity cuts of muon size spectra following the method introduced 20 years ago by the BASJE group [1]. As is well known the relationship between such equi-intensity cuts and the profile of longitudinal development of the muons is not as straightforward as in the case of the electromagnetic component, and is particular to the altitude of observation. This arises because the muon longitudinal development itself depends on the zenith angle and the nature of the primary particle, moreover observations are made in general above a muon threshold energy which is zenith angle dependent. Some reported calculations when compared with measurements appear to show significant discrepancies [2],[3]. We report here calculations of equi-intensity curves, based on simulated showers, for different fractions of Fe nuclei in an otherwise pure proton beam using a model for hadronic interactions consistent with the degree of scaling violation discussed in [4].

2. Model Used in the Simulations A model for p-p collisions was adopted which incorporates scaling violation for interactions of the leading particle at $E > 2\ 10^{13}$eV to the extent proposed in [4], with radial scaling assumed for all other interactions. Above 10^{11}eV the cross-section for hadron air-nucleus interactions was assumed to rise as $\sigma^{\text{inel.}} = \sigma_0(1+a\ell n^2 E)$, with values of the interaction lengths below this energy given by $\lambda_{\text{p-air}} = 90\ \text{gcm}^{-2}$ and $\lambda_{\pi\text{-air}} = \lambda_{\text{K-air}} = 120\ \text{gcm}^{-2}$. For heavy nuclei incident we assumed $\sigma^{\text{inel.}}_{\text{A-air}} = \pi r_0^2(A^{1/3} + A_{\text{air}}^{1/3} - \delta)^2$. The smaller elasticity [5] and larger multiplicity [6] reported for p-air nucleus collision was allowed for by taking $\eta_{\text{p-air}} = 0.31$ and $\langle m_{\text{p-air}}\rangle = 1.58\langle m_{\text{pp}}\rangle$. Although these additional particles arising from a nuclear target are in the central region and contribute little to the shower size they make a noticable contribution to the muon component at low energies. A Γ distribution was taken for the transverse momentum, whose mean, $\langle p_t\rangle$, was assumed to vary with the density of particles in rapidity space, consistent with recent accelerator data [7].

Three dimensional Monte Carlo simulations were made for proton and Fe nucleus primaries at different energies, at the vertical and at zenith angles of 30°, 40°, 50° and 60°. In fig.1 we show the average

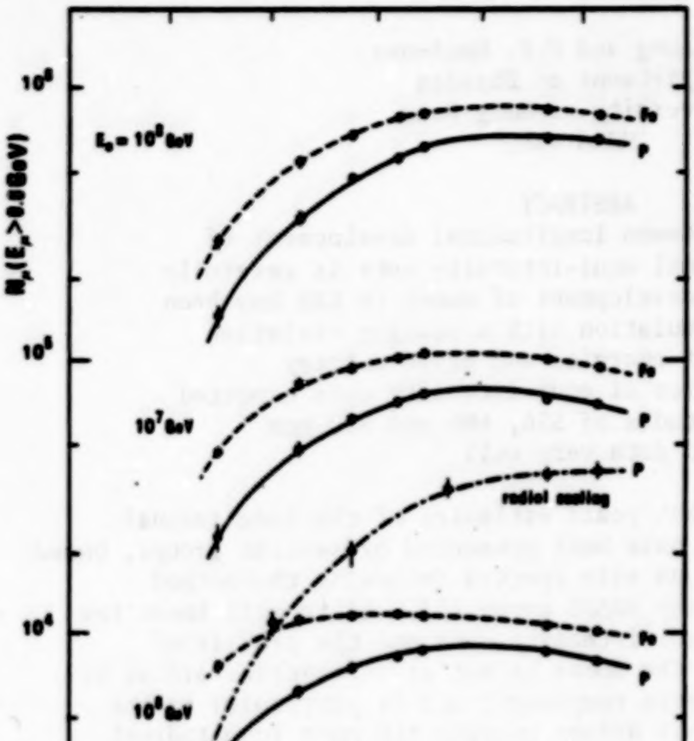

Fig. 1 Expected muon longitudinal development at fixed primary energies initiated by protons (solid curves) and iron dashed curves). The dot-dashed curve is for radial scaling model.

vertical longitudinal development of muons, $N_\mu(E_0,\theta=0,x,\varepsilon > 0.6GeV)$ at fixed energies, the case for protons where radial scaling is assumed at all energies is also shown for comparison; ε here is the muon threshold energy. These curves are generally similar to the calculations reported in [3].

3. Calculation of Equi-intensity Cuts To replicate the method used to derive equi-intensity cuts in the experiments would require the derivation of muon size spectra at different depths and zenith angles arising from particles selected from a primary spectrum of given slope and composition. This would involve an inordinate amount of computation, instead an approximate method is used. Because the muon decay probability depends on zenith angle, vertical longitudinal profiles cannot be used for constructing equi-intensity curves for comparison with experiment, unlike the case for the electron component. Longitudinal developments at different zenith angles at each depth must be used, in addition, as already mentioned, the relevant muon threshold energy must, in general, be taken as $\varepsilon_0 Sec\theta$ where ε_0 is the threshold for vertical muons. At a vertical depth x_0, when there is only one primary species present the experimental equi-intensity cuts correspond to $N_\mu(E_0,\theta,x = x_0 Sec\theta,\varepsilon>\varepsilon_0 Sec\theta)$ — assuming a unique relationship between

the energy of the primary E_o and muon size at θ, $J(N_\mu,x) = J(E_o(N_\mu,x))$ (fluctuations may be allowed for by considering instead root mean square sizes [8]). If we consider a primary beam containing two species, protons and Fe nuclei say, we have

$$J(N_\mu,x) = J_p(E_o^{(p)}(N_\mu',x)) + J_{Fe}(E_o^{(Fe)}(N_\mu,x)).$$

If the primary spectrum $J(E_o) = AE_o^{-\gamma}$ is assumed to contain protons, with a constant fraction k, and Fe nuclei only an equi-intensity curve is defined by

$$AE_o^{(p)-\gamma}[k+(1-k)(E_o^{(p)}/E_o^{(Fe)})^\gamma] = J_\mu, \text{ a constant.............}(1)$$

Since the range of primary energies of one species contributing to any one equi-intensity curve will not be very great we approximate $N_\mu^{(p)}(E_o,x) = E_o^\omega g_p(x)$, $N_\mu^{(Fe)}(E_o,x) = E_o^\omega g_{Fe}(x)$, where ω may depend on depth or zenith angle. Defining $\Lambda(x) = (g_p(x)/g_{Fe}(x))^{1/\omega}$ and using (1), we may write $N_\mu(x,J_\mu) = E_o'^\omega g_p(x)$, where $E_o' = E_o^{(p)}(N_\mu,x)[k+(1-k)\Lambda^{-\gamma}(x)]^{1/\gamma}$, $E_o^{(p)}(N_\mu,x) = (A/J_\mu)^{1/\gamma}$. Thus when k is not 0 or 1 equi-intensity curves should be constructed from the simulated longitudinal developments, not at a fixed E_o but at values of E_o' which depend on the depth.

4. Results Using the profiles simulated at different zenith angles values of the function Λ(x) could be obtained. Taking $A = 2.5 \times 10^6$,

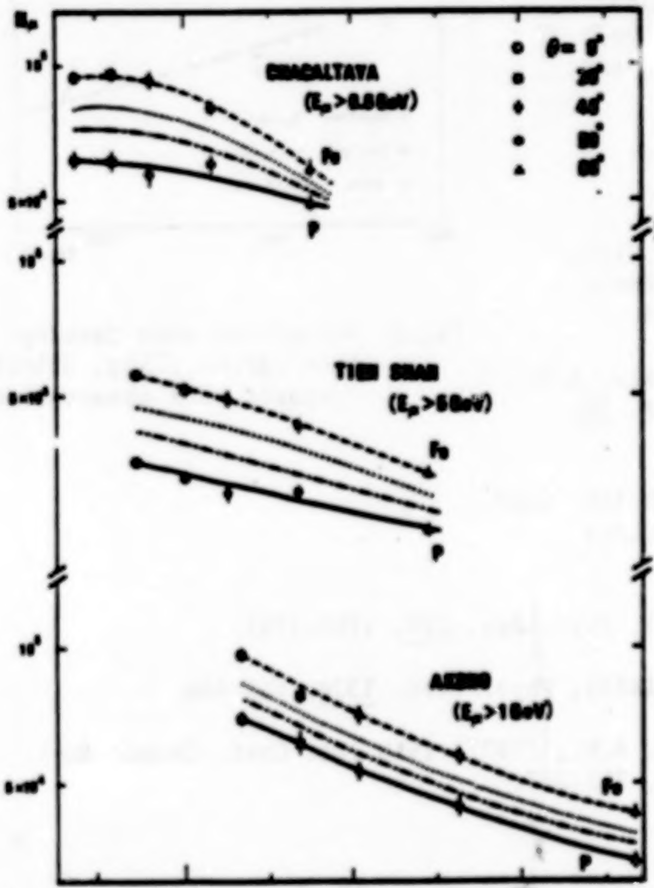

Fig.2 Expected muon longitudinal development for an integral intensity $J = 2.5 \times 10^{-8} m^{-2} s^{-1} sr^{-1}$ at Chacaltaya, Tien Shan and Akeno. The dot and dot-dashed curves correspond to 50% and 25% of iron in primary cosmic ray.

$\gamma = 2$ [8], expected equi-intensity curves for $J_\mu = 2.5\ 10^{-8} m^{-2} s^{-1} sr^{-1}$ at Chacaltaya, Tien Shan and Akeno have been calculated and are shown in fig.2, where a significant difference from the profiles at constant energy can be observed. Curves for 75%p, 25%Fe, normalised in each case to give a best fit to the data, are compared to experimental data from these experiments in fig.3. The relevance of these curves to the primary composition is noted in another paper (OG 5.2-12) at this conference.

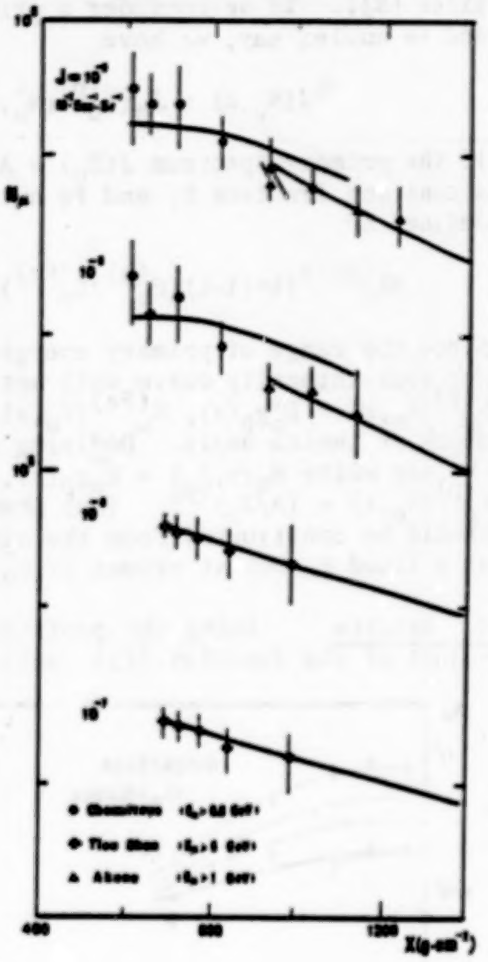

Fig.3 Normalised muon development curves (75%p, 25%Fe) compared with observations.

Acknowledgments We are grateful to Director of Computer Services, H.K. University Centre of Computer Studies and Applications for the provision of computing facilities.

References

[1] Bradt H., Clark, G., La Pointe, M., Domingo, V., Escobar, I., Kamata, K., Murakami, K., Suga, K., and Koyoda, Y., (1965), Proc. 9th Int. Conf. Cosmic Rays, London, 2, 715-717.

[2] Aguirre, C. et al., (1979), J. Phys. G: Nucl. Phys. 5, 151-157.

[3] Honda, M. et al., (1983), 18th Int. Conf. Cosmic Rays, Bangalore, Conference Papers, 11, 350-353.

[4] Wdowczyk, J. and Wolfendale, A.W., (1984), J. Phys. G: Nucl. Phys. 10, 257-272.

[5] Jones, L.W., (1983), 18th Int. Conf. Cosmic Rays, Bangalore, Conference Papers, 5, 17-20.

[6] Tasaka, S. et al., (1982), Phys. Rev. D25, 1765-1785.

[7] Breakstone, A. et al., (1983), Phys. Lett. 132B, 463-466.

[8] Gaisser, T.K. and Hillas, A.M., (1977) 15th Int. Conf. Cosmic Rays Plovdiv, Conference Papers, 8, 353-357.

N85-36007
HE 4.3-13

TOPOLOGICAL ASPECTS OF AGE PARAMETER

J.N. Capdevielle
Laboratoire de Physique Théorique, Bordeaux, France

and

J. Gawin
Institute of Nuclear Studies, Lodz, Poland

1. Introduction

The well known NKG function is a very useful tool to describe the lateral extension of the electromagnetic component in EAS ; however, in spite of non negligible qualities (simplicity, normalization by beta-function), it doesn't correspond exactly to the natural shape of the lateral electron distribution. Several bias may occur in size estimation if NKG is used without correction, for instance, contradiction between lateral and longitudinal development the lateral parameter $s_{\perp}$ being quite lower than the longitudinal one (1)(2). We emphasize here how the longitudinal age parameter s_t can be correlated with the information obtained from the lateral electron densities according to the conditions of use of the NKG function.

2. Local age parameter phenomenology

The theoretical age parameter s_t illustrates the declining stage of a shower and is determined as the saddle point in the inverse Mellin transformation. We have postulated that the NKG function, derived from diffusion equations fails to describe EAS data, mainly because a uniqueness of parameter s was assumed, and we have admitted local agreement with NKG function in small bands of distance by introducing the local age parameter

$$s(r) = \frac{1}{2x+1}\left((x+1)\frac{\partial \mathrm{Ln}\, f}{\partial \mathrm{Ln}\, x} + (6.5\,x + 2)\right) \qquad (f \equiv \mathrm{NKG})$$

$(x = r/r_o)$, r_o Molière radius. From two neighbouring points x_i, x_j, the lateral age parameter s_{ij} in $[r_i, r_j]$ is given by

$$s_{ij} = \mathrm{Ln}\,(F_{ij} X_{ij}^2 Y_{ij}^{4.5})/\mathrm{Ln}\,(X_{ij} Y_{ij})$$

where $F_{ij} = f(r_i)/f(r_j)$, $X_{ij} = r_i/r_j$, $Y_{ij} = (x_i+1)/(x_j+1)$.

If $r_i \to r_j$, $s_{ij} \to s(r)$ when $r = (r_i+r_j)/2$.

Different behaviour of lateral structure function were proposed from different analytical treatment of diffusion equations (3) or Monte-Carlo simulation of e.m. cascades (4). A convenient formula was advanced consisting to use NKG formula with a Molière radius reduced by a factor $m = 0.78-0.21\, s_t$ (for individual e.m. cascade). We observed for single e.m. cascade that s(r) had, versus (3) or (4) a behaviour similar to fig. 1 ; incorporating those results in EAS-3D simulation, we ascertained that this typical behaviour of s(r) survived in EAS lateral distribution for all sizes and levels.

ORIGINAL PAGE IS
OF POOR QUALITY

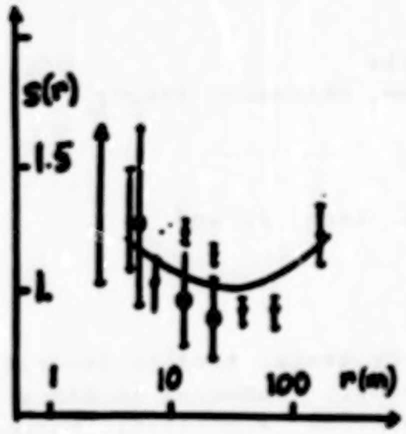

Fig. 1

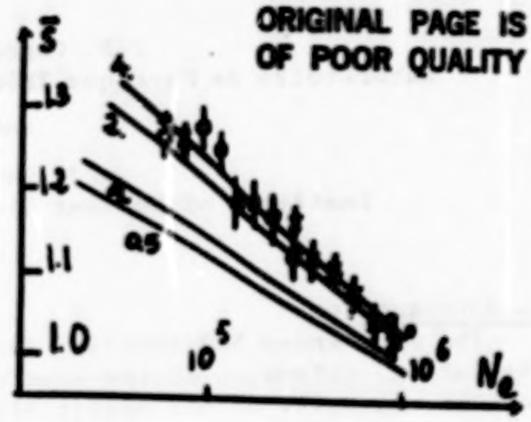

Fig. 2

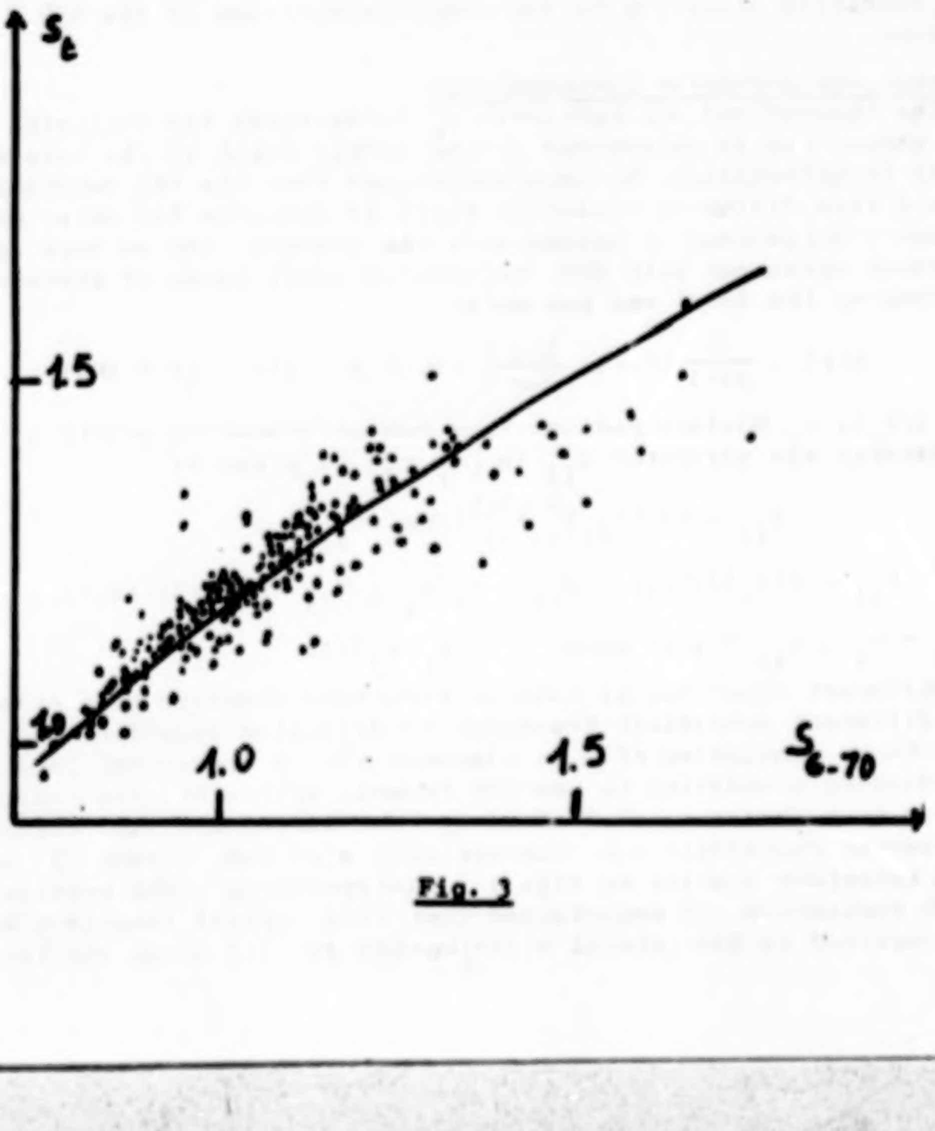

Fig. 3

Recently we developed a very detailed Monte-Carlo 3D-simulation, including all possible causes of deviation (for instance, the double body decay of each π^o, is completely described to produce energy and director cosines of each outgoing γ, $< p_t >$, is correlated with central rapidity density...) ; the model used for nuclear interaction is the multicluster phenomenological one described in HE 4.1-9,10. A surprising agreement is obtained with Akeno data (5) in favour of the parametrization (fig. 1)

$$s(r) = \alpha\xi^2 + \beta\xi + \gamma \quad , \text{ where } \xi = \mathrm{Ln}\,(r/r_o)$$

For a uniform density of detectors, the answer of an experimental array will be averaged on all the shower disk seen by the array. The radius R of this shower disk depends on the detector area (or density threshold) and it comes :

$$\bar{s} = \frac{1}{R}\int_0^R s(r)\,dr = \frac{1}{X}\,(\alpha F_1(X) + \beta G_1(X)) + \gamma \quad \text{with } X = R/r_o$$

where $F_1(X) = X\mathrm{Ln}^2 X - 2X(\mathrm{Ln}\, x - 1)$, $G_1(X) = X\mathrm{Ln}\, X - X$.
According to the shape of fig. 1, any attempt to estimate $\bar{s}$ in [0 - 50 m] and [50 - 150 m] will give the same value of the integral (6).

3. Comparison with experiment

The variation of $\bar{s}$ versus size has been calculated for MPM (nucleon primaries, θ = 22°5) at Akeno level (fig. 2). Four values of R have beer taken corresponding to 4 e^-/m^2, 2, 1, 0.5 e^-/m^2. The first value corresponding to 0.25 m^2 detector is in very good agreement with the experimental data. At Tian-Shan level, we have plotted the correlation between s_{6-70} and s_t, the first parameter being estimated by NKG function from numerical values simulated at 6 and 70 m (fig. 3) for different sizes between 10^4 - 10^6 particles. A general correlation appears : $s_t = 1.434\, s_{6-70}^{1/2} - 0.243$.

The correspondance giving s_t at Akeno and Moscow altitudes has been also obtained as $s_t = 1.246\, \bar{s}^{1/2} + 0.044$ and $s_t = 1.157\bar{s}^{1/2} + 0.183$. We note that with the present assumption included for e.m. cascade, the correlation is not independent on level (fig. 4).

4. Discussion

The behaviour versus r of s(r) is not smeared out by the hadronic cascade and survives in EAS (fig. 1). The agreement obtained previously with high multiplicity model is now obtained with the multicluster phenomenological model

(describing β-p data) up to 5.10^6 GeV (limit of our Monte-Carlo simulation) as well at Akeno for $\bar{s}$ and s(r) as in Tian-Shan for s_{6-70}. The age parameter data doesn't suggest between 2.10^4 - 5.10^6 GeV any increase of primary mass and supports better a nucleon dominance in primary cosmic rays.

References

1. S.C. Tonwar, 1981, Proc.17th Conf.on Cosmic Rays, Paris, rap. paper.
2. J.N. Capdevielle and J. Gawin, 1982, J.Phys. G8 (1982), 1317.
3. A.A. Lagutin, V.V. Uchaikin, 1979, Proc.16th Conf.on Cosmic Rays, Kyoto, 7, 18.
4. A.M. Hillas, 1981,Proc.17th Conf.on Cosmic Rays, Paris, 6, 244.

5. M. Nagano et al., 1984, J.Phys.Soc.Jap., 53, 1667.
6. F. Ashton et al., 1983, Proc.18th Conf.on Cosmic Rays, Bangalore, 11, 181.
7. M.V.S. Rao, 1983, Proc.18th Conf.on Cosmic Rays, Bangalore, 12, 449.
M. Nagano, 1983, Proc.18th Conf.on Cosmic Rays, Bangalore, 12, 475.

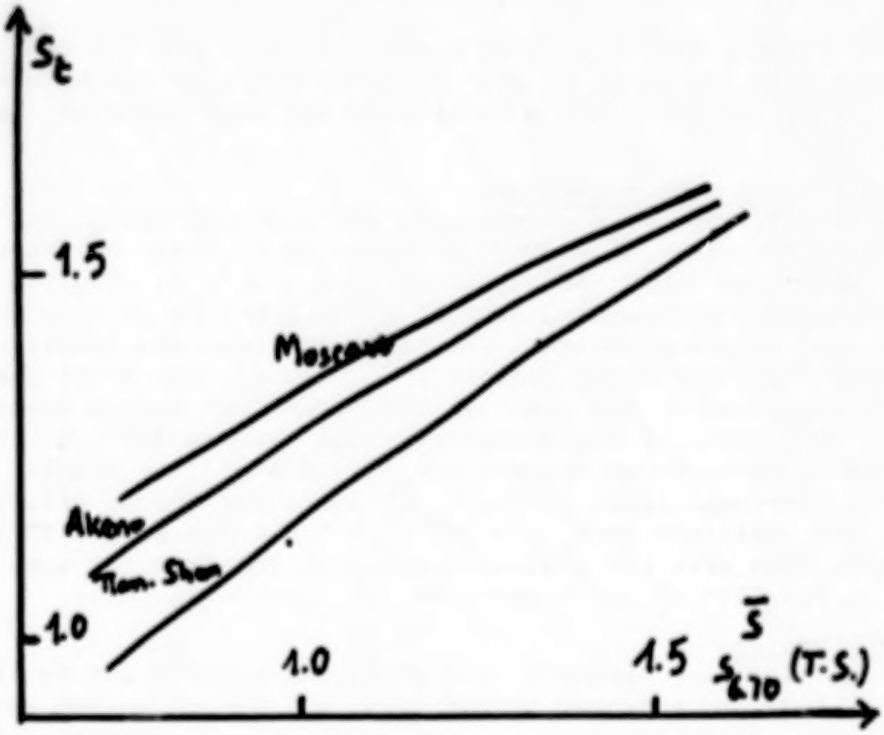

Fig. 4

N85-36008

MONTE CARLO SIMULATION OF E.A.S. GENERATED BY 10^{14}-10^{16} eV PROTONS

Fenyves, E.J. and Yunn, B.C.
University of Texas at Dallas
P.O. Box 830688
Richardson, TX 75083-0688

Todor Stanev
Bartol Research Foundation of the Franklin Institute
University of Delaware
Newark, DE 19716

1. Introduction

Detailed Monte Carlo simulations of extensive air showers to be detected by the Homestake Surface-Underground Telescope (1) and other similar detectors located at sea level and mountain altitudes have been performed for 10^{14}-10^{16} eV primary energies. The results of these Monte Carlo calculations will provide an opportunity to compare the experimental data with different models for the composition and spectra of primaries and for the development of air showers (2).

In the present paper we report on the results obtained for extensive air showers generated by 10^{14}-10^{16} eV primary protons.

2. Monte Carlo Simulation of the Hadronic Cascade

The interaction model used assumed inelastic cross sections increasing with energy as $\ln^{1.8}s$, which corresponds to a $\ln^2 s$ rise of the inelastic p-p cross section. The x distribution obeys radial scaling and is realized through the splitting technique suggested by A.M. Hillas. The K/π ratio is 0.09 and energy independent.

Transverse momentum distribution is of the form $p_\perp \exp(-Kp_\perp)$ and includes the "sea gull" effect. For $x < 0.2$, $K = \frac{2}{x + 1/4}$, while for $x > 0.2$ we used a constant exponent of -4.44 for pions.

The secondary particles are followed until they reach certain threshold energy levels: 1.7 TeV for muons, 0.01 and 0.1 TeV for electrons, gammas, and 0.1 TeV for hadrons.

3. Simulation of the Electromagnetic Cascades

The electromagnetic cascades generated by gammas and electrons are propagated to the height of detection by applying the parametrized analytical formulas for the longitudinal development and lateral distribution of the electron component obtained by Fenyves and Yunn in previous Monte Carlo simulations of electromagnetic cascades (3). The threshold energy levels for the electromagnetic cascade generating gammas and electrons were: 0.01 TeV for 10^{14} and 10^{15} eV primary protons, and 0.1 TeV for 10^{16} eV protons. The average number of gammas and electrons above the threshold per shower is given in Table 1. (Muons above 1.7 TeV are also included in the Table.)

Table 1

E_p(eV)	N_γ	N_e	N_μ
10^{14}	361 ± 8	3.9 ± 0.3	0.30 ±0.06
10^{15}	2612 ±61	31.9 ± 1.1	1.54 ±0.17
10^{16}	3015 ±78	34.9 ± 1.2	8.20 ±0.50

From the extrapolation of the gamma spectra below the threshold levels correction factors were calculated for the missing low energy electromagnetic cascades. The correction factors for the total number of electrons of the air shower are dependent on the depth and the primary proton energy varying between 1.010 and 1.021.

The geomagnetic effect was included in the calculation by stretching the east-west axis of each vertical electromagnetic cascade by $[1 + 0.05(\cos\lambda/P)^2]^{\frac{1}{2}}$ where λ is the geomagnetic latitude and P the pressure in atmospheres (4). The individual cascades were then folded together to form the electron component of the extensive air shower.

4. Results

We have run a total of 220 extensive air showers generated by 10^{14}, 10^{15} and 10^{16} eV primary protons in a standard atmosphere. As expected the longitudinal development of these showers could not be approximated well with the standard formula used for the electron component of electromagnetic cascades generated by single gammas (3)

$$N_e(E_o,E,t) = \frac{A(E,s)0.31}{\sqrt{y}} \exp\,[t(1-1.5\,\ln s)] \tag{1}$$

where t is the depth measured in radiation lengths (37.1 g/cm^2), $y = \ln E_o/\varepsilon_o$ (ε_o = 81 MeV),

$$s = \frac{3t}{t + 2y} \tag{2}$$

and A(E,s) is the fraction of electrons having energies larger than the electron threshold energy, E. (E=5MeV and A(5MeV,s)=0.67 were used in the present study (3).)

We could, however, fit N_e^{max} and t_{max} calculated from Eq.(1) simultaneously to the corresponding average values obtained for the 10^{14}, 10^{15} and 10^{16} eV showers by varying E_o, the energy of the cascade generating gamma. The longitudinal development of the simulated air showers was, however, increasing faster before t_{max}, and decreasing slower after t_{max} than the values calculated from Eq.(1). This is expected because the electromagnetic component of the air shower starts with a large number of gammas, and dies out slower after the maximum due to new electromagnetic cascades generated by the hadronic core.

According to this we modified Eqs.(1) and (2) simply by replacing t in both equations by

$$t' = t + \beta(t_{max} - t)t^\gamma \tag{3}$$

where β and γ are constants depending on the primary proton energy, and the second term increases or decreases the effective t' values as compared to t before or after the maximum, respectively.

The optimum E_o, β and γ values obtained for this parametrization for $E_p = 10^{14}$, 10^{15} and 10^{16} eV are given in Table 2. Fig. 1 shows the good agreement between the Monte Carlo simulated average values (dots with error bars) and the smooth curves calculated by using Eqs.(1) and (2) modified by Eq.(3) with the parameter values given in Table 2.

Table 2

E_p(eV)	E_o(eV)	β	γ
10^{14}	$5.2 \cdot 10^{13}$	0.0100	1.00
10^{15}	$6.4 \cdot 10^{14}$	0.0173	0.75
10^{16}	$6.9 \cdot 10^{15}$	0.0300	0.50

Eqs.(1), (2) and (3) can also be used to describe moderately inclined showers ($\theta \leqslant 30^\circ$). Then t in Eq.(3) is the slant depth measured from the top of the atmosphere. The energy of the single gamma, E_o, simulating the longitudinal development of the air shower is increasing with E_p, the energy of the shower as expected because of the increasing probability of charged pions and kaons to produce nuclear interactions rather than decay. The β and γ values can be easily interpolated for intermediate E_p values when plotted on a log-log or lin-log scale vs. E_p, respectively.

The lateral distribution of electrons of air showers generated by 10^{14}, 10^{15} and 10^{16} eV protons was compared with the modified NKG formula

$$f(\frac{r}{r'_M}) = C(s) \left(\frac{r}{r'_M}\right)^{s-2} \left(\frac{r}{r'_M} + 1\right)^{s-4.5} \quad ;(4)$$

where r'_M is about half of the Molière length length, r_M, as suggested by A. M. Hillas (5), and s is calculated by Eq.(2) modified by Eq.(3) with the parameters given in Table 2. A good agreement was found for not too large distances from the core, from r=1m to about 300m, as illustrated in Figs. 2, 3 and 4 for 850 g/cm^2, the height of the Homestake Telescope where r'_M=45m (3). Similarly good agreement was found for other heights too. At larger distances from the core, however, even the modified the NKG formula fails to agree with the Monte Carlo simulated data. Corrections for this effect will be discussed in a forthcoming paper.

The geomagnetic effect is relatively small at sea level but increasing with altitude. The east-west axis of vertical showers is stretched by a factor of 1.013 at sea level, and 1.019 at 850 g/cm^2. The relative difference between the $f(r/r'_M)$ values averaged in a cone ±45° around the east-west axis and in a cone ±45° around the north-south axis is increasing with r from about −0.015 at r=1m, to about −0.075 at r=1000m.

5. Acknowledgements

The authors are indebted to N. R. Davis, S. S. Liao and D. J. Suson for their valuable cooperation. This work has been supported by the National Science Foundation.

References

(1) Cherry, M.L. et al., (1981), 17th Int. Cosmic Ray Conf., Paris, 11, p. 421.
(2) Fenyves, E.J. and Cherry, M.L., (1983), Proc. Cosmic Ray Workshop, Utah, p.173.
(3) Fenyves, E.J., Lee, C.J. and Yunn, B.C., (1983), 18th Int. Cosmic Ray Conf., Bangalore, 11, p. 240.
(4) Greisen, K., (1956), Progr. in Cosmic Ray Phys., Vol. III, p.1.
(5) Hillas, A.M., (1983), private communication.

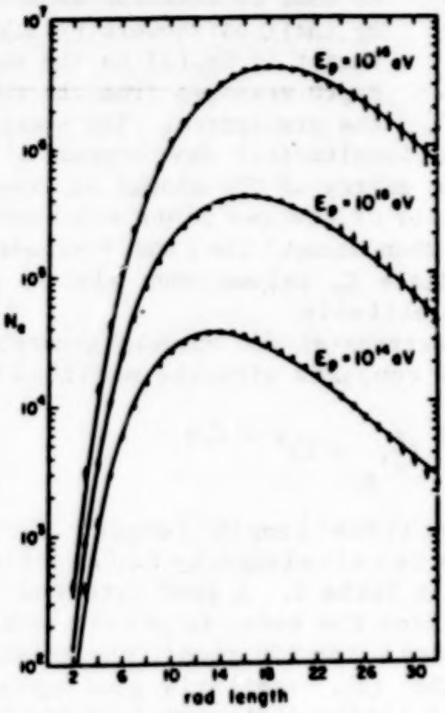

Fig. 1

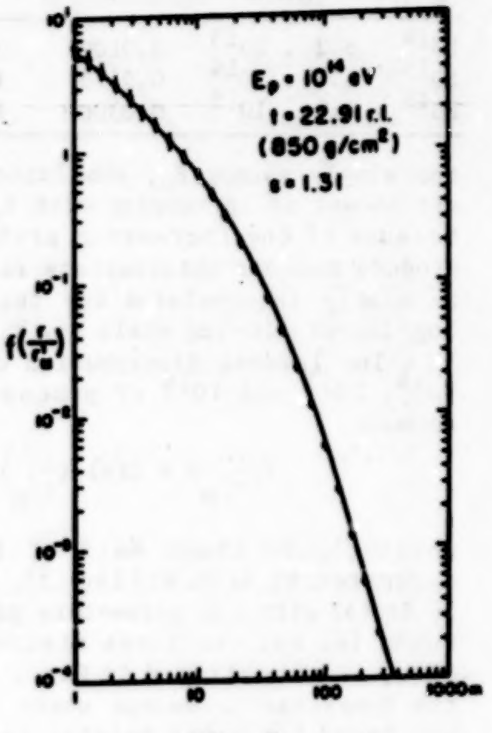

Fig. 2

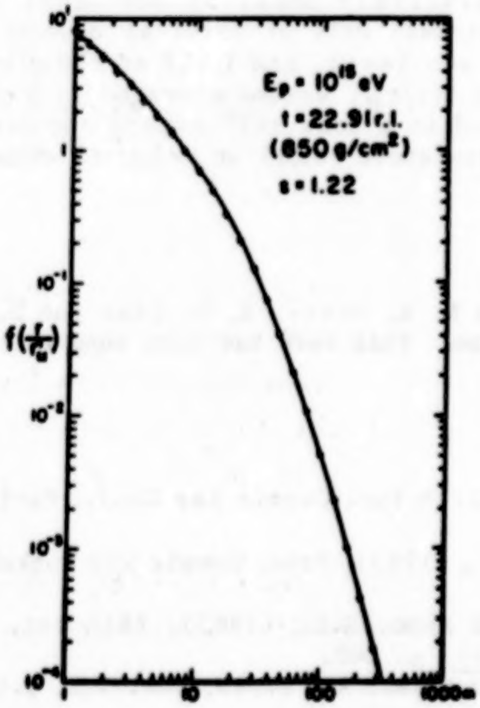

Fig. 3

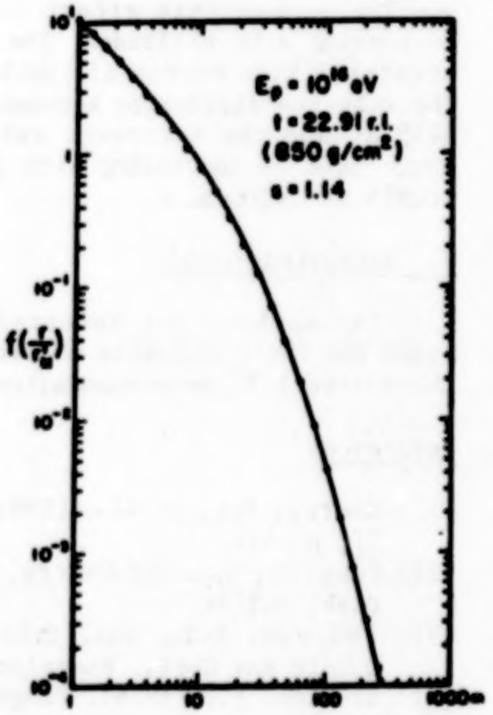

Fig. 4

N85-36009

LATERAL DISTRIBUTION OF CHARGED PARTICLES IN EAS

Dedenko L.G., Kulikov G.V., Solovjeva V.I., Sulakov V.P.
Institute of Nuclear Physics, Moscow State University,
Moscow 119899, USSR

1. Introduction. The calculations of lateral distribution of charged particles which allow for the finitness of energy of γ-quanta /1-3/, the inhomogeneity of the atmosphere /3,4/ and the experimental selection of EAS /5/ are needed to interpret correctly the experimental data /6,7/.

In /8,9/ calculations have taken into account the effect of finitness of energy of γ-quanta which produce the partial electron-photon cascades by substituting KR_m instead of R_m in NKG approximation where K has been found to be 0.56 from comparison with the experimental data. In /5,10-12/ new results on the lateral distribution of electrons in the partial cascades from γ-quanta have been obtained. The analysis /5/of results /11,12/ showed that the coefficient K can be regarded as a constant with the error of 5-10%. In /5/ the calculations have been carried out for such values of K as 0.75; 1, and $K = 1-0.5(1-y/16)$ for $y \leqslant 16$ and $K=1$ for $y > 16$ where $y = \ln(E_\gamma/1\ \mathrm{GeV})$. The last approximation of K was found to be most adequate from the comparison with the experimental data /6/ and it is used in this calculation. In /5/ the inhomogeneity of the atmosphere, muons and experimental selection were taken into account. In /5/ the calculation were done for EAS with size $N_e = 10^7$ at sea level. In this paper we extend the calculation on Ne from 10^5 to 10^7 for sea level and for Akeno level (920 $\mathrm{g.cm^{-2}}$).

2. Model and Method. The calculations were carried out in terms of the quark-gluon string model for hadron-hadron interactions /13-15/. The lateral distributions were calculated for primary protons and nuclei with A= 4,14,31,56 and the normal compositionΣ. The energy spectrum index was taken $\gamma_1 = 1.7$ at $E_1 \leq 3 \cdot 10^{15}$ eV and $\gamma_2 = 2.2$ at $E_2 \geq 10^{16}$ eV with smooth change between these two energies. The method includes the calculations of the two-dimensional functions and correlation matrixes for fixed Eo following by use of Beyes theorem and gaussian approximation for calculated functions to get the functions for fixed Ne and the zenith angle θ /16,17/. To allow for experimental selection the calculated functions for fixed Ne and θ were integrated on Ne and θ /5/. The experimental errors were taken into account by summing the physical correlation matrix with the matrix of errors, which consist of errors of $\sigma_{N_e}/N_e = 25\%$, $\sigma_{\rho}/\rho_e = 15\%$ and $\sigma_r/r = 10\%$ where ρ_e- density of electrons and r is distance from the shower axis. The approximation $R_m = 1.1\ R_m$ have been used to allow for the inhomogeneity of the atmosphere. The density of > 0.3 GeV muons and additional 27% of muon density to take into account the decay electrons and δ-electrons (according to our analysis and /18/) were added to electron density to get charged particle density.

3. Results and Conclusions. In Fig. 1 the calculated lateral distributions of charged particles for sea level are shown together with the experimental data /6/. One can see that in the limits of experimental errors the normal and proton primary compositions may agree with the experimental data /6/. Fig. 2 shows the analogous calculated functions for 920 g/cm^2 and Akeno experimental results /7/. To get the better agreement this time one should use a more steep electron lateral distribution in pure electron-photon cascades from γ-quanta than we have used. But our conclusion about primary composition made for sea level data is kept.

The authors wish to thank Prof. G.B.Khristiansen for informative discussions.

References

1. Gujavin V.V., IvanenkoI.(1960), Proc. 6th ICRC,Moscow v.2, p.253
2. Nishimura J. (1967) Handbuch der Physik, XL, VI/2.

3. Ivanenko I.P. et al. (1982) Izv.Akad Nauk SSSR, ser.phys. v.46, p.2433
4. Osipova L.N., Paskhalov Yu.I. (1979),Proc. 16th ICRC, Kyoto,v.9,p.232
5. Dedenko L.G. et al.(1985), Izv.Akad.Nauk SSSR, ser.phys. v. 49, No. 7
6. Khristiansen G.B. et al. (1983), Proc. 18th ICRC, Bangalore, No. v.11, p.197.
7. Nagano M. et al. J. Phys. Soc. Japan, 1984
8. Dedenko L.G. et al.(1975), Proc. 14th ICRC,Münich,v.8, p. 2731.
9. Dedenko L.G. et al.(1976), Brief Reps. on Physics, FIAN, No.1, p. 30
10. Hillas A.M., Papikens J.(1977), v.8, p.460,ICRC,Plovdiv
11. Lagutin A.A. et al. Proc. 16h ICRC,Kyoto, v.7,p.18
12. Vorobjev K.V. et al. (1982), Izv.Akad.Nauk SSSR,ser. phys. v.46, p.2437
13. Kaidalov A.B., Ter-Martirosjan K.A. (1984), Jadernaja Physika, v.39, p.1545
14. Anisovich V.V. et al. (1978), Jadernaja Phyzika,v.28, p. 1063
15. Kalmykov N.N., Khristiansen G.B. (1983), Proc. 18th ICRC, Bangalore, v.11, p.330.
16. Dedenko L.G. (1964), ZhETF, v.46, p.1859
17. Dedenko L.G., Zatsepin G.T. Proc. 6th ICRC, Moscow, 1960, v. 2, p.222.
18. Hayakawa S., (1969), Cosmic Ray Physics, part 1, Ed. by R.E. Marshak, v. XXII, John Wiley & Sons, New York.

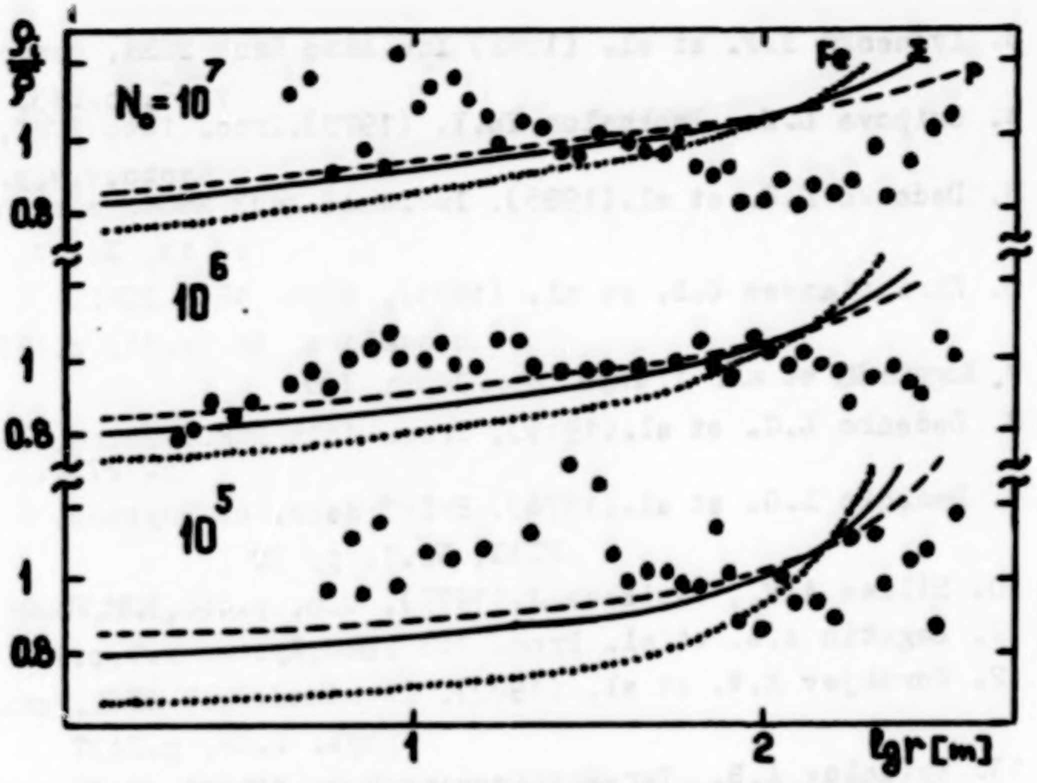

Fig.2. The lateral distribution of charged particles at 920 g cm^{-2}
($\bar{\rho} \sim (r/r_0)^{-a}(1+r/r_0)^{-b}$, $a=0.96$, $b=3.06$, $r_0=91.6$ m)

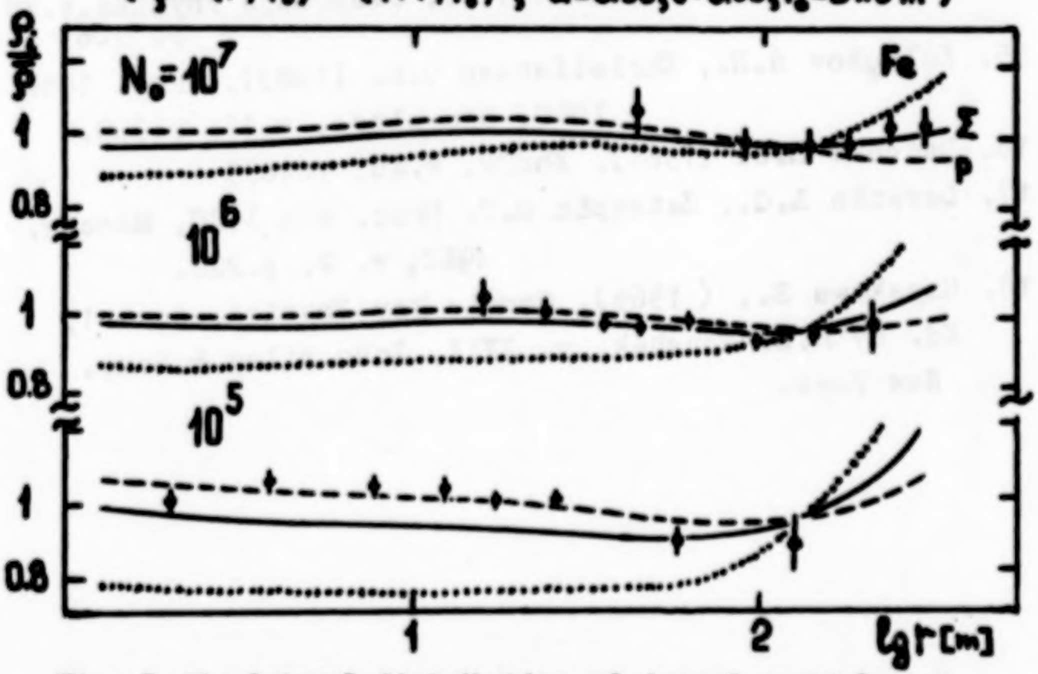

Fig. I. The lateral distribution of charged particles at sea level
($\bar{\rho} \sim (r/r_0)^{-a}(1+r/r_0)^{-b}$, $a=0.9$, $b=2.8$, $r_0=80$ m)

N85-36010

HE 4.3-16

LATERAL DISTRIBUTION OF HIGH ENERGY MUONS IN EAS OF SIZES $N_e \gtrsim 10^5$ and $N_e \gtrsim 10^6$.

Bazhutov Yu.N., Ermakov G.G., Fomin Yu.A., Isaev V.I., Jarochkina Z.V., Kalmykov N.N., Khrenov B.A., Khristiansen G.B., Kulikov G.V., Motova M.V., Proshkina I.P., Rukovichkin V.P., Solovjeva V.I., Sulakov V.P., Shkurenkov A.V. Trubitsyn A.V. and Vashkevich V.V.

Institute of Nuclear Physics, Moscow State University, Moscow, 119899, USSR.

Muon energy spectra and muon lateral distribution in EAS are investigated with the help of the underground magnetic spectrometer working as a part of the Moscow State University EAS array [1,2,3]. Before going to new results on EAS muons a general concept of the measurement should be mentioned. For every registered muon the data on EAS are analysed and the following EAS parameters are obtained: size N_e, distance r from the shower axis to muon, age parameter s. So the number of muons with energy over some threshold E_μ associated to EAS of fixed parameters are measured: I_{reg}. To obtain traditional characteristics-muon flux densities as a function of the distance r and muon energy E_μ i.e. muon lateral distribution and energy spectra which are widely discussed in terms of hadron-nucleus interaction model and composition of primary cosmic rays one should use the equation:

$$\frac{\Delta I_{reg}}{\Delta N_e \Delta r \Delta s} = t \cdot 2\pi r \int_0^{\theta_1(\varphi)} \int_0^{2\pi} d\cos\theta \, d\varphi \, I(\theta,\varphi) \cdot F(N_e,s) \, W^{EAS}_{reg}(N_e,r,s,\theta) \cdot W^{\mu}_{reg}\left[E_\mu, N_e, r, s, \sigma(E_\mu,\theta,\varphi)\right] \quad (1)$$

where $F(N_e,s)$ is known spectrum of EAS, $W^{EAS}_{reg}(N_e,r,s,\theta)$ is probability to register the EAS of specified parameters, W^{μ}_{reg} is probability to register muon of energy over E in magnetic spectrometer with effective area $\sigma(\theta,\varphi,E_\mu)$, $I(\theta,\varphi)$ is angular distribution of EAS, $\theta_1(\varphi)$ is spectrometer geometry limit on zenith angle θ, t is operation time. In our case probability is equal

$$W^{\mu}_{reg} = \left\{1 - \exp\left[-\rho_\mu(E_\mu,N_e,r,s,\theta)\,\sigma(\theta,\varphi,E_\mu)\right]\right\} \simeq \rho_\mu(E_\mu,N_e,r,s,\theta) \cdot \sigma(\theta,\varphi,E_\mu) \quad (2)$$

where $\rho_\mu(E_\mu,N_e,r,s,\theta)$ is muon flux density.

For final analysis only showers with $W^{EAS}_{reg} \geq 0,9$ ($0,9 \leq s$ $s \geq 1,6$) are selected. In this case the densities ρ_μ derived from experimental data are unbyased on age parameter. So equation (1) transforms to

$$\frac{\Delta I_{reg}}{\Delta N_e \Delta r \Delta s} = t \cdot 2\pi r \cdot F(N_e,s) \cdot \rho_\mu(E_\mu,N_e,r,s,\bar\theta) \cdot \sigma'(E_\mu); \; E_\mu, \mathrm{GeV} \sim \bar\theta = 9^\circ \quad (3)$$

where σ' equal to $\sigma' = \int_0^{\theta_1(\varphi)}\int_0^{2\pi} I(\theta,\varphi) \cdot \sigma(\theta,\varphi,E_\mu) \, d\cos\theta \, d\varphi$ is geometry factor $\sigma'(15)=.14$. In Table 1 the numbers of registered muons for threshold energies $E_\mu = 10, 200$ and 500 Gev are presented. EAS size ranges are $N_e 1$- 3.10^4-10^5 ($\langle N_e\rangle = 6.10^4$), $N_e 2$- $10^5-3.10^5$ ($\langle N_e\rangle = 1,6.10^5$) $N_e 3$- 3.10^5- [illegible] ($\langle N_e\rangle = 5.10^5$) $N_e 4$- $\geq 10^6$ ($\langle N_e\rangle = 3.10^6$).

ORIGINAL PAGE IS
OF POOR QUALITY

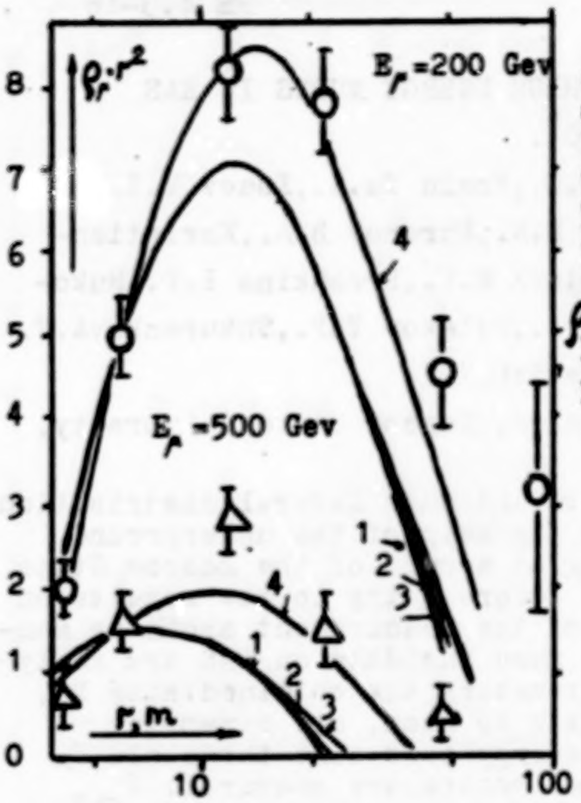

Fig.1 a

The data for muon threshold energies E_μ=200 and 500 Gev are corrected for MDM as in [1]. Muon lateral distribution (LD) shows weak dependance on EAS size. The following formula approximates the obtained data

$$\rho_\mu = K\cdot\left(\frac{N_e}{10^6}\right)^{\alpha}\cdot r^{-n}\cdot \exp\left[-r/r_0(N_e)\right]$$

where parameter α is equal

E_μ, Gev	50	100	200	500
α=	0,78	0,77	0,76	0,77
±	0,04	0,05	0,06	0,1

and

$$k = 1{,}3\cdot10^{4}/(E_\mu+250)^{1{,}4}$$

$$n = 0{,}55\cdot\left(\frac{E_\mu+2}{12}\right)^{0{,}1}$$

$$r_0 = \begin{cases} 80\left(\frac{E_\mu+2}{12}\right)^{-0{,}62}\cdot\left(\frac{N_e}{10^6}\right)^{0{,}05\pm0{,}05} & 50 \le E_\mu \le 200 \\ 10\pm3\ \text{m} & E_\mu = 500 \end{cases}$$

In Fig.1a the average LD of muons with E_μ=200 and 500 Gev are presented for $\langle N_e\rangle = 2\cdot10^5$.

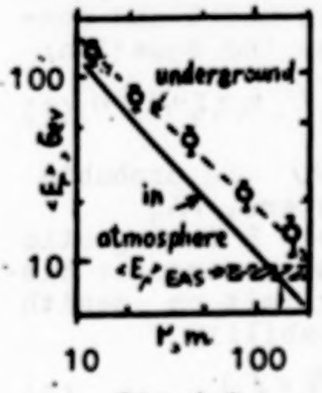

Fig.1 b

The mean muon energy as a function of distance r is presented in Fig.1b. Experimentally measured underground muon energy spectra were transformed to muon spectra in atmosphere. Solid line in Fig.1b presents mean muon energy in atmosphere at sea level. At the distance r=120±12m mean muon energy is equal to mean over EAS energy of muons, $\langle E_\mu \rangle$= 8±1 Gev,[3]. The ratio of positive and negative muon numbers was analysed for various distances r. Numbers of muons in differential ranges of energy are presented in Table2. It is seen that the ratio I_+/I_- does not deviate from 1 in statistical errors.

Table 1. Numbers of registered muons.

	r=0-8 m			r=8-16 m			r=16-32m			r=32-64m			r=64-128			r>128	
E_μ,Gev	10	200	500	10	200	500	10	200	500	10	200	500	10	200	500	10	200
All	359	94	35	556	92	30	980	87	21	952	29	5	301	3	1	55	0
[illegible]09	359	94	35	484	81	28	625	46	10	508	12	2	112	2	0	10	0
N_e-1	224	60	22	259	42	14	177	18	5	-	-	-	-	-	-	-	-
N_e-2	84	23	12	131	19	7	273	18	3	207	3	1	-	-	-	-	-
N_e-3	41	8	1	77	17	5	139	7	2	205	5	1	33	1	0	-	-
N_e-4	10	3	0	17	3	2	36	3	0	96	4	0	79	1	0	10	0

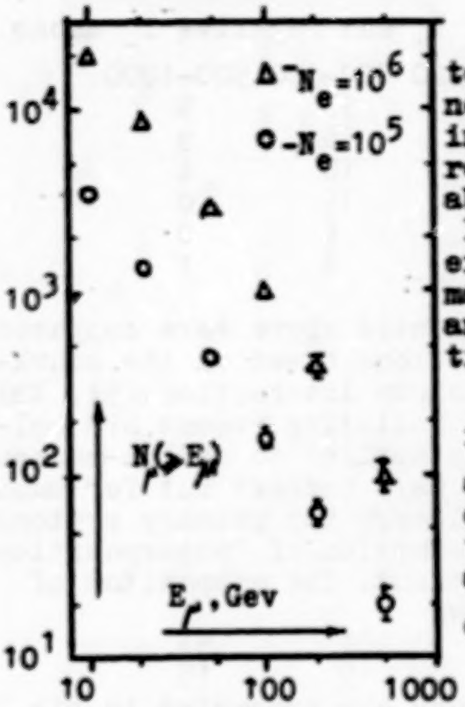

Fig. 2 a.

Comparison of LD of muons registered in E-W sectors of earth magnetic field and of muons registered in N-S sectors does not show difference in statistical errors (of about 10-20 %)for muon densities. It proves that for vertical showers deflection of muons in earth magnetic field is much less than angular spread of muon parent particles in acts of their generation.

Full numbers of muons $N_\mu(\geq E_\mu)$ in EAS of size $N_e = 10^5$ and $N_e = 10^6$ are presented in Fig.2a. The dependence $N_\mu(N_e)$ for the range of muon threshold energies $E_\mu = 10-500$ Gev and EAS of sizes $N_e = 6.10^4 - 3.10^6$ can be presented in form

$$N_\mu(N_e) \sim N_e^\alpha$$

with $\alpha = 0,78$ in experimental errors presented above.

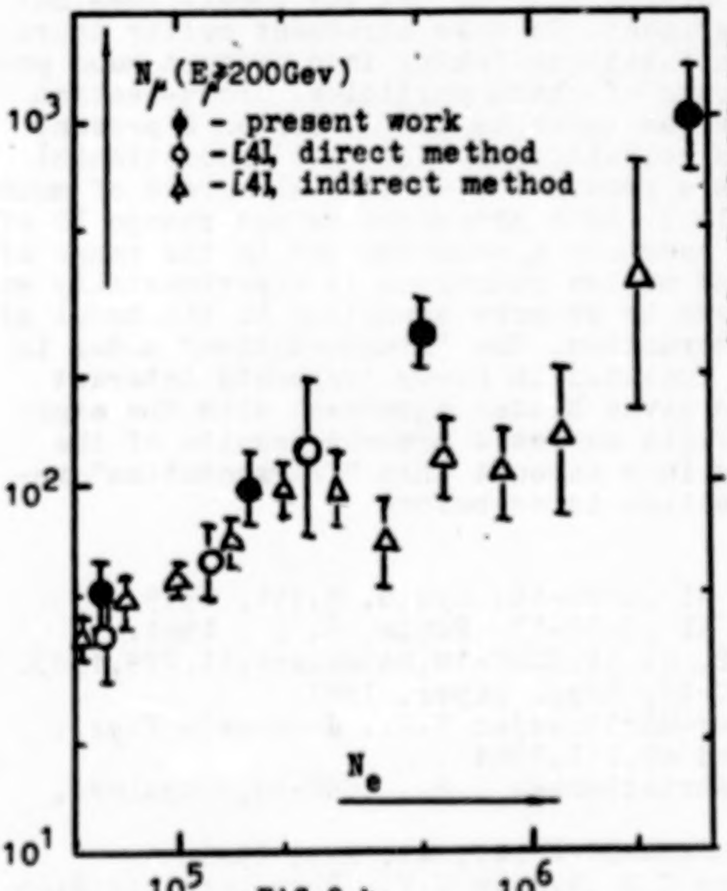

FIG.2 b

In Fig.2b our data on muons of threshold energy $E_\mu = 200$ Gev are compared to the data[4] of Indian group. The data[4] is recalculated to sea level taking the dependance N_e on depth x in atmosphere as

$$N_e \sim \exp(-x/180)$$

where x is in g/cm^2

One can see that our data do not confirm the change of the exponent α in $N_\mu(N_e)$ dependance obtained by indirect method in[4].

Table 2. Numbers of positive I_+ and negative I_- muons.

	E_μ Gev	10-50	50-100	100-200	200-500	500-1000
r < 16 m	I_+	161	97	77	57	9
	I_-	164	91	82	56	9
r=16-32m	I_+	174	75	51	18	4
	I_-	159	68	43	15	0
r ⩾ 32 m	I_+	224	69	16	6	0
	I_-	206	61	15	6	1

Experimental results presented above were compared to results of Monte-Carlo calculations based on the quark-gluon string theory of hadron-nucleon interactions[5]. This theory explains accelerator data including recent SPS collider data. In[6] this theory was applied to hadron-nucleus interactions. Calculations of EAS were carried out for muon production throughpion and kaon decays for primary protons and various primary nuclei in assumption of "superposition" model of nucleus-nucleus interactions. The composition of primaries was suggested as follows

A	1	4	14	21	56
%	40	15	15	15	15

Results of the calculations are presented in Fig.1a curves 1. One can see that for the highest measured muon threshold energies E_μ=200 and 500 Gev the theory does not agree with the experiment. To make agreement better there were carried out calculations taking into account muon production through decays of charm particles. Cross-section of charm production was taken as in[7]. Curves 2 present the results of this calculations. Soft jet production[8] was also checked as a reason for additional spread of muons. (curves 3 in Fig.1a). Both processes do not change LD of muons of threshold energies E_μ=200-500 Gev in the range of distances r close to median radius as is experimentally measured. Muon LD proved to be more sensitive to the model of nucleus-nucleus interaction. The "fragmentation" model in which nucleons not included in heavy fragments interact with target nucleus gives better agreement with the experimental data. In Fig1a curves 4 present results of the calculations taking into account this "fragmentation" model. Primary composition is as before.

Refrences.

1. Khrenov B.A., et al ,ICRC-16, Kyoto, 8,351, 1979.
2. Grishina N.V.,et al ,ICRC-17, Paris, 6, 3 , 1981.
3. Atrashkevich V.B., et al,ICRC-18,Bangalore,11,229,1983.
4. Rao M.V.S., ICRC-18, Rapp. paper, 1983.
5. KaidalovA.B.& Ter-Martirosjan K.A., Jadernaja Phys., 39,1514, 1983 and 40,211,1984 .
6. Kalmykov N.N.& Khristiansen G.B., ICRC-18,Bangalore, 11, 330, 1983.
7. Slavnov D.A., Jadernaja Phys., 41, 213, 1985.
8. Gribov L.V.,Levin E.M.,Ryskin M.V., Phys.Lett.,121B;65, 1983.

N85-36011

HE 4.4-1

ENERGY CALIBRATION OF THE FLY'S EYE DETECTOR

Baltrusaitis, R.M., Cassiday, G.L., Cooper, R., Elbert, J.W., Gerhardy, P.R., Ko, S., Loh, E.C., Mizumoto, Y., Sokolsky, P. & Steck, D.

Department of Physics, University of Utah, Salt Lake City, UT 84112

ABSTRACT

The methods used to calibrate the Fly's Eye detector in order to evaluate the energy of EAS is discussed below.

1. Introduction. The energy of extensive air showers (EAS) as seen by the Fly's Eye detector are obtained from track length integrals of observed shower development curves(1). eg

$$E_{em} = \frac{\epsilon_o}{X_o}\int N_e(x)dx$$

where E_{em} is the total energy of the shower dissipated in the electromagnetic channel, ϵ_o/X_o is the ratio of the critical energy of electrons to their radiation length in air(2) and $N_e(x)$ is the observed size of the EAS as a function of atmospheric slant depth x. The energy of the parent cosmic ray primary is estimated by applying corrections to account for undetected energy in the muon, neutrino and hadronic channels (3,4). These corrections amount typically to about 10% in the energy range 0.1-100 EeV (1 EeV = 10^{18} eV). Clearly, absolute values for E depend most critically upon the measurement of shower sizes $N_e(x)$. Knowledge of three essentially different processes are involved in leading to a measurement of $N_e(x)$. (i) An assessment of those factors responsible for light production by the relativistic electrons in an EAS and the transmission of light thru the atmosphere (ii) Calibration of the optical detection system, i.e., measuring and continually monitoring those factors required to convert measured electronic pulse integrals into absolute numbers of photons received by the Fly's Eye detector from the EAS light source and (iii) A knowledge of the trajectory of the shower which is necessary to convert apparent optical "brightness" into intrinsic optical brightness.

2. Light Production. The factors involving light production by EAS and transmission of light thru the atmosphere have been discussed in great detail in Ref.(1). These factors include:

(i) The Fluorescence Efficiency of Electrons in Air. Our values are taken from the work of Bunner(5).

We find that $\frac{d^2N_\gamma}{dl\,d\Omega} = \frac{N_f N_e}{4\pi}$ where N_f is the fluorescent yield in photons/electron/meter and N_e is the shower size. Roughly, $N_f \approx$ 4-4.5 photons/electron/meter depending on altitude and temperature(1).

(ii) The Production of Cerenkov Light. This factor has been calculated most recently by Elbert(6) who finds that

N85-36011

$$\frac{d^2N}{dl\,d\Omega}_{\gamma} = \frac{dN}{dl}_{\gamma}\,\frac{\exp^{-\theta/\theta_o}}{2\pi\sin\theta} \quad \text{and} \quad \theta_o = 0.83\,E_t^{-0.67}$$

where dN/dl is the Cerenkov photon yield per meter of air, θ is the emission angle and E_t is the Cerenkov threshold energy in air in MeV. We have measured the angular distribution of Cerenkov light with the Fly's Eye by observing light from the same EAS source simultaneously at different emission angles by Fly's Eye I and Fly's Eye II (separated by 3.3 km). We find that at altitudes corresponding to threshold energies of about 30 MeV our measured value of $\theta_o = 5.0 \pm 0.5°$ is in excellent agreement with the value $\theta_o = 4.87°$ obtained from Elbert's above expression.

(iii) The Scattering of Light. Both Rayleigh and Mie Scattering affect the transmission of light thru air. Our estimates for these effects are based respectively on the work of Flowers(7) and Elterman(8), they are discussd in detail in Ref.(1).

Finally, we show in Figure 1 an example of calculated relative photoelectron yields obtained by the Fly's Eye detector as generated by the various light production methods discussed above for a shower of size $N_e(x)$ whose total energy was 1 EeV observed at an impact parameter of 4 km.

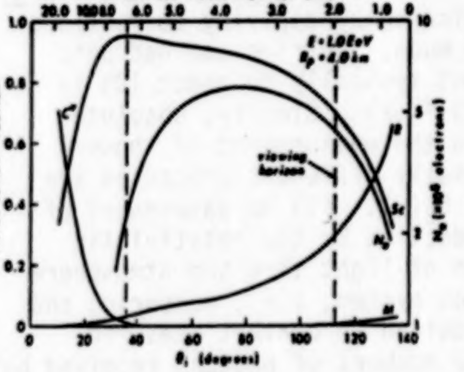

Figure 1. Relative photoelectron yields as a function of altitude (upper scale) and observed shower emission angle (lower scale). Sc=scintillation light, C=direct Cerenkov, R=Rayleigh and M=Mie Scattered Cerenkov light. N_e is the shower size.

3. Optical Calibration.

Converting measured pulse integrals into numbers of photons incident upon the Fly's Eye detector requires a knowledge of the overall efficiency-gain product εG_i of each of the approximately 1000 Fly's Eye data channels. An absolute measurement has been made on a single channel and the εG factors for all others determined by relative normalization. In situ Argon flash bulbs triggered on command by computer are used to continually monitor all εG factors during data taking at all times subsequent to the time of absolute calibration. Measured efficiency-gain factors are: $\varepsilon_{pmt} = 0.212 \pm .015$, $\varepsilon_{cone} = 0.80 \pm .05$ and $\varepsilon_{mirror} = 0.83 \pm .04$ giving an overall efficiency of $\varepsilon = 0.141 \pm .016$. The gain factor G includes PMT gains, preamp transconductance, finite cable DC resistence, charge-integrator input impedance and voltage-time input to digitized output conversion factors. The resultant overall gain is $G = 0.757 \pm .076$ mv/photoelectron. Hence, errors in absolute quanta measurements, δN_γ, are on the order of ± 16%.

4. Geometrical Reconstruction. The techniques of geometrically reconstructing an event seen either by Fly's Eye I alone or stereoscopically by Fly's Eyes I and II in coincidence have been discussed in Ref.(1). Essentially, the chief contribution of inaccurate geometrical reconstruction to uncertainty in energy measurement stems from inaccuracies in determining the shower impact parameter R_p, or distance of closest approach to the Fly's Eye I detector. These uncertainties are typically on the order of 5-10%. Hence, overall uncertainties in energy measurements from all factors listed above are expected to be on the order of ± 20%.

5. Tests. Several tests have been made to check the validity of all calculations and measurements of the energy determining factors described above.

(i) A Monte-Carlo simulation of the response of the Fly's Eye detector has been carried out in order to check the validity and self-consistency of the analysis procedure(1). Shown in Figure 2 is the Monte-Carlo response function for shower energies measured by the simulated detector. The effects of night sky noise fluctuations in measured pulse integrals have also been included. As can be seen from the plots, overall energy determinations appear to be accurate to within ± 20%.

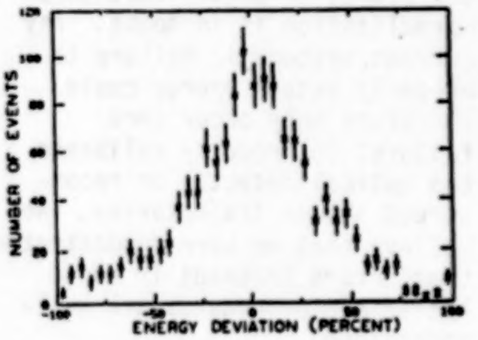

Figure 2. % Differences Between Measured Shower Energy and Known Monte-Carlo Imput Energy.

(ii) A pulsed nitrogen laser was positioned at Fly's Eye I at a variety of different zenith, azimuth angles and impact parameters. The scattered light from the upward-going laser light pulse simulates light emission from an EAS. Absolute light yields measured by the Fly's Eye for each laser pulse can then be used to calculate the number of photons in the upward-going beam after reconstructing its trajectory and calculating the amount of light both Rayleigh and Mie scattered from the beam as outlined above. Resultant estimates of the laser's photon output based on Fly's Eye measurements agree with direct measurements of its output to within ±20% and is virtually independent of scattering angles over a range of $20° < \theta < 120°$. The agreement implies that Fly's Eye optical calibration is well known and the treatment of Rayleigh and Mie scattering and light attenuation of a light beam propagating thru the atmosphere has been treated adequately.

(iii) About 500 showers have been observed steroscopically i.e., by Fly's Eye I and Fly's Eye II (separated by 3.3 km) in coincidence. Shown in Figure 3 is an example of a shower reconstructed steroscopically and whose longitudinal development sizes, $N_e(x)$, have been measured by data obtained by each detector. It is impossible to tell which data points belong to Fly's Eye I or Fly's Eye II. Again, since the light source was observed simultaneously from different emission angles as well as optical path lengths, the implication is that the angular distribution of both direct and scattered Cerenkov light, its relative strength to fluorescence light, and the effects of the atmosphere on light propagation is being treated properly.

(iv) During Fly's Eye prototype experiments, a direct intercalibration experiment of shower size measured by the Volcano Ranch experiment and the Fly's Eye optical detector was carried out at Volcano ranch(9). The obtained sizes in that experiment agreed to ± 10%. This intercalibration established the validity of the absolute values we currently use for the nitrogen fluorescence yield used to derive absolute shower sizes. It cannot, therefore, be argued that this normalization is in doubt. Any current systematic failure to properly assess energy could therefore only occur thru failures to properly calibrate the optical detector or reconstruct shower trajectories. We believe that we have demonstrated that errors inherent in these latter two procedures are well-understood.

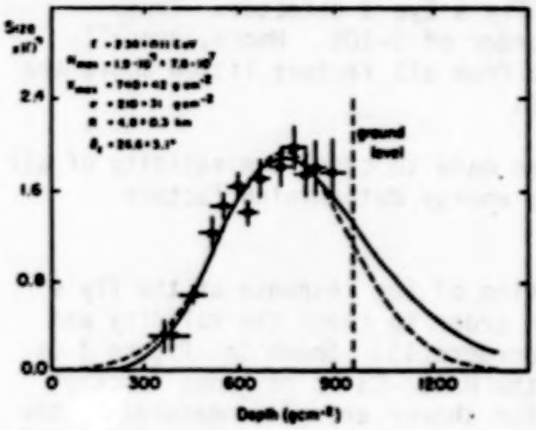

Figure 1. Longitudinal profile of an EAS observed by both Fly's Eye I and II simultaneously. Size estimates are composed of mixed data points, i.e., some from FEI, some from FEII.

6. Acknowledgements. We gratefully acknowledge the United States National Science Foundation for its generous support of this work under grant PHY8201089.

References.

1. Nuclear Instruments and Methods (submitted 1985).
2. Dozkenko, O.I. and Pomanskii, A.A., Soviet Physics JETP 18, 187 (1964)
3. Linsley, J., Spectra, Anisotropies and Composition of Cosmic Rays Above 1000 GeV, Proc. 18th Int. Conf. Cosmic Rays, Bangalore, India 12, 135 (1983).
4. Baltrusaitis, R.M., et al., paper HE 4.4-2 (this conference).
5. Bunner, A.N.,The Atmosphere As a Cosmic Ray Scintillator, PhD Thesis, Cornell Univ., Ithaca, N.Y. (1964).
6. Elbert, J.W., et al., Proc. 18th Int. Conf. Cosmic Rays, Bangalore, India 6, 227 (1983).
7. Flowers, E.C., et al, J. Appl. Meterology 8, 955 (1969).
8. Elterman, L. and Toolin, R.B., Handbook of Geophysics and Space Environments, Chapt. 7, Air Force Cambridge Research Labs, Office of Aerospace Research, USAF (1965).
9. Bergeson, H.E., et al., Phys. Rev. Lett. 39, 847 (1977).

THE STRUCTURE OF EAS AT E>0.1 EeV

Baltrusaitis, R.M., Cassiday, G.L., Cooper, R., Elbert, J.W.,
Gerhardy, P.R., Loh, E.C., Mizumoto, Y., Sokolsky, P., & Steck, D.

Physics Department, University of Utah, Salt Lake City, UT 84112

ABSTRACT

We have obtained the ratio of EAS total shower energy in the electomagnetic channel (E_{em})to the size of the shower at maximum development (N_{max}) from a direct measurement of shower longitudinal development using the air fluorescence technique(1). The values obtained agree closely with those estimated by Linsley(2). However, they are not inconsistent with values based upon track length integrals of the Gaisser-Hillas formula for shower development(3) or the known relation between shower energy and size at maximum for pure electromagnetic cascades. Using Linsley's estimates for undetectd shower energy(2) based on an analysis of a wide variey of cosmic ray data we obtain the following relation for total shower energy E vs N_{max}: $E=1.31\pm.14(N_{max}/10^9)^{0.990\pm.005}$GeV. Using the Gaisser-Hillas implied undetected shower energy fractions, we obtain $E=1.53\pm.16(N_{max}/10^9)^{0.99\pm.005}$GeV.

1. Introduction. The estimation of total EAS energy from shower size measurements at ground level depends, among other things, upon a knowledge of the conversion factor E/N_{max}(2,4). This factor has been derived by Linsley indirectly from a large body of existing cosmic ray data(2). In addition, it has been calculated from models of shower development incorporating scaling(3) and radial scaling(5). Values quoted range typically beween 1.3 and 1.7 GeV/particle for EAS energies in the range .01-100 EeV(1 EeV=10^{18} eV) the precise value being dependent primarily upon estimates of undetected shower energy in the non-electromagnetic channel. We present below the results of the E_{em} vs N_{max} relationship obtained from a direct integration of EAS longitudinal development profiles as measured by the Fly's Eye detector. We then infer values for the total shower energy relationship to N_{max} based upon Linsley's estimates of undetected shower energy from cosmic ray data(2) as well as estimates inferred from the Gaisser-Hillas parameterization of shower longitudinal development(3).

2. Measurement. The Fly's Eye detector has been described in detail elsewhere(1). Essentially, the detector observes the passage of EAS thru the atmosphere via nitrogen fluorescence. Shower sizes vs depth are calculated from measured light yields and experimentally determined shower trajectories(1). Electromagnetic shower energy, E_{em}, and shower size at maximum N_{max} is determined by fits made to resultant longitudinal development curves. Shower energy is given by:

$$E_{em} = \frac{\epsilon_0}{X_0} \int N_e(x)dx$$

where Ne(x) is the shower size vs depth and ϵ_o/X_o is the ratio of the critical energy of an electron to its radiation length in air, taken to be 2.18 MeV/electron g cm^{-2} (6). We note that, if a shower development curve is represented by an equivalent Gaussian then

$$\frac{E_{em}}{N_{max}} = \sqrt{2\pi}\,\frac{\epsilon_o}{X_o}\,\sigma$$

where σ is the equivalent Gaussian width of the curve.

We have selected a sample of approximately 1150 showers observed during a 3 year interval whose equivalent Gaussian widths were measured to an accurcy of better than ± 20% and whose total observed track lengths subtended an angle in the sky of greater than 60°. This selection criterion ensured a sample of showers whose longitudinal profiles were well-known and whose subsquent ratios of E_{em}/N_{max} were determined to within ± 20%.

3. Results. Shown in Table 1 are the results of the measured E_{em}/N_{max} ratios as a function of total shower energy E_{tot}.

Table I. E/N_{max} vs E_{tot}

Method	E_{tot}(EeV) .01	0.1	1.0	10.0
	E_{em}/N_{max} (GeV/electron)			
E&M Cascade(8)	1.12	1.18	1.25	1.31
Gaisser-Hillas(3)	1.13	1.20	1.28	1.34
Linsley(2)	1.06	1.12	1.17	1.22
Measured	1.11±.09	1.17±.10	1.19±.10	1.20±.10
	Missing Energy (% of E_{tot})			
Linsley(2)	19	13	9	6
Gaisser-Hillas(3)	31	27	22	18
	E_{tot}/N_{max} (GeV/electron)			
Measured(L)	1.37	1.34	1.31	1.28
Measured(GH)	1.16	1.60	1.53	1.46

In addition, we also show values of E_{em}/N_{max} derived in the following ways: (a) Pure electromagnetic cascades initiated by an electron (or photon) of energy E_{tot}, i.e.

$$N_{max} = \frac{0.31\ Em/\epsilon_o}{\sqrt{\ln(Em/\epsilon_o)-0.37}} \qquad (7)$$

(b) By integrating the Gaisser-Hillas shower development curve(3) we obtain:

$$\frac{Em}{N_{max}} = \frac{\epsilon_o}{X_o}\ \lambda\alpha^{-\alpha}\exp^{\alpha}\Gamma(\alpha+1)$$

where $\lambda = 70$ g cm^{-2} and $\alpha = 0.51\ln(E/\epsilon_o)-1$ (c) Linsley's estimated values quoted in ref.(2).

We note that the Gaisser-Hillas method yields E_{em}/N_{max} values remarkably close to those obtained from purely electromagnetic cascades. We also note that our measured values of E_{em}/N_{max} are in excellent agreement with the above estimates.

Finally, in order to convert E_{em}/N_{max} to E_{tot}/N_{max}, corrections for undetected shower energy (energy in the form of muons and neutrinos, undetected hadrons and nuclear excitation) must be applied. We have made such corrections in two ways primarily for the purposes of illustrating the uncertainties currently involved in accounting for total unobserved energy and thus obtaining the correct factors necessary to convert shower size measurements (or measurements of any other parameter basically dependent on the number of electrons in EAS) into total primary energy. The first estimate of missing energy is obtained directly from Linsley(2) who derives estimates of missing shower energy in a quite clever empirical fashion directly from measured electron and muon size spectra and the total assessed energy content of these respective components of the EAS. We have parameterized Linsley's estimates in the following way:

$$E_{em}/E_{tot} \equiv 0.99-.0782E_{tot}^{-0.175} \qquad E_{tot} \text{ in EeV}$$

This parameterization is valid for 1 PeV<E<100 EeV and the resultant undetected energy percentages listed in Table 1.

Finally, we note that the amount of undetected energy based on the Gaisser-Hillas formula for shower development can be obtained directly from the values listed in Table 1 for E_{em}/N_{max} and noting that the Gaisser-Hillas formula is based on a constant value for E_{tot}/N_{max} of 1.64 GeV/electron. Thus the apparent undetected energy percentages inferred from the Gaisser-Hillas parameterization are as shown in Table 1. Finally, we also list in Table 1 the resultant E_{tot}/N_{max} ratios based on applying each of the above missing energy percentages corrections to the resultant measured values of E_{em}/N_{max} obtained directly from Fly's Eye data.

We note that the Gaisser-Hillas parameterization with its large amount of implied missing energy is based on fits to simulated showers which incorporate a simple scaling model with constant cross section for EAS development. Such models tend to generate penetrating showers in which the amount of undetected energy would be anticipated to be less than for those models

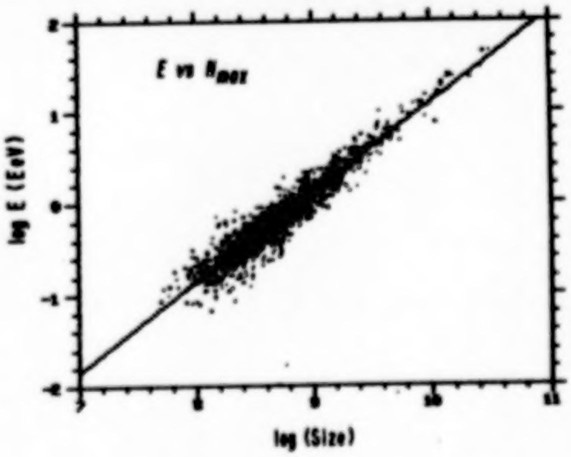

Figure 1. Scatter Plot of Total Shower Energy vs Shower Size at Maximum as Measured by the Fly's Eye Detector.

which led to more rapid shower development.

Finally, we show in Figure 1 a scatter plot of E_{tot}, assuming the Linsley estimates of missing shower energy, vs N_{max}. The best fit line is given by:

$$E_{tot}=1.31\pm.14\ (N_{max}/10^9)^{0.990\pm.005}\ \text{GeV}$$

the scatter in the data points is due both to detector resolution as well as intrinsic fluctuations. Future work will concentrate upon an extraction of the detector resolution function in order to determine how much intrinsic scatter there is in N_{max} and thus its effect on total energy measurements which depend essentially on a measure of that parameter.

4. Acknowledgements. We gratefully acknowledge the United States National Science Foundation for its generous support of this work under grant PHY8201089.

References.

1. Nuclear Instruments and Methods (submitted 1985).
2. Linsley, J., Spectra, Anisotropies and Composition of Cosmic Rays Above 1000 GeV, Proc. 18th Int. Conf. Cosmic Rays, Bngalore, India 12, 135 (1983).
3. Gaisser, T.K., and Hillas, A.M., Proc. 15th Int. Conf. Cosmic Rays, Plovdiv, Bulgaria 8, 353 (1977).
4. Bower, A.J. et al. J. Phys. G: Nucl. Phys. 9, L53 (1983).
5. Hillas, A.M., Proc. of the Cosmic Ray Workshop, Univ. of Utah, ed. T.K. Gaisser, Bartol Res. Foundation of the Franklin Inst. Univ. of DE, Newark, DE 16 (1983).
6. Dozhenko, O.I., and Pomanskii, A.A., Soviet Physics JET P 18, 187 (1964).
7. Rossi, B., High Energy Particles, Prentice-Hall Inc., Englewood Cliffs, N.J., Chapt. 5 (1952).

N85-36013

STANDARD VALUE FOR THE RADIATION LENGTH IN AIR

John Linsley
Department of Physics and Astronomy
University of New Mexico, Albuquerque, NM 87131
USA

ABSTRACT

Following the Paris ICRC I did some additional research on the radiation length in air, which was reported in *Proceedings of the Paris Workshop on Cascade Simulations*. However no standard value was recommended because a few calculations remained undone. These have now been finished. They give new values for t_o in atomic oxygen and nitrogen which are entirely free of dependence on the Thomas-Fermi approximate model. With the usual small corrections for atmospheric A and CO_2, these give $t_o|_{air} = 37.15$ g cm^{-2}, in close agreement with a value recommended by Dovzhenko and Pomanskii, but in contrast to $t_o|_{air} = 36.66$ g cm^{-2} obtained by Tsai using the Thomas-Fermi approximation.

1. Introduction. This concludes an inquiry concerning the radiation length in air, motivated by the importance of that unit in applying cascade theory to the interpretation of cosmic ray air shower data. The preceding installments provide background and more complete references (Linsley 1981a, 1981b).

2. Definitions. The radiation length t_o is customarily defined as follows:

$$(t_o)^{-1} = (N\sigma_o/A)[Z^2(L_{rad} - f) + ZL_{rad'}] \quad , \qquad (1)$$

where N is Avagadro's number, $\sigma_o = 4\alpha r_o^{\;2}$ (α the fine-structure constant, r_o the classical radius of the electron), A is the atomic weight and Z is the atomic number of the target atom, f corrects for use of the Born approximation, L_{rad} is the usual radiation logarithm given by

$$L_{rad} = \int_0^1 (1-F)^2 \frac{dq}{q} + 1 \quad , \qquad (2)$$

where q is the momentum transfer in units of $m_e c$ and F(q,Z) is the atomic form factor, and $L_{rad'}$, a quantity analogous to L_{rad}, takes into account collisions in which the scattering system is left in an excited state.

$$L_{rad'} = \int_0^1 S \frac{dq}{q} + 1 \quad , \qquad (3)$$

where S(q,Z) is the so-called incoherent scattering function. There is general acceptance of the Bethe-Maximon formula for f:

$$f(z) = z \sum_1^\infty n(n^2+z) \sim 1.202z - 1.0369z^2 + 1.008z^3/(1+z) \quad , \qquad (4)$$

where $z = (Z/137)^2$. For N and O, $f = 0.0031$ and 0.0041, respectively.

3. Evaluation of Structure Dependent Terms. The effect of atomic structure on t_o is expressed mainly through L_{rad}. It was shown by Bethe (1934) that the Z-dependence of L_{rad} is given essentially by

$$L_{rad} = \ln(aZ^{-1/3}) \quad , \tag{5}$$

where a is called the elastic screening coefficient. Using the Thomas-Fermi model he obtained the widely quoted value 183 for a_{TF}.* Recognizing the hazard in relying on a statistical model for an atom as light as N, Wheeler and Lamb (1939) recalculated L_{rad} for that element (and for hydrogen) using self-consistent wave functions of the Hartree-Fock type, obtaining a result equivalent to $L_{rad}|_{SCF} = 4.56$.

The need for taking into account inelastic scattering was noted first by Landau and Rumer (1938). Their estimate $L_{rad'} \sim L_{rad}$ underestimates $L_{rad'}$ by about 20% in case of elements as light as N and O, leading to errors in t_o of about 3%. A correct quantum mechanical formula equivalent to Eq. 3 was given by Wheeler and Lamb (1939). They used it to calculate $L_{rad'}$ for N (and for hydrogen) using both the Thomas-Fermi model and self-consistent wave functions. Their result in the latter case was equivalent to $L_{rad'}|_{SCF} = 5.47$.

More recently, values of F and S based on accurate self-consistent wave functions have been tabulated for all the elements over a complete range of q-values (Hubbell *et al.* 1975). Using these data and Eq's (2) and (3) I have calculated $L_{rad}|_{SCF}$ and $L_{rad'}|_{SCF}$ for O as well as N, obtaining 4.490, 5.253 for O, and 4.554, 5.347 for N (in good agreement with the results of Wheeler and Lamb), respectively.

4. The Radiation Length in Air. The radiation length in a complex substance is given by the following expression (Rossi 1952):

$$(t_o)^{-1} = \sum_i p_i/(t_o)_i \quad , \tag{6}$$

where p_i is the fraction by weight of the i-th atomic species. The data adopted here for calculating $t_o|_{air}$ are given in Table 1. The present result is $t_o|_{air} = 37.15$ g cm^{-2}.

---

* The alternative value 191, frequently quoted although it is erroneous, apparently entered the literature through being recommended by Oppenheimer to Serber (1938, 1981). (In Serber's 1938 paper it is attributed to Bartlett, who visited Oppenheimer's group at Caltech about the time the paper was being written.) The value of a has been recalculated recently, but it is questionable whether the new result, $a_{TF} = 184.15$ (Tsai 1974), is any more accurate than Bethe's, since the new calculation used an approximate parametrization of the Thomas-Fermi potential.

Table 1. Calculation of Radiation Length in Air

i	p_i	Z_i	A_i	f_i	$(L_{rad})_i$	$(L_{rad'})_i$	note
1	0.05	6	12.0111	0.0019	4.618	5.403	(a)
2	75.52	7	14.0067	0.0031	4.554	5.347	(b)
3	23.14	8	15.9994	0.0041	4.490	5.253	(b)
4	1.29	18	39.9480	0.0204	4.252	5.081	(a)

note (a): $L_{rad} = L_{rad}|_{TF} = \ln(183Z^{-1/3})$, $L_{rad'} = L_{rad'}|_{TF} = \ln(1194Z^{-2/3})$ (Tsai 1974)

note (b): $L_{rad} = L_{rad}|_{SCF}$, $L_{rad'} = L_{rad'}|_{SCF}$

5. Comparison with Previous Results. Values of t_o for C, N, O and A, as well as air, are compared in Table 2 with values recommended in widely quoted reviews: 1) by Dovzhenko and Pomanskii (1964), and 2) by Tsai (1974). (Tsai's article is the authority for values given in the *Particle Properties Data Booklet*.) The results by Tsai are based entirely on the Thomas-Fermi model. Dovzhenko and Pomanskii used their own SCF calculations of L_{rad}. For $L_{rad'}$ they used interpolated values based on Wheeler and Lamb's results for N.

Table 2. Radiation Length in C, N, O, A and air (units g cm^{-2})

material	Dovzhenko & Pomanskii	Tsai	present work
C	43.3	42.70	43.33
N	38.6	37.99	38.53
O	34.6	34.24	34.83
A	19.7	19.55	19.57
air	37.1	36.66	37.15

6. Remaining Questions. Out of 7 questions listed previously (Linsley 1981b) there are 2 which have not been given definitive answers:

1) How great is the molecular binding effect in N_2 and O_2?

2) What is the relation between t_o defined by Eq. 1 and the electromagnetic cascade unit X_o defined by $X_o = X_{max}/\ln(E/E_c)$, where E_c is the critical energy and X_{max} is the average depth of maximum development of simple cascades with energy E?

Regarding (1): Using the conventional definition of L_{rad} (Eq. 2), the value I reported previously for molecular nitrogen (Linsley 1981a) becomes 4.50, 1.2% *less than* the best SCF value for atomic nitrogen. On the other hand, Bernstein and Panofsky (1956) showed that in the complete screening limit the effect of molecular binding in hydrogen is to *increase* σ_{pair} by 2.8%.

Regarding (2): The point of the distinction is that the quantity appearing in the elongation-energy relation should logically be X_o rather than t_o. Clearly, X_o/t_o is independent of the stopping medium to a high degree of accuracy. Landau and Rumer (1938), for approximation A, and Snyder (1949), for approximation B of electromagnetic cascade theory, give $X_o/t_o = 1.01$. From tables given by Messel and Crawford (1970) I find $X_o/t_o = 1.04 \pm .02$. Can additional results of this kind be derived from existing work?

7. References.

Bernstein, D. and Panofsky, W. K. H. 1956, Phys. Rev. 102, 522.

Bethe, H. A. 1934, Proc. Cambr. Phil. Soc. 30, 524.

Dovzhenko, O. I. and Pomanskii, A. A. 1964, Sov. Phys. JETP 18, 187.

Hubbell, J. H., Veigele, W. J., Briggs, E. A., Brown, R. T., Cromer, D. T., and Howerton, R. J. 1975, J. Phys. Chem. Reference Data 4, 471.

Landau, L. and Rumer, G. 1938, Proc. Roy. Soc. (London) A166, 213.

Linsley, J. 1981a, Proc. 17th ICRC (Paris) 11, 246.

———— 1981b, Proc. Paris Workshop on Cascade Simulations, eds. J. Linsley and A. M. Hillas (Texas Center for the Advancement of Science and Technology, Albuquerque) p. 23.

Messel, M. and Crawford, D. F. 1970, *Electron-Photon Shower Distribution Function Tables* (Oxford, Pergamon Press).

Rossi, B. 1952 in *High Energy Particles* (Englewood Cliffs, NJ, Prentice-Hall).

Serber, R. 1938, Phys. Rev. 54, 317.

———— 1981, private communication.

Tsai, Y-S. 1974, Rev. Mod. Phys. 46, 815.

Wheeler, J. A. and Lamb, W. E. 1939, Phys. Rev. 55, 858, erratum 101, 1836 (1956).

LONGITUDINAL TRIAL FUNCTIONS AND THE COSMIC RAY ENERGY SCALE

N85-36014

John Linsley
Department of Physics and Astronomy
University of New Mexico, Albuquerque, NM 87131
USA

ABSTRACT

Formulae which have been proposed for representing the longitudinal profiles of cosmic ray air showers are compared, and the physical interpretation of the parameters they contain is examined. Applications to the problem of energy calibration are pointed out. Adoption of a certain especially simple formula is recommended, and its use is illustrated by means of examples.

1. Introduction. At all primary energies above $\sim 10^3$ GeV, incoming cosmic ray nuclei deposit more than half of their energy via the soft component. At the highest observed energies the fraction E_{EM}/E approaches 90-95%, where E_{EM} is the energy deposited by the composite electron-photon cascade resulting primarily from π_o decay γ-rays. The single most important step, therefore, in determining the cosmic ray energy scale for $E > 10^6$ GeV, where experiments above the earth's atmosphere currently give way to experiments using air showers, is measurement of E_{EM}.

The use of simple mathematical formulae to represent the *lateral* structure of extensive air showers began at an early stage in the study of shower phenomena (cf. Bethe quoted by Williams 1948), and such formulae continue to be useful tools. Analogous formulae for the *longitudinal* structure developed much later, possibly because accurate experimental data have taken much longer to obtain, and possibly because analytical methods have tended to be supplanted in recent years by Monte Carlo calculations.

With the advent of techniques for directly measuring the longitudinal profiles of individual air showers (Hammond *et al.* 1978, Grigoriev *et al.* 1979, Cassiday 1981, Cady *et al.* 1983) it seems an appropriate time to re-examine formulae that have been used to describe these profiles (Greisen 1956, Linsley 1967, Longo and Sestili 1975, Gaisser 1976 and 1979, Gaisser and Hillas 1977, Sass and Spiro 1978, Dyakonov *et al.* 1981). By analogy to formulae used for describing the lateral structure of various air shower components I will call them 'trial functions'. In case of lateral structure such functions have had an important role in comparing results of different experiments. One expects longitudinal trial functions to be useful in the same way. In case of the lateral structure of electrons, trial functions are also used in the conduct of experiments, to derive from raw data on shower density a global measure, the shower size N, as well as core location, age, and measures such as S_{600}. The corresponding step in dealing with profile data is to find N_m, long recognized as being one of the most reliable estimators of primary energy (Clark 1962), from data on N vs x. This step also yields x_m, the shower elongation, and may also yield the profile width σ_x. In case of the electronic lateral structure, trial functions are formulated in such a manner as to reflect the physical processes that govern cascade development. Thus core distances are expressed in Moliére units, and steepness is controlled by a parameter relating plausibly to shower age. One aspires to achieve similar success in case of the longitudinal structure.

2. Electromagnetic cascades. The longitudinal trial function proposed by Greisen (1956) provides a good illustration:

$$N = (0.31/\beta_o^{\frac{1}{2}})\exp[t(1 - \tfrac{3}{2}\ln s)], \text{ where } s = 3t/(t + 2\beta_o) \ . \qquad (1)$$

Clearly its structure was influenced in several ways by theoretical results obtained with diffusion equations (see Rossi 1952):

1) Thickness is measured in units of the radiation length ($t = x/x_o$).

2) Primary energy is measured in units of the critical energy E_c ($\beta_o = \ln(E/E_c)$).

3) There is a built-in elongation-energy relation, $x_m = x_o\beta_o$, which is approximately correct.

4) There is a built-in N_m relation, $N_m = (0.31E/E_c)/[\ln(E/E_c)]^{\frac{1}{2}}$, which is also approximately correct.

5) The shower age s is incorporated in an approximately correct manner.

The price paid for (5) is mathematical inconvenience. Expressions for N, Nt and Nt^2 cannot be integrated in closed form, so simple formulae for the track length integral, the average depth <x> and the profile width σ_x, provided by the exact theory, must be patched on *ad hoc*.

An alternative form is the gamma distribution, recommended in the current *Particle Properties Data Booklet* for representing results from EGS, a well known Monte Carlo program for simulating electronic cascades. Gamma distributions have been chosen independently by several workers to represent air shower profiles as well. Indeed, the choice has been unanimous, and this is the choice recommended here.

3. Mathematical properties of gamma distributions. I will write this distribution in the form

$$N = N_o\xi^q e^{-q\xi} \ , \qquad (2)$$

calling the numerical constant q the 'index'. The optimum values of ξ and N are given by

$$\xi_m = 1 \ , \qquad (3) \qquad\qquad N_m = N_o e^{-q} \ , \qquad (4)$$

while the mean value and variance are given by

$$\langle\xi\rangle = \frac{q+1}{q} \ . \qquad (5) \qquad\qquad \sigma_\xi^2 = \frac{q+1}{q^2} \ . \qquad (6)$$

The normalization is given by

$$\int N d\xi = \Gamma(q+1)/q^{q+1} \ , \qquad (7)$$

which admits approximation using Stirling's theorem

$$\int N d\xi \cong N_o(2\pi/q)^{\frac{1}{2}}e^{-q} = N_m(2\pi/q)^{\frac{1}{2}} \ . \qquad (8)$$

I propose to determine the parameters of (2) by using

1) the elongation-energy relation, x_m vs lnE (note from (3) that $\xi = x/x_m$),

2) a relation due to Kraushaar (1957) between the typical profile of an *individual* proton shower and the *average* profile of proton showers,

3) experimental data on σ_x, and on E_{EM}/E, the fraction of primary energy given to electrons.

First, however, I will show that (2) provides an excellent fit to electromagnetic cascade profiles.

4. Electromagnetic cascades revisited. Results of cascade theory in approximation B are (Rossi [illegible]):

$$x_m = x_o(1.01\beta + A), \quad \langle x\rangle = x_o(1.01\beta + B), \quad \sigma_x^2 = x_o^2(1.61\beta + C) \ , \qquad (9)$$

where $\beta = \ln(E/E_c)$ and A,B,C are constants ∿ 1 whose exact values depend on whether the primary particle is an electron or photon. Using (3) and substituting in (6) I solve for the index

$$q = 0.63 + D \ , \qquad (10)$$

where D = -0.4, 0.2 for primary electrons and photons, respectively. Substituting this result in (5), I find

$$\langle x\rangle - x_m = 1.6x_o \ , \qquad (11)$$

expressing the fact that the profile is unsymmetrical. To conserve energy the track length integral must equal E. Thus

$$\int(E_c/x_o)N dx = E \ . \qquad (12)$$

Using (8), which I solve for N_m, and again substituting for q and x_m,

$$N_m = (0.31E/E_c)/[\ln(E/E_c) - F]^{\frac{1}{2}} \ , \qquad (13)$$

where F = 1.7, 1.0 for primary electrons and photons, respectively. Results (11) and (13) are almost exactly the same as given by the detailed theory.

5. Application to air showers. One begins as in the preceding example, by letting $\xi = x/x_m$, where x_m is given by the elongation-energy relation. A reasonable choice for this is

$$x_m = A + D_{10}\log E \qquad (14)$$

with A = 159 g/cm^2 and D_{10} (elongation rate per decade) = 65 g/cm^2 (Linsley and Watson 1981; E is in GeV). The index q can be found as in the preceding example, using (6), but first I will show an alternative method illustrating a deep connection between gamma distributions and cascade processes.

It was pointed out by Kraushaar (1957) that the average number of electrons N at atmospheric depth x arising from a primary particle incident upon the top of the atmosphere is related as follows to the average number N_1 of electrons at thickness x' below a nuclear interaction of such a particle:

$$N(x) = \int_0^x N_1(x')\exp[-(x-x')/\lambda]dx'/\lambda \ , \qquad (15)$$

$$N_1(x) = [1 + \lambda(\partial/\partial x)]N(x) \ , \qquad (16)$$

where λ is the interaction mean free path of the particle, assuming that there are no fluctuations other than those in the starting level. Applying these, it is readily shown that *the condition for N and N_1 to be self similar*; meaning in this case for one to be a gamma distribution if the other one is, is the following:

$$q = x_m/\lambda \ . \qquad (17)$$

Substituting (17) in (6) one obtains a very interesting result,

$$\sigma_x^2 = \lambda^2 + \lambda x_m \ , \qquad (18)$$

which can be combined with (14), giving

$$\sigma_x^2 = (\lambda^2 + A\lambda) + \lambda D_{10}\log E \ . \qquad (19)$$

This says that if the energy dependence of λ is neglected, the energy dependence of σ_x^2 has the same form as that of x_m, just as it does in case of electromagnetic cascades. The energy dependence is described by a *rate*, analogous to the elongation rate, which is in fact proportional to the elongation rate. This new rate, which might be called the 'width rate' or 'spreading rate', is equal to λD_{10}.

An experimental result on σ_x has recently been reported by the Fly's Eye group. The value given, 220±33 g/cm^2 at 10^9 GeV (Baltrusaitis *et al.* 1985), agrees very well with a value derived from an average profile published by Grigoriev *et al.* 1983 for a slightly lower energy. Substituting the average of these results, and values of A and D_{10}, in (19), one finds $\lambda = 58$ g/cm^2.

This is appreciably greater than the mean free path for proton-air inelastic collisions found by other methods (see conference paper HE1.1-1). It is reasonable to assume that λ is greater than $\lambda_{pa,inel.}$ for the same reason that holds in similar cases: neglect of development fluctuations. This needs further study. Pending results of such a study, a reasonable estimate of σ_x^2 for energies other than 10^9 GeV is obtained by assuming that λ is constant with the value found above. Then

$$q = 3.36 + 1.12\log E\ , \quad (20) \quad \text{and} \quad \sigma_x^2 = 1.5\cdot10^4 + 3.8\cdot10^3\log E \quad (21)$$

The remaining parameter in (2), N_O, is found in the same manner as for electromagnetic cascades, using (7) or (8), keeping in mind, of course, that the track length integral equals E_{EM}, not E. The relation between E_{EM} and E is discussed in conference paper OG5.1-5 (or see Linsley 1983). A convenient formula representing results of that work is

$$E_{EM}/E = 1 - 2.8E^{-0.17} \text{ (E in GeV)} . \qquad (22)$$

References. BALTRUSAITIS *et al.* 1985, Phys. Rev. Lett. 54, 1875; CADY *et al.* 1983, Proc. 18th ICRC 11, 412; CASSIDAY 1981, *Proton-Antiproton Collider Physics* (Am. Inst. Phys.: New York) p. 528; CLARK 1962, J. Phys. Soc. Japan 17, Suppl. A-III, 286; DYAKONOV *et al.* 1981, Proc. 17th ICRC 6, 106; GAISSER 1976 private communication; 1979, *Proc. Air Shower Workshop Univ. Utah* (Bartol Foundation, Newark NJ) p. 57; GAISSER and HILLAS 1977, Proc. 15th ICRC 8, 353; GREISEN 1956, *Progress in Cosmic Ray Physics* (North-Holland: Amsterdam) Vol. 3; GRIGORIEV *et al.* 1979 ZhETP 30, 747; 1983, Proc. 18th ICRC 6, 204; HAMMOND *et al.* 1978, *Nuovo Cimento* 1C, 315; KRAUSHAAR 1957, *Nuovo Cimento Suppl.* 8, 623; LINSLEY 1967, Rev. Sci. Instrum. 38, 1268; 1983, Proc. 18th ICRC 12, 135 (see also paper OG5.1-4, this conference); LINSLEY and WATSON 1981, Phys. Rev. Lett. 46, 459; LONGO and SESTILI 1975, Nucl. Instrum. Meth. 128, 283; ROSSI 1952, *High Energy Particles* (Prentice-Hall: Englewood Cliffs NJ); SASS and SPIRO 1978, CERN $\bar{p}p$ Tech. Note 78-32; WILLIAMS 1948, Phys. Rev. 74, 1689.

EAS Developement Curve at Energy of 10^{16} - 10^{18}eV Measured by Optical Cerenkov Light

T.Hara, M.Daigo*, M.Honda, K.Kamata, T.Kifune, Y.Mizumoto**, M.Nagano, Y.Ohno and G.Tanahasni

Institute for Cosmic Ray Research, University of Tokyo, Tokyo, 188 Japan
* Wakayama Medical College, Wakayama-shi, Wakayama, 649-63 Japan
** Fujitsu Limited, 1-17-25, Shinkamata, Ohta-ku, Tokyo, 144 Japan

The data of optical Cerenkov light from extensive air shower observed at the core distance more than 1 Km at Akeno are reexamined. Applying the new simulated results, we reconstruct the shower developement curves for the individual events. For the showers of 10^{17} eV the average depth at the shower maximum is determined to be 660 ± 40 gcm^{-2}. The shower curve of average development is found to be well described by a Gaisser-Hillas shower development function with above shower maximum depth.

1. Introduction.

The Cerenkov light from EAS is one of the most important observables to know the EAS developement. In order to know the shower maximum depth for EAS of 10^{16} - 10^{18}eV, the Cerenkov pulse shapes from EAS's at more than 1Km from the core are observed at Akeno air shower array by using 3 large telescopes(1). The data were analyzed by using the relation between the characteristics of Cerenkov pulse and the average development of showers in previous paper(2). In this paper we reanalyze the data for the construction of shower development curve by taking into account the first interaction depth, which is found to be important in interpretation of Cerenkov pulse shape.

2. Simulation results.

The calculation of pulse shape of Cerenkov light from EAS was carried out with the same assumptions and procedures for showers of average developement as in ref.3 except the model of atmospheric attenuation of Cerenkov light. The fraction of light reaching the observation level can be expressed by $\exp(-x/\Lambda)$,where x is the path length of Cerenkov light in the atmosphere. A constant value Λ (18Km) was assumed in the previos paper but here we use the same model as that of Hillas(4), which is a function of atmospheric depth. The effect of the first interaction depth of primary cosmic rays to Cerenkov pulse shape was calculated with various interaction models. In this calculation, observation level is taken to be 700m a.s.l., where the telescopes are set in Akeno air shower array.

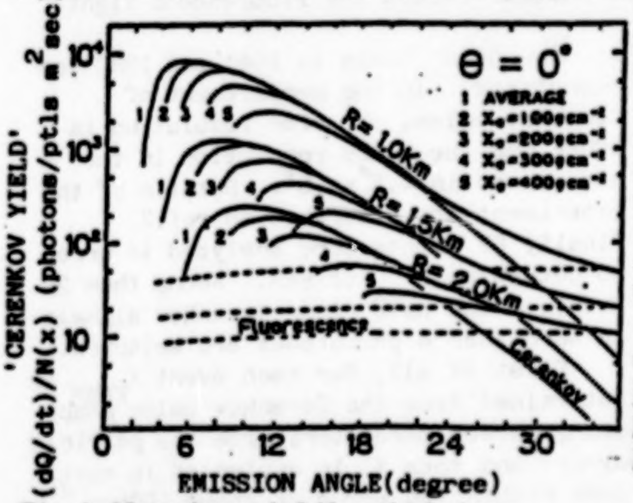

Fig.1 'Cerenkov yield' and photons from fluorescence.

2-1. Cerenkov yield per particle at the depth of photon source.

In fig.1 is shown 'Cerenkov yield',(dQ/dt)/N(x),observed number of Cerenkov photons

N85-36015

divided by the electron size at the light source level in the atmosphere. As shown in the previous paper the 'Cerenkov yield' is independent of the interaction models at 1 - 2 Km from the core. This is also indicated by Ivanenko et al. up to less core distance(700m)(5). This value is a function of the height of photon emission in the atmosphere(x), zenith angle of the shower(θ), distance from the core(R) and also the first interaction depth of the primary cosmic ray(X_0). The abscissa of fig.1 is the emission angle of Cerenkov light to the shower axis. The fluorescent light from EAS is also shown in fig.1. If above parameters are experimentally determined we can construct the shower curve in the atmosphere from the Cerenkov pulse shape using the relation of fig.1.

2-2. The EAS path length in the atmosphere corresponding to the full width at a half maximum of Cerenkov pulse.

The full width at a half maximum(FWHM) of Cerenkov pulse is well known to have a good relation to the longitudinal development of EAS, especially to the shower maximum depth, but it has a poor relation to X_0. Here we find a parameter which has a good relation to X_0, that is , X_{FWHM}, the atmospheric depth which the EAS passes through during the time of FWHM of Cerenkov pulse. Fig.2 shows the relation between them. The parameter of X_{FWHM} is a function of θ, R, X_0 and the shower maximum depth(X_{max}). Our calculation is made in the range of X_{max} from 450gcm^{-2} to 800gcm^{-2} for showers of average development. In fig.2 solid and chain lines show the relation of X_{FWHM} - X_0 for showers of extremely fast and slow development respectively in our calculation. The contribution of fluorescent light from EAS is also shown by broken lines for two extremely developed showers. Consequently showers concerned in the present paper distribute in the hatched regions in fig.2. If we know the value of X_{FWHM} we can estimate X_0 with an error of about 100gcm^{-2} for such showers that Cerenkov light photons exceed the fluorescent light.

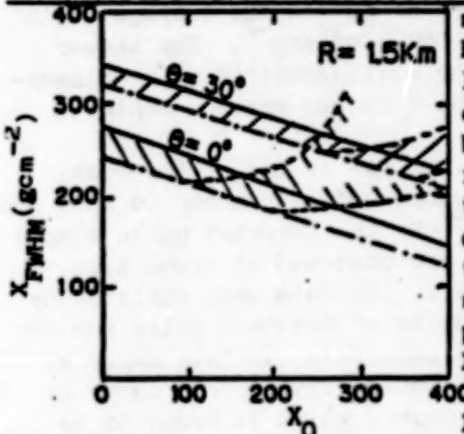

Fig.2 Relation between X_0 and X_{FWHM}.

3. Data analysis and results.

The data taken in 1981 and 1982 are reanalyzed. In the measurement of Cerenkov pulse, the time resolution is 100ns and the space resolution in the atmosphere is 4.5°x4.5°. Details of the experiment are described in ref.2. Finally 62 events were analyzed in order to determine X_{max} of EAS. Among them 38 events which have clear Cerenkov signals in more than 4 phototubes are selected.

First of all, for each event X_{FWHM} is determined from the Cerenkov pulse shape using shower parameters from the particle array and then X_0 is estimated in most case within the error of about 100gcm^{-2} by using the relation of fig.2. If we know X_0 we can construct the shower development

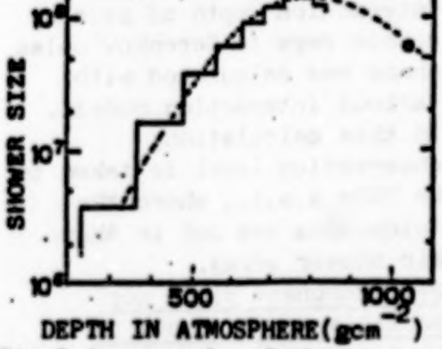

Fig.3 An example of shower curve determined from Cerenkov pulse wave.

ORIGINAL PAGE IS
OF POOR QUALITY

curve in the atmosphere from the Cerenkov pulse shape by using the relation of fig.1. Fig.3 shows an example of the shower development curve thus determined. In this experiment the space resolution in the atmosphere is limited by the time resolution of the registration system(100ns) for the Cerenkov pulse shape. In fig.3 open circle shows the shower size determined by the particle array for the event and broken line is a curve smoothly connected the data. From fig.3 we can determine both the depth of shower maximum and the maximum shower size(N_{max}). The primary energy(E_0) is obtained by multiplying N_{max} by a constant value of 1.4GeV(5).

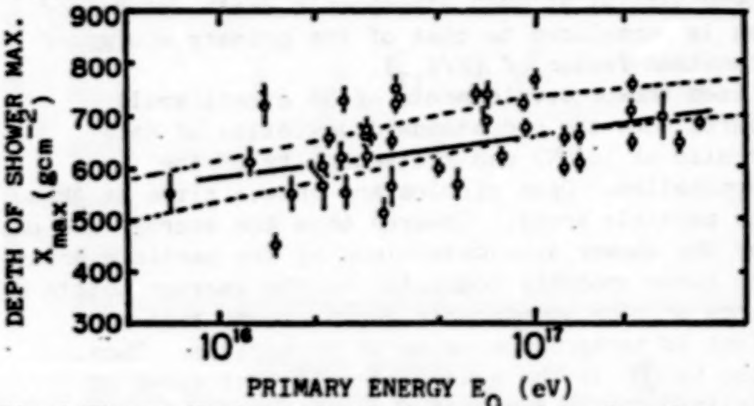

Fig.4 Shower Maximum depth determined by Cerenkov events.

Fig.4 shows the relation between X_{max} and E_0 for all events determined by the same procedure. The values of X_{max} for events which apparently penetrate in the atmosphere(X_0>100gcm^{-2}) are corrected by subtracting of X_0. The determination error of E_0 is estimated to be about ± 20% which is mainly due to the uncertainty of the background contribution to the data. In fig.4 solid line shows the least square fit for these data. Two broken lines show the region where almost all other experimental results are distributed(7). Our results seem to be consistent with other results. From fig.4 the average value of X_{max} at the primary energy of 10^{17}eV is 660 ± 40gcm^{-2}.

In order to know the average longitudinal development curve of showers, all data are normalized to the primary energy of 10^{17}eV(E_{17}) and to the maximum depth of 660gcm^{-2} using the average relation in fig.4 as follows.

(1) First the shower maximum depth of each event is moved to the average one of the same primary energy(E) in fig.4 and then the each atmospheric depth of the

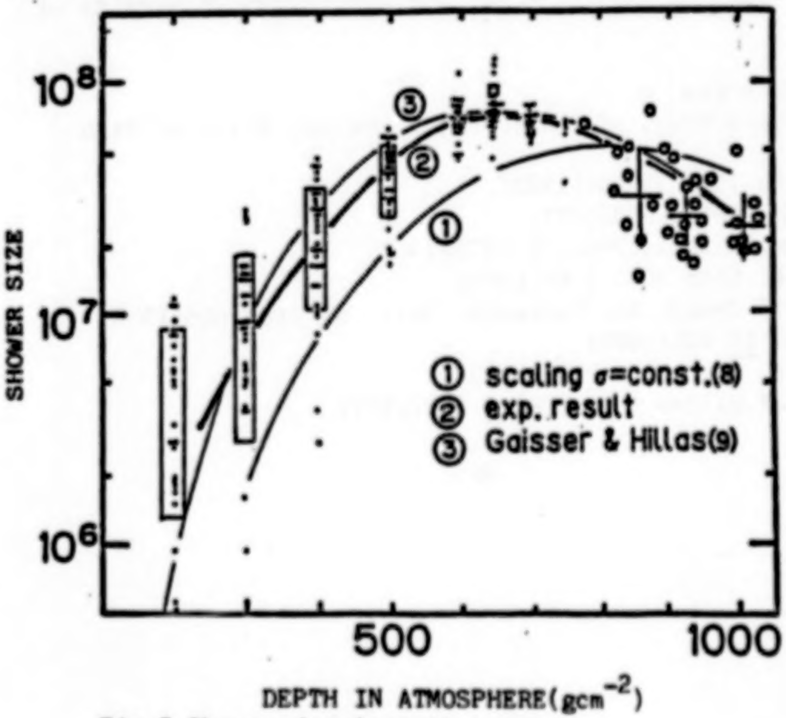

Fig.5 Shower development curve.

shower curve is normalized to that of the primary energy of 10^{17}eV.

(2) Secondly each shower size(N) at each atmospheric depth determined from the Cerenkov pulse is normalized to that of the primary energy of 10^{17}eV by dividing a constant factor of (E/E_{17}).

Fig.5 shows normalized shower developments of 38 events(small points). In fig.5 squares show the one standard deviation of data distribution in shower size of log(N) and the ambiguity of the atmospheric depth determination. Open circles are shower sizes at Akeno level determined by the particle array. Crosses show the average and one standard deviations for the shower size determined by the particle array. Thick solid line is the curve smoothly connected to the average points of shower size distributions at each atmospheric depth except that of 200gcm^{-2} where the effect of backgrounds seems to be serious. Then, thick solid line(denoted by ②) is the average development curve of showers of 10^{17}eV normalized to the depth at the maximum development .

In comparison with data two curves are shown in fig.5. One is the simulation by Ivanenko et al. with the assumption of primary proton and constant cross section with scaling law(8) and the other is the shower development function by Gaisser and Hillas(9) with 660gcm^{-2} for X_{max}. In most case, theoretical average curves are averaged over different starting points, and so can not directly be compared with our experimental one which is normalized at the depth of shower maximum. But when the depth of shower maximum is moved to the same one, the shape of shower development curve can be compared with our result except that in deep atmosphere. From fig.5 the average development of showers of energy 10^{17}eV is well described by the Gaisser-Hillas development function.

4. Acknowledgments. The authors would like to thank the member of Akeno group for their help. Analysis and calculation were done by FACOM M380 at the computer room of Institute for Nuclear Study, University of Tokyo.

References

1) Y.Mizumoyo and T.Hara Proc. of Cosmic Ray Workshop, Univ. of Utah p99(1983)
2) M.Daigo et al. 18th ICRC 11 406(1983)
3) T.Hara et al. 15th ICRC 8 308(1977)
4) A.M.Hillas J. Phys. G;Nucl. Phys. 8 1475(1982)
5) I.P.Ivanenko et al. 16th ICRC 9 88(1979)
6) A.M.Hillas Proc. of Cosmic Ray Workshop, Univ. of Utah p16(1983)
7) M.Nagano 18th ICRC 12 425(1983)
8) I.P.Ivanenko et al. 16th ICRC 9 83(1979)
9) T.K.Gaisser and A.M.Hillas 15th ICRC 8 353(1977)

N85-36016

HE4,4-8

MISSING ENERGIES AT PAIR CREATION

Ahmed Abu El- Ela
Department of Physics,Faculty of Science
Mansoura University , Mansoura , Egypt
Soad Hassan and Erich R.Bagge
Institut fuer Reine und Angewandte Kernphysik
der Universitaet Kiel , Olshausenstrasse 40-60
2300 Kiel , W.-Germany

ABSTRACT

Wilson cloud chamber measurements of the separated spectra of positrons and electrons produced by gamma quanta of 6.14 MeV are differing drastically from the theoretically predicted (identical) spectra by BETHE and HEITLER , but are in good conformity to those of a modified theory of pair creation by of one of the authors (B).

1. The experimental arrangement

A Wilson cloud chamber of the Blackett type (30 cm in diameter, 6 cm illuminated depth), filled with Helium at 1.2 bar gas pressure and a water alcohol mixture was operated to investigate pair creation by gammas of 6.14 ; 6.90 ; 7.11 and 8.87 MeV. These quanta will be emitted after irradiation of UREA (produced with highly enriched N15-nuclei) by the neutrons in the tangential hole of the 18 MW swimming pool reactor of the GKSS-Research-Centre Geesthacht near Hamburg. The cylindrical glass ring of the cloud chamber had a hole of 1 cm diameter, covered by a thin plexiglass foil to allow the gammas entering of the expansion room without passing the glass. Two Helmholtz coils produced inside the chamber a nearly homogeneous magnetic field of 703 Gauss (deviations from the homogeneity less than 1% wthin the illuminated volume). Helium was used to reduce the stopping power of the gas and also its motions due to its small expansion ratio (1.07 for $\kappa=1.67$). By this way positrons of energies above 30 KeV became measurable. But also below this limit pairs were still recognizable and could be distinguished from Compton electrons although the energies could not be determined precisely enough to present credible values.
The cloud chamber was installed at a distance of about 6 m from the reactor behind its 3.5 m concrete radiation shield. After an irradiation for at least one minute in the middle of the tangential hole a cartridge filled with 0.7 g UREA was transported within 3.2 sec to a lead bloc at the cloud chamber by a pressurised pipe line. A hole in the lead bloc "focussed" the gammas to a 25 μm gold foil inside the chamber.(Fig.1)

2. The evaluation method and the energy sum spectrum of the pairs

The particle pathes were photographed stereoskopally by two Hasselblad cameras at 12 cm distance of the optical axes and at a distance of one meter from the cloud chamber. About 4000 pictures were taken and 243 pairs on them have been evaluated on a Pulfrich stereokomparator by two persons (A,E.E. 121 pairs (see [1]) and S.H. 122 pairs) independly and under slightly modified calibrating conditions. The two separate measurements gave practically the same results for the positron- and electron-spectra.

In figure 2 we show here the energy sums of 122 pairs which demonstrate the energy deficits for the 3 lines at 6.14 ; 6.91 and 8.87 MeV by their asymmetries (soft rise of frequencies on the low energy side of the maxima and rapid fall down at higher energies). It should be noted that the 7.11 MeV-line has too low intensity and cannot be separated well from the 6.91-line.

3. The separated energy spectra of the positrons and the electrons

Figures 3 and 4 present the separated spectra of the positrons and electrons for 114 pairs (57 pairs by A.E.E. and the others by S.H.) of the 6.14 MeV-quanta. The corresponding spectra for the two types of particles, 69 pairs of the couple 6.90 and 7.11 MeV and 29 pairs for the 8.87 MeV-line, not shown here, are practically of the same behaviours. There is no question that the separated particle spectra are differing in a drastic way from the predictions of the well known theory of BETHE and HEITLER (dotted curves) [2] (1934), but are in a relatively good conformity to a modified theory of pair creation by BAGGE [3] (1977) (solid curves).

References

[1] Ahmed Abu El-Ela, Dr.rer.nat-thesis, university of Kiel 1984
Ahmed Abu El-Ela and Erich R.Bagge, Atomkernenergie/Kerntechnik, 45,208 (1984)

[2] H. A. Bethe and W.Heitler, Proc.Roy.Soc.,140,83 (1934)

[3] Erich R.Bagge Atomkernenergie/Kerntechnik,25,251-256 (1975)
26,73-75 (1975)
33,116-125 (1979)

ORIGINAL PAGE IS
OF POOR QUALITY

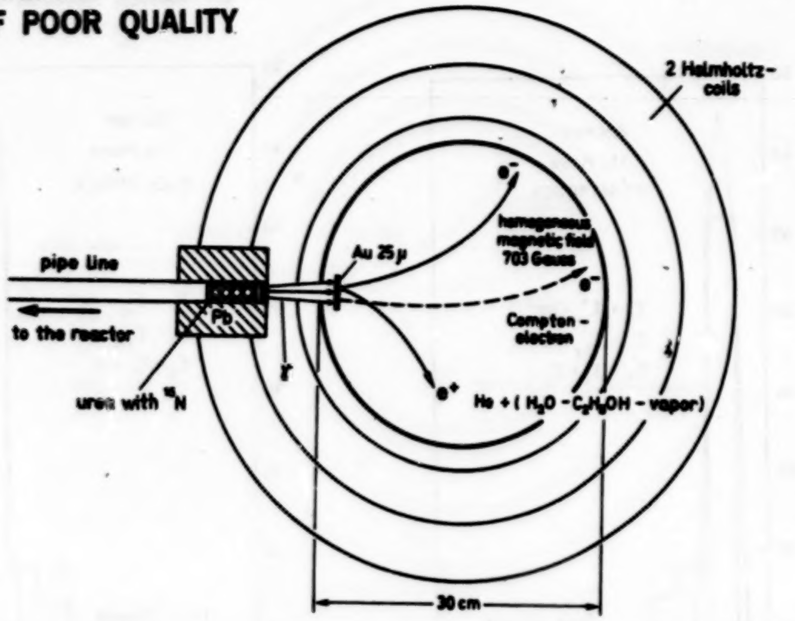
2 Helmholtz-coils
pipe line
to the reactor
Pb
urea with ^{15}N
γ
Au 25 μ
e^-
homogeneous magnetic field 703 Gauss
e^-
Compton-electron
e^+
He + (H_2O - C_2H_5OH - vapor)
30 cm

Figure 1. The Wilson cloud chamber arrangement with the Helmholtz coils, the pipe line for the cartrigde transport and the 25 μm gold foil as target for the pair production.

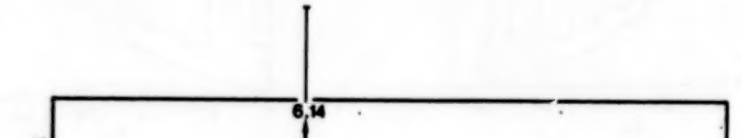

Figure 2. The energy sum spectrum of the positron-electron pairs produced by gamma quanta of 6.14; 6.90; 7.11 and 8.87 MeV. These quanta are emitted by ^{16}O-nuclei, generated by irradiation of ^{15}N-nuclei with the thermal neutrons of a swimming pool reactor and a subsequent β-decay of 7.13 sec lifetime.

ORIGINAL PAGE IS
OF POOR QUALITY

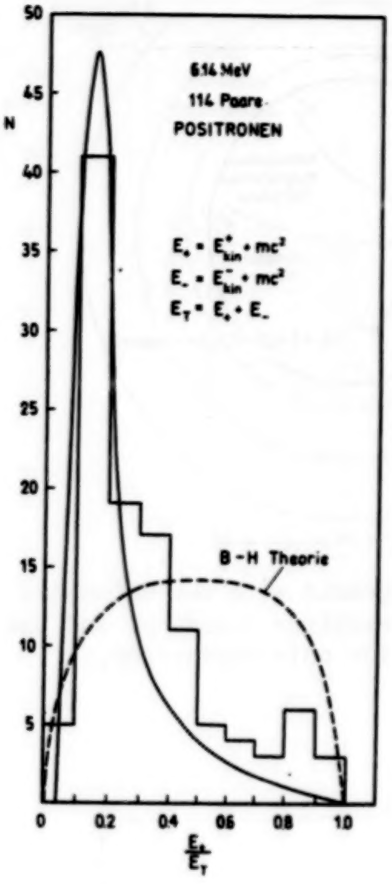

Figure 3.
The positron spectrum of 114 pairs created by 6.14 MeV quanta alone. Noteworthy is the high frequency of low kinetic energy positrons in full contradiction to BETHE and HEITLER's theoretically predicted (dotted) curve [2] .

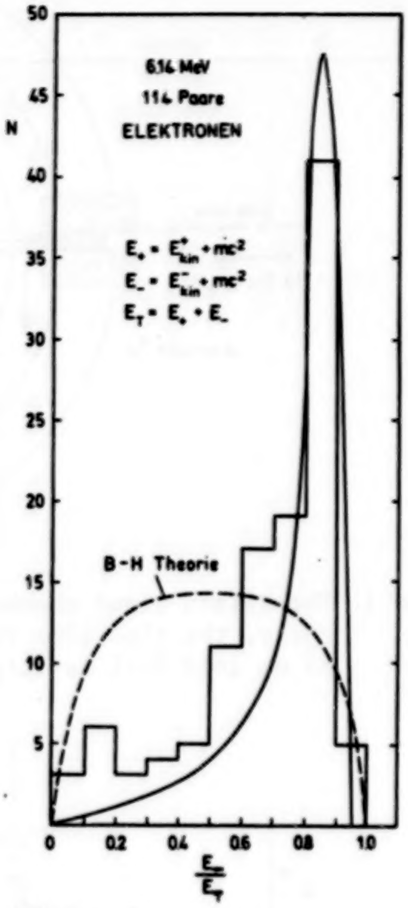

Figure 4
Here the corresponding electron spectrum of the same pairs as in figure 3 shows that these particles received mainly the highest possible energies at pair creation by the 6.14 MeV-quanta. There is no chance to say that positrons have identical spectra as BETHE and HEITLER's theory did it. The solid curves in the two figures 3 and 4 are derived in a modified theory of pair creation by BAGGE [3].

Transition Effect of Air Shower Particles in Plastic Scintillators

N85-36017

K.Asakimori and T.Maeda
Department of physics, Kobe University,
Nada-Ku, Kobe 657, Japan
T.Kameda
Kobe Women's University, Suma-Ku, Kobe 654, Japan
K.Mizushima
Kobe Women's Junior College, Chuo-Ku,
Kobe 650, Japan
Y.Misaki
Research Center for Nuclear Physics,
Osaka University, Ibaraki,
Osaka 567, Japan

ABSTRACT

Transition effect of air shower particles in the plastic scintillators near the core was measured by scintillators of various thickness. The air showers selected for the measurement were of size $\gtrsim 10^5$. Results obtained are as follows:

i) The multiplication of shower particles in the scintillators is less than 20% for that of 50mm thickness.

ii) Dependence of the transition effect on age parameter is not recognized within the experimental errors.

1. Introduction In order to obtain an accurate density of air shower partiles, it is essential to know the distortion caused by the materials which compose the detector and the surrounding container.

The transition effect of the shower particles due to plastic scintillators and iron plate of the container was investigated in detail (1), and multiplication of 10% was recognized near the core of air showers for the plastic scintillators of 50mm thickness.

However, some group reports that multiplication of > 50% for the scintillator of 50mm thickness exists near the core compared to that of 3mm thickness, and that the transition depends remarkably upon the age parameter (2).

To reveal the contradiction, transition effect in the scintillators was studied by comparison of the response of each scintillator of different thickness which piled up in layer above and bellow.

2. Experiment and Results. Four sets of detectors composed of two plastic scintillators of different thickness piled up above and bellow, were placed in the air shower array of Kobe University. All scintillators are of $0.25m^2$ area. The thickness of the plastic scintillators of each set is listed in Table 1. Measurement was carried out during the period from December 1983 to June 1984 and about 6000 showers which had size of $\gtrsim 10^5$ and zenith angle less than 30° were selected. Using these showers, the transition effect of the shower particles near the core (within 30m from the core) was studied.

Table 1 Combination of Thickness of scintillators (mm)

upper scintillator	30	10	3	3
lower scintillator	50	20	50	50

A multiplication (or absorption) factor was obtained by dividing particles of lower scintillator by those of upper one. Fig. 1 shows mean values of the multiplication factors as a function of distance from the core of the showers, having size $\gtrsim 10^5$ and age parameter $0.5 \leq s < 1.5$ In every case, mean value of multiplication factors exceeds one near the core, and decreases gradually as the distance increases, and becomes less than one at distance farther than 10m. None of the cases shows a multiplication factor exceeding by 20% near the core. Rate of multiplication (or absorption) is largest for the combination (30mm,50mm), and combinations (3mm,50mm) and (10mm, 20mm) are in order of decrease. These trends are well explained considering the cascade of electron components in the showers.

To study a dependence of shower age on the transition effect, showers were divided into 3 groups showers of age parameter $0.8 \leq s < 1.0$, $1.0 \leq s < 1.2$, and $1.2 \leq s < 1.4$, and for each group multiplication factor on the distance from the core were obtained.

Fig.2 represents the results, and the figure shows that any obvious dependence does not exist within the experimental errors

3.Discussion Four sets of detectors give us consistent values of multiplication factors each other, and we can safely say that the results mentioned above are in accordance with those obtained previously for scintillators of thickness 50mm does not exceed by 20%.

Our results are in disagreement with those of Akeno group. Disagreement may be caused by the different arrangement of detectors. We used the scintillators piled up directly,and they placed the thin scintillators independently among the array. Accordingly, their results reflect sharply the accuracy of location of the cores, compared to our cases.

Applying the results obtained by us and approximating the lateral distribution to NKG function, use of the plastic scintillators of thickness 50mm give us smaller value of age parameter by 0.03 independent of the values of age parameter, and it gives little effect on the shower size.

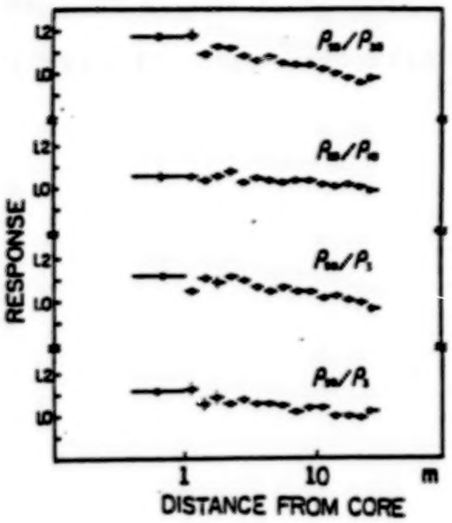
RESPONSE
1.2
1.0
1
10
m
DISTANCE FROM CORE

Fig.1

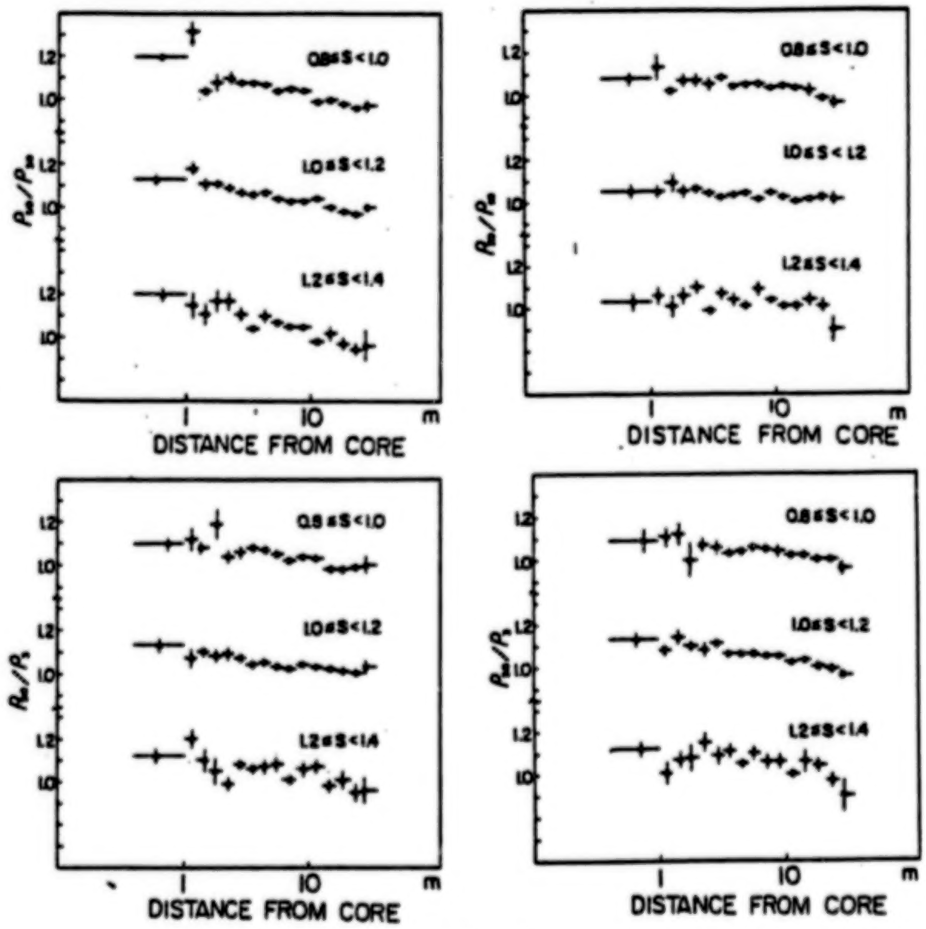
0.8≤S<1.0
1.0≤S<1.2
1.2≤S<1.4
1.2
1.0
1
10
m
DISTANCE FROM CORE

Fig.2

Reference

(1) K.Asakimori et al.: Proc. 16th Int. Conf. on Cosmic Rays, Kyoto 8 (1979) 252
(2) M.Nagano et al.: J.Phys. Soc. Jpn. 53 (1984) 1667

N85-36018

THE SYSTEM OF EAS TIME ANALYSIS

A.Z.KHALAFYAN, V.M.MKHITARYAN, J.S.OGANEZOVA

Yerevan Physics Institute, Markarian st. 2
375036, Yerevan, Armenia, USSR

G.L.BASHINDJAGHYAN, N.B.SINEV, L.I.SARYCHEVA

Institute of Nuclear Physics,
Moscow State University,
117234, Moscow, USSR

ABSTRACT

In studying the extensive air showers (EAS) it is important to have information for determining the EAS front shape, angle of incidence, disk thickness, particle distribution along the shower, on the delayed and EAS front advancing particles. The suggested system of the EAS time analysis allows one to determine the whole EAS longitudinal structure at the observation points. For this purpose the whole information from the detectors is continuously recorded in the memory with the memory cell switching in 5 ns, this enabling one to fix the moment of pulse input from the detector with an accuracy to ±2.5 ns. Along with the "fast" memory, a "slow" memory with the cell switching in 1μs is introduced in the system, this permitting one to observe relatively large time intervals with respect to the trigger (master) pulse with an appropriately lower accuracy (±0.5μs).

The methods of EAS structure analysis used at present are based on measuring the mutual delays between the operations of separate detectors or detector groups. One of the detectors switches on the time counter, and the other switches it off.

The suggested system principally differs from the existing ones by the fact that the information from each detector of the system is recorded continuously in the memory with memory cell switching in 5 ns.

At present, the system model connected to the EAS four detectors is tested on the PION installation.

As the memory capacity of each channel is limited, after filling all its cells (128 in the model) the further information is again recorded in the first cell, then in the second, and so on. Thus, every time moment in the channel memory there is an information on the particles striking the detector for the previous 128 x 5 = 640 ns.

After the input of the trigger, the output of which is determined by the experiment conditions, the memory cells switch for another 320 ns, the readout being feasible after that. The information about all the particles that passed through the system detectors before and after the trigger within ±320 ns is received by the computer. This time range may be extended by increasing the memory volume.

To extend the system possibilities, along with the "fast" memory a "slow" memory with cell switching in 1 μs is introduced in it (the time interval in the model is ±64 μs with respect to the trigger).

Apparatus. The signal from the scintillation detector photomultiplier (PMT) is fed to the amplifier-limiter A (fig.1) located in the close proximity to it, and then over the coaxial cable - to the memory block, where through the peaker P and shaper S is received by two shift registers Rg1 and Rg2.

Simultaneously, from the control unit CU the stable-frequency pulses are received, which in the phase inverter PI are separated into pulses of the same polarity, but out of phase by ½ period, that control the operation of Rg1 and Rg2 (K500UP141).

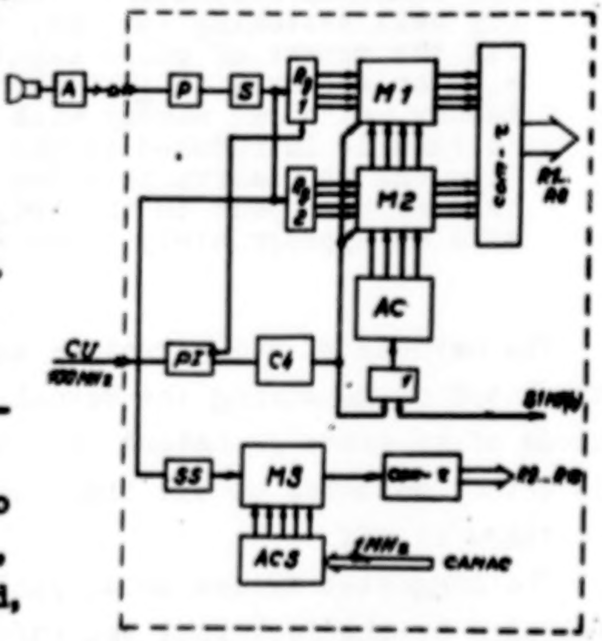

Fig.1. Block diagram of the time channel.

The real frequency of recording rises up to 200 MHz owing to register alternation. The recording from the registers in the memories M1 and M2 (K500PY145) of 64-bit capacity each is realized after filling the registers of 25 MHz frequency. (In the future, with appearance of more speedy microcircuits it will be possible to operate without shift registers and to record the information directly in the memory.) The record permitting pulses are received from the counter C4, and the simultaneous switching of M1 and M2 addresses - from the address counter AC.

The slow memory is organized analogously, but without shift registers. The address counter controlling the MS operation receives 1 MHz stable frequency pulses from the control unit.

The control unit (fig.2) is located in a separate module and is intended for the control of one crate memory blocks.

The quartz generator G produced 100 MHz pulses which are applied to the memory blocks through the key K and splitters. The fast shower master is received by the "stop" input of the control trigger CT. Having counted off 64 pulses of the generator G, the counter C64 closes the key K through the key K1, owing to which the information continues to be recorded in the memory cells for another 320 ns after the fast master input. If during 30 μs the main shower master is not received by the other CU input, then in 30 μs the fast master pulse will be applied to the CT "start" input. The key K

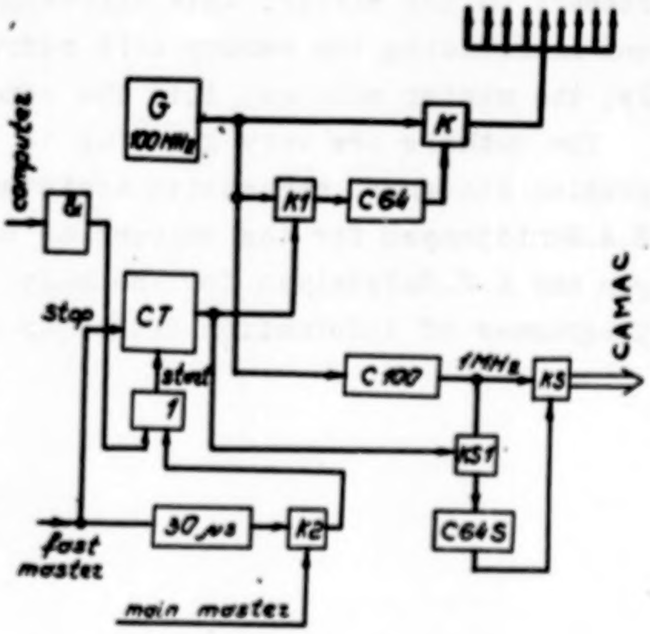

Fig.2. Control unit.

opens and the information from the detectors again starts to be recorded in the memory cells. And the main master input closes the key K2 and the CT remains in the "stop" position until from the computer a record permitting pulse is received that returns the CT to the "start" position.

The receipt of switch pulses to the slow memory is organized analogously. The keys KS and KS1 together with the counter C64S allow to generate 64 pulses more after the fast master input.

In reading, a fixed number of address switching pulses (64) from the computer is received by the same address counters. This allows one to start the readout from the cell in which the information was recorded at the most remote moment of time (-320 ns). The pulse number unambiguously reflects the information advance or delay time with respect to the master, this allowing one to operate without introducing the memory cell addresses and, particularly, the master address, into the computer.

The authors are very grateful to V.V.Avakyan for the problem statement and active assistance in the work, to E.A.Mamidjanyan for the support as well as to A.S.Beglaryan and K.S.Gabrielyan for the help in drawing up the programmes of information detection and processing.

N85-36019

ON THE DETERMINATION OF THE DEPTH OF EAS DEVELOPMENT MAXIMUM USING THE LATERAL DISTRIBUTION OF CERENKOV LIGHT AT DISTANCES < 150 m FROM EAS AXIS

N. Aliev, T. Alimov, M. Kakhkharov, B.M. Makhmudov,
N. Rakhimova, R. Tashpulatov
Samarkand State University, Samarkand, USSR

N.N. Kalmykov, G.B. Khristiansen, V.V. Prosin
Institute of Nuclear Physics, Moscow State University,
Moscow 119899, USSR

ABSTRACT

The Samarkand EAS array was used to measure the mean and individual lateral distribution functions (LDF) of EAS Cerenkov light. In the interval of distances $r = 20-150$ m, the functions are approximated to take the form $q(r) \backsim \exp(b \cdot r/10^4)$. The analysis of the individual parameters b has shown that the mean depth of EAS maximum and the variance of the depth distribution of maxima of EAS with energies of $\sim 2 \times 10^{15}$ eV can properly be described in terms of Kaidalov-Martirosyan quark-gluon string model (QGSM).

The Samarkand EAS array has been described in detail in /1/. The present work uses the experimental data obtained in 1983 when the EAS array consisted of 13 Cerenkov light detectors, each of which included from 7 to 10 FEU-49 photomultiplier tubes, arranged at distances of 15-120 m from the array center and 18 scintillators of 0.5-2 m^2 area each arranged at distances of 15-60 m from the array center. The showers were selected on the basis of their Cerenkov light. The events were selected for the analysis in which $\theta \leq 30°$ and the Cerenkov light flux density $q \geq 8$ photon/$cm^2 \cdot$eV in 6 detectors located at 60m and $q \geq 5$ photon/cm^2 eV in 3 detectors at 120 m.

The EAS axis positions and sizes were inferred from the scincillator data. The shower energy was derived from the Cerenkov light flux density at a 100-m distance from EAS axis. The analysis were made for the showers whose axes fell within a 60-m radius circles and the selection probability was > 90%.

During 45 hours of the array operations, 500 showers satisfying the above requirements were selected. The shower energies were from 10^{15} to 10^{16} eV.

Fig.1 shows the mean LDF for $E_0 = 3\times10^{15}$ eV. Fig. 2 exemplifies the individual LDF of Cerenkov light.

The LDF at small distances was proposed in /2,3/ to describe by the function of the form

$$q(r) \propto \exp(b \cdot r/10^4) \qquad (1)$$

We used this approximation with one parameter b to describe the mean and individual LDF. From Figs 1 and 2 it is seen that the approximation (1) can properly describe the experimental functions at distances of 20-150 m from EAS axis.

The Samarkand EAS array permits from 8 to 12 dots to be obtained in an individual shower at the above mentioned distances. In such a way, individual parameter b was found in each of 500 showers.

The results were interpreted quantitatively by mathematical simulation of experimental data. The EAS axis position and direction, energy, and depth of maximum were simulated as main parameters. The rest parameters, namely, EAS size Ne , the LDF parameters of Cerenkov light and charged particles, and densities in individual detectors, were treated as functions of the main parameters. The calculations allowed for the errors in measuring the angles and the flux densities of Cerenkov light and charged particles. The relationship of LDF to EAS maximum depth was taken from the calculations made in terms of the supracritical pomeron model described in detail in /4/. The parameter of the maximum depth distribution were taken from the calculations made in terms of the same model for mixed chemical composition of primary cosmic rays (40% of p and 15% of nuclei with A= 4,15,31, and 56 each):

$$\overline{X}_m = 504 + 75\,(\lg E_0 - 15)\ \mathrm{g/cm^2}$$

$$\sigma(X_m) = 85\ \mathrm{g/cm^2}$$

640 artificial showers were simulated. The simulation has shown that the accuracy of determining b in individual cases is $\Delta b = 18$.

To make sure that the LDF form reflects the depth of the maximum of an individual shower, we examined the correlation of the parameter b with the independent parameter, the particle number-to-energy ratio, which must also be sensitive to the depth of EAS maximum. Fig. 3 shows the experimental dots of the dependence b on lg(Ne/Eo). The correlation coefficient is 0.55+0.03. The curve in the figure is the regression line:

$$b = 153 + (102 \pm 7) \cdot (\log_{10}(N_e/E_0) + 9.7)$$

Fig. 4 shows the b distribution of individual showers with $E_o = 2 \times 10^{15}$ eV. In the distribution, $\bar{b} = 154 \pm 2$ and $\sigma(b) = 35 \pm 1$. The dashed line is the distribution obtained by simulating experimental data. In the distribution, $b = 154 \pm 2$ and $\sigma(b) = 33 \pm 1$. The experimental data coincide in practice with the calculation results for the above mentioned parameters of the maximum-depth distribution.

To test the sensitivity of the b distribution to the fluctuations of the maximum depth, the experimental data were repeatedly simulated at $\sigma(X_m) = 65$ g/cm^2, but at the same shape of the cascade curve. In this case $\sigma(b) = 26 \pm 1$, i.e. is much different from the experimental value.

It should be noted in conclusion that the procedure of finding X_{max} from LDF of Cerenkov light is in principle dependent on the model determining the cascade curve shape in the lower atmosphere.

References

1. Kalmykov et al. (1983),Proc. 18th ICRC,Bangalore,11,383
2. KuhlmannJ.D.et al.(1981) J.Phys. G,7, 183.
3. Petterson J.R.,Hilles A.M.(1983), J.Phys.G. preprint
4. Kalmykov N.N., Khristiansen G.B.(1983)Proc. 18th ICRC Bangalore, 11, 330.

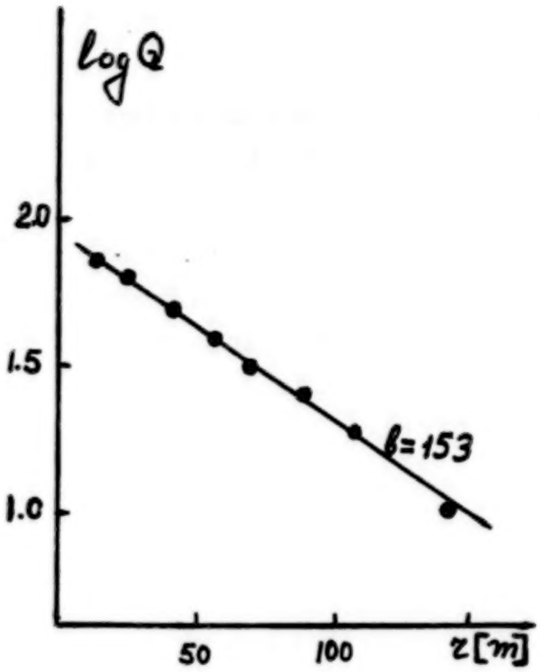

Fig 1.

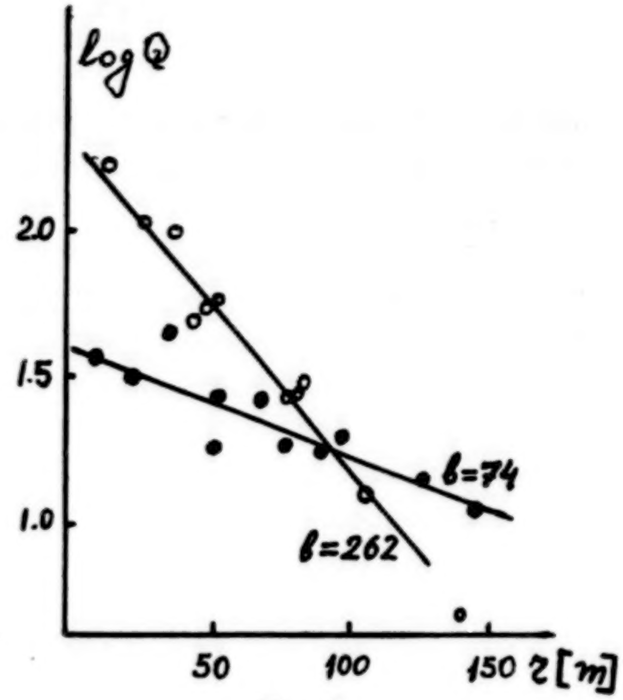

Fig 2.

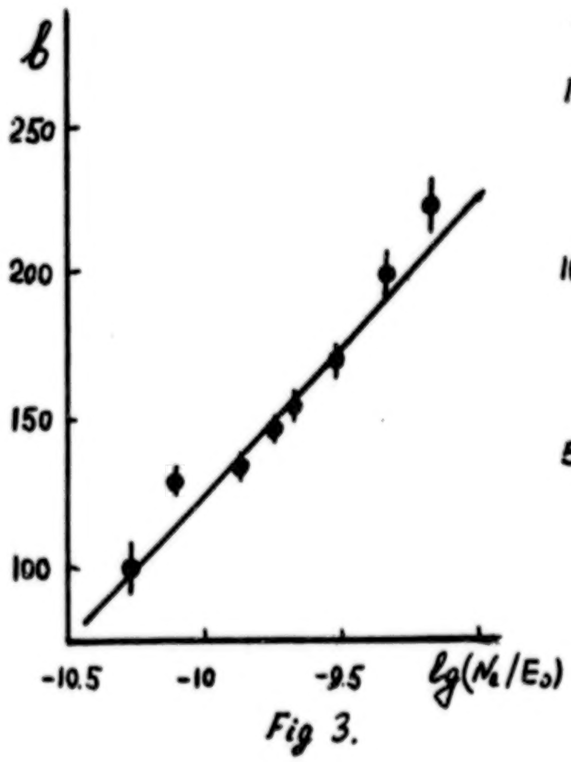

Fig 3.

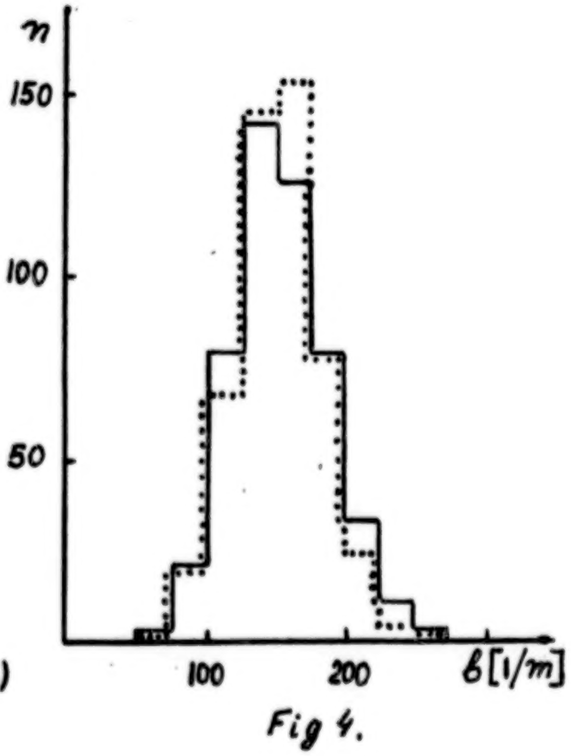

Fig 4.

N85-36020

STUDY OF THE ENERGY SPECTRUM OF PRIMARY COSMIC RAYS; EAS SIZE FLUCTUATIONS AT A FIXED PRIMARY ENERGY

N. Aliev, T. Alimov, N. Kakhharov, N. Khakimov, N. Rakhimova, R. Tashpulatov
Samarkand State University, Samarkand, USSR
G.B. Khristiansen
Institute of Nuclear Physics, Moscow State University, Moscow 119899, USSR

During the initial period of the Samarkand EAS array operations (1981) the showers were selected on the basis of charged-particle flux density /1/, and during the subsequent periods (1982-1983) the showers were selected on the basis of Cerenkov light flux density /2/. Such a procedure has made it possible to measure the shower energy, to estimate the EAS size fluctuations at a fixed primary energy, and to experimentally obtain the scaling factor K(Ne, Eo) from the EAS size spectrum to the primary energy spectrum. In 1983 six scintillators of area $S = 2\ m^2$ each were added to the array. The scintillators were placed at the verteces of a right hexagon at 60-m distances from the EAS array center. The fluctuations of EAS sizes in the showers of fixed primary energies and the scaling factors K(Ne,Eo) were inferred from the data obtained in 1983.

The showers with zenith angles $<30^\circ$ were selected. The EAS axis positions were inferred from the amplitude data of the scintillators. The primary energy Eo was determined by the method of least squares for the known EAS axis position (inferred from the scintillator data) using the data of the Cerenkov detector located at 80-150 m (100m on the average) from EAS axis. In this case the NKG function was taken to be the mean lateral distributions function (LDF) of charged particles, while the Cerenkov light LDF was assumed to be of the form proposed in /3/ with the parameters found using the Samarkand EAS array.

The calculations /4/ have shown that the Cerenkov light flux fluctuations at 100 m from EAS axis, q_{100}, do not exceed 10% at a fixed EAS energy, so the parameter q_{100} may be used to estimate the EAS-generating primary particle- energy.

Fig. 1 compares between the calculated and experimental data on the fluctuations of sizes Ne of EAS with fixed Eo. The mean energy of such showers is $3x10^{15}$ eV. The standard deviation lgNe is $\sqrt{D(\lg Ne)} = 0.31 \pm 0.02$. The figure also shows the distribution calculated in terms of the supracritical pomeron model (SPM) allowing for the difference between the hadron-nucleon and hadron-nucleus interactions (the solid line). The calculations were made in case of mixed chemical composition (40% of p and 15% of nuclei with A= 4, 15, 31, and 56 each) distributed through the $0^\circ - 30^\circ$ zenith angles. To imitate the instrumental errors, each values of Ne was added a random number distributed normally with a variance equaling the squared instrumental error. The instrumental error in the values of Ne, σ_{Ne}, was taken to be 0.15 Ne .

The so obtained distribution shows the stardard deviation $\sqrt{D(\lg Ne)} = 0.31 \pm 0.01$ (for the pure proton composition of primary cosmic rays, $\sqrt{D(\lg Ne)} = 0.34 \pm 0.01$.

Fig. 2 shows the Ne dependence of the scaling factor from Ne to (Ne, Eo) in the showers with fixed values of Eo and Ne, Also shown are the results of the model calculations of the scaling factors in case of complex chemical composition for various models of EAS development. The SPM gives a good agreement with experimental data.

The Ne spectrum was scaled to the primary spectrum using the K(Ne,Eo) approximation of the form

$$K\ (Ne,Eo) = Eo/Ne = (0.57)0.06) x 10^6 (Ne/10^6)^{-0.1 \pm 0.02}$$

The approximation was obtained as follows. Experimental data were used to find only the absolute value of K(Ne,Eo), while the Ne dependence of K(Ne,Eo) was inferred from the SPM calculations.

During 160 hours of its operations (at clear moonless nights), the EAS array detected 10240 showers which gave 7-fold coincidences in the scincillators located at 30 m (see / 1/)from the array center. Out of the events detected, the showers were selected in which the charged-particle density was at least 2 particle/m^2 in the scintillators at 30 m from the array center. A 6 particle/m^2 density was required in the central scintillator. After such a selection, 7233 showers remained. Of them, 3380 showers were with zenith angles $\leqslant 30^\circ$. For the purposes of final analysis the showers were selected whose detection probability is >0.9 within a 20-m circle for Ne = $(2.5-4.0)\times10^5$ and within a 30-m circle for Ne 4×10^5. Such showers amounted to 920 and were used to construct the EAS size spectrum. This spectrum can be approximated by the the functions

$$F(>Ne) = (3.45 \pm 0.20)\times 10^{-10}(Ne/10^5)^{-1.47\pm0.05}\ cm^{-2}s^{-1}sr^{-1}$$

for $2.5\times10^5 \leqslant Ne < 6\times10^5$ and

$$F(>Ne) = (1.15 \pm 0.30)\times 10^{-9}(Ne/10^5)^{-2.10\pm0.09},\ cm^{-2}s^{-1}sr^{-1}$$

for $9.0\times10^5 \leqslant Ne < 3.2\times10^6$.

The experimental scaling factor found in the showers with fixed Ne was used to scale from the measured EAS size spectrum to the primary EAS energy spectrum which can be approximated by the functions.

$$F(>Eo) = (1.9\pm0.3)\times 10^{-10}(Eo/10^{15})^{-1.63\pm0.09}\ cm^{-2}s^{-1}sr^{-1}$$

for $1.5\times10^{15} \leqslant Eo < 3.5\times10^{15}$ eV and

$$F(>Eo) = (5.2\pm0.8)\times 10^{-10}(Eo/10^{15})^{-2.30\pm0.12}\ cm^{-2}s^{-1}sr^{-1}$$

for $5.2\times10^{15} \leqslant Eo < 2.0\times10^{16}$ eV.

Fig. 3 shows the primary cosmic ray spectra obtained with the Samarkand EAS array and elsewhere /5-8/.

REFERENCES

1. Makhmudov B.M. et al.(1979) Proc.16th ICRC, Kyoto, v.9, p.61
2. Kalmykov N.N. et al. (1983) Proc. 18th ICRC, Bangalore, v.11, p.383.
3. Diminstein O.S. et al.(1981) Proc. 17th ICRC, v.11, p.242, Paris
4. Alimov T.A. et al. (1982) Izv.Acad.Nauk SSSR, ser.fiz.46, 1815.
5. Grigorov N.L. et al.(1972) Rescarch XII Akademie Verlag, Berlin
6. Vernov S.N., Khristiansen G.B. Proc.13th ICRC, PA, p.345 , 1969
7. Nagano M. et al. (1984). J.Phys.G. Nucl.Phys.10, 1295.
8. Kirov I.N. et al.(1982) Iyv.Akad.Nauk SSSR, ser.fiz.46, 1827.

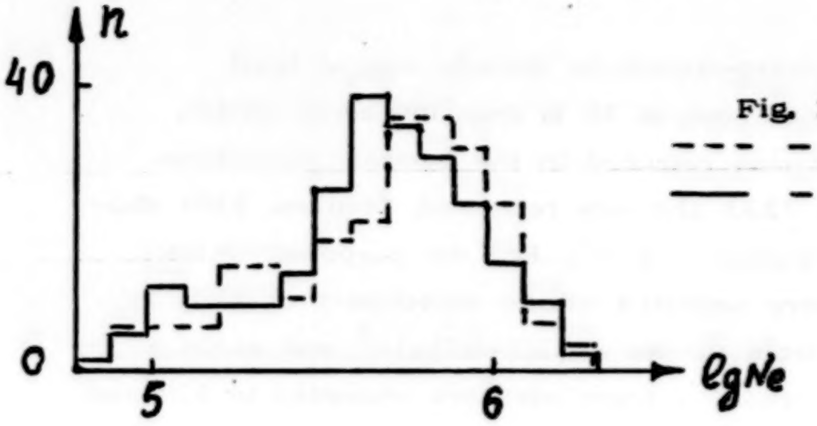

Fig. 1.

- - - - experimental data

—— SPM calculations

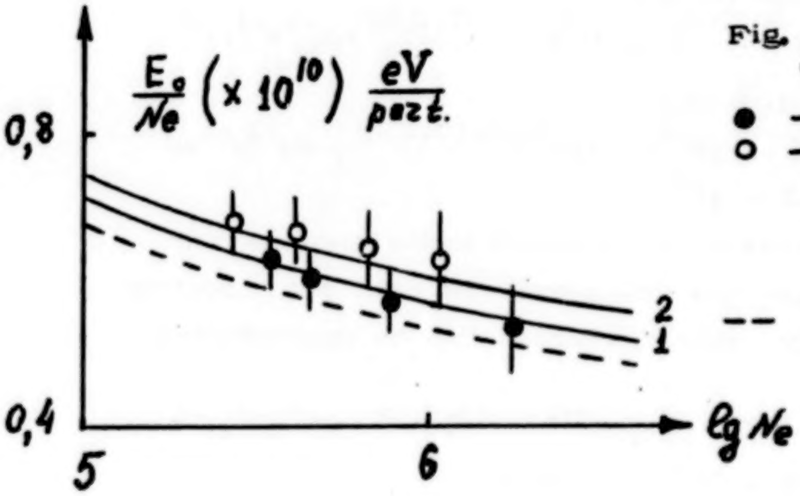

Fig. 2.

experimental data

● — fixed Ne

○ — fixed Eo

SPM calculations

1 - fixed Ne

2 - fixed Eo

— — CKP calculations

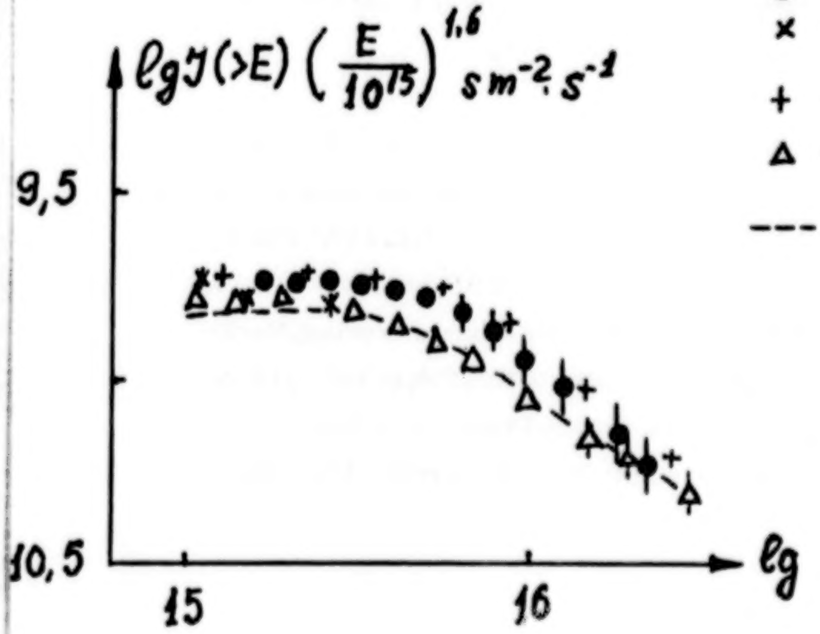

Fig. 3.

● — the present work

× — /5/

+ — /6/

Δ — /8/

- - - - /7/

STUDY OF THE SHOWER MAXIMUM DEPTH BY THE METHOD OF DETECTION OF THE EAS CERENKOV LIGHT PULSE SHAPE

N85-36021

N. Aliev, T. Alimov, M. Kakhkharov, N. Khakimov,
B.M. Makhmudov, N. Rakhimova, R. Tashpulatov

Samarkand State University, Samarkand, USSR

G.B. Khristiansen, V.V. Prosin, V.Yu. Zhukov

Institute of Nuclear Physics,Moscow State
University, Moscow 119899, USSR

ABSTRACT

The report presents the results of processing the data on the shape of the EAS Cerenkov light pulses recorded by the EAS array of the Samarkand University in 1983. The pulse FWHM is used to find the mean depth of EAS maximum.

In 1983 the Samarkand EAS array consisted of 13 integral detectors of Cerenkov radiation arranged as was described in /1/ and 18 scintillators arraged symmetrically around the array center, with 6 instruments located on each of the circles of 15, 30, and 60-m radii. The detector of Cerenkov pulse shape was installed at 250 m from the array center and included 13 photomultiplier tubes of the XP-2041 type. The detector is described in more detail in /2/.

The pulse shape was recorded with a 6LOR-04 oscillographic recorder, as described in /2/, and sometimes with the AFI-16 digital analyzer of pulse shape described in /3/. The digital analyzer recorded the instantaneous values of the pulse amplitude at 16 points with a 2-6 ns step which was selected automatically depending on the detected pulse duration. The digital analyzer threshold was above the oscillograph threshold.

The total resolution time of the recorders was estimated as the minimum duration at half-maximum of the Cerenkov light pulses whose amplitude is 2 times as high as the threshold amplitude.

Such duration proved to be 7.5 ns for the oscillograph and 6.5 ns for API-16.

The showers were selected using their Cerenkov light. Some 2500 showers accompanied by the oscillograph pulses and about 1500 showers accompanied by the digital analyzer pulses were detected.

For the purpose of processing we selected EAS with $\theta < 30°$ and the photon flux densities in 6 detectors at the 60-m distance from the array center $q > 8$ photon/cm^2·eV, at the 120-m distance from the array center $q > 5$ photon/cm^{2}eV, in the pulse shape detector $q > 3$ photon/cm^{2}eV for the oscillographic recording and $q > 5.3$ photon/cm^2 eV for the digital recording.

The EAS arrival directions were inferred from the readings of the detectors at $r = 60$ m. The axis coordinates and the EAS size were determined from the readings of the scintillators. The energy was found from the Cerenkov light flux density at a 100-m distance from EAS axis. The processing procedure is described in detail in /4/.

The results were obtained using the showers whose axes fall inside the array ($r < 60$ m) at a > 200 m distance from the pulse shape detector. The selection probability calculated allowing for the fluctuations of the Cerenkov light LDF is > 0.9. In such a way, we have selected 55 events recorded with the oscillograph and 28 events recorded with the digital analyzer. The FWHM of the pulses were measured for all the events. The depths of the individual shower maxima were inferred from the duration and the distance from EAS axis using the method described in /2/.

In terms of energy, all the events were broken into three groups. The mean depths of the maxima for the three groups are shown in Fig. 1 which also presents the results obtained earlier with the EAS arrays at Samarkand /2/, Yakutsk /5/, Tien-Shan /6/, in Japan (Akeno)/7/, and Australia (Adelaida) /8/.

A certain systematic shift of the dots obtained with the Samarkand EAS array may be explained by the transition from the density-based selection of showers ag 60 m from the array center /2/ to the density-based selection at r=120 m. Our calculations /11/ have shown that the latter selection is closer to the selection of showers with a fixed energy.

A good agreement is observed with the data obtained at Tien-Shan and in Japan. The data of /8/ may be significantly distorted by the shower selection effects, as was noted in the work /9/ carried out using the same EAS array.

Fig. 1 shows the results of calculating the depths of EAS maxima in terms of the supracritical pomeron model described in /10/ for primary protons and complex chemical composition (40% of p and 15% of nuclei with A= 4,15,31, and 56 each). A good agreement of the dots of this works and of the dots obtained in /6,7/ with the theoretical dependence for the complex chemical composition can be seen. The dots obtained with the Yakutsk EAS array at $E_o > 10^{17}$ eV do not contradict the dependence either. At lower energies the Yakutsk dots deviate from the dependence by 2 statistical errors. This is probably due to the poor allowance for the erros arising from the application of the photomultiplier tubes of a high time resolution (~ 2 3ns) for EAS with $E_o < 10^{17}$ eV.

REFERENCES

1. Kalmukov N.N.,et al.(1983).Proc.18th ICCR,11,383,Bangalore.
2. Alimov T.A. et al.(1983).Proc.18th ICCR,11,387, Bangalore.
3. Nazansky V.Ya., Sheingeziht A.A., Preprint Inst.Nucl.Phys., Sob.Brunch, Acad.Sci. USSR,Novosibirsk
4. Alimov T. et al., Proc. This Conference
5. Prosin V.V. (1980). Thesis for Candidate Degree,MGU.
6. Kvashnin A.N., et al.(1983). 18th ICCR,11,394, Bangalore.
7. Inone N.,et al.Proc. 18th ICCR,11,402, Bangalore.
8. Thornton G.J. ,R.W. Clay,J.Phys.Rev.Lett.43,p.1622,1979.
9. Liebing D.F. et al.(1984) J.Phys.G. Preprint
10. Kalmykov N.N.,G.B. Khristiansen ,(1983),Proc. 18th ICCR,11, 330, Bangalore.
11. Aliev N.A. et al.(1983) Proc.18th ICCR,11,391,Bangalore.

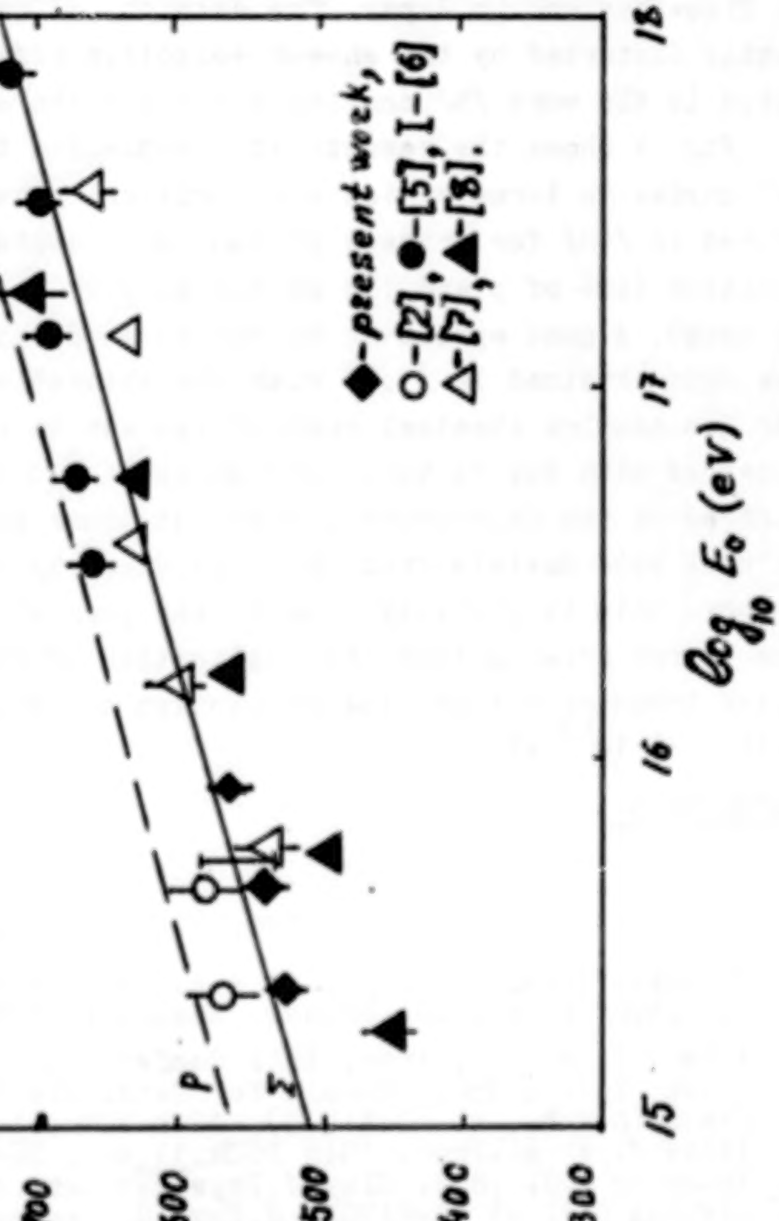

X_m (g·cm^{-2})
300
400
500
600
700
$\log_{10} E_0$ (eV)
15
16
17
18
P
E
◆-present week,
○-[2], ●-[5], I-[6]
△-[7], ▲-[8].

HE 4.4-16

N85-36022

ANALYSIS OF CERENKOV PULSES RECORDED SIMULTANEOUSLY AT TWO SITES.

D.F. Liebing* and J.R. Patterson

Physics Department, University of Adelaide,
Adelaide, South Australia, 5001.

*Present address: Physics Department,
Iowa State University, Ames, Iowa.

ABSTRACT

The agreement between measured distances to maximum for ~ 49 simultaneous Cerenkov pulse profiles from different sites is ± ~ 0.1 km near 4.5 km and ± 0.5 km near 7 km. Uncertainty in depths of maximum are ~ ± 10 g cm^2 and ± 30 g cm^{-2} respectively. Usually the Hillas-Patterson simulation is able to fit both pulse shapes satisfactorily using a single N(x) profile.

1. Introduction. Measurement of the widths of optical Cerenkov pulses from cosmic ray air showers has proved to be a most useful means of studying shower development, in particular the distance to maximum. Several theoretical studies have been published including that by Patterson and Hillas[1] (1983) which forms the basis of the present study. Because of a lack of published data on simultaneous measurements on individual cosmic ray showers, the theories have not previously been tested for consistency of measured distances or for the goodness of the fit with a single longitudinal development curve, N(x).

2. Experimental Data. We make use of part of an extensive data set obtained by Liebing[2] at Buckland Park in 1981-82 in which detectors were located at 200 m North of the centre of the air shower array and 200 m South East. The Cerenkov pulses were obtained in coincidence with showers recorded by the array for which a full NKG shower analysis giving directions, core locations, and hence radial distances, and shower sizes was available. Each detector comprised a 125 mm diameter fast-response photo-multiplier (Philips XP2040, with S11 response) and mechanically collimated at 45° from the zenith, the cut-off being sharp. Few showers detected have greater inclinations than 40°. Short wide-band ($\gtrsim$ 400 MHz or 2 ns rise time) cables (with no preamplifiers) and independently triggered storage oscilloscopes (Tektronix 7834) were used with photographic recording. Impulse responses (~ 5.0 and 5.7 ns FWHM, non-oscillatory and non-Gaussian[1]) were routinely checked for each system using the narrowest sky pulses. Because of a 2s dead time associated with each oscilloscope trigger, a dead time ~ 30% was associated with each system.

Of ~ 138 analysed pulses recorded at the 200 m N site and 166 at the 150 m N site, and ~ 170 at the 200 m SE site, a subset of 49 showers were observed with analysable pulses in two sites. A full analysis of these data treating the systems as quite independent and looking at the variation of depths of maximum with shower size is given in ref. 3. It clearly showed the effect of array selection effects in the data which arise because of the limited dynamic range of the optical detectors and the array bias. However, these are not relevant to the present discussion, except to say that many pulses were lost either because they went off scale or did not trigger the oscilloscopes.

Three representative showers were studied in detail and fits to the experimental profiles are given in figures 1, 2 and 3. They were chosen because the radial distances from the two detector sites were markedly different. Few usable pulses were observed further than 250 m from the shower axis; and sensitivity of the pulses to shower development becomes much less inside 150 m. We also imposed the requirement that for reliable shower analysis, the core should fall inside the perimeter of the array. On the figures the full lines are the oscilloscope traces and show the effect of sky background pulses especially at the more distant site.

3. Theoretical Fits. Hillas[4] has described a method of mapping back from the pulse profiles to the N(x) profiles using absolute timing, not available in these cases. However, a timing zero can be fixed for each pulse by using the width of the pulse to determine the distance to maximum first. In a preliminary investigation we found the N(x) profile derived from the data very sensitive to the sky noise and divergent below the maximum. This was not surprising as Patterson and Hillas[1] showed that the pulse profile was very insensitive to large changes in shower attenuation. The alternative approach adopted therefore was, knowing the measured distance to maximum, to select the closest match from a library of previously simulated N(x) profiles by Hillas[4] which varied in depth of maximum but not very much in shape. Primary energies of 10^{15}, 10^{16} and 10^{17} eV were available, but do not markedly affect the shape.

The simulation calculation of pulse shape was then performed including the photomultiplier resolution for angles 0°, 15°, 30° or 40° and radial distances increasing by 25 m steps. The simulations are not very sensitive to zenith angle so the closest angle was chosen. However, the shape appropriate to the measured radial distance was interpolated graphically from the calculation. The results are fairly sensitive to the radius, which is subject to ± 5 m errors and small changes in distance to maximum.

The theoretical fits are shown as dashed lines and enable the agreement with experiment to be checked over the full profile, whereas it is more usual to be only concerned with the Full Width at Half Maximum. For this comparison the theoretical pulse has been normalized to the experiment at the peak and the relative times adjusted to give the best fit.

The agreement in shape on the rising edge and near the top of the pulse is considered fairly satisfactory. There is a tendency for the theory to underestimate the flux in the tail. This cannot be attributed to a slower attenuation in the N(x) profile because the preliminary study showed the required N(x) to diverge. It arises partly because of the limitation in the simulation to 10 GeV subshowers. The simulation in fig. 1 using 100 GeV subshowers improves the fit in the tail of the pulse.

4. Conclusion. Comparison of simulation fits for a single N(x) development profile to experimental pulses at the different sites has shown satisfactory agreement with the Patterson-Hillas simulations. Independent estimates of distance to maximum indicate errors of ± ~ 0.1 km near 4.5 km and ± 0.5 km near 7.0 km, again consistent with predictions[1]. These correspond to errors in depth of maximum of approximately 10 g cm^2 and 30 g cm^{-2} respectively.

Acknowledgements. We acknowledge the contribution of colleagues including Dr. A.M. Hillas, University of Leeds, and Drs. Gerhardy, Gregory and Clay. The work was supported by the Australian Research Grants Scheme.

References.
1. Patterson, J.R. and Hillas, A.M., (1983), J. Phys. G., 9, 323.
2. Liebing, D.F., (1983), PhD Thesis, University of Adelaide.
3. Liebing, D.F., Clay, R.W., Gregory, A.G. and Patterson, J.R. (1984), J. Phys. G., 10, 1283.
4. Hillas, A.M., (1982) J. Phys. G., 8, 1475.

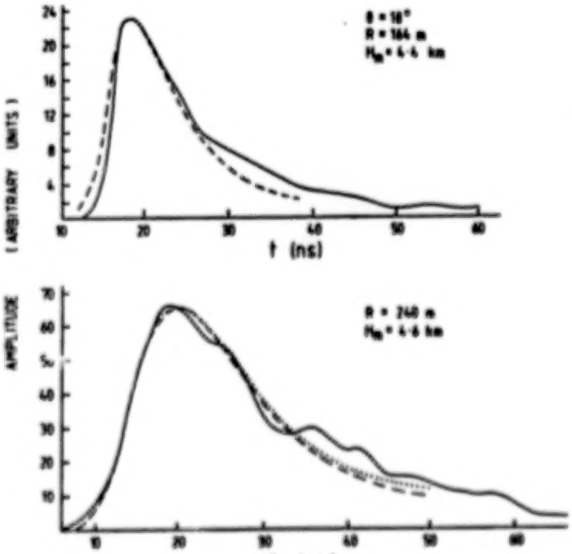

Fig. 1 shows a comparison of the experimental trace (full lines) for a shower with $N_e = 4.6\times10^6$, $E = 2\times10^{16}$ eV and S=1.28, and the Patterson-Hillas simulation using 10 GeV subshowers (dashed lines) and 100 GeV subshowers (dotted). The N(x) profile used[1] has $H_m = 4.5$ km, and depth of maximum 640 gcm^{-2}.

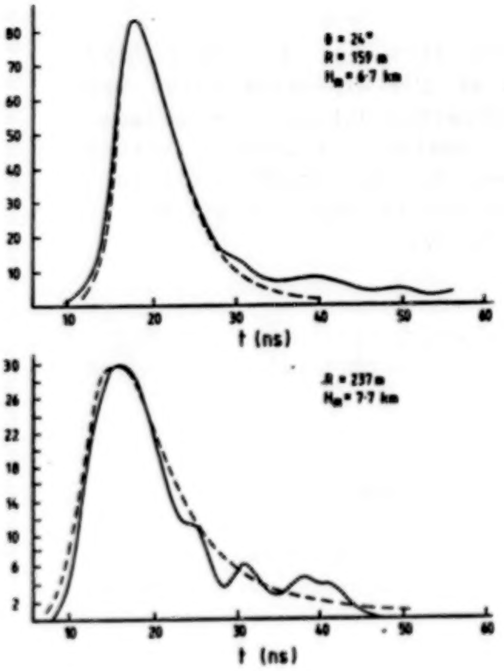

Fig. 2. shows a comparison of experiment and simulation for a shower with N_e = $6x10^5$, E = $8x10^{15}$ eV and S= 1.56. The N(x) profile has H_m = 7.4 km and depth of maximum 470 gcm^{-2}.

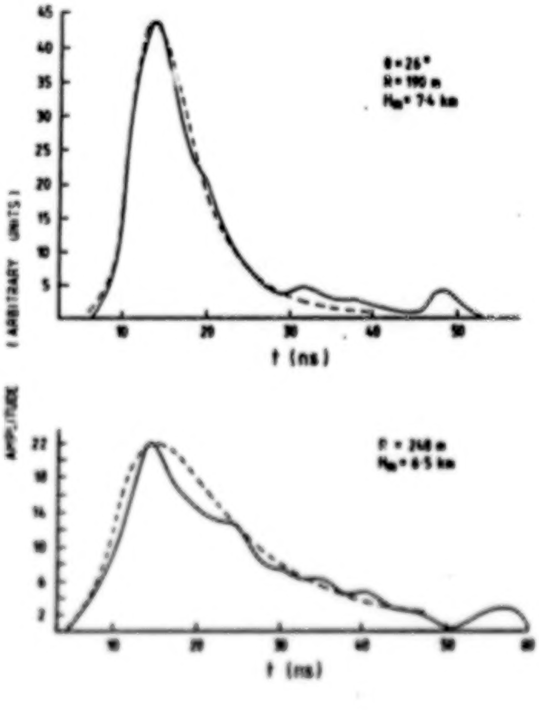

Fig. 3 shows a comparison and experiment and simulation for a shower with Ne = 1.7 x 10^6, E= $3x10^{16}$ eV and S= 1.19. The N(x) profile has HM = 7.4 km and depth of maximum 490 gcm^{-2}.

PRELIMINARY RESULTS OF THE CERENKOV EAS FLASHES OBSERVATIONS ON THE MULTI-MIRROR INSTALLATION OF THE CRIMEAN ASTROPHYSICAL OBSERVATORY

B.M.Vladimirsky, Yu.L.Zyskin, Yu.I.Neshpor,
A.A.Stepanian, V.P.Fomin, V.G.Shitov

Crimean Astrophysical Observatory
p/o Nauchny, 334413, Crimea, USSR

Abstract

A short description of the facility designed for the study of angular resolution of light in the EAS flashes is communicated. The threshold energy of the facility is about 3×10^{12} eV. The data on the angular distribution of light in a flash and the ratio of the flux in the UV ($\lambda < 300$ nm) and visual region as a function of the distance to the axis of a shower are given. Obtained results are compared to the published computations.

1. Introduction.

It is commonly assumed, that the main obstacle to increase the sensitivity of Cerenkov EAS detectors for gamma-quanta registration is the charged particles background.

It was Grindlay [1] who made the first attempts to reduce the registered background of cosmic rays. Turver [2] suggested to reduce the background by using spaced detectors. The experiments in Tata institute, India, showed, that spaced detectors permit to determine the direction of the primary particle (or quantum) on the sky with the accuracy up to $0\overset{\circ}{.}3$ [3] .

In [4] we proposed a method of discrimination of gamma-showers from proton-showers. This method is based in principle on different angular dimentions of these showers. But since the difference is rather scanty, it needs an optical system which allows to obtain the image of the flash with high (minimum $0\overset{\circ}{.}1$) angular resolution. Besides, we suggested in [4] to use the difference in UV region of shower ligh spectrum ($\lambda < 300$ nm) for gamma and proton showers.

2. Description of the facility located at the Crimean observatory.

The facility was described in short in the Proceedings of Ban-

N85-36028

galore Conference [5] . The results given hereafter are obtained on the installation consisting of six similar elements. Each of them comprizes 4 spherical mirrors 1.2-m in diameter. Nineteen PMs are located in the focal plane of each of the four elements (see Fig.1). The light is transmitted to the photocathodes by means of light conductors. The signals from 4 elements being directed in parallel are summarized within each channel, digitized and then stored in the computer memory. Any 2-channel coincidence from 7 central was adopted as a muster-pulse.

Two other telescopes also being directed in parallel were used for UV region of flash spectrum with solar-blind PM. Summarized signal yeild from these two elements is also digitized and recorded in the computer memory. The diameter of the light spot from the point source at the focal plane is $0^{\circ}.1$.

3. The results of the observations.

The observations of the EAS flashes were carried out in November - December, 1984. More than 1000 Cerenkov flashes have been registrated. But for the further analysis only those were selected whose maximal amplitude coincided with one of 7 central pixels. The final sampling constituted 644 events. The energies of primary particles responsible for a flash lie, according to estimations within the range $(3-6)\times10^{12}$ eV.

We have calculated the values of $a^2=\sum_{i=1}^{19}(x_i-\bar{x})^2A_i$ and $b^2=\sum_{i=1}^{19}(y_i-\bar{y})^2A_i$ where A_i is the amplitude of flash in the i-channel, x is the coordinate axis directed along the large axis of ellipsoid of Cerenkov flash, and y is the coordinate axis along the small axis; that gives $\bar{x}=\sum_{i=1}^{19}x_i\frac{A_i}{\sum A_i}$ and $\bar{y}=\sum_{i=1}^{19}\bar{y}_i\frac{A_i}{\sum A_i}$ Fig.2a shows the frequency distribution with respect to a and Fig.2b gives the value of b/a. The mean value of a equals to $0^{\circ}.40\pm0^{\circ}.02$ and $(b/a)=0.69\pm0.01$.

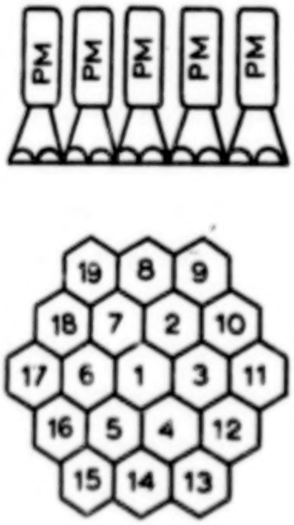

Figure 1.
The configuration of pixels with PM at the focal plane.

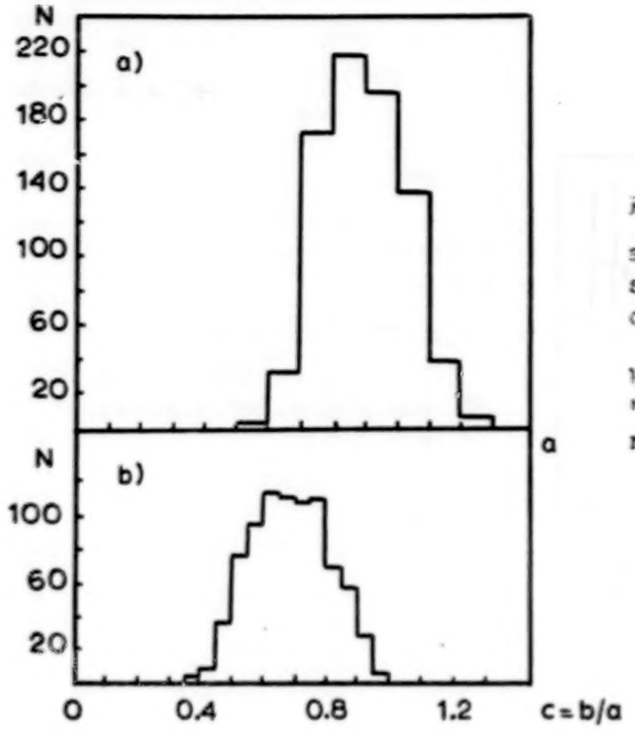

Figure 2.

Frequency distribution :

a) of the effective dimension of the large semiaxis of the flash ellipsoid,

b) of the semiaxis ratio. "N" corresponds to the number of flashes.

For the given values of b/a the flashes amplitudes ratios were obtained for the rim Ae zone to central Ac zone. Here the central zone is adopted as a pixel with maximum amplitude together with the adjucent pixel having the highest amplitude. All other pixels are considered as "rim". Therefore Ae/Ac parameter can be considered as a characteristic of angular distribution of light in a flash. It approaches to "y" computed in [4] .

The obtained distribution is presented on Fig.3a. According to this distribution, the mean value of Ae/Ac depends on b/a variation. The value b/a is distance-dependent: the larger the distance from detector to the axis, the smaller the value of b/a. Here one can see the magnitude of dispersion D(Ae/Ac) of individual estimates. It corresponds to (30-40)% of the estimated value.

Fig.3b shows the ratio of the UV flux Au to the flux in visual region Av as a function of b/a. The dispersion of Au amplitude is high and compatible with the mean value within the given interval. The error of the mean value of Au/Av is presented here.

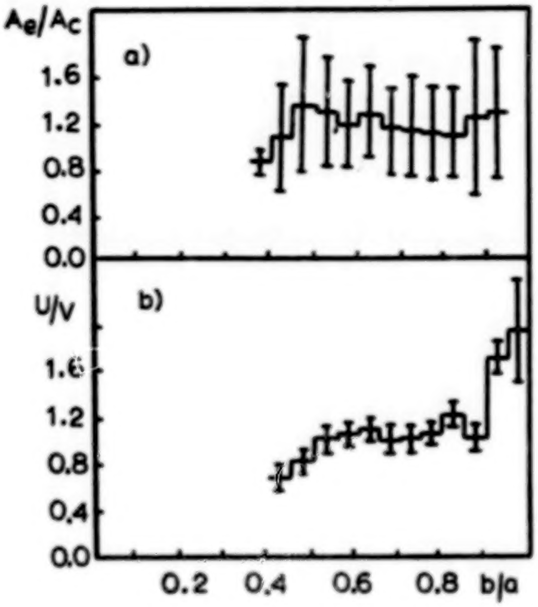

Figure 3.
The dependence of the semiaxes ratio b/a :

a) the amplitude ratio Ae/Ac

b) the ratios of amplitudes in UV and "visible" flashes at random units.

Near the EAS axis the UV flux is much stronger than at large distances. We should note, that detailed information on UV flashes needs further enlargement of mirror surfaces detecting UV-light.

4. Discussion and results.

The obtained data on flash angular dimension are in good agreement with our earlier calculations [4] . These measurements are compatible with the data of Plyasheshnikov and Bignami [6] , the accord is rather high. For instance, according to [6] a=0°.42 and in our computations a-0°.40, although our data is still crude.

As far as we know, the UV flashes have never been registrated so far. So, just the fact of their registration seems to be of importance. We think, that the perspective of gamma and proton showers discrimination is realistic.

References.

1. Grindlay J.E. 1975, Smithsonian Astrophys.Obs.Spec.Rep. N 334.
2. Gibson A.I. et al., 1981, Phil.Trans.R.Soc.Lond. A 301, 635.
3. Gupta S.K. et al., 1982, Proc. of Intern.Workshop on VHE Gamma-Ray Astronomy, Ootacamund, Sept.20-25, 1982, p.295.
4. Stepanian A.A., Fomin V.P., Vladimirsky B.M. 1983, Izv. Krimsk. Astrophys. Obs., 66, 234.
5. Fomin V.P. et al., Proc. 18-th Intern. Cosmic-Ray Conf. Bangalore, India, 1983, v.6, p.223.
6. Plyasheshnikov A.V., Bignami G.F. Nuovo Cim. 1985, in press.

N85-36024

HE 4.4-18

THE EXPERIMENTAL CASCADE CURVES OF EAS AT $E_0 > 10^{17}$ eV OBTAINED BY THE METHOD OF DETECTION OF CHERENKOV PULSE SHAPE

Yu.A. Fomin, N.N. Kalmykov, G.B. Khristiansen, M.V. Motova,
Yu.A. Nechin, V.V. Prosin, V.Yu. Zhukov
Institute of Nuclear Physics, Moscow State University,
Moscow II9899, USSR

N.N. Efimov, V.M. Grigoriev, E.S. Nikiforova,
Institute for Cosmophysical Research and Aeronomy,
Yakutsk 67789I, USSR

Since recently we have systematically studied the individual cascade curves of EAS with $E_0 > 10^{17}$ eV /I-3/ by the method of detection of EAS Cherenkov light pulses proposed initially in /4/.

The scintillators located at the center of the Yakutsk EAS array within a 500-m radius circle were used to select the showers and to determine the main EAS parameters (the axis coordinates, the azimuthal and zenith angles φ and θ, and the primary energy E_0) /5/. The individual cascade curves N(t) were obtained using the EAS Cherenkov light pulses satisfying the following requirements: (I) the signal-to-noise ratio $f_m/\sigma_n \geq 15$, where f_m is the amplitude of pulse, σ_n is the r.m.s. value of night sky noises, (2) the EAS axis-detector distance $r_\perp \geq 350$ m, (3) the zenith angle $\theta \leq 30^\circ$, (4) the probability for EAS to be detected by scintillators $W \geq 0.8$. Condition (I) arises from the desire to reduce the amplitude distortion of Cherenkov pulses due to noise and determines the studied range of EAS sizes, N(t). The resolution times of the Cherenkov pulse shape detectors are $\tau_0 \approx 23$ ns which results in distortion (broadening) of a pulse during the process of the detection. The restrictions $r_\perp \geq 350$ m and $\theta \leq 30^\circ$ permit to select the Cherenkov pulses with relatively high $\tau_{0.5}$ (the half-width of non-distorted pulses). We estimated the distortion of pulses due to the finiteness of τ_0 value. It was shown that the rise time of pulse becomes greater as $\tau_{0.5}/\tau_0$ ratio decreases; at the same time the tail does not vary within 5% accuracy. The results were used in order to correct the experimental pulses.

Since the moment of intersection of the observation level and the EAS axis is not fixed experimentally, the Cherenkov pulse is measured on the scale of relative time τ. In order to determine the absolute time τ_A it is necessary to use the results of theoretical calculation /6/ which permit to find the difference of values τ^N_{mA} and τ^f_{mA}, where τ^N_{mA} is the time moment when the light corresponding to EAS maximum is detected and τ^f_{mA} is the time corresponding to the Cherenkov pulse maximum: $\Delta\tau_m(t_m, r_\perp) = \tau^N_{mA}(t_m, r_\perp) - \tau^f_{mA}(t_m, r_\perp)$, where t_m is the EAS maximum depth in the atmosphere. The value of t_m can be determined from the half-width $\tau_{0.5}$ of the given pulse /7/ and can be used to find τ^N_{mA} in accordance with formulae of /2,3/. Then one obtains the time $\tau^f_{mA} = \tau^N_{mA} - \Delta\tau_m$ corresponding to the maximum of experimental Cherenkov pulse. The theoretical functions /2,3/ used for the transformation of the Cherenkov pulse $f(\tau_A, r_\perp, \theta)$ to the cascade curve N(t) are independent, to within a 5% accuracy, on the adopted model of EAS development and the primary composition. This is illustrated by the function $\Delta\tau_m(t_m, r_\perp)$ shown in Fig. I for the high-multiplicity model (HMM) and for the quark-gluon strings (QGS) model for a primary proton (A=I) and a primary iron nucleus (A=52) /6,8/. These functions depend only on the angle distribution of EAS electrons /7/.

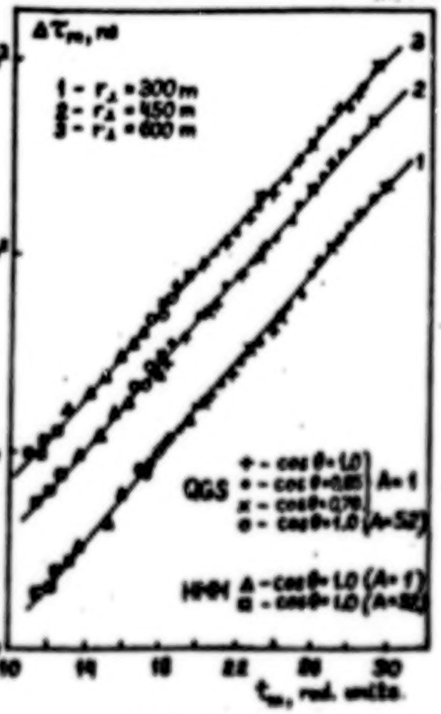

Fig. I

26 showers with Cherenkov pulses satisfying to above men-

tioned requirements were selected. It should be noted that I0 showers out of 26 exhibited the Cherenkov pulses in two detectors at different distances from EAS axis under condition $f_m/\sigma_n \geq 15$. For these events the r.m.s. errors $\sigma_m = \sqrt{D(t_{m_I} - t_{m_2})}$ = I.2 radiation units, where t_{m_1} and t_{m_2} are depths of EAS maximum determined from two Cherenkov pulses. The errors $\sigma_{0.25}$ for the depths corresponding to the points on the ascending branch of the cascade curve at the 0.25 N_m level (N_m is the EAS size in the maximum) $(t_{0.25})_I$ and $(t_{0.25})_2$ is somewhat higher and is about I.6 radiation units.

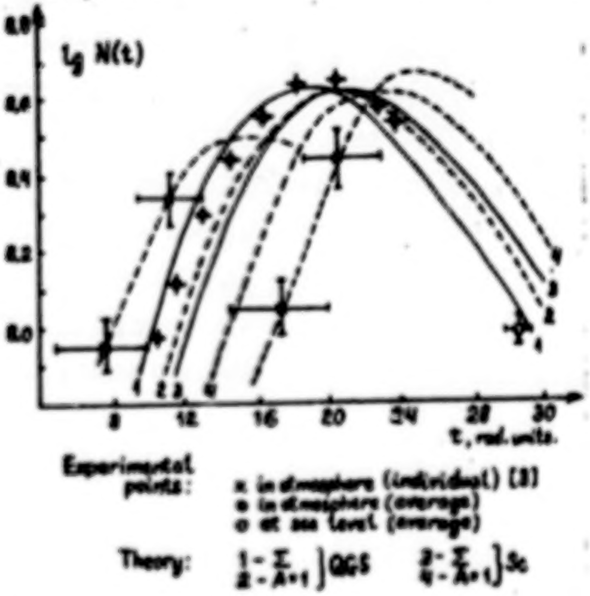

Fig. 2

Fig. 2 presents the mean cascade curve constructed using 26 individual cascade curves in EAS size units N(t). To construct the cascade curves in the absolute units N, the detectors of Cherenkov pulse shape were calibrated by comparing the pulses detected in them with the Cherenkov light flux densities P_c [cm^{2}eV] detected by the time-integral Cherenkov light detectors of the Yakutsk array /5/; $S = mP_C$, where S [mm,ns] is the Cherenkov pulse area measured initially on millimetre scale of amplitudes and on nanosecond sweep of oscillograph, m is calibration factor (which permits to express the amplitudes of pulses in units of flux density [cm^{-2}ns^{-I}eV^{-I}]). After that, using the theoretical functions /2,3/ one obtains the cascade curves N(t) for the number of shower electrons. The accuracy of the calibration factor m, hence of the EAS size N(t), is 25% and arises mainly from the accuracy of the absolute calibration of the integral detectors. The EAS size in the maximum of the mean cascade curve is $\overline{N}_m$ = (4.5 ±

± I.I).10^8. Fig. 2 also shows the point corresponding to the mean EAS size at sea level $\overline{N}_s = (0.95 \pm 0.06).10^8$ inferred from the data of the Yakutsk EAS array scintillators. The energy of individual cascade curves was also determined on the basis of the parameter ρ_{600} /9/, The mean cascade curve energy is $\overline{E}_0 = (7.0 + 2.0).10^{17}$ eV. The correlation coefficient between E_0 and N_m inferred from 26 experimental cascade curves is $\bar{K} = \overline{(E_0/N_m)} = (1.60 \pm 0.08).10^9$ for r.m.s. error 30% related mainly to the apparatus errors of determination of E_0 and N_m.

The comparison by the Pearson method between the experimental cascade curve and the theoretical curves calculated in terms of the scaling model (Sc) /6/ and the QGS model /8/ under various assumptions concerning the chemical composition of primary cosmic rays exhibits a better agreement of the experimental data with the QGS model for complex chemical composition (QGS, Σ) ($P(\chi^2) = 0.07$). Other versions of the theory are in a poorer agreement with the experimental data ($P(\chi^2) \leq 0.01$).

References

I. Grigoriev V.M. et al. Pis'ma ZhETF (1979) 30, II, 747
2. Kalmykov N.N. et al. Proc. I7th ICRC (198I) 6, II4
3. Grigoriev V.M. et al. Proc. I8th ICRC (1983), 9, 204.
4. Fomin Yu.A., Khristiansen G.B. Sov.Nucl.Phys. (197I) I4, 642.
5. Glushkov A.V. et al. Characteristics of EAS from Ultrahigh energy cosmic rays, Yakutsk, 1976, p.45
6. Grishina N.V. et al. Proc. I6th ICRC (1979) 9, I.
7. Berezhko I.A. et al. Sov.Nucl.Phys. (1979), 30, 4I5.
8. Kalmykov N.N., Fomin Yu.A., Khristiansen G.B. Sov.Nucl. Phys. (1985) 4I, 947.
9. Vasiliev I.V. et al. Cosmic Rays of Energies above 10^{17}eV Yakutsk, 1983, p.I9.

N85-36025

LATERAL-ANGULAR AND TEMPORAL CHARACTERISTICS OF EAS OPTICAL RADIATION

Chuykova T.A., Galkin V.I., Ivanenko I.P., Roganova T.M.
Institute of Nuclear Physics, Moscow State University,
Moscow 119899, USSR

The paper presents characteristics of the direct and scattered components of electron-photon shower optical radiation for distances $R \geqslant 500$ m from the shower core to a detector, allowing for the Cerenkov and fluorescent mechanism of photon generation. The results of calculations can be employed to clarify the techniques for determination of the shower parameters detected by both installations registering fluorescent light and those recording Cerenkov light.

1. Introduction. Optical radiation has been used for many years to investigate the lateral EAS development/1,2/. Each new more accurate and/or detailed consideration of the optical component leads, as a rule, to decreasing uncertainties in the determination of shower parameters and sometimes allows finding new characteristics of the shower optical image, which are more sensitive to the nuclear interaction parameters at superhigh energy or to the shape of the primary cosmic ray spectrum than those used earlier/3/.

One of these improved considerations has been reported in /4,5/ where "contamination" of the fluorescent component of EAS optical radiation by scattered Cerenkov light has been examined, and both lateral-angular and temporal characteristics of the shower optical image has been presented. The author of /4,5/ devides the Cerenkov light registered by a detector into three components: direct(non-scattered) light, scattered light, and fluorescent light, thus assuming that fluorescent photons, unlike to Cerenkov ones, would not scatter in the atmosphere(i.e. the fluorescent light being always only direct). When considering the scattered component, the author confines himself to a single scattering; as a model of longitudinal development of EAS with $E_0=10^{17}-10^{18}$eV the author have used a cascade curve of a shower induced deep in the atmosphere by a gamma-ray of $E_0=2\cdot10^{11}$eV, with the hope that this simplification would not considerably distort the relative contributions of various optical radiation components. The papers /4,5/ furthermore have not presented the temporal characteristics of a direct Cerenkov component. Since the results obtained using the above noted approximations, on one hand, are only preliminary and, on the other hand, seem to be important and interesting, we attempted to consider this group of phenomena with the help of simulating program of a different type.

2. The present paper approach. A separate consideration of the Cerenkov and fluorescent components undoubtedly gives an additional information of their relative contributions, however most of modern installations are incapable of dis-

* C-4

tinguishing the nature of photons arriving at a detector.

We performed calculations for a 3000-8000Å wavelength-band. Since large distances($R \gtrsim 500$m) from the core to a detector are considered at which the characteristic temporal scale of a pulse is ~100 ns, the time of fluorescent photon reemission can be neglected in the first approximation. Thus, in the situation of interest for us the differences between the two components reduce to their angular characteristics which practically do not affect the simulation algorithmic aspect. So, a unified source of photons is used composed of Cerenkov and fluorescent sources with appropriate angular characteristics and intensities, and the photon transfer from this source to a detector is considered as usually introducing the photon time delay:

$$cT = r - r_0 + H_0 \eta_0 \left(\frac{\exp(z/H_0)-1}{\cos\theta} - \frac{\exp(z_0/H_0)-1}{\cos\theta_0} \right), \text{ where } H_0 = 7.5\text{km} \quad (1)$$

is the exponential atmosphere depth; $\eta_0 = 2.9 \cdot 10^{-4}$ is the diversity from a unity of an atmosphere refrection index at sea level; $\vec{r}_0 = (r_0, \theta_0, \psi_0)$ being the shower generation point; $z_0 = r_0 \cos\theta_0$; $\vec{r} = (\vec{r}, \theta, \psi)$ is the point under consideration; $z = r\cos\theta$; the spherical coordinate system is bound to a detector.

As far as a large core distances region is concerned a simple shower model-that of a moving point-is valid, i.e. we neglect the electron lateral distribution and take into account their angular distributions only. The direct optical radiation component is calculated on average. Use is made of a model of the angular distribution/6/, $f(\theta)$ where α is calculated using moments $\overline{\theta^2}$ also present in /6/. The cascade curve approximation used is

$$N(\varepsilon_0, \varepsilon, s) = \frac{\varepsilon_0^s}{(1+\varepsilon)^s} \cdot \frac{1}{q(s)} \quad (2)$$

where $\varepsilon = E D^{1/s}(s)/\beta$, $\varepsilon_0 = E_0 D^{1/s}(s)/\beta$, $\beta = 81$ MeV, D(s) and q(s) are the known cascade functions from /7/.

For the Cerenkov component E is the threshold energy of Cerenkov light, and for the fluorescent component $E = 0$. A charged particle is assumed to produce 5 photons over a meter of path due to the fluorescent mechanism. The scattered component was Monte-Carlo simulated. Over each segment of the shower trajectory, approximately 0.1 c.u. long, 6x13 photons(6 cells over the azimuth and 13 cells over the polar angle) were radiated and followed till their arrival at a detector, till their absorption by the Earth's surface, till their leaving the atmosphere or till their departure from a detector to a distance larger than some value. When arriving at a detector, a photon was given a weight factor proportinal to the overall light amount radiated by the shower electrons over a fixed trajectory segment and to the weight of angular cell from which centre of mass the photon has been radiated. The differential cross section of scattered light was, as in /4,5/, proportional to $(1+\cos^2\chi)$, where χ is the scattering polar angle. The data on the scattering length (molesular Rayleigh and aerosol) were taken from /8/. The detector comprised 200 temporal bins each of 10 ns and one integral bin for delays > 2000 ns. The angle 2π ster was devided into 120 bins (12 equal-size bins over the azimuth anglex10 equal-size bins over the polar angle) covering different solid angles(.04 ster to .08 ster). Though the program can simulate inclined showers, the present paper reports on the results for the vertical electron-photon showers with $E_0=10^{17}$eV for distances R=.5, 2.0, 8.0 km from detector. For a better comparison with the results of /4,5/ we considered production depth 119 g/cm^2(H=16.1 km) that yields t_m=896 g/cm^2 and the same distance $H_{obs}-H_m$=1.2 km, as in /4,5/. For each R the data on scattered light were obtained by averaging over 10 showers.

3.Simulation results. The lateral-angular distribution of the light in Fig.1(the solid curves are for the present calculation, the dash-dot ones - /4,5/- the sum of direct Cerenkov and fluorescent photons, the dashed curves are for scattered Cerenkov light/4,5/). All the data are divided by detector solid angles; The data /4,5/ are furthermore multiplied by $5\cdot10^5$ to allow for the differences in primary energies. The present paper data were selected from the bins facing the shower core. Unlike to the data /4,5/, our curves for scattered light do not reveal such an abrupt rise with zenith angle, though an increase of scattered light in the overall flux is noticeable even at R=.5 km that is explained by a decreasing contribution of the Cerenkov mechanism. At R=8 km, the two sets of data are the most similar, though some differences in intensity are observed which can be explained by the diversity between the cascade curves and solid angles of detectors in /4,5/ and present paper.

Fig.2 shows the data on FWHM τ of scattered light pulses. FWHM of the scattered component, according to our calculation, is noticeably broarder than that of the direct one(multiple scattering really matters) and increases with R, though slower than FWHM of the direct component. In the present paper FWHM increases with zenith angle similar to that in /4/. Fig.3 shows tipical pulses for the direct and scattered components(integrated over all bins facing the shower core).

References

1. Jelly J. Cerenkov radiation, Moscow, 1960.
2. Nesterova N.M., Chudakov A.E., 1962, JETP, 42, vyp6,1622.
3. Galkin V.I., Makarov V.V., 1983, 18th ICRC, v.6, 236.
4. Protheroe R.J., 1982, J. Phys. G., v.8, L165.
5. Protheroe R.J., 1983, Proc. 18th ICRC, v.6, 240.
6. Belyaev A.A. et al. Electron-photon showers in cosmic rays at superhigh energies, 1980, Moscow.
7. Belenky S.Z. Avalanche processes in cosmic rays, 1984, Moscow.
8. Martynov A.Ya. Course of applied astrophysics, 1964, Moscow.

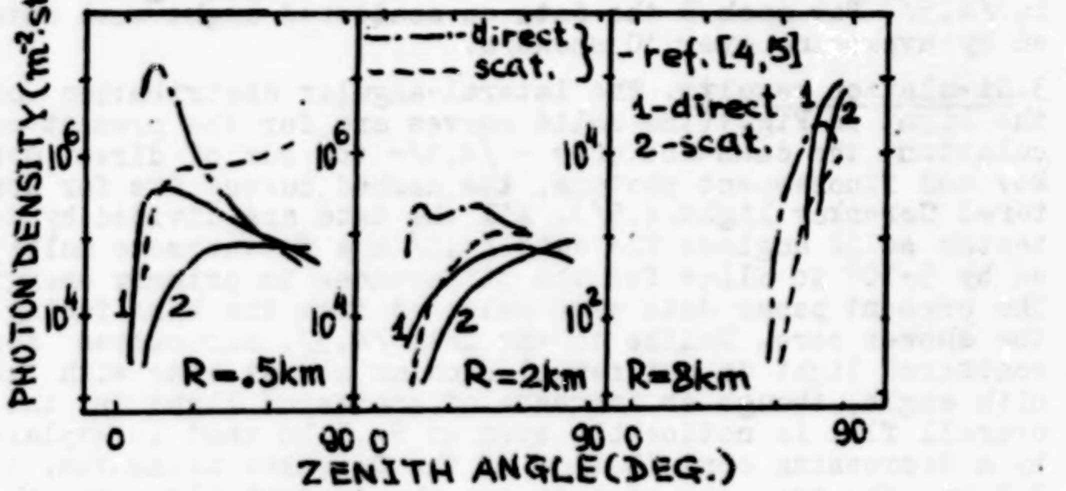

FIG. 1

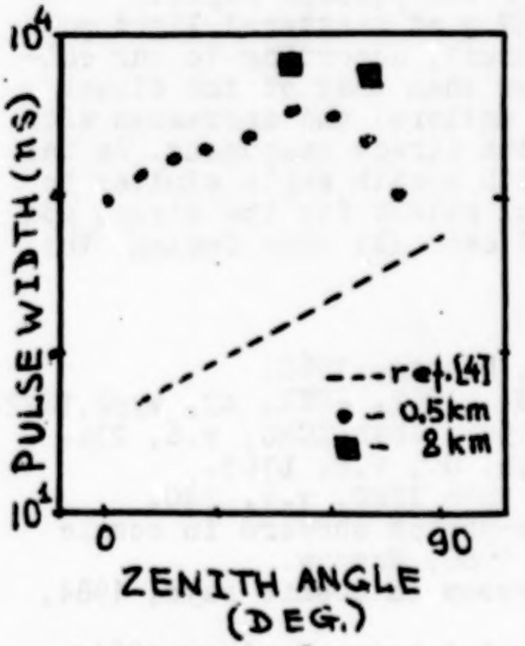

FIG. 2

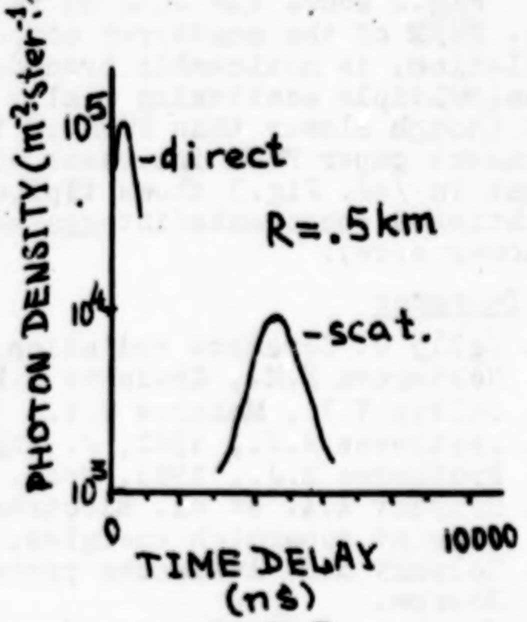

FIG. 3

N85-36026

THE IDENTIFICATION OF GAMMA RAY INDUCED EAS

P. R. BLAKE and W. F. NASH
Department of Physics, University of Nottingham, U.K.

Abstract

Recently Stanev et al have suggested that some of the penetrating particles in "gamma-induced" EAS from Cygnus X-3 observed by the Kiel EAS group using a single layer of flash-bulbs under 880 g cm^{-2} concrete, may be "punched through" photons rather than muons. This paper presents an analysis of the shielded flash-tube response from EAS detected at Haverah Park. The penetration of the electromagnetic component through 20 cm of Pb has been observed at core distances $\lesssim$ 10 m.

1. Introduction Experiments carried out by the Kiel group [1] indicated an excess of showers of size $N \geq 10^5$ arriving from the direction of Cygnus X-3. Further, these showers exhibited the 4.8 hour modulation characteristic of well-determined X-ray measurements. The excess EAS were assumed to be primary γ induced. Simulations by Wdowczyk et al [2], and McComb et al [3] comparing the muon densities from proton and gamma initiated showers of the same primary energy predicted that gamma induced showers would produce about 10% of total muons compared with proton induced showers.

Samorski and Stamm [4] (1983) used the Kiel array to investigate the muon content of the EAS produced by these "gammas" in the range $10^{15} - 10^{16}$ eV. The EAS detector consisted of 28 scintillator detectors of 1 m^2 each at distances up to 100 m from the centre of the array. A neon hodoscope of effective area 21.5 m^2 under 880 gm/cm^2 of concrete was used as a muon detector for muons of energy > 2 GeV.

In comparing the average number of muons in "on" and "off" source showers at core distances of approximately 10 m, they concluded that the difference in muon content of the two kinds of EAS was very small (< 20%). The densities of muons in the source showers appeared to increase more rapidly with shower size and fell more rapidly with core distance than normal showers.

Recently Stanev et al [5] carried out simulations in an attempt to explain this apparent discrepancy in the behaviour of "gamma induced" showers. Their calculations agreed with the work of McComb et al [3] in that only at $E_p > 10^{18}$ eV will photo production contribute a significant number of muons. In the primary energy range of the Kiel experiment, however, the number of photoproduced muons should still be very significantly less than the muon number in hadronic showers. Consequently Stanev et al investigated the number of photons that might "punch through" the 880 gm/cm^2 of concrete shield at approximately 10 m from the shower core. They concluded that only 30% of the muon density might be explained in terms of "punch through" gammas, assuming an overall detection efficiency for gammas of 40% for the neon flash bulbs.

2. Experimental Arrangement For several years the Nottingham group working at the Haverah Park EAS Array operated a detector of crossed neon flash tubes interleaved with lead absorber in order to identify and measure the arrival directions of muons.

The detector is shown in Figure 1. The top two boxes of crossed flash tubes (3.34 m²) have 5 cm of lead between them. The next two layers of flash tubes (4.18 m²) were covered by a further 5 cm and 10 cm of lead. Thus not only could the muons be clearly identified but the degree of accompaniment under 5, 10 and 20 cm of lead could be observed. The threshold energy for muons to penetrate the whole stack was approximately 350 MeV. Although this was less than that of the Kiel group, the number of cascade lengths of the total lead absorber compared with the concrete absorber was not significantly different.

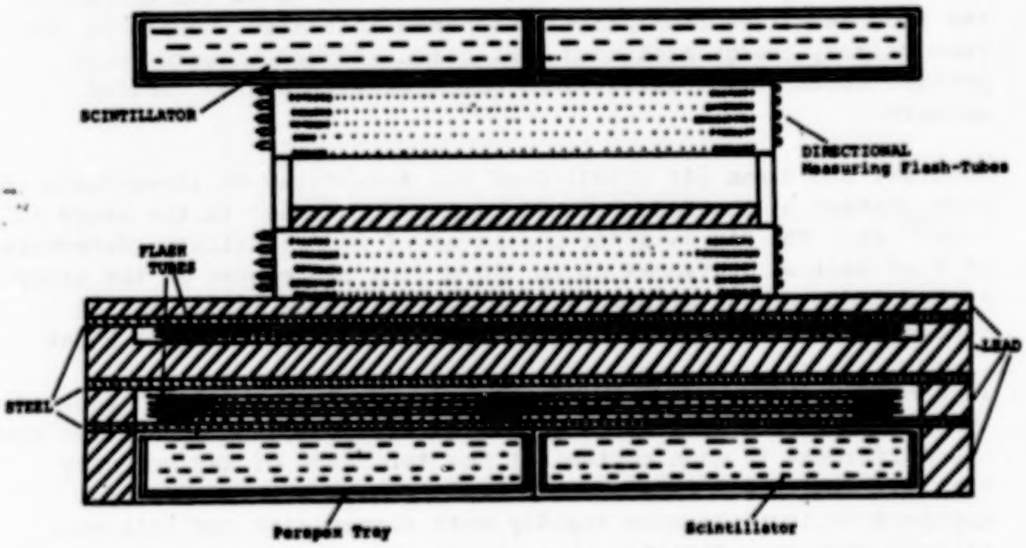

FIGURE 1 The neon-flash tube muon detector

3. Analysis of Data Normally EAS with $E_p \geq 10^{17}$ eV were recorded and for this "punch through" study EAS have been selected with well determined core distances such that 20 m < R < 100 m. The sandwich of flash tubes and absorber enabled the muons to be unambiguously identified. The number of muons detected in the shower was measured along with the degree of electromagnetic punch through accompaniment (excluding obvious muon-induced knock-ons and bursts), under 5, 10

ORIGINAL PAGE IS
OF POOR QUALITY

and 20 cm of lead. The water Cerenkov response at the same position in the EAS was also measured.

Figure 2 shows the frequency distribution of the electron accompaniment per muon capable of penetrating at least 5 cm of lead for two core distances, viz 20 m < R < 35 m and 20 m < R < 100 m. It is seen that within the statistical limits of the sample there is no significant change with limitation of the core distance to 35 m. The detected accompaniment per muon per flash tube layer under 5, 10 and 20 cm of Pb was found to be 2.48, 0.14 and 0.02 respectively. It is seen therefore from these observations that the degree of "punch through" from "normal" showers for 10 cm and 20 cm of lead is insignificant beyond 20 m from the axis. However this result may be attributed to the low photon energies found in EAS at these core distances.

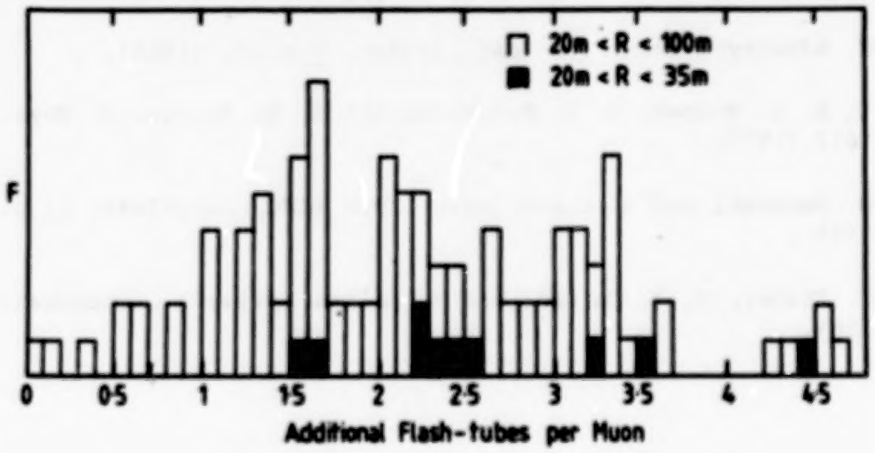

FIGURE 2 Frequency distribution of electron accompaniment/muon

It should be noted that the Kiel measurements applied to core distances around 10 m and the Stanev calculations were for such small core distances. It is in this region of the EAS that photons of energies 10-100 GeV have a significant probability of causing punch-through effects. For a period of time, apart from being triggered by the 500 m Air Shower Array at Haverah Park the muon flash tube detectors were also triggered from large bursts (detected by the fully-shielded scintillator) in "local" showers. The details of these showers was not determined directly but it was possible by determining the muon/electron density ratio to identify EAS falling within about 10 m of the core.

For these events the ratio of the number of detected accompanying "punch-through" particles to the number of muons was found to be approximately 2:1. With the limitations of the technique it would appear that the degree of accompaniment capable of "punching through" 20 cm of lead is significant at core distances $\lesssim$ 10 m.

4. Conclusion Analysis of the data obtained with a crossed flash tube/scintillator array indicates that the degree of "punch-through" accompaniment of muons from EAS of $E > 10^{17}$ eV for $R > 20$ m capable of penetrating 20 cm of lead and being detected by flash-tubes is negligible. However there is a strong indication that within a core distance $R \leq 10$ m there is a significant increase in such accompaniment. Thus in order to reduce the possible contamination of observations from such an effect it is therefore clear that observations of the muon content of showers should be made at core distances ≥ 20 m. If observations are to be made at core distances of < 10 m then the detector must be capable of unambiguously identifying muons.

References

[1] M. Samorski and W. Stamm, Ap. J. 268 L17 (1983).

[2] J. Wdowczyk, Proc. 9th ICRC, London, 2 p.691 (1965).

[3] T. S. L. McComb, R. J. Protheroe and K. E. Turver, J. Phys. G 5 1613 (1979).

[4] M. Samorski and W. Stamm, Proc. 18th ICRC, Bangalore, 11 p.244 (1983).

[5] T. Stanev, T. K. Gaisser and F. Halzen (private communication) 1984.

N85-36027

Muons in gamma showers

Todor Stanev[*] *and Ch. P. Vankov*[*]

Bartol Research Foundation of the Franklin Institute, University
of Delaware, Newark, DE 19716

Francis Halzen

Department of Physics, University of Wisconsin-Madison, Madison,
WI 53706

ABSTRACT

We study muon production in gamma-induced air showers, accounting for all major processes. For muon energies in the GeV region the photoproduction is by far the most important process, while the contribution of $\mu^+\mu^-$ pair creation is not negligible for TeV muons. The total rate of muons in gamma showers is, however, very low.

1. Introduction

There are two types of processes involved in generation of muons in electromagnetic showers: photoproduction and direct creation of muon pairs. In the photoproduction muons are generated through production and subsequent decay of mesons, thus in addition to the photoproduction cross-section one has to account for the meson interaction cross-section and the interaction-decay competition. At higher energies and in dense atmosphere mesons interact rather than decay and the resulting muon spectrum is steeper than the photoproduction one by one power of the energy. Directly produced muons are not affected by the production depth and their spectrum is a convolution of the photon energy spectrum and the pair creation cross-section.

We shall briefly discuss the cross-sections of both types of processes, introduce the techniques used in the calculations and show the muon production spectra for fixed primary energy. We shall use such spectra to estimate the total muon rates resulting from the observed gamma-ray fluxes of point sources.

2. Photoproduction and muon pair creation cross-sections.

Figure 1[*] shows the energy dependence of the photoproduction cross-section in air used in the calculation. It interpolates gamma-proton data and assumes a $A^{0.91}$ dependence on atomic number. After the resonance region below 1 GeV the cross-section shows a very slow logarithmic rise with the incident photon energy. A constant diffractive cross-section of 194 μb is asumed to result in ρ production. The electron photoproduction cross-section is shown on the same graph with dash line. Although this process has a significant cross-section, it does not contribute much to the muon production because the spectrum of the radiated virtual photons is very soft and the energy loss to photoproduction is small.

The lower part of the figure shows the cross-section for direct production of $\mu^+\mu^-$ pairs by photons in air. This process is analoguous to the creation of electron-positron pairs and in the assymptotic case of full screening of the nucleus field by the atomic electrons $\sigma_{\mu^+\mu^-}/\sigma_{e^+e^-}=(m/\mu)^2$. In addition to that the screening parameter $\zeta_\mu=\zeta_e(\mu/m)^2$ and the assymptotic cross-section for muon pairs is achieved for $E_\gamma >> 1$ TeV. In the very interesting region between 1 and 10 TeV the cross section increases by a factor of two. The corresponding process of muon pair production by electrons is of higher order and its cross-section is smaller at least by a factor of α.

All cross-sections shown on Fig. 1 are very small. Even at 1000 TeV their values are 2.4 and 2.1 *mb* for photoproduction by photons and electrons and 11.7 *μb* for muon pairs compared to the 502 *mb* cross section for e^+e^- pairs. Only a very small fraction of the shower energy goes into these channels and we can still use the cascade theory to estimate the shower size.

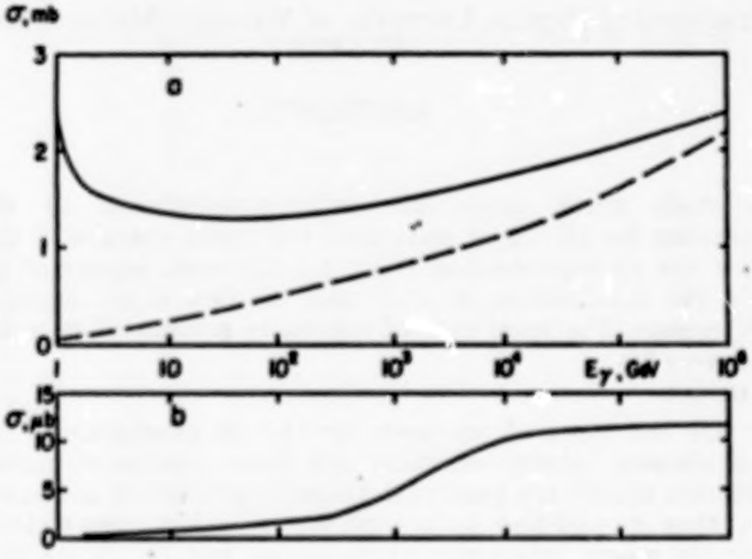

Fig. 1. Cross-sections for photoproduction by photons and electrons (dash line)$^{(a)}$ and for muon pairs creation$^{(b)}$ in air. Note the difference in the units (*mb* for photoproduction and *μb* for pair creation.

3. Calculational technique.

We have used two methods to calculate the muon production in gamma showers due to photoproduction. An electromagnetic Monte Carlo program was used to calculate the photoproduction at fixed primary gamma ray energy and all photoproduction events were recorded. Then the data files were treated with a hadronic Monte Carlo simulation program, which followed the muon production and propagation to the appropriate threshold energies. Results from these runs for GeV muons were discussed in Ref. 1. The same approach was used in Ref. 2 to calculate the number of TeV muons in gamma showers.

A numerical integration including the photoproduction energy spectrum and the three first generations in the hadronic cascades was also performed to check the Monte Carlo calculation and to extend the results for GeV muons to higher primary energies.

To calculate the number of muons with energy greater than E_μ in gamma showers of primary energy E_0 due to creation of muon pairs one has to evaluate the integral

$$N(>E_\mu) = \int_{E_\mu}^{E_0}\int_{E_\mu}^{E_0} \frac{dN_\gamma(E_0,E_\gamma)}{dE_\gamma}\sigma_{\mu^+\mu^-}(E_\gamma,E)\,dE\,dE_\gamma$$

where dN/dE_γ is the total number of γ rays in the shower. We evaluated the integral using the tracklength (total number of particles with energy E_γ in the cascade) given by Rossi [3] $g_o^{(\gamma)}(E_o,E_\gamma)=0.572E_o/E_\gamma^2$.

4. Results

The calculation confirmed that the number of GeV muons in gamma showers is at least one order of magnitude smaller than the number of muons in hadronic showers. For muon energy > 2 GeV we obtained a factor of 25 in the muon content of hadronic and electromagnetic showers for shower sizes between 10^5 and 10^6 particles at sea level. We also found that the fluctuations in the muon production are very large and most of the gamma showers will have only half of that amount of muons.

At muon energies below 1 GeV, where the muon decay is extremely important, the number of photoproduced muons grows in the same shower size region faster than linearly with the energy. We agree with the conclusions of McComb et al. [4] that at energies around 10^{18} eV the photoproduction will significantly contribute to the number of low energy muons.

Fig. 2 compares the production spectra of muons by photoproduction and muon pair creation in gamma showers with primary energy of 10^6 GeV. Photoproduced muons have integral energy spectrum of E^{-2} and directly created muons of $E^{-0.80}$. If the same trend continues at higher muon energies the production spectra will cross over at muon energies 10 TeV. At energy 3 TeV directly produced muons contribute about 1/4 of the total muon number.

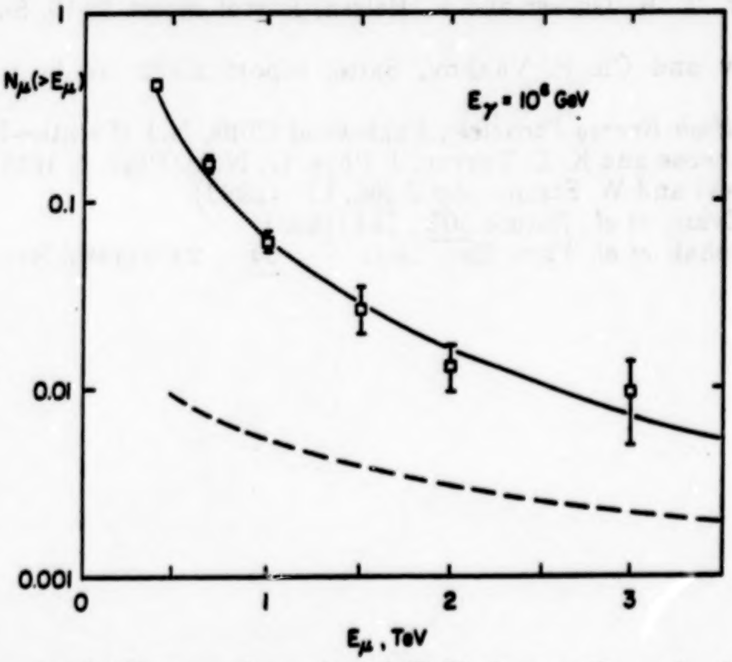

Fig 2. Muon production spectrum in 10^6 GeV showers through photoproduction and muon pairs creation (dash line).

5. Discussion and conclusion.

One can now use the flux of high energy γ rays measured at Kiel [5] $N(>E_\gamma)=6\times10^{-7}E_\gamma(GeV)^{-1.11} photons.cm^{-2}.s^{-1}$ with cut-off at 10^7 GeV as suggested by the measurement at Haverah Park [6] and calculate the flux of muons at different depths underground due to both photoproduction and pair creation. The vertical muon flux resulting from this photon flux at depths 2 and 4 km.w.e. underground are respectively 1.60×10^{-13} and $2.05\times10^{-14} cm^{-2}\times s^{-1}$. These rates are very low and the expected muon rates in a 1000 m^2 detector are respectively 45 and 6 yr^{-1}. For the 0.92 yrs running time of the 9 m^2 Soudan [7] detector the expected number of muons from gamma showers is 0.4.

Gamma showers are inefficient in producing muons in the TeV as well as in the GeV region. The photon induced air showers are "mu-poor" and this feature can be used as identification signature. It is not possible to understand the underground muon signals from point sources[7] as a result of photon showers in the atmosphere.

Acknowledgements

The authors gratefully acknowledge the participation of T.K. Gaisser in this work through numerous discussions and reading the manuscript.

This work was funded in part by the U.S. Department of Energy under contract DE-AC02-76ER00881 (F.H.) and by the National Science Foundation under Grant PHY-8410989 (T.S.) and the U.S.-Bulgaria Cooperative Research Program (Ch.P.V.). Ch.P.V. would like to thank Bartol Research Foundation for its hospitality.

References

(*) Permanent address: Institute for Nuclear Research and Nuclear Energy, Sofia 1184, Bulgaria.

(1) T. Stanev, T. K. Gaisser and F. Halzen, Bartol report 85-10, Submitted to Phys.Rev.D.
(2) T. Stanev and Ch. P. Vankov, Bartol report 85-22, To be published in Phys.Lett.B.
(3) B. Rossi, *High-Energy Particles* , Englewood Cliffs, N.J. (Prentice-Hall, 1952).
(4) R. J. Protheroe and K. E. Turver, J. Phys. G: Nucl. Phys. 5, 1613 (1979).
(5) M. Samorski and W. Stamm, Ap J 268, L17 (1983).
(6) J. Lloyd-Evans *et al.*, Nature 305 , 784 (1983).
(7) M. L. Marshak *et al.*, Phys. Rev. Lett. 54 , 2079 (1985) Rev. Lett.

N85-36028

HE 4.5-4

MUON SPECTRUM IN AIR SHOWERS INITIATED BY GAMMA RAYS

S.A. Stephens
Tata Institute of Fundamental Research
Homi Bhabha Road, Bombay 400005, India

R.E. Streitmatter
NASA/GSFC, Maryland 20771, U.S.A.

ABSTRACT

We have derived an analytic representation for the invariant cross-section for the production of charged pions in γP interactions by making use of the available cross-sections. Using this the abundance of muons in a gamma ray initiated air shower is calculated.

1. Introduction. Total hachonic cross-section of γ-rays at energies greater than a few GeV is about two hundred times smaller than hadron inelastic cross-section. Therefore, hadron production by γ-ray showers in the atmosphere is neglected for the study of muons. However, the discovery of pure γ-ray air showers from Cygnus X-3 [1] has renewed interest in this study, because of the observed muon content in these air showers is not very small compared to those from hadron showers. We have attempted in this paper to derive an analytic representation for the invariant cross-section for the production of charged pions in γ-P interaction, using the available data. Making use of this, the pion production spectrum in the atmosphere is calculated for an air shower initiated by γ-rays and muon spectrum at different depths is determined.

2. γ-P Inclusive Cross-section. The frame in which particle production is symmetric in γ-P interaction is found to be the one in which the ratio, Q, of the target momentum to the beam momentum is larger than 1. Experiments performed at energies >a few GeV show that the value of Q lies between 2 and 3 [2-5]. However, at low energies, where P_{33} and D_{13} resonances dominate, the threshold is consistent with that of centre of mass system (CMS) with Q = 1. Therefore, we assume in our investigation that Q is energy dependent of the form

$$Q = 1. + 2. \exp(-m_p/E_\gamma) \qquad (1)$$

From a study of the observed invariant cross-section for the production of charged pions, we obtained a representation of the type

$$E \frac{d^3\sigma}{dp^3} = f(E_\gamma) \exp(-C_1\mu) . \exp(-C_2 x^{-1.5})/\{1.+C_3/(1-p^*/p^*_{max})\} \ldots \qquad (2)$$

Here $\tilde{x} = \sqrt{\{x'^2_{11} + Q(p^2_\perp + m^2_\pi)/S\}}$ and $\mu = \sqrt{(p^2_\perp + 9m^2_\pi)}$, where $x'_{11} = p'_{11}/p^*_{max}$, C_1, C_2 and C_3 have values 6.93, 3.4 and 0.03 respectively. The longitudinal momentum in the Q-system is given by

$$p'_{11} = \{p(S'+m_p^2)-E(S'-m_p^2)\} / 2m_p \sqrt{S'} \qquad \ldots \qquad (3)$$

In the above expressions $S = m_p(m_p+2E_\gamma)$, the square of the invariant mass and $S' = m_p(m_p+2QE_\gamma)$. The last term in Eqn. (2) makes sure that the momentum of pions p^* in CMS does not exceed the maximum allowed momentum p^*_{max}. It is clear that Eqn. (2) is symmetric in Q system except at large values of $\tilde{x}$ due to this restriction.

We have shown in Figure 1, the invariant cross-section for the production of $(\pi^+ + \pi^-)$ as a function of $x^*_{11} = p^*_{11}/p^*_{max}$ for various values of $p_\perp$ at E_γ values 18 and 6 GeV [3,6]. The general fit to this data using Eqn. 2 is very good. Notice that the invariant cross-section does not peak at $x^*_{11} = 0$. The measured $2\int E(d^3\sigma/dp^3)p_\perp\, dp_\perp$ is shown in Fig. 2, for various $p_\perp$ intervals. The filled circles, triangles and squares correspond to respectively data from 9.3, 4.7 and 2.8 GeV. The data plotted in this figure relate to π^- production only. Here again one finds that the overall fit to the data is remarkably good.

The form of the function $f(E_\gamma)$ is $A[1+g(E_\gamma)]$. In order to evaluate this, we have adopted the following procedure. In the energy region between about 2.5 and 20 GeV, we have made use of the measured cross-sections given in Figures 1 and 2 and the observed π^+/π^- ratio of ≈ 1.1 [2,3,6]. For the rest of the energy region, we have made use of the observed multiplicity in PP collisions with the assumption that multiplicity depends only on the available energy in CMS. It is found that at large E_γ values the observed $< m_\pi >$ agrees well with that calculated using PP data [7,8]. However, in the region, where ρ production dominates, the $< m_\pi >$ in γP interaction is larger. Therefore, at low energies, we have smoothly fitted from the observed data at 2.8 GeV to one pion production region. By setting $<m_\pi^\pm> \sigma_T = 2\pi \int\int^{p^*_{max}} (Ed^3\sigma/dp^3)\, p_\perp\, dp_\perp/E^*$ and using the observed σ_T values [9,10], we found that A=4.7 and $g(E_\gamma)$ as

$$\begin{aligned} g(E_\gamma) &= 3350\,(E_\gamma+10)^{-3.5} && E_\gamma \geq .86 \text{ GeV} \\ &= 125\,\exp(-5.6\,E_\gamma) && .725 \leq E_\gamma \leq .86 \\ &= 3.5\,E_\gamma^{1.5} && .625 \leq E_\gamma \leq .725 \qquad \ldots \qquad (4) \\ &= 1.73 && .49 \leq E_\gamma \leq .625 \\ &= 1620\,\exp(-14E_\gamma) && .315 \leq E_\gamma \leq .49 \end{aligned}$$

The above expressions approximately characterize Δ(1232), N(1520) and N(1680) resonances well within a few percent.

From our investigation, we need to know the cross-section for γ-air nuclei interactions. In order to obtain information on this, we have examined the asymptotic total cross-sections for γP, γD, πP, πD, KP, KD, PP, PD, $\bar{P}P$ and $\bar{P}D$ interactions [10]. It is found that photo-hadron cross-section scales exactly as other hadron-hadron cross-sections with atomic number of the target. Therefore, we made use of the scaling for proton interactions and obtained γ-air inclusive cross-section as $\sigma_T < A >_{air}/1.8$.

ORIGINAL PAGE IS
OF POOR QUALITY

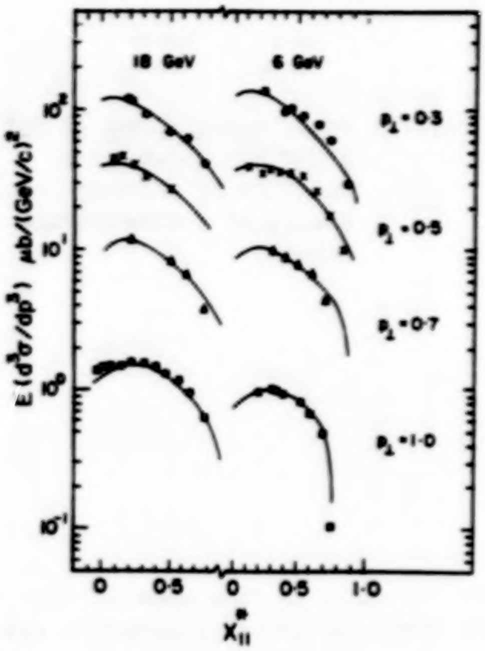

Fig. 1 *Invariant cross-section for $(\pi^+ + \pi^-)$ is shown as a function x^*_{11} for E_γ = 18 and 6 GeV*

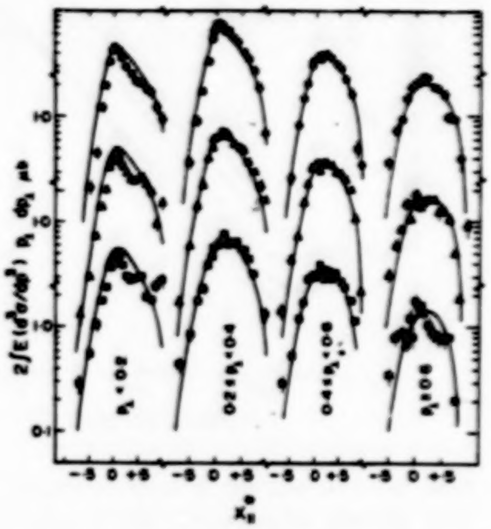

Fig. 2 *π^- invariant cross-section integrated over $p_\perp$ is shown for different $p_\perp$ intervals. The filled circles, triangles and squares correspond to E_γ = 9.3, 4.7 and 2.8 GeV respectively.*

3. Muon Production in γ-ray Showers. Pion production spectrum in the atmosphere is given by

$$P_\pi(E,x) = \iint J_\gamma(E_\gamma,x)\,dE_\gamma \;.\; \{2\pi\ (E\ d^3\sigma/dp^3)p_\perp\ d\theta \quad \dots \qquad (5)$$

Here, the photon spectrum J is obtained using one dimensional propagation of cascade initiated γ-rays in the atmosphere without approximations [11]. From this the spectra of pions and muons in the atmosphere are calculated by taking into account the decay, energy loss processes and the 2nd generation of pions as described by Stephens [12].

In Figure 3, we show the preliminary results based on a representation of invariant cross-section, which has the same form as that for π^0-inclusive production. The integral flux muons is shown as a function of primary γ-ray energy for different energy thresholds and for a few sample depths. It is seen that the total muon flux is small at all depths and therefore, the observed large flux of muons with γ-ray showers associated with Cygnus X-3 [1] could be due to other reasons.

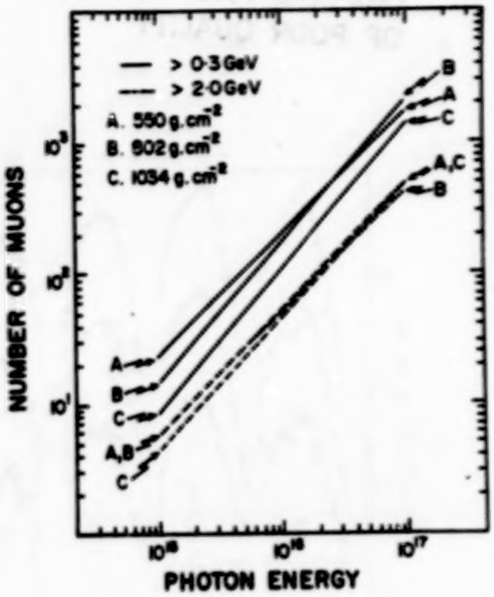

Fig.3 Total muons above .3 and 2 GeV are shown as a function of primary γ-ray energy at 3 atmospheric depths.

One of the possible explanation for this anomaly is that some of the air shower electrons and photons, which continue their propagation are registered by the muon detectors.

References

[1] M. Samorski and W. Stamm, Ap.J., 268, L17 (1983)
[2] P. Rankin, Ph.D. Thesis, Imperial College, London (1982)
[3] A.M. Boyarski et al., Phys. Rev., D14, 1733 (1976)
[4] K.C. Moffeit et al., Phys. Rev., D5, 1603 (1972)
[5] G. Alexander et al., Phys. Rev., D8, 712 (1973)
[6] H. Burfeindt et al., Nuclear Phys., B74, 189 (1974)
[7] G.D. Badhwar et al., Phys. Rev. D15, 820 (1977)
[8] S.A. Stephens and G.D. Badhwar, Ap.Sp. Sci., 76, 213 (1981)
[9] T.A. Armstrong et al., Phys. Rev., D5, 1640 (1972)
[10] M.A. Benitez et al., Rev. Mod. Phys., 56, No.2 (1984)
[11] R.E. Streitmatter and S.A. Stephens (This Conference)
[12] S.A. Stephens, Proc. 16th ICRC (Kyoto), 10, 90 (1979)

HE 4.5-5

N85-36029

DEVELOPMENT OF ELECTROMAGNETIC CASCADES IN THE ATMOSPHERE INCLUDING THE LANDAU-POMERANCHUK-MIGDAL EFFECT

R. E. Streitmatter and S. A. Stephens*
NASA/Goddard Space Flight Center, Greenbelt, MD 20771, U.S.A.

ABSTRACT

Numerical solutions have been obtained for the one-dimensional atmospheric electromagnetic cascade diffusion equations, including the LPM and screening effects. Spectra produced by primary gamma rays of various energies are given at a number of depths in the atmosphere.

1. Introduction. As the first step in a program to calculate the muon content of gamma-ray-induced atmospheric showers (1), we have carried out numerical solutions of the 1-dimensional electromagnetic cascade diffusion equations (2).

We have attempted to carry out a calculation with a minimum of approximation. The Landau-Pomeranchuk-Migdal (LPM) effect (3,4) on pair-production and bremsstrahlung cross sections has been included. The LPM cross sections were calculated using the formalism of Bowen *et al.* (5). Atmospheric densities were taken from the U. S. Standard Atmosphere. Constant collisional energy loss was included. Lastly, the effects of incomplete screening (6) were included.

The diffusion equations were integrated using the Runge-Kutta method. An initial condition of a single gamma ray vertically incident on the atmosphere was used. Electron and photon spectra down to 10 MeV were found throughout the atmosphere. Solutions have been obtained for incident gamma ray energies ranging from 10^{14} to 10^{19} eV. As a check, the LPM and incomplete screening effects can be removed, yielding the classical complete screening cross sections. In this case, the solutions obtained agree with Approximation B.

Figure 1 shows the atmospheric development of the integral electron spectra above 10 MeV for 6 incident gamma ray energies. Generally, the effects of the LPM cross sections on the integral spectrum are most pronounced at shallow atmospheric depths. For a 10^{19} eV incident gamma, at 550 g/cm^2 the ratio of the Approximation B integral spectrum (not shown here) above 10 MeV to the integral spectrum of Figure 1 is 1.56. At 1034 g/cm^2, the same ratio is 0.95.

Figures 2 and 3 show the differential electron spectra at 550, 700, 800, 900, and 1034 g/cm^2 for incident 10^{14} and 10^{16} eV gammas, respectively. While there are differences between this spectra and the corresponding Approximation B spectra at the 15 percent level, only above 10^{18} eV do the differential electron and photon spectra sharply and progressively deviate from the Approximation B spectra. Figure 4a shows the differential electron spectra induced by a 10^{19} eV gamma, again at the same 5 atmospheric depths as the previous figures. Figure 4b, plotted to the same scale, shows the Approximation B spectra.

---

* Tata Institute of Fundamental Research, Bombay, INDIA

References

1. Stephens, S. A., and Streitmatter, R. E., This Conference, HE 4.5-4.
2. Rossi, B., 1952, High Energy Particles, 214.
3. Landau, L. and Pomeranchuk, I., Dokl. Akad. Nauk SSSR, 1953, 92, 535.
4. Migdal, A. B., Phys. Rev., 1956, 103, 1811.
5. Bowen, T., et al., 1979, At. Data Nucl. Data Tables, 24, 495.
6. Bernstein, I. B., 1956, Phys. Rev., 80, 995.

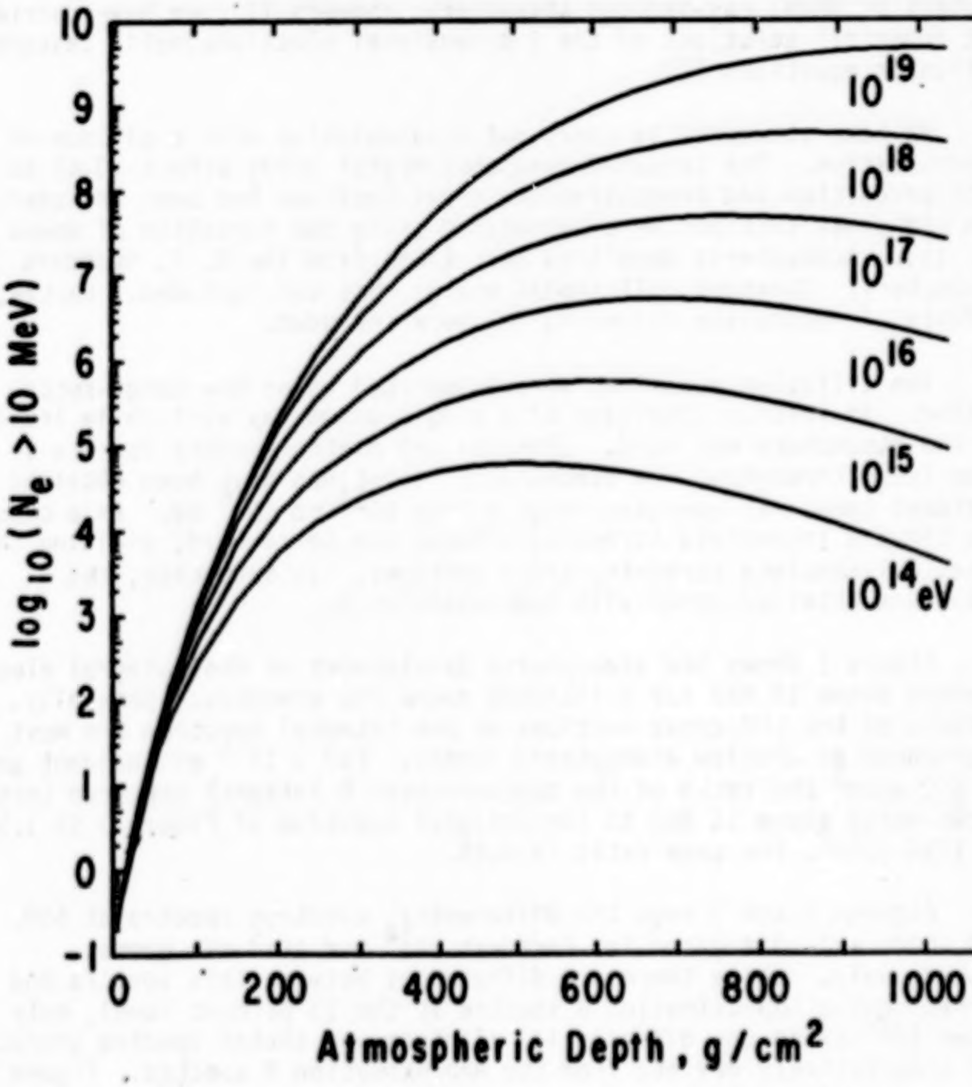

Figure 1.

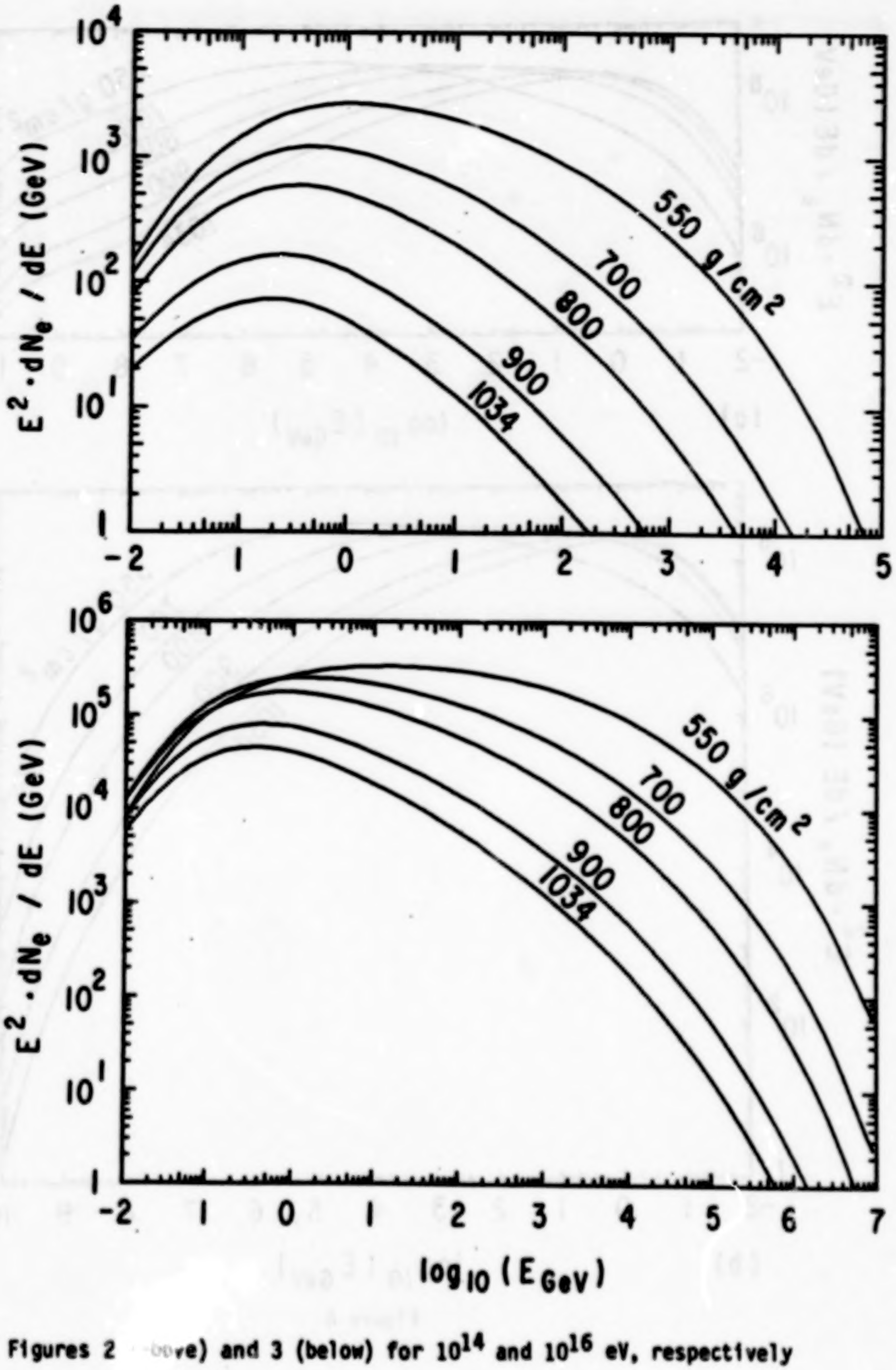

Figures 2 (above) and 3 (below) for 10^{14} and 10^{16} eV, respectively

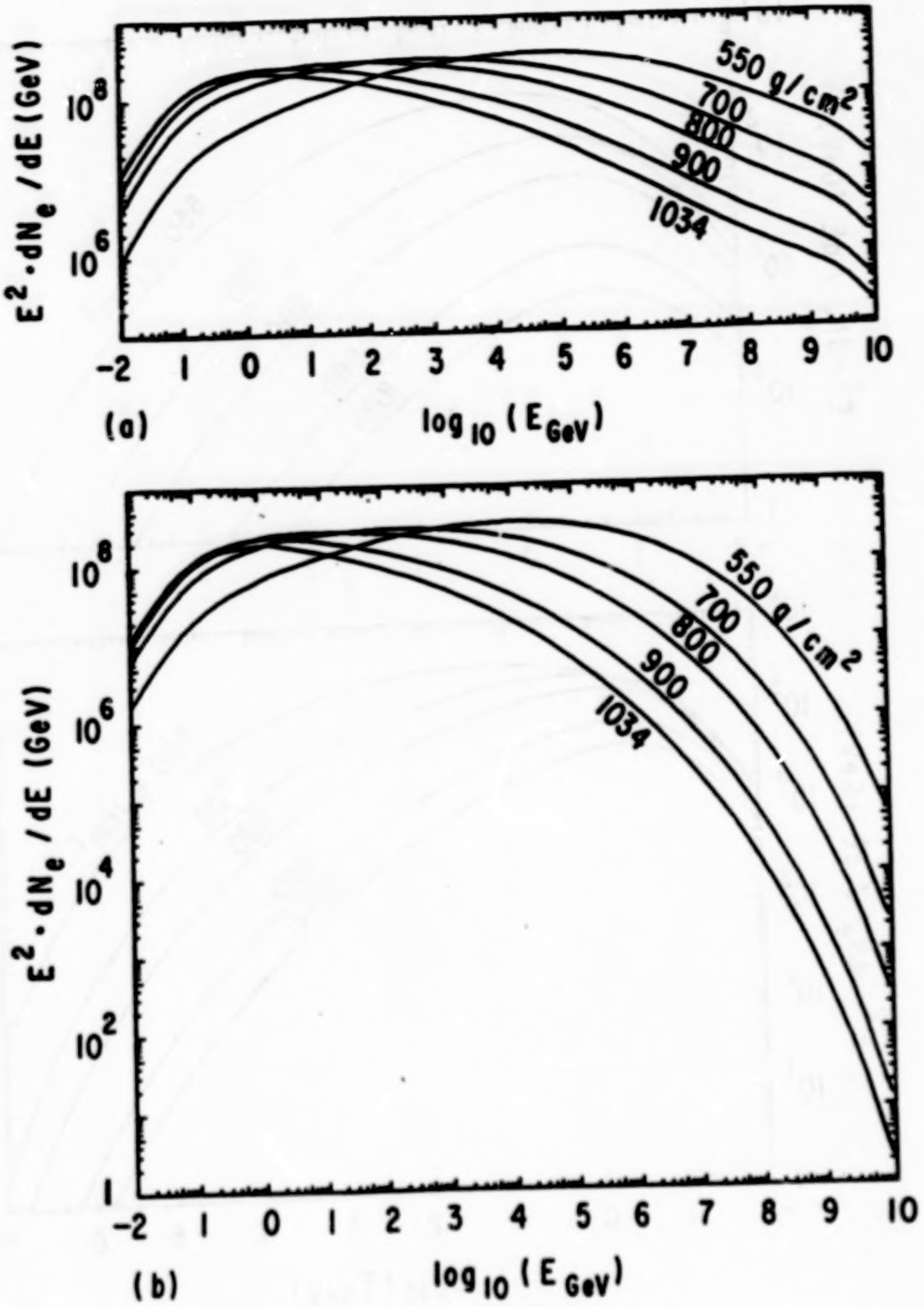
$E^2 \cdot dN_e/dE$ (GeV)
10^8
10^6
550 g/cm^2
700
800
900
1034
-2
1
0
1
2
3
4
5
6
7
8
9
10
(a)
$\log_{10}(E_{GeV})$
$E^2 \cdot dN_e/dE$ (GeV)
10^8
10^6
10^4
10^2
1
550 g/cm^2
700
800
900
1034
-2
1
0
1
2
3
4
5
6
7
8
9
10
(b)
$\log_{10}(E_{GeV})$

Figure 4

N85-36030

HE 4.5-6

ELECTROMAGNETIC AND MUONIC STRUCTURE OF SHOWERS INITIATED BY GAMMA-RAYS AND BY HADRONS

A. M. Hillas
Physics Department, University of Leeds,
Leeds LS2 9JT, UK

ABSTRACT

(a) If photon cascades develop by the usual mechanisms, there should indeed be notable differences between the structure of showers due to photon and hadron primaries, as regards muon densities and lateral distributions of some detector signals.

(b) The muon content of showers from Cygnus X-3, observed at Kiel, cannot be understood in this way. One remedy is to postulate arbitrarily a strong hadronic interaction of photons in the TeV region. This would utterly change the nature of electromagnetic cascades, but surprisingly does not at first sight seem to be in conflict with air shower observations.

1. Two questions concerning gamma-ray initiated showers

(i) Can the structure of extensive air showers (10^{15} - 10^{16} eV) be used to distinguish those that are initiated by primary gamma-rays from the normal proton- or nucleus- initiated showers? This would help in observations of point sources such as Cygnus X-3. The low muon content of gamma showers has been regarded as their most obvious hallmark, with different shower "age" as another possible distinguishing feature. However,

(ii) can one understand the observation by Samorski & Stamm (1) that showers from Cygnus X-3 (whose primaries are undeflected and stable, and hence presumably photons) have about 2/3 of the normal density of penetrating particles (muons of 2 GeV or more) at ~10 m from the shower axis?

If the directional particle fluxes being reported from various proton decay experiments are confirmed, they indicate that the radiation from Cygnus X-3 has important interactions that are not yet understood.

2. Calculation of shower development

A 3-dimensional Monte-Carlo simulation is used to follow all particles (electrons, photons, nucleons, pions, muons — but omitting kaons) down to 0.05 MeV, and to determine the signals produced in 5-cm-deep scintillators and 120-cm-deep water Cerenkov detectors (as used at Haverah Park). (The average response of such detectors — covered by a thin wood roof — to the relevant particles and energies was calculated beforehand, but, as a check, the shower particles were followed into a 120-cm-deep lake on reaching the ground, where their Cerenkov emission was noted and the ionization loss in the top layer was also noted to check the scintillator response.)

Assumptions about hadronic interactions of photons: Up to several GeV, $\sigma(\gamma, \text{air nucleus} \rightarrow \text{hadrons}) = 6.4\,\sigma(\gamma, \text{deuteron})$. The intermediate states produced in the well-known resonances below 1 GeV were taken to decay isotropically (in c.m.s.) as an approximation, in 2-body stages. However, these resonances are of little importance in EAS: most of the muons resulting (via pion decay) are of such low energy that they stop — and certainly none is above 2 GeV. From 10 GeV to 200 GeV the cross-section is taken to be 1.42 mb, and then to rise rather like p-p cross-sections — i.e. $1.42\,(1 + 0.0273u + 0.01u^2)$ mb, where $u = \ln(E/200\,\text{GeV})$. Interacting photons are taken to behave very much like pions.

Assumptions about hadron interactions. Two models of hadronic interactions are used: (a) a radial scaling model (with rising hadron-nucleon cross-sections), based on detailed accelerator data up to 1 TeV, but making the approximation of working with scaling in the laboratory frame of reference (thus underestimating a little the particles below ~1 GeV); (b) a modification in which a greater multiplicity of low-x particles is generated (but without a large reduction in the fragmentation-region particles) at collision energies above ~1 TeV, and fewer leading pions are produced. These two variants are thought to bracket the true main features of interactions. Roughly speaking, the first model with a large content of very heavy nuclei in the primary beam, or the latter with largely protons, would account for many air shower features.

3. Proton-initiated and gamma-initiated showers

Figure 1 shows the apparent particle densities ρ at various axial distances, in showers produced by normal primaries of 10^{14}, 10^{15}, 10^{16} and 10^{17} eV per nucleon, and by gammas of 10^{15} and 10^{16} eV, all at 15° zenith angle. All are normalized to 10^{16} eV energy, by plotting $r^2\rho/E_{16}$, where $E_{16} = E_{prim}/10^{16}$ eV. Particle densities recorded by deep water tanks, and muon densities above 0.4 GeV (as at Haverah Park). Graphs 1(a) and 1(b) use the two different hadronic interaction models. Muon densities, in the lower part of the graphs, are shown by thinner lines. The gamma showers (-.-.-.-) differ from the proton showers by having a very much lower muon density — as expected from calculations by Wdowczyk long ago (2), and this helps to make the overall particle density fall more steeply beyond 200m — though this effect is less marked in scintillators.

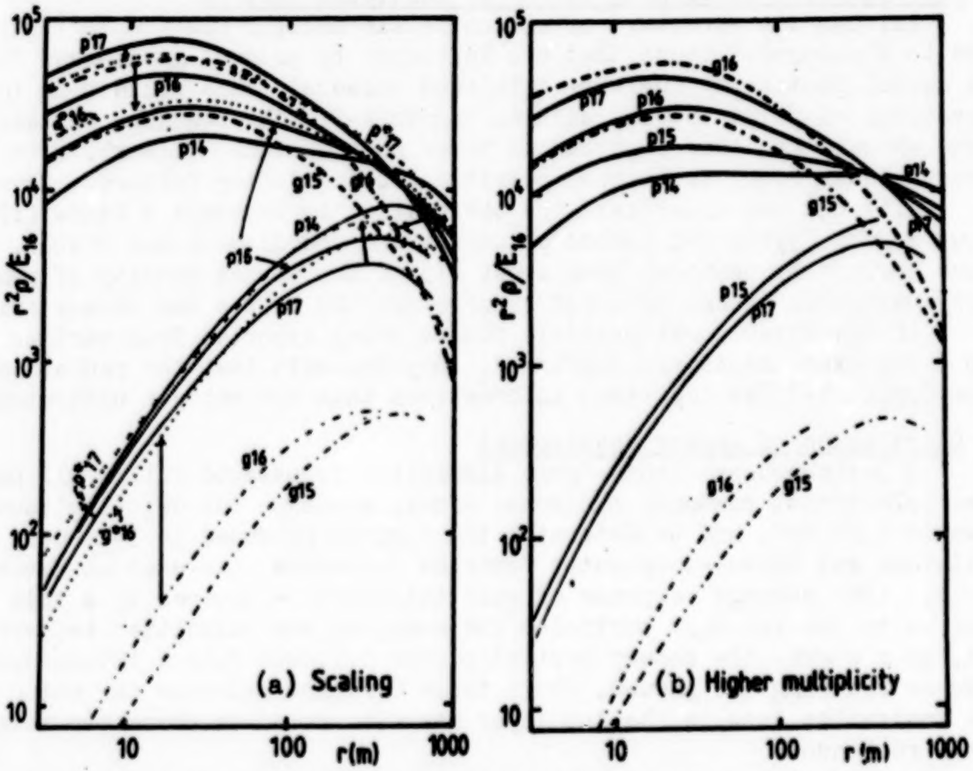

Figure 1: Particle densities (in water tank) and muon densities in proton and gamma-initiated showers at 15° to vertical (Sea level).

ORIGINAL PAGE IS
OF POOR QUALITY

As an alternative to muon detection may be to compare particle densities recorded by deep and shallow detectors, the ratio of (120 cm) water tank signal (ptcle. density) to (5 cm) scintillator density is plotted in Figure 2 for 10^{16} eV proton showers (line and dashed curve show results from the two models) and gamma showers (dotted curve). Mean ratios in showers of ~3×10^{16} eV at ~13° zenith angle have been observed for ordinary real showers (filled circles: J. Perrett & A. A. Watson, private communication), and agree fairly well with expectation. (The sensitivity to the proportion of heavy nuclei is not calculated here, but is not a major factor in the present comparison.) Measurements are required beyond 100m with very large detector areas to make use of the expected peculiarities of individual gamma showers.

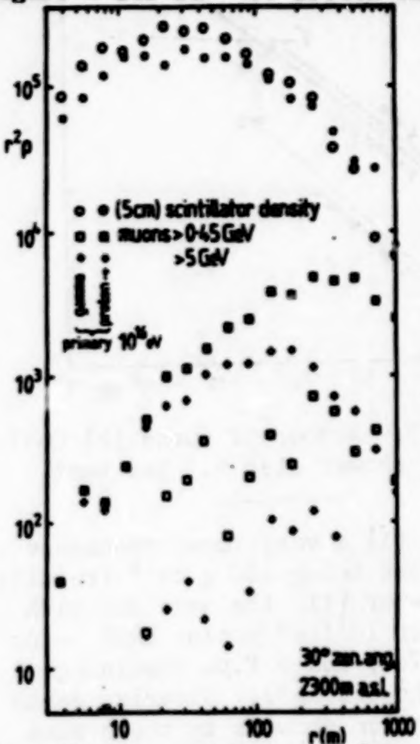

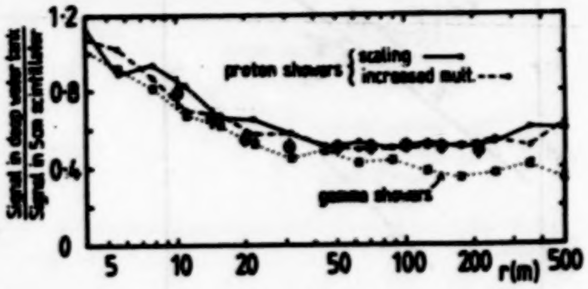

Figure 2 (↑). Ratio of particle densities recorded by two detectors in proton and gamma showers at various axial distances. (Sea level: zenith angle 15°: energy 10^{16} eV or thereabouts.)

← Figure 3. Predicted particle densities ρ in proton (filled symbols) and gamma showers (open symbols) of 10^{16} eV at high altitude site (2300 m). Showers at 30° zenith angle. Detectors are 5-cm scintillators.

Figure 3 shows what is expected (from the scaling model) at a high level observing station (2300m altitude), looking at 10^{16} eV gamma showers and proton showers at 30° zenith angle (typical for Cygnus X-3). Scintillator particle densities are plotted. The statistical accuracy of this simulation run for gamma showers is too low to give a good determination of their muon densities, though the shape of the muon curve should be very similar to the curves in Figure 1.

4. Do gamma-rays produce hadrons much more frequently?

This would, of course, invalidate the previous graphs.

Figure 4 shows the density of muons above 2 GeV at 10m from the shower axis, interpolated from the calculations for protons (line p – both models agree here) and gammas (line g). A line for iron primaries (Fe) is also shown. The Kiel results (1) for nuclear and (presumed) gamma showers are marked. There is a huge discrepancy. So, do electrons or photons of high energy generate pions or muons readily by some unknown process? Would this not wreck all interpretations of air showers?

To begin an exploration of the latter question, a quite arbitrary large addition has been made to the hadronic cross-section for photons at

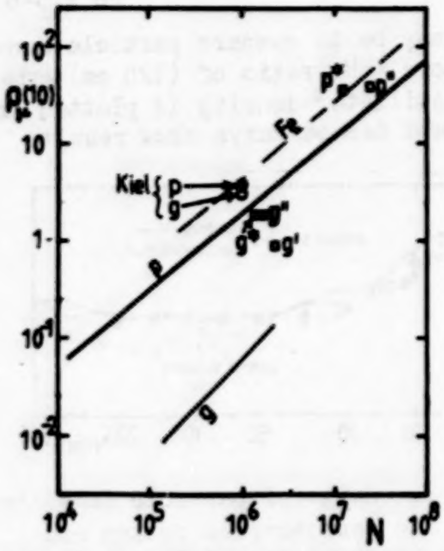

Figure 4. Densities of muons (>2 GeV at 10 m from shower axis in nuclear (p,Fe) and gamma (g) showers.

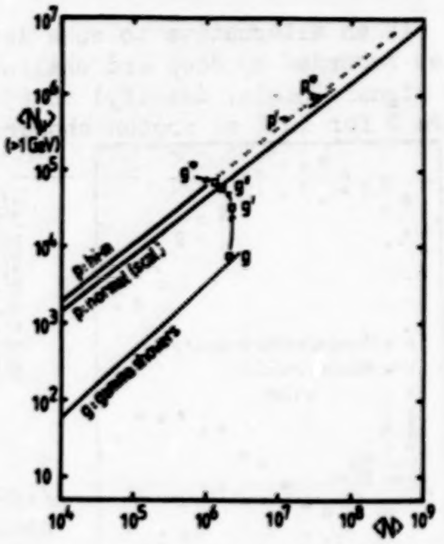

Figure 5. Number of muons (>1 GeV) & total shower size N. See text.

high energy (no change below 1 TeV) — either (i) a very broad resonance at a few TeV, the interaction m.f.p. at its peak being 100 g cm^{-2} (result: muon density in gamma showers shown as g') — or (ii) the same but with m.f.p. 40 g cm^{-2} at peak (g" , and point p" for 10^{17} eV proton EAS) — or (iii) cross-section having threshold above 1 TeV, and m.f.p. remaining at 100 g cm^{-2} above 10 TeV (g* and, for proton showers, p*). Clearly, gamma showers are now hardly distinguishable from proton showers by their muon content — and their lateral distributions become more similar. (See Fig. 1: the line ...... shows the modified 10^{16} eV gamma showers, g*, and the line — — — shows the resulting change to the structure of ordinary 10^{17} eV proton showers. The latter are in fact a surprisingly good fit to observations!)

One would expect the N_μ-N_e relationship for showers to be spoiled — perhaps $N_\mu \propto N_e$ now? Figure 5 shows that this is not the case. (The mean N_μ (E_μ>1 GeV) is plotted against total number of particles (N) in the shower. For the purpose of this simple test only the averages <N> for fixed $E_{primary}$ are plotted, without applying the small correction for primary spectrum selection bias.) Such an (arbitrary) assumption about photon interactions would also be expected to ease the problem of accounting for the ratio of multi-TeV hadrons and gammas in the atmosphere.

The alternative of considering direct muon production, or production via charm rather than by pions, has not been explored. Pions have the advantage of putting their energy into many lower-energy muons, after cascading.

Such a large hadron-like cross-section has no theoretical justification: can it really be possible? It would perhaps not have been noticeable in emulsion calorimeters with short (Pb) radiation lengths.

References

1. Samorski, M. & Stamm, W. (1983) 18th Int. C. R. Conference, Bangalore, 11, 244-7.
2. Wdowczyk, J. (1965) 9th Int. Conf. on Cosmic Rays, London, 2, 691-3

N85-36031

HE 4.5-7

THE MUON CONTENT OF GAMMA-RAY SHOWERS

P.G. Edwards and R.J. Protheroe
Department of Physics, University of Adelaide
Adelaide, South Australia 5001

Abstract. We report the result of a calculation of the expected number of muons in γ-ray initiated and cosmic ray initiated air showers using a realistic model of hadronic collisions in an effort to understand the available experimental results and to assess the feasibility of using the muon content of showers as a veto to reject cosmic ray initiated showers in ultra-high energy γ-ray astronomy. We also consider the possibility of observing very-high energy γ-ray sources by detecting narrow angle anisotropies in the high energy muon background radiation.

1. *INTRODUCTION.* With the recent observation of ultra-high energy (UHE) γ-rays from Cygnus X-3 (Samorski and Stamm, 1983a; Lloyd-Evans *et al.*, 1983), Vela X-1 (Protheroe *et al.*, 1984) and LMC X-4 (Protheroe and Clay, 1985), together with the detection of excess air showers from the direction of the Crab Nebula (Dzikowski *et al.*, 1983; Boone *et al.*, 1984), it is timely to examine the muon content of extensive air showers (EAS) initiated by primary γ-rays to investigate the possibility of: (a) using a "normal" muon content to veto some fraction of cosmic ray (CR) showers; and (b) detecting γ-ray sources at very-high energies through observing narrow angle anisotropies in the muon background radiation.

Measurements of the muon content were made in two of the recent source observations, that of Cygnus X-3 by the Kiel group (Samorski and Stamm, 1983b) and that of the Crab by the Lodz group (Dzikowski *et al.*, 1983). Early predictions of muons in γ-ray EAS (Karakula and Wdowczyk, 1963; Wdowczyk, 1965; Braun and Sitte, 1965) together with later work on muons of photoproduction origin in CR EAS by McComb *et al.* (1979), had led us to expect that at 10^{15}–10^{16} eV energies γ-ray initiated EAS would have a muon content about one tenth of that of proton-initiated EAS. The ratio of muon number in the excess EAS to that in CR EAS was measured to be somewhat higher in the two recent experiments, however: about 0.6 for the observation of the Crab and about 0.7 for the Cygnus X-3 observation. This surprising result appeared to preclude the possibility of using a "normal" muon content to veto CR events in UHE γ-ray astronomy.

A number of deep underground muon detectors are now being commissioned to search for muons produced by the interaction of extraterrestrial neutrinos and an estimate of the flux and neutrino light curve for Cygnus X-3 has recently been made by Gaisser and Stanev (1985). If a significant number of muons are produceed in the atmosphere as secondaries by γ-ray showers at very-high energies, it may also be worth searching for narrow angle anisotropies in the sea-level muon background radiation as an alternative to the atmospheric Cerenkov technique. Searches of this type were conducted some years ago (Allkofer *et al.*, 1981) although not specifically for γ-ray sources.

To consider these questions we have recently performed a new calculation of the muon content of γ-ray initiated EAS using a realistic model of high energy hadronic interactions. Details of the calculation are given by Edwards *et al.* (1985).

2. *MUONS IN GAMMA-RAY SHOWERS.*

The integral energy spectra of muons we obtain at an atmospheric depth of 1130 g cm^{-2} are given in Fig. 1 for average γ-ray and proton initiated EAS for primary energies in the range 10^{11} - 10^{17} eV and 10^{15} - 10^{17} eV respectively. The atmospheric depth chosen is appropriate to the Kiel (sea level) observation of Cygnus X-3. In the Kiel and Lodz experiments, the muon measurements were obtained at fixed shower size rather than at fixed primary energy. For a realistic comparison, then, we have calculated the mean muon number for showers of given size by performing a numerical integration over primary energy taking account of fluctuations in longitudinal development. For primary CR a broken power law energy spectrum was adopted with a differential exponent of -2.7 steepening to -3.1 above 3×10^{15} eV. For γ-rays, the spectrum adopted had a differential exponent of -2 and was cut off at 10^{17} eV. The results are given in Fig. 2 and show that the ratio of the muon number in γ-ray initiated EAS to that in proton initiated EAS is about 0.1. If the primary composition at 10^{15} - 10^{17} eV energies is mixed or is enriched in heavy nuclei, however, the ratio would be less than 0.1. From these results then it would appear that the muon component of EAS could usefully be employed to veto against CR initiated EAS in UHE γ-ray astronomy.

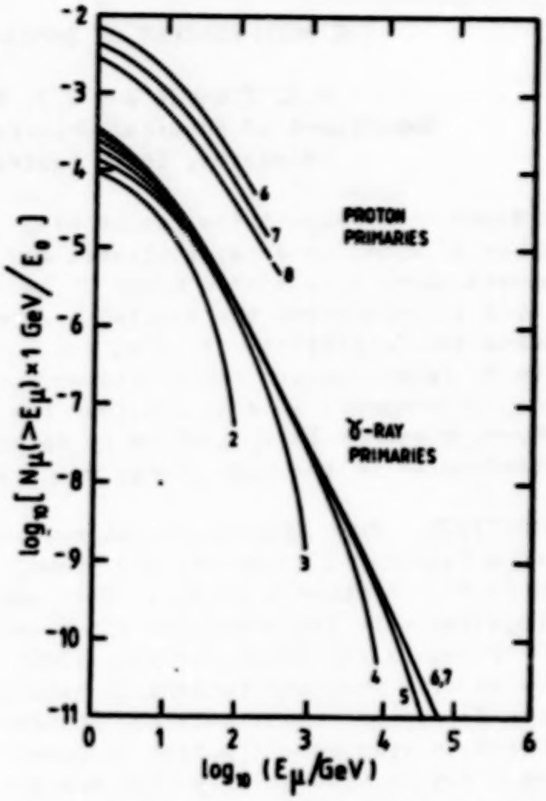

Fig. 1. Integral energy spectrum of muons in average proton and γ-ray initiated EAS divided by primary energy E_0. Numbers attached to the curves are $log_{10}(E_0/GeV)$.

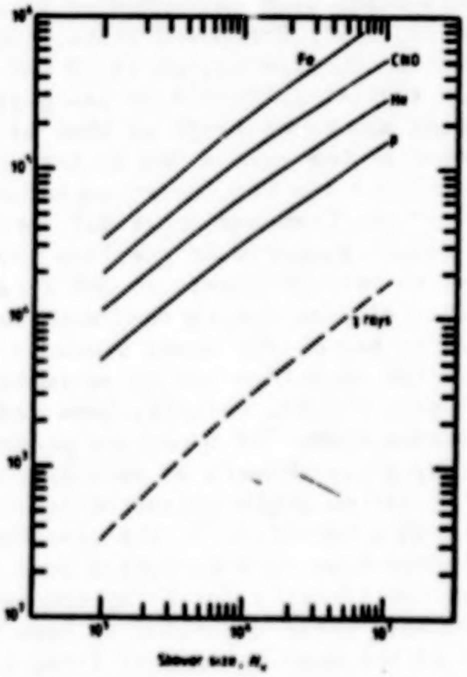

Fig. 2. Average muon number (>1 GeV) at fixed shower size at an atmospheric depth of 1130 g cm^{-2} in γ-ray and nucleus initiated EAS. (Reproduced from Edwards *et al.*, 1985).

3. *GROUND LEVEL MUON FLUX.* The flux of atmospheric muons due to γ-rays from Cygnus X-3 has been calculated by convolving the muon energy spectra in γ-ray showers (Fig. 1) with the γ-ray energy spectrum of Cygnus X-3. For this we took an E^{-2} differential photon spectrum normalised to the integral flux above 3×10^{15} eV reported by Lloyd-Evans *et al.* (1983):

$$N(E) = 4.5\times10^{-4}(E/\mathrm{GeV})^{-2} \quad (\mathrm{photons\ m^{-2}\ s^{-1}\ GeV^{-1}}). \qquad (1)$$

The resulting integral muon spectrum is shown in Fig. 3 assuming the γ-ray spectrum of equation (1) continues to a cut-off energy of: (a) 10^{16} eV; (b) 10^{17} eV; (c) 10^{18} eV. Whether this muon flux can be seen significantly above the background for a given exposure (area x time) depends on the accuracy with which the muon directions recorded reflect the γ-ray arrival directions. The angular uncertainty is likely to be made up of two parts for high energy muons: (i) uncertainty in muon track reconstruction in the detector; and (ii) angular spread due to transverse momentum imparted to parent pions. For the background muon intensity summarised by Allkofer *et al.* (1971), and assuming that γ-rays are present over 1/100th of the orbital period, the exposure required to detect muons due to γ-rays from Cygnus X-3 with 99% confidence is shown in Fig. 4 for various detector track resolutions.

4. *DISCUSSION.* From the present calculations the Kiel and Lodz results are inconsistent with the excess EAS detected by these groups being due to γ-rays. For the nearer of the two sources, the Crab, Dzikowski *et al.* (1983) have already suggested the possibility that the excess EAS are due either to neutrons

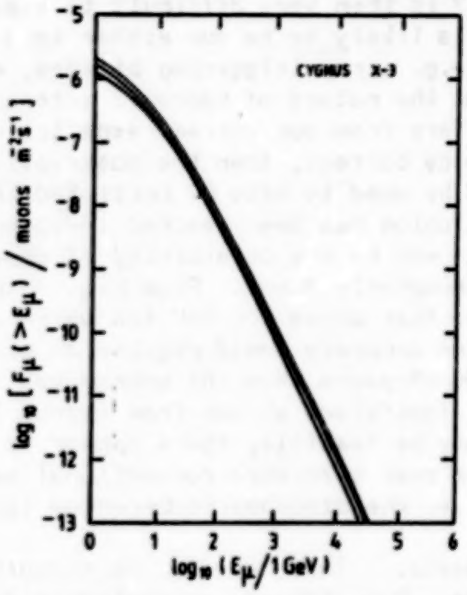

Fig. 3. Integral flux of atmospheric secondary muons due to gamma-rays from Cygnus X-3. The three curves given correspond to different assumptions about the high energy cut-off energy in the γ-ray spectrum (see text).

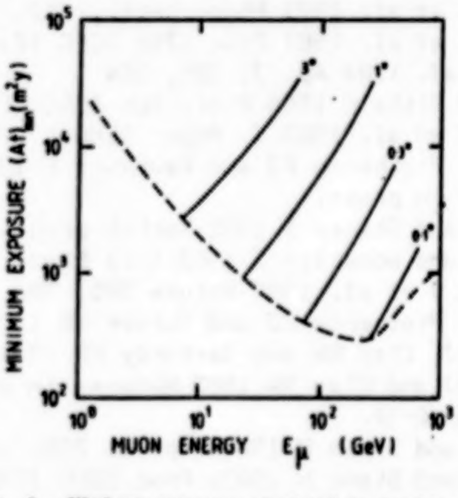

Fig. 4. Minimum expusure required as function of muon energy threshold and muon track reconstruction accuracy (the numbers attached to the curves). A lower limit is imposed by the angular spread of muons due to tranverse momentum (assumed to be: $\theta \sim \langle p_t \rangle c/E_\mu$) and by Poisson statistics and is indicated by the broken line.

or protons, energetics arguments strongly favouring the latter alternative. The present calculations would also favour the excess EAS being due to protons or light nuclei: a ratio of 0.7 could easily be obtained if the excess events are due to protons and light nuclei from the Crab Supernova and if the galactic CR are of mixed composition at these energies (i.e. the CR's produced during the Crab supernova had a somewhat lighter composition than average). For Cygnus X-3, protons or nuclei can be ruled out because the excess EAS are observed in phase with the orbital motion of the system and it appears fairly certain that the excess EAS from Cygnus X-3 are indeed due to γ-rays. The observed ratio of muons in these EAS to that in CR EAS of 0.7 is then very difficult to explain. We conclude then that the discrepancy is likely to be due either to a systematic effect in the experiment (e.g. array triggering biasses, etc.) or alternatively, may indicate that the nature of hadronic interactions at 10^{14} - 10^{16} eV energies differs from our current expectations. If the first possibility turns out to be correct, then the observation of a "normal" muon content in an EAS could be used to veto CR initiated EAS in UHE γ-ray astronomy. A similar conclusion has been reached independently by Stanev *et al.* (1985).

We turn now to the possibility of observing γ-ray sources through detecting atmospheric muons. From Fig. 4 the best energy range to examine appears to be that above 100 GeV for which a detector with a 0.1° track reconstruction accuracy would require an exceptionally large exposure, in excess of 300 m^2-years when the source was in the field of view, in order to detect a significant excess from Cygnus X-3. While technically such an experiment may be feasible, there appear to be few (if any) advantages of such a system over over more conventional methods of very-high energy γ-ray astronomy (i.e. the atmospheric Cerenkov technique).

Acknowledgements. This research is supported by the Australian Research Grants Scheme. P.G. Edwards acknowledges receipt of a Commonwealth Postgraduate Research Award.

REFERENCES

Allkofer OC *et al.* 1971 Phys. Lett., 36B, 425
Allkofer OC *et al.* 1981 Proc 17th ICRC (Paris) 9, 174
Boone J *et al.* 1984 Ap. J. 285, 264
Braun O and Sitte K 1965 Proc. 9th ICRC (London) 2, 712
Dzikowski T *et al.* 1983 J. Phys. G:Nucl. Phys. 9, 459
Edwards PG, Protheroe RJ and Rawinski E 1985 J. Phys G: Nucl. Phys. (letter) in press.
Gaisser TK and Stanev T 1985 Bartol preprint BA-85-12
Karakula S and Wdowczyk J 1963 Acta Phys. Polonica 24, 231
Lloyd-Evans J *et al.* 1983 Nature 305, 784
McComb TJL, Protheroe RJ and Turver KE 1979 J. Phys. G:Nucl. Phys. 5, 1613
Protheroe RJ, Clay RW and Gerhardy PR 1984 Ap. J. 280, L47
Protheroe RJ and Clay RW 1985 Nature, in press. See also these proceedings paper OG2.6-10.
Samorski M and Stamm W 1983a Ap. J. 268, L17
Samorski M and Stamm W 1983b Proc 18th ICRC (Bangalore) 11, 244
Stanev T, Gaisser TK and Halzen F 1985 preprint
Wdowczyk J. 1965 Proc. 9th ICRC (London) 2, 691

N85-36032

HE 4.5 - 9

THE HUMP IN THE CERENKOV LATERAL DISTRIBUTION OF GAMMA RAY SHOWERS

S. Sinha and M.V.S. Rao
Tata Institute of Fundamental Research, Bombay 400005, India

ABSTRACT

The lateral distribution of atmospheric Cerenkov photons emitted by gamma ray showers of energy 100 GeV is calculated. The lateral distribution shows a characteristic hump at a distance of ~ 135 meter from the core. The hump is shown to be due to electrons of threshold energy 1 GeV, above which the mean scattering angle becomes smaller than the Cerenkov angle.

Introduction : We have reported earlier[1] the calculation of the lateral distribution of Cerenkov radiation at sea-level emitted by showers initiated by gamma rays of energy 100 GeV incident at the top of the atmosphere. The lateral distribution shows a characteristic shoulder at a distance of ~ 125 m from the core. This shoulder has been seen by various authors [2-4] but not by Browning and Turver[5]. Our calculation did not include the effect of Rayleigh and aerosol scattering and ozone absorption on the Cerenkov photons and the effect of the geomagnetic field on the electrons. Also the effect of temperature variation in the atmosphere was not included in this calculation.

Further calculations were done in which the effect of Rayleigh, aerosol scattering and ozone absorption have been included but not the geomagnetic field as the effect due to this is found to be small [4]. Also the effect of temperature variation is now included. The resulting lateral distribution still shows the hump at a distance of ~135 m from the shower core. Investigations on the nature and origin of the shoulder are reported in the present paper.

Method of Calculation

The treatment of the soft cascade is essentially similar to calculations of Vatcha[6]. For photons both pair production and Compton scattering processes are considered while for electrons bremmstrahlung, multiple Coulomb scattering and ionisation losses are taken into account.

Everywhere corrections have been applied for the screening effect. The value of the radiation length in air used is 37.2 gms/cm^2. For the atmosphere a realistic model is taken. The relation between the height h (in meters) and the depth x (gms/cm^2) in the atmosphere is given by

$$h = (6740 + (2.5 \ln X) \ \ln (1030/X)$$

The scale height is thus dependent on depth

The most important effect is that of multiple Coulomb scattering. Both the single and multiple Coulomb scattering are considered for particles of energy below I GeV and for particles with energy above 1 GeV only the multiple Coulomb scattering is taken into account since inclusion of single scattering term for these particles has negligible effect on the

Cerenkov photon lateral distribution. The refractive index, n, of air is given by

$n = 1 + 0.0002926\ (X/1030)\ (273.2/T)$ where T, the atmospheric temperature (°k) is

$$T = 204 + 0.091\ X$$

Each photon and electron (or positron) is treated by Monte Carlo method from the point of its production to the next interaction point until either one of the following conditions is satisfied (a) its energy falls below 1 MeV, (b) it starts moving horizontally or backwards, or (c) it emerges below the observation level.

For the calculation of the Cerenkov emission it is assumed that the electron moves in a straight path to a certain distance (this distance varied for different sets of calculations) and does not suffer any energy loss in between. This energy loss, is, however, taken into account for following the electrons in the cascade.

The Cerenkov photon lateral distribution is calculated in the following manner . For each straight section of the electron path the Cerenkov photons emitted are confined between two cones having vertices at the two ends of the straight section. These two cones intersect the observation plane in two ellipses. The Cerenkov photon density is calculated by assuming uniform distribution within the two ellipses and is accumulated at some fixed points which happen to fall in between the two ellipses. The points lie along the X-axis at distances from 10 m to 220 m from the core. The average Cerenkov lateral distribution at sea-level for the wave length interval 300 nm to 650 nm is obtained, from a total of 100 showers.

Different sets of calculations have been carried out with and without including the effect of Rayleigh, aerosol scattering and ozone absorption of the Cerenkov photons. For this purpose, the data given by Eltermann 7 is used. A fourth degree polynomial is fitted to Eltermann's data for interpolation to intermediate distances.

Results

The lateral distribution without absorption (a) and with absorption (b) are shown in Fig.1. The lateral distribution shows the characteristic hump at ~ 135 m from the core. It is quite clear that inclusion of the effect of absorption does not reduce the prominence of the hump at all.

Such a hump in the lateral distribution was noticed in the calculations of Zatsepin and Chudakov and Patterson and Hillas whereas it is absent in that of Browning and Turver. The hump present in the calculation of Zatsepin and Chudakov is less prominent than in ours and Patterson and Hillas see a hump whose height is intermediate between ours and that of Zatsepin and Chudakov.

Patterson and Hillas suggest that the extraordinary prominence of the hump in our first calculation may result because of the fact that we have taken very large slab thickness ($5 \times 10^{-4} \times E$ for E less than 1 MeV, 1 radiation length above 1 GeV) while treating the Coulomb scattering. In our present calculations we have used very small slab thickness, sometimes as small as 0.003 radiation length. Still the shape of the hump remains unchanged. (Fig.2)

We have calculated the Cerenkov photon lateral distribution produced by particles with energy greater than 1 GeV and by particles with energy less than 1 GeV separately (Fig.2). The lateral distribution due to lower energy particles shows a very weak shoulder. The lateral distribution due to particles having energy greater than 1 GeV shows a very strong shoulder. These are the particles for which the r.m.s. scattering angle due to Coulomb scattering is less than the Cerenkov emission angle. The contribution to the lateral distribution from different depths in the atmosphere from electrons of energy greater than 1 GeV and less than 1 GeV is shown in Fig.3 (a) and (b) respectively.

The product of the height of production of the Cerenkov photons from electrons of energy greater than 1 GeV and the Cerenkov angle remains almost constant (between 110 and 140 m) for a fairly large range of the height of production of the Cerenkov photons (between 7 and 20 Km). The hump is essentially a consequence of this and is due to the contribution from particles of energy of greater than 1 GeV where the scattering angle becomes smaller than the Cerenkov angle.

Conclusions

We have shown that the hump in lateral distribution of Cerenkov photons at sea level in electromagnetic cascades of energy 100 GeV, remains essentially unaffected even after taking into account the Rayleigh and aerosol scattering and ozone absorption, and reducing the atmospheric slab thickness to very small values in the treatment of scattering of high energy electrons. The hump is essentially due to particles of energy greater than 1 GeV where the mean scattering angle becomes smaller than the Cerenkov angle.

References

1. B. S. Acharya et al., Proc. Intl. Workshop on Very High Energy Gamma Ray Astronomy, Ootacamund (Eds.P,V. Ramana Murthy and T. C. Weekes) 1982, p.303.

2. V. I. Zatsepin and A. E. Chudakov, Zh. Eksperim.I.Teor.Fiz,42,1622(1962 English Translation. Soviet Physics-JETP, 15,1126 (1962).

3. G. Rieke, Smithsonian Astrophysical Observatory Space Report No.301(1969).

4. J. R. Patterson and A. M. Hillas, J. Phys.G.Nucl.Phys. 9 (1983)1433-1452.

5. R. Browning and K. E. Turver, Nuovo Cimento, 38A,223 (1977).

6. R. H. Vatcha, Ph.D. Thesis, University of Bombay (1972).(Unpublished).

7. L. Elterman 1968 US Airforce Cambridge Research Laboratory Report AFCRL-68-0153.

ORIGINAL PAGE IS
OF POOR QUALITY

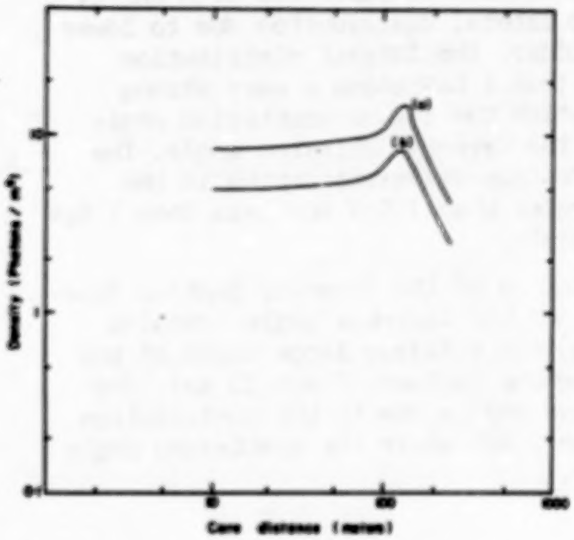

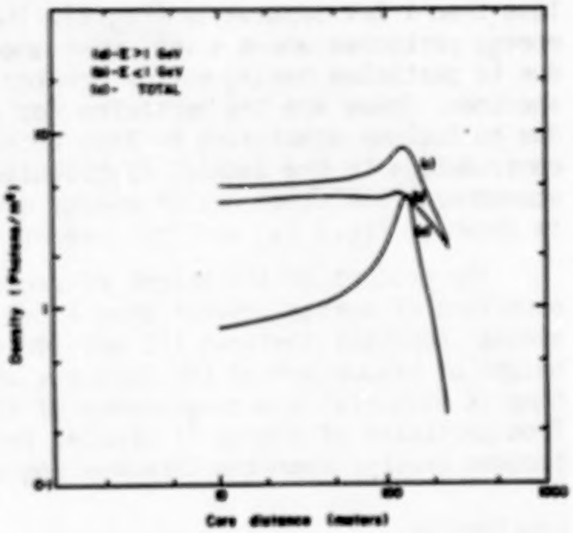

Fig.1. Lateral distribution of Cerenkov photons (a) without absorption, (b) with absorption

Fig.2. Lateral distribution of Cerenkov photons due to particles of energy (a) > GeV (b) < 1 GeV and (c) total

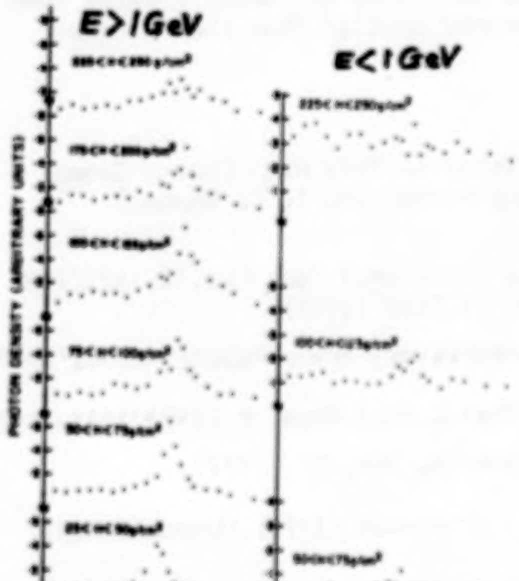

Fig.3 Contribution to lateral distribution of Cerenkov photons from different depths in the atmosphere due to particles having energy (a) > 1 GeV (b) < 1 GeV.

HE4.5-10

N85-36033

SIMULATION OF GAMMA-INITIATED SHOWERS

Yo.Stamenov and Kh. Vancov
Institute for Nuclear Ressearch and Nuclear Energy
BG-1784 Sofia, Bulgaria
T. Vodenicharova
Department of Physics, Institute for Foreign Students
BG-1111 Sofia, Bulgaria

Abstract

The main average characteristics of muon,electron and hadron components of exstensive air showers were calculate using a standart model of nuclear interaction. The obtained results are in good agreement with Tien Shan experimental data.

1. Introduction. The method of analysis of the onomaly in the development and structure of exstensive air showers /EAS/ gives the real possibility[1] for experimental investigation of gamma-quanta with high energy in the primary cosmic radiation. On the basis of Tien Shan experimental data was shown[2], that EAS poor in muons and high energy hadrons are initiated by gamma-quanta with energy - 10^{15} eV.

2. Method. The development of electron-photon component with a threshold energy of 500 MeV in homogenous atmosphere was simulated with help of Monte-Carlo method. The primary energy of the initiated photon was $E_\gamma=10^{15}$ eV.

The probability for realization of the cross-section:

$$\sigma_{\gamma p}(E) = 114.3 + 1.647\, \ln^2 (0.0213 E)$$,where $\sigma_{\gamma p}$ is in μb

and E in GeV.

It was supposed, that the nuclear cascade, initiated by a proton with the same energy as the correspondent photon energy, starts in the point of the photonuclear interaction. Further there were used the differential energy spectra of pions for different deepnesses in the atmosphere[4] in attempt to evolute the analogous spectrum for the observation level 700 g. cm^{-2}. By this way were calculated the total number of muons with energy $E_\mu > 5$ GeV too.

The energy flux carried by the electron-photon component of the same type of EAS was estimated with help of the lateral distribution function $\mathcal{E}_{e\gamma}[r,s]$[5] of the average energy per electron. In this case the correspondent energy flux density is:

$$\rho_E(r,s) = \rho_e(r,s)\, \mathcal{E}_{e\gamma}(r,s)$$

$$= \left[N_e/(m R_m)^2\right] f_{NK}(r/mR_m\,,\, s)$$,were $\rho_e(r,s) =$

is the modifed[6] NK funktion of the lateral distribution of electrons in a shower.

3. Results. The average energy of the hadron component E in EAS, initiated by a primary gamma-quanta with energy 10^{15} eV was estimated for the threshold energy of the Tien Shan experimental data - $E_{htr} > 3.8$ GeV:

$$E_{htr}(> 3.8\,GeV) = 1.62 \cdot 10^{12}\, eV$$

Only ~3% of the primary energy were transfered as energy of the electron-photon component and there are ~11.5 GeV in each photonuclear interaction.

The number of muons with $E_\mu>5$ GeV in the same showers was estimated as $N_{\mu\gamma}(E_\mu>5$ GeV$)=555$.

4. Discusion. The total number of muons $N_{\mu\gamma}$ in gamma-initiated shower with energy-6.10^{14} eV was estimated with help of a semiemperical method[2] as 255 for the Tien Shan experimental data. Taken into account the $N_\mu(E)$ dependance[4] we obtain $N_{\mu\gamma}(6.10^{14}eV)=361$. The average relation between total numbers of muons in gamma-initiated $N_{\mu\gamma}$ and normal $N_{\mu A}$ showers was estimated as $\left(\bar{N}_{\mu\gamma}/N_{\mu A}\right)=0.047$. Taken into account the total muon fluctuations for the Tien Shan experiment[2] we can obtain the threshold value for the selection of muon poor showers:

$\left(N_{\mu\gamma}/N_{\mu A}\right)=0.15$, what is in good agreement with the semiemperical value 0.11[2].

The energy of the electron-photon component transfered in the Tien Shan calorimeter[7] is:

$$E_{ec}=2\pi\int_{0.2m}^{3m}dr\,r\,\rho_E(r,S)=6.94.10^{13}eV$$

The correspondent part of the energy of hadron component was estimated as $E_h=3.7\ 10^{11}$ eV, taken into account the results[7, 8] about the lateral distributin of hadrons with different energies. So is the average value of the relation[2] $(E_h / E_e)=5.3\ 10^{-3}$ and including the total fluctuation of (E_n / E_e) for Tien Shan experiment[2] we obtain for the threshold value for hadron poor shower selection (E_h / E_e) $=1.5\ 10^{-2}$, which confirms the semiemperical value $1.42\ 10^{-2}$ too.

5. Conclusions. The results of the present calculation confirms the criteria, adopted by the analysis[2] of the Tien Shan experimental data, for selection of muon and hadron poor showers as gamma-initiated showers with energy $\sim 10^{15}$ eV

6. Acknoweledgments. The authors are thankful to Dr. A. Erlykin and Dr. S. Ushev for many fruitful discussions

References:

1/ Maze R. , Zavadzki A.; 1960, Nuovo Cimento, 17 5, 625-633

2/ Nikolsky S. , Stamenov Y. , Ushev S. , 1984, Adv. Spac. Res. v. 3, 10-12 , 131-134

3/ Bezrukov L. B. , Bugaev E. V. , 1981 Proc. ICCR, Paris, v. 7, 90-93

4/ Dedenko L. G. , 1965, Preprint FIAN A-69

5/ Danilova T. V. , Erlykin A. D. , 1984 Preprint FIAN N°15

6/ Dedenko L. G. , Nikolsky S. I. , Stamenov Y. N. , 1976 , Short Reports FIAN , 1 , 30

7/ Romakhin V. A. , Nesterova N. M; 1979, Trudy FIAN v. 109, 77-108

8/ Vernov S. N. et. al; 1970, Acta Sci. Hungaricae, 29 Suppl. v. 3, 429

N85-36034

HE 4.5-11

PHENOMENOLOGICAL CHARACTERISTIC OF THE ELECTRON COMPONENT IN GAMMA-QUANTA INITIATED SHOWERS

Nikolsky S.I.[*], Stamenov J.N.[**], Ushev S.Z.[**]
[*] P.N.Lebedev Physical Institute,Moscow,USSR
[**] Institute for Nuclear Research and Nuclear
Energy,Sofia,Bulgaria

ABSTRACT

The phenomenological characteristics of the electron component in showers initiated by primary gamma-quanta were analyzed on the basis of the Tien Shan experimental data.It is shown that the lateral distribution of the electrons in gamma-quanta initiated showers can be described with NKG - function with age parameter $\bar{S} = 0{,}76 \pm 0{,}02$,different from the same parameter for normal showers with the same size $\bar{S} = 0{,}85 \pm 0{,}01$.The lateral distribution of the correspondent electron energy flux in gamma-quanta initiated showers is steeper as in normal EAS.

I.Introduction

The phenomenological characteristics of the electron component of EAS contains information about the primary particle which has initiated the shower /1,3/.Particularly, the muon and hadron components in the extensive air showers, generated by primary gamma-quanta,are practically absent because the photonuclear processes cross-section are relatively small in comparison with the hadron-hadron interactions cross-sections,which are responsible for the normal showers.

In our earlier papers /4-6/ the investigation results are discussed of primary gamma-quanta with energy of $\sim IO^{I5}$ eV with the help of the method of muon and hadron poor-shower selection on the basis of the Tien Shan experimental data, obtained during an effective running time $\sim I,8.IO^{4}$h.

2. Results

The lateral distributions of the electron flux in the selected muon and hadron poor-showers were described in the distance interval $5 \div I80$ m from the axis by means of standard NKG-function with age parameter $\bar{S}_{\perp} = 0,76 \pm 0,02$. On the other hand, the normal showers with the same size have electron lateral distribution, characterized with the age parameter $\bar{S}_{\perp} = 0,85 \pm 0,0I$. In this case, the gamma-initiated showers are also younger that the showers with the same size but generated by primary nucleons and nucleis. Taking into account the relation $S = S_{\perp} + \Delta S$, where $\Delta S = 0,I5 \div 0,20$ /7/, it is necessary to suppose that the development maximum of the gamma-initiated showers is localized deeper in the athmosphere. This supposition is confirmed by the comparison of the experimental data /8/ about the height of the maximum in proton initiated showers with energy IO^{I5} eV - $X_{max} \approx 450$ g.cm^{-2} with the cal-

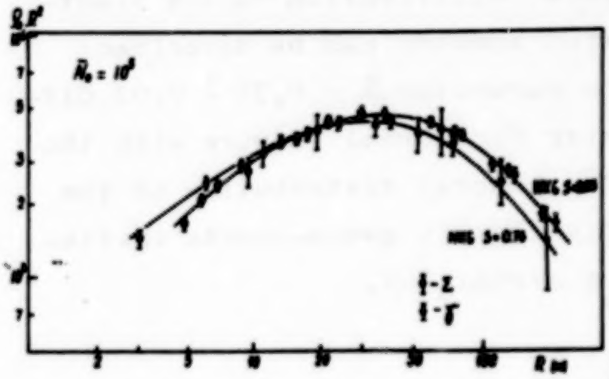

culation result for the electron-photon cascades in the athmosphere, assuming the same energy of the primary photon - $X_{max} \approx 600$ g.cm^{-2} /9/.

The lateral distribution of the electron energy flux in gamma-initiated and normal showers were analyzed too in the distance interval $0,2 < r < 5$ m /fig.2/.

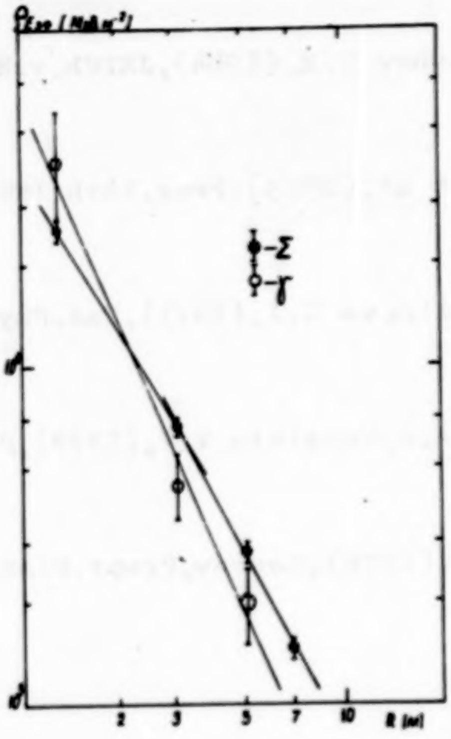

It is shown that the lateral distribution in normal proton or nuclei initiated showers were described by the same functions as in /IO/:

$\rho_{Eef} \sim r^{-I,53}$ $0,2 < r < 3$ m

$\rho_{Eef} \sim r^{-I,9}$ 3 m $< r < 7$ m

but in gamma-initiated showers

$\rho_{Eef} \sim r^{-2,0}$ $0,2 < r < 3$ m.

The absence of flattening of the lateral distribution of the energy flux in the central part of the pure electromagnetic showers is a natural consequence of the absence of transverse momenta of secondary hadrons in the high energy hadron interactions.

References

I. Nikolsky S.I, (I970), Trudy FIAN, v.46, 900.

2. Stamenov J.N, (I982), Thesis of doctor, FIAN, Moscow.

3. Khristiansen G.B, Kulikov G.V et al, (I975), "Cosmicheskoe

izluchenie sverhvisokoii energii",Moscow.

4. Stamenev J.N,Ushev S.Z et al,(1983),Proc.18th ICRC,v.6, pp.54-57.
5. Nikolsky S.I,Stamenov J.N,Ushev S.Z,(1984),Adv.Space Res,v.3,10-12,pp.131-134.
6. Nikolsky S.I,Stamenov J.N,Ushev S.Z,(1984),JETPh,v.87, 1/7/,pp.18-36.
7. Dedenko L.G,Nesterova N.M et al,(1975),Proc.14th ICRC, v.18,2731-2736.
8. Antonov R.A,Ivanenko I.P,Tulinova Z.I,(1973),Yad.Phyz., v.18,pp.554-559.
9. Pljasheshnikov A.V,Lagutin A.A,Uchaikin V.V,(1979),Proc. 16th ICRC,v.7,pp.1-6.
10. Aseikin V.S,Kirov I.N et al,(1976),Moscow,Prepr.FIAN142.

abstract N85-36035 HE 4.5-13

A Three-dimensional Monte Carlo Calculation of the Photon initiated Showers and Kiel Result

A. Okada and Y. Muraki

Inst. for Cosmic Rays, Univ. of Tokyo, Tanashi, Tokyo 188

abstract

The Kiel experimental results indicate an exsistence of the ultra high-energy gamma-rays coming from Cyg. X-3. However the result indicates that the number of the muons included in the photon initiated shower is the same as the number included in the proton initiated showers. According to our Monte Carlo calculation as shown in the graph of underpart, the number of muons included in the photon initiated showers should be less than 1/15 of the proton's [See also Proceed. 17th ICRC 7 (1983),54.].

The previous simulation was made under one dimensional approximation. This time we report the result of three dimensional calculation by oral and ICRR preprint.

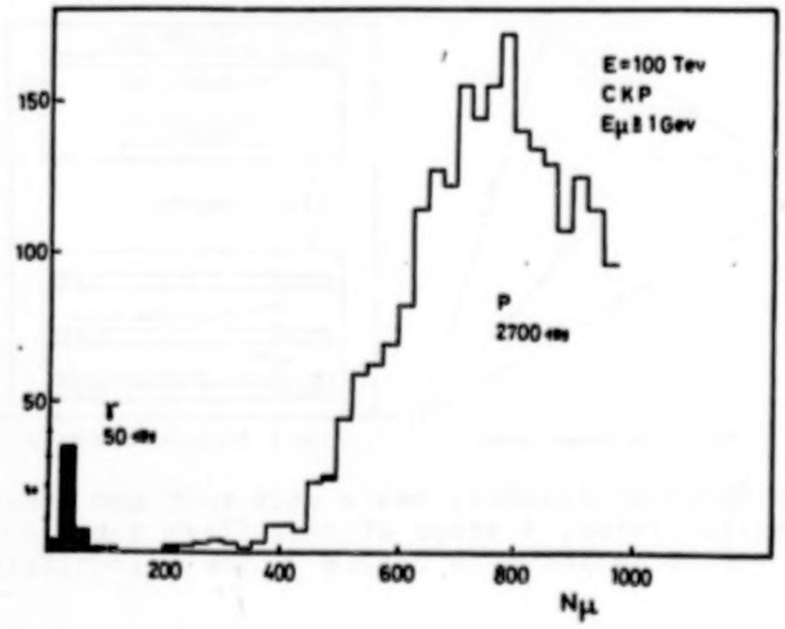

N85-36036
HE 4.5 - 14

Construction of a Cosmic Ray Air Shower Telescope

L.K. Ng and S.K. Chan
Physics Department, University of Hong Kong
Hong Kong

Abstract

The telescope under construction is mainly for the purpose of locating the arrival directions of energetic particles and quanta which generate air showers of sizes 10^5 - 5.10^6. Both fast timing method and visual track method are incorporated in determining the arrival directions. The telescope is composed of four stations using scintillators and neon flash tubes as detectors. The system directional resolution is better than 1.5°.

1. Introduction. Application of medium-size shower arrays in astronomical observations is exemplified by the Kiel experiment[1] in the detection of high energy gamma rays from Cygnus X-3. This type of continuous observation using ground-base air shower arrays may yield more fruitful results, if it is participated by more stations spreading out at various latitudes. For long term observations, such telescope could be less elabourate than Kiel's. The requirements may just be high directional resolution and ability to measure the muon/electron density ratios of individual showers, in addition to the usual determination of lateral distributions and age parameter. This paper reports a simple air shower telescope which meets the above requirements.

2. Detection system. It consists of four detector assemblies (a required minimum), which are at sea level and arranged as shown in figure 1.

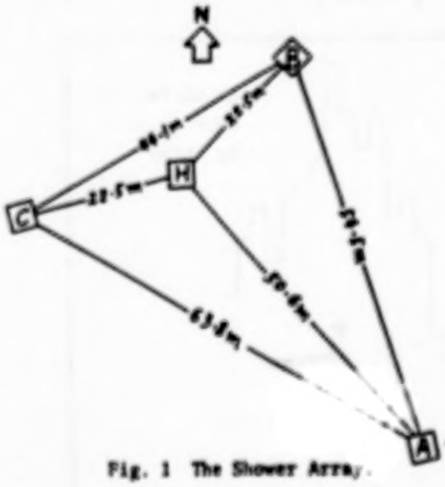

Fig. 1 The Shower Array.

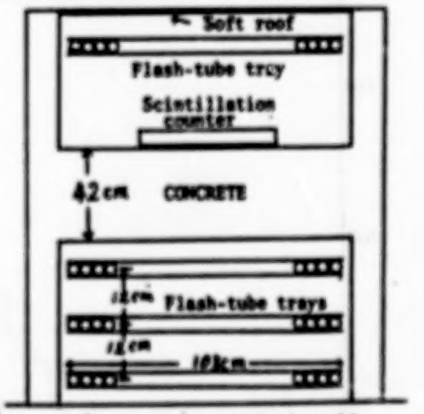

Fig. 2 The Detector Assembly.

Each detector assembly has a soft roof and contains a plastic scintillator, 4 trays of neon flash tubes and an absorber medium as shown in figure 2. The scintillator has a minimum geometry of 0.5m x 0.5m x 0.05m and is viewed by two 2" photomultipliers in contact with the scintillator. For precise arrival time determination, anti-jitter preamplifiers described in another conference paper (HE 4.7 - 9) are used.

Each of the four flash-tube trays consists of 48 close packed tubes. Each tube has a geometry of 2m x 1.9cm dia. and when it fires, its output electromagnetic signal is picked up by a latch. There are 4 x 48 latch units in an assembly providing 24 bytes of data per shower per assembly. Clearly, the top tray is for shower density measurement and the bottom three trays are for muon density and direction measurements.

3. Electronics. For each shower, data required from the system include information from the flash tubes, the particle arrival times, and the event time and date. Block diagram of the electronic system is given in figure 3. Communication between each assembly and the central processing station is linked by transceiver buses throughout. A master pulse is produced by 4-fold coincidence of the scintillator outputs (2μs window). The master pulse is used to reset the flash-tube latches, to fire the flash tubes by triggering the UHT pulsing unit, and to start the data acquisition subroutine in the microcomputer.

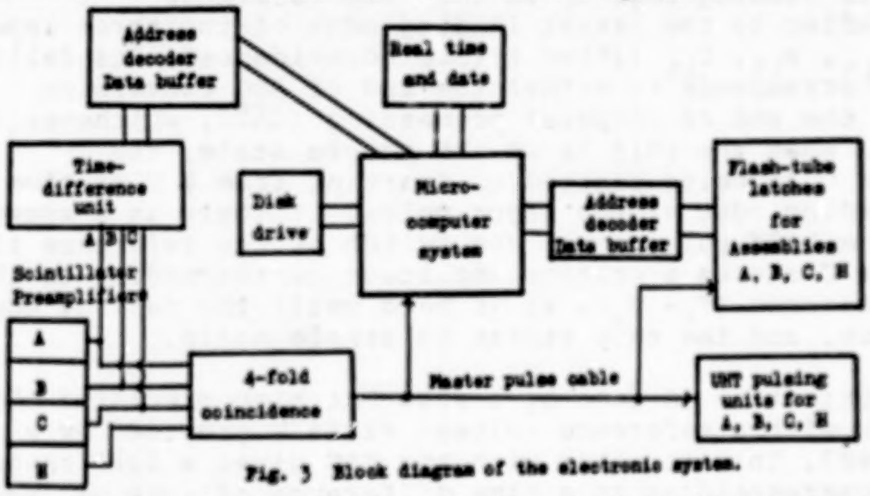
Address decoder Data buffer
Real time and date
Time-difference unit
A B C
Scintillator Preamplifiers
Disk drive
Micro-computer system
Address decoder Data buffer
Flash-tube latches for Assemblies A, B, C, H
A
B
C
H
4-fold coincidence
Master pulse cable
UHT pulsing units for A, B, C, H

Fig. 3 Block diagram of the electronic system.

However, the key part of the electronic system is the time-difference unit which determines the relative arrival time of particles falling at the scintillators. The arrival time is precisely related to the leading edge of the output pulse from the anti-jitter preamplifier. This leading edge is free from distortion during transmission, because the signal cable is terminated by a matched pair of driver/receiver.

The time-difference unit contains three sets of time-to-amplitude converter(TAC) and analogue-to-digital converter(ADC). The leading edge of an input pulse from one of the assemblies A, B, C is compared with a common time reference, and the difference is then digitized by the TAC and ADC. The TAC and time reference circuits are shown in figure 4.

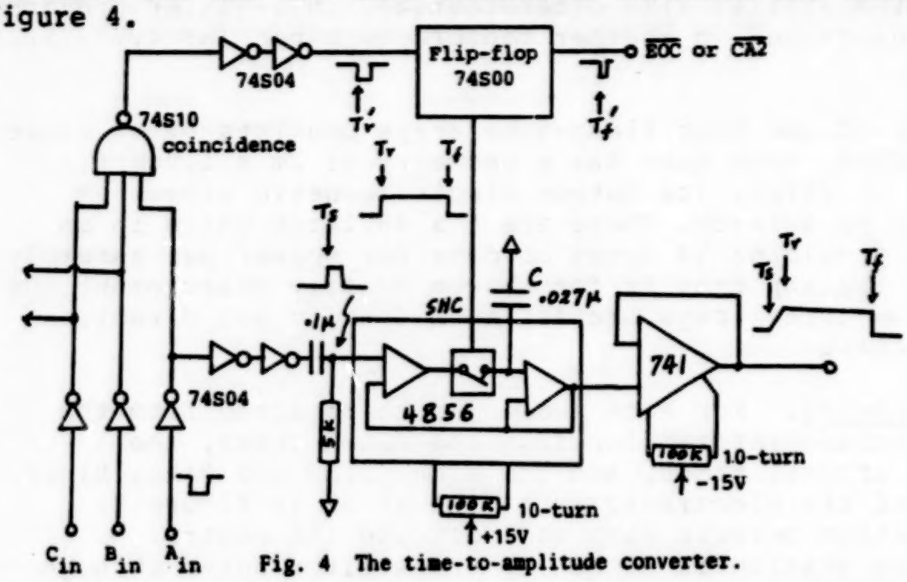

Fig. 4 The time-to-amplitude converter.

The TAC is a sample/hold chip (Teledyne Philbrick 4856) with a charging rate ~1.5 V/μs and a drift rate ~0.8 mV/s at the hold state, using a low leakage capacitor C of 0.027 μf. The hold pulse (at SHC) is generated by a fast flip-flop as shown. Its leading edge T_r is the time reference corresponding to the latest leading edge of the three input pulses A_{in}, B_{in}, C_{in} (after triple coincidence). Its falling edge T_f corresponds to either the end of ADC conversion ($\overline{EOC}$) or the end of computer processing ($\overline{CA2}$), whichever is the last. When the chip is at the sample state, the capacitor C is being charged up starting from 0 V at time T_s, the leading edge of the input pulse. If there is a shower event, the hold pulse opens the switch at the reference time T_r. Hence C stores a voltage amplitude corresponding to the time difference ($T_r - T_s$). It is held until the falling edge T_f sets in, and the chip starts to sample again.

Digitization is done by a slow but high precision ADC (MC14514) with a reference voltage +2.48 V provided by a chip MC1403. This together with the TAC gives a full range of 1999 corresponding to a time difference of 1768 ns. Hence the time resolution is better than 1 ns. The unit is calibrated by using a fast CRO and a signal generator. The various fixed time delays are also determined similarly.

From the geometry in figure 1, a time difference of 2.9ns corresponds to ~1° zenith angle. Hence the directional resolution is mainly determined by the time fluctuation in the scintillation counters, including photomultipliers and preamplifiers. The fluctuation is not expected to exceed 4ns. Therefore, the directional resolution is better than 1.5°.

4. Shower rate and efficiency. The minimum trigger density at each scintillator is 4 m^{-2}. Using the differential intensity spectrum[2],

$$j(N) = 1.95.10^{6} N^{-2.7} \quad ,$$

The shower rate is estimated by the expression,

$$\phi = \frac{2\pi}{\alpha+2} \int j(N) A(N) dN, \text{ with } \alpha = 8.6 \text{ at sea level,}$$

and is presented below.

Shower size $(N - N+\delta N)$	$A(\bar{N})$	$\bar{N}^{-2.7} A(\bar{N}) \delta N$
9.2 E4 - 1 E5	1.0 E1	0.03 E-7
1 E5 - 2 E5	3.0 E2	4.87 E-7
2 E5 - 3 E5	2.05 E3	6.31 E-7
3 E5 - 4 E5	4.10 E3	4.76 E-7
4 E5 - 5 E5	6.10 E3	3.47 E-7
5 E5 - 6 E5	8.00 E3	2.61 E-7
6 E5 - 7 E5	1.05 E4	2.16 E-7
7 E5 - 8 E5	1.24 E4	1.73 E-7
8 E5 - 9 E5	1.47 E4	1.46 E-7
9 E5 - 1 E6	1.67 E4	1.22 E-7
1 E6 - 2 E6	2.40 E4	7.78 E-7
2 E6 - 3 E6	4.20 E4	2.58 E-7
3 E6 - 4 E6	5.70 E4	1.32 E-7
4 E6 - 5 E6	6.80 E4	0.77 E-7

Total 41.07 E-7

Hence the shower rate is $\phi(>9.2.10^{4}) = 4.7 \text{ hr}^{-1}$.

The effective area of each flash-tube tray is 1.73 m^2 and the expected efficiency of the tubes is ~85%. Hence on the average, the minimum number of shower particles recorded from each tray is 4 x 1.73 x 0.85 = 5.9. The directions of the muon tracks in a muon-rich shower can be used to check the shower direction obtained by the time-difference method.

5. Acknowledgement. The authors are grateful to Professor D.J. Newman for his support and encouragement.

References.

1. Samorski M and Stamm w, Ap.J. Lett. 268 (1983) L17.
2. Hillas A M et al, Phys. Reports, 20C (1975) 79.

An Underground Cosmic Ray Muon Telescope for Observation of Cosmic Ray Anisotropy

Y.W. Lee and L.K. Ng
Physics Department, University of Hong Kong
Hong Kong

N85-36037

Abstract

A telescope housed in a tunnel laboratory has an overburden of 573 hg cm^{-2} and is located under the centre of a saddle-shaped landscape. It is composed of triple layers of proportional counters, each layer of area~4m x 2m and their separation 0.5m. Events are selected by triple coincidence and software track identification. The telescope is in operation for over a year and the overall count rate is 1280 hr^{-1}. The structure and operation of the system is reported.

1. Introduction. Construction of a cosmic ray muon telescope in a road tunnel laboratory on Hong Kong Island was proposed in 1979[1] for the purpose of measuring high energy cosmic ray sidereal variations in the light of similar experiments at Poatina[2] and Utah[3]. The work was delayed due to the tunnel construction, but was finally in operation since August 1983.

The laboratory site is under a saddle-shaped landscape with a vertical rock overburden of 573 hg cm^{-2}(including the atmospheric depth). Two hill peaks of height ~420m limits the East-West zenith view. The North-South profile of the 'saddle' is given in figure 1. With the detectors (proportional counters) placed along E-W direction, 23 directional bins are obtained in the N-S profile.

The experiment is expected to run continuously for three more years in order to obtain statistically significant data. A preliminary data analysis is given at this Conference (OG5.3-9). This paper only reports on the structure and operation of the system.

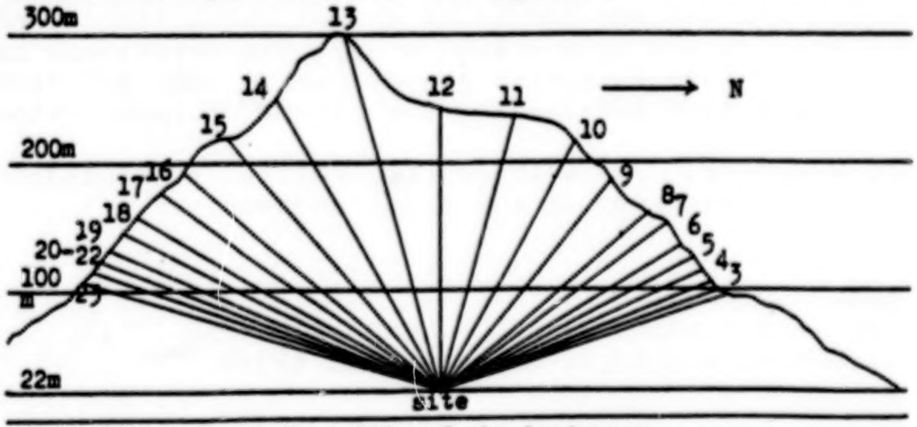

Fig. 1 The N-S profile of the landscape.

2. Detection system. Large area proportional counters (2m x 7.6cm dia.) are used. The counter body is made of 0.16cm thick stainless steel with 50 µm stainless steel anode wire under 100g tension. The tube is filled with a standard P-10 gas at 1 atmospheric pressure. Figure 2 shows the arrangement of the counters with 48 tubes in one layer. The whole assembly is covered by lead sheets to minimize soft radiation from the tunnel rocks.

The counters are operated at the limited proportional region (EHT = +2600 V) and the single count rate is ~80 s^{-1}. Operation of the counters is indicated hourly by a monitor spectrum described in later sections. Long term drift due to slow aging is found insignificant.

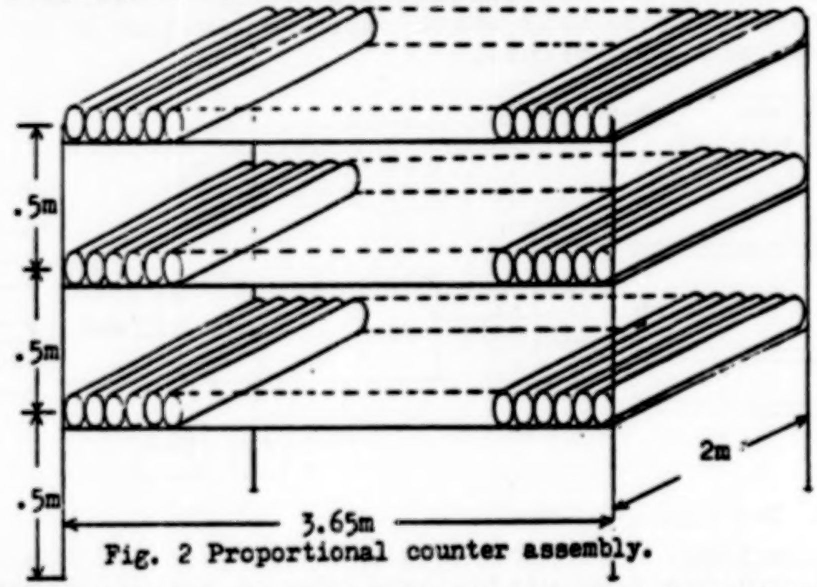
.5m
.5m
.5m
3.65m
2m

Fig. 2 Proportional counter assembly.

3. Electronics. Each proportional counter has its own preamplifier, and they are binned together with 4 counter in one bin shown in figure 3. For more precise track identification, counters in the middle layer are binned in two ways A and B as shown.

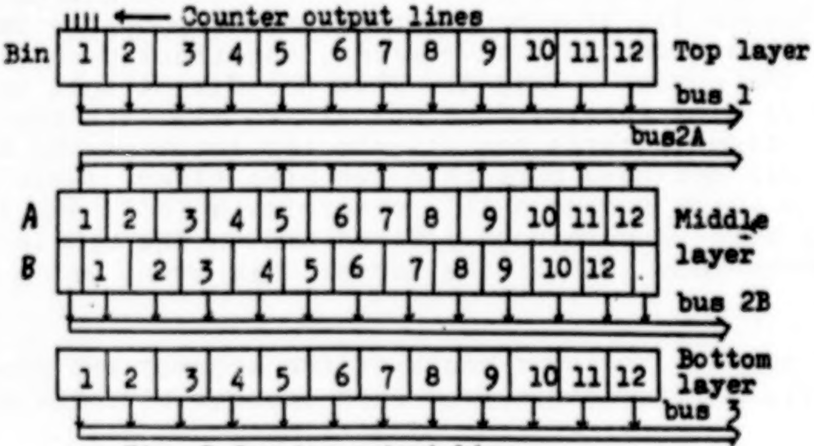
Counter output lines
Bin
1 2 3 4 5 6 7 8 9 10 11 12
Top layer
bus 1
bus2A
A
1 2 3 4 5 6 7 8 9 10 11 12
Middle layer
B
1 2 3 4 5 6 7 8 9 10 12
bus 2B
1 2 3 4 5 6 7 8 9 10 11 12
Bottom layer
bus 3

Fig. 3 Counter output bins.

The digital system mainly consists of counter latches, a triple coincidence system and three microprocessor systems MPS (Motorola 6800) as shown in figure 4.

The coincidence unit with window 1.14 µs provides the required master pulse which commands holding of the counter information in the latches and starts a series of operations in the three MPS systems. The wires in each input bus to the coincidence unit are ORed before entering the unit. MPS1 reads the latched counter information and sends the raw data to the remote system MPS2. If MPS2 is busy, the data is temporarily held in the MPS1 output buffer. MPS2 accumulates hourly a muon directional spectrum and a monitor spectrum of individual bin counts. It also keeps time and date; and for visual checking, it can provide an option of slow video display of particle tracks in a current event. The triple coincidence rate, the two spectra and the time and date are finally transfered to MPS3 which stores them hourly in floppy disks and hard prints.

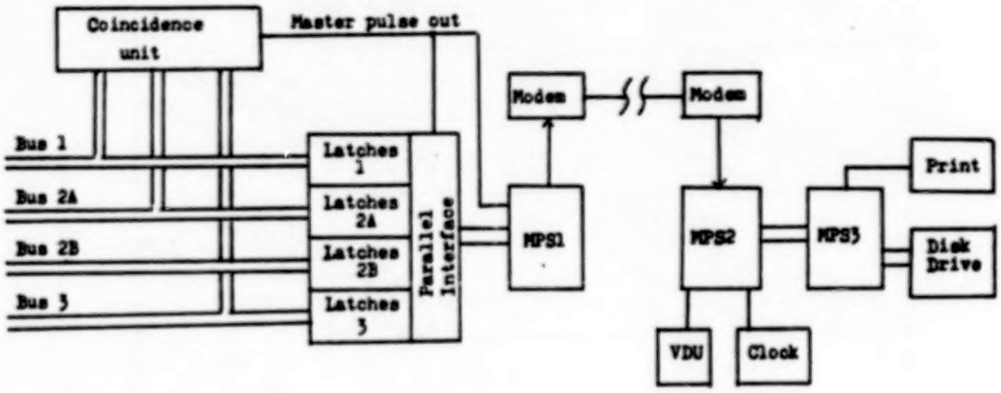

Fig. 4 The digital system.

4 Data collection. From the single count rate and the triple coincidence time window, the chance rate is about 800 hr^{-1}, which is very significant when compared with the corrected event rate of 1280 hr^{-1}. Hence software particle track identification is carried out in MPS2 as follows:

The counter bins in each layer are labelled from 1 to 12 (see figure 3). If a muon traverses Bin p on the top layer and Bin q on the bottom layer, the track direction is given by the number N = (p-q). Thus the directional spectrum contains 23 bins ranging from N = -11 to +11. The track identification criteria are (i) the top layer or the bottom layer should not have more than two bins fired. (When a bin fires, its latch stores a '1', otherwise a '0'); and (ii) the track must pass through a fired bin on the middle layer, either among bins in A if the number N is even, or in B if N is odd).

The monitor spectrum contains the accumulated counts during triple coincidence from each counter bin. The count rate in each bin therefore depends on the bin location. But the spectral shape should not vary if the counters are operating normally. This determines the data reliability.

5. Comparison and discussion. The table below compares the experimental system with those at Utah and Poatina.

	Hong Kong	Utah	Poatina
Site latitude	22.2° N	40.6° N	41.8° S
Effective depth/hg cm^{-2}	573	486	365
Vertical threshold muon energy/GeV	157	121	~80
Median regidity/GV	1915	1500	~1000
Effective area/m^2	7	37	4
Total counts	$1.27.10^7$	$1.52.10^8$	--

From the particle track identification criteria, it is obvious that showers and local bursts are excluded and so are the chance events. However, the second particle identification criterion was considered to be too restrictive which could exclude some genuine events due to deviation in the counter alignment. This criterion was then relaxed by including the neighbouring bins on the middle layer. This relaxation only results in a chance coincidence of 1.4 counts per hour. The merit of this system over a scintillator system is that all particle tracks are identified first before acceptance.

6. Acknowledgement. We are grateful to the Hong Kong Royal Observatory for the continuous supply of meteorological data , the Public Works Department and the Transport Department of Hong Kong for the construction and maintenance of the tunnel laboratory.

References.

1. Ng L K et al, Proc. 16th ICRC (Kyoto) 4 (1979) 232.
2. Fenton A G et al, Proc. 15th ICRC (Plovdiv) 11 (1977) 242.
3. Bergeson HE et al, Proc. 16th ICRC (Kyoto) 4 (1979) 188.

N85-36038

HE 4.5-16

NUCLEAR CASCADES IN ELECTROMAGNETIC SHOWERS PRODUCED BY PRIMARY GAMMA-QUANTA IN THE ATMOSPHERE.

Danilova T.V., Erlykin A.D., Mironov A.V., Tukish E.I.
P.N.Lebedev Physical Institute, Leninski pr. 53,
Moscow, 117924, USSR.

Distributions have been calculated for the number of electrons N_e, number of muons with the energy above 5 GeV N_μ and the energy of hadron component E_h in electromagnetic showers, produced by primary gamma-quanta with energies 10^{13} - 10^{16} eV, incident on the atmosphere at zenith angles $\theta \leq 30°$ and observed at the mountain level 700 g/cm^2. The mean number of nuclear interactions of photons with the energy above 5 GeV is about 0.3 per each TeV of the primary energy and nuclear cascades take out in average about 2% of the total shower energy. The mean number of 5 GeV muons for the electromagnetic shower is (2-5)% from the number of muons in EAS with the same number of electrons at the observation level. Similar value for the total energy of hadron component is also (2-5)%. N_μ and N_e values as well as E_h and N_e don't correlate at the fixed primary energy E_γ^o. Between N_μ and E_h there is a positive correlation at the given E_γ^o.

Simulation of nuclear cascades arising when the electromagnetic shower propagates through the atmosphere has been undertaken in connection with the works on high energy gamma-astronomy carried out at the Tien-Shan EAS array /1/. Similar study is planned at ANI array /2/. The difference between the present set of calculations and that carried out in pioneer works of Wdowczyk /3/ is in their orientation onto Tien-Shan and ANI arrays, i.e. the observation of showers at the mountain level 700 g/cm^2, higher muon threshold energy - 5 GeV and the usage of hadron component as an additional criterium for the selection of pure electromagnetic showers.

Electromagnetic showers were simulated for primary gamma-quanta with energies 10^{13}, 10^{14}, 10^{15} and 10^{16} eV, incident on the atmosphere isotropically in the zenith angle interval $\theta \leq 30°$. The total number of electrons at the level 700 g/cm^2 was determined after the sampling of the first interaction point and of the value $\cos\theta$ by means of approximation formulae of Greisen /4/ or Klimakov-Pavlov /5/. Then the development of the electromagnetic shower in the atmosphere was followed by steps $\Delta z=10$ g/cm^2. The probability for photons $\Gamma(E^{o}_{\gamma}, >5$ GeV, $z)$ to have photonuclear interaction in ide the step was estimated according to formulae of the Approximation A of the cascade theory: $W=1-\exp(-\Gamma(E^{o}_{\gamma}, >5 \text{ GeV}, z/\cos\theta)\cdot\sigma_{\gamma A}\cdot\Delta z/\cos\theta)$. If this probability exceeded 0.1, then the step Δz was reduced by 2, and the procedure repeated. The cross-section of the photonuclear interaction with air atoms $\sigma_{\gamma A}$ was taken constant and equal to 2 mb. When such a photonuclear interaction occured, then the energy of the photon giving rise to the nuclear cascade was sampled within the photon spectrum at the depth z, calculated also by means of Approximation A formulae. The number of 5 GeV muons and the energy of the hadron component in that nuclear cascade, reaching the observation level 700 g/cm^2, were calculated on the base of simulation results, obtained for the "tails" of nuclear cascades with the help of the routine for small EAS simulation /5/. The result obtained for all partial nuclear subcascades in one and the same electromagnetic shower were summarized. For 10^{13}, 10^{14} and 10^{15} eV primary energy 1000 showers were simulated, for 10^{16}-100.

N_e-distributions for simulated showers are shown in the fig.1a. Arrows indicate mean values in these distributions. It is necessary to notice that approximation formulae /4/ give higher values of N_e compared with /5/, which differ by 1.35 at 10^{13} eV and by 1.07 at 10^{16} eV. In the fig.1a results are given, obtained by formulae /4/. It is interesting to note the change of the distribution shape, when E^{o}_{γ} increases. It is due to the shower maximum, approaching the observation level at $E^{o}_{\gamma}=10^{16}$eV and to the different impact of deep penetrations of primary gamma-quantum on N_e, when the shower in the mean is either after the maximum

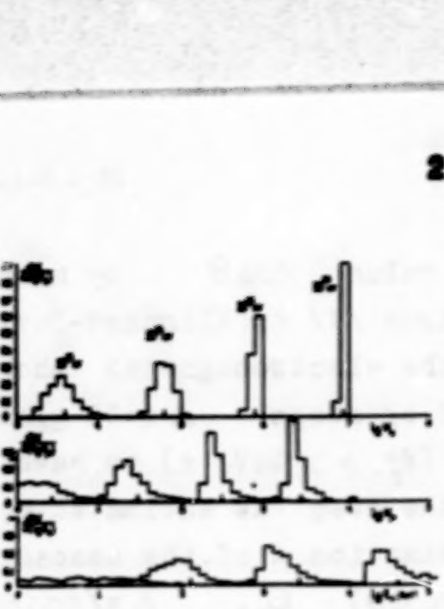

Fig.1.

or in the maximum of its development.

The simulation showed that the number of photonuclear interactions with energies above 5 GeV is proportional to the primary energy E^{o}_{γ} with a good accuracy. The proportionality coefficient is o.358 TeV^{-1} at 10^{13} eV and 0.247 TeV^{-1} at 10^{16} eV, i.e. it is equal to about 0.3 interactions per each TeV of the primary energy. The same concerns the fraction of the total energy, carried out by photons, initiating nuclear cascades in the shower. It is 0.015 at 10^{13}eV and 0.027 at 10^{16} eV, i.e. about 2% of the primary energy in the average.

In figures 1b and 1c distributions are shown for the number of 5 GeV muons and the energy of the hadron component reaching the observation level 700 g/cm^2. Arrows indicate again mean values of $\overline{N}_{\mu}$ and $\overline{E}_{h}$ in the distributions. It is seen that the muon number fluctuates less than the energy of the hadron component. In the figure 2 distributions of the muon number and of the hadron energy in the electromagnetic shower with E^{o}_{γ}=10^{15} eV are shown in comparison with similar distributions for ordinary nuclear EAS with the same N_e. The latter distributions were obtained in the paper /6/. It is seen that N_{μ} and E_{h} distributions for electromagnetic and nuclear EAS are principally rather well separated from each other. Ratios of their mean values, shown in the fig.3, vary from 2.0% at 10^{13} eV up to 4.5% at 10^{16} eV for N_{μ} and from 1.4% at 10^{13} eV up to 5.0% at 10 ^{16} eV for E_{h}, i.e. are about (2-5)% for both values. However since

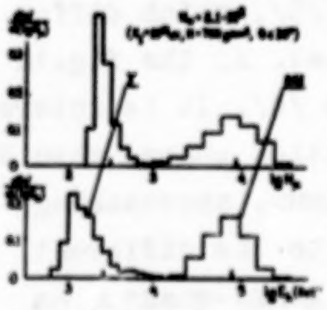

Fig.2.

the absolute number of muons with the energy above 5 GeV in electromagnetic showers is relatively small (~300) for $E_\gamma^0=10^{15}$ eV and they are widely spread over the area, then it is usually difficult to identify electromagnetic showers by muons. It is possible to make this only at arrays with good resolution in the region of muon-poor showers, that is by means of large area of muon detectors about several hundreds of m^2. The identification of electromagnetic shower by the energy of the hadron component is more reliable, since this energy is considerably more concentrated around the shower core. The calorimeter area about several tens of m^2 is enough for such identification.

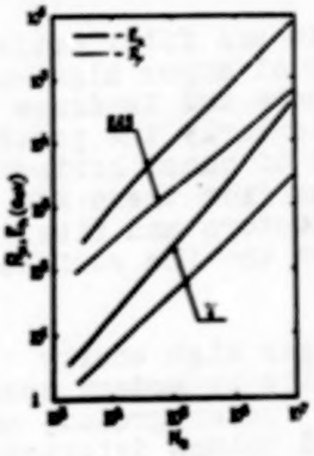

Fig.3

The simulation showed also that N_μ and N_e values, as well as E_h and N_e don't correlate with each other at the fixed value of E_γ^0. At the same time there is a strong positive correlation between N_μ and E_h at the fixed E_γ^0.

References.

1. Stamenov J.N., Ushev S.Z. et.al. 18 ICRC, 1983, Bangalore, 6, 54; Adv. Space Res., 1984, 3, 10.
2. Danilova T.V. et al. 18 ICRC, 1983, Bangalore, 5, 520.
3. Wdowczyk J. IX ICRC, 1965, London, 2, 691.
4. Greisen K. in "Progress in Cosmic Ray Physics" ed. by J.G.Wilson, Amsterdam, 1954, 3.
5. Klimakov A.P., Pavlov A.A. "Elementary particles and cosmic rays", 1976, 4, 35, Moscow, Atomizd. (in Russian).
6. Danilova T.V. et al. 17 ICRC, 1981, Paris, 6, 146.

N85-36039

HE 4.6-2

ON THE POSSIBILITIES OF LARGE-SCALE RADIO AND FIBER OPTICS DETECTORS IN COSMIC RAYS,

G.A.Gusev, M.A.Markov, I.M.Zheleznykh
Institute for Nuclear Research,the USSR
Academy of Sciences, Moscow, USSR

ABSTRACT

Different variants of radio and fiber optics detectors for registration of super high energy cascades in the atmosphere and in dense media are discussed. Particularly the possibilities for investigation of quasi horizontal EAS and simulated muons from these EAS with the help of radio detectors and fiber optics detectors located on the ice surface are considered.

1. Introduction. The problems of super high energy physics and astrophysics not accessable by modern accelerators require creation of surface, under ground, and deep under water super large area and volume detectors. The particles with energy up to $E \simeq 10^{28}$ eV (particularly neutrino) could be created in the evolution of the stable (or long life-time) elementary black holes with Planck's masses and dimensions [1-3] which could have been formed in early Universe. Such absolutely cold black holes ($T \to 0$) could have external mass ($\sim 10^{28}$ eV) determined by the electric charge or the rotational moment.

2. Different Radio Detectors. In recent years several variants of super large radio detectors [3-7] were proposed based on the principle of the registration of the cascade coherent radio emission which was proposed as early as 1961 [8]. We note three possibilities.

The first possibility is founded on the reflection of EAS radio emission from the Earth and ionosphere producing the augmentation of the region where EAS radio emission may be received, up to $10^{4}-10^{5}$ km^{2}. The second possibility is founded on some crust transparency for cascade radio emission created by the neutrino in the crust and spreading out in the atmosphere (RAMAND-A) [3,6,7]. The last possibility (RAMAND-I) [5,7] is founded on the use for example of antarctic ice in which radio emission absorption for frequencies up to 1 GHz is very small (for temperature -50°C in the frequency band 0,5-1 GHz the attenuation is about 10 dB/km).

Particularly a radio detector with volume 10^{11} m^3 could be used for determination of electron antineutrino fluxes in the energy region $6\cdot10^{15}$ eV with the help of the reaction $\tilde{\nu}_e + e^- \rightarrow W^- \rightarrow$ hadrons in the W-boson resonance region and for determination of Pγ-neutrino fluxes [7,9] with energy ~10^{19} eV (compare also optic registration of Pγ-neutrino cascades spreading out in the atmosphere [10]).

3. Large-scale radio detectors for quasi horizontal EAS and muons. Here we consider the possibility of complex radio installation for EAS muons registration by its cascade radio emission in the ice simultaneously with the EAS radio emission. We also discuss the utilization of fiber optics detectors for EAS registration.

It is known that EAS muon spectra (see for example [11] have high energy muon component. Its cascades in the volume 1 km according to [11] have statistics of the order of 10 events per year per steradian for cascade energies above $5\cdot10^{14}$eV. This allows to registrate simultaneously EAS with energy more than $3\cdot10^{18}$eV and muon cascade with energy more than

$5\cdot10^{14}$eV(for effective noise temperature ~1000°C) with probability of the order of 1.

Complex radio detector is shown in Fig.1. Such radio detector has two parts: EAS radio detector (domain 1) and EAS muon cascade radio detector in the ice (domain 2). These parts are placed so that for EAS axe in the domain 1 in the zenith angle region $60^\circ-80^\circ$ the radio spot from the muon cascade with deepness of 500m is projected on the domain 2. The radio detector has 50 antennas (separated from each other on a distance of 500m) with the amplifiers in the frequency band of 30-70MHz, so 7-10 channels receive a signal as much as 30-20dB above the atmosphere noise for EAS energy of 10^{19}eV [3]. Muon cascade radio detector has 50 antennas (placed on a distance 250m) with the amplifiers in the frequency band of 200-100MHz, so for cascade energy about $5\cdot10^{14}$ eV 10-20 channels receive the signal with signal noise ratio ~ 10dB [5].

We consider the possibility of changing EAS radio detector by fiber optics detector. The idea of such detector consists in the registration of the optic Cherenkov radiation of the electrons crossing the light guide. The optic emission guided in the fiber can propagate with small absorption at large

ORIGINAL PAGE IS
OF POOR QUALITY

distances to the photomultiplier (with small photocathode). It is known that after passing the distance of 1 cm in dense matter an electron in the optic region lets 200 Cherenkov photons. For a fiber of the diameter 0,5 mm this will give 10 photons and for an aperture of 0,3 10% of photons will be guided exepting some EAS electrons coming from directions along and normaly to the fiber. So one electron produces one photon guided in the fiber. For a cable consisting of 10 fibers of diameter 0,5 mm the calculation gives 200 photons at the photocathode, if the EAS axe is at distance of 250 m from the cable (EAS energy being $\sim 10^{19}$ eV). If the photomultiplier effectiveness is roughly 10% then there will be registrated 20 one electron pulses during some units microseconds. At Fig.2 the complex detector with EAS fiber optics detector (threshold is about 10^{18} eV) is presented.

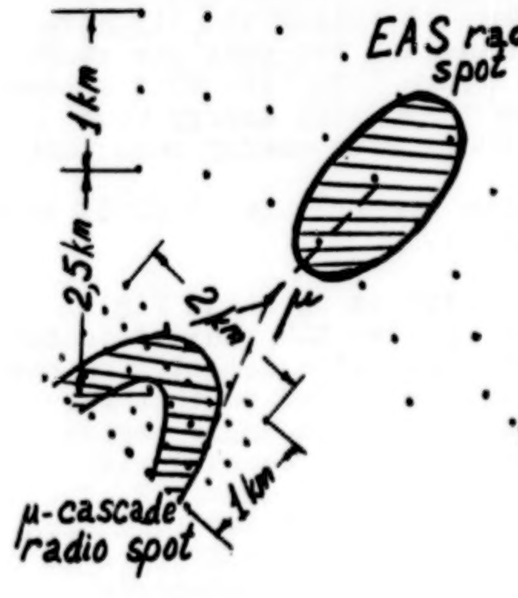

Fig.1. Complex Radio Detector for Quasi Horisontal EAS and Muons.

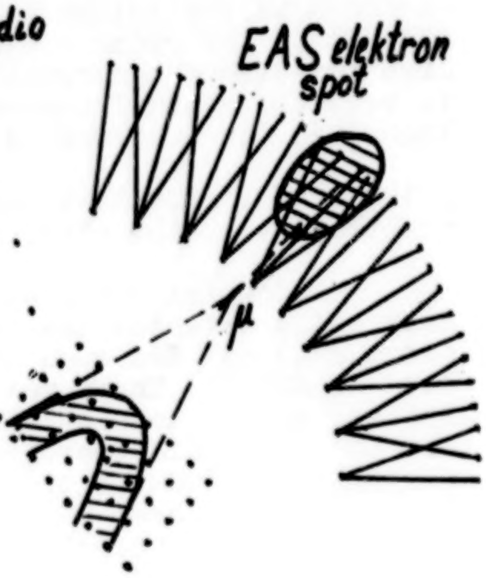

Fig.2. Complex Detector with EAS Fiber Optics Detector.

4. Conclusion. Complex detector placed on the ice surface may be important instrument for research of neutrino, primary composition of cosmic rays, promt muon creation at super high energies and etc.

5. Acknoledgements. We wish to thank A.E.Chudakov and L.G.Dedenko for an useful discussion.

References

1. Markov M.A., On the Upper Limit of the Cosmic Ray Energy Spectrum (DUMAND-type experiments). Preprint INR.P-0197 Moscow 1981.
2. Markov M.A., Zheleznykh I.M. Proc. 1979 DUMAND Workshop at Khabarovsk and Lake Baikal (ed. J.Learned, Honolulu) p.177.
3. Dedenko L.G., Markov M.A., Zheleznykh I.M. Proc. 1981 Int.Conf. Neutrino Phys. and Astrophys.ed. R.Cense, E.Ma, A.Roberts, Maui, Hawaii, 1981, v.2, p.292.
4. Gusev G.A., Dedenko L.G., Markov M.A., Zheleznykh I.M. Pisma JETP, 1982, v.36, p.316.
5. Gusev G.A., Zheleznykh I.M. Pisma JETP, 1983, v.38, p.505.
6. Gusev G.A., Zheleznykh I.M. Uspekhi Fisich.Nauk, 1984, v.143, p.499.
7. Gusev G.A., Dedenko L.G., Zheleznykh I.M. Paper presented at Neutrino-84, Dortmund, 1984.
8. Askaryan G.A. JETP, 1961, v.41, p.616.
9. Gusev G.A., Krystev P., Zheleznykh I.M. Paper presented at Int. Seminar "Quark-84", 1984.
10. Linsley J. Paper presented at 18-th ICRC, India 1983.
11. Kitamura T. DUMAND Workshop at Khabarovsk and Lake Baikal, ed.J.Learned, 1979, p.234.

Radio Signals from Very Large Showers

Suga K.* and Kakimoto F.
Department of Physics, Tokyo Institute of Technology
Meguro, Tokyo 152, Japan

Nishi K.
The Institute of Physical and Chemical Research
Wako, Saitama 351, Japan

ABSTRACT

Radio signals from air showers with electron sizes in the range 1×10^7 to 2×10^9 have been detected at 50kHz, 170kHz and 1,647kHz at large core distances in the Akeno 20km^2 air-shower array. The field strength is higher than that expected from any mechanisms hitherto proposed.

1. Introduction. An experiment is being made to detect low-frequency radio signals from air showers observed in the Akeno 20km^2 air-shower array at large core distances. The motivation is a discussion on the possibility made by one of the present authors(K.S) at the Bangalore Conference in 1983(1) to observe giant air showers by detecting the low-frequency radio signal radiated from the electric current of air-shower particles due to the negative excess during the longitudinal development. And the experiment is an effort in seeking a method to detect air showers at a great core distance, which provides a huge effective area suitable to observe super giant air showers of very low flux beyond the 2.7K Greisen-Zatsepin cut-off, even if exists(2).

2. Experimental. Antennas are located in the yard of a closed primary school at a distance of about 2km from the center of the Akeno 20km^2 air-shower array(3), and the receivers and recording apparatus are set in the classroom. The recording of radio signals is made by a master pulse from the array sent through an optical-fiber cable.

Following two kinds of antennas are operated simultaneously:

(a) Ball antenna(4). A inverted metal cup, whose capacity to the ground is about 10pF, is fixed to the top of vertical glass-fiber pole of 10m and the potential difference of radio signal between the cup and the ground is measured. The preamplifier is enclosed in the metal cup, and the frequency response is flat from several Hz up to 10MHz with a gain of unity.

(b) Vertical wire antenna. A thin wire is stretched vertically along a glass-fiber pole of 10m. The preamplifier is set just above the ground, and the input stage consists of a capacity of 100pF parallel to a resistor of 20MΩ to the ground. The frequency response is flat from a few kHz up to 10MHz with a gain of 2.5.

The output of the preamplifier is sent through a co-axial cable(3C2W) to a receiver in the classroom. Following three kinds of receivers are operated alternately:

(i) Sony CRF1 commercial radio receiver(10kHz-30MHz). The output signal

---

*Present address: Department of Physics, Meisei University, Hodokubo 337, Hino-shi, Tokyo 191, Japan

from the AM detection circuit is recorded at frequencies of 50kHz, 170kHz and 1647kHz. The bandwidth is ±7kHz at -50dB.
(ii) Sony ICF2001 commercial radio receiver(150kHz-30MHz). The output signal from the AM detection circuit is recorded at frequencies of 170kHz and 1647kHz. The bandwidth is almost same as the above receiver(i).
Following three kinds of recorders are operated alternately:
(I) Storage oscilloscope (Tektronix 7834, 400MHz).
(II) Storage oscilloscope (Tektronix 466, 100MHz).
(III) 1-100kHz passive band pass filter(BPF), low noise amplifier(×100, NF circuit LI75A), 17.4kHz active band elimination filter(BEF) and FFT (fast Fourier transform) signal analyser(100kHz, 12bit, Iwatsu SM-2100C).
The display on CRT is made by a master pulse from the air-shower array and, then, the photograph is taken. The sensitivities of all combinations of the antennas and the commercial receivers are confirmed to be almost same at frequencies from 10kHz to 2MHz.

3. Recorded radio signals. Air showers accompanying radio signals observed well beyond the background noise at the output of commercial radio receiver are plotted with large open circles and those unaccompanying radio signals are plotted with small full circles in figure 1(170kHz) and figure 2(50kHz) for air showers with secθ(θ) smaller than 1.30(40°).

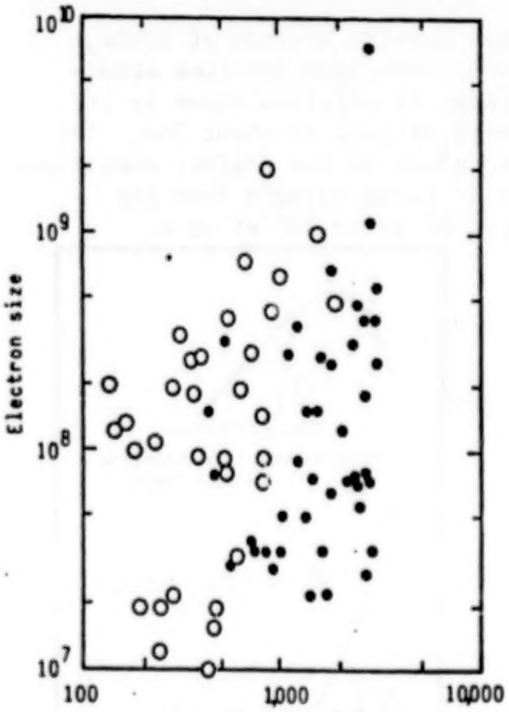

Fig. 1

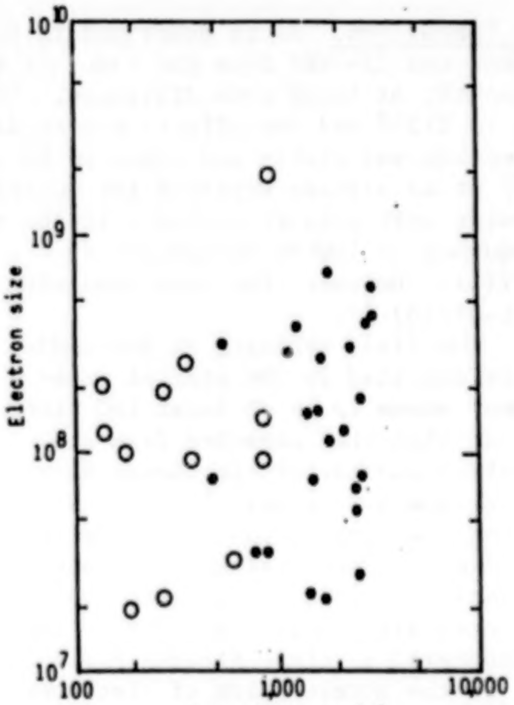

Fig. 2

The effective core distances for showers with zenith angles larger than 40° are somewhat longer. Radio signals were observed at 1647kHz up to almost same core distances as at 50kHz. The effective core distances seem to be independent of the weather condition, such as clear sky, fog, cloud, rain,snow, humidity, temperature, and radio signals have been observed stabely during the intermittent operation in every months from December 1984 to May 1985.

The operation with the FFT signal analyser has been made in order to obtain information on the shape of radio pulse. The 1-100kHz BPF is used to cut intense local MF broadcasts and the 17.4kHz BEF an intense local VLF radio signal. A radio signal stored in the FFT signal analyser with a master pulse from the air-shower array undergoes the Fourier transform, and the real and imaginary parts at frequencies corresponding to man-made radio waves are erased. Then, after the inverse Fourier transform is applied, the reconstructed signal is displayed on CRT and is photographed. A wave packet was observed for a shower with the associated radio signal at the output of the commercial radio receiver. From these patterns of observed wave packets, the main component of frequencies of the radio signal associated with the air shower in the present experiment seems to be above 100kHz of the limit of the signal analyser, although the shape of the radio pulse is not known at present.

The field strength of the radio pulse observed in the present experiment can not be estimated accurately for lack of the knowledge of the pulse shape and due to an application of commercial radio receivers. However, the calibration of the radio receivers with pulses of various shapes and lengths seems to indicate that the field strength of the radio pulse peak may be higher than several mV/m at largest core distances where the radio signals were observed well beyond the background noise level as shown in figure 1 and figure 2.

4. Discussion.

As is described in section 3, radio signals of 50kHz, 170kHz and 1647kHz from the same air showers have been detected simultaneously at large core distances. The range of electron sizes is 1×10^7 to 2×10^9 and the effective core distance extends to about 2km. The detection was stable and seems to be independent of the weather condition. Clay et al already reported the detection of radio signals from air showers with primary energies in the range 10^{15}eV to 10^{16}eV at a frequency of 100kHz (bandwidth 80 kHz)(5). However, the detection was unstable(5)(6).

The field strength of the radio pulse detected in the present experiment seems to be at least 100 times higher than that expected from the electric current of air-shower particles due to the negative excess during the longitudinal development. The field strength seems to be also at least 10 times higher than that expected from local reduction of the atmospheric electric field(A.E.F.) due to the acceleration of electrons produced by ionization of air-shower particles in A.E.F. discussed by Wilson(7). A plausible mechanism to produce radio signals detected in the present experiment seems to be radiation from electrons produced by ionization of air-shower particles in the atmosphere due to the acceleration in A.E.F.. The field

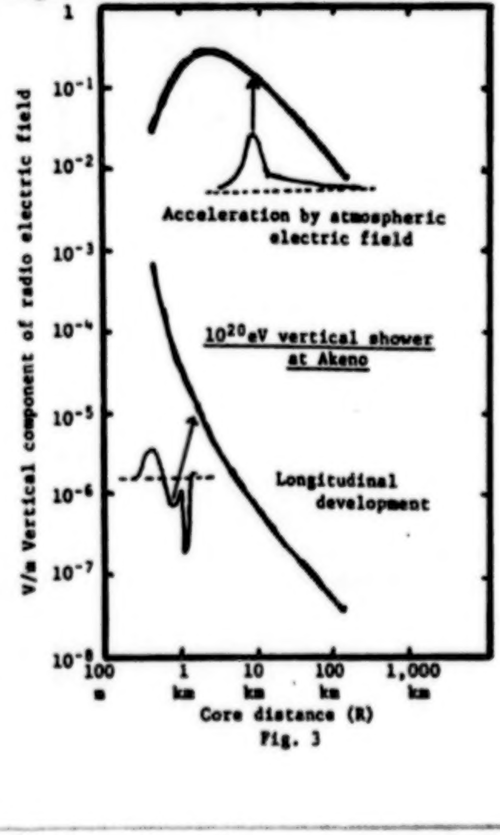

Fig. 3

strength of this radio pulse estimated for a vertical air shower with primary energy of 10^{20}eV observed at Akeno is shown in figure 3, together with that of radio pulse expected from the net negative current of air-shower particles during the longitudinal development. The slow tail of the radio pulse also shown in the figure is due to the acceleration of ions produced by ionization of air shower particles in A.E.F. and contains a frequency component from several tens of Hz to 0.1Hz. This extremely low-frequency component is very important, since the frequencies of the Schumann resonance (earth-ionosphere cavity resonance) are 8Hz and 14Hz for the ground mode and the second mode, respectively. An experiment is undertaken with the ball antenna, a 20Hz passive low pass filter, the low noise amplifier, an active 5-20Hz BPF and the FFT signal analyser.

It is clear that further work to observe many air showers with electron sizes larger than 10^9 is required to examine whether this low-frequency radio method is promising for providing a huge effective area of detection. It is also important to check whether the mechanism tentatively suggested above is accepted. For that purpose, the shape of radio pulse will be examined with a wave form recorder(20ns sampling, 10 bit) connected to the FFT signal analyser.

5. Acknowledgments. The authors wish to express their sincere thanks to Prof. T. Ogawa of Department of Physics of Kōchi University for his suggestion of the ball antenna and to Prof. T. Kamata and Mr. H. Jindō of Institute for Atmospherics Research of the Nagoya University for their suggestion of the vertical wire antenna. The authors are deeply grateful to the staffs of the air-shower group of Institute for Cosmic Ray Research of the University of Tokyo, especially Prof. M. Nagano and Dr. M. Teshima, for their operation of the air-shower array and their analysis of the air-shower data.

References

1. Kaneko T. et al: Proc. 18th Int. Cosmic Ray Conf.(ICRC), Bangalore, 11 (1983) 428
2. Baltrusaitis R. M. et al: Phys. Rev. Lett.54 (1985) 1875
3. Teshima M. et al: This Conference OG 9.4-8
4. Ogawa T.: Contr. Geophys. Inst., Kyoto Univ., 13 (1973) 111
5. Clay R. W. et al: Proc. 13th ICRC, Calgary, 4 (1973) 2420
6. Clay R. W. et al: Proc. 14th ICRC, München, 8 (1975) 3039
7. Wilson R. R.: Phys. Rev. 108 (1957) 155

N85-36041

HE 4,6-4

ON THE PRODUCTION MECHANISM OF RADIO_PULSES FROM LARGE EXTENSIVE AIR SHOWERS

Datta, Mrs. P. and Pathak, K.M.
Department of Physics, Gauhati University,
Gauhati - 781 014, ASSAM, INDIA.

1. **Introduction** : None of the theories (1,2,3 & 4) put forward so far to explain the radio-emission from EAS, has been successful to give satisfactory explanation of all the experimental data obtained from various laboratories over the globe. It is apprehended that emission mechanism at low and high frequencies may be quite different (5). This calls for new theoretical look into the phenomenon.

Using basic equations of Kahn & Lerche (1) and a much sophisticated model for shower structure, Castagnoli et al. (2) calculated the radiation field at a point outside the disc of charges. They, however, calculated the radiation field due to current and excess charge only. In this paper, the requltant field inside the disc of charges, due to current and dipole moment have been calculated afresh using the technique adopted by Castagnoli et al. (2), from very low to very high frequencies.

2. **Methods** : The radiation field at a distance R from the axis of the shower disc can be obtained by phase mixing the contributions from the various rings of charges. For a point lying inside the disc of charges of radius Ro at a distance R from the axis, the point will be an outer one w.r.t. the disc of radius R and an inner one w.r.t. the annular ring of inner radius R and an outer radius Ro. Accordingly, effects of the disc of radius R and the annular ring are to be taken into account.

The current field at a distance R from the axis (R<Ro) :

(A) Current field due to the disc of radius R :

$$E_c'(R) = -\frac{Ke\times10^{8}}{2C(29.4)^2}\times2\pi\times0.4N\times H_0^{(1)}(K\alpha R)\int_0^R J_0(K\alpha r)r^2\left(\frac{r}{29.4}\right)^{-0.75}\left(\frac{r}{29.4}+1\right)^{-3.25}\left(1+\frac{r/29.4}{11.4}\right)dr \cdots (1)$$

(B) Current field due to the annular ring of inner radius R and outer radius Ro :

$$E_c''(R) = \frac{-Ke}{2C}\frac{J_0(K\alpha R)}{(29.4)^2}\times10^5\times2\pi\times0.4N\int_R^{R_0} H_0^{(1)}(K\alpha r)r^2\left(\frac{r}{29.4}\right)^{-0.75}\left(\frac{r}{29.4}+1\right)^{-3.25}\left(1+\frac{r/29.4}{11.4}\right)dr \cdots\cdots (2)$$

The dipole field at a distance R from the axis (R < Ro) :

(C) Dipole field due to the disc of radius R :

$$E_p'(R) = iK\alpha e\tau\pi\frac{0.4N\times10^{8}}{40(29.4)^2}H_0^{(1)\prime}(K\alpha R)\int_0^R J_0(K\alpha r)r^2\left(\frac{r}{29.4}\right)^{-0.75}\left(\frac{r}{29.4}+1\right)^{-3.25}\left(1+\frac{r/29.4}{11.4}\right)dr \cdots\cdots (3)$$

(D) Dipole field due to the annular ring of inner radius R and outer radius Ro :

$$E_p''(R) = iK\alpha e\tau\pi\frac{0.4N}{40(29.4)^2}\times10^5 J_0'(K\alpha R)\int_R^{R_0} H_0^{(1)}(K\alpha r)r^2\left(\frac{r}{29.4}\right)^{-0.75}\left(\frac{r}{29.4}+1\right)^{-3.29}\left(1+\frac{r/29.4}{11.4}\right)dr \cdots\cdots (4)$$

The vector sum of E_c' , E_c'' , E_p' & E_p'' will give the resultant field.

3. __Results__ : Equations (1) to (4) have been integrated numerically at various frequencies for R=40 m, Ro=100 m and E= 10^{16} eV. Theoretical frequency spectra of (i) the present work, (ii) Hough, as well as the experimental data of different workers normalised at 80 MHz with the theoretical curve of Hough (4), are shown in Fig.1.

4. __Discussion__ : Experimental results of different workers (6,7, 8) support the presence of a plateau region in the frequency range (40-60)MHz. For frequencies above 80 MHz, experimental data of the present group, within experimental error, agree with the present calculation. But in the low frequency region (< 10 MHz), none ofthe experimental results support any of the theoretical predictions. It seems to indicate that below 80 MHz besides geomagnetic mechanism,

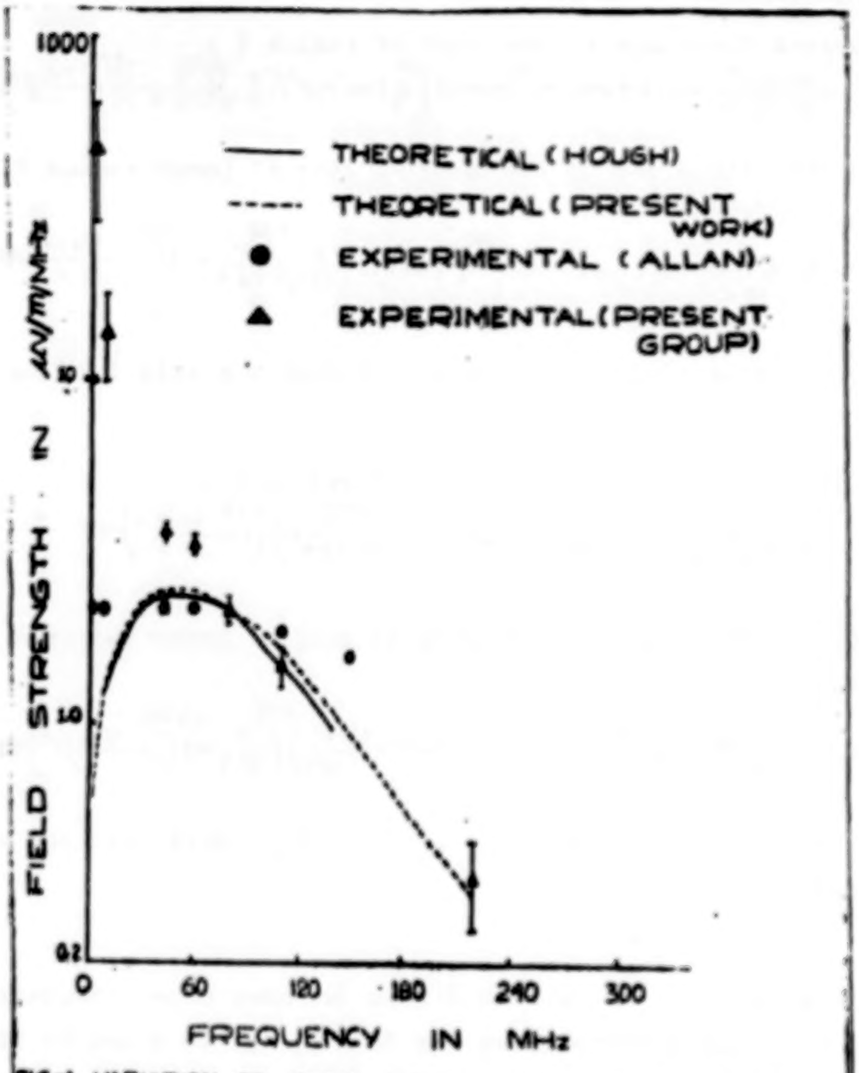

FIG-1. VARIATION OF RADIO FIELD STRENGTHS WITH FREQUENCIES

some other mechanism/s are also involved. Nature of variation of experimental data with frequency shows gradual decrease of the effect of theabove unknown mechanism/s towards 80 MHz.

5. Conclusions : Theoretical as well as the experimental results of the present authors and also of other workers indicate that the frequency spectrum is rather flat in the fruquency range (40-60)MHz. Above 80 MHz, the radio-emission can be explained with the help of geomagnetic mechanism. But at very low frequency ($<$ 10 MHz), mechanisms other than geomagnetic are involved.

6. **Acknowledgements** : The authors thank the Department of Atomic Energy, (BRNS), Govt. of India for funding the project.

References :

1. Kahn, F.D. and Lerche, I., (1966), Proc. R. Soc. A 289, 206.

2. Castagnoli, C. et al., (1969), Nuo. Cim. LXIII B, N.I, 373

3. Allan, H.R., (1971), Prog. Elem. Part. & C.R. Phys., 10 , 171

4. Hough, J.H., (1973), J. Phys. A., 6 , 892.

5. Borah, B. et al., (1983), Proc. ICRC, 6 , 249.

6. Borah, B. et al., (1983), Proc. ICRC, 6 , 245.

7. Allan, H.R. et al., (1970), Nature, Lond. 227.

8. Mandolesi, N. et al., (1976), J. Phys. A., 9 , 815.

* * *

HE 4.6-5

A NEW STUDY ON THE EMISSION OF EM WAVES FROM LARGE EAS

PATHAK K.M. & MAZUMDAR G.K.D.
Physics Department, Gauhati University,
Gauhati-781014, Assam, INDIA

1. Introduction. Studies on Cosmic Ray Showers of energy $E_p \gg 10^{16}$ eV have been continuously pursued since 1970 in Gauhati University, Assam (1). With an GM counters array. EM waves-both at optical Čerenkov and at Radio frequencies (from 2 to 220 MHz) - associated with the showers have been studied in this laboratory. Experimental results obtained reveal the following features:

(i) Frequency spectrum of Radio as well as Cerenkov pulses decreases with increasing pulse heights.
(ii) Field-strength of radio pulses decreases with increase in frequency.
(iii) Radio pulses are polarised in E-W direction. The high value of polarization ratio at 9 MHz appears to confirm the predominance of geomagnetic effect on emission mechanism.
(iv) Studies on the correlation coefficients of emission between radio pulses of different frequency pairs from the same shower indicate:
(a) There is no correlation between low ($\ll$80 MHz) and high ($\gg$80 MHz) radio frequencies.
(b) The positive correlation coefficient between the frequency pairs below 80 MHz (eg. 9-60 MHz) and negative correlation coefficient between any frequency pair below and above 80 MHz (eg. 9-220, 60-80, 60-110 MHz) confirm that the production mechanism of radio pulses below and above the cut off frequency ($\sim$80 MHz) may perhaps be different.
(c) There is no correlation between the emission of optical Čerenkov radiation and radio pulses at different frequencies.

The above observations have tempted us to repeat the whole experiment with a sophisticated particle detector array with facilities for corelocation and energy determination of individual showers. In this paper the new array and the core detection technique along with a few of the sampled parameters, obtained so far, are reported.

2. Methods. (a) The array. The present array consists of seven plastic scintillators (50cm x 50cm x 5cm each) the outermost is located at 100 m from the array centre. Fig 1 gives the schematic diagram of the array used along with

ORIGINAL PAGE IS
OF POOR QUALITY

the positions of the antennas and Čerenkov detector.

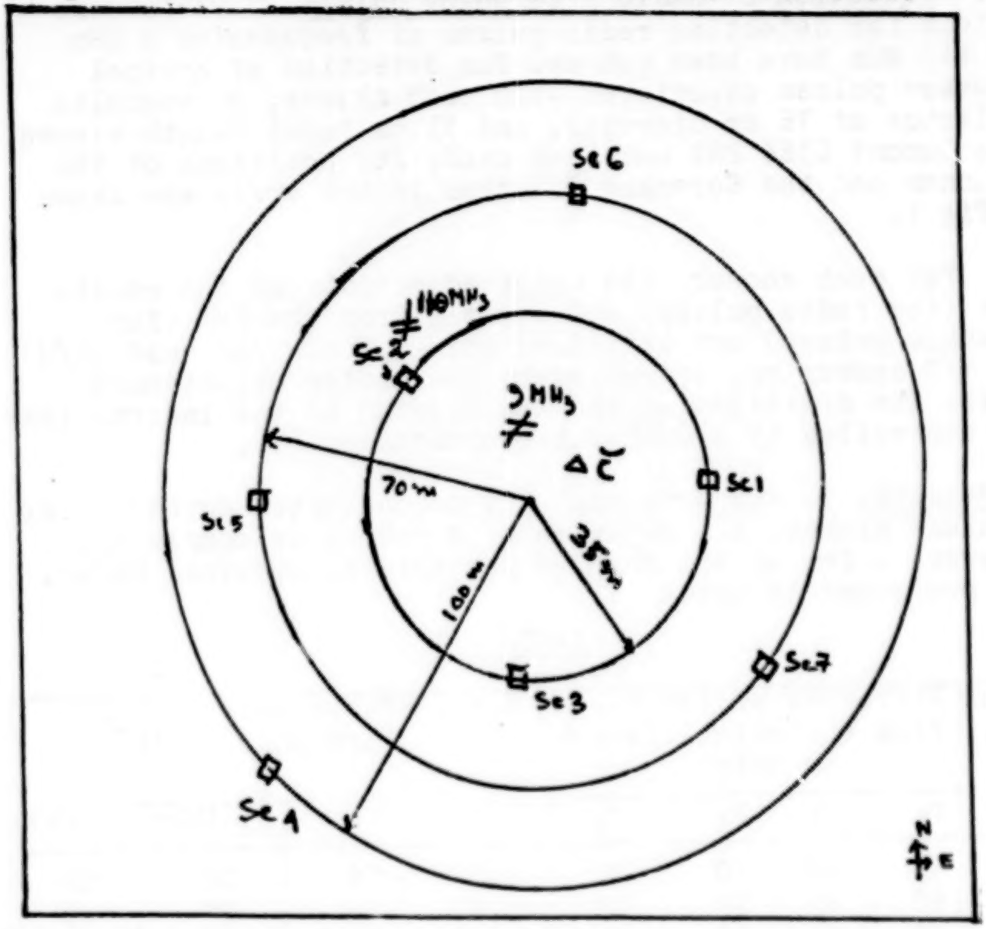

Fig 1. The array. Sc 1-Sc 7 - Positions of scintillators ≠ -positions of Antennas, Δ -position of Č detector.

2.(b) Core location. Each shower can be specified by four parameters viz size (N), co-ordinates of the core (x_0, y_0) and the age (s). Therefore, measurements of four particle densities are, in principle, enough to evaluate these parameters. We assumed NKG lateral distribution for particles given by $\Delta = Nf(r,s)/R_1^2$. It is evident from this that by taking the ratio of densities between any two detectors the parameter N can be eliminated. Numerical calculations using computer (Ellipse 316), give a set of curves i.e. locii of the shower axes producing different density ratios. With these sets of locii, assuming different 'S' values, one can locate the shower core within ±3.3 metres.

The above method has been applied in locating the core of each individual shower. Using a microprocessor-based detecting system (2), the density distribution and hence, energy of each detected shower has been estimated.

2.(c) Detection of Radio & Ćerenkov pulses. Two antenna systems for detecting radio pulses at frequencies 9 MHz and 110 MHz have been set up. For detection of optical Cerenkov pulses associated with each shower, a parabolic reflector of 76 cm diameter, and 13 cm focal length viewed by a Dumont 6364 PMT has been used. The positions of the antennas and the Cerenkov detector in the array are shown in **Fig** 1.

For each shower, the detected outputs of the receivers (for radio pulses) and signals from the PMT (for Ćerenkov pulses) are digitized using sample and hold (S/H) and A/D converter, triggered by the master coincidence pulse. The digitization and the storing of the informations are controlled by a 8085 A microprocessor (2).

3. Results. As the data can only be collected during clear moonless nights, the experiment is yet to be completed. However, a few of the sampled parameters, obtained sofar, are presented in Table 1.

TABLE - 1

Event No.	Distances of the cores from the scintillators in metre				$E_p \times 10^{16}$ in eV	Pulse heights (arb.unit) x 10^{-2}		
	r_1	r_2	r_3	r_4		9MHz	110MHz	Optical
1	55	60	10	80	4.30	75	26	58
2	50	45	28	80	3.57	96	20	40
3	80	53	56	30	0.80	67	26	44
4	65	13	65	105	6.70	80	16	60
5	64	64	105	68	5.90	60	26	30
6	60	60	10	71	0.50	50	20	28
7	62	58	40	68	3.20	70	28	30
8	70	65	40	80	1.20	60	30	40
9	68	60	25	68	4.80	78	30	26
10	45	50	20	65	0.70	65	20	37

r_1, r_2, r_3, r_4 are the distances of the core from Sc 1, Sc 2, Sc 3 and Sc 4 respectively.

4. Conclusions. The work is in progress and we hope to get adequate data within a couple of months or so to test our earlier observations as mentioned in the introduction.

5. Acknowledgements. The authors thank the Department of Atomic Energy (BRNS), Govt. of India for funding the project, and the TIFR, Bombay for some equipments. They al also like to thank the Institute of Advance Studies in Science and Technology (Assam Science Society) for partial funding of the project.

References.

1. Pathak K.M. et al (1982) Proc. of the International workshop on V.H.E.G.R. Astronomy 309.
2. Mazumdar G.K.D. et al (1985) XIX ICRC Papers code HE 4.6-13

AIR FLUORESCENCE DETECTION OF LARGE AIR SHOWERS BELOW THE HORIZON

Peter Halverson and Theodore Bowen
Department of Physics
University of Arizona, Tucson, AZ 85721, USA

In the interest of exploring the cosmic ray spectrum at energies greater than 10^{18} eV, where flux rates at the earth's surface drop below 100 yr^{-1} km^{-2} sr^{-1}, cosmic ray physicists have been forced to construct ever larger detectors in order to collect useful amounts of data in reasonable lengths of time. At present, the ultimate example of this trend is the Fly's Eye system[1] in Utah, which uses the atmosphere around an array of skyward-looking photomultiplier tubes. The air acts as a scintillator to give detecting areas as large as 5000 km^2 sr (for highest energy events). This experiment has revealed structure (and a possible cutoff) in the ultra-high energy region above 10^{19} eV.[2]

The success of the Fly's Eye experiment provides impetus for continuing the development of larger detectors to make accessible even higher energies. However, due to the rapidly falling flux, a tenfold increase in observable energy would call for a hundredfold increase in the detecting area. But, the cost of expanding the Fly's Eye detecting area will approximately scale linearly with area.

It is for these reasons that the authors have proposed a new approach[3] to using the atmosphere as a scintillator; one which will require fewer photomultipliers, less hardware (thus being less expensive), yet will provide position and shower size information.

The Side-Looking Air Shower Detector. As shown in Fig. 1, the Side-Looking Detector (SLD) consists of an array of at least three SLD stations, each containing six photomultipliers, a large cylindrical focusing mirror, and some associated electronics such as PMT power supplies, digitizing modules, and communication equipment (to transmit the digital data to the base station).

Each SLD station would look almost horizontally, dividing the atmosphere into a stack of three wedges 60 degrees wide and 0.2 degrees thick. The three detector stations are identical and are located at the three corners of an equilateral triangle, so their fields of view overlap. Since the detector stations are expected to be able to detect 10^{19} eV events up to 30 kilometers away, our detecting area would be about 380 km^2. If we can detect larger events up to 35 km away, then our detector area will grow to 520 km^2. A cosmic ray shower descending through the atmosphere above the detecting area successively passes through the three wedges of air, whereupon near-ultraviolet photons from excited nitrogen molecules are emitted.

As shown in Fig. 2, the photons are collected by the mirrors in the SLD stations and are focused onto long strips of acrylic that have been doped with the wavelength-shifting chemical BBQ. The BBQ absorbs the ultraviolet photons and re-emits them as green photons, which travel down the plastic strips to PMT's at each end. The PMT's convert the light from the BBQ to photoelectrons which, after being waveform digitized, are transmitted to the base station for data

ORIGINAL PAGE IS
OF POOR QUALITY

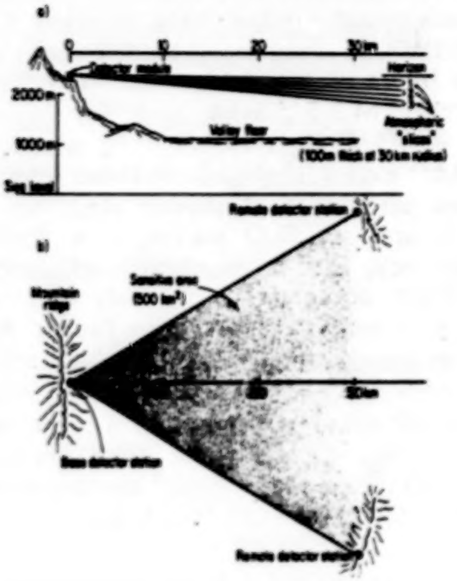
a)
0
10
20
30km
Detector module
Horizon
2000m
Atmospheric "slices"
Valley floor
1000m
(100m thick at 30km radius)
Sea level
Remote detector station
b)
Mountain ridge
Sensitive area (500 km²)
30km
Base detector station
Remote detector station

Fig. 1. Proposed side-looking air fluorescence detector to observe $E \geq 10^{19}$ eV air showers. (a) Side view (Vertical scale: X10), showing three slices or wedges (opening angles ~0.2°) viewed by each station. Viewing angles are set below the horizon to reduce background light; (b) Plan view, showing suggested triangular coverage of three stations, each having a horizontal viewing wedge angle of 60°.

analysis. The amplitude and timing information in the light pulses resulting from the passage of the cosmic ray shower contains information about the shower's location, orientation, and energy. The location and distance from the detector stations of the shower can be determined by accurately comparing the arrival times of the light pulses at each station and for each wedge. By comparing the arrival times of the photons in the upper and lower wedges at each station, the orientation of the shower may be determined. Once the distance of the shower from the SLD stations has been computed, the size of the light pulses can be used to compute the shower size. With stations located at the three corners of a triangle, the corrections required for atmospheric light attenuation can be computed from the data, as well as from calibration light flashes sent from one station to another. The calibration flashes would also synchronize the timing at the remote stations.

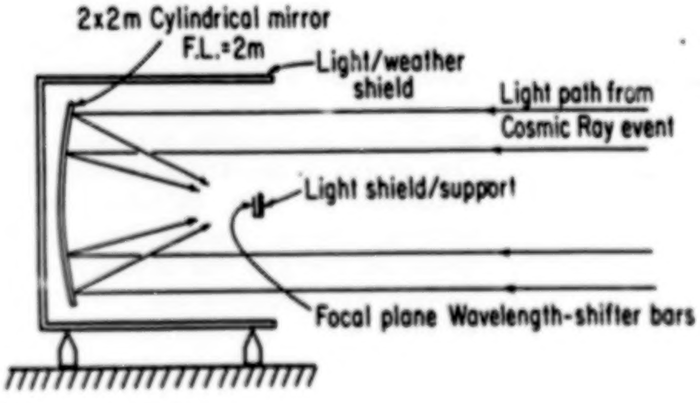
2x2m Cylindrical mirror
F.L.=2m
Light/weather shield
Light path from Cosmic Ray event
Light shield/support
Focal plane Wavelength-shifter bars

Fig. 2. Side view of proposed SLD station.

Design Equations. If S is the number of photoelectrons due to the shower, and $b\tau$ is the number of photoelectrons due to background light in time interval τ, then the fractional error is given by $\sigma(S)/S=(S+b\tau)^{1/2}/S$, which must be $<<1$ for a useful measurement. It is convenient to define a figure of merit M, which is the square of the reciprocal of the fractional error; $M \equiv S^2/(S+b\tau) >> 1$ for a useful measurement. It can be shown that $M = K_1/[(1/\delta)+K_2(1+(\ell/r\delta)^2)^{1/2}]$, where $K_1 = [qN_eA\epsilon]/[4\pi r \exp(\alpha r)]$, and $K_2 = [4\pi\beta I_{sky}\Delta\lambda\phi r^2 \exp(\alpha r)]/[qN_ec]$. In these equations, q = no. of optical air fluorescence photons per meter of shower electron track (~3), N_e = no. of shower electrons, A = area of SLD mirror, ϵ = combined wavelength shifter and photocathode efficiency, α = attenuation coefficient for light transmission in air, r = distance from detector to shower, I_{sky} = no. photons/m^2-s-sr-Å in night sky (~4x10^8), β = intensity reduction factor due to viewing below horizon (~0.4), $\Delta\lambda$ = effective bandwidth of detector (~90 nm), ℓ = lateral size of shower (~100 m), c = speed of light, ϕ = horizontal opening angle of viewing wedge (1.047 rad), and δ = its vertical opening angle. As δ increases, M approaches a maximum possible value, K_1/K_2, because the time interval τ increases with δ. If $A\epsilon$ is chosen to be 0.25 m^2 and N_e is 8×10^9 electrons for an event at r = 30 km, then $K_1/K_2 = 9.3$ and $M = 4.9$ if $\delta = 0.2°$ (τ~0.5 μs).

The Scintillation Efficiency of Air. We have carried out a small experiment using ground-level muons in the laboratory to confirm that the yield of photons per meter, q, into a PMT with bialkali response is 3.2±0.5 photons/meter. A black box was employed so Cherenkov photons would be absorbed; most ground-level muons are near or below the Cherenkov threshold in air, so the black walls appear to reduce the Cherenkov component to a negligible level relative to air fluorescence. The yield was obtained from the counting efficiency for single-photoelectron pulses in a 5 inch RCA 4522 PMT viewing 20.3 cm of path.

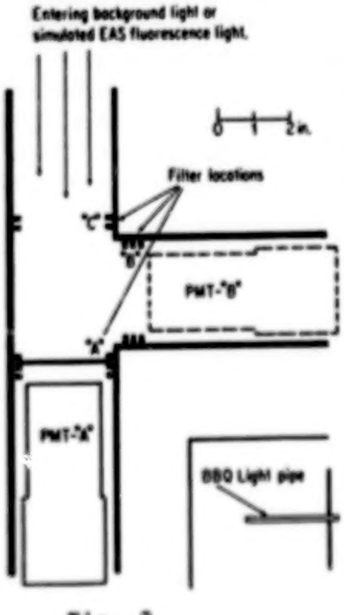
Entering background light or simulated EAS fluorescence light.
0 1 2 in.
Filter locations
"C"
"B"
"A"
PMT-"B"
PMT-"A"
BBQ Light pipe

Fig. 3.

The Effect of Filters on Signal and Background. The apparatus used in making these measurements is shown in Fig. 3. The transmission coefficient of each filter was measured by comparing the output current of an RCA 6655A photomultiplier having S11 response with and without the filter in place. Two sets of data were gathered: filter performance on background light, as observed from Mount Hopkins, and filter performance on light from each of the major air fluorescence lines, as produced by a monochrometer. Table I shows the factor by which the figure-of-merit, M, is predicted to improve with the use of each filter. The emission spectrum predicted by Bunner[4] was employed in the calculations. The distance between the air shower and the detector must be specified because the attenuation due to Rayleigh scattering significantly modifies the source spectrum.

Since the signal-to-background ratio tends to be smallest for the most distant events, the UG-5 and U330 filters have the most favorable characteristics among those listed. Filtering also attenuates the signals; this must be considered along with the improvement factors. If a filter with ≥70% transmission for the 3914 and 4000 Å bands could be found, it would be better than any of those listed in Table I.

Table I. Expected figure-of-merit improvement factors for various filters.

Event Distance [km]	Filter: UG-1	UG-5	U330	U340
0	5.0	4.8	4.6	4.1
4	4.4	4.5	4.2	3.3
16	2.7	3.5	3.3	1.4
32	1.6	2.8	2.7	0.5

The Effect of Viewing Below the Horizon. The background light intensity I_T, below the horizon at Mount Hopkins, Arizona was compared with the dark night sky intensity I_0. At each angle, the distance to the valley floor could be calculated. Figure 4 shows I_T/I_0 as a function of the g/cm^2 of air between the detector and the valley floor. As shown by the curves, the data seem to agree with a model in which the below-horizon background is due to Rayleigh-scattered light; for this model I_T/I_0 approaches 0.5 for infinite air thickness.

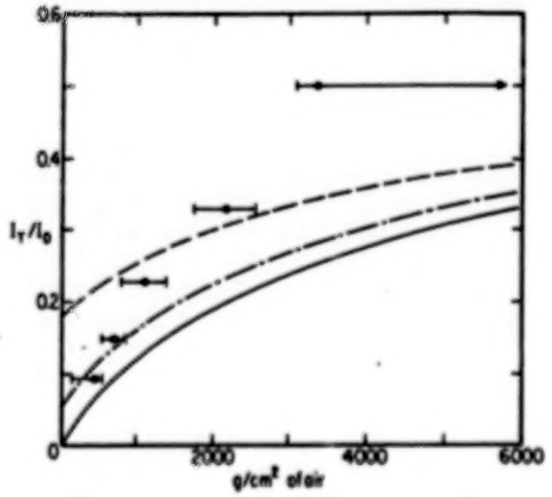

Fig. 4, Plot of scattered light observed at Mt. Hopkins as a function of air thickness to the ground. The theoretical curves are for 0%, 5%, and 18% (solid, dot-dashed, and dashed, respectively) ground reflectivities.

Conclusion. Filters and below-horizon viewing may offer important advantages for an economical side-looking air fluorescence detector.

Acknowledgments. The authors thank Charles Bridges for his assistance with the measurements. This work is supported by NSF Grant No. PHY-82-07697.

1. R. Cady et al., "The Fly's Eye," Report UUHEP-83/11, University of Utah, 1983.
2. R. M. Baltrusaitis et al., Phys. Rev. Lett. 54 (1985).
3. T. Bowen and P. Halverson, Proceedings of Workshop on Cosmic Ray and High Energy Gamma Ray Experiments for the Space Station Era, Baton Rouge, LA, 17-20 October 1984.
4. A. N. Bunner, "Cosmic Ray Detection by Atmospheric Fluorescence," Thesis, Cornell University, 1966.

INVESTIGATION OF COSMIC RAYS IN VERY SHORT TIME SCALES

J. Peltonen, E. Valtonen, J.J. Torsti, H. Arvela, M. Lumme,
M. Nieminen and E. Vainikka

Wihuri Physical Laboratory, University of Turku, and
Department of Physical Sciences, University of Turku,
SF-20500 Turku, Finland

ABSTRACT

We have constructed a fast databuffer system, where cosmic ray events in the Turku hadron spectrometer, including particle arrival times, are recorded with time resolution of 100 ns. The databuffer can be read continuosly by a microprocessor, which preanalyses the data and transfers it to the main computer. The time span, that can be analysed in every detail,is a few seconds.

The high time resolution enables a study of time correlated groups of high energy particles. In addition the operational characteristics of the spectrometer can be monitored in detail.

1. The spectrometer

The Turku hadron spectrometer consists at present of a double neutron monitor combined with plastic scintillators. The spectrometer has been used to measure the energy spectra of neutrons and protons in the energy range .05 - 1000 GeV. Detailed description of the apparatus and its future development is given in paper /1/ presented at this conference.

2. The data collection system

Two identical microprocessor units are used in the Turku hadron spectrometer to collect the cosmic-ray events. Both units can record the status of the spectrometer with time resolution of 50 μs. This time resolution already enables a detailed study of very rapid cosmic-ray phenomena. It is also possible to study the spectrometer characteristics in detail.

The two microprocessor units have different tasks. Unit 1 calculates the hadronic spectra and monitors the hadron and muon flows through the spectrometer. Unit 1 is programmed to study energy dependent variations of hadron and muon intensities in time scales > 30 s. A detailed description of the microprocessor 1 and of its software was given in /2/.

Unit 2 can be used parallel with unit 1. Its time resolution can be improved by adding a fast data buffer. This data buffer records spectrometer events, including particle arrival times, with time resolution of 100 ns.

The overall diagram of the data collection system is given in fig. 1.

2.1. A fast data buffer

The heart of the buffer memory is a DUALPORTED FIFO-memory type IDT-7201-S-80-C from Integrated Device Tecnology (identical to better known MK4501 from Mostek) This memory component is very handy in data buffering applications. The READ-WRITE-operations can be done truly asyncronously and independently. Besides, these new memories are fast (cycle time 100 ns or even better) and easily cascadable.

The schematics of the data buffer is given in fig. 2. The 8 parallel FIFOs form a memory of 64*512. This memory can be triggered from 6 sources. On every trigger the logic generates a common WRITE-pulse and 64-bits of data is latched in, including the data of the time counters. The status and control signals are connected to microprocessor, which can acces the READ-side of the FIFOs.

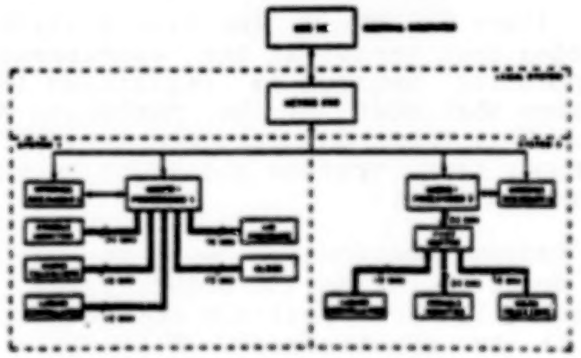

Fig. 1. The overall diagram of the control system.

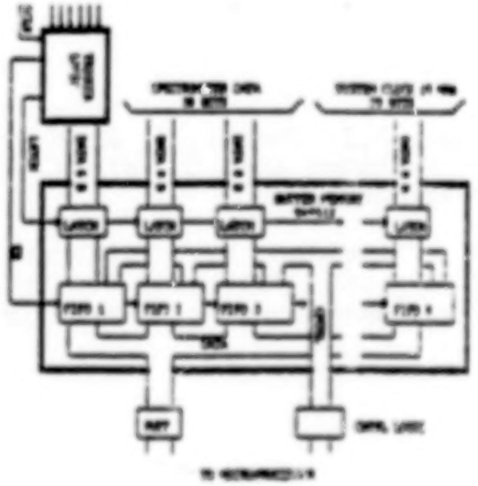

Fig. 2. Schematic of the data buffer.

ORIGINAL PAGE IS
OF POOR QUALITY

---

3. Some results and discussion

Until now, the system 2 has been used only for some simple, mainly instrumental measurements. Two examples of these measurements are shown in figures 4 and 5. The study of more interesting problems, like long tails of extensive air showers and time behaviour and detection of high energy bursts (γ-ray bursts) requires longer measurements.

In fig.3 , the measured time intervals between charged particles coming into our spectrometer are shown. According to Poisson-statistics we should have exponential distribution of the form $A*\exp(-kt)$. As one can see from figure 3, the measured time distribution is strictly Poissonian when $t > 20\ \mu s$. At shorter time intervals there is, however, an excess of events, compared with the Poisson distribution. We believe that most part of these events can be explained by afterpulses from the photomultipliers. The exact portion of afterpulses and the role of some other possible phenomen in these events are being investigated.

In fig. 4, there is shown the time distribution of charged particles that arrive at the spectrometer before the first evaporation neutron is registered in the monitors. It can be seen that most of the particles arrive at times $t < 250\ \mu s$. This time distribution is important, since we separate muons from protons and pions by assuming certain maximum reaction delay.

The Turku hadron spectrometer will be used in future as a central detector of an air shower array /1/ . In addition, there will be position and direction sensitive detectors in the spectrometer. With the fast recording system described and with some additional electronics we can analyse cosmic ray showers and bursts in detail.

References

/1/ E. Valtonen, J.J. Torsti, H. Arvela, M. Lumme, M. Nieminen, J. Peltonen and E. Vainikka, paper HE 4.6-8 in this conference,

/2/ Lumme, M., Nieminen, M., Peltonen, J., Torsti, J.J., Vainikka, E., and Valtonen, E., Proc. 18th Int. Conf. Cosmic Rays, Bangalore, 8, 182-5 (1983).

ORIGINAL PAGE IS
OF POOR QUALITY

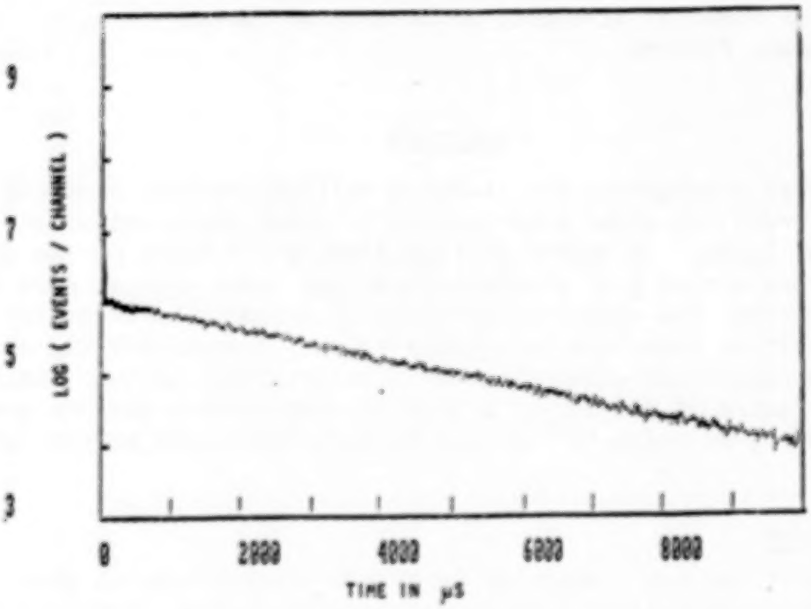

Fig. 3. The time interval distribution of charged cosmic-ray particles in the Turku hadron spectometer.

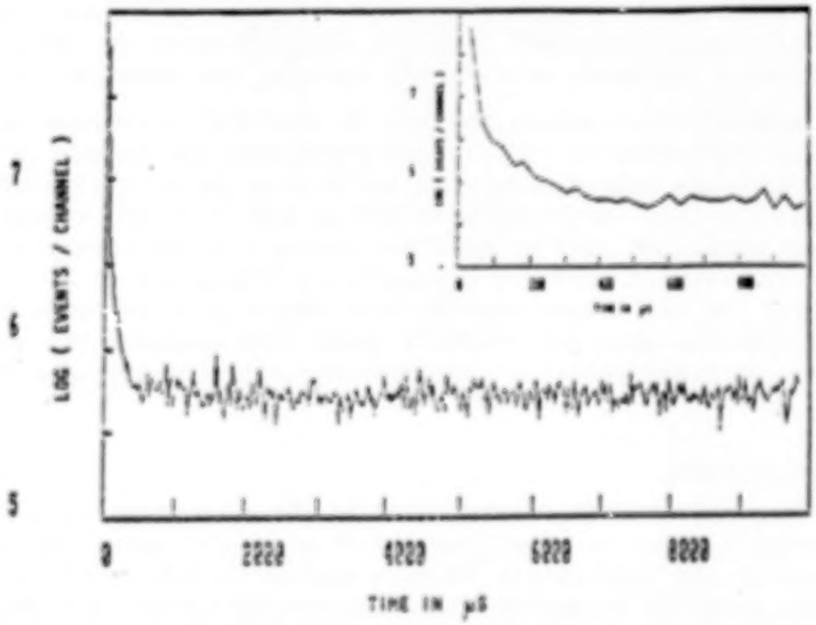

Fig. 4. The time distribution of charged particles arriving at the spectrometer before the first neutron is detected in the neutron monitors. This time distribution is used to separate protons and pions from muon background.

N85-36045

HE 4.6-8

A FACILITY FOR INVESTIGATION OF MULTIPLE HADRONS AT COSMIC-RAY ENERGIES

E. Valtonen, J.J. Torsti, H. Arvela, M. Lumme, M. Nieminen, J. Peltonen, and E. Vainikka

Wihuri Physical Laboratory, University of Turku and
Department of Physical Sciences, University of Turku,
SF-20500 Turku, Finland

ABSTRACT

An experimental arrangement for studying multiple hadrons produced in high-energy hadron—nucleus interactions is under construction at the university of Turku. The method of investigation is based on the detection of hadrons arriving simultaneously at sea level over an area of a few square metres. The apparatus consists of a hadron spectrometer with position-sensitive detectors in connection with a small air shower array. The position resolution using streamer tube detectors will be about 10 mm. Energy spectra of hadrons or groups of simultaneous hadrons produced at primary energies below 10^{16} eV can be measured in the energy range 1-2000 GeV.

1. Introduction

Measurements of the exact shape of cosmic-ray hadron spectra give information on the properties of high-energy hadron—nucleus interactions. Recently, energy spectra of charged and neutral hadrons were measured at sea level in the range 0.05-1000 GeV /1/. Particularly interesting is the spectrum of pions, because the few previous measurements made at sea level have given contradictory results /2,3,4/. Nieminen et al. /1/ estimated pion spectrum assuming an identical shape of neutron and proton spectra above 5 GeV and a proton-to-neutron ratio of 1.05. Even then, above 50 GeV only upper bound was obtained for pion spectrum. This was due to simultaneous incidence of multiple hadrons, not necessarily pions.

Incidence of several simultaneous hadrons in sea-level detectors was earlier studied theoretically /5/. It was shown that the frequency of occurrence of multiple hadron events is noticeable above total hadron energies of about 100 GeV increasing with energy and is strongly dependent on the detector area. The role of multiple hadrons in the interpretation of air shower results was recently discussed by Sreekantan et al. /6/. At high energies the air shower results were found to be severely distorted if these events were not properly taken into account. The present report concerns an experimental arrangement for studying multiple hadron production.

2. Hadron spectrometer

Front view of the hadron spectrometer used in the experiment is shown in figure 1. Central part of the spectrometer is a double neutron monitor. Effective depth of the lead target in each monitor is 270 gcm^{-2}. Evaporation neutrons produced in hadron—lead-nucleus collisions are detected with 16 BF$_3$-counters with an average efficiency of 12.5 % /7/. In addition to the double neutron monitor, five liquid scintillation counters (100×100×0.7 cm^3), viewed from two sides by photomultipliers, are used to measure the energy of electromagnetic cascades produced in the spectro-

*

C-5

meter. The thicknesses of the four iron absorbers shown in fig. 1 are 1.2 cm, 5 cm, 10 cm, and 10 cm, starting from the top. The total depth of lead and iron in the spectrometer is 4.5 interaction mean free paths of hadrons. The measurement of energy of incident hadrons is based on recording the multiplicities of neutrons produced in each monitor and on the pulse heights observed in the liquid scintillators due to electromagnetic cascades. The spectrometer can be used in the energy range 1-2000 GeV.

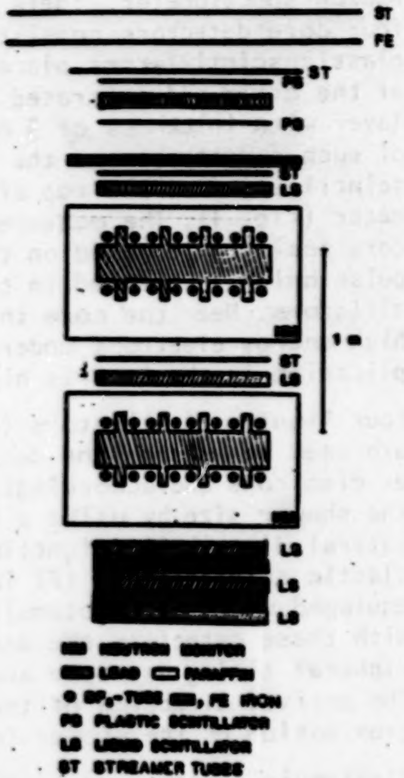

Fig. 1. Front view of the hadron spectrometer.

3. Position-sensitive detectors

Three layers of streamer tubes at the top of the spectrometer (fig. 1) are used to determine the number of simultaneously incident charged hadrons. The uppermost tube layer is unshielded while the other two are shielded against low-energy electrons by lead and/or iron layers. The active areas of these three detectors are 4.0, 1.7, and 1.0 m^2. The streamer tubes are of the same type as those of the Mont Blanc detector described by Iarocci /8/. The basic element is an 8-cell plastic profile coated with graphite. The dimensions of a cell are $0.9 \times 0.9 \times 120$ cm^3. The diameter of the Be-Cu anode wires is 100 µm and the gas filling is a mixture of 75 % isobutane and 25 % argon. Two-dimensional read-out from each three tube planes by perpendicular induction strips enables the determination of positions and number of incident particles. To solve mirror ambiguities, the induction strips of successive tube planes are rotated by 45° with respect to each other. By using digital read-out, the position resolution will be about 10 mm. In addition, the angle of incidence of particles can be measured with an accuracy of about 2 degrees. The read-out electronics are based on commercial Camac system. A special circuit has been designed, which triggers the read-out in case a selected number (≥ 2) of charged particles traverses the sreamer tube layers.

A fourth layer of streamer tubes is installed between the two neutron monitors (fig. 1). This detector enables measurement of positions of showers produced in hadron cascades in the upper monitor. Thus, also the number of neutral hadrons incident on the spectrometer and interacting in the lead target can be determined.

4. Air shower array

The air shower array which will be constructed in connection with the hadron spectrometer is shown in figure 2. The shower parameters to be measured are core position, size, and arrival direction of a shower. The principal idea is to study hadrons near the shower core. The core position is determined using the method proposed by Bergamasco et al. /9/. This method enables the signals from the core detectors to be used as a master trigger for the other instruments in case the core falls in an appropriate distance (≲20 m) from the hadron spectrometer. There are in total four core detectors consisting of two plastic scintillators placed one on top of the other and separated by a lead layer with thickness of 5 cm. An example of such a detector are the two plastic scintillators at the top of the spectrometer (fig. 1). The measurement of the core position is based on the relative pulse heights observed in the two scintillators. Near the core the number of high-energy electrons undergoing multiplication in the lead is high.

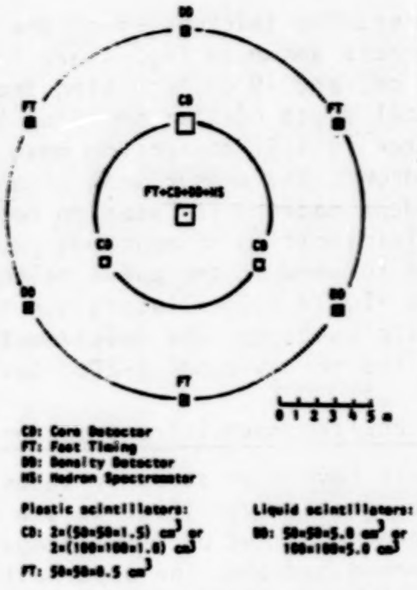

Fig. 2. Air shower array.

Four liquid scintillators (DD in fig. 2) are used to measure the density of shower electrons and accordingly to estimate the shower size by using a theoretical lateral distribution function. Four plastic scintillators (FT in fig. 2) are equipped with fast photomultipliers. With these detectors the arrival times of the shower front in each peripheral timing detector are measured with respect to the central detector. The arrival direction of the shower is then estimated using plane approximation of the shower front.

Electronic system used to measure all the pulse heights and time differences is based on Camac equipment. Microcomputers are used to read the data and store it on floppy disks. Hadron cascade model of Lumme et al. /10/ is being extended to include electromagnetic component in order to calculate response of the array as well as the accuracy of shower size, core position and arrival time measurements.

5. Discussion

Assuming that multiple cosmic-ray hadrons arriving simultaneously at sea level are produced in the last collision of a high-energy hadron in the atmosphere, the height of production will be a few hundred metres and particles detected over an area of 1 m^2 at sea level are emitted into very narrow cone (≲1 mrad). The higher is the collision point in the atmosphere, the narrower is the emission cone. Accordingly, such events of multiparticle production are detected, where the relative transverse momentum of the particles is very small. Using the experimental arrangement described above, intensities and energy spectra of groups with various numbers of hadrons can be studied. Restricting to single particles, the exact shape of energy spectra of cosmic-ray hadrons (e.g. pions) can be measured. Investigation of lateral distribution of particles produced in the same collision and emitted into a narrow cone is also possible, fixing the center of the group to the position of the most energetic particle. This can be estimated by determining the number of charged particles in hadron cascades observed under the first neutron monitor using analog read-out of the streamer tubes or possibly simply by observing the physical size of the clusters produced by the developing cascades.

Multiple high-energy hadrons observed without accompanying air showers are thought to be produced in diffractive excitation processes. In these processes the primary particle retains most of its energy thus preventing the development of a shower. Recently, however, a model of coherent production of hadrons with small transverse momentum from nuclear targets was advocated by Berlad and Dar /11/. The mechanism was attributed to the decay of resonances produced in Coulomb excitation. By measuring intensities of groups of simultaneous hadrons, energy dependence of cross sections of coherent production can be studied and their possible contribution to the rising total cross section estimated. Even the relative contribution of single and double diffractive excitation can be studied on the basis of observed single and double clusters of particles.

Multiple hadrons have been earlier investigated in air showers /6/ and at very high energies (> 1 TeV) by several groups using emulsion chambers. In the present experiment occurrence of multiple hadron events is studied both in air showers and without accompanying air shower. Furthermore, also low-energy (∝1 GeV) hadrons are taken into account. Primary energy range covered by the experiment is from 1 TeV upto about 10000 TeV. Properties of multiple production in air showers are of great importance and could explain, at least in part, for example the observed increase of transverse momentum with energy.

References

/1/ Nieminen, M., Torsti, J.J., Valtonen, E., Arvela, H., Lumme, M., Peltonen, J., and Vainikka, E., J. Phys. G 11, 421 (1985).

/2/ Brooke, G., Meyer, M.A., and Wolfendale, A.W., Proc. Phys. Soc. 83, 871 (1964).

/3/ Diggory, I.S., Hook, J.R., Jenkins, I.A., and Turver, K.E., J. Phys. A 7, 741 (1974).

/4/ Ashton, F. and Saleh, A.J., Proc. 14th Int. Conf. Cosmic Rays, Munich, 7, 2507 (1975).

/5/ Arvela, H., Lumme, M., Nieminen, M., Peltonen, J., Torsti, J.J., Vainikka, E., and Valtonen, E., J. Phys. G 10, 695 (1984).

/6/ Sreekantan, B.V., Tonwar, S.C., and Viswanath, P.R., Phys. Rev. D 28, 1050 (1983).

/7/ Arvela, H., Torsti, J.J., and Valtonen, E., Nucl. Instrum. and Methods 192, 467 (1982).

/8/ Iarocci, E., Nucl. Instrum. and Methods 217, 30 (1983).

/9/ Bergamasco, L., Castagnoli, C., Dardo, M., and Saavedra, O., Nuovo Cimento 2C, 453 (1979).

/10/ Lumme, M., Nieminen, M., Peltonen, J., Torsti, J.J., Vainikka, E., and Valtonen, E., J. Phys. G 10, 683 (1984).

/11/ Berlad, G. and Dar, A., Phys. Rev. D 21, 3133 (1980).

N85-36046

HE 4.6-9

A POSSIBLE EAS ARRAY ABOVE THE SOUDAN II DETECTOR

K. Sivaprasad
Department of Physics & Astronomy
University of Maryland
College Park, MD 20742
(On leave from TIFR, Bombay, India)

ABSTRACT

Multiple high energy muons, when studied with a large area detector, can be useful in the study of the composition of Cosmic Rays at energies ~10**14 eV. The Soudan II detector, primarily designed to detect nucleon decay, is located ~600 m deep underground and has dimensions 16m X 8m X 5m(height), and is made up of drift tubes. The minimum muon energy needed to penetrate that depth is ~500 GeV.

We have used a set of simulated EAS to calculate the rate of muon associated events, using a trigger array with the number of detectors varying from 37 to 127 (the radius of acceptance varying from 50m to 100m). The number of simulated showers, initiated by different nucleii(mass A) used in the calculations, is given in the following table.

A	$E_o >$:	50 Tev	100 Tev	400 Tev	1600 Tev
1		711	917	711	-
4		-	306	1100	-
14		-	-	686	120
24		-	-	629	149
56		-	-	1100	88

The association rate is seen to be a strong function of the multiplicity of muons in the detector. The difference in the rates of association of proton and nucleii induced showers rises rapidly with multiplicity. More detailed decoherence studies, which is possible with this high resolution detector, and correlation with shower chartacteristics is under progress.
Flux considerations dictate that a minimum radius of 100m for the EAS array is essential for the method to be useful.

N85-36047

FAST SCINTILLATION COUNTER SYSTEM AND PERFORMANCE

Sasaki,H., Nishioka,A., Ohmori,N., Kusunose,M.
Kochi University, Kochi, Japan
Nakatsuka,T.
Konan University, Kobe, Japan
Horiki,T.
The Institute of Physical and Chemical Research, Woko, Japan
Hatano,Y.
Institute for Cosmic Ray Research, University of Tokyo, Tokyo, Japan

§1. Introduction.

At the investigation of the arrival time distribution, it is very important to measure the pulse wave-form precisely as much as possible and still the observation by fast pulse technique has attracted the attention of many researchers.(1),(2),(3),(4)

Experimental study of the fast scintillation counter(FS) system to observe a shower disk structure at Mt.Norikura are described in this paper, especially on the system performance and a pulse wave-form by a single charged particle. Some improvements were made on a few points. As reported at the previous conference, the photomultiplier tube pulse (PT-pulse, at Bangalore called a knot pulse) is appeared at the leading edge of the main pulse. To remove this PT-pulse from the main pulse , we changed the frame of the scintillator vessel (1) and have made the fast triggering system to decrease the dead time which came from the use of the function of the self triggering of the storage oscilloscope(OSC). To provide a new field on the multi-parameter study of the EAS, the system response of our FS system also improved as a results of many considerations.

§2. Experimental.

For the fast triggering system , four $0.25m^2$ trigger fast scintillation counters (TFS) were used for the air shower trigger and two $0.0625m^2$ TFS used for the identification of a single particle at the present work, where the photomultiplier is the same one for the FS(R329-02,Hamamatsu). A block diagram of developed fast trigger system and the FS system is shown in Fig. 1. Four constant fraction timing discriminators (CFTD) were added last year, where its propagation delay is $\sim$10nS ,time walk is $\sim$1.5nS and the out put pulse width was set to 80nS, because of the usage for the EAS trigger.

Used plastic scintillators for the FS to measure pulse wave-forms, are the polymerization type ternry plastic scintillator plates($50x50x5cm^3$) with the same lot(CI LTD). To avoid diffused reflection, the inside wall of the scintillator vessel is covered with a sheet of black paper except for the bottom. The signal outputs from the FS were connected to a storage oscilloscope(TS8123,IWATSU) with a 15m 10D2V cable and a 5cm 58 U/G cable and terminated to 50Ω by the terminator(BB50M1 frequency range is DC$\sim$3GHz) at the entrance of the storage main amplifier . Coincidence output signal triggers the storage OSC of the external trigger mode, first of all, and when the service request signal through GPIB control Bus is transmitted from the storage OSC to the personal computer, the computer begins to control the GPIB data Bus. It takes about 12 seconds per one record.

By the way,the definition of the pulse wave-form parameters, such as a rise time, FWHM and FWTM, are illustrated in Fig. 2. As the FWTM represents a thickness of shower disk, we must pay attention to the definition.

§3. Performance of the FS system.

As the measuring method of the time response of the system , we adopted the Cerenkov light signal observation from the acrylic acid resin plate (50x50x5cm^3) with the same vessel and the photo-tube as for the FS scintillator. Fig.3(a) shows the arrangement of the Cerenkov detector. A single charged particle does not pass through the photo-tube , so the influence of the PT-pulse (e.g. Č light signal at the photocathode made by borsilIicate glass with a conceve surface, 1mm to 6.7mm thick) is avoidable . Most of the obtained pulse wave-form have a small ringing pulse train , gradually decreasing their amplitude , at the trailing edge of the main pulse which may be due to high frequency component contained in the main pulse . But the pulse height of the first ringing pulse is less than 10% of the main peak . The result of the time response is tabulated in Table 1 .

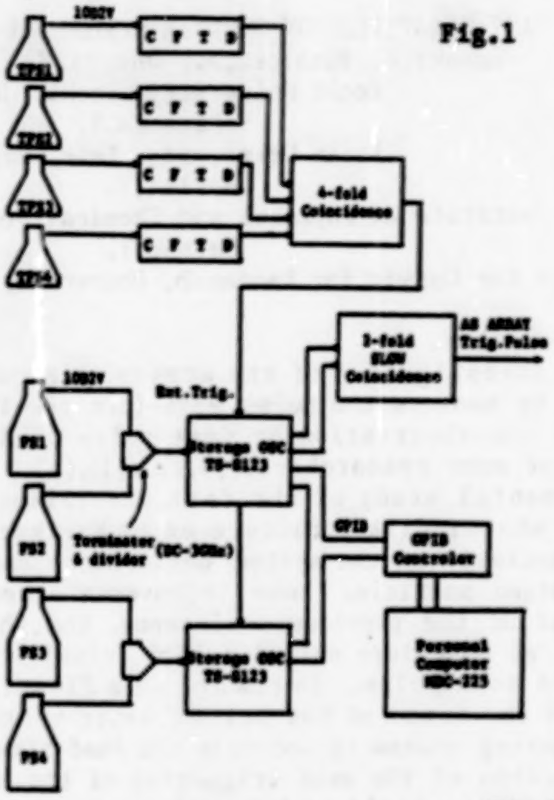
Fig.1
1082V
C F T D
C F T D
C F T D
C F T D
TFS1
TFS2
TFS3
TFS4
4-fold
Coincidence
3-fold
SLOW
Coincidence
AS ARRAY
Trig.Pulse
Ext.Trig.
1082V
FS1
FS2
FS3
FS4
Storage OSC
TS-8123
Storage OSC
TS-8123
Terminator
& divider
(DC-3GHz)
GPIB
GPIB
Controller
Personal
Computer

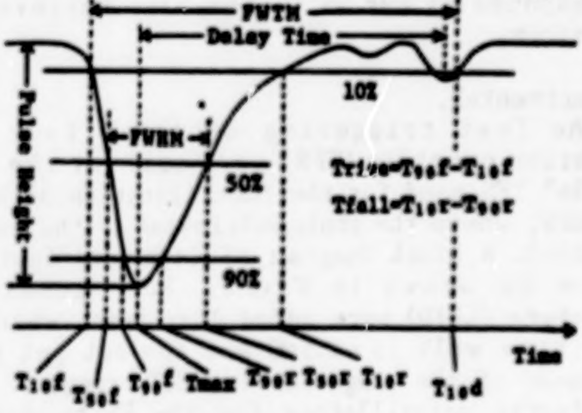
Fig.2
FWTM
Delay Time
FWHM
Pulse Height
10%
50%
90%
Trise=T90f-T10f
Tfall=T10r-T90r
Time
T10f
T50f
T90f
Tmax
T90r
T50r
T10r
T10d

§4. Pulse wave-form of the FS by a single charged particle.

On the pulse wave-form measurement of the scintillation counter had been done mainly by the time spectrometer with a time to pulse height converter(TPHC) and the results show a smooth curve.(5) This pulse wave-form is an averaged one , so we must be handle with caution. On the other hand, the single particle response of the system must be known at the time when we discuss the arrival time distribution of the shower particles. Then, we observed the pulse wave-forms for single particles with the detector arrangement shown in Fig.3(b). TFS1,and TFS2 were installed as to avoid the PT-pulse occurrence.

The experimental results are shown in Fig.4. Various time response data in this work are listed in Table 1 ,where parenthesized values show the standard deviation. Our data are quite sufficient one, because the maximum rise time of the storage OSC 3.5nS (Commercial data) is larger than our Cerenkov data.

Fig.3(a)

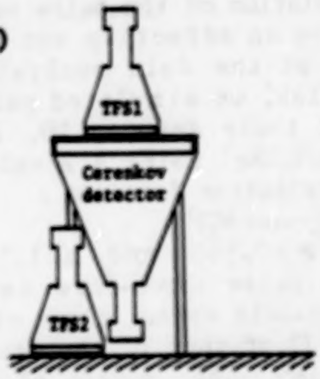

Fig.3(b)

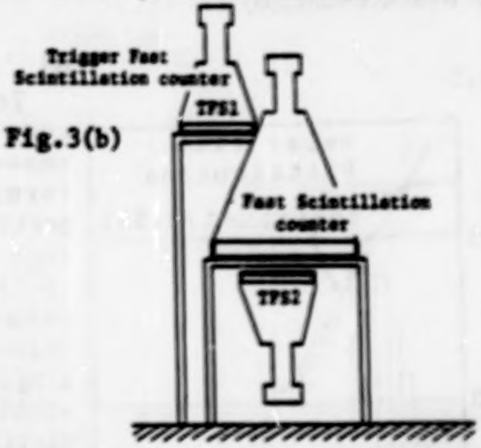
Trigger Fast Scintillation counter
TFS1
Fast Scintillation counter
TFS2

Table 1

Mode of Experiment	Rise Time (nS)	F W H M (nS)	Comment
Cerenkov Detector	2.68 (±0.3)	4.31 (±0.15)	present work
PT pulse	2.51 (±0.2)	4.37 (±0.2)	present work
Single particle	3.54 (±1.18)	7.18 (±2.03)	present work
Averaged Single particle	3.57	7.43	present work
PT pulse	2.5~3.5	5.2~5.5	Kobe Group Ref(2)
Single particle	4.3~4.5(0.9~1.3)	8.6~8.8(1.7~1.8)	Kobe Group Ref(2)

Fig.4

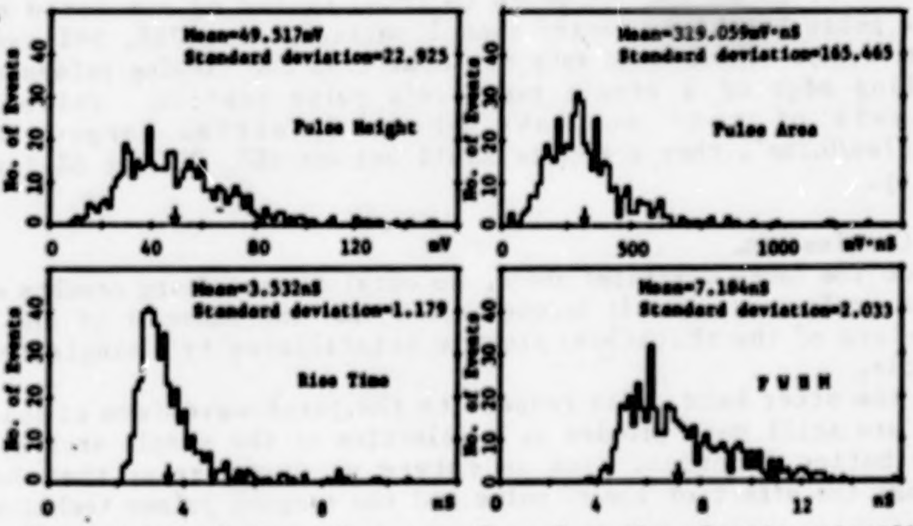

The fluctuation of the pulse wave-form from the plastic scintillator is larger than what we expected and this tendency is obvious at glauce of individual pulse profile. The rate of subpeaks, at the condition that the peak height of a subpeak is greater than the 10% of the average peak height, is about 82%, and at the condition that larger than the 33% of the main the rate is about 48%. In the former case that is P.H.(subpeak)≥0.1xPH(mainpeak), the rate is affected by the small ringing pulse. At the case P.H.(sub)≥0.33xP.H.(main), the influence by the ringing pulse is small and the delay time distribution of subpeaks in this case is shown in Fig.5. This delay time distribution is expressed as

$$F = A\exp(-t/\tau_0) \; : \; \tau_0 = 3.56\text{nS} .$$

the value τ_0=3.56nS is quite reasonable as compared with the fall time measurement.(6)

Fig.5

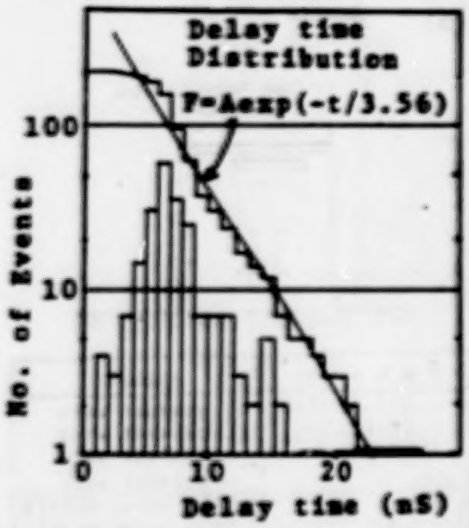

§5. Simulation of the pulse wave-form.

To give an effective and practical comment at the data analysis of the shower disk, we simulated pulse wave-forms at their density 10, 20 and 40 particles/0.25m² using a sample arrival time distribution function :

$f(t)=\frac{1}{\sqrt{2\pi}\sigma}\exp(-\frac{(t-m)^2}{\sigma^2})$

,where σ =0.5nS and m=1.5nS, and observed pulse wave-form data for a single particle whose values of area are within 17% of that of the average area distribution. The number of simulated pulse wave-forms for density 10, 20 and 40 are 21, 23 and 16 events, respectively.

The average values of the obtained rise time , and the FWHM, are somewhat larger than those of the measured for a single particle. Analysis shows, also, that the ratio of the sub peaks to total number of simulated events whose pulse height is larger than 1 particle, are 38%, 59% and 81%, respectively. Those high rate may come from the ringing pulses at the trailing edge of a single particle's pulse profile. While as an analysis of the subpeaks whose densities larger than 2 particles/0.25m², they are quite small and are 10%, 27% and 6% for each density.

§6. Conclusions.

From the facts described above, we obtained satisfying results on the system performance and it becomes clear that the behavior of the pulse wave-form of the thick(5cm) plastic scintillator by a single charged particle.

On the other hand, with respect to the pulse wave-form simulation there are still many problem as a selection of the sample arrival time distribution function. And in future we must devise that how to decrease the effect of the PT pulse and the ringing pulses technically.

References.

(1) Sasaki,H. et al :in this conference HE 4.7-1.
(2) Yoshida,M. et al :J.Phys. Soc. JAPAN, 53(1984)1983
(3) Sakuyama,H. et al :Proc. 18th Int. Cosmic Ray Conf,Bangalone 11(1983)88
(4) Mincer,A.I. et al:Proc. 18th Int.Cosmic Conf,Bangalone(1983)264
(5) Moszynski,M. and Bengttson,B. N.I.M. 158(1979)1
(6) Yates,E.C. and Crandall,D.G.: IEEE TRANS. Nuclear Science June(1966)153

Performance of a local electron density trigger to select extensive air showers at sea level.

T. Abbas, T. Madani and F. Ashton
Dept. of Physics, Durham University, Durham, England.

Abstract

Time coincident voltage pulses in the two closely spaced (1.6m) plastic scintillators have been recorded. Most of the recorded events are expected to be due to electrons in EAS whose cores fall at some distance from the detectors. This result is confirmed from a measurement of the frequency distribution of the recorded density ratios of the two scintillators.

Introduction. A threshold local electron density selection requirement is the simplest method of detecting extensive air showers. With this system the minimum shower size (and hence primary energy) that produces a threshold trigger is reasonably well defined but for a given recorded density, showers with a wide spread of core distance and shower size can satisfy the trigger requirement. Near the shower core (<1m) the electron density is believed to increase more rapidly with decreasing core distance than at larger core distances and it is possible that small core distance showers could be selected by a density ratio requirement.

Experimental arrangement and results. EAS were selected by a twofold coincidence Δ_A ($\geq 27.5m^{-2}$). Δ_B ($\geq 27.5m^{-2}$) between two plastic scintillators A and B each of area 80 x 50 cm = $0.4m^2$, their long sides being parallel and their centres being separated by a distance of 1.6m. For each trigger the number of particles N_A and N_B traversing each scintillator was recorded using a computerised data acquisition unit and figure 1 shows the frequency distribution of the density ratio N_A/N_B and also N_B/N_A. It is seen that the most probable value of the frequency ratio is close to unity in both cases and that the distributions show a long tail. The peaking of the density ratio at a value close to unity is consistent with the known slope of the electron density lateral structure function as a function of core distance and the estimates of the median core distance of showers that produce a local electron density greater than some threshold value are shown in table 1 (Ashton and Parvaresh, 1975).

The data can also be used to evaluate the integral density spectrum of electrons at sea level and the result is shown in figure 2 where the minimum of the two recorded densities was used in evaluating the integral spectrum. For density thresholds in the range $2\text{-}40m^{-2}$ the integral spectrum was measured directly by counting the rate of twofold coincidences. It is seen from figure 2 that the present measurements are consistent with the best estimate given by Greisen (1960) for $\Delta > 27.5m^{-2}$ but that for smaller densities a somewhat larger rate is observed. Also shown in figure 2 is the response of the two counters A and B measured individually to the global cosmic ray flux where the output pulse height from either detector is plotted in terms

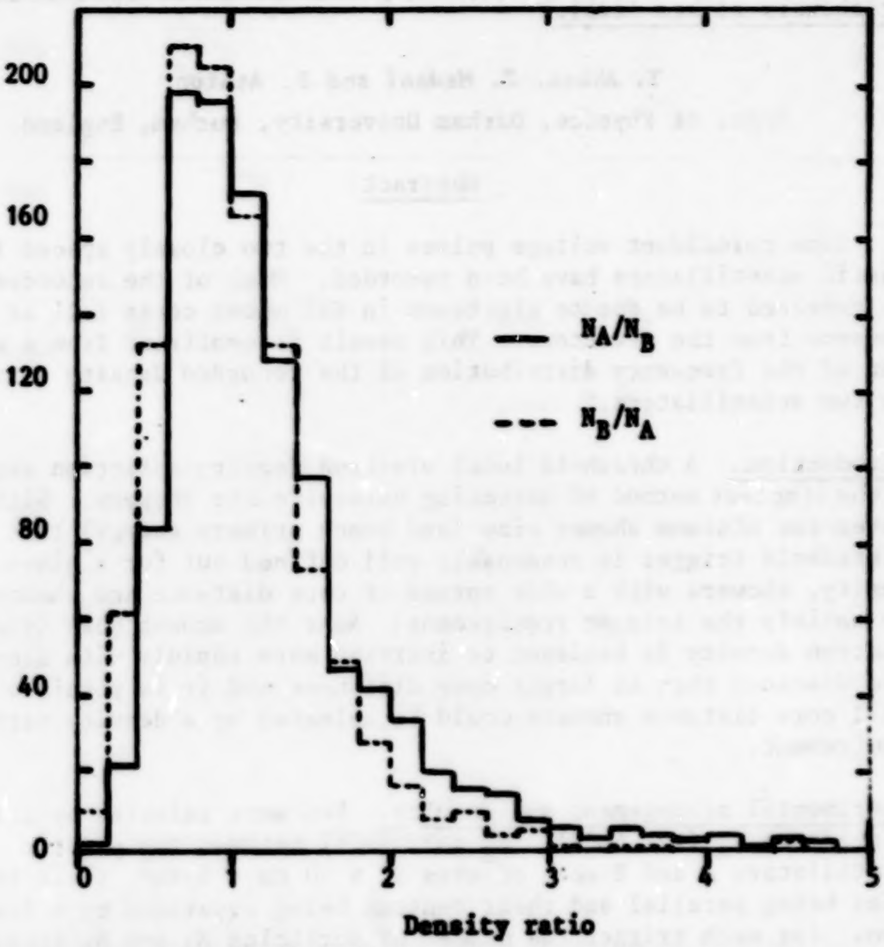

Figure 1. Frequency distribution of the ratio N_A/N_B where N_A, N_B are the number of particles traversing scintillators A and B which each have area $0.4m^2$. EAS were selected by requiring $\geqslant 11$ particles to traverse both scintillators simultaneously and the ratio N_A/N_B is evaluated if both N_A and N_B satisfy $11 \leqslant N \leqslant 134$ as the passage of >134 particles through either scintillator saturated the recording system. Total number of shower triggers =1184. Number of evaluated density ratios =1122. i.e. 62 shower triggers saturated at least one channel of the recording system. Number of observed triggers with $N_A/N_B>5$ and hence not plotted in the figure =10 (N_A/N_B = 8.1, 10.3, 7.6, 8.1, 5.5, 6.4, 7.7, 8.6, 6.2, 6.4). Also plotted is the ratio N_B/N_A (dashed histogram). Number of observed triggers with $N_B/N_A>5$ =2 (N_B/N_A=6.2,5.7).

of the equivalent density of particles traversing it. Extrapolating the measured distributions suggests that for $\Delta \geqslant 600m^{-2}$ EAS could be selected using only a single detector rather than the coincidence between two detectors as used in the present work.

ORIGINAL PAGE IS
OF POOR QUALITY

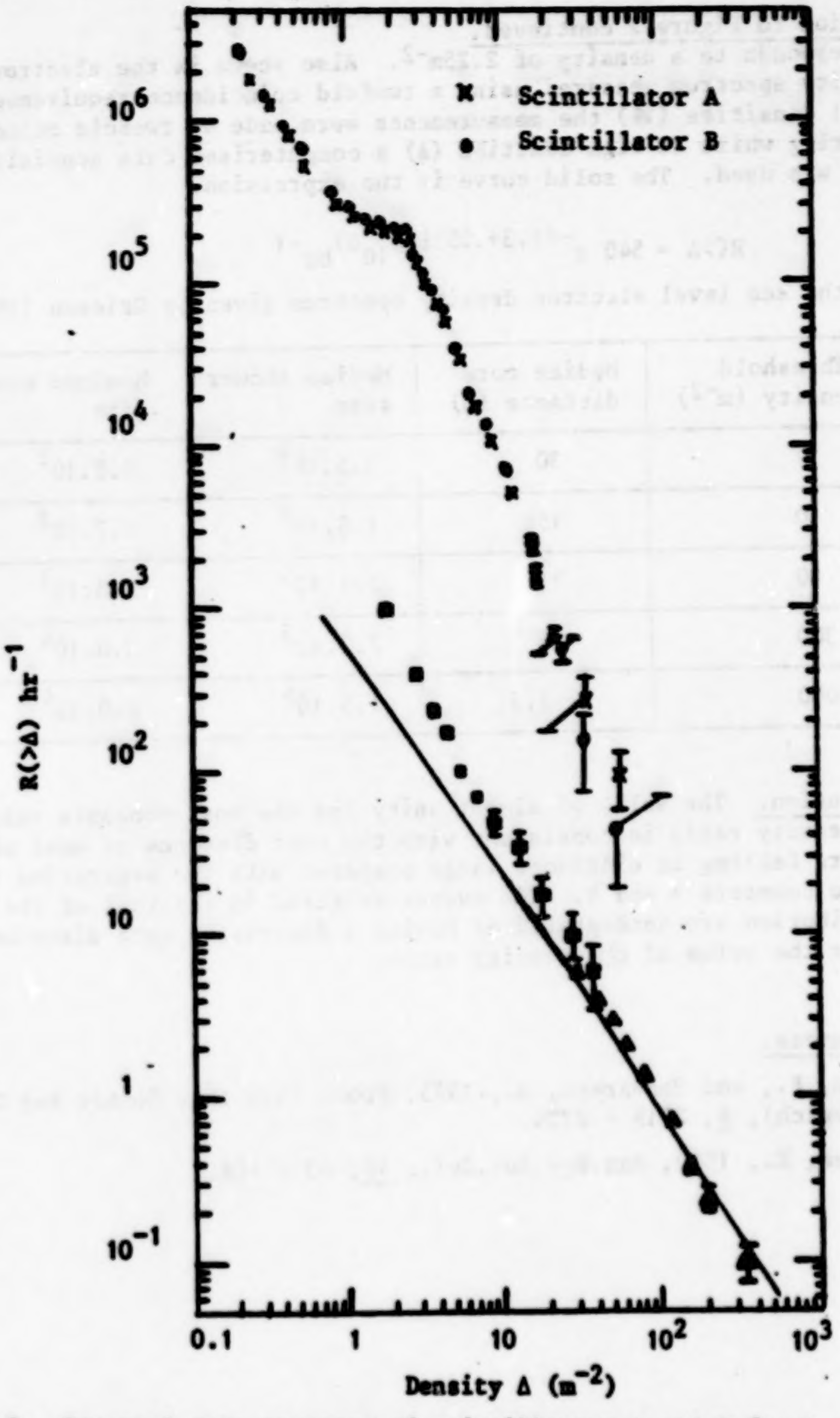

Figure 2. Integral rate response of scintillators A and B (each of area $0.4m^2$) to the global cosmic ray flux. The pulse heights recorded by each scintillator have been converted to the number of equivalent particles traversing the scintillator at normal incidence and then expressed in terms of the density of equivalent particles incident on the scintillator. The traversal of the scintillator by single particles

Caption to Figure 2 continued.
corresponds to a density of $2.25\mathrm{m}^{-2}$. Also shown is the electron density spectrum measured using a twofold coincidence requirement. At small densities (■) the measurements were made by twofold coincidence counting while at high denities (▲) a computerised data acquisition unit was used. The solid curve is the expression.

$$R(>\Delta = 540\ \Delta^{-(1.3+.055\log_{10}\Delta)}\mathrm{hr}^{-1}$$

for the sea level electron density spectrum given by Griesen (1960).

Threshold density (m^{-2})	Median core distance (m)	Median shower size	Minimum shower size
1	30	$3.5.10^4$	$8.0.10^2$
10	15	$1.5.10^5$	$1.7.10^3$
40	11	$2.1.10^5$	$5.5.10^3$
300	6	$7.0.10^5$	$3.0.10^4$
1,000	3.5	$1.5.10^6$	$8.0.10^4$

Conclusion. The value of almost unity for the most probable value of the density ratio is consistent with the core distance of most of the showers falling at distances large compared with the separation (1.6m) of the counters A and B. The events observed in the tail of the distribution are interpreted as having a decreasing core distance, the larger the value of the density ratio.

References.

Ashton, F., and Parvaresh, A., 1975, Proc. 14th Int. Cosmic Ray Conf. (Munich), 8, 2719 - 2724.

Griesen, K., 1960, Ann.Rev.Nuc.Sci., 10, 63 - 108.

ORIGINAL PAGE IS
OF POOR QUALITY

N85-36049

HE 4.6-15

MICROPROCESSOR -BASED SINGLE PARTICLE CALIBRATION OF SCINTILLATION COUNTER

MAZUMDAR G.K.D. & PATHAK K.M.
Department of Physics ,Gauhati University
Gauhati -781014 ,ASSAM ,INDIA

ABSTRACT

A microprocessor-based set-up fabricated and tested for the single particle calibration of the plastic scintillator.The single particle response of the scintillator is digitised by an A/D converter,and a 8085 A based microprocessor stores the pulse heights.The digitised informations are printed with a printer. Facilities for CRT display and cassette storing and recalling are also made available .

The details of fabrication along with same results are presented in this paper.

1.Introduction. The system described here is designed to calibrate the plastic scintillators used in an EAS array in Gauhati University,Assam. The different aspects and significance of the study are already reported elsewhere (1) .In this paper the design and the experimental set-up relating to the detection and recording of the scintillator responses due to single muons are reported .

2.Methods. Fig. 1 shows the experimental set-up for the calibration of the scintillators .

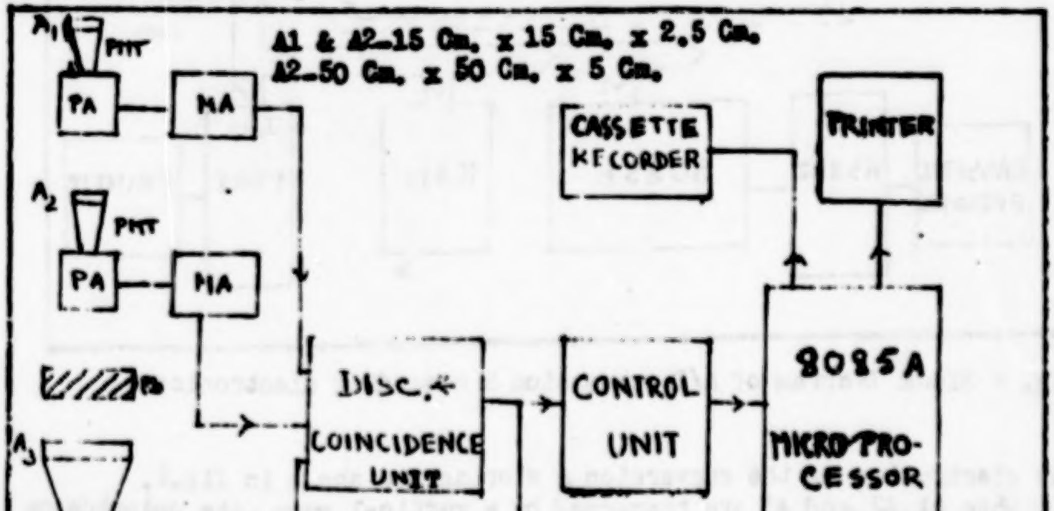
A1 & A2-15 Cm. x 15 Cm. x 2.5 Cm.
A2-50 Cm. x 50 Cm. x 5 Cm.
A_1
PMT
PA
MA
A_2
PMT
PA
MA
Pb
A_3
PMT
PA
MA
INT
S/H
A/D
DISC. & COINCIDENCE UNIT
CONTROL UNIT
CASSETTE RECORDER
PRINTER
8085A MICRO PROCESSOR

Fig.1:- The Experimental set-up .

N85-36049

ORIGINAL PAGE IS
OF POOR QUALITY

It consists of three plastic scintillators A1,A2,& A3.The Scintillator A3 which is to be calibrated ,is placed under a 20 Cm.thick lead block. Each scintillator is viewed by a 6364 PMT of 12.5 Cm. diameter.

The analog signals from each PMT are talcen out from an inverting pre-amplifier (PA) fabricated using a MOSFET 3N 200 and two HF transisters BF115. The details of the amplifier system including sample-and-hold are reported elsewhere (2).

The output from the PA is input to the main amplifier (MA) by low loss cables .The MA out put is integrated by an integrator (INT) and the integrated signal is sampled and held by a sample-and-hold (S/H) consisting of two LF 398 and 74 series TTL circuits.The S/H is actuated by a logic step derived from the Discriminators & coincidence unit. This unit comprises of three discriminators using Three 710 & one CD 4068 .This unit is triggered by the MA out put. The analog out put of the S/H is digitised by an A/D converter 0816 and is controlled by a 8085 A microprocessor .

The microprocessor controls the detection and recording of the events.

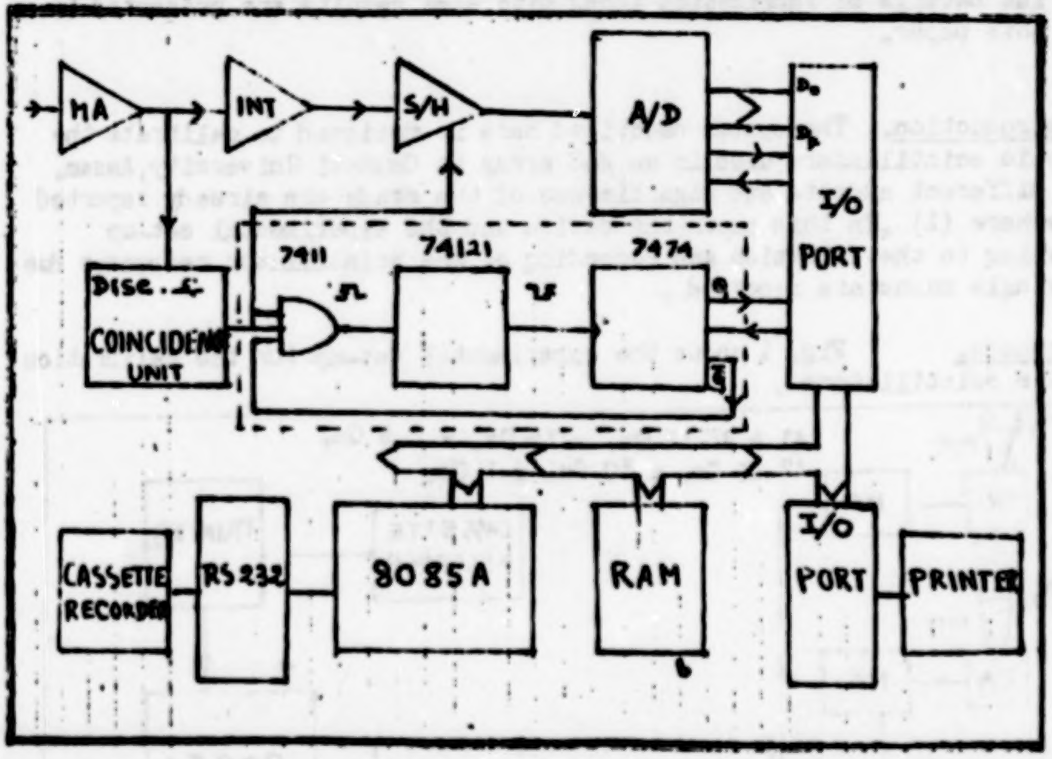

Fig. 2 Block Diagram of A/D conversion & recording electronics.

The electronics of the conversion & storing are shown in fig.2.

When A1,A2,and A3 are traversed by a vertical muon ,the coincidence pulse, On receipt of the coincidence pulse,the S/H holds the input analog signal and at the same time a positive pulse is generated by the AND gate 7411 of the control unit .The rising edge of this pulse triggers a monoshot 74121 to give a negative pulse at the out put.

ORIGINAL PAGE IS
OF POOR QUALITY

This pulse is connected to the clock input of the flipflop (F/F) 7474 and Q and $\overline{Q}$ are set to high and low states respectively. $\overline{Q}$ is connected to the other input of the AND gate and it does not give any pulse till Q is reset to high state .

The high output of the F/F interrupts the microprocessor and it sends a start conversion pulse to the A/D .The 8-bit data bus of the A/D is coupled to the one of the I/O ports of the processor.The microprocessor sends a clear pulse after storing the digitised information in a RAM and it resets the F/F to be ready for the next event.

With the help of another port, the stored informations are printed out.T-he interface RS 232 is provided for cassette recording /CRT display .

3.Results & Discussion. Fig.3 shows the pulse height distribution obtained with the present set-up .The most probale pulse height for single particle is found to be 0.45 ± .05Volts.

The number of electrons collected at the anode of the PMT is calculated using the relation Q = NPM where N is the number of photon produced by the incident particle of energy E which dissipates dE energy in scintillator .P is photon transfer efficiency .M - over all gain of the PMT . Q is also calculated from the most probable pulse height and it is found to tally with the theoretical value within experimental error.

The response of the scintillator over different regions is also studied and is found to have variation less than 10% with a slight decrease towards the edge.

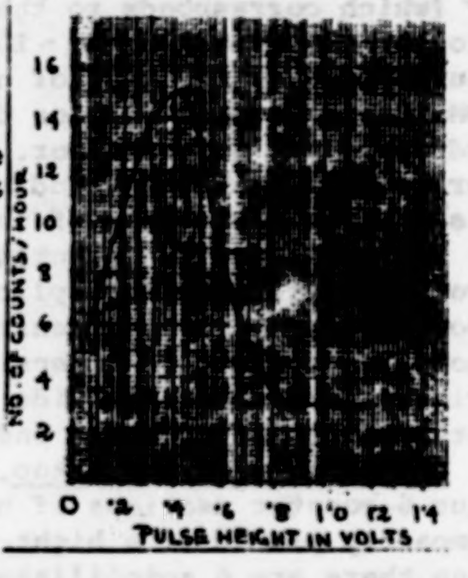

Fig.3 Pulse height distribution

4.Conclusions. The technique developed has been used in estimating the numberdensity in an air shower array for studying emission of EM waves from EAS.

The method,which can be very well used in place of an expensive Multichannel-Pulse-height-analyser (MCPHA),is useful for small laboratories .

5.Acknowledgements. The authors thank the Department Atomic Energy (BRNS), Govt. India for funding the project, and the TIFR,Bombay for for some equipments .They also like to thank the Institute of Advance Studies in Science and Technology (Assam Science Society) for partial funding of the project.

References
1.Pathak K.M. etal (1982) Proc. of the International Workshop on V.H.E.G. R. Astronomy 309 .
2.Mazumdar G.K.D. etal(1982)Proc. XVIII ICRC T 8 204.

N85-36050

HE 4.6-14

SAMARKAND COMPLEX SETUP FOR INVESTIGATION OF COSMIC RAY VARIATION IN THE ENERGY RANGE OF $7\ IO^{9} - IO^{15}$eV

Dorman L.I.
Institute of Terrestrial Magnetism, Ionosphere and Radio Wave Propagation, USSR Academy of Sciences, I42092 Troitsk, Moscow Region, USSR

Valikhodzhaev F., Makhmudov B.M., Sirodzhev N., Tashpulatov R.
Samarkand State University, Uz.SSR, Samarkand, USSR

I. Abstract. The Samarkand complex setup is aimed at the study of cosmic ray variations in a wide energy range from $7.IO^{9}$ eV (which corresponds to the geomagnetic threshold in the region of Samarkand) up to ~IO^{15}-IO^{16}eV. The setup consists of four 6-counter sections of neutron supermonitor with counters SNM-I5 and 48 scintillator detectors (Im^2 each) placed under and above the supermonitor. The effective area of the setup for recording neutrons and muons is 24 m^2. The setup can register time variations of the following cosmic ray components: I) the total neutron counting rate, 2) counting rates for neutrons of different multiplicity, 3)soft-muon fluxes, 4)hard-muon fluxes at various zenith and azimuth angles, 5) electron-photon component, 6) extensive air showers (EAS) induced by primary particles in a wide energy range and accompanied or not accompanied by muons and neutrons.

2. Description of the setup. The complex setup consists of four 6-counter sections of neutron supermonitors which are compactly placed at a hight of I m. Under and above each section there are 6 scintillator detectors with an effective area of I m^2 each. The dimensions of each section are 3I5 x 222 x x 52 cm^3 and the weight is about I3 tons. The generator of neutrons is made of lead (an effective area in one section is ~6.2I m^2), and the retarder and reflector of neutrons was made of polyethylene. Neutrons are detected by Soviet neutron counters SNM-I5 (effective length ~200 cm, diameter-I5 cm, filled with a gas BF_3 up to a pressure of 20 cm Hg, the concentration of IO_B isotope in boron reaches 80 %, operating voltage ~ 2600-2800 B, proper radioactive background ≤I %). Plastic scintillators with reflectors and photomultipliers placed at the top of reflectors are used as detectors of charged particles (electrons, muons, protons). After amplification, formation, and discrimination, pulses from detectors come to the general logic scheme in which different components are selected (neutron, electron-photon, muon, EAS with different accompanying). The results of the selection come into a multichannel recorder with a punch out on the paper tape and digitiser.

3. Recording of single and multiple neutrons. The developed electronics makes it possible to sort out events induced by single and multiple neutrons and to block pulses from electrons and muons in neutron counters /I/. Bearing in mind the coupling coefficients for single and multiple neutrons one can say that the Samarkand neutron supermonitor is sensitive to promary cosmic rays in the energy range from 7 to several tens of GeV, with an effective energy of about I5 GeV. The total counting rate for neutrons is expected to be about IO^6 pulses/hr, which corresponds to the rms statistical error σ = = 0.I%/hr; for 5-minute data this corresponds to $\sigma \sim$ 0.3-0.4 %/5 min., which is quite sufficient for statistical investigation of cosmic ray scintillations. The counting rate for neutrons of multiplicity m=2 is $\sim$ I.3 IO^5 pulses/hr, which provides $\sigma \sim$ 0.3%/hr; for m=3 the counting rate is $\sim$4 IO^4 pulses/ /hr, which gives $\sigma \sim$ 0.5%/hr; for the sum m=4 and 5 the counting rate is $\sim$ 2.IO^4 pulses/hr and $\sigma \sim$ 0.7 %/hr, and for m=6 the counting rate is $\sim$ 4.IO^3 pulses/hr and $\sigma \sim$ 2 %/hr. These accuracies show that the data on high multiplicities can be used only for the investigation of long-period variations and statistical analyses, and also of short-time variations with a large amplitude (powerful Forbush decreases, effects of solar flares).

4. Recording of soft muons. It is well known (see the review /I/) that in a neutron supermonitor about 7 % of pulses are induced by soft negative muons which form on lead nuclei the mesonic atoms with a subsequent capture of muons and a formation of several neutrons. Such events can be discriminated by pulse anticoincidence in the upper and lower scintillators and by retarding pulse coincidence in a neutron supermonitor. The expected counting rate for soft muons is about I.3 IO^5 pulses/hr, which corresponds to $\sigma \sim$ 0.3 %/hr. This will make it possible to study in detail the meteorological variations of soft muons which are of great theoretical and practical interest.

5. Recording of the electron-photon and muon components. Summation of the counting rates of upper scintillators provides information on time variations of the total ionising component with a high statistical accuracy ($\sigma \sim$ 0.02% for a 5-minute interval). Subtraction from this counting rate of the flux of hard and soft muons gives data on variations of the electron-photon component. Further, the use of a scintillator system for selecting the respective double coincidences between individual upper and lower scintillator detectors gives exclusively valuable information about time variations of hard muon fluxes which arrive at different zenith and azimuth angles. After the quality of the work is analised, analogous

channels of coincidences which correspond to one and the same zenith and azimuth angles are summed up. The large effective area of the setup allows us to obtain observational data with so small statistical errors (smaller than 1 % for 5-minute data) that we can very reliably use the recording even at large zenith angles which correspond to primary cosmic rays with an energy $\geq 10^2$ GeV. The data on time variations of hard muon fluxes from different directions yield much information about variations of atmospheric, geomagnetic and extraterrestrial origin with an energy of $10^{10} - 10^{12}$ eV.

6. Recording of different types of extensive air showers. Pulses from each of the 48 upper and lower scintillators, as well as from 24 neutron SNM-15 counters come to a logic system which sorts out the following events: a) various combinations of coincidences only of upper scintillators - recording of counting rate for EAS of different power which correspond to primary particles of energies $10^{13} - 10^{16}$ eV; b) recording of EAS of different power accompanied by muons; c) recording of EAS of different power accompanied by neutrons.

7. Meteorological and coupling coefficients. With an account of the geometry of the setup and its geographical position, each of the components mensioned above in 3-6 is characterized by the following coefficients: β_i - a barometric coefficient for the i-th component of a setup; $\alpha_i(h)$, the density of temperature coefficient, where h is pressure at a corresponding isobaric level; $W_i(R)$, the coupling coefficient depending on the rigidity R of primary particles (see /1/, /2/, /3/).

8. Application of generalized spectrographic method for the analysis of observational data. A continuous recording of fluxes of single and multiple neutrons, soft muons, electron-photon component, fluxes of hard muons from different directions and frequencies of different types of EAS with essentially different meteorological coefficients and different coupling coefficients makes it possible to use the generalized spectrographic method /4/ for obtaining separate information about variations of atmospheric, geomagnetic, and extraterrestrial origin. The method consists in the fact that for each i-th component recorded by a complex setup for each time moment t one derives an equation for an observed variation of the counting rate

$$\frac{\delta I_i(t)}{I_{i0}} = \beta_i \delta h_0(t) + \int_0^{h_0} \alpha_i(h)\,\delta T(h,t)\,dh - \delta R_c W_i(R_c) + \int \frac{\delta D(R,t)}{D_i(R)} W_i\,dR \qquad 1)$$

ORIGINAL PAGE IS
OF POOR QUALITY

where the intensity variation $\delta I_i(t) = I_i(t) - I_{ic}$, variation of the air column mass above the setup may differ considerably from the pressure $\delta h_0(t) = h_0(t) - h_0$, temperature variation $\delta T(h,t) = T(h,t) - T_0(h)$, variation of geomagnetic cutoff rigidity $\delta R_c(t) = R_c(t) - R_c$ and variation of the primary spectrum $\delta D(R,t) = D(R,t) - D_0(R)$. Here the first two terms on the right imply variations of atmospheric origin, the third term determines variations of geomagnetic origin, and the fourth term - variations of extraterrestrial origin. The solution of a system of equations of the type (I) by the method described in /4/ for the above-mentioned set of components of a complex setup allows us to obtain continuously the information about $\delta h_0(t)$, $\delta T(h,t)$, $\delta R_c(t)$ and $\delta D(R,t)/D_0(R)$, i.e. in the end, about the processes in the atmosphere /2/ and magnetosphere /5/ of the Earth and in cosmic space /6/; the information of space-time variations of the energy spectrum of primary CR will be obtained in a wide energy range from 7 10^9 eV to 10^{15} - 10^{16} eV.

REFERENCES

I. Dorman L.I. Experimental and Theoretical Principles of Cosmic Ray Astrophysics. Nauka, I975.
2. Dorman L.I. Meteorological effects of cosmic rays. Nauka, I972.
3. Dorman L.I. Cosmic Rays: variations and space exploration. Amsterdam, I974.
4. Dorman L.I. Proc. I5-th ICRC, vol.4, 28I, Plovdiv, I977.
5. Dorman L.I., Smirnov V.S., Tyasto M.I. Cosmic rays in the magnetic field of the Earth. Nauka, I97I.
6. Dorman L.I. Variations of galactic cosmic rays. Izd. MGU, I975.

N85-36051

RADIO WAVE EMITTED BY AN EXTENSIVE AIR SHOWERS IN 10KHZ TO 1MHZ REGION

Jun Nishimura
The Institute of Space and Astronautical Science
Komaba, Meguro, Tokyo, Japan

ABSTRACT

An importance of radio wave in a frequency range less than 1MHz has been discussed by Suga at the time of the Bangalore Conference. In this paper, an estimate of radio intensities at 10KHz, 100KHz and 1MHz has been made on the basis of the Kahn-Lerche theory. An emphasis is made that negative charge excess in a shower gives main contribution for low frequency radio emission, in spite of the importance of the contribution of transverse current in the geomagnetic field in higher frequency range. An estimate is also made for radio intensity produced when the shower hits the ground. Contribution of this process seems to be important at large distance say beyond 1km from the shower axis.

1. INTRODUCTION

The radio wave emitted from extensive air showers has been studied since 1965 in the frequncy range of 30 to 60MHz. However, since lateral spread of the radio wave intensity was found to be steep, such studies have not been considered to be promising to detect low frequency large showers.
In a low frequncy range around 1MHz, only a few studies have been reported. Moscow and Yakutsk group (V.B.Atrashkevich et al: 1973) reported that strong radio wave of 1.9MHz with 1 to 25 micro V./M.MHz were observed for showers of $6x10^6 < Ne < 1.7x10^8$ at distances from 600m to 1300m.

Suga proposed possible detection and importance of radio wave at frequency range less than 1MHz (K.Suga: 1983). He discussed contribution of charge excess in an extensive air shower for emission of the radio wave in this range, and also discussed possible emission process when this excess charge hits the ground. Similar treatement to estimate the contributions of these processes have also been performed recently by Sakata.(T.Sakata: 1985).

Since these results seem to be promising to detect low frequency large showers, we examined the contribution on the basis of Kahn-Lerche treatement, in which we can estimate radio intensity more easily, such as to include effect of emission angle of the radio wave from shower axis. The comparison is made for the degree of the each contribution by excess charge, dipole and transverse current, and shows

excess charge gives the most important contribution between these processes in frequncy range less than 1MHz.
Radio wave emission when the excess charge hit the ground is also treated by using the formulae of the transition radiation. Contribution for the radio intensity by this process is much larger than other processes below 1MHz. We estimate a few times of 100 micro V/M.MHz or more at 1km from the shower axis for a shower of 10^{20} eV.

2. RADIO WAVE EMISSION IN A LOW FREQUENCY RANGE.

The radio wave emission from an extensive air shower has been treated by Kahn and Lerche on the basis of the Maxwell equation.(F.D.Kahn and I.Lerche:1965). They discussed the contributions from three process, i.e. charge excess, dipole and transverse current in the geomagnetic field.
They obtained a fourier transformed field strength due to each process as, in the notation of their paper:

a) Charge excess

$$E(k)= -ie\Delta/2\cdot(k\alpha)J_o(k\alpha a)H_o^{(1)\prime}(k\alpha r) \quad (1)$$

b) Dipole

$$E(k)= -iM/2\cdot(k\alpha)^2 J_o(k\alpha a)(H_o^{(1)\prime}(k\alpha r)/k\alpha r+H_o^{(1)}(k\alpha r)) \quad (2)$$

c) Current

$$E(k)= -J/2\cdot kJ_o(k_\alpha a)H_o^{(1)}(k\alpha r). \quad (3)$$

Here Δ, M and J are the excess charge, dipole moment and current in an extensive air shower. k, α, a, and r are the wave number, Cerenkov angle, radius of shower disk and the distance of the observation point from the shower axis.

If the number of the shower particles changes with altitude as exp(-Lx), where L and x are the absorption coefficient and depth of the atmosphere measured in unit of length, another process for emission of radio wave arises.
$k\alpha$ in eq.(1) should be replaced, in this case, as

$$((k_\alpha)^2+2ikL+L^2)^{1/2}. \quad (4)$$

The relative importance of each term in eq(4) depends on the radio concerned. Since L is of the order of 1/1km= 10^{-5}/cm, α =.024 and k= 2×10^{-4}/cm at 1MHz, contribution of $k\alpha$ in eq.(4) becomes small in these frequency range. Thus the radio emission is mainly due to the charge acceleration rather than the Cerenkov process as illustarted in Fig.1. The effect of change of number of shower particles with altitude becomes predominant in the low frequncy radio waves.

Due to this situation, degree of the contribution of charge excess becomes important compared with that of other process in the low frequency range as seen from formulae (1),(2) and (3). The emission angle α is also changed to about $(L/K)^{1/2}$, giving a large angle spread compared with Cerenkov angle.This results wide lateral spread of radio pulse, and gives us a possibility to detect large extensive air showers efficiently. The relative importance of each process for intensities at various frequencies are shown in Table 1.

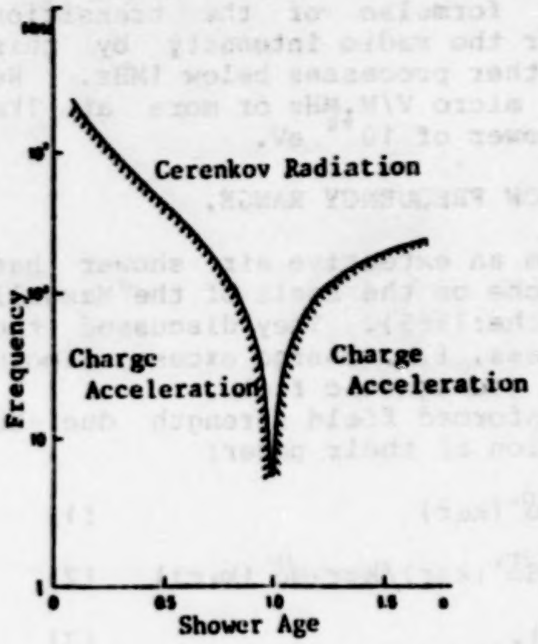

Fig.1. Relative importance of Cerekov emission and charge acceleration.

Table 1
Relative contribution of each process ($L = 10^{-5}$ / cm)

Freq.(MHz)	Excess charge	Dipole	Current
100	1	0.57	2.2
1.0	1	0.053	0.24
0.1	1	0.0169	0.074

Here we refer to the values of Δ , M and J in the paper (M. Fujii and J. Nishimura: 1968). This clearly indicates the importance of the charge excess in the low frequncy range, and we can estimate the radio intensity by only taking this process.

3. RADIO PULSE WHEN SHOWER PARTICLES HIT THE GROUND

When shower particles hit the ground, radio pulse is emitted by excess charge in the shower. This is just the same process known as the transition radiation. Since the shower disk hits the ground with a time duration of 0.1 to 1 micro sec. depending on the inclination of the shower axis. Only the radio wave of frequency less than 1 to 10MHz are emitted coherently. The radio pulse intensity is

$$W(f,\theta)dfd\Omega = e^2/\pi c \cdot |\cos\theta| dfd\Omega \quad , \qquad (5)$$

where f is the frequency of the radio wave, and θ is the zenith angle of the shower axis. If N charged particles are involved, e in the eq.(5) should be replaced by Ne.

ORIGINAL PAGE IS
OF POOR QUALITY

4. NUMERICAL RESULTS AND DISCUSSIONS

Referring to the formula in section 2, 3, numerical evaluations are made and shown in Fig 2, 3. Here we assume number of shower particles changes with altitude as :

$$N = No.\exp(-x^2/2(\sigma c)^2),$$

where σ is around 5 micro sec. for a vertical incident shower. The calculated radio intensity is 100 to 1000 micro V/m.MHz for a shower of 10^{20} eV and is similar to those orders of magnitude obtained by Suga and Sakata.

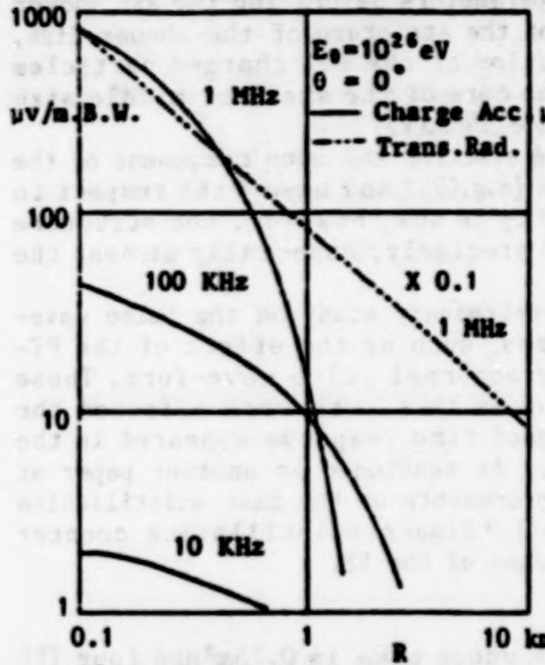

Fig.2. Radio intensity per band width of each Frequency. Vertical incident Shower.

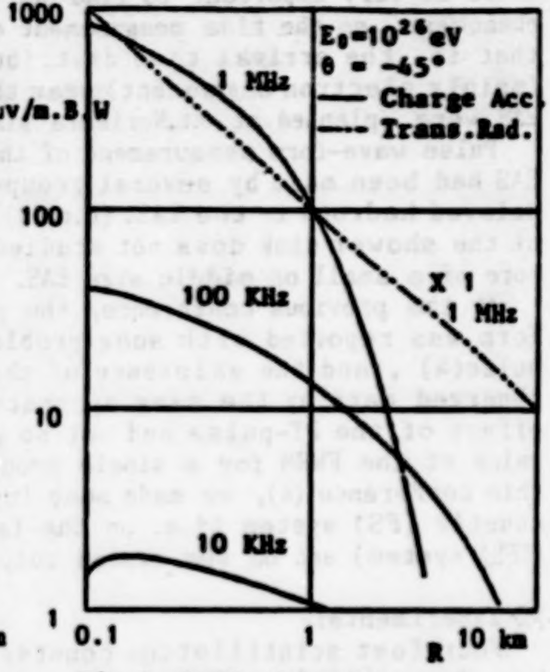

Fig.3. Radio intensity of shower with Zenith angle of -45 degrees.

The transition radiation emitted by charge excess in shower gives the most predominant contribution at a distance beyond 1km. Since the intensity of transition radiation is known to be changed as $(\sqrt{\varepsilon} - 1/\sqrt{\varepsilon} + 1)$, where ε is a dielectric constant of the ground, which indicate that radio intensity is affected by condition of the ground. Other processes to emit the radio wave are proposed by Suga and Sakata. Contribution of those processes will be discussed at the time of the conference.

References

Atrashkevich,V.B. et al : 1973, Proc. 13th ICRC 2399
Fujii M. and Nishimura.J. : 1968, Proc. 11th ICRC 710
Kahn F.D. and I.Lerche : 1966 Proc. Roy. Soc. A289, 206
Sakata T.: 1985, in this issue
Suga K. : 1983, Proc. 18th ICRC Vol 11. 428.

N85-36052

THE STRUCTURE OF THE SHOWER DISK OBSERVED AT MT. NORIKURA

Sasaki,H.,Nishioka,A.,Ohmori,N.,Kusunose,M.
Kochi University, Kochi, Japan
Nakatsuka,T.
Konan University, Kobe , Japan
Horiki,T.
The Institute of Physical and Chemical Research, Wako, Japan
Hatano,Y.
Institute for Cosmic Ray Research, University of Tokyo, Tokyo, Japan

§1 Introduction.

It is very important to find out parameters describing the air shower phenomena, so the fine measurement of the structure of the shower disk, that is, the arrival time distribution of the all charged particles (mainly electron component) near the core of the small or middle size EAS were planned at Mt.Norikura since 1982.(1)

Pulse wave-form measurement of the electron and muon component of the EAS had been made by several groups (e.g.(2)) and also with respect to delayed hadrons in the EAS. (e.g.(3)) Up to now, however, the structure of the shower disk does not studied precisely, especially at near the core of a small or middle size EAS.

At the previous conference, the preliminary study on the pulse wave-form was reported with some problems, such as the effect of the PT-pulse(4) , and the existence of the abnormal pulse wave-form. These observed data by the same apparatus as this work were affected the effect of the PT-pulse and not so good time response appeared in the value of the FWHM for a single muon. As mentioned in another paper at this conference (4), we made some improvements on the fast scintillation counter (FS) system (i.e. on the fast trigger scintillation counter (TFS) system) and on the system response of the FS.

§2 Experimental.

Four fast scintillation counters whose area is $0.25m^2$ and four TFS have been added to Mt.Norikura EAS array as shown in Fig. 1. The triggering requirement for this run was that four TFS counters show the pulse height greater than 4 particles/$0.25m^2$ at the same time whose allowable time delay is 80nS for each TFS.

Approximately 6200 showers were caught for this work in last summer.

Digitized data by storage oscilloscope were transmitted to the personal computer through the GPIB bus and were recorded on the floppy disk. To measure the rise time of the pulse, some improvements were made. First, we change the design of the FS vessel to as shown in Fig. 2, because this change means the increase of

Fig. 1

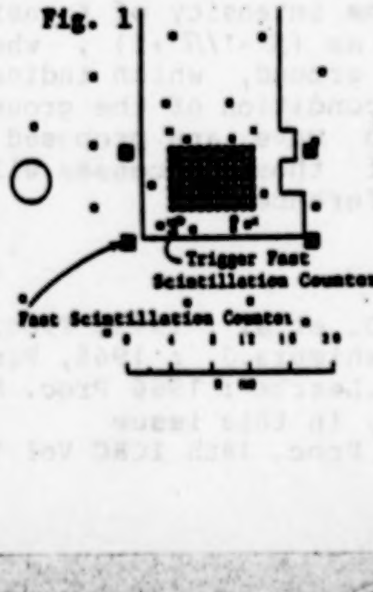
Trigger Fast Scintillation Counters
Fast Scintillation Counter
0
10
20
m

Fig. 2

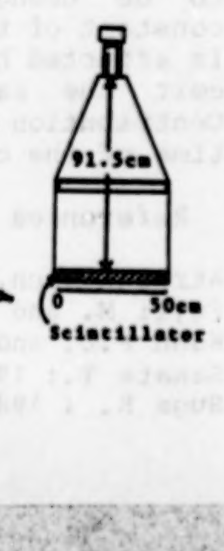

time difference between the prompt PT-pulse and the main scintillation pulse. So we can easily eliminate such a pulse shape data that affected by the PT-pulse. Secondary, the dynode chain of the resistance (i.e. voltage distribution ratio) for the photo-tube was improved to that for the pulse linearity measurement, consequently, the effect of a saturation of pulse height was avoided. Finally, we changed a high voltage to feed the photo-tube up to about 1900 volts, from 1550 volts at the previous experiment, and if the time response characteristics has the same tendency as for the photo-tube 931A, circular cage type, the rise time of the photo-tube (R329-02) may be improved about 0.5nS (i.e. the rise time become 2.1nS).

The definition of the various parameters of the pulse wave-form are reported in another paper at this conference (4). About the definition of the FWHM, care must be taken, because only when the time of the 50% of the main peak pulse height is found at the trailing edge of the main peak, the FWHM is obtained.

§3 Experimental Results.

3.1 Rise time, FWHM and FWTM

Fig. 3 (a),(b),(c) show the rise time, the FWHM and the FWTM distributions of the fast scintillation counter FS1 against the lateral distance from the shower axis to FS1, where size region is 10^6 to $2*10^6$,age is greater than 0.2 and zenith angle is less than 30°, the core distance

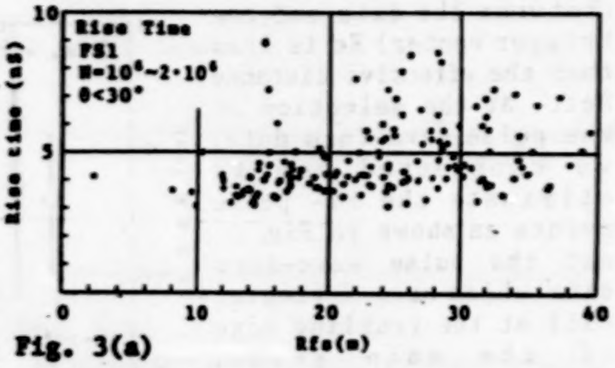

Fig. 3(a)

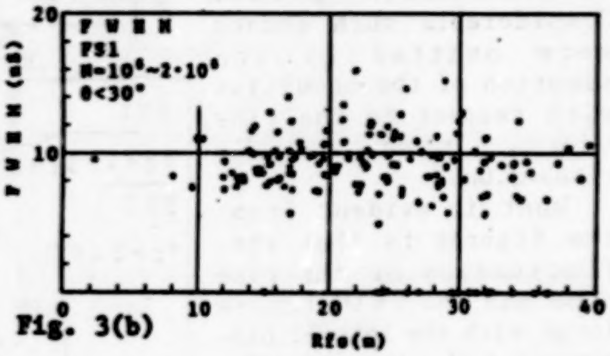

Fig. 3(b)

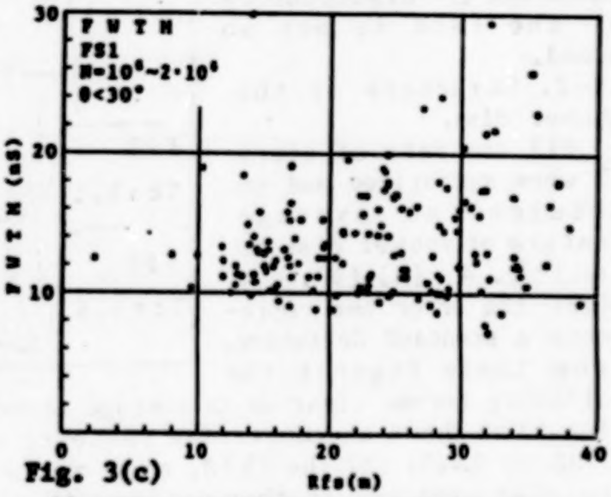

Fig. 3(c)

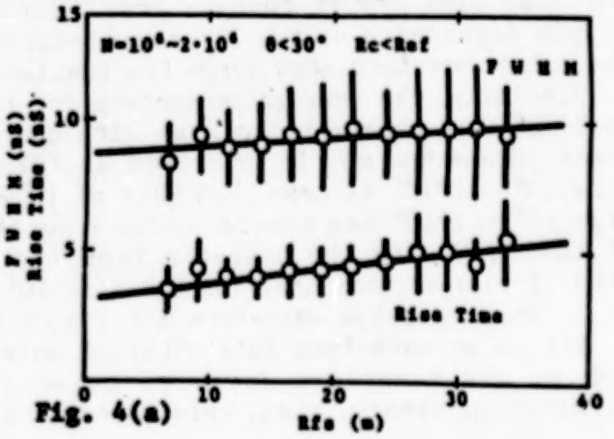

Fig. 4(a)

(between the axis and the trigger center) Rc is less than the effective distance Ref. At the selection of the pulse wave-form data, we considered how to eliminate the PT- pulse events as shown in Fig. 5 and the pulse wave-form data which have a ringing tail at the trailing edge of the main pulse. Considerable such events were omitted by the adoption of the condition with respect to the rise time, that is T-rise>=3.0nS.

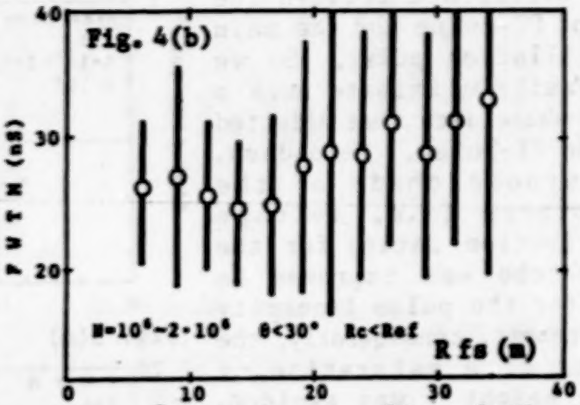

What is evident from the figures is that the fluctuation of the rise time and the FWTM become large with the lateral distance but the distribution of the FWHM is not so broad.

3-2. Structure of the shower disk.

All the data of every FS were summarized and we obtained an average feature of shower disk as in Fig. 4 (a),(b),(c), where the error bar represents a standard deviation. From these figures the following become clear as an average structure of the EAS disk. (A) The rise time shows an increasing tendency with a lateral distance from 3.5nS to 5.4nS. (B) The FWTM, also shows the same tendency as that of the rise time and it changes from 25nS to 33nS. (C) The FWHM has slight dependence on the lateral distance. (D) All the parameters of the pulse wave-form show large fluctuations for each shower.

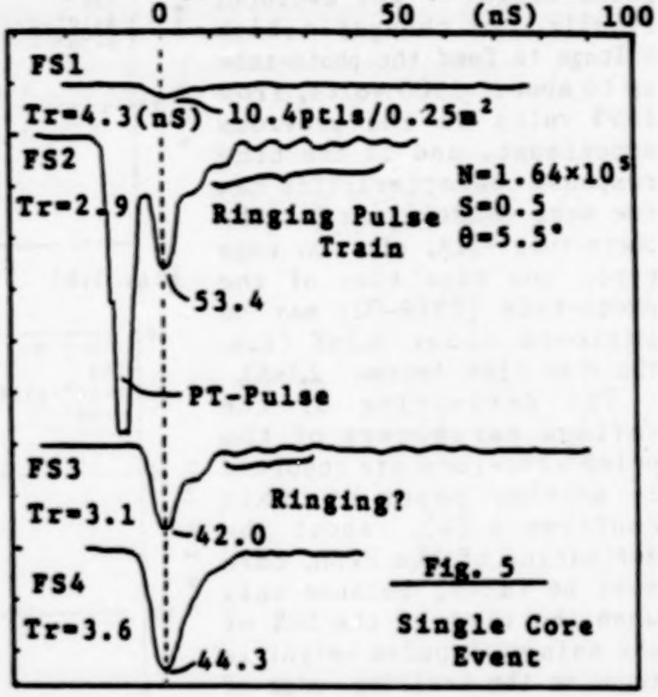

Fig. 5 Single Core Event

Similarly, the average parameters for the EAS whose size region is 10^5 to $2*10^5$ were obtained. Compared with above results, size dependence of these parameters may be described as follows. (A) The rise time of the size $10^6 \sim 2*10^6$ is less than that of $10^5 \sim 2*10^5$. (B) The FWHM of the size $10^6 \sim 2*10^6$ has greater value than that of 10^5. (C) The variation of the FWTM with the distance from the axis for the size region 10 2*10 is larger than that for the size $10^6 \sim 2*10^6$.

3-3. Observed pulse wave-form and its core structure.

All pulse wave-form data obtained were printed again by a computer and we found various types of pulse profiles. The core maps of interesting events, also, were obtained and 40 showers whose core hit

ORIGINAL PAGE IS
OF POOR QUALITY

the central array were analysed up to now, together with the pulse data. Fig. 6 shows an example of the multi-core event that all of the pulse wave-form of this event have a subpeak at time=26.0nS~27.4nS delayed from the main peak time. On the other hand, an example of the single core event is shown in Fig. 5. The pulse wave-form from the FS2 has a PT-pulse and also has a ringing pulse train. This event has not any coincident subpeak whose time allowance was 2.5nS around the time of the biggest subpeak.

Fig. 6

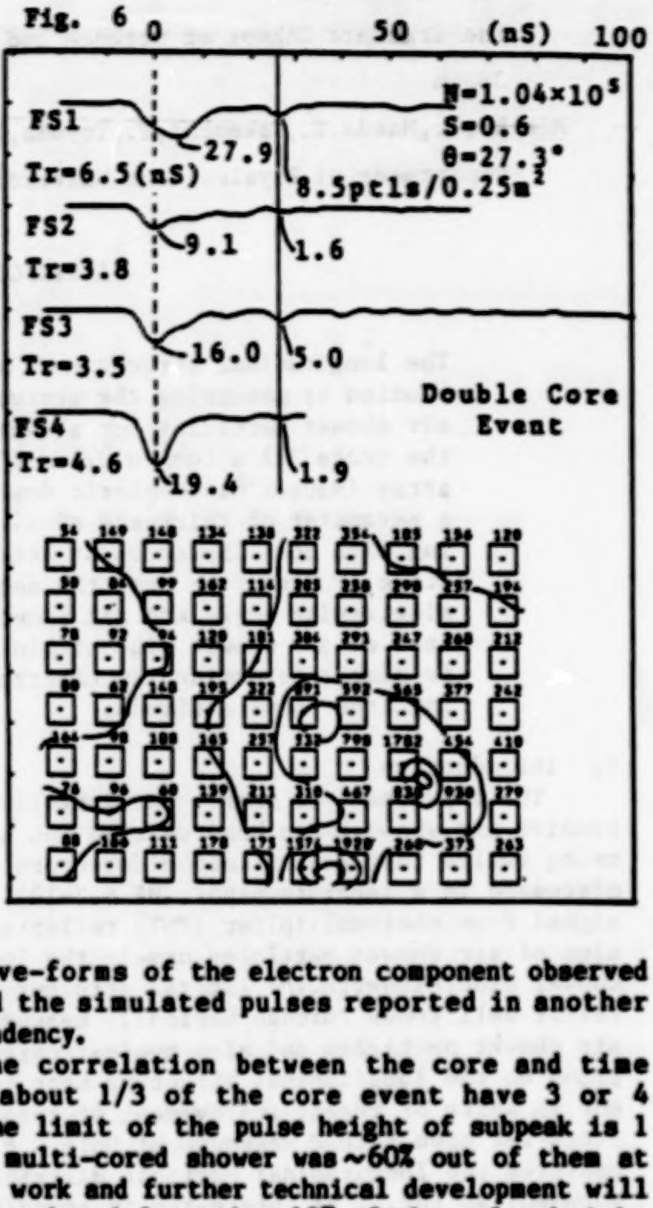

§4 Conclusions.

(A) The average structure of the shower disk became clear and further analysis will be continued with respect to the size and age dependence of the pulse wave-form parameters.

(B) Considerable pulse wave-forms of the electron component observed have two decay constant and the simulated pulses reported in another paper (4) also have same tendency.

(C) Rough analysis on the correlation between the core and time structure, it seems that about 1/3 of the core event have 3 or 4 coincident subpeaks where the limit of the pulse height of subpeak is 1 particle. And the rate of a multi-cored shower was ~60% out of them at the size 10^5~10^6. Simulation work and further technical development will be necessary, because small subpeak less than 10% of the pulse height may be under the influence of the ringing pulse appeared in the single particle pulse.

References

(1) Sasaki,H. et al.: Proc. 18th Int. Cosmic Ray Conf., Bangalore 11(1983) 205

(2) Tamura,T. et al.: Proc. 18th Int. Cosmic Ray Conf., Bangalore EA-1.2 18(1983) 133

(3) Mincer,A.I. et al.: Proc. 18th Int. Cosmic Ray Conf., Bangalore 11(1983) 264

(4) Sasaki,H. et al.: in this conference, HE 4.6-10

STRUCTURE OF AIR SHOWER DISC NEAR THE CORE

N85-36053

Inoue,N.,Kawamoto,M.

The Graduate School of Science and Technology,Kobe University,
Japan

Misaki,Y.,Maeda,T.,Takeuchi,T.,Toyoda,Y.

Department of Physics,Kobe University,Japan

ABSTRACT

The longitudinal structure of air shower disc has been studied by measuring the arrival time distributions of air shower particles for showers with electron size in the range $3.2 \times 10^{5.5}$ to $3.2 \times 10^{7.5}$ in the Akeno air-shower array ($930 gcm^{-2}$ atmospheric depth).The average FWHM as a parameter of thickness of air shower disc is increasing with core distances at less than 50m.At present stage,it cannot be seen the dependence on electron size,zenith angle and air shower age.The average thickness of air shower disc within core distance of 50m is almost determined by electromagnetic cascade starting from lower altitude.

1. Introduction

The experiment to search for long-lived massive particles in extensive air showers has been carried out in the Akeno air-shower array, using twelve fast scintillation detectors at intervals of 5m,will be discussed in a separate paper (HE 6,2-10).The time profile of the signal from photomultiplier (PMT) reflects the arrival time distribution of air shower particles,namely the longitudinal structure of air shower disc.Hitherto,the lateral structure of air shower particles is rather well known through basically measurement of lateral density of air shower particles and also nuclear cascade theory.However,informations on the longitudinal structure near the core (<50m) are not abundant in spite of recent improvement of recording apparatus and additive parts for nano second measurement.Only,C P Woidneck et al (1975) measured the longitudinal particle distribution from the time delay measurement,so far.It is interested in studying the thickness,the curvature of air shower disc and also their fluctuations in order to discuss the longitudinal development of air shower and primary compositions.The preliminary results on average thickness of air shower disc and its dependence on zenith angle and air shower age are presented in this paper.

2. Experimental

Twelve scintillation detectors were located at the S2 area in the Akeno air-shower array at intervals of 5m as discribed in separate paper (HE 6,2-10).The group A consisted of two $0.25m^2$ scintillation detectors with 2" fast PMTs and a $1m^2$ scintillation detector with 5" fast PMT.Signals fed to an adding circuit through co-axial cables (11C4AF) with different length of 50m,63m and 75m,and then added signals were recorded by a 100MHz storage oscilloscope.The group B and C were also same systems as mentioned above.The time response of the whole 0.25 m^2 scintillation detector system for single relativistic particle was 4.9ns in rise time (t_r :time from 10% to 90% of the maximum signal) and 10.6ns in Full Width at Half Maximum (t_w).That of the whole $1m^2$ scintillation detector system was also 6.2ns and 15.2ns in t_r and t_w ,respectively.

The work was performed in conjunction with the air-shower array. Signals from each groups were stored in three storage oscilloscopes if the heights of three signals from the triggering detectors (A-1,B-1 and C-1) were higher than a given level and coincided in time with one another.The stored signals were read out to a floppy disk by simultaneous master pulse from the air-shower array.

3. Analysis and Result

Observation was made from May to October of 1984.Total running time was 88days and the total number of events triggered was about 6300.The analysis was made on 2142events recorded by B-2 detector.The arrival direction (θ and φ),the electron size (N_e),the core location and the age parameter (s) of an air shower were determined according to the procedure adopted by the air-shower group of Institute for Cosmic Ray Reserch of the University of Tokyo.We excluded the signals whose peaks of some showers were out of the storage oscilloscope frame and also whose peaks were smaller than given level corresponding to four relativistic particles.In this paper,the arrival time distributions of air shower particles with N_e in the range $3.2 \times 10^{5.5}$ to $3.2 \times 10^{7.5}$ and sec θ in the range 1.0 to 1.3 are reported.

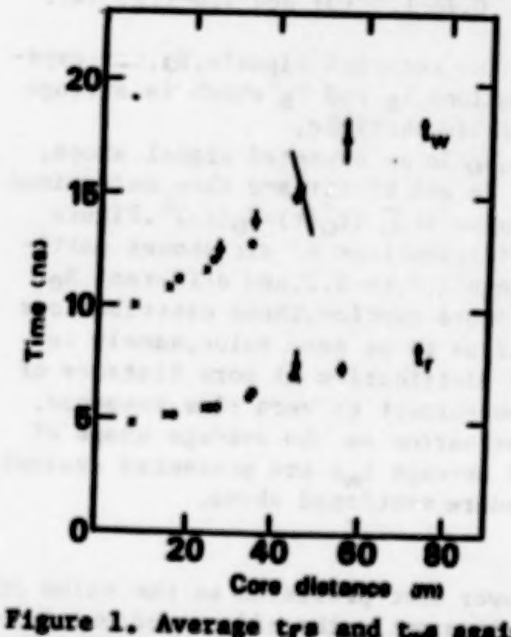

Figure 1. Average t_rs and t_ws against core distance for showers with sec θ of 1.0-1.2 and N_e of $3.2 \times 10^{5.5}$– $1.0 \times 10^{6.0}$(X),$1.0 \times 10^{6.0}$– $3.2 \times 10^{6.5}$(●), $3.2 \times 10^{6.5}$– $1.0 \times 10^{7.0}$(O) and $1.0 \times 10^{7.0}$– $3.2 \times 10^{7.5}$(■).

The average values of t_r and t_w plotted against core distances are shown in figure 1. As is seen in this figure,both values increase with increase in core distances.On the other hand ,dependence of these values on N_e cannot be seen from this figure.As often pointed out,average t_ws have some biases at core distances larger than those presented here in each N_e bins.They are caused by small number of incident particles (less than about ten particles),and consequently,average t_ws are estimated to be rather small values. We have been confirmed carefully unbiased regions of core distances in regard to each N_e bins.

Figure 2(a) shows the average values of t_w for showers with N_e in the range $3.2 \times 10^{6.5}$

to 1.0 x $10^{7.0}$, core distances in the range 20m to 50m and sec θ in the range 1.0 to 1.1, 1.1 to 1.2 and 1.2 to 1.3. Figure 2(b) shows dependence of average t_w on s for showers with sec θ in the range 1.0 to 1.2, and same N_e and core distance bins as figure 2(a). Average number of incident particles to the detector in these three core distance bins is about 50, 25 and 12 for sec θ in the range 1.0 to 1.2 and for s in the range 0.75 to 1.25. Average particle number adopted in figure 2(a), (b) is the same values within errors regardless of different s and sec θ.

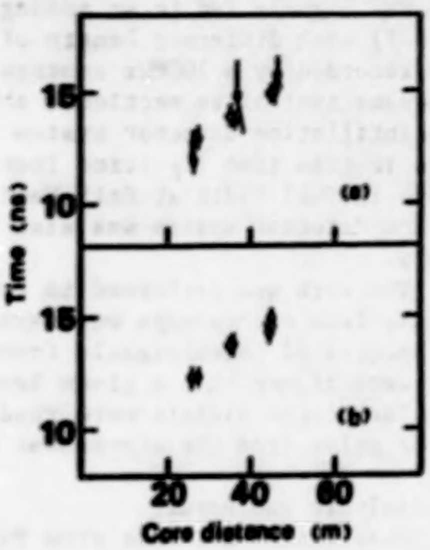

Figure 2. Average t_ws against core distance for showers with N_e of 3.2 x $10^{6.5}$- 1.0 x $10^{7.0}$. (a) shows the dependence of average t_w on sec θ; 1.0-1.1 (○), 1.1-1.2 (●) and 1.2-1.3 (■). (b) shows the dependence of average t_w on age parameter (s); 0.75-1.0 (○) and 1.0-1.25 (●).

These quantities (t_f and t_w) derived from recorded signal shape are distorted due to the decay time of plastic scintillator, the transit time spread in PMT and the response in storage oscilloscope. Accordingly, the average signal shapes have to be reduced to a system with zero time response in order to discuss the true thickness of air shower disc. We assume the function V_e for the arrival time distribution of air shower particles as

$$V_e(t)=\exp(-a(t)) \times (1-\exp(-b(t)))$$

The average signal shape derived from the recorded signals, V_o, can express as the convolution of the two functions V_e and V_s which is average shape corresponding to single relativistic particle.

$$V_o'(t)=\int_0 V_s(t-t') \times V_e(t')\,dt'$$

Here, V_o' is an expected signal shape. Calculation was made by two parameter (a and b) fit, and then determined these parameters giving the minimum value of $\sum (V_o'(t)-V_o(t))^2$. Figure 3 shows the corrected arrival time distributions of air shower particles for showers with sec θ in the range 1.0 to 1.2, and different N_e and core distance bins as showed in figure caption. These distributions presented here are normalized their areas to be same value, namely to same number of incident particles. The distribution at core distance of 10m to 20m have a large ambiguity when correct to zero time response, because the average signal shape is as narrow as the average shape of single particle. In figure 4, corrected average t_ws are presented against core distances derived from the procedure mentioned above.

4. Discussion

The average thickness of air shower disc presented as the value of t_w is increasing with core distances. Apparently, the effects of multiple Coulomb scattering and transvers moments of the particles contribute to broaden the thickness with increase in core distances. On the other hand, the contribution of high energy interaction and primary compositions through the longitudinal development of air shower particles to the value of t_w is not obvious as is seen in figure 2(a) and (b). It seems

ORIGINAL PAGE IS
OF POOR QUALITY

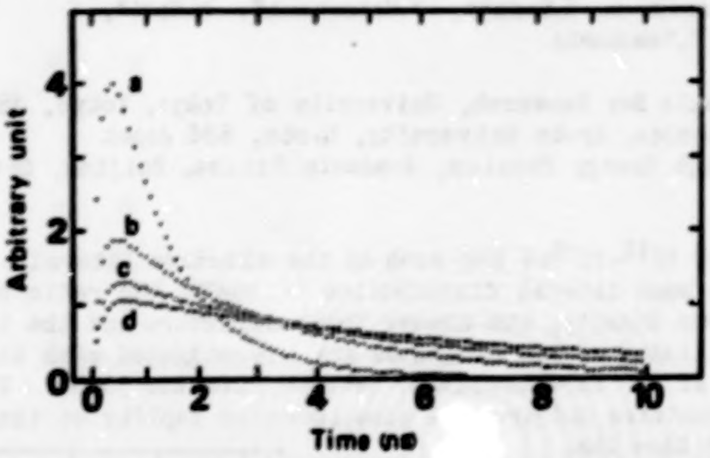

Figure 3. Corrected arrival time distributions of air shower particles for showers with sec θ of 1.0-1.2 and
(a) N_e of $3.2 \times 10^{5.5}$ - $1.0 \times 10^{6.0}$ for core distances 10m-20m
(b) N_e of $1.0 \times 10^{6.0}$ - $3.2 \times 10^{6.5}$ for core distances 20m-30m
(c) N_e of $3.2 \times 10^{6.5}$ - $1.0 \times 10^{7.0}$ for core distances 30m-40m
(d) N_e of $1.0 \times 10^{7.0}$ - $3.2 \times 10^{7.5}$ for core distances 40m-50m

that the thickness at core distance less than 50m is almost determined by electromagnetic cascade starting at lower atmosphere. However, the detailed discussions should be done after a comparison of the whole shape of arrival time distribution, especially on the part of tail and also those at larger core distances, which are seemed to include the information of upper atmosphere. Furthermore, it is necessary to compare with an elaborate three-dimensional shower simulation.

We are going to process the data obtained simultaneously in an air shower by twelve detectors in order to expect higher accuracy and also to study the uniformity of thickness.

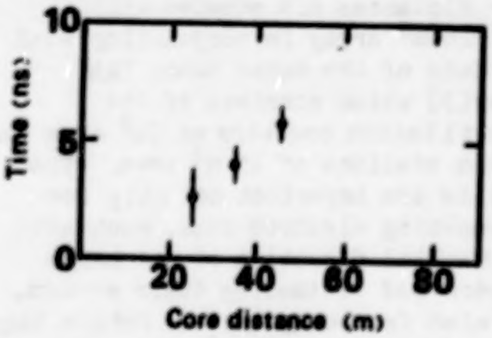

Figure 4. Corrected average t_ws against core distance derived from the arrival time distributions shown in figure 3.

References

Kawamoto, M. et al; HE 6,2-10 of this conference.

Woidneck, C.P. et al: J.Phys. A:Math.Gen. 8(1975)997.

N85-36054

Properties of 10^{18}-10^{19}eV EAS at far core distance

M.Teshima*, M.Nagano, T.Hara, Y.Hatano, N.Hayashida, C.X.He**
M.Honda, F.Ishikawa, K.Kamata, Y.Matsubara*, M.Mori*,
H.Ohoka and G.Tanahashi

Institute for Cosmic Ray Research, University of Tokyo, Tokyo, 188 Japan
*Department of Physics, Kyoto University, Kyoto, 606 Japan
**Institute of High Energy Physics, Academia Sinica, Beijing, China.

Abstract

Properties of 10^{18}-10^{19}eV EAS such as the electron lateral distribution, the muon lateral distribution (E>1GeV), the ratio of muon density to electron density, the shower front structure and the transition effects in scintillator of 5cm thickness are investigated with the Akeno $4\text{km}^2/20\text{km}^2$ array at far core distances between 500m and 3000m. The fluctuation of densities and arrival time increase rapidly at the core distances farther than 2km.

1. Introduction

The 4km^2 array has been in continuous operation for two years[1] and the expanded array of 20km^2[2] from the end of 1984. Properties of 10^{18}-10^{19}eV extensive air shower(EAS) at far core distances are studied with $4\text{km}^2/20\text{km}^2$ array in conjunction with the data of the dense Akeno 1km^2 array[3] which consists of 151 scintillation counters of 1m^2 area and 9 muon stations of 25 m^2 area. The results are important not only for determining electron size, muon size and arrival direction of the large showers and estimating their errors, but also for designing the future huge surface array of 100km^2 area. The reliability of the Linsley proposal for the detection of giant air shower with "mini array"[4] is also discussed using the data obtained.

The data observed with 4km^2 array during a period between Dec. 1982 and Oct. 1984 and with 20km^2 between Sep. 1984 and May. 1985 are analysed. During this operation time about 250 EAS of energies above 10^{18}eV are observed.

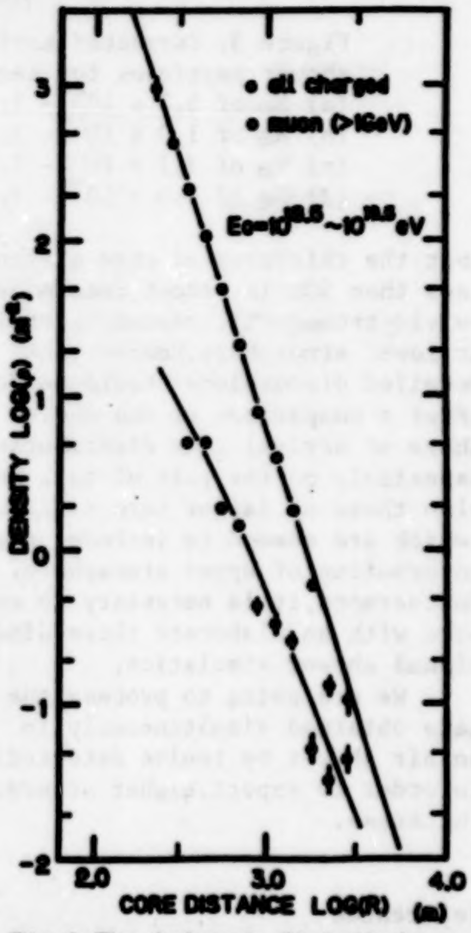

Fig.1 The lateral distribution of electrons and muons.

2. The lateral distribution of electrons(LDE)

The LDE is expressed by the function with two parameters α and η [5].

$$\rho_e(R) = C(R/R_m)^{-\alpha}(1+R/R_m)^{-(\eta-\alpha)}. \quad R_m = 91.6\text{m} \text{ ; Moliere unit.} \quad \text{---(1)}$$

α is 1.2, to which our experiments is not sensitive. η can be measured precisely with many detectors. For the EAS of 3×10^{18}eV η is about 3.8. The LDE becomes steeper as the energy increases and is expressed by

$$\eta = 3.80\pm0.05+(0.10\pm0.05)\mathrm{LOG}(E/10^{19}\mathrm{eV}) \quad \text{-----------(2)}$$

between 100m and 1000m. This energy dependence is a little larger than the result reported by Linsley[6].

At core distances above 1km, the LDE becomes steeper than the extraporation of the above formula. In fig.1 the average LDE of $10^{18.5}$eV-$10^{19.5}$eV for vertical EAS is shown.

The fluctuations of electron densities after subtrqcting statistical ones(Poisson) are shown by solid lines in fig.2(a) and expressed as a function of core distances as follows.

$$\Delta\rho\, e(R)/\rho\, e(R) = 0.20x(1+R/1500)^{2.0}. \quad \text{---------------(3)}$$

At core distances near 2km, the fluctuations become about 100%.

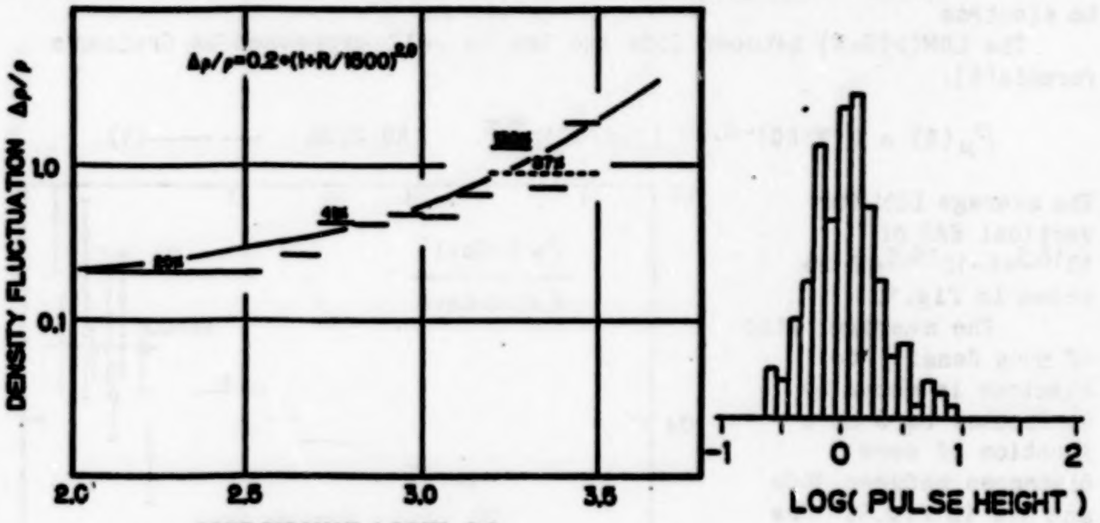

(a) (b)

Fig.2 The fluctuation of electron densities(a). The broken line is derived from pulse height distribution of single particles. That is shown in (b).

3. Ionization losses in scintillator at far core distances

At far core distances the fluctuations of electron densities become larger. The following causes are possibly related to its increment; the transition effect in scintillator, slow neutrons, large core angle distributions of electrons or broad arrival time distribution of electrons. The last one is important when the densities are measured by one detector of large area.

The transition effect in scintillator is examined by comparing the ionization losses of 16 scintillation detectors of $1m^2$ area with 5cm thickness and those of 25 detectors of $0.25m^2$ area with 0.3cm thickness. The ratio of them is 1.05±0.05 and the transition effect is negligible.

The slow neutrons may be partly responsible, since the delayed pulses are frequently observed at far from the core[7].

We are measuring the density with the logarithmic amplifier by discriminating the exponential pulse of decay constant 10 μsec. Therefore the successive particle incidence with broad arrival time distribution described in section 5 may contribute to the fluctuation. The fluctuation due to this is estimated to be about 5% at 1km and 60% at 2km, which are less than the observed values. The pulse height distribution of a single particle which traverse the scintillator is measured at core distances around 2km and is shown in fig.2(b). This distribution is obtained with 151 scintillators of 1km^2 array when the average density is smaller than 0.2 per detector. Therefore this distribution shows the energy loss distribution of a single particle and is free from the pile up of the exponential pulses. The FWHM is about 100% and is the same with the value of Eq(3). This shows that the large density distribution is not due to the spurious one of the used amplifier.

The large core angle distribution of electrons is expected to be originated from multiple scattering, which is also concerned with time structure of shower front reported in section 5.

4. The lateral distribution of muons(LDM) and the ratio of muon density to electron

The LDM(>1GeV) between 200m and 3km is well expressed by Greisen's formula[6].

$$\rho_\mu(R) = C(R/R0)^{-0.75}\ (1+R/R0)^{-2.5}, \qquad R0=280m \quad \text{---------(4)}$$

The average LDM for vertical EAS of $10^{18.5}$eV-$10^{19.5}$eV is shown in fig.1.

The average ratio of muon density to electron is shown by horizontal bars as a function of core distances between 100m and 3km in fig.3. The points with error bars are the individual events which are observed by using the detectors of 1km^2 array triggered by 20km^2 array. The average ratio at core distances between 2km and 3km is 0.20±0.01, but the fluctuation of each event is large.

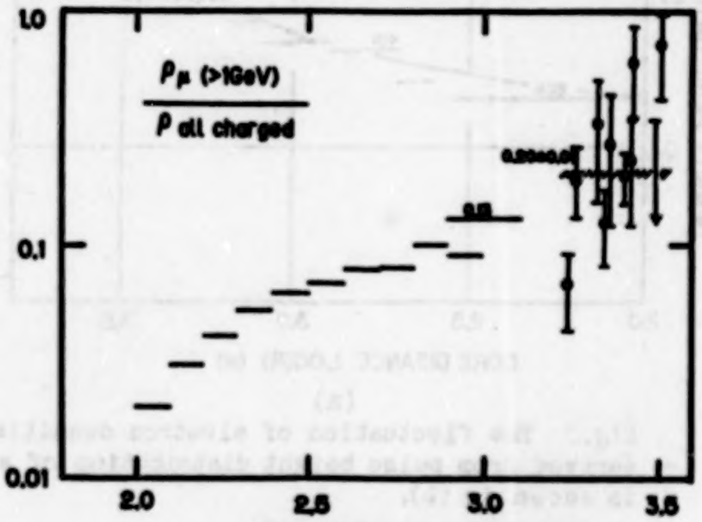

Fig.3 The ratio of muon density to electron.

5. The time structure of shower front

The arrival time of the fastest particle of each detector is measured to determine the arrival direction of EAS. There are 53 fast timing channels with 10nsec resolution in 1km^2 array and 23 channels with 20nsec in 20km^2. The time structures of shower front are studied by using these 76 channels. Our information is the arrival time of the fastest particle, but it gives the shower front structure at far from the core where the average density per detector is less than 1.

In fi[illegible] the dispersion of arrival time is shown. The dispersion increases rapidly at core distances above [illegible] and deviates from the extrapolation of the formula given by Linsley[4]. The curvature of shower front shows the similar tendency.

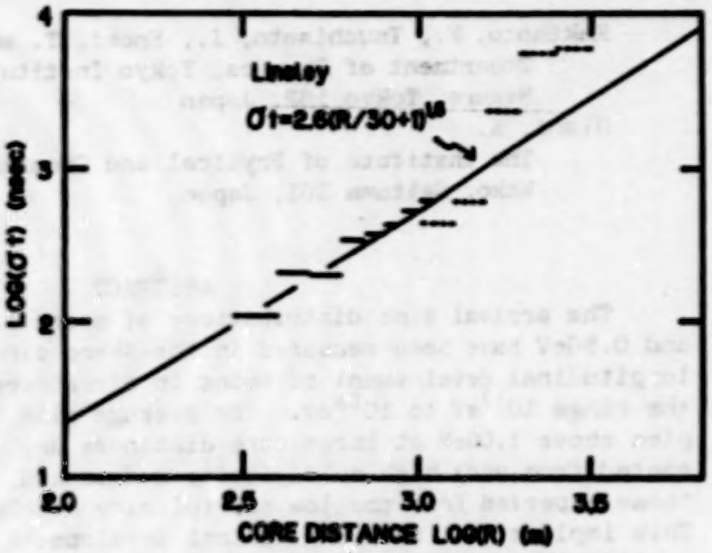

Fig.4 The thickness of shower front.

6. Discussion and Conclusion

At core distances above 1km, the LDE becomes steeper than the extraporation of that within 1km. The density fluctuation increases with distances and exceeds 100% above 2km. The causes of the increment of fluctuations are possibly related to the broad arrival time distribution and the large core angle distribution originated from multiple scattering of electrons. The curvature and the thickness of shower front increase more rapidly above 2km. Therefore, it is necessary to arrange the detectors within 1km spacing.

The observation of Giant Air Shower with "mini array" proposed by Linsley[4] has serious limitations, because the lateral distribution of electrons becomes steeper and its fluctuations become large above 1km. Furthermore fraction of low energy muons to total charged particles fluctuate largely in shower to shower. This method requires the detectors of large area.

Acknowledgements

The authors wish to thank the other members of Akeno A.S. Group for their help and fruitful discussions. The analysis was carried out with FACOM M380 at the Computer Room of Institute for Nuclear Study, University of Tokyo.

Reference

[1] T. Hara et al., Proc. 18th ICRC, Bangalore 11 (1983) 276.
[2] M. Teshima et al., This conf., La Jolla OG 9.4-8
[3] T. Hara et al., Proc. 16th ICRC, Kyoto 8 (1979) 135.
[4] J. Linsley, Proc. 18th ICRC, Bangalore 12 (1983) 135.
[5] J. Linsley, Proc. 15th ICRC, Plovdiv 12 (1977) 56.
[6] K. Greisen, Ann. Rev. Nucl. Sci. 10 (1960) 63.
[7] F. Kakimoto et al., This conf., HE4.7-5.

Longitudinal development of muons in large air showers studied from the arrival time distributions measured at 900m above sea level

N85-36055

Kakimoto, F., Tsuchimoto, I., Enoki, T. and Suga, K.*
Department of Physics, Tokyo Institute of Technology,
Meguro, Tokyo 152, Japan
Nishi, K.
The Institute of Physical and Chemical Research,
Wako, Saitama 351, Japan

ABSTRACT

The arrival time distributions of muons with energies above 1.0GeV and 0.5GeV have been measured in the Akeno air-shower array to study the longitudinal development of muons in air showers with primary energies in the range 10^{17}eV to 10^{18}ev. The average rise times of muons with energies above 1.0GeV at large core distances are consistent with those expected from very high multiplicity models and, on the contrary, with those expected from the low multiplicity models at small core distances. This implies that the longitudinal development at atmospheric depths smaller than 500gcm^{-2} is very fast and that at larger atmospheric depths is rather slow.

Comparison of the mean arrival times of muons with energies above 0.5GeV and the calculation made by McComb et al suggests no serious contribution of muons arising from photon-nucleus collisions to the arrival time distributions of muons with energies above 0.5GeV.

1. Introduction

The Bolivian Air Shower Joint Experiment (BASJE) group and the Tokyo Institute of Technology group carried out a series of experiments to study the longitudinal development of electrons and that of muons by measuring the arrival time distributions both of atmospheric Cerenkov light and of muons, at widely separated atmospheric depths of 550gcm^{-2}(Mt. Chacaltaya) and 930gcm^{-2}(Akeno). The longitudinal development of muons derived from the experiment at Chacaltaya and that of electrons derived from both experiments at Chacaltaya and at Akeno have already been published(1),(2),(3).

In the present paper, we report on the arrival time distributions of muons with energies above 1.0GeV in air showers with primary energies in the range 10^{17}eV to 10^{18}eV observed in the Akeno air-shower array. Also reported in the paper are arrival time distributions of muons, with a lower threshold energy of 0.5GeV, in air showers around 10^{18}eV. On this basis an estimate is made of the contribution of muons arising from photon-nucleus collisions (photoproduced muons) to the arrival time distributions of muons with energies above 0.5GeV, by comparing the mean arrival times of muons calculated by McComb et al(7) with those measued in the present experiment.

2. Experimental

The first run (May 1981-December 1982) was made to measure the arrival time distributions of muons with energies above 1.0GeV in air showers with primary energies around 10^{17}eV. The result of this run was already reported(4).

---

*Present address: Department of Physics, Meisei University,
Hodokubo 337, Hino-shi, Tokyo 191, Japan

In the second run (January 1983-October 1984) the measurement was made both at the M4 muon station ($E_\mu > 1.0$GeV) and at the ME3 muon station ($E_\mu > 0.5$GeV), which were separated by 100m from each other. Four 4m^2 shielded scintillation detectors were operated along with a 4m^2 unshielded scintillation detector at each station (hereafter called muon detector and electron detector, respectively). The inside wall of muon detector was covered with black paper while that of electron detector was painted white, and a 5in fast photomultiplier with 14 stages (Hamamatsu Photonics R1250) viewed a scintillator in the detector. Signals from four muon detectors were added in a circuit through a coaxial cable (11C4AF). A signal from the electron detector was delayed by 1.8μs through a coaxial cable (8C4AF) and then added in the circuit. This combined signal was fed to a waveform recorder (Biomation 8100) with a sampling interval of 20ns. When the local trigger pulse generated by the passage of at least one particle through the electron detector was coincident with a master pulse from the Akeno 4km^2 air-shower array(5), which observed an air shower with electron size larger than $10^{7.5}$, the combined signal was stored in the recorder.

The time response of the whole system was 16.2ns for rise time between 20% and 70% of the integrated full signal from the muon detector (T_{20-70}).

3. Arrival time distributions of muons with energies above 1.0GeV

In figure 1 average values of T_{20-70} for muons with energies above 1.0 GeV in the second run are presented against core distances, where the data are free from biases arising from the requirement for the local trigger and the limited dynamic range of the pulse height in the recording system. Also shown in the figure are values of T_{20-70} calculated from four models for primary protons with energies of 10^{18}eV and secθ of 1.1. As is seen in the figure, the average values of T_{20-70} at small core distances are consistent with those calculated from low multiplicity models, while high multiplicity models reproduce the present T_{20-70} consistently at large core distances, indicating that the observed values of T_{20-70} at all core distances seem not to be explained by any single model as in the case of lower primary energies(4). Since the showers observed in the present experiment were classified by their electron sizes, the sample of showers with a given electron size observed in the Akeno array contains showers initiated at the top of the atmosphere with a particular primary energy as well as those from lower primary energies starting at the deeper atmosphere. This fact was already confirmed from the measurement of atmospheric Cerenkov light at Akeno(3). Considering this fluctuation, a model with an enhanced $E^{1/2}$ multiplicity law reproduces the observed values of T_{20-70} better than a model with an $E^{1/2}$ multiplicity law at largest core distances.

4. Comparison of both arrival time distributions of muons above 0.5GeV and 1.0GeV

The average values of T_{20-70} for muons with energies above 0.5GeV are longer than those with energies above 1.0GeV by about 50% for showers with electron sizes in the range $10^{8.0}$ to $10^{8.5}$ and secθ in the range 1.0 to 1.2, as shown in figure 2. It is worth noting that the average values of T_{20-70} for muons above 0.5GeV are almost consistent with those above 0.42GeV obtained by the Nottingham group in the Haverah Park array(6), if the differences of the system time response and the threshold energy of muons in the two experiments are allowed for.

In figure 3 the mean arrival times of muons above 0.5GeV and those above 1.0GeV were calculated from observed muon signals and are compared with those estimated from the mean arrival times and lateral distributions of photoproduced and normal muons above 0.3GeV at sea level calculated by McComb et al(7) using a scaling model for proton and iron-initiated showers. After allowing for differences of the threshold energy of muons and the atmospheric depth between the calculation and the present experiment, we would conclude that the longitudinal development of muons in air showers with primary energies around 10^{18}eV is faster than that calculated by McComb et al using a scaling model and primary iron, furthermore the proportion of photoproduced muons to all muons above 0.5GeV must be much smaller than that calculated by these authors.

5. Discussion and conclusions

The observed values of T_{20-70} at small core distances are consistent with those calculated from low multiplicity models while at large core distances these observed values of T_{20-70} are well explained by high multiplicity models. According to the present calculation, the average production depth of muons arriving at the time intervals of T_{20-70} decreases with increasing core distance. We may conclude, therefore, that the longitudinal development of muons in air showers with primary energies in the range 10^{17}eV to 10^{18}eV is as fast as expected from an enhanced $E^{1/2}$ multiplicity law from 200gcm^{-2} to 500gcm^{-2} and is rather slow beyond that atmospheric depth. This conclusion is consistent with that derived from the arrival time distributions of muons in air showers with primary energies above 10^{17}eV observed at Chacaltaya(1) and of atmospheric Cerenkov light from air showers with primary energies in the range 5×10^{15}eV to 2×10^{17}eV observed at Akeno(3) as well as at Chacaltaya(2).

The fact that photoproduced muons appear to make no significant contribution to the arrival time distributions of muons with energies above 0.5GeV means that the character of particle interactions may be conveniently studied by measuring the arrival time distributions of muons above 0.5GeV, instead of 1.0GeV, and comparing them with calculations for normal muons. This way is important to reduce the cost of the shielding material of muon stations with large area in a large air-shower array.

References

(1) F. Kakimoto et al: J. Phys. G: Nucl. Phys. 5(1983)339.
(2) N. Inoue et al: J. Phys. G: Nucl. Phys. 11(1985)669.
(3) N. Inoue et al: J. Phys. G: Nucl. Phys. 11(1985)657.
(4) T. Tamura et al: Proc. of 18th ICRC, Bangalore, 6(1983)133.
(5) T. Hara et al: Proc. of 18th ICRC, Bangalore, 11(1983)276.
(6) P.R. Blake et al: J. Phys. G: Nucl. Phys. 8(1982)1605.
(7) T.J. McComb et al: J. Phys. G: Nucl. Phys. 5(1979)1613.

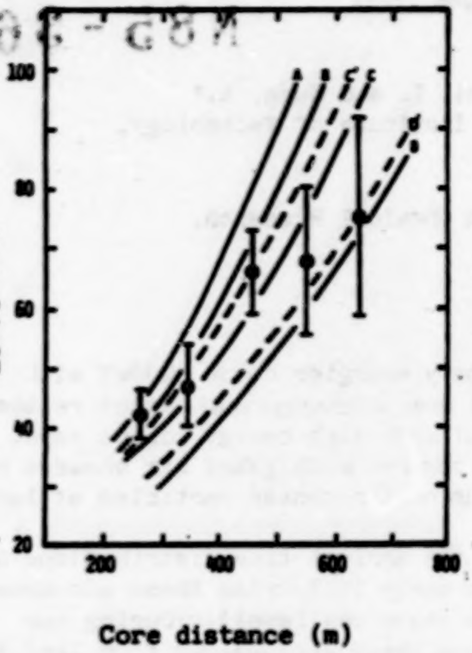

Figure 1. The average T_{20-70} of the arrival time distributions of muons with energies above 1.0GeV for showers with N_e of $10^{8.0}$-$10^{8.5}$ and secθ of 1.0-1.2 compared with those calculated from A: scaling model, B: a model with an $E^{1/4}$ multiplicity law, C: a model with an $E^{1/2}$ multiplicity law and D: a model with an enhanced $E^{1/2}$ multiplicity law and with first-interaction depths of 40gcm^{-2} for A-D and 120gcm^{-2} for C'-D'.

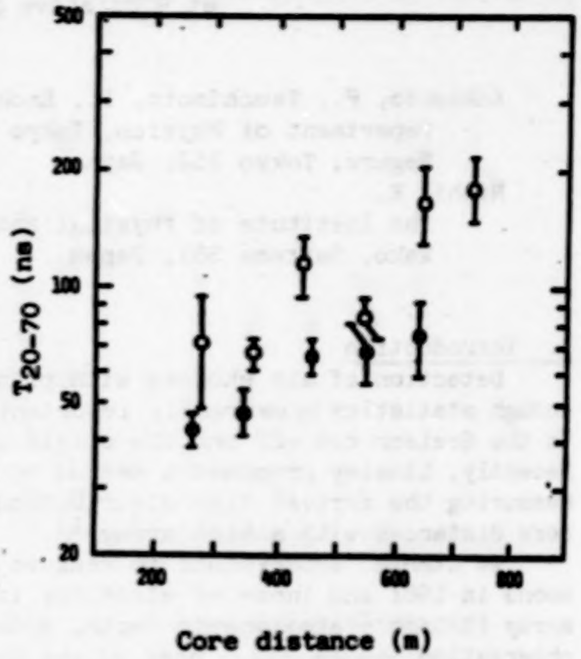

Figure 2. The average T_{20-70} of the arrival time distributions of muons with energies above 0.5GeV (○) and those above 1.0GeV(●).

Figure 3. Mean arrival times of muons with energies above 0.5GeV (○) and those above 1.0GeV(●) for showers with N_e of $10^{8.0}$-$10^{8.5}$ and secθ of 1.0-1.2 against core distances compared with those of muons above 0.3GeV estimated for primary protons (———) and for primary irons (- - -) with energies of 10^{18}eV and secθ of 1.0.

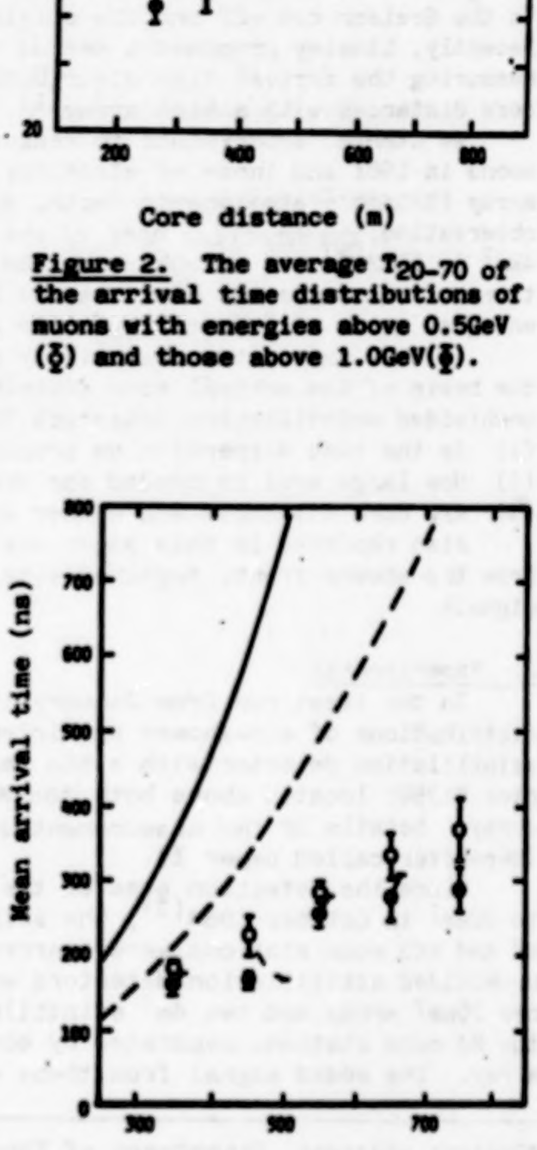

Arrival time distributions of electrons in air showers with primary energies above 10^{18}eV observed at 900m above sea level

N85-36056

Kakimoto, F., Tsuchimoto, I., Enoki, T. and Suga, K.*
Department of Physics, Tokyo Institute of Technology,
Meguro, Tokyo 152, Japan
Nishi, K.
The Institute of Physical and Chemical Research,
Wako, Saitama 351, Japan

1. Introduction

Detection of air showers with primary energies above 10^{19}eV with enough statistics is extremely important in an astrophysical aspect related to the Greisen cut off and the origin of such high energy cosmic rays. Recently, Linsley proposed a method to observe such giant air showers by measuring the arrival time distributions of air-shower particles at large core distances with a mini array(1).

We started experiments to measure the arrival time distributions of muons in 1981 and those of electrons in early 1983 in the Akeno air-shower array (930gcm^{-2} atmospheric depth, 900m above sea level). During our observation, the detection area of the Akeno array was expanded from 1km^2 to 4km^2 in 1982(2) and to 20km in 1984 . Now the arrival time distributions of electrons and muons can be measured for showers with primary energies above 10^{19}eV at large core distances.

In this paper, the possibility of Linsley's proposal is examined on the basis of the arrival time distributions of particles measured with unshielded scintillation detectors for following three points:

(1) Is the time dispersion as proposed by Linsley a stuitable parameter?
(2) How large area is needed for the detector?
(3) Are core distances and shower sizes determined accurately enough?

Also reported in this paper are signals delayed by longer than 1μs from the shower front, together with a discussion on the nature of these signals.

2. Experimental

In the first run from January 1983 to October 1984, the arrival time distributions of air-shower particles was measured using a 4m^2 unshielded scintillation detector with a 5in fast photomultiplier (Hamamatsu Photonics R1250) located above both the N4 and NE3 muon stations in the Akeno array. Details of the measurement are described in the preceding paper(4) (hereafter called paper I).

Since the detection area of the Akeno array was expanded from 4km^2 to 20km^2 in October 1984(3), the scintillation detectors located at the N4 and NE3 muon stations were rearranged. In this second run four 4m^2 unshielded scintillation detectors were installed near the center of this new 20km^2 array and two 4m^2 scintillation detectors were located above the N4 muon station, separated by about 2km from the center of the new array. The added signal from these detectors was stored in the waveform

---

*Present address: Department of Physics, Meisei University,
Hodokubo 337, Hino-shi, Tokyo 191, Japan

recorder (Biomation 8100) with a sampling interval of 50ns in each station, when the local trigger pulse generated by a passage of at least one particle through any one of the detectors was coincident with a master pulse from the array to observe air showers with electron sizes larger than $10^{8.0}$.

The time response of the whole system in the first run was 39ns for rise time between 20% and 70% of the integrated full signal (T_{20-70}), while this value in the second run became larger due to the larger sampling interval of the recorder but this is not serious for observation of the arrival time distributions of particles at large core distances.

3. Arrival time distributions of particles at large core distances

On the basis of the observed arrival time distributions, the time dispersion (σ) proposed by Linsley as well as the rise time (T_{20-70}) were calculated for each shower. Average values both of σ and T_{20-70} are plotted against core distances in figure 1(a) and (b), respectively, for air showers with electron sizes from $10^{8.0}$ to $10^{8.5}$ and secθ from 1.0 to 1.2 in the first run. Also shown in figure 1(a) is the value of σ given by Linsley's empirical formula. Although the average values of σ obtained at core distances smaller than 500m are larger than the value of σ by Linsley, those at large core distances are consistent with each other. As is seen in figure 1(b) average values of T_{20-70} show a steeper dependence on the core distance than those of σ.

Though the sample of showers is limited at present, time dispersions for showers with electron sizes above $10^{8.0}$ observed in the two runs are plotted against core distances in figure 2. A large fluctuation in σ is seen at given core distances. The distribution of σ depends upon the number of observed particles. For a sample of showers with electron sizes of $10^{8.0}$-$10^{8.5}$ at core distances of 500-600m, the standard deviation of σ is 100ns for more than 10 particles while 30ns for more than 30 particles.

4. Signals delayed by longer than 1μsec

Signals, which correspond to the passage of more than 0.5 particles, delayed by longer than 1μs from the shower front have been seen in 15% of arrival time distributions measured for showers with electron sizes larger than $10^{8.0}$. Figure 3 shows the delay time distribution for air showers with electron sizes from $10^{8.0}$ to $10^{8.5}$ and secθ from 1.0 to 1.2. The frequency decreases monotonously up to 4μs with delay time while, after that time, this frequency is almost constant up to 10μs. The frequency of accidental signals is as low as $8\times10^{-4}(4m^2\cdot1\mu s)^{-1}$. Moreover, during first run, we observed five interesting showers in which one or successive delayed signals appeared in both the arrival time distribution of muons and that of electrons with almost same delay times, one of which is shown in figure 4(a), and observed one shower in which four successive delayed signals appeared in both arrival time distributions of electrons with almost same delay times at the N4 and NE3 muon stations separated by 100m from each other, which is shown in figure 4(b).

5. Discussion and conclusion

From the fluctuation in the time dispersions (σ) shown in figure 2, we may tentatively argue that the core distance and the shower size would be determined within an accuracy of 100-150m and $^{+120}_{-70}$%, respectively, if the number of particles observed in the detectors exceeds ten and the core distance is around 1.5km. However, it should be mentioned from the present analysis that the value of time dispersion (σ) is more sensitive to the existence of delayed particles than that of T_{20-70} and the values of T_{20-70} show a steeper dependence on core distance than that of σ. Needless to say, it is most importnat to accumulate the sample of showers and examine further the dependence of the dispersion on the electron size and the zenith angle to make a final conclusion on the possibility of the proposal made by Linsley.

The delayed signals observed in the present experiment seem to be explained qualitatively as originated from low-energy neutrons which made interactions in the scintillator. However, the successive delayed signals as described at the end of §4 look very interesting and more samples should be necessary to clarify their origin.

__References__

(1) J. Linsley: Research Reports UNML-6/11/83, UNML-6/15/83 and UNML-6/20/83(1983)

(2) T. Hara et al: Proc. of 18th ICRC, Bangalore, __11__(1983)276.

(3) M. Teshima et al: OG 9.4-8 in this Conference.

(4) F. Kakimoto et al: HE 4.7-4 in this Conference.

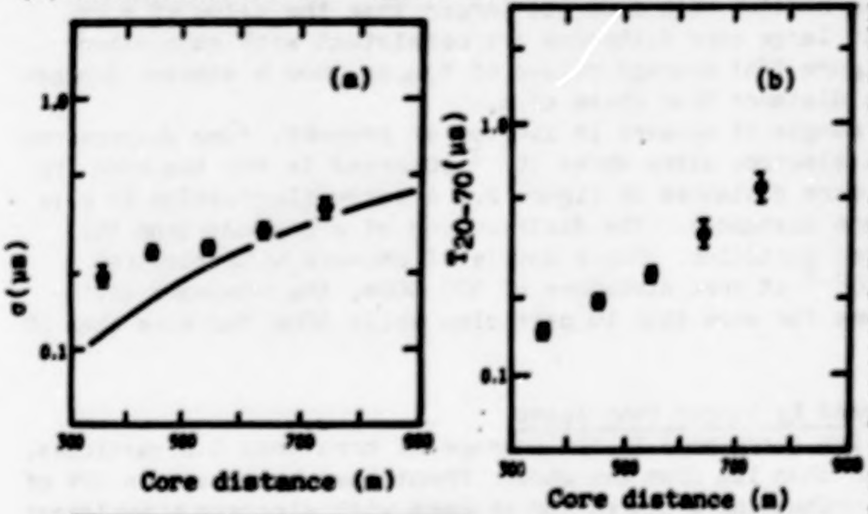

__Figure 1.__ The average σ (a) and T_{20-70}(b) of the arrival time distributions of particles in the first run for showers with electron sizes from $10^{8.0}$ to $10^{8.5}$ and secθ from 1.0 to 1.2. A curve in (a) is given by Linsley's empirical formula (σ(ns)=$2.6(1+R/30m)^{1.5}$, R:core distance)

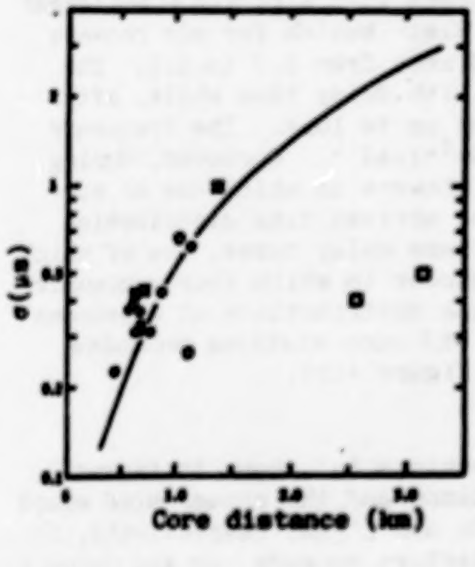

__Figure 2.__ Time dispersions (σ) of the arrival time distributions of particles for showers with electron sizes above $10^{9.0}$ observed in the first run(●,○) and in the second run(■,□). The number of particles observed in the unshielded detectors: ≥10 for ● and ■; <10 for ○ and □. Time intervals in the arrival time distributions of particles, within which time dispersions were calculated; 2.4μs for ● and ○; 10μs for ■ and □. A curve is given by Linsley's formula.

ORIGINAL PAGE IS
OF POOR QUALITY

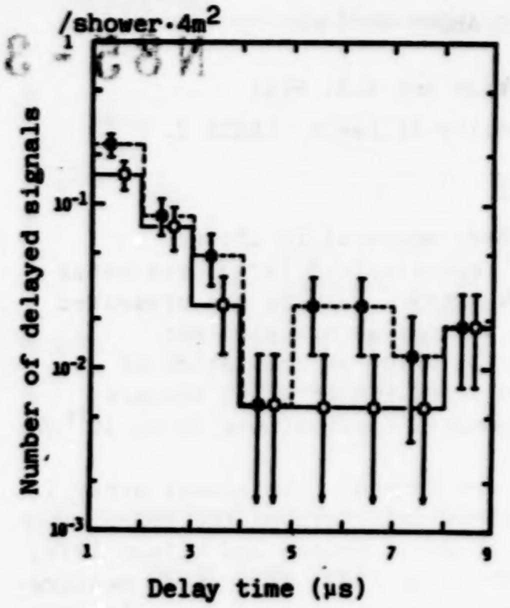

Figure 3. Delay time distribution of signals delayed by longer than 1.0µs observed in the arrival time distributions of particles for air showers with electron sizes from $10^{8.0}$ to $10^{8.5}$ and secθ from 1.0 to 1.2. ●: more than 0.5 particles; ○: more than 1.0 particle.

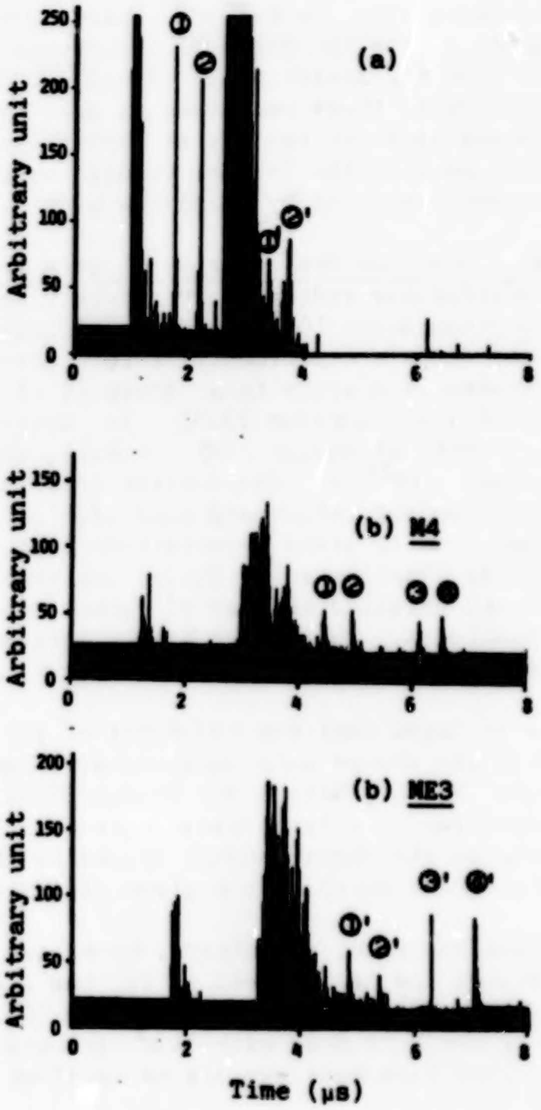

Figure 4(a). Delayed signals observed both in the shielded detectors (①: t_d=0.76, n_d=14.8; ②: t_d=1.18, n_d=15.7) and in the unshielded detector (①': t_d=0.70, n_d=2.6; ②': t_d=1.12, n_d=3.2) at ME3 station for air shower with N_e of 3.7×10^8, θ of 15.2° and R of 327.3m. t_d: delay time in µs and n_d: the number of delayed particles. Time between both signals from the shielded detectors and the unshielded one is 1.8µs as described in paper I. Under-shoot in the figure is due to overloading in the amplifier of the recorder.

(b). Delayed signals observed in the unshielded detector both at M4 station (①: t_d=1.48, n_d=2.3; ②: t_d=2.00, n_d=2.4; ③: t_d=3.16, n_d=1.7; ④: t_d=3.56, n_d=2.0) and ME3 station (①': t_d=1.56, n_d=1.5; ②': t_d=2.04, n_d=0.9; ③': t_d=3.00, n_d=1.6; ④': t_d=3.76, n_d=4.4) for air shower with N_e of 2.8×10^9, θ of 8.1° and R of 697.3m from M4 and of 665.6m from ME3.

THE THICKNESS OF THE SHOWER DISC AS OBSERVED IN SHOWERS PRODUCED BY PRIMARIES ABOVE 10^{19} eV

N85-36057

M.A. Lawrence, A.A. Watson and A.A. West
Department of Physics, University of Leeds, LEEDS 2.

ABSTRACT

The thickness of the shower disc has been measured in showers initiated by primaries of energy $> 10^{19}$ eV using the large area water Cerenkov detectors of the Haverah Park array. Results are presented which (a) provide supporting evidence for the accuracy of our analysis procedures in giant showers, (b) offer an evaluation of Linsley's mini-array technique for the detection of giant showers and (c) extend earlier work on developmental fluctuations above 10^{19} eV.

1. Introduction. A unique feature of the Haverah Park shower array is the large area ($34\ \mathrm{m}^2$) of the water-Cerenkov detectors of the 500 m array. These have been used in a succession of studies (Watson and Wilson 1974, Lapikens 1977, Walker and Watson 1981, 1982 and 1983) to provide measurements of the thickness of the shower disc as a function of core distance ($r > 250$ m), zenith angle ($\theta < 40^{\circ}$) and energy ($E > 2 \times 10^{17}$ eV). In particular these measurements were amongst the first to be used to demonstrate the reality of shower-to-shower fluctuations in large showers. Here we describe further results which have been deduced about giant showers produced by primaries with $E > 10^{19}$ eV.

2. Check on the accuracy of core location above 4×10^{19} eV. There is considerable contemporary interest in the shape of the cosmic ray energy spectrum above 10^{19} eV (e.g. Hill and Schramm 1985) and, despite considerable experimental effort world-wide, the shape of the spectrum remains in dispute (e.g. Bower et al 1983, Diminstein et al 1982, Horton et al 1983, Linsley 1983). In particular the Yakutsk group have reported no events of energy $> 10^{20}$ eV while the other three groups all claim events $> 10^{20}$ eV. The Yakutsk group have suggested that errors in core location and inadequate knowledge of the water-Cerenkov structure function have lead to gross over-estimates of the energy of some Haverah Park events (Vasilev et al 1983). We briefly describe a simple check, based on our detailed studies of shower disc thickness, which refute this hypothesis. This check has in fact been used in our work for many years and has been alluded to before (e.g. Lapikens 1977, Cunningham et al 1980).

It is found that the thickness of the shower disc increases with distance from the shower axis independent of detector type (Linsley and Scarsi 1962, Baxter, Watson and Wilson 1965). This arises because the source of particles at a large axial distance is essentially a line source. Furthermore as the shower energy increases the 'line-source' moves deeper in the atmosphere so that at a given distance the disc will become thicker.

These features, and others, have been quantified in the Haverah Park work through the measurement of $t_{1/2}$, the risetime of the signal in the water-Cerenkov detectors between 10 and 50% of full height. So far all of the work has been done with $34\ \mathrm{m}^2$ detectors and the majority of data is derived from measurements on oscilloscope records.

The easiest and most common way to over-estimate the size of an air-shower is to misplace the core at greater than the correct distance from the centre of the array. The steepness of the lateral distribution, combined with the wide-spacing of detectors, make this an important and well-recognized problem. The shower disc thickness allows a check on the accuracy of the assigned core: if the core is placed too far from the array centre then the measured risetime will appear to be anomalously fast. The risetime of the pulse thus acts as an independent check on the core location analysis.

Figure 1: Plot of risetime against distance for events listed in Table 1.

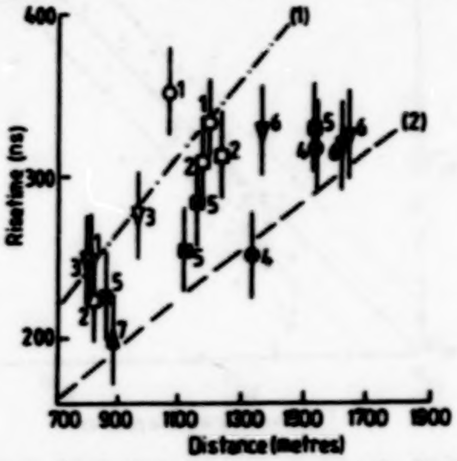

Table 1

	MR	θ	1D	Ep/eV
(1)	9597348	11°	1	6.7×10^{19}
	19384465	9°	2	5.1×10^{19}
	21220296	13°	3	4.2×10^{19}
(2)	9160073	30°	4	1.6×10^{20}
	12701723	29°	5	1.4×10^{20}
	16632298	34°	6	1.1×10^{20}
	17684312	35°	7	9.8×10^{19}

Events included in the Haverah Park energy spectrum (Brooke et al OG5.1-3) with $\theta < 40^\circ$, $E > 4 \times 10^{19}$ eV and for which risetime measurements are available above are shown in Figure 1. The lines are for 11° and 32° but are appropriate to the 139 events with $5 \times 10^{18} < E < 4 \times 10^{19}$ eV $(\overline{\log E} = 19.0)$ from which the regression relation

$$t_{\frac{1}{2}}\,(\text{ns}) = ((0.71 \pm .01) - (0.47 \pm .10)\sec\theta)\,r + (55 \pm 8)$$

was derived. The points, on average, lie above this line as expected; specifically $\Sigma\sigma(\theta,r)/\sigma_m(t_{\frac{1}{2}})$ is +8.3 for the 18 risetimes measured in 7 events. Checks made in this way on the vast majority of showers with $E > 5 \times 10^{18}$ eV and $\theta < 40^\circ$ underpin our confidence in the existence of primary cosmic rays above 5×10^{19} eV.

3. The mini-array method. Linsley (1983 and this conference OG-9) has proposed a cheap and novel method of detecting giant air-showers through the simultaneous measurement of shower disc thickness, density and direction at a small (~ 50 m) shower array. His proposal was based on empirical data from the Volcano Ranch array obtained by averaging over many showers. We find this idea attractive and are presently instrumenting the peripheral arrays at Haverah Park for this purpose (Brooke et al 1983). As an interim step we have attempted to evaluate the potential of the method using existing data.

Events of known primary energy $> 5 \times 10^{18}$ eV and with at least one risetime measurement were selected. Using the zenith angle determined from the 500 m array detectors and the known regression line for giant showers (section 2 above) the distance of the core from each detector was estimated and hence, from the known density and assumed lateral distribution, the primary energy was derived. In Figure 2 the primary energy, E(t), derived from risetime measurement is compared with that from our normal analysis, the dashed lines indicating factors of two about the 1:1 line. Data for two threshold density cuts are shown.

Figure 2: Plots of energy derived from risetime against energy derived from conventional analysis.

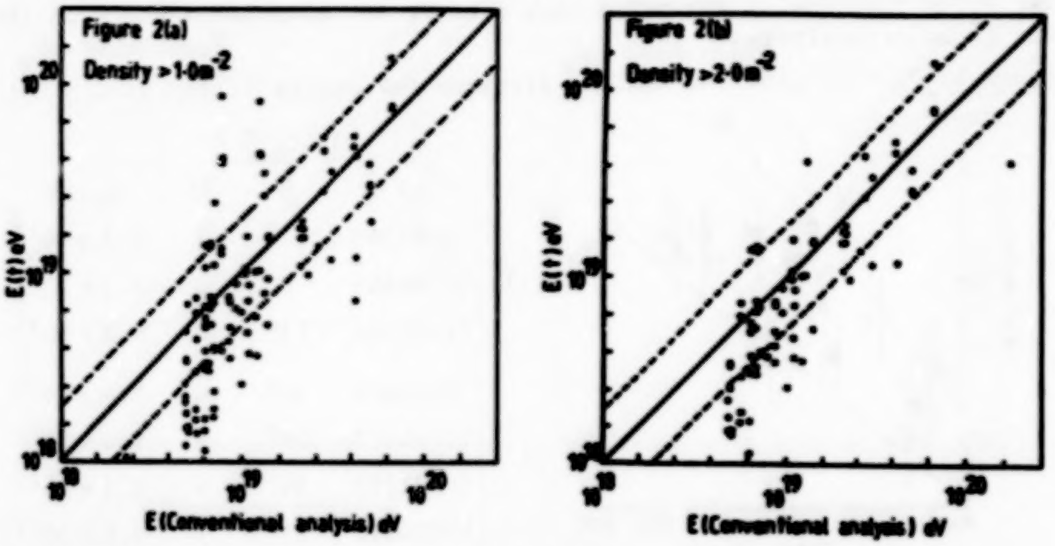

An unweighted straight line fit to the points above 10^{19} eV yields gradients of 0.9 ± 0.2 and 1.2 ± 0.2 and the rms scatters about these lines are 100% and 75% for the two threshold density cuts respectively. A number of factors contribute to the spread in E(t) and some of these will be discussed in the context of risetime measurement at 1 km in a 10^{19} eV shower at 30°.

(a) Zenith angle uncertainty. For the showers used above the typical zenith angle uncertainty is about 3°. However for realistic mini-arrays (such as those already set up at Haverah Park) $\Delta\theta \simeq 5^{\circ}$ (Brooke et al 1983). For a density recorded at 1 km this leads to an uncertainty in E(t) of about 30%. It is possible that with suitable calibration improved zenith angle uncertainties might be achieved. Present work in optimizing angular resolution for UHE γ-ray astronomy might have spin-off here.

(b) Density threshold. The density threshold for the events in Figure 2(a) was set at $> 1\,\mathrm{m}^{-2}$ (34 vertical equivalent muons). A detailed analysis of measurement errors shows that for the reference shower being discussed here $\sigma \simeq 20$ ns with the major contribution coming from the finite size of the density sample. This leads to an rms error in r of about 100m and to an rms error in E(t) of about 35%. The error in the risetime from this cause will vary as $1/\sqrt{\rho}$, where ρ is the density.

(c) Between shower variations. There are fluctuations in the longitudinal development of individual air-showers. These are unavoidable and cannot be overcome by new experimental techniques. For the reference shower $\sigma \simeq 20$ ns so that again the error in the deduced E(t) is $\sim 35\%$.

These three factors when combined in quadrature predict an rms spread in E(t) of $\sim 60\%$ for a 10^{19} eV observed at 1 km and 30° with water-Cerenkov detectors of $34\,\mathrm{m}^2$ area. With smaller area detectors the situation will be worse, but we propose to evaluate the problem using the sub-arrays at Haverah Park which are located 2 km from the centre of the array. Each, consisting of 4 x 13.5 m^2 water-Cerenkov detectors, spaced at 50 or 150 m, is presently used to record small local showers (> 10^{15} or 10^{16} eV) as well as being slaved by the giant array trigger. A single mini-array will have a collecting area of ~6 km^2 at 10^{18} eV for a 1 m^2 threshold so that a x3 enhancement of our present system will be achieved at low cost. The uncertainties in energy measurement discussed above suggest that the mini-array technique will be more useful in the investigation of anisotropy at the highest energies than for the accurate determination of the cosmic ray spectrum.

The above evaluation refers to the use of $t_{\frac{1}{2}}$ to measure the disc thickness. In fact Linsley (1983) proposed the use of the dispersion and there will be differences of detail between an evaluation of that parameter and the present one.

4. Developmental Fluctuation. We have used our sample of 51 events above 10^{19} eV to estimate the fluctuation in the mean depth of maximum at 3×10^{19} eV. Details will be given elsewhere but the method is essentially that discussed in Walker and Watson (1983). The rms fluctuation in X_m, $\{X_m\}$, is found to be 33 ± 8 g cm^{-2}, consistent with our previous work. The tendency for $\{X_m\}$ to decrease with energy and the conclusion that pure Fe can be excluded above 10^{19} eV are reinforced.

5. Acknowledgements. Extensive discussion with Bob Reid is gratefully acknowledged as is the financial support of the Science and Engineering Research Council.

References

Baxter, A.J., Watson, A.A. and Wilson, J.G. (1965) Proc. 9th Int. C.R. Conf. (London) 2, 724.
Bower, A.J. et al (1983) J. Phys. G 9, L53.
Brooke, G. et al (1983) Proc. 18th Int. C.R. Conf. (Bangalore) 9, 420.
Cunningham, G. et al (1981) Proc. 16th Int. C.R. Conf. (Paris)
Diminstein, O.S. et al (1982) Bull. Naush. Info. Yakutsk 9, 537.
Hill, C.T. and Schramm, D. (1985) Phys. Rev. D31, 564.
Horton, L. et al (1983) Proc. 18th Int. C.R. Conf. (Bangalore) 2, 128.
Lapikens, J. (1977) Proc. 15th Int. C.R. Conf. (Plovdiv) 8, 1978.
Linsley, J. (1983) Proc. 18th Int. C.R. Conf. (Bangalore) 12, 135.
Linsley, J. and Scarsi, L. (1962) Phys. Rev. Lett. 9, 123.
Vasilev, I.V. et al (1983) 'Cosmic Rays with Energy > 10^{17} eV', published by Yakutsk Branch of Academy of Science USSR, EDK537.591, p.19.
Walker, R. and Watson, A.A. (1981) J. Phys. G 7, 1297.
Walker, R. and Watson, A.A. (1982) J. Phys. G 8, 1131.
Walker, R. and Watson, A.A. (1983) Proc. 18th Int. C.R. Conf. (Bangalore) 6, 114.
Watson, A.A. and Wilson, J.G. (1974) J. Phys. A 7, 1199.

N85-36058

HE 4.7-7

METHODS FOR ROOF-TOP MINI-ARRAYS

Wayne E. Hazen and Eric S. Hazen*
Randall Laboratory of Physics, University of Michigan
Ann Arbor, MI 48109, USA
*ETC Inc., Middleton WI 53562, USA

1. Introduction. In order to test the idea of the Linsley effect mini array (1) for the study of giant air showers, it is desirable to have a trigger that exploits the Linsley effect itself. In addition to the trigger, it is necessary to have a method for measuring the relative arrival times of the particle swarm selected by the trigger. Since the idea of mini- arrays is likely to appeal to small research groups, it is desirable to try to design relatively simple and inexpensive methods, and methods that utilize existing detectors.

Thus far we have designed for clusters of small detectors where the operation is in the local particle density realm where the probability of >2 particles per detector is small. Consequently, we can discriminate pulses from each detector and thenceforth deal mainly with logic pulses.

This report describes the key circuits that have been built and the results of preliminary tests. Results from a preliminary run with a small shower array are presented in another conference paper (2). Expected rates of data collection are calculated in paper HE 4.7-8.

2. Method. Pulses from the photomultiplier (PM) of each detector are fed to discriminators (after preamplification if desirable). The discriminators can be single level or double level (CFD) if desirable enough to warrant the extra circuitry. The discriminator outputs are then "shaped" to 20 ns length and combined by an OR element. The OR'd output is fanned-out to the trigger circuit and to a 100 MHz time shift register.

For a study and utilization of the Linsley effect itself a time window of 2 µs is sufficient, but we can also provide an additional 2 µs of analog display (with lower time resolution) by means of a 30 MHz pulse form digitizer,[3] if we want to look for delayed pulses. Both of the above are also readily lengthened by adding more shift-register IC's.

(A) The trigger circuits are of two sorts. The first is digital and simply counts the number of pulses that arrive within a 2 µs gate that is opened by each pulse. (With the "singles" counting rates we need in order to have satisfactory particle detection efficiency, the accidental rates can be kept manageable.) If the number of pulses within the window satisfies the preset requirement, a trigger is generated at the end of the 2 µs gate. The circuit is shown in Fig. 1.

The above trigger has the advantage of simplicity, but it cannot count pulses that are closer together than 30 to 40 ns. There-

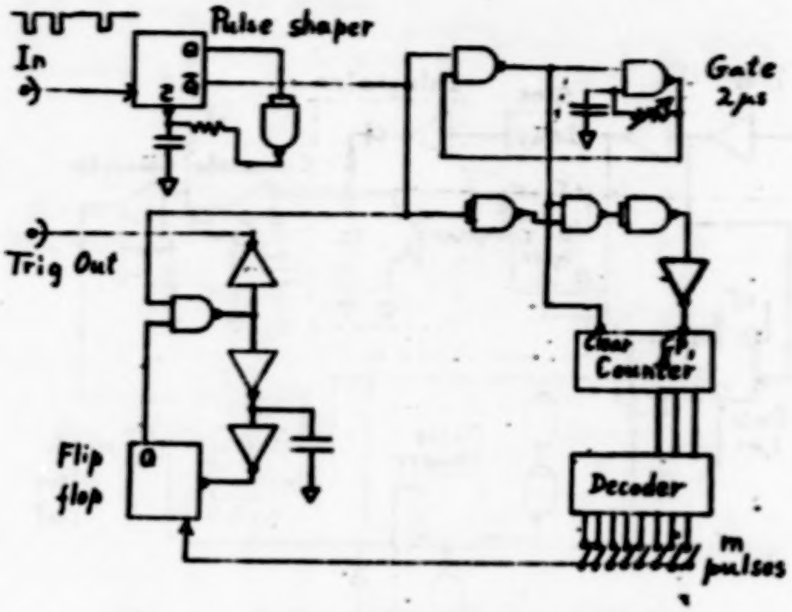

Fig. 1 Pulse-train trigger; digital.

fore, we have built a second type of trigger. Again, each arriving particle, i.e., pulse on the OR line, opens a 2 µs gate. But this time the gate is for an analog device that integrates the time occupied by following pulses (if any). This system has the advantage of partially "resolving" overlapping pulses. The circuit is shown in Fig. 2. Again, a trigger is generated at the end of the 2 µs gate if the preset requirement is met.

(B) The relative time record is obtained from a 100 MHz time shift register that holds 2 µs of information. The register is stopped and read out when a trigger is received from (A). The register is composed of four 25 MHz elements with a 50 ns multitap TTL delay IC to phase shift among the registers. The circuit is shown in Fig. 3.

3. Applications. The above circuit elements are being used by the cosmic ray group of L.K. Ng at Hong Kong (2) in conjunction with a cluster of eight 1/4 m^2 scintillators. There are plans underway to use this method in parallel with the main shower experiment of the Cosmic Ray Group of the Institute of High Energy Physics at Beijing. We also hope to use it for calibrations at some of the existing large shower arrays.

This work has been supported by grants from the Rackham Graduate School of the University of Michigan and the U.S. Department of Energy.

References

[1] Linsley, J (1983) Research Report UNML 6/83.
[2] Ng, LK et al., Paper at this conference.
[3] Crosby, DA and MacAdam KB (1981), Rev. Sci. Inst. 52(2) 297.

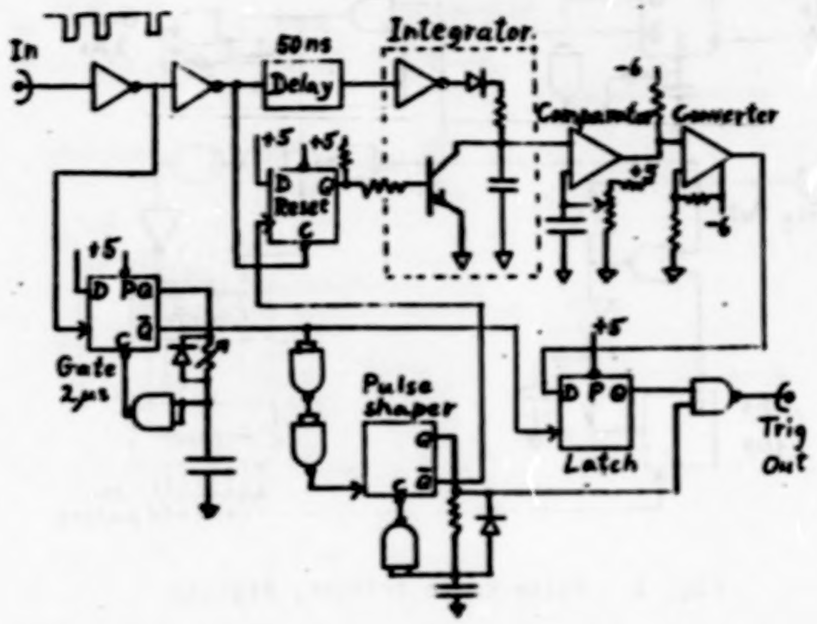
In
50ns
Delay
Integrator
-6
Comparator
Converter
+5
D Q
Reset
C
+5
D P Q
C Q̄
Gate 2μs
Pulse shaper
Q
Q̄
C
+5
D P Q
Latch
Trig Out
-6

Fig. 2 Pulse-train trigger; integrated width.

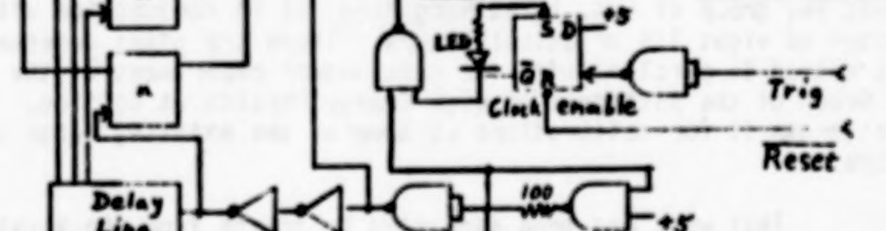
In
D Q
Flip-
flops
Flip-flop
Shift Registers
TDC 1005
D0
1
Out
2
3
Data Adv
LED
+5
S D
Q̄ R
Clock enable
Trig
Reset
Delay Line
50ns
100
+5
25
25 MHz

Fig. 3 100 MHz shift register.

N85-36059

EXPECTED RATES WITH MINI-ARRAYS FOR AIR SHOWERS

Wayne E. Hazen
Randall Laboratory of Physics
University of Michigan
Ann Arbor, MI 48109, USA

1. Introduction. As a guide in the design of mini-arrays used to exploit the Linsley effect in the study of air showers, it is useful to calculate the expected rates. The results can aid in the choice of detectors and their placement or in predicting the utility of existing detector systems. Furthermore, the potential of the method can be appraised for the study of large showers. Specifically, we treat the case of a mini-array of dimensions small enough compared to the distance of axes of showers of interest so that it can be considered a point detector.

The input information is taken from the many previous studies of air showers by other groups. The calculations will give: (a) the expected integral rate, $F(\sigma,\rho)$, for disk thickness, σ, or rise time, $t_{1/2}$, with local particle density, ρ, as a parameter; (b) the effective detection area $A(N)$ with $\sigma(\min)$ and $\rho(\min)$ as parameters; (c) the expected rate of collection of data $F_L(N)$ versus shower size, N. The latter is flatter than the number spectrum because the detection area increases with N.

2. Method. The required input relations are:

(a) the shower disk thickness, $\sigma = Br^{\beta}$ (1), which is a passable form for the large values of core distance, r, of interest here;

(b) the particle density distribution, $\rho = CNr^{-n}$ (2), where N is the total number of particles and, again, the simple form is adequate for our purposes;

(c) the number spectrum, $F(N) = DN^{-\gamma}$, or $f(N) = -\gamma DN^{-\gamma-1}$ (3), where a constant value of γ is an approximation adequate to our purposes.

(A) The frequency of Linsley events is obtained from

$$F(\sigma,\rho) = \int_{N(\min)}^{\infty} A(N)f(N)dN \qquad (4)$$

where

$$A(N) = \pi\left(r^2_{(\max)} - r^2_{(\min)}\right) \qquad (5)$$

and $r(\min) = (\sigma/B)^{1/\beta}$ from (1) (6) and $r(\max) = (CN/\rho)^{1/n}$ from (2) (7) and, finally, $N(\min) = (1/C)B^{-n/\beta}\,\sigma^{n/\beta}\,\rho$ (8) which comes from $A(N(\min)) = 0$ (see (5) above).

The result is:
$F(\sigma,\rho) = \pi C^{\gamma}B^{(n\gamma-2)/\beta}\,D(1-\gamma/(\gamma-2/n))\,\rho^{-\gamma}\,\sigma^{(2-n\gamma)/\beta}$ (9), where the constants are defined in (1), (2), and (3) above.

(B) The effective detecting area, $A(N)$, obtained from (5), (6), and (7), is $A(N) = \pi C^{2/n}\rho^{-2/n}N^{2/n} - \pi B^{-2/\beta}\,\sigma^{2/\beta}$ (10).

(C) The expected rate of collection of data versus shower size is

$$F_L(N) = \int_{N}^{\infty} A(N)f(N)dN \qquad (11)$$

which gives: $F_L(N) = \pi C^{2/n} D[\gamma/(\gamma-2/n)] \rho^{-2/n} N^{-\gamma+2/n} - \pi B^{-2/\beta} D \sigma^{2/\beta} N^{-\gamma}$ (12).

The Haverah Park Group reduce their data to energy of the incident primary and, therefore, give an energy spectrum, F(E), rather than a shower size spectrum, F(N). The rate calculations above are directly applicable with N replaced by E, since the approximations are about equally valid.

3. Numerical Results. In order to get a tentative idea of actual rates, values for the constants were obtained from a brief survey of the literature.

For (1), we have Linsley's fit to his Volcano Ranch data[1], which has been corroborated by others as far as average values are concerned. Thus $\sigma = 2.6(1 + r/30)^{1.5}$ (nsec) gives $\sigma = 1.58\times10^{-2}\ r^{1.5}$ (nsec) that is, $B = 1.58\times10^{-2}$ and $\beta = 1.5$.

For (2), the Akeno Highlands data with scintillators reported at Bangalore[2] seem appropriate since they are for large showers and extend out to r > 1000m. The constants in (2), for large r, are C = 853 and n = 3.8 for ρ to be in particles/m^2.

For (3), the reviews by Hillas[3] give summaries of determinations of the frequency shower-size spectrum. The constants obtained for (3) for large showers are D = 318 and $\gamma = 1.7$.

The above are plotted in Figs. 1 and 2. Some rates for accidentals (see below) are also shown.

In the case of the deep water Cerenkov detectors of Haverah Park, $t_{1/2}$ replaces σ in (1). The constants in (1), determined from the data in the World Catalogue[4], are B = 0.14 and β=1. The constants obtained[5] for (2) are $C = 7.8\times10^{-9}$ and n = 3.5. As stated earlier, it is convenient to do (3) in terms of E (of the primary) in place of shower size, N. The constants become[5] $D = 3.5\times10^{27}$ and $\gamma = 2.17$, when E is in eV. The results are also plotted in Figs. 1 and 2.

4. Accidental Rate. A basic limitation to the sensitivity of the method is due to accidental time clustering of pulses that are unrelated. The accidental rate, R, of occurrence of m pulses within a time window τ when the rate is f can be written $R = f^m \tau^{m-1}$.

The particle rate J×S (where J is the omni-directional flux and S the total detector area) can be a good approximation to f with the usual sort of detectors used in shower studies. There is generally a shoulder in the free running pulse height distribution and consequently a minimum pulse height, P_v, can be chosen such that the particle detection efficiency is high and signal/noise is also high (Fig. 3). The pulse rate is then approximately equal to the particle rate. Since σ is the FWHM value, the effective window width, τ, is, say, ~1.5σ.

We then have $R = (JS)^m (1.5\sigma)^{m-1}$ (13). In Fig. 1, we show examples for m=4 and two areas, S=2 or 4m^2, that we are using in exploratory runs. The particle densities are then ρ=1 or 2m^{-2}, and the singles rates f = 300 or 600 s^{-1}. (The accidental rate for m=3 is dominated by $\mu\to e$ plus a single!)

ORIGINAL PAGE IS
OF POOR QUALITY

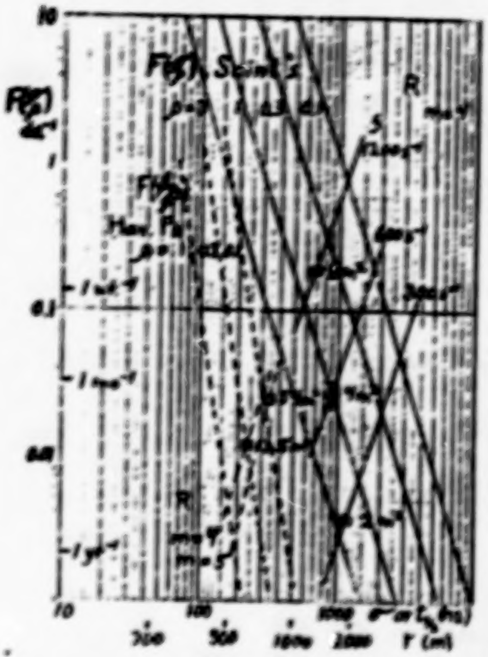

Fig. 1

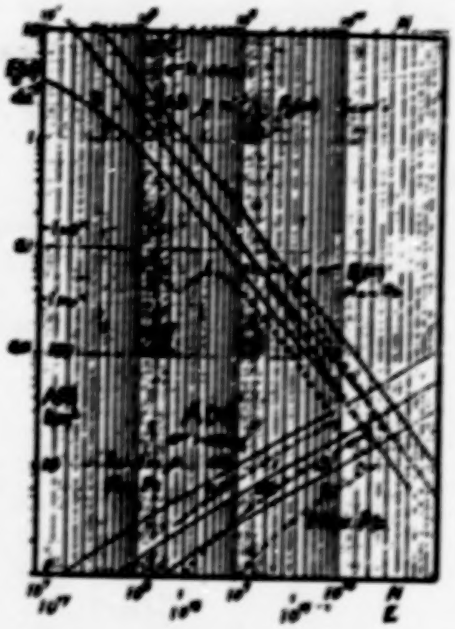

Fig. 2

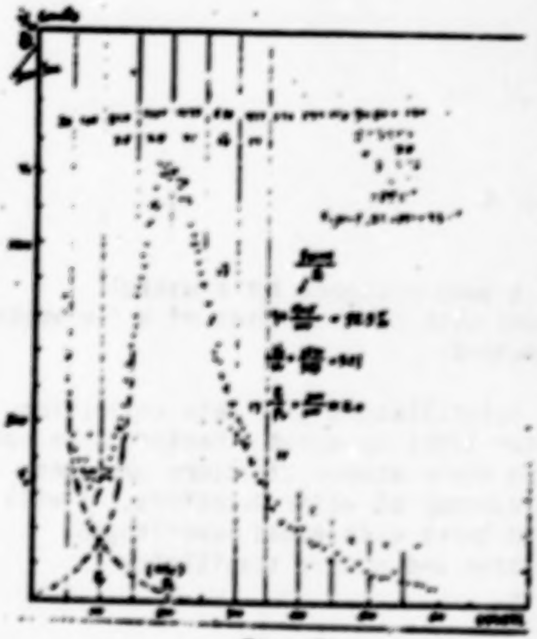

Fig. 3

5. Conclusions. The above predictions show that it is necessary to go down to low particle densities, ρ, in order to get a good rate for large showers. But, to limit the uncertainties, the size of the particle sample, =m, cannot be too small. Thus, the total detector area, S (=m/ρ) must be as big as feasible. However, as the area is increased, the "singles" rate increases with consequent increase in accidental rate.

The relationships among the above are implicit in Fig. 1. It may be more graphic to use total detector area, S, as abscissa with m and σ as parameters. This is done in Fig. 4, with shower rate F(S), solid lines, and accidental rate R(S), dashed lines, as ordinates. Numerical values of the parameters, m and σ, are written near the lines.

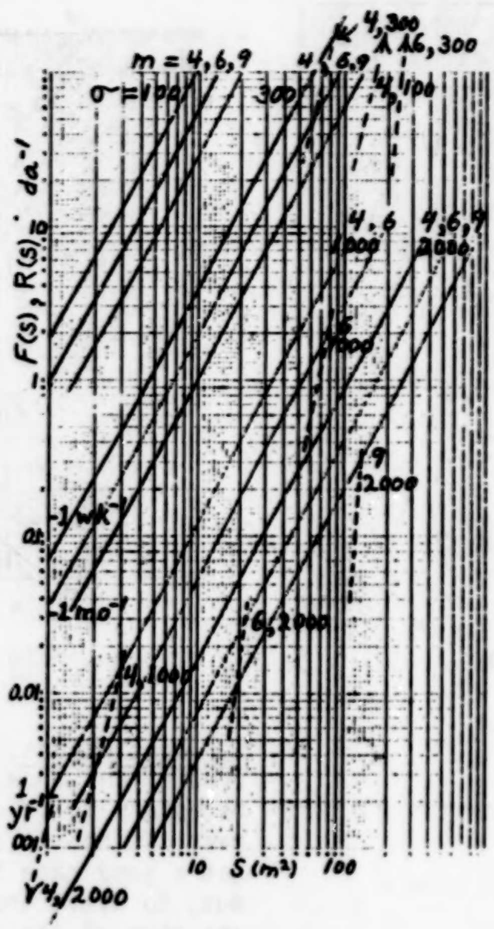

Fig. 4

It is seen that there is a good prospect for a useful "window" for exploratory observations with running times of a few weeks even with an area of a few square meters.

From Fig. 1, we see that scintillators give data collection rates larger than deep Cerenkov water tanks by about a factor three out to the distances of a few kilometers where shower structure has been measured. In view of the relative economy of water detectors, it will be desirable to develop medium depth tanks with added wave-length shifter, aiming for low-energy electron and photon sensitivity comparable to their muon sensitivity.

References

1. Linsley, J. (1983) Research Report UNML 6/83.
2. Hara, T. et al. (1983) ICCR 11, 276.
3. Hillas, A.M. (1975) Phys. Reports 20c, 79.
4. Haverah Park (1980) Catalogue of Cosmic Rays, IPCR Itabashi, Tokyo.
5. Edge, D.M. et al. (1973) J. Phys. A 6, 1612.

Fast Scintillation Counter Preamplifier for the Observation of Linsley Effect

L.K. Ng
Physics Department, University of Hong Kong
Hong Kong

Abstract

A fast preamplifier circuit has been designed and thoroughly tested for the purpose of observing the air shower arrival directions including the Linsley effect. The circuit intends to eliminate the time jitter due to variation of scintillation counter signal amplitudes. It assumes that the output signals from one counter system have the same rise time. On this basis, error arising from time jitter is removed by voltage discrimination at about half signal amplitudes. Detailed description of the circuit is reported.

1. Introduction. In the investigation of cosmic ray extensive air showers, it is often required to determine the particle arrival time at various detection stations of a shower array, in order to find the shower arrival direction. This applies to our observation of the Linsley effect in large air showers described in a paper (HE 4.7-10) at this conference, and to the determination of the shower arrival directions incident on our shower telescope given in another paper (HE 4.5-14) at this conference.

Large area plastic scintillators are commonly used for the above purpose because of their fast response to traversing shower particles. However, the signals obtained from a scintillation counter has a finite rise time typically in the range of 10 ns - 100 ns. Its magnitude depends chiefly on the counter geometry which affects the optical paths, and on the quality of the photomultiplier. This finite rise time gives rise to time jitter when signals of varying amplitudes are subjected to a constant voltage discrimination as illustrated in figure 1. Hence, for precise arrival time measurement, this time jitter cannot be overlooked. An anti-jitter preamplifier is therefore designed.

2. Design principles. Two criteria are adopted for the present design: (i) the rise time of counter output signals is assumed to be a constant characteristic of the counter system, and (ii) there is no signal pile-up at the counter output with proper choice of the output RC coupling. These criteria ensure that the pulses to be processed by the preamplifier are of proper shape. From criterion (i), if each pulse is discriminated at its half signal amplitude, the time relation between the incidence of a particle and the leading edge of the discriminated output pulse is a

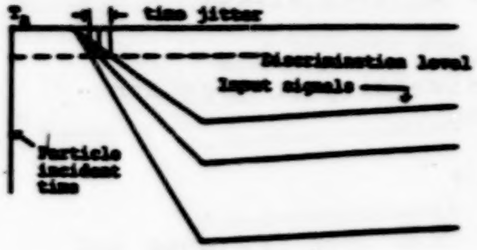
T_a
time jitter
Discrimination level
Input signals
Particle incident time

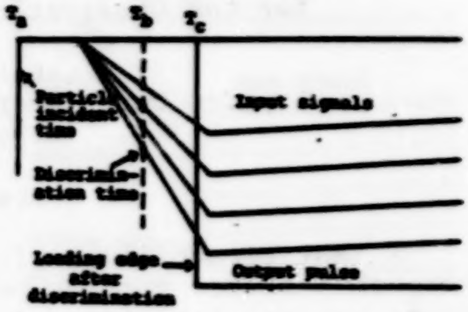
T_a
T_b
T_c
Particle incident time
Input signals
Discrimination time
Leading edge after discrimination
Output pulse

Fig.1 Time jitter due to fixed voltage discrimination.

Fig.2 Discrimination at the half signal amplitude.

constant as illustrated in figure 2. The time relation is indicated by the particle incident time T_a, the time at half amplitude T_b and the leading edge T_c of the discriminated output. The delay time (T_c - T_a) is a constant independent of signal amplitudes. The discrimination is done at half signal amplitudes, because the slope of the leading edge of the input signal is sharpest at this position.

To achieve the above result, the the following design is carried out:

a. In order to provide a reference voltage equal to the half amplitude of an input signal, one branch of the input is connected to a simple 1:1 potential divider, so that the signal amplitude is halved and its peak level can then be used as a reference voltage.

b. Since the reference voltage must be established before the arrival of the input pulse at the discriminator input, another branch of the input is connected to a long coaxial cable in order to delay the input signal for a fixed interval of time t_d. The time relation between the reference voltage signal and the delayed signal is shown in figure 3.

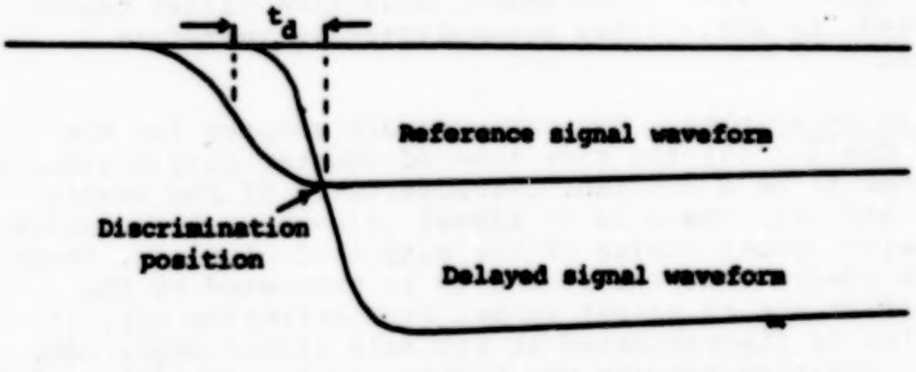
t_d
Reference signal waveform
Discrimination position
Delayed signal waveform

Fig.3 The time relation of the signal waveforms.

c. The above discriminator (called A) cannot eliminate noises since the reference voltage diminishes with input signal amplitudes. Hence a separate discriminator (called B) with fixed reference valtage is required to exclude noise signals. The output signal from this discriminator B can be shaped , which serves as a strobe pulse to gate the discriminator A.

Two important conditions in the timing must be observed: the leading edge of the strobe pulse must arrive the discriminator A earlier than the time T_b given in figure 2; and the width of the strobe pulse must not be so wide as to include the trailing edge of any input signal to A. The first condition is obviously required as T_b is the reference time. This condition can be met by adjusting the length of the coaxial cable. The second condition is required because the trailing edge of the input signal crosses very gently over the reference voltage level and hence any ripple at the crossing point will give rise to multiple pulses after discrimination. Such phenonemon can be eliminated if the strobe gate of A is closed before the crossing time occurs. This condition can be met by narrowing down the strobe pulses.

3. Circuit details. Based on the above conditions, the preamplifier circuit designed is presented in figure 4. The negative photomultiplier pulses after passing through a Darlington stage, enter two d.c. level shifters in parallel. The d.c. levels of the level shifters are separately controlled by two potentiometers P1 and P2. The

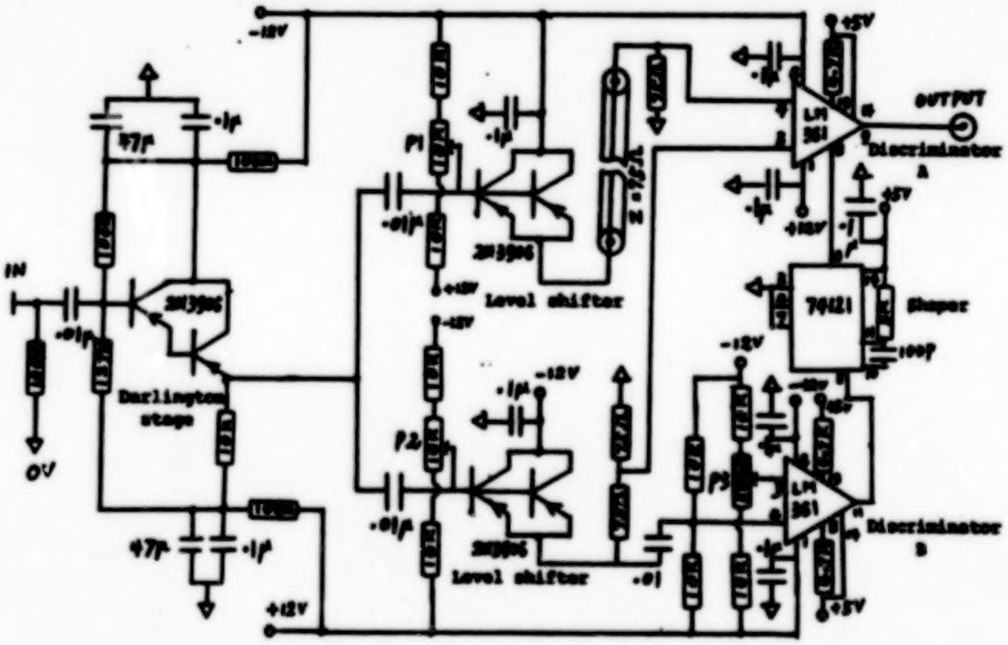
-12V
47p
·1μ
IN
·01μ
2N3906
Darlington stage
0V
47p
·1μ
+12V
P1
·1μ
·01μ
2N3906
+12V
Level shifter
-12V
·1μ
-12V
P2
·01μ
2N3906
Level shifter
·01
+5V
·1μ
LM 361
OUTPUT
Discriminator A
·1μ
+12V
+5V
74121
Shaper
100P
-12V
P3
LM 361
Discriminator B
+5V

Fig.4 The anti-jitter preamplifier circuit.

shifters provide sufficient power to drive the coaxial cable and the potential divider respectively.

The fixed reference voltage of the discriminator B is controlled by the potentiometer P3. Output pulses from B are shaped by a monostable shaper and the strobe pulses obtained then gate the discriminator A as required.

4. Discussions. It should be noted that in the discriminator A, the base line voltage of the signal input must be slightly higher than that of the reference voltage input for the discriminator to work. This fixed voltage difference causes slight deviation of the reference voltage from the true half amplitude level. Since the difference is not proportional to the input signal amplitude, a jitter can therefore be introduced. This jitter obviously depends on the rise time of the photomultiplier signals, but is very small, (well within 5 ns for a large rise time of 100 ns).

It should also be pointed out that the circuit is sensitive to high frequency ringing. Therefore, decoupling capacitors are found at various power supply points. The shortest ground path is required for each of these capacitors. The recommended layout of the printed board is to have the circuit on one side of the board only and the other side a ground plane.

HE 4.7 - 10

A Mini-array for Large Air Showers

L.K. Ng and S.K. Chan
Physics Department, University of Hong Kong
Hong Kong

W. Hazen and E. Hazen
Physics Department, University of Michigan
U.S.A.

Abstract

A mini-array that utilizes the Linsley effect is proposed for the measurement of large air showers. An estimate of the detectable shower rates for various shower sizes is made. Details of the detection and data collection systems are also described.

1. Introduction. Interest in the measurement of large air showers has been enhanced by the conflicting result reported in 1982 (Yakutsk[1]). However, since intensities of large air showers are extremely low and only a few large centres are able to do the measurement, it was proposed by J. Linsley[2] that more independent measurements could be done with rooftop mini-arrays by making use of the particle arrival time distributions (Linsley effect). This idea has been pursued by us, and the present proposed system is the result after looking into various problems associated with such mini-arrays.

2. Theorectical estimation. To be able to measure the arrival time distribution, at least two particles per event are required. With a mini-array of 2 m^2, a threshold density of the shower particles arriving at this mini-array should be $\rho_1 = 1\ m^{-2}$. Using the differential intensity expression,

$$j(N,\theta) = j(N)\cos^{\alpha}\theta \ ,$$

with $\alpha = 8.6$ at sea level, the shower rate for large showers with size N to N+δN should be

$$\begin{aligned}\phi(N)\delta N &= 2\pi j(N)A(N)\delta N \int_0^{\pi/2}\cos^{\alpha+1}\theta\sin\theta d\theta \\ &= \frac{2\pi}{\alpha+2}\, j(N)A(N)\delta N,\end{aligned}$$

where A(N) is the area containing the cores of all the air showers detected by the mini-array. Hence the integral shower rate is

$$\phi(>N_{min}) = \frac{2\pi}{\alpha+2}\int_{N_{min}}^{\infty} j(N)A(N)dN.$$

The area A(N) is an annular ring with its outer radius determined by the density threshold $\rho_1 = 1\ m^{-2}$ and its inner radius determined by the minimum time spread σ_1 selected. Therefore, it has the form,

$$A(N) = \pi\left[\left(\frac{CN}{\rho_1}\right)^{2/n} - \left(\frac{\sigma_1}{B}\right)^{2/\beta}\right]$$

Hillas' integral intensity spectrum[3] ,

$$J(>N) = 8.10^{-12}\,(N/10^8)^{-1.7}\ m^{-2}sr^{-1}s^{-1}$$

is used to determine j(N), and Linsley's empirical formula[2],

$$\sigma(ns) = 2.6\left(\frac{r}{30} + 1\right)^{1.5} \quad \text{with r in m}$$

is used to relate the time spread σ to the core distance r from the mini-array. The lateral distribution of electrons at Akeno for large showers,

$$\rho = 5.10^{-5}\,N\,(r/r_0)^{-3.8} \quad \text{with } r_0 = 79\ m$$

is used to relate ρ to r.

The final expression for the shower rate is given by

$$\phi(>\sigma_1,\ >\rho_1) = 9.07.10^{6}\rho_1^{-1.7}\sigma_1^{-2.97}\,day^{-1},$$

and the values are tabulated below.

$\rho_1(m^{-2})$	$\sigma_1(ns)$	N_{min}	Shower rate (day^{-1})
1	50	$9.07.10^5$	81.6
1	100	$6.25.10^6$	10.4
1	200	$3.04.10^7$	1.33
1	300	$8.49.10^7$	0.40
1	400	$1.76.10^8$	0.17

Table I

3. Detection system. From the estimation given in Table I, it is clear that a mini-array so constructed should be able to pick out the very few large air shower events from a swarm of irrelevant events including the counter noises, the background soft radiations and the small air showers. Fast electronics is also required for the determination and collection of the arrival time spread.

In order to eliminate the large number of small air showers, a minimum time spread σ_1 has to be assigned. According to Table I, for a mini-array of 2 m^2, a minimum acceptable shower size of $9.07.10^5$ requires a minimum time spread σ_1 equal to 50 ns.

A mini-array of 2 m^2 is then assembled which consists of 8 pieces of plastic scintillators each with dimensions 0.5m x 0.5m x 0.05m. In view of the small particle density encountered, each scintillator is not expected to receive more than one particle at a time from a shower.

Each scintillator is viewed by two 5" photomultipliers, the signal coincidence of which practically eliminates all the counter noises. In order to exclude the background soft radiations, the array is shielded by thin sheets of galvanized iron (0.5mm thick). Particle track identification may be found necessary at a later stage to acertain genuine large shower events. This can be done by sandwiching the array by 4 layers of small diameter proportional counters.

The mini-array is placed in another small air shower array system, which may provide additional information on the nature of showers received.

4. __Fast electronics__. Precise measurement of the particle arrival time is essential in this experiment, and hence an anti-jitter preamplifier per counter is employed to remove the time jitter between the particle arrival time and the signal output time. The preamplifier as shown in figure 1 is a slightly modified version of the circuit described in another paper (HE 4.7 - 9), and the modification provides another coincidence input from a second photomultiplier.

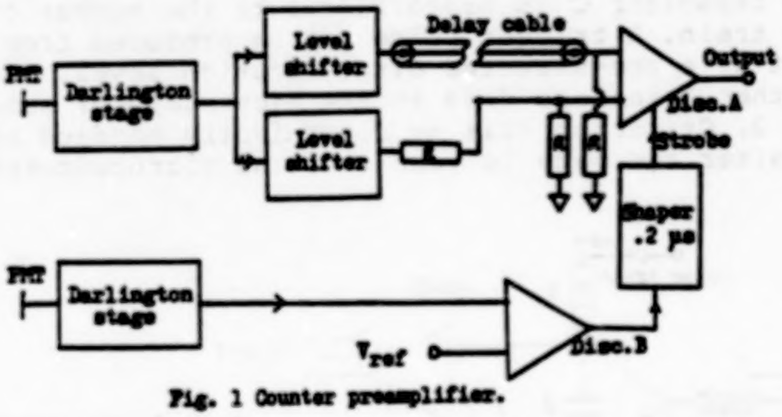

Fig. 1 Counter preamplifier.

Outputs from the eight counter preamplifiers are individually shaped to narrow pulses of 20 ns each, and then combined together to give a train of narrow pulses per shower. The time delay in each of the 8 channels from the particle arrival to the pulse output after combination has been equalized by adjusting the length of the delay cable in each preamplifier. The number of pulses in the train depends on the number of counters giving out particle signals, and the relative positions of the pulses in the train depend on their particle arrival time. The circuit block diagram is given in figure 2.

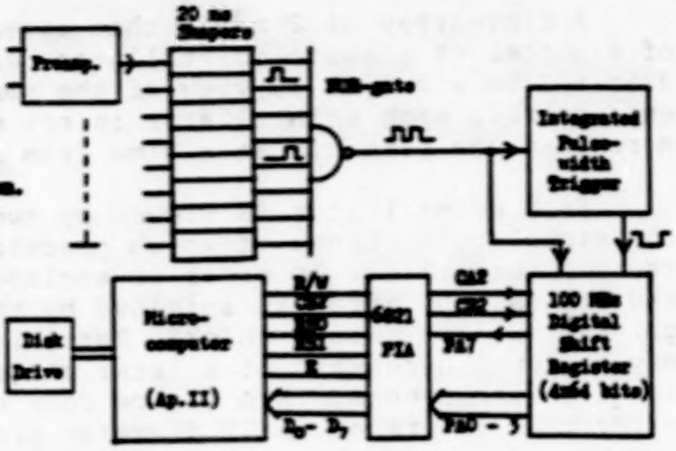
20 ns Shapers
Preamp.
NOR-gate
Integrated Pulse-width Trigger
Disk Drive
Micro-computer
(Ap.II)
R/W
R
6821
PIA
$D_0 - D_7$
CA2
CB2
PB7
PA0 - 3
100 MHz Digital Shift Register (4x64 bits)

Fig. 2 The electronic system.

The pulse train is temporarily stored in a set of four shift registers. The shift registers have 4 x 64 bits in total and hence can readily store 2 µs of information. the clock rate for accepting the pulse train is equivalent to 100 MHz. Consequently, it provides a time resolution of 10 ns in the measurement of particle arrival time.

The criteria for recording a pulse train temporarily stored in the shift registers are (i) at least two pulses are found in the train, and (ii) the time spread of the pulses should not be less than σ_1. Criterion (i) is dealt with by means an integrated pulse-width trigger circuit. Its basic element is given in figure 3. The charge accumulated in the capacitor C is proportional to the number of pulses in the train. A trigger pulse can be produced from the circuit at a pre-selected discrimination level. The trigger pulse then transfers data to the microcomputer shown in figure 2. Criterion (ii) is conveniently handled by software means after the data is read into the microcomputer.

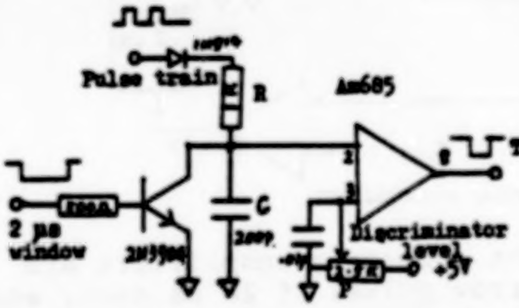
Pulse train
R
Am685
Trigger
C
2 µs window
Discriminator level
+5V

Fig.3 The integrator.

The above system has been assembled and thoroughly tested.

Reference.

1. Diminstein O S et al, 8th Eur.Cosmic-ray Symp.(Rome),1982
2. Linsley J, (preprint).
3. Hillas A M et al, Phys. Reports, 20C (1975) 79.
4. Hara T et al, Proc. 18th ICRC (Bangalore), 11 (1983) 276.

A NOTE ON SOME STATISTICAL PROPERTIES OF RISE TIME PARAMETERS USED IN MUON ARRIVAL TIME MEASUREMENTS

D.J. van der Walt and E.J. de Villiers
PU-CSIR Cosmic Ray Research Unit,
Department of Physics,
Potchefstroom University for CHE,
Potchefstroom, 2520.
South Africa.

N85-36062

1. Introduction

Most investigations of the muon arrival time distribution in EAS during the past decade made use of parameters which can collectively be called rise time parameters. We will follow the definition of Blake et al. (1981) and define the rise time parameter $T_{A/B}$ as the time taken for the integrated pulse from a detector to rise from A% to B% of its full amplitude. The use of these parameters are usually restricted to the determination of the radial dependence thereof. This radial dependence of the rise time parameters are usually taken as a signature of the particle interaction characteristics in the shower. As these parameters have a stochastic nature, it seems reasonable to us that one should also take notice of this aspect of the rise time parameters. The aim of this paper is therefore to present a statistical approach to the rise time parameters, as this has not been done in the past.

2. Order statistics and rise time parameters

From the definition of $T_{A/B}$ it is reasonable to assume that on the average A% of the total number of particles which gave rise to the output pulse from the detector have arrived in the time $T_{0/A}$. A sample quantile of order p is defined as follows: Let $(X_1, X_2 \ldots X_n)$ be a random sample of size n of a random variable X with probability density function (pdf) f(t). Let $(X_1^{(n)}, X_2^{(n)} \ldots X_n^{(n)})$ be an arrangement of $(X_1, X_2 \ldots X_n)$ such that $X_1^{(n)} \leq X_2^{(n)} \leq \ldots X_n^{(n)}$. $X_i^{(n)}$ is called the i-th order statistic. The sample quantile of order p, $0<p<1$, is defined to be the order statistic $X_k^{(n)}$ for which $k = [np] + 1$, where $[np]$ is the greatest integer not larger than np. This definition states that a fraction p of the sample values is less than $X_k^{(n)}$. This corresponds exactly to the definition of $T_{0/A}$. The rise time parameter $T_{A/B}$ corresponds therefore to the difference between two order statistics of the sample. The statistical properties of $T_{A/B}$ can therefore be determined from the properties of the difference between two order statistics.

We now give a number of properties which are very useful. The following notation is used: $f_k^{(n)}(t)$ is the pdf of $X_k^{(n)}$, $W_{k\ell}^{(n)}(t)$ is the pdf of $X_\ell^{(n)} - X_k^{(n)}$, F(t) is the distribution function of the random variable X, i.e. $F(t) = P(X \leq t)$, and $g^{(n)}(t)$ is the pdf of the arrival times of muons with respect to the first detected muon.

(i) $f_k^{(n)}(t) = C f(t) [F(t)]^{k-1} [1-F(t)]^{n-k}$ with $C = n!/(k-1)!(n-k)!$

(ii) $W_{k\ell}^{(n)}(t) = C \int_0^\infty f(t) f(x+t) [F(t)]^{k-1} [F(x+t)-F(x)]^{\ell-k-1} [1-F(x+t)]^{n-k} dx$

with $C = n!/(k-1)!(n-k)!(\ell-k-1)!$

(iii) $\lim_{n\to\infty} P(|X_k^{(n)} - a_p| \geq \varepsilon) = 0$ for $\varepsilon > 0$, $k = [np] + 1$, and a_p is the population quantile of order p.

(iv) $\lim_{n\to\infty} f_k^{(n)}(t) = N\left[a_p, \frac{p(1-p)}{nf^2(a_p)}\right]$ (Fisz(1963))

(v) $\lim_{n\to\infty} W_{k\ell}^{(n)}(t) = N\left[a_q - a_p;\ \frac{p(1-p)}{nf^2(a_p)} + \frac{q(1-q)}{nf^2(a_q)} - \frac{a_p a_q}{nf(a_p)f(a_q)}\right]$ (Swanepoel (1985)).

(vi) $\lim_{n\to\infty} g^{(n)}(t) = f(t)$ (Van der Walt (1984)).

Property (iii) states that the sample quantile converges stochastically to the population quantile. Properties (iv), (v) and (vi) give the limiting distributions of $f_k^{(n)}(t)$, $W_{k\ell}^{(n)}(t)$ and $g^{(n)}(t)$. The rise time parameters will then also have the above properties.

The significance of these results is further that it is possible to examine specific properties of the rise time parameters without having to simulate air showers. It must be made clear at this point that points (i) to (vi) does not add directly to the understanding of the physics involved in shower development. We feel, however, that it gives one a firm basis from which one can understand the properties of the measured rise time parameters.

Discussion

Consider, for example, property (iii). For the case of EAS, the arrival of the hypotherical shower front can be considered as the time t=0 from which timing measurements can be made. In this case $f(t) = 0$ for all $t \leq 0$, and we can allow p to be equal to zero. Then $X_1^{(n)}$, corresponds to the zeroth order sample quantile while $a_p = a_o = 0$. We then have $\lim_{n\to\infty} P(|X_1^{(n)} - 0| \geq \varepsilon) = 0$, which means that the arrival time of the first detected muon with respect to the shower front converges stochastically to zero. This means that for large samples one can consider the first detected particle as the time t = 0. Property (vi) is equivalent to what has just been said.

In figure 1 we show the arrival time distribution of muons together with the arrival time distribution of muons when the first detected muon was taken as the time t = 0. The difference at small delays is due to the fact that the sample size was only ten.

In figure 2 we present the relationship between $\langle X_2^{(5)} - X_1^{(5)}\rangle$ and $\langle X\rangle$ for the case when f(t) is a gamma density function. The same relationship was found to exist for larger samples. Is is also possible to show that this linear relationship exists for a wide variety of density functions. In figure 3 we present the relationship between $\langle X_{10}^{(10)} - X_1^{(10)}\rangle$ and $\langle X\rangle$ for shower simulation data. $X_i^{(10)}$ is the i-th order statistic for a sample of 10 muon arrival times measured in a detector and $\langle X\rangle$ is the mean muon arrival time. It can be seen that the relationship is also linear even though we do not know the parametric form of the muon arrival time distribution. This example also illustrates that it is not necessary to determine the properties of the rise time parameters through the simulation of air showers. It should also be noted from figure 2 that $\langle X_\ell^{(n)} - X_k^{(n)} \rangle$ does not determine $\langle X \rangle$ uniquely. This is an example of some of the limitations of rise time parameters.

Conclusion

With the above examples we have tried to illustrate that there exist a statistical basis for the rise time parameters. We believe that the statistical properties of rise time parameters may be of use not only for the analysis of experimental data but also for the planning of experiments.

References

1. Blake, P.R.; P.J. Connor, D.M. Mann, W.F. Nash, B. O'Connell and R.B. Strutt: Nuclear Instruments and Methods, 188 (1981).

2. Fisz, M.: Probability Theory and Mathematical Statistics, 3rd edition, John Wiley and Sons (1963).

3. Swanepoel, J.W.H. (1985). Personal communication.

4. Van der Walt, D.J. (1984). D.Sc.Thesis, Potchefstroom University.

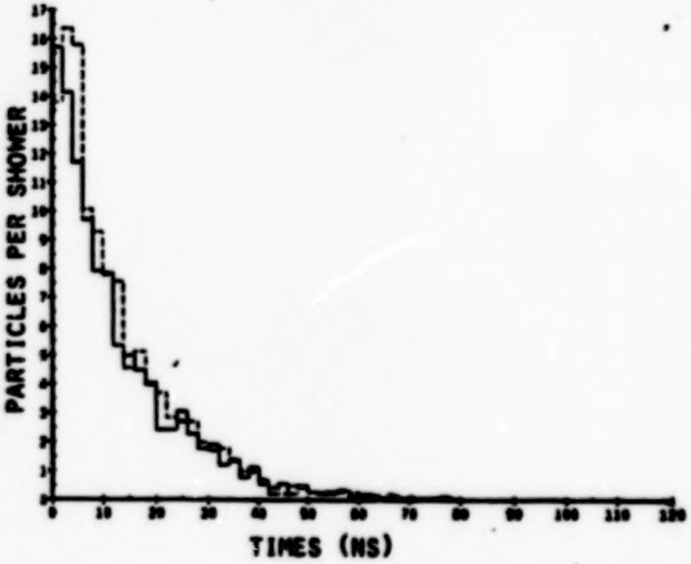

Figure 1 Comparison between $g^{(10)}(t)$ and $f(t)$ for 14 Fe-initiated showers. — $f(t)$, --- $g^{(10)}(t)$. $110\text{m} \leq R \leq 120\text{m}$, $E_\mu \geq 1$ GeV

ORIGINAL PAGE IS
OF POOR QUALITY

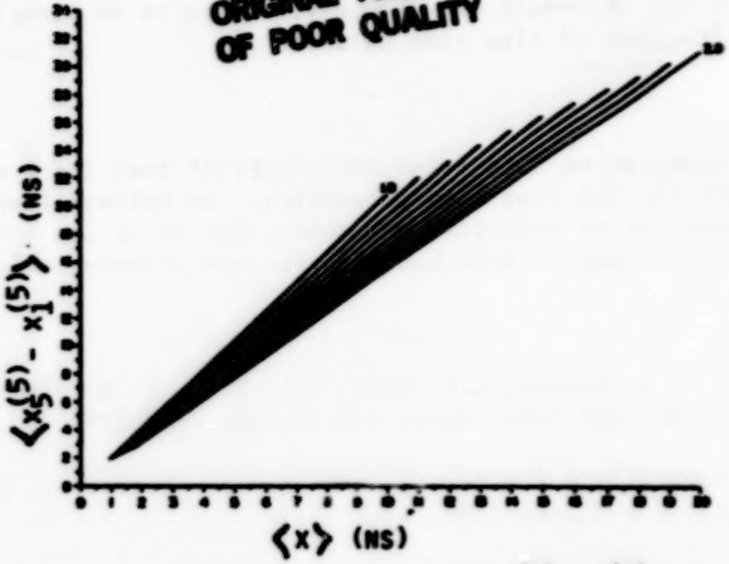

Figure 2 Relationship between $\langle X_5^{(5)} - X_1^{(5)}\rangle$ and $\langle X\rangle$ for a number of gamma random variables for which $1 \leq \langle T\rangle^2/\sigma_1^2 \leq 2$.

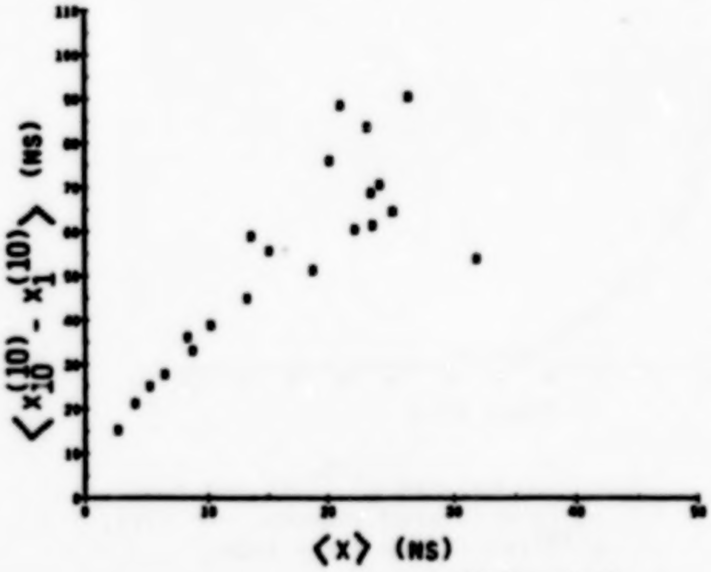

Figure 3 Relationship between $\langle X_{10}^{(10)} - X_1^{(10)}\rangle$ and $\langle X\rangle$ for 14 Fe-initiated showers. $E_\mu \geq 1$ GeV.

N85-36063

HE4.7-13

SUB-LUMINAL PULSES FROM COSMIC RAY AIR SHOWERS

John Linsley
Department of Physics and Astronomy
University of New Mexico, Albuquerque, NM 87131
USA

ABSTRACT

Some of the signals produced by air showers in scintillators possess a distinctive feature, a 'sub-luminal pulse' (SLP) following the normal one with a time delay of approximately 1.5 r/c. The average amplitude of the SLP corresponds to an energy deposit of about 50 MeV, three times as much as is deposited in a typical scintillator by vertical minimum ionizing muons. The SLP account for approximately 5% of the energy deposited in the atmosphere by air showers with energy > 10^{10} GeV at impact parameters > 1 km. Assuming with Greisen that these pulses are due to neutrons travelling with a speed slightly less than c, they provide a unique means of estimating E_h, the energy deposited by slow hadrons, in showers of this very high energy. On the other hand, if not allowed for properly, these pulses are liable to cause errors in estimating the impact parameters of large showers from pulse width observations.

1. Introduction. There are two reasons for regarding the phenomenon reported here as more than a mere curiosity: 1) it may prove to be useful as an additional indicator of primary mass, and 2) if it is not taken into account properly it can cause errors in estimating shower size from measurements of particle density and arrival time spread by means of a mini array (Linsley 1983).

When air showers (AS) were first observed at very large values of the impact parameter it was found that signals produced in thin scintillators were unexpectedly broad (Linsley *et al.* 1961, Linsley and Scarsi 1962). Recently some of the records of the experiment were re-examined in connection with a controversy about very large AS with E > 10^{10} GeV (Bower *et al.* 1982, 1983). Such records (oscilloscope photographs) still exist for more than 500 events registered during 1962-63, including 16 which were qualified, by satisfying the above energy condition, for inclusion in the *Catalogue of Highest Energy Cosmic Rays* (Linsley 1980). The experimental method as it relates to the present discussion is described by Linsley and Scarsi (1962); for a complete bibliography see (Linsley 1980).

2. Observations. It was noticed that the scintillator signals from these AS frequently possess a sort of after-pulse, called for reasons explained below an SLP (sub-luminal pulse). To account for the name, signals with delays < r/c can be produced by 'luminal' particles travelling at essentially the speed of light. Almost all particles in AS are of this type. Signals with greater delays require that the observed energy be transported from the shower core at 'sub-luminal' velocities appreciably < c. For r > 1 km such signals are easily recognized in the Volcano Ranch data

(double pulse resolving time ∿ 3 μs). Sixteen of them were discovered while re-examining the events listed in the *Catalogue*. Tracings are shown in Fig. 1, together with tracings of a typical bandwidth-limited (BWL) test pulse and a typical train of 1 MHz timing pulses.

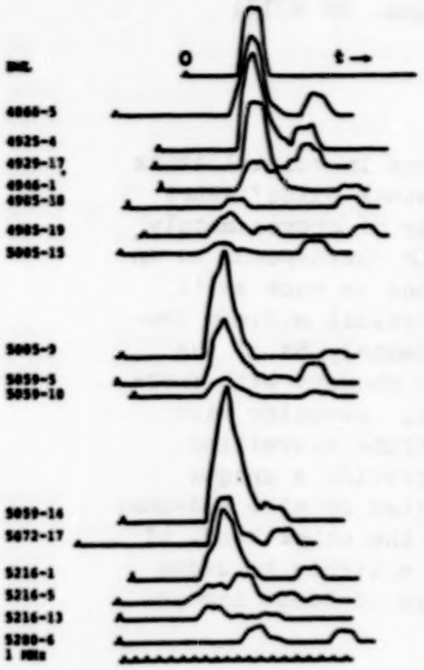

Fig. 1. Scintillator signals showing SLP, identified by event No. and channel No., with a typical bandwidth-limited test pulse (BWL) and a typical train of 1 MHz timing pulses.

In order to rule out instrumental effects such as photomultiplier after-pulsing as the source of delayed pulses, the following tests were made:

1) All 1962-63 AS signals in the same size range as signals preceding the Fig. 1 SLP were scanned for the presence of delayed pulses. (The pulses preceding the SLP have integrated charge values 4 to 40 times the average for vertical minimum ionizing muons.) In 132 cases out of 1648 the prompt pulse was followed after 3 to 10 μs by a well defined delayed pulse (DP). It was determined that the fraction of DP was the same within statistical errors for all 19 channels corresponding to the 19 scintillators making up the Volcano Ranch array.

2) The 1648 DP candidates were then sorted according to shower size, using bins a factor of 2 in width. It was found that the showers in the two lowest-size bins (41 candidate pulses) had no DP, and that showers in the next higher bin (169 candidates) had only 3 DP. The fraction of DP in larger showers increased steadily as shown in Fig. 2, reaching a value ∿ 0.2 for the highest 3 bins.

While it is not quite true that pulses of a given size from large showers are *identical* to pulses of the same size from smaller showers, the differences there are, in average pulse duration, fail to account for the strong shower size dependence seen in Fig. 2. Ignoring therefore the differences there are, in pulse duration, I take it that the fraction of DP in small-shower pulses gives an upper limit for the percentage of DP that might be spurious. I conclude that no more than 10% of the DP in large showers (size $N > 10^9$) are in fact instrumental, or accidental.

In case of very large showers (highest 3 bins) about half of the DP are sub-luminal. The trend seen in Fig. 2 can be explained as follows:

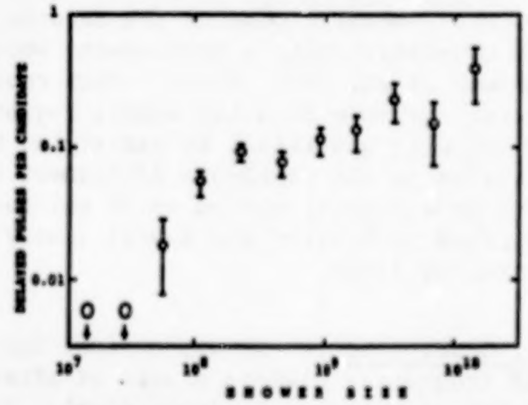

Fig. 2. Fraction of signals with delayed pulses vs shower size, for densities 4-40 particles per 3.26 m² scintillator area.

as one goes from very large showers to smaller ones (right to left in the figure) the impact parameter corresponding to the accepted range of pulse amplitudes decreases, and so does the critical delay separating the luminal and sub-luminal regimes. By the time one reaches shower size $3 \cdot 10^8$, nearly all DP (which are required to have delays $> 3\ \mu s$ so as to be clearly resolved) are sub-luminal. As one goes to still smaller sizes the SLP begin to merge with the prompt pulses, until finally (for $N < 3 \cdot 10^7$) all of them have merged, and no more DP are found using the definition adopted here.

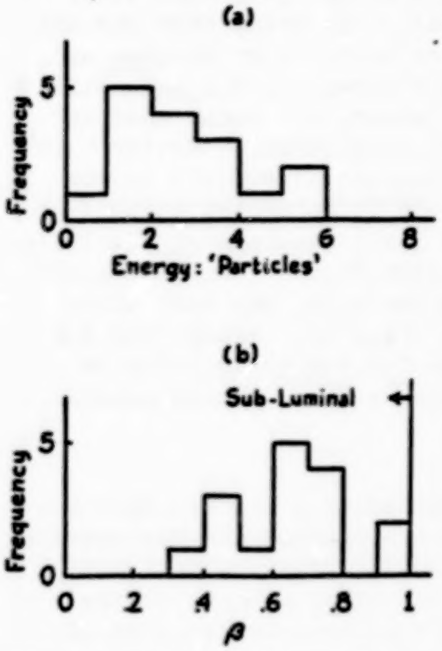

Fig. 3. Distribution of deposited energy (a) and transport velocity (b) for 16 SLP.

3. Results and discussion.

The amplitudes of the Fig. 1 SLP (apparent particle densities) show that the average amount of energy deposited in the scintillators is about 50 MeV, 3 times as much as is deposited by a vertical minimum ionizing muon (see Fig. 3a). If the scintillations are produced by heavily ionizing secondaries, as the low transport velocity suggests may be the case, then the actual deposited energy will be somewhat higher because the response of the plastic scintillator to heavily ionizing particles is nonlinear (Korff 1962).

The time at which the earlier pulse begins (see Fig. 1) corresponds to passage of the shower plane, a plane perpendicular to the axis through the central portion of the particle swarm, determined by means of detectors at relatively small core distances. In most cases the SLP (latest pulse) has no structure; its shape indicates that the energy is deposited in a time interval too small to be resolved. Exceptions are 5216-5 and possibly 4860-5. In case of 4929-17 the latest pulse is a superposition of 2 BWL signals. Only the later, larger one satisfies the condition: delay (with respect to the shower plane) $> r/c$. With two exceptions, the one just noted and 5059-14, the SLP seem to be completely resolved from the normal particles by that condition alone. Additional evidence that SLP are a distinct phenomenon is given by Fig. 3b. The most frequent examples are not the ones that just marginally satisfy the selection condition, they are those with time delay $\sim 1.5\ r/c$ ($\beta \sim 0.7$).

Fig. 4 shows the ratio of SLP to normal particles in various r intervals, for all signals with particle density $< 10\ m^{-2}$ (hence sufficiently undistorted by the electronic system for DP to be recognizable) and $r > 1$ km. The average ratio is $(1.6 \pm 0.4)\%$, and there is no evidence of any r dependence. This fact, and the fact that SLP occur in AS with zenith angles in a broad range (7° to 55° for this sample) suggests that the component which causes them is in equilibrium with the normal particles. Under this assumption the energy deposited in the form of SLP amounts to about 5% of the primary energy. (The scintillation plastic

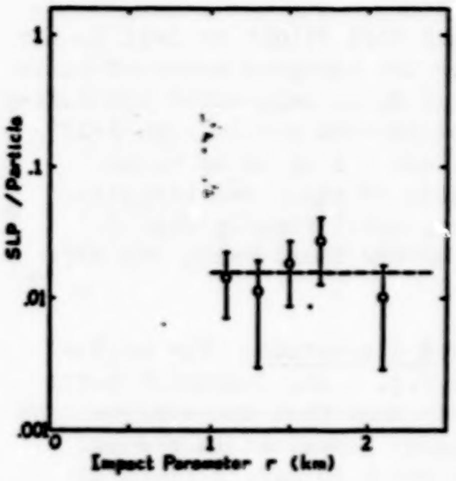

Fig. 4. Abundance of SLP vs impact parameter.

has a composition similar to air.) The explanation of Fig. 2 offered above is based on the same assumption.

4. Conclusions. Commenting on the result of Linsley and Scarsi (1962) in the light of his own observations using similar equipment, Greisen opined that "some of the delayed pulses with large delays...are due to neutrons travelling at a speed slightly lower than light" (Greisen 1962). Assuming that SLP and the pulses referred to by Greisen are the same, and accepting his suggestion as to their cause, one notes that for AS with much lower total energies $\sim 10^6$ GeV the percentage dissipated by low energy hadrons is estimated to be 4 or 5% (Greisen 1956, Zatsepin *et al.* 1963), which agrees at face value with the estimate from Fig. 4. But the equilibrium hypothesis needs further testing. In any case, one must still explain the amplitude and delay distributions (Fig. 3). Aside from the present work the only experimental evidence on low energy nucleons in showers with energy > 10^6 GeV is from data taken with a neutron monitor at the Yakutsk array (Kozlov *et al.* 1981).

Acknowledgement. The re-examination of old records was started during a visit to the University of Leeds, assisted by the Science and Engineering Research Council (UK) through the award of a Senior Visiting Fellowship. Discussions with Alan Watson, Michael Hillas and other members of the Leeds AS group played an important part in gaining an understanding of SLP. Rosalind Mendell kindly provided information about the response of organic scintillators to recoil protons. This work was supported in part by the National Science Foundation.

References. BOWER, A.J., REID, R.J.O. and WATSON, A.A. 1982, Proc. 8th European Cosmic Ray Symposium (Rome) paper B 1.4; BOWER, A.J., CUNNINGHAM, G., LINSLEY, J., REID, R.J.O. and WATSON, A.A. 1983, J. Phys. G: Nucl. Phys. 9, L53; GREISEN, K. 1956, *Progress in Cosmic Ray Physics*, ed. J.G. Wilson (North-Holland: Amsterdam) 3, 1; 1962, Proc. 5th Interamerican Seminar on Cosmic Rays (Lab. Fisica Cosmica, UMSA, La Paz, Bolivia) 2, XLVII-2; KORFF, S. 1962, *ibid.* (same page); KOZLOV, V.G., KUZMIN, A. I., MIGUNOV, V.M., SKRIPIN, G.V. and UPOLNIKOV, A.A. 1981, Proc. 17th Int. Cosmic Ray Conf. (Paris) 6, 210; LINSLEY, J., SCARSI, L. and ROSSI, B. 1961, Phys. Rev. Lett. 6, 485; LINSLEY, J. and SCARSI, L. 1962, Phys. Rev. 128, 2384; LINSLEY, J. 1980, *Catalogue of Highest Energy Cosmic Rays*, ed. M. Wada (Inst. Phys. Chem. Res., Tokyo: World Data Centre C2) 1, 3; 1983, Proc. 18th Int. Cosmic Ray Conf. (Bangalore) 12, 135; ZATSEPIN, G. T., NIKOLSKII, S.I. and KHRISTIANSEN, G.B. 1963, Proc. 8th Int. Cosmic Ray Conf. (Jaipur) 4, 100.

THICKNESS OF THE PARTICLE SWARM IN COSMIC RAY AIR SHOWERS

John Linsley
Department of Physics and Astronomy
University of New Mexico, Albuquerque, NM 87131
USA

ABSTRACT

The average dispersion in arrival time of air shower particles detected with a scintillator at an impact parameter r is described with accuracy 5-10% by the empirical formula $\langle\sigma\rangle = \sigma_{to}(1 + r/r_t)^b$, where $\sigma_{to} = 2.6$ ns, $r_t = 30$ m and $b = (1.94\pm.08) - (0.39\pm.06) \sec\theta$, for $r < 2$ km, $10^8 < E < 10^{11}$ GeV, and $\theta < 60°$. (E is the primary energy and θ is the zenith angle.) The amount of fluctuation in σ_t due to fluctuations in the level of origin and shower development is less than 20%. These results provide a basis for estimating the impact parameters of very large showers with data from very small detector arrays (mini-arrays). The energy of such showers can then be estimated from the local particle density. The formula also provides a basis for estimating the angular resolution of air shower array-telescopes (conference paper OG9.5-6).

1. Introduction. The particles making up an air shower (AS) travel in a swarm which is remarkably compact near the shower axis. Within 10 m of the axis the thickness is only a meter or two (Bassi *et al.* 1953). But when the thickness was measured at much greater distances it was found unexpectedly to be much greater, tens to hundreds of meters (Linsley *et al.* 1961, hereafter LSR; Linsley and Scarsi 1962, hereafter LS). This result, like the earlier one, was derived from arrival time measurements with scintillators. In reporting it primary emphasis was given to $t_{1/2}$, the median delay with respect to the shower plane. This is a plane perpendicular to the axis through the central portion of the particle swarm, determined from timing data at relatively small distances. It was shown that for a given impact parameter r, the median delay decreases with increasing zenith angle θ, and it was pointed out that by a simple kinematic argument the median time delay of the essentially unscattered muon component (observed in the same experiment using a shielded scintillator) provides an estimate of the median production height of the muons (LS).

This behavior at large distances was soon confirmed by J.G. Wilson and his collaborators using an array of deep water Cerenkov detectors at Haverah Park. Painstaking studies showed that $t_{1/2}$ measured with these detectors depends not only on θ but also on primary energy (Baxter *et al.* 1965, Walker and Watson 1981). They showed, moreover, that for given θ and E, $t_{1/2}$ fluctuates, presumably as a result of variability in starting points and subsequent development of AS, possibly also because of differences in mass of the primary particles (Walker and Watson 1982).

The early results near the axis have been confirmed (Woidneck and Böhm 1975, Sakayama and Suzuki 1981), but until recently no further results had been reported on arrival times measured with scintillators at large distances, nor had data been published on measures of thickness other than $t_{1/2}$ (and $\langle t\rangle$, the average particle delay). Presently there is renewed interest in AS thickness at large core distances for 3 reasons:

1) a disagreement between the S(600) spectrum (equivalent to the primary cosmic ray energy spectrum) reported by a group in Yakutsk (Diminstein *et al.* 1982) and similar results obtained in the Volcano Ranch and Haverah Park experiments (Bower *et al.* 1983). It has been suggested that this may result from some peculiarity of the Yakutsk electronic system related to signal durations (Bower *et al.* 1982),

2) the presence of so-called SLP's (sub-luminal pulses) observed with scintillators, apparently caused by the low energy nucleon component of AS (Linsley 1984),

3) a suggestion for using pulse widths to measure AS impact parameters, increasing by an order of magnitude the area that can be made sensitive to 10^{20} eV cosmic rays for a given cost (Linsley 1983, Brooke *et al.* 1983, Hazen and Hazen 1983, Clay and Dawson 1984).

In response to this interest, records from the Volcano Ranch experiment (oscilloscope photographs) have been re-examined. Given here are results from this re-examination, together with new results derived from previously published Volcano Ranch data (LSR, LS).

2. Arrival Time Dispersion. In some applications, notably (3) above, the shower plane may not be well determined by the data, so an appropriate measure of shower thickness is the separate event arrival time dispersion defined by $\sigma_t = [\int(t-\langle t\rangle)^2 p(t)dt]^{\frac{1}{2}}$, rather than $t_{\frac{1}{2}}$, where p(t) is the probability of a particle arriving in time interval dt. Volcano Ranch records provide 3 avenues by which estimates of σ_t can be obtained:

1) a previously published set of signals from a certain unusually large AS, notable because they afford good statistical accuracy at quite large impact parameters,

2) previously published arrival time histograms for single particles in smaller AS, affording good statistical accuracy at smaller impact parameters,

3) original photographic records of 16 especially large AS from 1962-63.

It is shown that an empirical formula which fits the data at smaller impact parameters (average small AS, data set 2 above) is consistent with the data at larger impact parameters (set 1). It is then shown by means of the previously unpublished data (set 3) that the single large AS is in fact typical, and that pulse width fluctuations are tolerably small. Data set 3, containing events with θ ranging from 7° to 55°, also yields the zenith angle dependence of $\langle\sigma_t\rangle$.

Data set 1 consists of 8 graphically deconvoluted signals from scintillators at impact parameters > 1.3 km. The estimates of core location, size and energy for this event (LSR) have since been revised on the basis of a detailed study of shower structure (Linsley 1977). The final values used here are given in the *Catalogue of Highest Energy Cosmic Rays*, together with values of many subsidiary quantities for the same event, No. 2533 (size $1.1\cdot10^{10}$ particles, $E = 5.6\cdot10^{19}$ eV, $\theta = 42°$; Linsley 1980). For the present purpose the signals were sorted into 2 groups according to r, and those in each group were combined. For each group the dispersion is given in Table 1 with standard estimates of the statistical error.

Table 1. Width of signals, AS No. 2533

av. r (km)	No. of particles	mean delay (ns)	dispersion (ns)
1.45	91	840 ± 60	610 ± 45
1.80	33	1260 ± 200	1140 ± 140

It was stated in LSR that this event is typical, meaning that 1) to first order the arrival time distribution is independent of shower size or zenith angle, depending only on r, and 2) for given N, θ, r the fluctuations in this distribution due to variability in starting points, development, etc. are relatively small. If this is correct then the dispersion values given in Table 1 will be consistent with those obtained by the method of LS, in which distributions for various r intervals were built up from single particle delays for many AS with widely ranging values of N (shower size) and θ. Results on dispersion were not given in that article, so they have now been calculated from the single particle delay histograms that were given. The new results are listed in Table 2. Inspection shows that they are reasonably consistent with those for the one large event (Table 1), and that all of the data, including data at small core distances referred to in the Introduction, can be represented by the empirical formula

$$\langle\sigma_t\rangle = \sigma_{to}(1 + r/r_t)^b \qquad (1)$$

with $\sigma_{ot} = 2.6$ ns, $r_t = 30$ m, and $b \sim 1.5$. When these fixed values are taken for σ_{ot} and r_t, the value of b controls the fit at large distances. A best value for b will be determined next from data set 3.

The original records for all years of Volcano Ranch operation except the last one (1962-1963) have been lost, so it is not possible to reexamine the record of event No. 2533. Records still exist, however, for more than 500 large AS, including 16 which satisfied the condition ($E > 10^{19}$ eV) for being listed in the *Catalogue of Highest Energy Cosmic Rays*. The proposed method of determining r (and hence E) from σ_t and S (integrated particle density) at a single location was tested using these 16 events (Linsley 1983). An intermediate result of the test is another set of σ_t values given in Table 3. Because they belong to different events these values will reveal whether fluctuations of σ_t are likely to be troublesome. By agreeing fairly well on average with Table 1 they show that No. 2533 is indeed typical of AS with $E > 10^{19}$ eV. By agreeing on average with Table 2 they show that $\langle\sigma_t\rangle$ hardly changes between 10^{17} and 10^{19} eV.

Table 2. Width of single particle arrival time distribution

r (km)	No. of particles	mean delay (ns)	dispersion (ns)
0.46	62	238 ± 20	152 ± 10
0.55	202	271 ± 17	242 ± 12
0.65	289	307 ± 16	280 ± 12
0.75	193	330 ± 24	329 ± 17
0.85	161	534 ± 35	448 ± 25
0.95	167	475 ± 39	508 ± 28
1.10	169	649 ± 50	671 ± 36
1.35	88	683 ± 73	660 ± 50

The Volcano Ranch array consisted of 19 detectors. For events such as these most of them were struck by one or more particles. The first step was to select in an unbiased manner one pulse per event. It should not be too small because of statistical errors nor too large because of electronic distortion. The one chosen in each case is the one with greatest S such that $S < 7\ \mathrm{m}^{-2}$. The number of particles contributing to the various AS pulses ($n = AS\cos\theta$, where A is the detector area, 3.26 m^2) ranges from 6 to 22, averaging 12. The values of r range from 0.9 to 2.0 km, averaging 1.4 km.

The AS pulses and a bandwidth-limited (BWL) test pulse were digitized and the dispersions were calculated. The dispersion of the input signal was taken as $(\sigma_{obs}^2 - \sigma_{BWL}^2)^{\frac{1}{2}}$. Sub-luminal pulses, present in 2 cases, were disregarded in calculating σ_{obs}. Thanks to an astute anonymous reviewer it was noted that the data of Table 3 contain useful information about the zenith angle dependence of $<\sigma_t>$. A convenient way to express this is through the parameter b in (1), by letting $b = b_1 + b_2 \sec\theta$. By use of least squares one obtains $b = (1.94 \pm .08) - (0.39 \pm .06) \sec\theta$. Using this expression in (1), there is excellent agreement between Tables 1, 2 and 3. The individual values of $\sigma_t/<\sigma_t>_{calc}$ have about 3 times the variance expected from the simple statistical errors. The excess variance is due in part to systematic differences in primary energy and possibly primary mass, in part to random instrumental errors, and in part to AS fluctuations. By neglecting the first two types of contribution one obtains an upper limit of 20% for the amount of fluctuation in σ_t due to fluctuations in level of origin and shower development.

Table 3. Width of separate event arrival time distributions

serial number	θ (deg)	r (km)	No. of particles	dispersion (ns)
4827	28	1.3	17	490 ± 80
4835	31	1.7	10	1040 ± 230
4860	12	1.3	19	710 ± 120
4882	40	2.0	9	880 ± 200
4906	25	1.1	19	1090 ± 180
4925	7	1.3	12	690 ± 140
4929	55	1.4	11	200 ± 40
4946	37	1.2	13	760 ± 150
4985	39	1.3	9	690 ± 170
5005	23	1.3	10	860 ± 190
5051	40	1.2	9	350 ± 80
5059	31	1.6	6	1550 ± 450
5072	32	0.9	18	540 ± 90
5171	54	1.2	10	380 ± 90
5216	16	1.3	22	920 ± 140
5280	52	1.5	8	750 ± 190

3. Conclusions. Eq. 1 with $\sigma_{to} = 2.6$ ns, $r_t = 30$ m, and $b = (1.94 \pm .08) - (0.39 \pm .06) \sec\theta$ represents the average dispersion in arrival time of AS particles as measured with scintillators when SLP's are excluded. The dispersion is not strongly energy dependent over the range $10^8 < E < 10^{11}$ GeV. The fluctuation in σ_t due to fluctuations in level of origin and shower development is less than 20%.

References. BASSI *et al.* 1953, Phys. Rev. 92, 441; BAXTER *et al.* 1965, Proc. 9th ICRC 2, 724; BOWER *et al.* 1982, Proc. 8th European Cosmic Ray Symposium, paper B-1.4; BOWER *et al.* 1983, J. Phys. G: Nucl. Phys. 9, L53; BROOKE *et al.* 1983, Proc. 18th ICRC 8, 140; CLAY and DAWSON 1984, Aust. J. Phys. 37, 309 (includes data for intermediate distances); DIMINSTEIN *et al.* 1982, *Bull. Nausho-technithekoj Informasii* (Yakutsk) 9, 537 and Proc. 8th European Cosmic Ray Symposium, paper B-1.2; HAZEN and HAZEN 1983, Proc. 18th ICRC 6, 14; LINSLEY *et al.* 1961, Phys. Rev. Lett. 6, 485; LINSLEY and SCARSI 1962, Phys. Rev. 128, 2384; LINSLEY 1977, Proc. 15th ICRC 12, 56, 62, 89; 1980, *Catalogue of Highest Energy Cosmic Rays*, ed. M. Wada (Tokyo: World Data Centre C2) 1, 3; 1983, Univ. New Mexico Research Note UNML-6/20/83; 1984, J. Phys. G: Nucl. Phys. 10, L191; SAKAYAMA and SUZUKI 1981, Proc. 17th ICRC 11, 309; WALKER and WATSON 1981, J. Phys. G: Nucl. Phys. 7, 1297; 1982, J. Phys. G: Nucl. Phys. 8, 1131; WOIDNECK and BÖHM 1975, J. Phys. A: Math, Nucl. Gen. 8, 1004.

STUDY OF THE TIME-DIFFERENTIATED PARTICLE FLUX DENSITY AT VARIOUS DISTANCES FROM EAS AXIS

V.G. Atrashkevich, R.J. Chernykh, Yu.A. Fomin, G.K.Garipov,
G.B. Khristiansen, G.V. Kulikov, A.P. Lebedev, S.J.Matsenov,
V.J. Nazarov, A.A. Silaev, V.J. Solovyeva, V.P. Sulakov,
A.V. Trubitsyn, O.V. Vedeneev
Institute of Nuclear Physics, Moscow State University,
Moscow 119899, USSR

This work is devoted to studying the EAS time structure with the enlarged EAS array of the Moscow State University. The array was described earlier in /1,2/.

The time measurements are made using 22 scintillators which form 13 rectanges of 180x190 m^2 size covering the entire array area. The array was triggered by a signal of 4-fold coincidences of the pulses from the detectors forming each of the rectangles.

The data presented below were obtained during 2200 hours of the array operation in 1984.816 showers to which at least 14 of 22 scintillator detectors responded were selected among all the detected showers. The coordinates of the EAS axis in the observation plane and the EAS sizes were determined by the maximum likelihood method using a computer /1/ on the assumption that the electron LDF is of the NKG form. 492 showers in the interval of EAS size $Ne = 5x10^6 - 2x10^8$ ($\bar{N}e = 1.7x10^7$) with zenith angles $\theta \leq 45°$ and axes within the array were analyzed.

The spatial orientation of the shower axis was determined using only the data of four scintillators included in the rectangle containing shower axis (it is called central system). The shower axis angles θ, φ were found on the assymption of a plane shower front /2/. The front plane was drawn through the central system detector with the maximum detected density of the charged particle flux. The delays of the particle arrivals at the detectors τ were